ISSN 0021-9673

VOL. 672 NOS. 1 + 2 JUNE 24, 1994
COMPLETE IN ONE ISSUE

JOURNAL OF CHROMATOGRAPHY A

INCLUDING ELECTROPHORESIS AND OTHER SEPARATION METHODS

ELSEVIER

JOURNAL OF CHROMATOGRAPHY A

INCLUDING ELECTROPHORESIS AND OTHER SEPARATION METHODS

Scope. The *Journal of Chromatography A* publishes papers on all aspects of **chromatography, electrophoresis** and related methods. Contributions consist mainly of research papers dealing with chromatographic theory, instrumental developments and their applications. In the *Symposium volumes*, which are under separate editorship, proceedings of symposia on chromatography, electrophoresis and related methods are published. *Journal of Chromatography B: Biomedical Applications* —This journal, which is under separate editorship, deals with the following aspects: developments in and applications of chromatographic and electrophoretic techniques related to clinical diagnosis or alterations during medical treatment; screening and profiling of body fluids or tissues related to the analysis of active substances and to metabolic disorders; drug level monitoring and pharmacokinetic studies; clinical toxicology; forensic medicine; veterinary medicine; occupational medicine; results from basic medical research with direct consequences in clinical practice.

Submission of Papers. The preferred medium of submission is on disk with accompanying manuscript (see *Electronic manuscripts* in the Instructions to Authors, which can be obtained from the publisher, Elsevier Science B.V., P.O. Box 330, 1000 AH Amsterdam, Netherlands). Manuscripts (in English; *four* copies are required) should be submitted to: Editorial Office of *Journal of Chromatography A*, P.O. Box 681, 1000 AR Amsterdam, Netherlands, Telefax (+31-20) 5862 304, or to: The Editor of *Journal of Chromatography B: Biomedical Applications*, P.O. Box 681, 1000 AR Amsterdam, Netherlands. Review articles are invited or proposed in writing to the Editors who welcome suggestions for subjects. An outline of the proposed review should first be forwarded to the Editors for preliminary discussion prior to preparation. Submission of an article is understood to imply that the article is original and unpublished and is not being considered for publication elsewhere. For copyright regulations, see below.

Publication information. *Journal of Chromatography A* (ISSN 0021-9673): for 1994 Vols. 652–682 are scheduled for publication. *Journal of Chromatography B: Biomedical Applications* (ISSN 0378-4347): for 1994 Vols. 652–662 are scheduled for publication. Subscription prices for *Journal of Chromatography A*, *Journal of Chromatography B: Biomedical Applications* or a combined subscription are available upon request from the publisher. Subscriptions are accepted on a prepaid basis only and are entered on a calendar year basis. Issues are sent by surface mail except to the following countries where air delivery via SAL is ensured: Argentina, Australia, Brazil, Canada, China, Hong Kong, India, Israel, Japan, Malaysia, Mexico, New Zealand, Pakistan, Singapore, South Africa, South Korea, Taiwan, Thailand, USA. For all other countries airmail rates are available upon request. Claims for missing issues must be made within six months of our publication (mailing) date. Please address all your requests regarding orders and subscription queries to: Elsevier Science B.V., Journal Department, P.O. Box 211, 1000 AE Amsterdam, Netherlands. Tel.: (+31-20) 5803 642; Fax: (+31-20) 5803 598. Customers in the USA and Canada wishing information on this and other Elsevier journals, please contact Journal Information Center, Elsevier Science Inc., 655 Avenue of the Americas, New York, NY 10010, USA, Tel. (+1-212) 633 3750, Telefax (+1-212) 633 3764.

Abstracts/Contents Lists published in Analytical Abstracts, Biochemical Abstracts, Biological Abstracts, Chemical Abstracts, Chemical Titles, Chromatography Abstracts, Current Awareness in Biological Sciences (CABS), Current Contents/Life Sciences, Current Contents/Physical, Chemical & Earth Sciences, Deep-Sea Research/Part B: Oceanographic Literature Review, Excerpta Medica, Index Medicus, Mass Spectrometry Bulletin, PASCAL-CNRS, Referativnyi Zhurnal, Research Alert and Science Citation Index.

US Mailing Notice. *Journal of Chromatography A* (ISSN 0021-9673) is published weekly (total 52 issues) by Elsevier Science B.V., (Sara Burgerhartstraat 25, P.O. Box 211, 1000 AE Amsterdam, Netherlands). Annual subscription price in the USA US$ 4994.00 (US$ price valid in North, Central and South America only) including air speed delivery. Second class postage paid at Jamaica, NY 11431. **USA POSTMASTERS**: Send address changes to *Journal of Chromatography A*, Publications Expediting, Inc., 200 Meacham Avenue, Elmont, NY 11003. Airfreight and mailing in the USA by Publications Expediting.

See inside back cover for Publication Schedule, Information for Authors and information on Advertisements.

0021-9673/94/$07.00

Printed in the Netherlands

VOL. 672, NOS. 1 + 2 JOURNAL OF CHROMATOGRAPHY A JUNE 24, 1994

CONTENTS

(Abstracts/Contents Lists published in Analytical Abstracts, Biochemical Abstracts, Biological Abstracts, Chemical Abstracts, Chemical Titles, Chromatography Abstracts, Current Awareness in Biological Sciences (CABS), Current Contents/Life Sciences, Current Contents/Physical, Chemical & Earth Sciences, Deep-Sea Research/Part B: Oceanographic Literature Review, Excerpta Medica, Index Medicus, Mass Spectrometry Bulletin, PASCAL-CNRS, Referativnyi Zhurnal, Research Alert and Science Citation Index)

REGULAR PAPERS

Column Liquid Chromatography

Gas Chromatography

(Continued overleaf)

Contents (continued)

SHORT COMMUNICATIONS

Column Liquid Chromatography

Gas Chromatography

JOURNAL OF CHROMATOGRAPHY A

VOL. 672 (1994)

JOURNAL OF CHROMATOGRAPHY A

INCLUDING ELECTROPHORESIS AND OTHER SEPARATION METHODS

ELSEVIER

Amsterdam – Lausanne – New York – Oxford – Shannon – Tokyo

J. Chromatogr. A, Vol. 672 (1994)

0021-9673/94/$07.00

Printed in the Netherlands

ELSEVIER

Journal of Chromatography A, 672 (1994) 1–10

JOURNAL OF CHROMATOGRAPHY A

Modeling of radial heterogeneity in chromatographic columns Columns with cylindrical symmetry and ideal model☆

Tong Yun[a], Georges Guiochon*[,b]

[a]*Department of Chemical Engineering, University of Tennessee, Knoxville, TN 37996-1503, USA and Division of Analytical Chemistry, Oak Ridge National Laboratory, Oak Ridge, TN 37831-6120, USA*

[b]*Department of Chemistry, University of Tennessee, Knoxville, TN 37996-1503, USA and Division of Analytical Chemistry, Oak Ridge National Laboratory, Oak Ridge, TN 37831-6120, USA*

(First received December 6th, 1993; revised manuscript received February 11th, 1994)

Abstract

Elution band profiles are calculated for radially heterogeneous cylindrical columns, assuming an infinite rate of mass transfer kinetics and no axial dispersion. Steady-state flow-rate is assumed, with a given, cylindrical radial distribution of the velocity. Parabolic, cuspal and cosinusoidal distributions were studied, all three with either the velocity maximum or minimum in the column center. In all cases, strong changes in the band profiles appear for velocity distributions in which the ratio of the maximum to the minimum velocity is as low as 1.05. Some of the profiles obtained appear to be similar to experimental profiles.

1. Introduction

The theory of chromatography has always assumed so far that the column is radially homogeneous, that the feed is evenly spread over the entire column cross-section and that plug flow is achieved throughout the column [1–5]. Accordingly, the mass balance equation is written and solved in a single space dimension, and the mathematical problem studied has only two dimensions, the column length and the time. However, even analytical chromatographic columns are not homogeneous. There are a few scattered reports in the literature showing significant variations of the mobile phase velocity across the column cross-section, probably caused by a lack of homogeneity of the packing density [6–8]. Preliminary results [9] obtained in our laboratory lead to the same conclusion.

Analytical columns are typically 0.46 cm I.D. and 10–30 cm long, so they are 20 to 60 times longer than they are wide. Even in this case, Knox and Parcher [10] have shown that trans-column equilibration is a comparatively slow process, much slower than axial migration. So, in practice, most sample molecules injected in the center of the column never come close to the column wall. In such a case, radial diffusion cannot even out the effects of fluctuations of the column characteristics related to an inhomogeneous packing density, if these fluctuations take place over a distance significant compared to the column radius. Column heterogeneity causes

* Corresponding author. Address for correspondence: Department of Chemistry, University of Tennessee, Knoxville, TN 37996-1503, USA.

☆ Presented at the *22nd Annual Meeting of the Spanish Chromatography Group, Barcelona, October 20–22, 1993.*

0021-9673/94/$07.00
SSDI 0021-9673(94)00144-X

local fluctuations of the external porosity, the permeability, and the retention factors. It probably explains a large part of the plate height contribution attributed to eddy diffusion [11].

If even an analytical column cannot be considered as homogeneous, a preparative column, typically several inches to a few feet in diameter, and rarely more than 2 or 3 ft. (1 in. = 2.54 cm, 1 ft. = 30.48 cm) long, certainly cannot. Accounting for the local fluctuations in the packing density becomes necessary. This problem has been identified by Giddings [12] long ago. Its solution does not raise major difficulties of principle, but requires the answers to a number of practical problems. The straightforward solution would be to write and solve the mass balance equation of chromatography in a three-dimension space, but this would require an enormous amount of computing power, even though the number of meshes needed in the grid would be much smaller in the two radial directions than along the column axis. Furthermore, the solution of this problem requires the definition of proper boundary conditions, *i.e.*, of the distribution of the packing heterogeneity, a parameter which is usually not available. Finally, experiments show that the efficiency of wide-bore preparative columns is not much below that of analytical columns packed with the same stationary phase. The influence of the column heterogeneity on the profile of large-size samples cannot be important when the profiles obtained with preparative columns remain close to those observed for analytical columns operated at the same loading factor. Thus, a simple correction would be useful in most cases. The general problem does not have to be solved at this stage.

Preparative columns are cylindrical. The lack of stability of the packing observed in numerous cases, the formation of important voids at the top of the bed after operating times ranging from a few days to a few weeks have been attributed by their operators to the lack of bed support by the column wall [13,14]. This suggests that if the bed is heterogeneous, the first approximation for a distribution of the packing density should be cylindrical. Indeed, a cylindrical distribution of the mobile phase velocity in analytical [6–8] or narrow-bore columns [9] is in agreement with experimental results. The long-term stability of the packing bed requires a form of dynamic compression. A number of axial and radial compression columns are currently in use. Because of its geometry, the radial compression columns must be cylindrical with a good degree of approximation. Accordingly, the study of the behavior of band profiles under linear and non-linear conditions in cylindrical, heterogeneous columns would be a satisfactory approximation, and the solution of the chromatographic problem in this case would give an excellent idea of the degree to which column heterogeneity can affect the performance of preparative columns. The advantage of this approach is to reduce the problem to a two-space dimension one, decreasing considerably in the process the amount of computing power required for the calculation of numerical solutions.

If we assume a cylindrical symmetry for the column, the packing is not homogeneous in the radial direction, but the distribution profile is the same in all planes passing through the column axis. As a consequence, the packing density, the column external porosity, and its permeability are constant along any parallel to the column axis. Hence, the mobile phase velocity will be everywhere parallel to the column axis and constant along a parallel to this axis. Because chromatographic columns are always used after proper equilibration between the stationary and the mobile phases, we do not need to solve a time-dependent hydraulic equation. It is legitimate to assume a stable cylindrical distribution of the mobile phase velocity, related to the permeability distribution, and to consider the distribution of the mobile phase velocity as a part of the boundary conditions.

The simplest model of non-linear chromatography is the ideal model. In this model, constant equilibrium of the studied component between the stationary and the mobile phase is assumed. Furthermore, the axial dispersion, due to molecular diffusion and to eddy dispersion is neglected. A linear column operated with these assumptions would have an infinite efficiency. A third assumption of the ideal model is plug flow

distribution. In this work, we investigate what happens if this third assumption is relaxed. We study the band profiles observed in a column where axial and radial dispersion are neglected, and where local phase equilibrium is reached constantly, but where there is a cylindrical distribution of the mobile phase velocity.

2. Theory

In this work, we assumed that the column has an infinite efficiency and that the equilibrium isotherm is given by the Langmuir equation. We divide the column in an infinite number of concentric annular columns of thickness d_r and radius r between 0 and R_c, the column radius. The velocity is constant in each of these annular columns, so its contribution to the elution profile is derived by applying the solution of the ideal model. The elution profiles of the sample on each column are identical, but their breakthrough times are shifted since the velocity varies from annular column to annular column. Summation of these individual contributions over the column radius will give the elution profile as recorded by a conventional detector. It will be possible also to represent the elution of isoconcentration surfaces in order to illustrate the propagation of the zones. We discuss successively the elution profile of the ideal model in the case of the Langmuir isotherm, the velocity profiles selected and the derivation of the profiles.

2.1. The ideal model of chromatography

The ideal model assumes a linear column with an infinite efficiency. In this case the mass balance of a compound is written

$$\frac{\partial C}{\partial t} + F \cdot \frac{\partial q}{\partial t} + u(r) \cdot \frac{\partial C}{\partial z} = 0 \tag{1}$$

where C and q are the local concentrations in the mobile and stationary phases, respectively, F is the phase ratio [$F = (1 - \epsilon)/\epsilon$, with ϵ total column porosity], and $u(r)$ is the mobile phase velocity. Since we assume constant equilibrium between the two phases, q and C are related by the equilibrium isotherm, and given by the Langmuir equation

$$q = \mathrm{f}(C) = \frac{aC}{1 + bC} \tag{2}$$

where a and b are numerical coefficients characterizing the compound studied and the stationary phase. The local concentrations C and q are functions of the two spacial coordinates, z and r and of time, t: $C = C(z,r,t)$. The initial condition is

$$C(z, r, t = 0) = 0 \tag{3}$$

indicating that at time $t = 0$, the column is equilibrated with the pure mobile phase. The boundary condition is the injection of a rectangular concentration pulse of width t_p and height C_0

$$C(z = 0,r,t) = C_0 \text{ for } 0 < t \leq t_p \tag{4a}$$

$$C(z = 0,r,t) = 0 \text{ for } t_p < t \tag{4b}$$

Wilson [15] and DeVault [1] have shown that, for a convex upwards isotherm such as the Langmuir model, the elution profile has two different sides, a front shock and a rear diffuse boundary [16]. This phenomenon arises from the fact that, in the ideal model, a velocity can be associated to each concentration. Thus, if we consider a linear (*i.e.*, homogeneous) column, any concentration propagates along a straight line in the z,t space (z = column length, t = time). The rear, diffuse profile is given by the equation

$$t(r,C) = t_p + t_0(r)\left(1 + F \cdot \frac{\mathrm{d}q}{\mathrm{d}C}\right) \tag{5a}$$

$$= t_p + t_0(r)\left(1 + \frac{aF}{(1 + bC)^2}\right) \tag{5b}$$

where $t_0(r)$ is the hold-up time, now function of the radial position [$t_0(r) = L/u(r)$, where L is the column length], and $t(r, C)$ is the retention time of the concentration C along the cylinder of radius r coaxial with the column. Eq. 5a applies to any isotherm, and Eq. 5b to the Langmuir model. The profiles end with the elution of the concentration 0, at time

$$t_R(r, C=0) = t_p + t_0(1 + aF) = t_p + t_{R,0}(r) \quad (5c)$$

with $aF = k'_0$, the classical retention factor under linear conditions. The retention time of the concentration shock is also the retention time of the band maximum. In the case of a Langmuir isotherm, it is given by [5,16]

$$t_R(r) = t_p + t_0(r) + [t_{R,0}(r) - t_0(r)]\left(1 - \sqrt{L_f}\right)^2 \quad (6)$$

where L_f is the loading factor or ratio of the sample size to the sample amount needed to saturate the column. This column saturation capacity is proportional to the amount of stationary phase in the column and to the ratio a/b of the two coefficients of the Langmuir isotherm. The maximum concentration of the local elution profile is

$$C_M = \frac{\sqrt{L_f}}{b(1 - \sqrt{L_f})} \quad (7)$$

It is independent of the radial position, but this maximum concentration is eluted at time $t_R(C_M, r)$, which depends on r.

2.2. Velocity distribution

The exact distribution of the mobile phase velocity across the column is extremely complicated. It reflects the complexity of the packing structure. The velocity is 0 inside each particle and along its surface. Between particles, it raises very rapidly from the particle surface to the core of the channels, with rapid fluctuations in direction and intensity, as it is probable that more or less stable eddies take place inside some of the minute holes between particles. Any tractable model must simplify drastically the actual flow-rate distribution by considering averages.

The simplest model is the one currently used, the velocity is averaged over the entire column cross-section area by dividing the flow-rate by either πR_c^2 or by the actual cross-section area available to the stream, $\pi\epsilon_e R_c^2$, with ϵ_e the external porosity (approaches favored in hydraulics), or by the cross-section area of the column available to the mobile phase, $\pi\epsilon R_c^2$ (approach favored by chromatographers when they consider the mobile phase flow velocity, $u = L/t_0$). It is legitimate to average out the local fluctuations of the mobile phase velocity over short distances because dispersion may smooth out the concentration gradients caused by these velocity fluctuations (*e.g.*, fluctuations on the scale of the particle diameter). However, this approach precludes from taking into account the large-scale fluctuations of the velocity which cause warping, undulations or other large-scale distortions of the radial shape of the band profiles which may not be smoothed out by dispersion without major loss in column efficiency, or which just subsist until elution of the zone.

In order to account for the effect of large-scale fluctuations in the bed density, we need a more sophisticated model. We assume that the velocity can be averaged out locally, over a scale large compared to the particle size, but small compared to the column radius. Since for the sake of simplicity, we assume the column to have a cylindrical symmetry, we shall consider three cylindrical distributions for the mobile phase velocity, a parabola, two parabolas with a cusp at the column center, and a cosine symmetrical around the column center (Fig. 1). These profiles are referred to later as FLOW-1 (Fig. 1a and b), FLOW-2 (Fig. 1c and d) and FLOW-3 (Fig. 1e and f), respectively. Each velocity profile is characterized by the ratio of the maximum to the minimum velocities. For each distribution, we considered the two possible cases, with either a maximum (u_M) or a minimum (u_m) of the mobile phase velocity in the column center. For each distribution, the calculations were carried out with three different ratios of the maximum to the minimum flow velocity. To permit an easy comparison of the results, the flow velocity distributions were normalized, to achieve in all cases the same value for the mobile phase flow-rate

$$F_v = \int_0^{R_c} 2\pi r u(r)\, dr \quad (8)$$

Thus, the cross-section average velocities, hence the column hold-up times, are the same for all distributions, provided the average velocity be

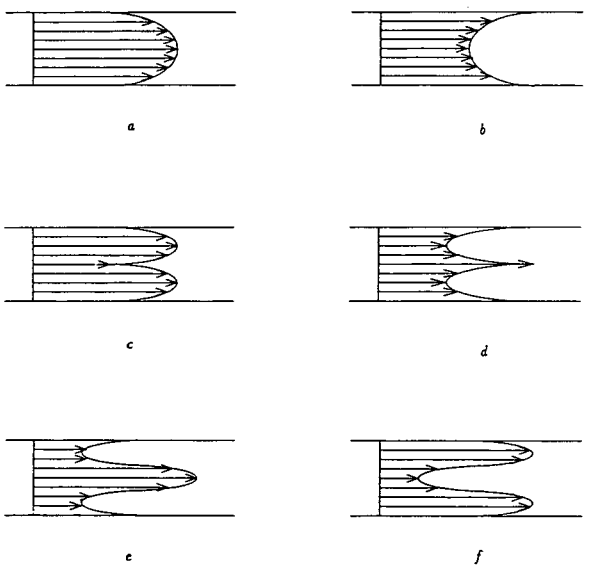

Fig. 1. Velocity distributions used for the band profile calculations (not to scale). (a) FLOW-1, parabolic distribution, $u_C > u_W$. (b) FLOW-1, parabolic distribution, $u_C < u_W$. (c) FLOW-2, cuspal distribution, $u_C < u_M$. (d) FLOW-2, cuspal distribution, $u_C > u_m$. (e) FLOW-3, cosinusoidal distribution, $u_C > u_W$. (f) FLOW-3, cosinusoidal distribution, $u_C < u_W$. u_C = Flow velocity at the column center; u_W = flow velocity along the wall.

defined from the first moment of an unretained band profile.

The velocity distributions are assumed to be fully developed and stable in each case, the velocity being constant along any parallel to the column axis. The possible contribution of transient effects at both ends of the column, where the velocity profile may be different from what it is in the column, under steady-state conditions, are neglected. Also neglected is the radial distribution of the injection profile. A piston injection profile is assumed. The effect of a radial distribution of the injection is discussed in the next section. Finally, the effect of the difference in viscosity between the pure mobile phase and the sample solution inside the moving band is also neglected. Calculations carried out in the case of an homogeneous column [17] have shown that this effect is small unless the sample concentration is very high and the viscosity of the sample is much higher than that of the mobile phase.

The parabolic distribution was chosen for its simplicity. It affords the simplest possible departure from column homogeneity. It is important to understand that the parabolic profile considered here has nothing to do with the Hagen–Poiseuille velocity profile observed in an empty tube. Although the velocity is certainly 0 at the column wall, there are no reasons for it to be smaller at a few particle diameters from the wall than at the column center, unless there is a significant gradient of packing density. In fact, as we show later, the ratio of the maximum to the minimum "local averaged" velocities as defined above which is observed in an actual preparative column is probably lower than 1.1. The other two distributions were selected because experimental results [6–9] suggest that the mobile phase velocity is indeed not constant across the column, and tends to be distributed approximately with a cylindrical symmetry, but also that the maximum velocity is located neither at the column center nor along the wall, but on a near circle having a diameter slightly larger than the column radius.

2.3. Injection profile and velocity profile

In this paper, we study the influence on the elution profile in the ideal model of a radial distribution of the velocity in the column combined with a flat injection profile. This combination is equivalent to that of a constant velocity across the entire column (flat velocity profile) with a radial distribution of the concentration at the injection, so the band profiles obtained will be similar. It is easy to prove this by comparing two experiments, one done with a column having a velocity profile, $u_0(r)$, and a flat injection profile (Fig. 2, dotted line), the other a flat velocity profile and an injection profile such that the injection pulse front shock enters into the column at time $t(r)$ and its rear shock enters the column at $t_p + t(r)$ (Fig. 2, solid line). The elution time of the front shock on the first column will be given by Eq. 6, and the retention time of the concentration C on the rear diffuse

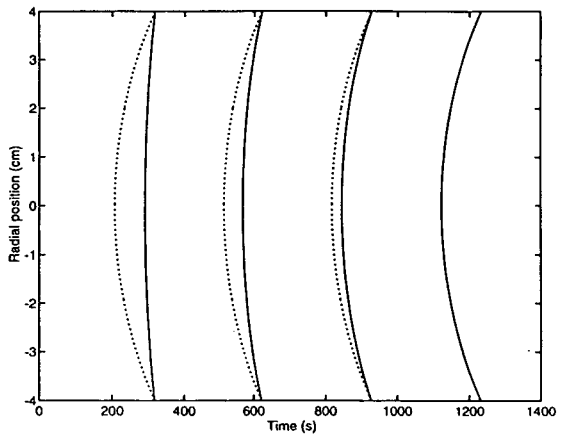

Fig. 2. Comparison between the radial distributions of the concentration obtained with a flat injection in a non-homogeneous column (solid lines) and a nonplanar injection in an homogeneous column with a flat velocity profile (dotted lines). Each profile gives the time of arrival of the front concentration shock as a function of the radial position. The different profiles correspond to different locations along the column (5, 10, 15 and 20 cm). The profile is unchanged for a non-planar injection in an homogeneous column, since there is no radial dispersion in the ideal model. The profile becomes increasing curved for a planar injection in a non-homogeneous column, because the effect of the velocity profile is cumulative.

boundary by Eq. 5b. For the second column, a similar equation can be written, giving the radial distribution of the retention time of the concentration C

$$t_R(r) = t_p + [t_0 + t(r)]\left[1 + k_0'\left(1 - \sqrt{L_f}\right)^2\right] \quad (9)$$

where $t_0 = L/u_0$ is now constant, because the velocity profile is flat (in Fig. 2) and $t(r)$ is the radial profile of the injection. The two radial and axial distributions of all the concentrations C in the elution bands on the two columns will be identical provided

$$\frac{L}{u_0} + t(r) = t_0(r) = \frac{L}{u_0(r)} \quad (9a)$$

$$t(r) = L\left[\frac{1}{u_0(r)} - \frac{1}{u_0}\right] \quad (9b)$$

Eq. 9b is the relation of equivalence between the injection profile in a column with a flat velocity profile and a column with a flat injection and a velocity profile, for them to give the same elution profile.

Accordingly, solving one problem is equivalent to solving the other one, in the framework of the ideal model, because there is no radial dispersion. The equivalence would be approximate in columns having a high efficiency, because the same combination of radial and axial dispersion coefficients would lead to different results in the two columns. Using Eq. 9b would also permit the derivation of an injection profile which would permit the calculation of a band profile affected by both a velocity distribution and an injection distribution. It could also permit the calculation of an injection distribution which would cancel the effects of a known velocity distribution, if it were practical to implement an injection with a complex injection profile.

2.4. Calculation of the elution profiles

The column is divided into n concentric annular columns of thickness $\Delta r = R_c/n$ and of radius r between 0 and R_c. In each annular column, the velocity is constant. The concentration profile at the end of each annular column is derived by applying the solution of the ideal model. The elution profile for the whole column is calculated by summing up the differential amounts eluted from all the annular columns at any given time and reporting this amount to the total volume of mobile phase in the corresponding differential slice of the column

$$\bar{C}(t) = \frac{\sum_{i=1}^{n} 2\pi r_i \Delta r\, u(r_i) C(r_i,t)}{\sum_{i=1}^{n} 2\pi r_i \Delta r\, u(r_i)} = \frac{\sum_{i=1}^{n} r_i \Delta r\, u(r_i) C(r_i,t)}{\sum_{i=1}^{n} r_i \Delta r\, u(r_i)} \quad (10)$$

where $\bar{C}(t)$ is the cross-section average concentration, r_i is the radius of the ith annular column, $u(r_i)$ is the velocity distribution and $C(r_i,t)$ is the solution of the ideal model for the ith annular column. The calculations were done with a value of n equal to 50. The chromatograms obtained are reported in the dimensionless coordinates of the Langmuir model, as $b\bar{C}$ *versus* $(t - \bar{t}_0)/$

$(t_{R,0} - \bar{t}_0)$, where $\bar{t}_0$ and $\bar{t}_{R,0}$ are the average hold-up time and the average limit retention time at infinite dilution. Both average retention times are calculated from the cross-section average mobile phase velocity. Thus, the chromatograms depend only on the velocity distribution and the loading factor.

The concentration profile given by Eq. 9 would be recorded by a detector which would mix and homogenize the entire column stream. In practice, no detector could possibly operate this way without introducing a significant amount of axial dispersion. More probably, the detector would see only part of the column effluent and give a different chromatogram depending on the exact location of the streamlet on which it operates, and one different from the actual average concentration profile. The corresponding sources of errors are not discussed in this paper.

3. Results and discussion

The calculations were carried out for two values of the loading factor, 1 and 10%. The band profiles obtained for each velocity distribution, with these two values, are presented on the same figure. The results are shown in Figs. 3–8, corresponding to the parabolic (Figs. 3 and 4), the cuspal (Figs. 5 and 6) and the cosine (Figs. 7 and 8) velocity distributions, respectively.

A quick glance at these figures shows that the band profile is very sensitive to the nature of the velocity distribution and, in each case, to the amplitude of the velocity fluctuation across the column. All the figures have a few common features, however. First, they share the angular sharpness resulting from the lack of apparent dispersion which is observed for all the profiles derived from the ideal model. Secondly, except in extreme cases, the profile remains highly unsymmetrical, with a steep front and a diffuse rear boundary. Thirdly, the influence of the velocity distribution on the band profiles is more important for the lower value of the loading factor than for the higher one. Fourthly, an important fraction of this rear boundary remains

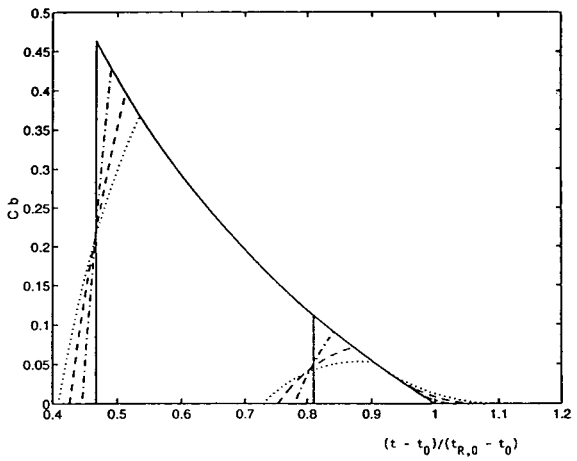

Fig. 3. Band profiles obtained with the velocity distribution in Fig. 1a. Solid line, $u_C/u_W = 1$; dashed-dotted line, $u_C/u_W = 1.05$; dashed line, $u_C/u_W = 1.10$; dotted line, $u_C/u_W = 1.15$. Right profiles, $L_f = 1.0\%$; left profiles, $L_f = 10\%$.

unchanged, whatever the velocity distribution and its amplitude. Finally, the bands end at a finite retention time, another characteristic of the ideal model and of its lack of dispersion.

Comparison of Figs. 3 and 4 (parabolic velocity distribution) shows a great similarity, indicating that, in this case, the nature of the distribution is more important than whether the

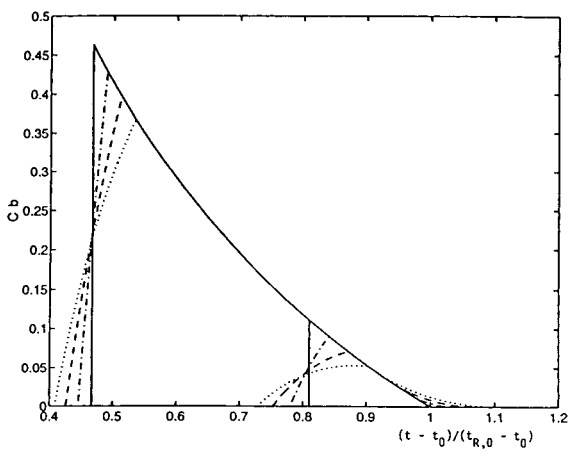

Fig. 4. Fig. 4. Band profiles obtained with the velocity distribution in Fig. 1b. Solid line, $u_W/u_C = 1$; dashed-dotted line, $u_W/u_C = 1.05$; dashed line, $u_W/u_C = 1.10$; dotted line, $u_W/u_C = 1.15$. Right profiles, $L_f = 1.0\%$; left profiles, $L_f = 10\%$.

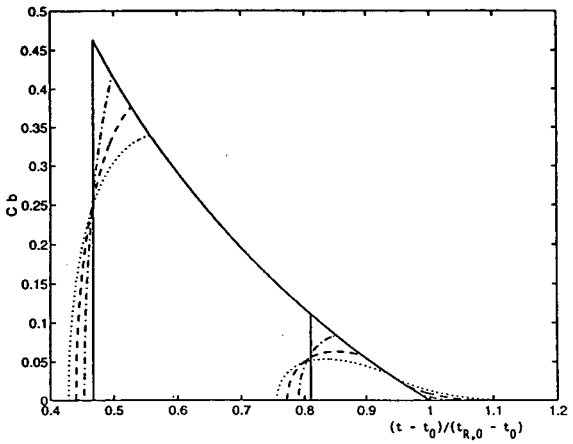

Fig. 5. Band profiles obtained with the velocity distribution in Fig. 1c. Solid line, $u_M/u_C = 1$; dashed-dotted line, $u_M/u_C = 1.05$; dashed line, $u_M/u_C = 1.10$; dotted line, $u_M/u_C = 1.15$. Right profiles, $L_f = 1.0\%$; left profiles, $L_f = 10\%$.

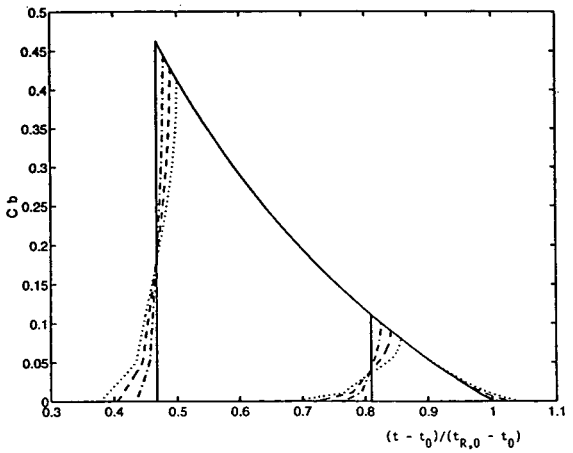

Fig. 7. Band profiles obtained with the velocity distribution in Fig. 1e. Solid line, $u_M/u_m = 1$; dashed-dotted line, $u_M/u_m = 1.05$; dashed line, $u_M/u_m = 1.10$; dotted line, $u_M/u_m = 1.15$. Right profiles, $L_f = 1.0\%$; left profiles, $L_f = 10\%$.

maximum velocity is in the center or close to the wall. For low or moderate velocity ratios, the front is slightly slanted but still nearly a straight line. The time between the beginning of the elution of the band and the elution of its maximum is nearly independent of the loading factor. Accordingly, the profiles of the small size sample bands are more strongly distorted than the heavily overloaded ones. At large velocity ratios, the front still begins as a straight line, then it curves at approximately half the height of the ideal band profile. The band tails slightly, as if the column efficiency had become finite, but still

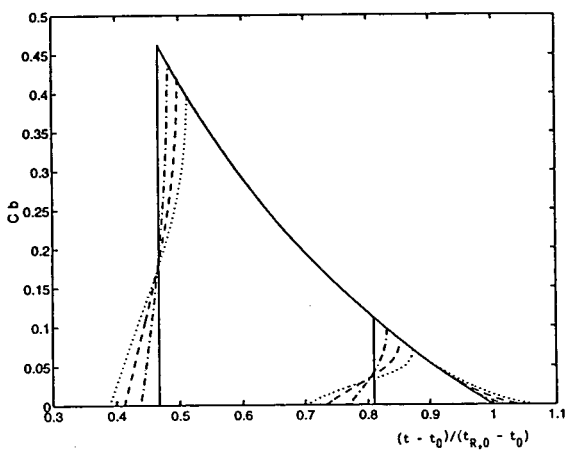

Fig. 6. Band profiles obtained with the velocity distribution in Fig. 1d. Solid line, $u_C/u_M = 1$; dashed-dotted line, $u_C/u_M = 1.05$; dashed line, $u_C/u_M = 1.10$; dotted line, $u_C/u_M = 1.15$. Right profiles, $L_f = 1.0\%$; left profiles, $L_f = 10\%$.

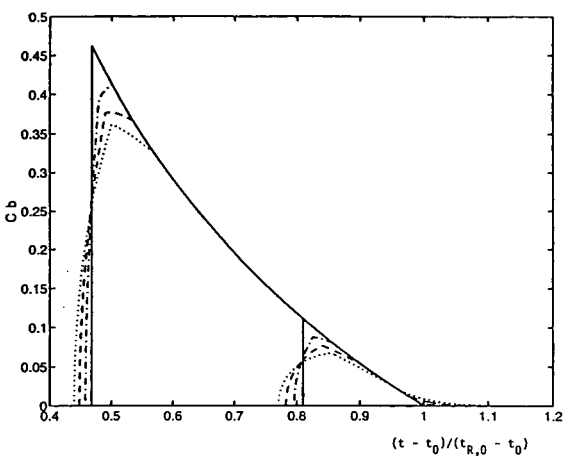

Fig. 8. Band profiles obtained with the velocity distribution in Fig. 1f. Solid line, $u_M/u_m = 1$; dashed-dotted line, $u_M/u_m = 1.05$; dashed line, $u_M/u_m = 1.10$; dotted line, $u_M/u_m = 1.15$. Right profiles, $L_f = 1.0\%$; left profiles, $L_f = 10\%$.

elution is entirely finished after a finite time. As expected [5], the rear of the band is the same for the two sample sizes.

Comparison of Figs. 5 and 6 shows a behavior significantly different from the one observed in the previous case. The band profile is strongly different depending whether the velocity is maximum at the column center (Fig. 5) or at half the column radius (Fig. 6). This is due to the fact that, by contrast with the previous case, the contributions of the different concentric regions of the column cross-section to the profile have significantly different weights. In the former case, the front begins as a shock, to turn backwards, with a slope which decreases rapidly with increasing velocity ratio. At the lower value of the loading factor, the band is nearly flat towards its maximum. The band tail is the same as for the parabolic distribution. In the latter case (Fig. 6), the band begins smoothly, and quite earlier than in the former case (Fig. 5). Beyond its half-height, the profile becomes nearly vertical. This difference is explained by the fact that the regions around the column center and the wall where the velocity is extreme has a much lower surface area than the annular region where the velocity is near its other extreme. Accordingly, the band maximum is quite sharp.

Finally, the comparison of Figs. 7 and 8 shows a situation much closer to the second case than to the first one. The main difference between Figs. 5 and 7, or Figs. 6 and 8, respectively, is in the more progressive rise of the beginning of the band front.

It is also important to observe that in all cases the band width at half-height is barely affected by the importance of the spread of the velocity distribution for a 10% loading factor. It is noticeably increased for the 1% loading factor, but even then the relative change is moderate. The baseline band width is more significantly increased. Thus, the band distortion, and especially the amount of tailing caused by a non-homogeneous packing, may have more serious effects than revealed by mere studies of band widths and apparent column efficiencies. For actual columns, the effect might not be easy to recognize unless the velocity spread is large.

Radial dispersion can relax the concentration gradients arising from large-scale velocity differences over short distances. After a time t, a Dirac pulse in an homogeneous cylindrical tube becomes a Gaussian of variance $\sigma^2 = 2Dt$. Thus, the Fick number, $Fi = z^2/2Dt$, is used to characterize the extend of relaxation of a concentration gradient by dispersion. A Fick number of 1 corresponds to a distance equal to $\sqrt{2Dt}$.

In an actual chromatographic column, the radial dispersion coefficient includes contributions of the molecular and eddy diffusions similar to those involved in the axial dispersion coefficient, but does not include any contributions of the resistance to mass transfer inside the particles nor of the kinetics of adsorption/desorption [7,10]. Accordingly, D_r can be estimated to be between one half and one fifth of $D_a = HL/2t_0 = Hu/2$, depending on the mobile phase velocity (where D_a and D_r are the axial and radial dispersion coefficients, respectively). The distance over which a concentration gradient can be relaxed during the band migration is of the order of $\sqrt{HL/2}$ to $\sqrt{HL/5}$. With values of the column HETP in the 20 to 50 μm range and typical column lengths being around 20 cm, we obtain 0.14 cm, which is indeed small compared to the diameter of most preparative columns. It is barely a quarter of the diameter of conventional analytical columns. Indeed, Knox and Parcher [10] have shown that if a point-like injection is performed at the column center, the elution zone never sees the wall of a conventional column.

The worse chromatogram we have obtained so far, with a radial compression column severely mistreated by raising the inlet pressure above the compression pressure to induce the formation of cracks in the packing [18], is shown in Fig. 9. As this figure illustrates, actual overloaded elution profiles may look somewhat as predicted using a cylindrical velocity distribution (compare the profile in Fig. 9 and the high concentration profiles corresponding to a velocity ratio of 1.05 in Figs. 5 and 8). Nevertheless, in view of the profiles generated in this study, the degree of homogeneity which can be achieved when packing large-diameter preparative columns appears to be more than satisfactory. It seems to corre-

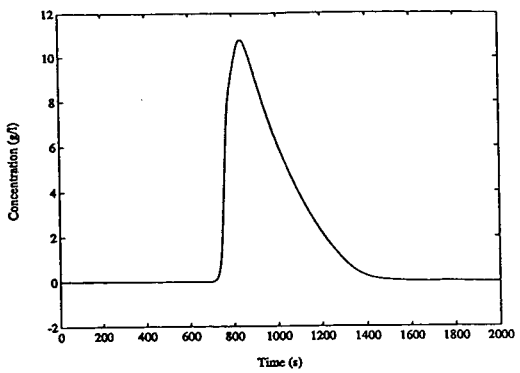

Fig. 9. Experimental band profile obtained with a worn out 17.5 × 7.5 cm radial compression column packed with IMPAQ RG1020C_{18}. Mobile phase methanol–water (40:60), 74 ml/min. Sample, 3.88 g phenol.

spond to velocity distributions where the range of velocity across the column does not exceed 5 to 10% of the average velocity.

4. Conclusions

The ideal model shows that major distortions of the band profiles arise whenever the mobile phase velocity changes significantly across the section of the column. It is rare that experimental profiles exhibit the large deformations which are associated with variations of the local velocity over the column width of the order of 10 to 15%. Thus, a comparison between the results of experiments and those of the calculations discussed in this work tends to show that actual columns are relatively homogeneous. However, the ideal model is not realistic, as we know from studies of classical, homogeneous columns. A radial velocity distribution creates a radial concentration gradient which will be relaxed to some extent by radial dispersion. The actual deformation of the band profiles caused by a non-homogeneous packing distribution will be less than predicted by the ideal model. Further work using a model taking both axial and radial dispersion into account is in progress and will be reported later.

Acknowledgements

This work has been supported in part by grant CHE-9201663 of the National Science Foundation and by the cooperative agreement between the University of Tennessee and the Oak Ridge National Laboratory. We acknowledge the continuous support of our computational effort by the University of Tennessee Computing Center.

References

[1] D. DeVault, *J. Am. Chem. Soc.*, 65 (1943) 532.
[2] E. Glueckauf, *Proc. Roy. Soc.*, A186 (1946) 35.
[3] H.-K. Rhee, R. Aris, N.R. Amundson, *Phil. Trans. Roy. Soc. (London)*, A267 (1970) 419.
[4] F. Helfferich and G. Klein, *Multicomponent Chromatography —A Theory of Interference*, Marcel Dekker, New York, 1970.
[5] G. Guiochon, S. Golshan-Shirazi and A.M. Katti, *Fundamentals of Preparative and Non-Linear Chromatography*, Academic Press, Boston, MA, 1994.
[6] J.H. Knox, G.R. Laird and P.A. Raven, *J. Chromatogr.*, 122 (1976) 129.
[7] C.H. Eon, *J. Chromatogr.*, 149 (1978) 29.
[8] R.M. Wightman, *Anal. Chem.*, 60 (1988) 2334.
[9] T. Farkas and G. Guiochon, *J. Chromatogr.*, submitted for publication.
[10] J.H. Knox and J.F. Parcher, *Anal. Chem.* 41 (1968) 1599.
[11] J.H. Knox, *J. Chromatogr. Sci.*, 15 (1977) 352.
[12] J.C. Giddings, *J. Gas Chromatogr.*, 1 (1962) 12.
[13] H. Colin, in G. Ganetsos and P.E. Barker (Editors), *Preparative and Production Scale Chromatography*, Marcel Dekker, New York, 1993, p. 11.
[14] R.M. Nicoud and M. Perrut, in G. Ganetsos and P.E. Barker (Editors), *Preparative and Production Scale Chromatography*, Marcel Dekker, New York, 1993, p. 47.
[15] J.N. Wilson, *J. Am. Chem. Soc.*, 62 (1940) 1583.
[16] R. Aris and N.R. Amundson, *Mathematical Methods in Chemical Engineering*, Vol. 2, Prentice Hall, Englewood Cliffs, NJ, 1973.
[17] A. Felinger and G. Guiochon, *Biotechnol. Progr.*, 9 (1993) 450.
[18] M. Sarker and G. Guiochon, *J. Chromatogr.*, submitted for publication.

ELSEVIER

Journal of Chromatography A, 672 (1994) 11–24

JOURNAL OF CHROMATOGRAPHY A

Role of local antibody density effects on immunosorbent efficiency

Anuradha Subramanian[a], Kevin E. Van Cott[a], Dean S. Milbrath[b], William H. Velander*[,a]

[a]*Department of Chemical Engineering, Virginia Tech University, Blacksburg, VA 24061, USA*
[b]*3M Bioapplications, 3M Center, St. Paul, MN 55144, USA*

(First received November 17th, 1993; revised manuscript received February 14th, 1994)

Abstract

This study evaluates the effect of immobilized antibody density on the performance of an immunosorbent. In contrast to previous studies that emphasize the correlation of high volume averaged antibody density with immunosorbent performance, we have studied the effects of locally high antibody density and spatial distribution on the antigen binding efficiency under conditions of dynamic loading and elution. The distribution of an anti-human Protein C monoclonal antibody immobilized on 3M Emphaze AB1 Biosupport Medium was evaluated. The distribution of immobilized antibody was controlled by a two-step sequence of permeation and reaction. Labeled antibody was visualized by immunofluorescence. Conditions of low pH, low temperature, and the presence of a competitor nucleophile sufficiently depressed the Thiele modulus for coupling to enable permeation of the antibody. The adsorption of the permeated antibody was enhanced by the presence of 0.75 *M* Na_2SO_4, and then the pH was raised to achieve rapid covalent coupling. Bead-averaged antibody densities of 1–11 mg/ml of hydrogel support were studied. Immunosorbents containing more evenly distributed antibody gave a two- to three-fold greater antigen binding efficiency than those with locally high antibody densities. No appreciable changes in mass transfer characteristics were observed using breakthrough analysis for immunosorbents with distributed *versus* locally high antibody density.

1. Introduction

Immunoaffinity chromatography is a process in which the binding affinity of an antigen (Ag) to a parent antibody is used as the basis for separation, where one of the species is immobilized. Monoclonal antibodies (mAbs) can be selected for a high degree of avidity for an antigen and gentle elution conditions [1–3]. While being a powerful tool for protein purification, the high cost of mAb production and low volume averaged antigen binding efficiency ($\langle \eta_{Ag} \rangle$) of immobilized mAbs makes immunoaffinity chromatography an expensive purification technique. The development of methods that increase the antigen binding efficiency can make immunosorbents more cost effective both at laboratory and industrial scales.

Antigen binding efficiency can be affected by the orientation and localized density of the immobilized antibodies [1,3]. At high localized densities the antigen binding sites of the antibodies may be in sufficient proximity to cause steric hindrance and restricted access of antigen

* Corresponding author.

0021-9673/94/$07.00
SSDI 0021-9673(94)00164-5

Table 1
Summary of immobilized antibody density effects

Reference	Support	mAb/Antigen	Density (mg/ml)	Efficiency (%)
Eveleigh and Levy [6]	Sepharose 4B	Anti-HSA/HSA	1.5	27
			22	10.5
Fowell and Chase [7]	Sepharose 4B	Anti-β-galactosidase/ β-galactosidase	0.3	5.5
			13.8	5.5
Tharakan *et al.* [8]	Sepharose CL2B	Anti-FIX/FIX	1.6	61
			9.67	17
Katoh [9]	Sepharose 4B	Anti-BSA/BSA	1	22
			30	15
Katoh [9]	Activated CH Sepharose 4B	Anti-BSA/BSA	2	18
			25	10
Katoh [9]	Formyl Cellulofine	Anti-BSA/BSA	2	30
			20	10
Strauss *et al.* [10]	CM BioGel A	Anti-FIX/FIX	0.71	20
			15.83	8
Strauss *et al.* [10]	Affi-Gel 202	Anti-FIX/FIX	0.58	28
			19.52	8

to the binding site on the antibody [3]. It also has been postulated that restricted access to the support interior can be caused by high densities of immobilized protein near the surface [4,5]. However, immunosorbent performance is usually correlated with volume-averaged antibody densities ($\langle \rho_{mAb} \rangle$, mg antibody/ml of resin or hydrogel), not local immobilized densities (ρ_{mAb}).

Many researchers have observed lower immunosorbent activity at high volume averaged antibody densities (Table 1). Antibody density effects similar to those that occur in agarose-based supports have also been reported in silica supports [11–14]. In all the immunoaffinity systems reported, the efficiency of the immobilized antibody decreased or remained constant as immobilized antibody density increased. None of the above studies distinguished between $\langle \rho_{mAb} \rangle$ and ρ_{mAb}. This work evaluates the relationship between $\langle \rho_{mAb} \rangle$, ρ_{mAb} and the performance of immunosorbents.

2. Theoretical background

Most protein immobilization on particulate supports is done in a batch mode where intraparticle diffusion is the rate-limiting mass transfer step. Modelling studies have shown that it is primarily the ratio of the reaction rate to the intraparticle diffusion rate that governs the distribution of immobilized antibody [15–18]. The Thiele modulus (Φ^2) is a dimensionless group derived from the governing equations modelling the simultaneous processes of intraparticle diffusion and reaction [15–18]. Φ^2 is of the form

$$\Phi^2 = \frac{R^2 k C}{D_{eff}} \quad (1)$$

where k is a coupling reaction rate coefficient, C is the ligand concentration, R is the radius of the bead support, and D_{eff} is the effective diffusivity of the protein in the matrix.

The distribution of immobilized mAbs within a support matrix can be controlled by changing the Thiele modulus (Φ^2) for the coupling reaction. The rate of diffusional transport of protein into the matrix is primarily determined by the characteristic length over which diffusion will occur (R^2) and by D_{eff}. For low solids content hydrogels, D_{eff} of proteins may be on the order of magnitude of that in a purely aqueous environment, essentially not affected by pH 4–9, and a weak function of temperature. Tyn and Gusek

[19] have compiled experimental values of protein diffusivities and predictive correlations of the form

$$D_{eff} = f(T, 1/M_r) \quad (2)$$

Once mAb is delivered to reactive sites within the support matrix, the rate of the mAb coupling can be divided into a sequence of adsorption and then covalent reaction. mAb concentration may be seen as the major driving force for the adsorption step. Previous studies have shown that increasing the adsorption of proteins onto matrices also increases the yield of immobilized protein [20–22]. We have used Na_2SO_4 to enhance adsorption of mAbs onto Emphaze AB1 and increase coupling efficiencies [20]. Once adsorbed, the rate of coupling of ligand (*i.e.*, mAb) to the reactive matrix is a strong function of pH and temperature. For example, the lysyl residues of a protein (pK_a about 10) will become markedly better nucleophiles at pH greater than about 9. Conversely, the activated (electrophilic) sites on the matrices will have an optimal pH range where competition between acid-catalyzed hydrolysis at low pH and base-catalyzed hydrolysis at high pH will compete with the coupling reaction with lysyl residues.

The functional form of the rate of the combined adsorption and coupling reaction (R_c) for protein near the reaction site can be expressed as the following:

$$R_c = \frac{k \cdot f1(C_{mAb} \cdot N_{sites})}{C_{mAb} + f2(N_{sites})} \quad (3)$$

$$k = k_0 \, e^{-E_{act}/RT}$$

where we view k as a strong function of pH (E_{act} is the activation energy). The number of reactive sites (N_{sites}) will strongly affect R_c. The radial profile of N_{sites} has not been well studied, but we note that the nature of many derivatization procedures may well result in a higher concentration of reactive sites near the edge of beaded supports relative to that found in the bead interior. If the functions f1 and f2 of Eq. 3 are assumed to be first order with respect to N_{sites} as described by Michaelis–Menten or Langmuir adsorption kinetics [21], then R_c can be decreased by lowering the N_{sites} available for mAb immobilization. We have achieved this by simultaneous reaction with a nucleophilic competitor such as a primary amine like Tris.

The process of immunosorption onto a support matrix can be mechanistically viewed as diffusional transport of antigen to the immobilized mAb followed by adsorption and complexation steps. A rate limitation due to mass transfer was not evidenced by the Ag breakthrough and wash profiles (Fig. 4a–d). Thus, we here emphasize the effects of ρ_{mAb} on the kinetics of Ag binding and its relationship to the pointwise antigen binding efficiency $[\eta_{Ag}(r)]$ and then to the bead-average functional efficiency $(\langle \eta_{Ag} \rangle)$. For clarity, we first discuss the elementary reaction steps for antigen capture by mAb in solution, and then we will extend the concept to the more complex situation of immobilized mAb. The elementary reactions steps for antigen capture by mAb in solution can be described by

$$Mab + Ag \underset{k_{r1}}{\overset{k_{f1}}{\rightleftharpoons}} [Mab \cdot Ag_1] \quad (4a)$$

$$[Mab \cdot Ag_1] + Ag \underset{k_{r2}}{\overset{k_{f2}}{\rightleftharpoons}} [Mab \cdot Ag_2] \quad (4b)$$

$$R_{ic} = R_{id} \approx 0 \quad (4c)$$

$$K_{eq1} \equiv \frac{C_{mAb \cdot Ag_1}}{C_{mAb} C_{Ag}} = \left(\frac{k_{f1}}{k_{r1}}\right)_{solution} \quad (4d)$$

$$K_{eq2} \equiv \frac{C_{mAb \cdot Ag_2}}{C_{mAb \cdot Ag_1} C_{Ag}} = \left(\frac{k_{f2}}{k_{r2}}\right)_{solution} < K_{eq1} \quad (4e)$$

The elementary reactions for filling the first antigen binding site are given by Eq. 4a. The elementary reactions for filling the second antigen binding site are given by Eq. 4b. At conditions near to that of equilibrium binding, the sum of the forward (R_{ic}) and backward (R_{id}) reactions rates for each site is approximately zero (Eq. 4c). Based upon protein structure [23], the two Ag binding sites on an empty mAb molecule are assumed to be kinetically indistinguishable. It is only when a large Ag is bound to the first site that a kinetic distinction between the first and second Ag binding site of an individual mAb molecule becomes necessary.

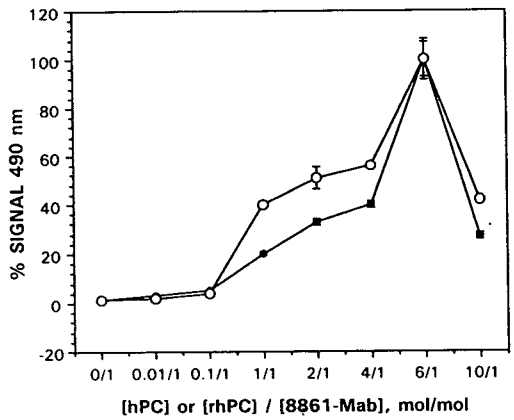

Fig. 1. Binding experiments. Increasing concentrations of (●) hPC and (○) rhPC were incubated with 8861-mAb (0.032 μM) for 1 h at 25°C, and then added to rabbit anti-hPC coated wells. After 1 h of incubation at 37°C, goat anti-mouse IgG HRP conjugate was added to the wells and incubated for 1 h. The hPC–or rhPC–8861-mAb complex was detected and quantified with OPD and reading at 490 nm.

From the solution phase experiments presented here (Fig. 1), we conclude that K_{eq2}, which describes the equilibrium filling of the second antigen binding site, is less than K_{eq1} (Eq. 4e). An increase in % ELISA (enzyme-linked immunosorbent assay) signal as a function of increasing molar concentration of either human Protein C (hPC) or recombinant hPC (rhPC) is indicative of the relative avidity of the two antigen binding domains for hPC or rhPC. Fig. 1 suggests that a large concentration driving force (corresponding to a stoichiometric ratio of Ag:mAb = 6:1) is required to overcome the decreased avidity for filling of the second Ag binding site in solution. This behavior is typical of the mAb we have studied for binding large Ags such as hPC ($M_r = 62\,000$).

The rate expressions for R_{ic} and R_{id} are functions of C_{mAb}, C_{Ag}, $C_{mAb\cdot Ag_1}$, $C_{mAb\cdot Ag_2}$, and the elementary forward (k_{f1}, k_{f2}) and backward (k_{r1}, k_{r2}) rate coefficients. For solution phase mAb–Ag reactions the equilibrium constants defined for K_{eq1} and K_{eq2} can be related to k_{f1}/k_{r1} (Eq. 4d), and k_{f2}/k_{r2} (Eq. 4e). In an analogous way, the combined forward (R_{ic}) and backward (R_{id}) reactions rates can be related to the respective K_{eq1} and K_{eq2} for Ag in equilibrium with immobilized mAb. Under conditions where Ag diffusional transport is not rate limiting, the forward rate of immunocapture (R_{ic}) of Ag by a mAb immobilized with proper orientation can be given by

$$R_{ic} = k_{f1}\rho_{mAb}C_{Ag} + k_{f2}\rho_{mAb\cdot Ag_1}C_{Ag} \tag{5a}$$

$$k_{f1} = k_{f1,0}\exp\left[-\frac{E_{act,0}\cdot f1(\rho_{mAb}, \rho_{mAb\cdot Ag_1}, \rho_{mAb\cdot Ag_2})}{RT}\right] \tag{5b}$$

$$k_{f2} = k_{f2,0}\exp\left[-\frac{E_{act,0}\cdot f2(\rho_{mAb}, \rho_{mAb\cdot Ag_1}, \rho_{mAb\cdot Ag_2})}{RT}\right] \tag{5c}$$

where a kinetic expression of the local solution phase concentration of antigen (C_{Ag}) and the local solid phase concentrations of immobilized mAb (ρ_{mAb}) and mAb–Ag complexes ($\rho_{mAb\cdot Ag_1}$, $\rho_{mAb\cdot Ag_2}$) is proposed. The expressions for the two rate constants k_{f1} and k_{f2} govern the high avidity of the first Ag binding site and the lesser relative avidity of the proximal Ag binding sites due to intra/intermolecular steric hindrance by neighboring mAbs or a sufficiently large Ag occupying that first site. Conceptually, intramolecular and intermolecular steric hindrances of the Ag binding site result in a higher activation energy in R_{ic} that is needed to "push" the antigen into a combined state with the mAb. Hence, f1 (Eq. 5b) and f2 (Eq. 5c) serve as scaling factors to increase the unhindered activation energy $E_{act,0}$ for Ag binding as ρ_{mAb}, $\rho_{mAb\cdot Ag_1}$, and $\rho_{mAb\cdot Ag_2}$ are increased. We assume that $E_{act,0}$ is the same for solution phase or immobilized mAb having proper orientation. Note that R_{ic} becomes highly dependent upon intraparticle position if ρ_{mAb} varies with position.

At equilibrium, the pointwise antigen binding efficiency $\eta_{Ag}(r)$ can be related to K_{eq1} and K_{eq2}

through $\rho_{mAb\cdot Ag_1}$, $\rho_{mAb\cdot Ag_2}$. Antigen binding efficiency $\eta_{Ag}(r)$ is defined by

$$\eta_{Ag}(r) \equiv \left[\frac{\rho_{mAb\cdot Ag_1} + \rho_{mAb\cdot Ag_2}}{\rho_{mAb}}\right]_{r=r} \cdot \frac{1\,\text{mol mAb}}{2\,\text{mol Ag}} \cdot 100\% \quad (6)$$

At conditions of equilibrium, Eq. 6 can be rewritten in terms of the defined equilibrium constants that are analogous to those given by Eqs. 4d and e, but that are now written in terms of the solid-phase concentrations of immobilized mAb and mAb–Ag complexes (ρ_{mAb}, $\rho_{mAb\cdot Ag_1}$, $\rho_{mAb\cdot Ag_2}$).

$$\eta_{Ag}(r) = [K_{eq1}C_{Ag}\{1 + K_{eq2}C_{Ag}\}]_{r=r} \cdot \frac{1\,\text{mol mAb}}{2\,\text{mol Ag}} \cdot 100\% \quad (7)$$

Note that if the functional forms of both R_{ic} and R_{id} are known, they are relatable to $\eta_{Ag}(r)$ by K_{eq1} and K_{eq2}. Finally, $\eta_{Ag}(r)$ is integrated over the whole volume of the bead (V) to give the bead-average functional efficiency ($\langle\eta_{Ag}\rangle$).

$$\langle\eta_{Ag}\rangle = \frac{\int_V \eta_{Ag}(r)\,dV}{\int_V dV} \quad (8)$$

$\langle\eta_{Ag}\rangle$ is the most commonly used measure of immunosorbent efficiency [6–10]. From Eq. 4c and Eqs. 6–8, a local increase in R_{ic} relative to R_{id} will result in an increase in $\eta_{Ag}(r)$; those mAbs with very slow R_{ic} due to locally high ρ_{mAb} will have lower $\eta_{Ag}(r)$.

3. Methods

3.1. Materials and reagents

Murine pH- and EDTA-dependent anti-human Protein C monoclonal antibodies (8861-mAb and 7D7B10-mAb) were provided by the American Red Cross (Rockville, MD, USA). Rabbit antisera against human Protein C, affinity-purified goat anti-mouse (whole molecule), and sheep anti-goat, goat anti-mouse immunoglobulins conjugated to horseradish peroxidase (HRP) were purchased from Sigma (St. Louis, MO, USA). Goat anti-human Protein C antisera was purchased from American Diagnostics (Greenwich, CT, USA). Emphaze AB1 Biosupport Medium was provided by 3M (3M Bioapplications, 3M Center, St. Paul, MN, USA). Immulon II microtiter plates were purchased from Fisher Scientific (Pittsburgh, PA, USA) hPC was provided by the American Red Cross. rhPC was isolated from transgenic porcine whey using ion-exchange and immunoaffinity chromatography [24]. JB4 histological embedding kit was purchased from Polysciences (Warrington, PA, USA). Texas red acid chloride labeled anti-mouse antisera was purchased from Vector Laboratories (Burlingame, CA, USA). *o*-Phenylenediamine–2HCl (OPD) tablets were purchased from Abbott Laboratories (Chicago, IL, USA). Immunoaffinity chromatography was performed with C_{10} columns from Pharmacia (Piscataway, NJ, USA). A Rainin data acquisition system along with a Knauer spectrophotometer was used to monitor column-mode separations. All other reagents were purchased from Sigma at the best grade available.

Emphaze AB1 ($d_p = 60\ \mu m$) is a polymer-based affinity support, synthesized by a copolymerization reaction of 2-vinyl-4,4-dimethyl-1,3-oxazolin-5-one and methylenebisacrylamide at various ratios to yield a rigid and macroporous support for bioseparations [20]. The azlactone functionality readily undergoes a ring-opening reaction with nucleophiles (ex:–NH_2 moieties on the antibody/proteins) to yield stable covalent linkages. The stability of the reactive azlactone functionality under a wide range of pH and temperature makes Emphaze AB1 Biosupport Medium a suitable support for this study.

3.2. Emphaze AB1 immunosorbent preparation

Reference coupling procedure [R] [20]

8861-mAb was incubated for 1 h at room temperature (RT) with dry azlactone beads in coupling buffer (0.05 *M* sodium phosphate–0.75 *M* Na_2SO_4, pH 7.0) containing 1–10 mg of antibody to yield 1–3 ml of immunosorbent. For target densities of 1–2 mg mAb/ml of gel a final

mAb concentration of 0.8–1.0 mg mAb/ml was used, and for target densities of 3–10 mg mAb/ml of gel, a final mAb concentration of 3 mg/ml was used. Residual reactive sites were blocked with ethanolamine. The beads were then washed with 0.5 *M* NaCl and equilibrated with loading buffer for protein immunosorption. Supernatants from all blocking and wash steps were saved for mAb determination by ELISA. The columns were analyzed for mAb leaching during chromatographic runs by ELISA.

Alternate immobilization strategy [A] (two-step method)

8861-mAb (at the same final mAb concentrations as the reference method) was incubated with dry azlactone beads at pH 4.0 for 10 min at 4°C in the presence of 0.5 *M* Tris–HCl and in the absence of Na_2SO_4 in a binary buffer system (50 m*M* acetate, 0.5 *M* Tris–HCl). At the end of the permeation step, the salt concentration was raised to 0.75 *M* Na_2SO_4 and the reaction was allowed to proceed for an additional 10 min. The pH was increased to 9.0 with 1 *M* NaOH and the reaction was allowed to proceed for another 40 min at 4°C at pH 9.0 (a total of 60 min at 4°C). The reference blocking protocol was followed. The supernatants from all blocking and wash steps were assayed for mAbs by ELISA. Columns were analyzed for mAb leaching during chromatographic runs by ELISA.

3.3. Effect of pH/competitor on coupling efficiency

Small-scale experiments (final immunosorbent volume of 40–50 μl) were conducted to determine the pH-dependent mAb coupling efficiency of Emphaze AB1 biosupport medium at 4°C. A ternary buffer system of acetate, phosphate and pyrophosphate (50 m*M* each, 0.75 *M* Na_2SO_4) was adjusted to a final pH of 4–9 with either HCl or NaOH. 7D7B10-mAb (200 μg) was suspended in the ternary buffer at the indicated pH, and dry azlactone beads were added to the reaction tubes. A target $\langle \rho_{mAb} \rangle$ of 5 mg/ml gel was used in these experiments, and the reactions were run in duplicate. To monitor the extent of reaction, the reaction was terminated at 5, 15, 30 min. Supernatant was drawn off for mAb determination by ELISA. The effect of Tris–HCl (0.1 *M*, 0.5 *M*) and salt (Na_2SO_4) on the mAb coupling efficiency at pH 4.0 was determined by similar methods. The condition leading to the slowest rate of immobilization was selected for the first step of our alternate immobilization strategy.

3.4. Chromatography

Columns (I.D. = 1 cm) were packed with approximately 1 ml of 8861/Emphaze AB1 immunosorbent, cleaned with at least 10 column volumes of 2 *M* NaSCN, and then equilibrated with at least 20 column volumes of loading buffer (20 m*M* sodium citrate, 80 m*M* sodium chloride, pH 6.5). After equilibration, pure rhPC at a concentration of 1–2 mg/ml was loaded at about 1 ml/min [linear velocity (u_o) = 1.3 cm/min] until the breakthrough front leveled off. The columns were then washed with the loading buffer until baseline was reached. Bound rhPC was eluted with either a two-step sequence of a pH 10 buffer (0.1 *M* sodium bicarbonate, 0.15 *M* sodium chloride, pH 10) and then 2 *M* NaSCN, or by a single 2 *M* NaSCN elution. All chromatographic fractions were saved for rhPC determination by ELISA.

3.5. Assays

Determination of mAb

Immulon II microtiter plates were coated with 100 μl/well of 1:200 diluted anti-mouse whole molecule in 0.1 *M* $NaHCO_3$ (pH 9.3) for 24 h at 4°C. Wells were washed with 12.5 m*M* Tris–0.05 *M* NaCl–0.05% Tween (TBS–Tween) and the residual reactive sites were blocked with TBS–0.1% BSA (TBS–BSA) for 20 min at RT. Dilutions of standard and samples in TBS–BSA were added to the wells and incubated for 20 min at 37°C. After incubation wells were washed and 1:1000 diluted HRP-conjugated goat anti-mouse IgG was added to the wells and incubated for 20 min at 37°C. Wells were washed and OPD substrate was added to each well. The colorimet-

ric reaction was stopped after 3 min by the addition of 1.5 *M* H_2SO_4 to each well. The plates were read at 490 nm using an EL308 Bio-Tek Microplate reader. The amount of antibody immobilized on the support matrix and the amount of antibody leaching were evaluated by this assay.

Determination of Protein C by polyclonal ELISA

Immulon II plates were coated overnight with 100 μl/well of 5 μg/ml of rabbit anti-human Protein C in 0.1 *M* $NaHCO_3$, pH 9.3 at 4°C. Wells were washed with TBS–Tween. 100 μl of standard and samples in the dilution buffer (TBS–0.1% BSA, pH 7.0) was added to all the wells and incubated at 37°C for 20 min. Wells were washed four times and the bound PC was detected by a sandwich of goat anti-human protein C and HRP-conjugated sheep anti-goat IgG. The plates were read at 490 nm.

Binding experiments

Immulon II plates were coated overnight with 100 μl/well of 5 μg/ml of rabbit anti-human Protein C in 0.1 *M* $NaHCO_3$, pH 9.3 at 4°C. The wells were then washed with TBS–Tween and residual reactive sites were blocked with TBS–BSA for 15 min at RT. Solutions of 0.032 μ*M* 8861-mAb (final concentration) with increasing amounts of hPC or rhPC ranging from 0.04 to 0.32 μ*M* (final concentration) were pre-equilibrated for 1 h at 25°C, and 100 μl of the mAb/hPC or rhPC mixture were added to the IgG-coated wells and incubated at 37°C for 1 h. After washing with TBS–Tween, 100 μl of 1:1000 diluted HRP-conjugated goat anti-mouse IgG was added to the wells. After a 1 h incubation and washing, OPD was added to each well, the reaction was quenched with 1.5 *M* H_2SO_4 after 3 min, and the plate was read at 490 nm.

Immunofluorescent staining of Emphaze AB1 beads

The distribution of mAb in azlactone beads at various densities was determined immunofluorescent microscopy. Texas Red labeled anti-murine IgG (whole molecule) was bound to azlactone beads by the reference as well as two-step procedures at targeted densities of 1, 3 and 8 mg mAb/ml of hydrogel. Dehydrated beads were infiltrated and embedded in JB-4 embedding resin according to manufacturer's instructions. Cross-sections, 10 μm thick, were cut from the block using an LKB automatic microtome. Fluorescent photomicrographs were taken using Kodak Ektar 1000 film.

4. Results

4.1. Binding experiments

The binding of divalent Fab domains on 8861-mAb to hPC (from human plasma) or rhPC was evaluated by ELISA. Fig. 1 presents the ELISA signal resulting from the immunocapture of the (r)hPC–8861-mAb complex formed in solution. Each sample was run in triplicate, error bars are imperceptible for some data. A low and relatively constant response resulted at molar Ag:mAb ratios up to 0.1:1 for both hPC and rhPC. The signal then gradually increased for both rhPC and hPC for molar Ag:mAb ratios from 1:1 to 4:1. A sharp maximum in absorbance was observed at an Ag:mAb ratio of 6:1. rhPC was used for our studies because of the availability of rhPC and the similar avidity of 8861-mAb to hPC and rhPC.

4.2. Effect of pH/competitor on coupling kinetics

To gain a better understanding of the impact of surface density of immobilized mAb on the functional efficiency, we have developed an immobilization strategy to yield a uniform distribution of mAbs throughout the bead cross-section. The distribution of mAbs within the porous support was achieved by controlling both the Thiele modulus for mAb immobilization and by simultaneous titration of reactive sites with a nucleophilic competitor (Tris).

The effect of pH on mAb coupling efficiency (total mAb immobilized/total mAb input) for small-scale columns (40–50 μl) is shown in Fig.

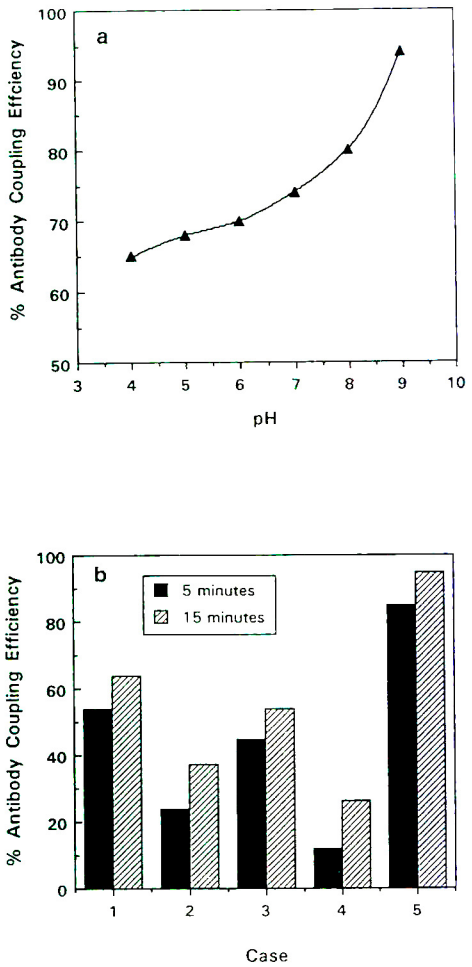

Fig. 2. (a) Effect of coupling pH on mAb immobilization efficiency. Murine EDTA dependent anti-hPC mAb (7D7B10-mAb) was incubated in a ternary buffer (50 m*M* acetate, phosphate, and pyrophosphate) with 0.75 *M* Na_2SO_4 for 30 min at pH 4, 5, 6, 7, 8, 9. Immobilizations were performed as outlined in the Methods section. mAb in feed and coupling step supernatants was assayed by ELISA described in Methods. mAb coupling efficiency is defined as the ratio of total mAb bound to the total mAb input. (b) Effect of salts/Tris on mAb immobilization efficiency. Murine EDTA dependent anti-hPC mAb (7D7B10-mAb) was incubated in 50 m*M* acetate buffer (pH 4.0) both in the presence and absence of 0.75 *M* Na_2SO_4. Immobilizations were performed in the presence of 0.1 or 0.5 *M* Tris–HCl as outlined in the Methods section. mAb coupling efficiency is calculated as in Fig. 3a. Case 1: 0.1 *M* Tris–0.75 *M* Na_2SO_4, 4°C. Case 2: 0.5 *M* Tris–0.75 *M* Na_2SO_4, 4°C. Case 3: 0.1 *M* Tris–0.0 *M* Na_2SO_4, 4°C. Case 4: 0.5 *M* Tris–0.0 *M* Na_2SO_4, 4°C. Case 5: 0.05 *M* sodium phosphate–0.75 *M* Na_2SO_4/pH 7.0, RT.

2a. Immobilization of 7D7B10-mAb at pH 4.0 yielded a mAb coupling efficiency of 65% with a $\langle \rho_{mAb} \rangle$ of 3.2 mg/ml. mAb coupling efficiency increased with pH, with an efficiency of 95% obtained at pH 9.0 to yield a $\langle \rho_{mAb} \rangle$ of 4.8 mg/ml of gel.

The effect of salts, nucleophilic competitor species (*i.e.*, Tris), and temperature on mAb coupling efficiency is shown in Fig. 2b. A target mAb density of 5 mg/ml was used in these experiments. mAb immobilized at pH 7.0 (0.75 *M* Na_2SO_4, no Tris) at RT for 15 min resulted in an average mAb coupling efficiency of 95% (Case 5). Immobilization of mAbs at pH 4 in the presence of 0.75 *M* Na_2SO_4 with Tris at 0.1 *M* and 0.5 *M* gave average mAb coupling efficiencies of 64% (Case 1) and 37% (Case 2), respectively. Upon elimination of Na_2SO_4, coupling at pH 4 and in the presence of 0.1 *M* Tris and 0.5 *M* Tris yielded average mAb coupling efficiencies of 54% (Case 3) and 26% (Case 4), respectively. mAbs incubated at pH 4.0, 0.5 *M* Tris, 4°C for 10 min in the absence of Na_2SO_4, followed by incubation in 0.75 *M* Na_2SO_4 for 10 min and a step change to pH 9.0 at 4°C gave a coupling efficiency of 90% with a $\langle \rho_{mAb} \rangle$ of 4.3 mg/ml.

Table 2
8861-mAb coupling efficiencies

Target density (mg/ml gel)	Actual density (mg/ml gel)	Coupling effiency (%)
Two-step coupling		
1.1	0.9	82
4.5	3.2	71
10	5.7	57
20	9.3	47
Reference coupling		
1.1	1.1	100
2.3	2.2	96
12	11.8	98

Emphaze AB1 immunosorbents were prepared by both reference and two-step methods as described in the Methods section. mAb coupling efficiency was determined as a ratio of the total mAb bound to total mAb challenge.

4.3. Analysis of coupling efficiencies

Table 2 summarizes the mAb coupling efficiencies obtained for larger columns (1–3 ml) with the alternate immobilization (A) and the reference protocol (R) recommended by the manufacturer. The immunosorbents prepared with both methods at similar target $\langle \rho_{mAb} \rangle$ were challenged with the same solution concentration of mAb. Incubation with lower concentrations of mAb ($\langle$0.1 mg/ml) at the same total mAb challenge gave lower coupling efficiencies (data not shown).

Using the reference protocol (R), 8861-mAb was immobilized at mAb densities (mg mAb/ml of hydrogel) ranging from about 1–12 mg mAb/ml of gel. A coupling efficiency of about 100% was obtained for a density of 1.1 mg 8861-mAb/ml of hydrogel. Coupling efficiencies of 96% and 98% were obtained for 8861-mAb immobilized at 2.2 and 11.8 mg/ml of hydrogel, respectively (Table 2).

Immunosorbents were prepared using the two-step procedure (A) with targeted mAb densities of 1–20 mg/ml. A coupling efficiency of 90% was achieved at mAb density of 1.0 mg/ml of hydrogel. However, at higher targeted mAb densities lower coupling efficiencies were obtained. Coupling efficiencies of 71, 57 and 47% were obtained for targeted mAb densities of 4.5, 10, 20 mg mAb/ml of hydrogel, respectively (Table 2).

Leaching of mAbs from the immunosorbents prepared by both the reference and two-step procedures was measured by mAb ELISA on the elution fractions from the first two chromatographic runs. Both A- and R-type columns (for all columns having about 1–12 mg mAb/ml support) gave a similar leaching of mAb; less than about 0.8 μg mAb per mg of rhPC was found in 2 *M* NaSCN eluates where rhPC was loaded at about 50% of theoretical capacity of the column.

4.4. Immunofluorescent staining results

Texas Red labeled antibodies were immobilized according to reference (R) and alternate immobilization procedures (A) at targeted $\langle \rho_{mAb} \rangle$ of 1–8 mg/ml, respectively. Photomicrographs of 10 μm thick bead cross-sections with mAb density of 5–6 mg/ml using fluorescent microscopy are shown in Fig. 3a and b. Beads made with the reference procedure (R) gave a shell-like profile of fluorescent signal in the outer 10 μm of the bead radii (Fig. 3a). Beads made with the alternate procedure (A) gave a more even distribution of the fluorescent signal throughout the cross section (Fig. 3b).

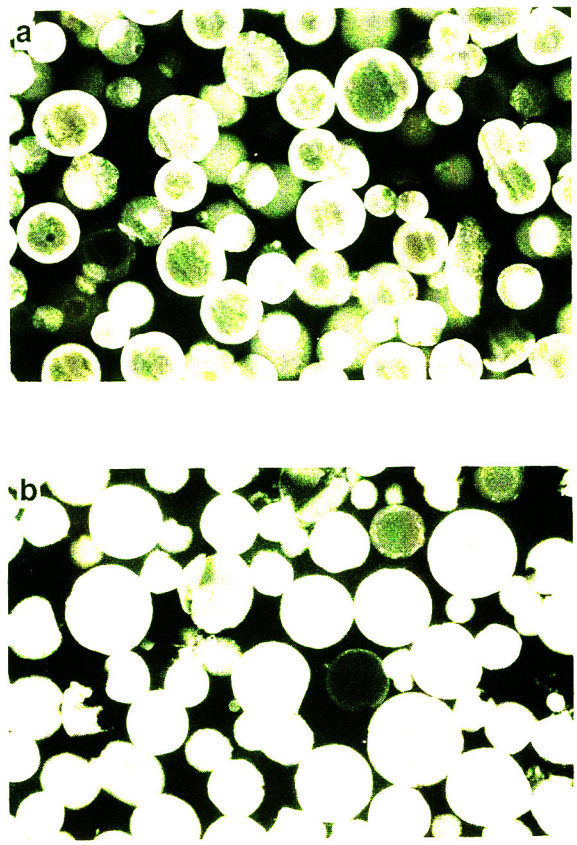

Fig. 3. Texas Red labeled beads. Texas Red labeled anti-mouse IgG was reacted with Emphaze AB1 by the reference and two-step procedures. Fluorescently labeled beads were sectioned as detailed in Methods section and viewed under fluorescent light. Panel a presents an immunosorbent prepared via the reference method at a $\langle \rho_{mAb} \rangle$ of 6.0 mg/ml. Panel b presents an immunosorbent prepared via the alternate immobilization strategy (two-step method) at a $\langle \rho_{mAb} \rangle$ of 5.5 mg/ml.

Table 3
Performance of immunosorbents under breakthrough loading

mAb density (mg/ml)	Run No.	CV[a] (ml)	Flow-rate (ml/min)	Ag loaded (mg)	PC eluted (μg)	Efficiency (η_{Ag}) (%)
Two-step coupling						
0.9	1	1.0	1.0	11	156	22
	2	0.86	0.86	8.0	141	23
3.2	1	1.0	1.0	12	1407	55
	2	1.0	1.0	30	1595	62
9.3	1	1.0	1.0	28	4891	65
	2	1.0	1.0	50	4402	59
Reference coupling						
1.1	1	1.0	1.0	21	180	20
	2	1.0	1.0	8.0	234	26
2.2	1	0.86	0.86	35	471	31
	2	0.86	0.86	12	429	28
11.8	1	1.0	1.0	28	2092	22
	2	1.0	1.0	50	2700	28

Emphaze AB1 immunosorbents described in Table 2 were challenged with pure rhPC in 20 m*M* sodium citrate, 80 m*M* NaCl, pH 6.5. The concentration of rhPC in the feed ranged from 1–2 mg/ml. In each experiment columns with $<\rho_{mAb}>$ of 0.9 (A) and 1.1 (R) mg/ml columns were loaded with 10 CVs of feed, 3.2 (A) and 2.2 (R) mg/ml columns were loaded with 15 CV of feed, and 9.3 (A) and 11.8 (R) mg/ml columns were loaded with 25 CVs of feed. Antigen was eluted from the column by a pH 10 elution (0.1 *M* $NaHCO_3$, 0.15 *M* NaCl, pH 10) followed by a 2 *M* NaSCN elution, the two elution fractions being summed to give the total rhPC eluted. The elution fractions were analyzed by ELISA. Antigen binding efficiency of immunosorbents is defined as the percent of the theoretical maximum binding capacity, assuming a 2:1 antigen to antibody stoichiometry.
[a] CV = Column volume.

4.5. Breakthrough analysis

Table 3 gives operating conditions and antigen binding efficiencies obtained from breakthrough experiments. The antigen-binding efficiencies were calculated using the total amount of rhPC eluted from the sequence of pH 10 and 2 *M* NaSCN elutions. Since the 8861-mAb is an IgG-2A class immunoglobulin, antigen binding efficiency ($\langle\eta_{Ag}\rangle$) of the immobilized mAb was calculated by assuming a binding stoichiometry of two Ags per immobilized mAb. Average antigen-binding efficiencies of 23, 30 and 25% were obtained for 1.1 (R), 2.2 (R), and 11.8 (R) mg/ml columns, respectively. Average antigen-binding efficiencies of 23, 59 and 62% were obtained for 0.9 (A), 3.2 (A), and 9.3 (A) mg mAb/ml of support, respectively.

Fig. 4 shows typical breakthrough and elution profiles at 280 nm for rhPC loaded on 8861-mAb immunosorbent columns made by either reference (R) or two-step (A) methods. The shapes of the breakthrough profiles and respective 2 *M* NaSCN eluate profiles were similar for immunosorbents having comparable $\langle\rho_{mAb}\rangle$. The NaSCN product eluates spanned about 2 column volumes for the 0.9 (A) and 1.1 (R) mg/ml columns. The NaSCN product eluates spanned about 4 column volumes for the 9.3 (A) and 11.8 (R) mg/ml columns, with the two-step column (9.3 mg/ml) having about a three-fold higher binding efficiency, as determined by ELISA.

5. Discussion

In general, Φ^2 is much greater than 1 for most protein immobilization procedures [25], and thus the rate of coupling is much faster than the rate at which protein is delivered into and transported throughout the bead. For example, in the absence of a competitor nucleophile, a shell of

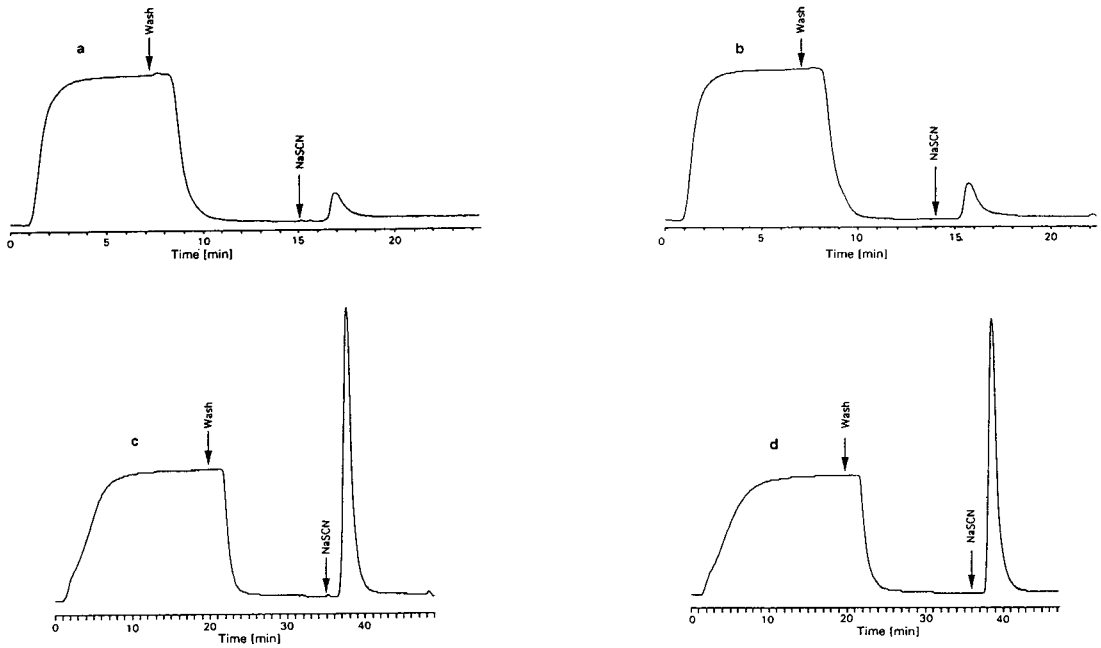

Fig. 4. Breakthrough loading of pure rhPC on Emphaze AB1 immunosorbents. Columns (I.D. = 1 cm) were packed with immunosorbents referred to in Table 2 and loaded with pure rhPC at 1 ml/min. After washing, rhPC was eluted with 2 *M* NaSCN. (a) Two-step procedure, $\langle \rho_{mAb} \rangle = 0.9$ mg/ml, flow-rate = 1 ml/min, column volume = 0.86 ml, $C_{Ag} = 1.1$ mg/ml. (b) Reference procedure, $\langle \rho_{mAb} \rangle = 1.1$ mg/ml, flow-rate = 1 ml/min, column volume = 0.79 ml, $C_{Ag} = 1.1$ mg/ml. (c) Two-step procedure, $\langle \rho_{mAb} \rangle = 9.3$ mg/ml, flow-rate = 1 ml/min, column volume = 1 ml, $C_{Ag} = 1.0$ mg/ml. (d) Reference procedure, $\langle \rho_{mAb} \rangle = 11.8$ mg/ml, flow-rate = 1 ml/min, column volume = 1.2 ml, $C_{Ag} = 1.0$ mg/ml. The amount of rhPC eluted was determined by ELISA

high density, fluorescently labeled mAb results at immobilization conditions of $\Phi^2 > 1$ (Fig. 3a). This is in part due to the high N_{sites} that occurs on Emphaze AB1 [0.25 meq/g of Emphaze AB1 (technical data on 3M Emphaze AB1 from 3M Corporation)] as well as in many other activated supports. In the case of Emphaze AB1 as well as several other activated supports (data for other supports not shown), we have found that the simultaneous conditions of low pH, low temperature and the presence of a competitor nucleophile greatly lower the coupling efficiency and enable permeation. In this work we did not directly determine if pore blockage by anchored antibody occurs at fast reaction/slow permeation conditions, or if there is just such an excess of sites to react that no antibody remains to diffuse in. However, mAb coupling yields for the reference method were greater than 96% for loadings up to about 12 mg/ml. This indicates that pore blockage at the outer edge of the support by antibodies does not occur. Rather a great excess of sites is present and thus antibody is reacted to completion before it can penetrate by diffusion.

Increased permeation was seen in the more evenly distributed fluorescently labeled mAb that was immobilized and visualized in bead cross-sections (Fig. 3b). We conclude that conditions of $\Phi^2 \langle 1$ were achieved by the low pH conditions and presence of Tris. We note that coupling efficiencies of about 40–60% still resulted at pH 4. The addition of 0.5 *M* Tris reduced the coupling efficiency to about 20–30% at pH 4. While both Tris and the lysyl residues are much less nucleophilic at lower pH, some reaction still occurs, probably by an acid-catalyzed mechanism. The Tris effectively inactivates those sites which would be likely to react with

the protein. We note that while the amine group of Tris and lysine would both be fully protonated at low pH, Tris is a very small molecule and thus "kinetically" more nucleophilic species (via acid catalyzed mechanism) than a lysyl residue tied to a large and less mobile protein molecule. Thus, Tris will be more likely to terminate a given site under acid catalyzed mechanism than a lysyl residue on a protein. We here used Na_2SO_4 to assure adsorption after permeation, and a shift to conditions of rapid reaction gave coupling efficiencies of 60–80% for $\langle \rho_{mAb} \rangle$ equal to about 6 mg/ml or less (Table 2). For the 1–6 mg/ml support mAb loadings, the combined levels of mAb and Tris were still probably less than N_{sites}. However, less than 50% yields were obtained at $\langle \rho_{mAb} \rangle$ of about 9 mg/ml, and therefore the combined levels of mAb and Tris were on the order of N_{sites}. For practical applications, the Tris concentration may need to be optimized to achieve a balance between ρ_{mAb} and higher coupling efficiencies at high $\langle \rho_{mAb} \rangle$.

Because $\langle \eta_{Ag} \rangle$ can be related to kinetic phenomena described by R_{ic} and R_{id}, both the reference and two-step immunosorbents were exposed to similar Ag concentration driving forces in each set of Ag breakthrough experiments. The steep return to baseline absorbance during the wash step of these breakthrough experiments supports our assumption that the Ag binding reactions are essentially irreversible. We have purposefully chosen 2 *M* NaSCN elution conditions for the chromatograms in Fig. 4 to elicit fast desorption kinetics and make R_{id} very large relative to R_{ic}. Past studies with 8861 immunosorbents used a pH 10 elution step [24,26]. These previous studies at pH 10 resulted in broad and tailing peaks, which is indicative of conditions where R_{id} is a rate-limiting process relative to mass transfer. It is noted that shell-type and distributed forms of immobilization at similar $\langle \rho_{mAb} \rangle$ yield similar elution profiles at given loading and elution conditions (Fig. 4), although the characteristic length needed to permeate all mAb sites with Ag is much different (Fig. 3a and b). Furthermore, the narrow peak widths obtained using NaSCN as an eluate indicate that any increased penetration needed to access interior mAb sites does not affect the Ag mass transfer rate within a high $\langle \rho_{mAb} \rangle$ immunosorbent. It appears that the amount of mAb which leaches into the 2 *M* NaSCN eluates is similar in either A or R reaction methods. This indicates that the percentage of covalently attached and physiosorbed mAb is similar for either R or A type immobilizations.

Our method of immobilization has enabled study of the relationship between $\langle \rho_{mAb} \rangle$ and ρ_{mAb} to $\langle \eta_{Ag} \rangle$. High $\langle \rho_{mAb} \rangle$ immunosorbents prepared by the reference method have two- to three-fold lower values of $\langle \eta_{Ag} \rangle$ than the two-step method (Table 3). This behavior was found over a range of $\langle \rho_{mAb} \rangle$ from about 3 to 11 mg mAb/ml support, but not for $\langle \rho_{mAb} \rangle$ less than 3 mg mAb/ml. We note that the highest combined levels of C_{mAb} and N_{sites} occur near the edge for both the reference and two-step methods during the initial contacting of the mAb with the matrix. Thus, we expect that significant reaction may occur even at bead average conditions of $\Phi^2 \langle 1$ to form locally high ρ_{mAb} at the outer edge of the beads ($r = R$). Coupling yields of about 20–30% after the first step of the two-step method (at bead average conditions of $\Phi^2 \langle 1$) probably represent mAb that has coupled near the edge at high ρ_{mAb}. The similar appearance of fluorescent-photomicrographs of bead cross sections of the two-step or reference immunosorbents at a labeled $\langle \rho_{mAb} \rangle$ of less than 3 mg mAb/ml supports this conclusion for most mAb coupled at about $r = R$. These analyses showed a narrow band of similar fluorescent signal near the edge of the bead cross-sections for two-step and reference methods (data not shown). In terms of Eqs. 4c and 5a–c, the ρ_{mAb} at about $r = R$ is sufficiently high to reduce the ratio of R_{ic} to R_{id} at that radial position.

Congruently, the two- to three-fold higher $\langle \eta_{Ag} \rangle$ found at about 3 mg/ml or greater in two-step relative to reference immunosorbents is consistent with the locally lower ρ_{mAb} at $r \langle R$, as evidenced by the more evenly distributed fluorescent signal seen in Fig. 3B. Thus, the lower $\langle \eta_{Ag} \rangle$ seen for reference relative to two-

step immunosorbents at ρ_{mAb} greater than about 3 mg/ml is kinetically consistent with a lower ratio of R_{ic} to R_{id} for a large percentage of the immobilized mAb. In summary, it is primarily the mAb immobilized away from the surface by the two-step method at $\langle \rho_{mAb} \rangle$ greater than about 3 mg/ml that benefit from higher $\langle \eta_{Ag} \rangle$ due to locally lower ρ_{mAb}.

This present work establishes the highly non-uniform distribution of mAbs and $\eta_{Ag}(r)$ in immunosorbents, and thus the oversimplifications in previous modelling studies presenting the effects of mass transfer and sorption kinetics on intraparticle concentration profiles of bound Ags [27]. Due to the high values of $\langle \eta_{Ag} \rangle$ we have achieved with our two-step method ($>50\%$), we have proposed a bivalent kinetic model for mAb–Ag interactions (Eq. 5a), rather than the traditional univalent Langmuir model presented in most modelling studies [27]. A more detailed evaluation of kinetic and mass transport effects using similar but more specific functional forms for R_{ic} (Eqs. 5a–c) and R_{id} (not given) is beyond the scope of this work, but is currently being studied to gain further insight into the role of mAb coupling on immunosorbent performance.

6. Conclusions

In the above discussion, we have hypothesized that intermolecular steric hindrance of Ag-combining sites of immobilized mAb by other proximally immobilized mAb and associated Ag–mAb complexes exists and is superimposed upon the inherent intramolecular steric hindrance by bound Ag. The local mAb density in an immunosorbent is a more critical parameter than bead-average mAb density in immunoaffinity chromatography. mAb coupling methods with a large Thiele modulus during permeation will likely result in a shell-type profile with high localized densities. Using a two-step strategy, where the Thiele modulus is low during the permeation step, a more even distribution of immobilized mAb can be achieved at high $\langle \rho_{mAb} \rangle$. This modified coupling method results in increased binding efficiency at high $\langle \rho_{mAb} \rangle$, increasing the overall usefulness of the resulting immunosorbent. The improvement is not strongly related to nor results in mass transfer restrictions in the 60 μm diameter beads studied, and thus is related to changes in the kinetics of Ag adsorption.

7. Acknowledgements

This work was supported by NSF grant BCS-9011098 AMD-2. K.E.V.C. was supported in part by the DuPont PhD Fellowship. The technical assistance of K. Hess and T. Moore is greatly appreciated. The gift of 8861-mAb and 8861-mAb immunopurified hPC from the ARC is greatly appreciated.

8. References

[1] H.A. Chase, *Chem. Eng. Sci.*, 39 (1984) 1099.
[2] C.L. Orthner, R.D. Madurawe, W.H. Velander, W.N. Drohan, F.D. Battey and D.K. Strickland, *J. Biol. Chem.*, 264 (1989) 18781.
[3] W.H. Velander, A. Subramanian, R.D. Madurawe and C.L. Orthner, *Biotechnol. Bioeng.*, 39 (1992) 1013.
[4] K.E. Dennis, D.S. Clark, J.E. Bailey, Y.K. Cho and Y.H. Park, *Biotechnol. Bioeng.*, 26 (1984) 892.
[5] Md.M. Hossain and D.D. Do, *Chem. Eng. J.*, 34 (1987) B35.
[6] J.W. Eveleigh and D.E. Levy, *J. Solid-Phase Biochem.*, 2 (1977) 45.
[7] S.L. Fowell and H.A. Chase, *J. Biotechnol.*, 4 (1986) 1.
[8] J.P. Tharakan, D.B. Clark and W.N. Drohan, *J. Chromatogr.*, 522 (1990) 153.
[9] S. Katoh, *Trends Biotechnol.*, 5 (1987) 328.
[10] W.M. Strauss, G.J. Broze, J.P. Miletich and H.R. Null, *Biotechnol. Appl. Biochem.*, 9 (1987) 462.
[11] P.D. Weston and R. Scorer, *Affinity Chromatogr.*, (1978) 207.
[12] S.R. Narayanan and L.J. Crane, *Trends Biotechnol.*, 8 (1990) 12.
[13] J.R. Sportsman and G.S. Wilson, *Anal. Chem.*, 52 (1980) 2013.
[14] D. Wu and R.R. Walters, *J. Chromatogr.*, 458 (1988) 169.
[15] D.D. Do and J.E. Bailey, *Chem. Eng. Commun.*, 12 (1981) 221.

[16] R. Scharer, Md.M. Hossain and D.D. Do, *Biotechnol. Bioeng.*, 39 (1992) 679.
[17] Md.M. Hossain, D.D. Do and J.E. Bailey, *AIChE J.*, 32 (1986) 1088.
[18] D.D. Do, D.S. Clark and J.E. Bailey, *Biotechnol. Bioeng.*, 24 (1982) 1527.
[19] M.T. Tyn and T.W. Gusek, *Biotechnol. Bioeng.*, 35 (1990) 327.
[20] P.L. Coleman, M.M. Walker, D.S. Milbrath, D.M. Stauffer, J.K. Rasmussen, L.R. Krepski and S.M. Heilmann, *J. Chromatogr.*, 512 (1990) 345.
[21] J.B. Wheatley and D.E. Schmidt, Jr., *J. Chromatogr.*, 644 (1993) 11.
[22] P.L. Coleman, M.W. Walker and D.S. Milbrath, *US Pat.*, 5 200 471, April 6, 1993.
[23] P.M. Alzari, M.-B. Lascombe and R.J. Poljak, *Ann. Rev. Immunol.*, 6 (1988) 555.
[24] T. Morcol, R.M. Akers, J.L. Johnson, F.C. Gwazdauskas, J. Knight, H. Lubon, W.N. Drohan and W.H. Velander, *Ann. N.Y. Acad. Sci.*, 721 (1994) 218.
[25] A. Borchert and K. Buchholz, *Biotechnol. Bioeng.*, 26 (1984) 727.
[26] K. Kang, D. Ryu, W.N. Drohan and C.L. Orthner, *Biotechnol. Bioeng.*, 39 (1992) 1086.
[27] M.A. McCoy and A.I. Liapis, *J. Chromatogr.*, 548 (1991) 25.

ELSEVIER

Journal of Chromatography A, 672 (1994) 25–33

JOURNAL OF CHROMATOGRAPHY A

Immunoaffinity purification of recombinant hepatitis B surface antigen from yeast using a monoclonal antibody

Alberto Agraz*[,a], Carlos A. Duarte[b], Lourdes Costa[c], Lilia Pérez[d], Rolando Páez[a], Vivian Pujol[a], Giuvel Fontirrochi[e]

[a]*Biopharmaceutics Development Department, Center for Genetic Engineering and Biotechnology, P.O. Box 6162, Havana, Cuba*

[b]*Immunotechnology Division, Center for Genetic Engineering and Biotechnology, P.O. Box 6162, Havana, Cuba*

[c]*Quality Control Department, Center for Genetic Engineering and Biotechnology, P.O. Box 6162, Havana, Cuba*

[d]*Hepatitis B Vaccine Production Unit, Center for Genetic Engineering and Biotechnology, P.O. Box 6162, Havana, Cuba*

[e]*Center for Genetic Engineering and Biotechnology, Camaguey, Cuba*

(First received September 13th, 1993; revised manuscript received January 14th, 1994)

Abstract

A murine monoclonal antibody developed for the purification of recombinant hepatitis B surface antigen was immobilized on a chromatographic support and used to adsorb and purify the recombinant antigen from yeast. The adsorption–elution behaviour was first investigated using monoclonal antibody-coated enzyme-linked immunosorbent assay plates and performing adsorption, washing and elution procedures with different elution agents. It was found that 3 *M* KSCN and 8 *M* urea at neutral pH disrupted antigen–antibody interactions in both systems. The procedure for washing the immunoaffinity column was optimized, using different salts and detergents. The best results were obtained by applying the starting material in 1 *M* NaCl and washing with the same buffer. The use of 0.1% sodium deoxycholate in the washing buffer reduced about 20-fold lipopolysaccharide contamination in the eluates as compared with washing without detergent. The relationship between bed height and the adsorption capacity of the column was studied, and it was found that the dynamic capacity decreased twice on reducing its length/diameter ratio tenfold. The recovery of antigen was not affected by increasing the flow-rate up to 25 cm/h but decreased at higher values. Using the optimum conditions, the affinity column was able to purify the recombinant hepatitis B surface antigen to more than 90% purity and a 65% antigen recovery was obtained.

1. Introduction

Immunoaffinity chromatography with monoclonal antibodies (mAbs) has been widely used for the purification of proteins. It has proved to be a powerful tool in several purification procedures, mainly because of the high selectivity of this technique.

Some important aspects have to be considered when an immunoaffinity column is prepared for large-scale purification, including the choice of the solid support, ligand coupling chemistry, ligand coupling density, capacity for the ligand and the product, washing and elution agents, column geometry and flow-rate. In order to improve the performance of the immunoadsorbent, all these parameters must be carefully studied and optimized.

* Corresponding author.

0021-9673/94/$07.00
SSDI 0021-9673(94)00047-D

The nature of antigen–antibody binding can vary to a great extent between different mAbs, even when they are directed against the same antigen. For that reason, once a new mAb, specific for the protein of interest, is obtained, the thermodynamic performance of its interaction with the antigen should be investigated in order to evaluate it usefulness as a ligand.

This kind of study is better performed using enzyme-linked immunosorbent assay (ELISA) or radioimmunoassay (RIA), where the action of a wide range of agents can be investigated and those best suited for this specific system can be selected. Another correct, although more tedious, approach consists in performing adsorption–elution studies in batch, using microamounts of immunoaffinity supports. Low-affinity mAbs are generally preferred because they allow the use of mild elution steps using low denaturing conditions and agents, such as extreme pH values, amines and organic solvents.

Another important element in this technique is the washing step, which diminishes the proportion of undesired, non-specifically bound molecules (contaminant proteins, endotoxins, etc.). Such molecules can be adsorbed on the immunogel by hydrophobic or electrostatic interactions. Most commonly used washing agents include concentrated salts, detergents and chaotropic salts.

The hepatitis B surface antigen (HBsAg) is a well characterized protein of the hepatitis B virus envelope. About 100 molecules of this M_r 24 000 monomeric form are assembled into 22-nm particles. These particles are stabilized by disulphide bonds [1], and contain carbohydrates and lipids [2]. The gene encoding for the antigenic protein has been cloned and expressed in bacteria [3,4], animal cells [5–8], vaccinia virus [9] and yeast [10–17]. Several purification procedures have been described [1,18–23], some of them using immunoaffinity chromatography.

This paper presents the results of the immunoaffinity purification, using mAb CB-HEP.1, against recombinant hepatitis B surface antigen (r-HBsAg), which is included in a vaccine preparation against the hepatitis B virus. The influence of several chromatographic parameters, such as washing and elution agent, flow-rate and column geometry, on the immunoaffinity performance was also analysed.

2. Experimental

2.1. Materials

All chemicals were of analytical-reagent grade. Sodium deoxycholate was obtained from Fluka (Buchs, Switzerland) and Triton X-100 and Tween 20 from BDH (Poole, UK). Other chemicals were purchased from Merck (Darmstadt, Germany).

2.2. Source of r-HBsAg

r-HBsAg was produced by fermentation of a recombinant strain of *Pichia pastoris* (C-226) in saline medium supplemented with glycerol, and its expression was induced with methanol. The r-HBsAg was recovered and submitted to initial purification steps as described previously [21]. Briefly, the cells were harvested by centrifugation and disrupted on a bead mill (KDL type; WAB, Basle, Switzerland). The disruption buffer contained 20 m*M* Tris–HCl (pH 8.0), 3 m*M* EDTA, 0.3 *M* NaCl, 3.0 *M* KSCN and 10 g/l sucrose. The homogenate was submitted to acid precipitation by adding 1 *M* HCl down to pH 4.0 and centrifuged at 10 000 *g* for 30 min. The supernatant was placed in contact with Hyflo Super Cell (a flux calcined grade of Celite filter aid) equilibrated to the same pH (4.0) under continuous stirring. Adsorption was allowed to take place for 2 h and the Hyflo Super Cell was separated by centrifugation. After washing the matrix twice with two Hyflo Super Cell volumes of 0.2 *M* KSCN solution, the antigen was eluted with 20 m*M* Tris–HCl–3 m*M* EDTA–100 g/l sucrose (pH 8.2). With the described procedure, a semi-purified material of about 10–25% purity was obtained. This was used as the starting material for all immunoaffinity experiments.

2.3. Monoclonal antibody

Mab CB-HEP.1, secreted by the hybridoma cell line 48/1/5/4, has been characterized previ-

ously [24]. This hybridoma was shown to secrete IgG2b and IgM antibodies having the same specificity against HBsAg. The clone used for this work was selected because of its lower secretion of the IgM component. The antibodies were purified from ascites by protein-A affinity chromatography. The purity of the final antibody preparation (IgG + IgM) was more than 90% and the content of IgM less than 3%, both assessed by sodium dodecyl sulphate–polyacrylamide gel electrophoresis (SDS-PAGE) under reducing conditions.

2.4. Binding and elution of the antigen using 96-well plates

A poly(vinyl chloride) microplate (Dinatech, Cambridge, UK) was coated with 100 μl per well of 10 μg/ml CB-HEP.1 Mab in 0.1 *M* sodium hydrogencarbonate buffer (pH 9.6) overnight at 4°C. mAb solution was removed and the blocking step was performed using 100 μl per well of 1% fat-free milk in phosphate-buffered saline (PBS) for 30 min at 37°C. Subsequently, 100 μl per well of 200 ng/ml purified r-HBsAg diluted in PBS + 1% fat-free milk and 0.5% Tween 20 was added. After incubation for 1 h at 37°C, the plate was washed three times using 0.05% Tween 20 in PBS. Elution from the plate was carried out by adding 100 μl per well of different eluting agents: (a) 8 *M* urea in PBS, (b) 4.5 *M* $MgCl_2$ in PBS, (c) 10% dioxane, (d) 20 m*M* Tris(hydroxymethyl)aminomethane(Tris)–50% ethylene glycol adjusted to pH 11.6 with NaOH, (e) 20 m*M* Tris adjusted to pH 11.6 with NaOH, (f) 0.2 *M* glycine–HCl (pH 3.5), (g) 3 *M* KSCN and (h) 3 *M* GuSCN (where Gu = guanidine). The plate was washed five times in the same manner as described before and incubated at 37°C for 1 h with 100 μl of anti-HBsAg sheep polyclonal antibody–peroxidase conjugate. After washing, the plate was developed using 100 μl of 0.05% *o*-phenylenediamine and 0.015% hydrogen peroxide in citrate buffer (pH 5.0). The reaction was stopped after 20 min with 50 μl of 1.25 *M* H_2SO_4. The plate was finally measured on a Multiskan system (Titertek, Helsinki, Finland) at 492 nm. Each condition was assayed twice in two different tests.

The percentage of elution (E) was calculated as $E = [100 - (M - B/C - B)] \cdot 100$, where M is the absorbance at 492 nm, B is the absorbance without HBsAg and C is the absorbance of a control (eluted with PBS).

2.5. Binding and elution of the antigen using immunoaffinity columns

Sepharose CL-4B (Pharmacia–LKB, Uppsala, Sweden) was activated by the CNBr method and kindly supplied by Dr. L. Rodés (Department of Chemistry of Solid Surfaces, CIGB, Havana, Cuba). The CB-HEP.1 mAb was coupled as recommended by the manufacturer. The ligand coupling density was determined by measuring the total protein before and after the coupling reaction, and it was about 5 mg/ml of gel for all experiments if not specified otherwise.

The gel was packed on a K 16/20 column (5 cm × 1.6 cm I.D.) and equilibrated with 20 m*M* Tris · HCl–3 m*M* EDTA (pH 7.8). The column was loaded with an excess of semi-purified r-HBsAg preparation in the same buffer and washed using about five column volumes of starting buffer containing 1 *M* NaCl. After washing, the column was eluted with the corresponding eluting agent. The elution peak was monitored (280 nm) and collected for all experiments. The eluting agents tested were (a) 8 *M* urea, (b) 4.5 *M* $MgCl_2$, (c) 10% dioxane, (d) 50% ethylene glycol–20 m*M* Tris adjusted to pH 11.6 with NaOH, (e) as (d) without ethylene glycol, (f) 0.2 *M* glycine–HCl (pH 3.5), (g) 3 *M* KSCN and (h) 3 *M* GuSCN. All eluting solutions except (d), (e) and (f) contained 20 m*M* Tris–HCl buffer (pH 7.8) if another pH is not specified. The flow-rate was 25 cm/h. The immunogel was replaced each time and three runs were performed for each condition.

2.6. Optimization of washing step

The immunogel was packed on a K 16/20 column (10 cm × 1.6 cm I.D.) at 25 cm/h and equilibrated using 20 m*M* Tris · HCl–3 m*M* EDTA (pH 7.8). The column was loaded up to 85% of its maximum capacity with semi-purified r-HBsAg. Subsequently, different washing pro-

cedures were tried: (A) first with 0.1% sodium deoxycholate and then with 1 *M* NaCl, (B) first with 10% sucrose and then with 1 *M* NaCl, (C) first with 0.5% Triton X-100, second with 0.3 *M* GuHCl–0.3% Triton X-100, third with 0.5 *M* NaCl–0.2% Triton X-100 and finally with 1 *M* NaCl, (D) first with 0.5% sodium deoxycholate and then with 1 *M* NaCl, (E) first with 1 *M* NaCl, second with 0.5 *M* KSCN and finally with 1 *M* KSCN, (F) first with 0.1% Tween 20 and then with 1 *M* NaCl, (G) first with 1 *M* NaCl, second with 0.1 *M* GuHCl and finally with 0.2 *M* GuHCl, (H) the sample was pre-incubated on 0.1% sodium deoxycholate, applied in this same buffer and then washed with 1 *M* NaCl and (I) 1 *M* NaCl was added to the loading sample, then washed with 1 *M* NaCl. All washing buffers contained 20 m*M* Tris·HCl (pH 7.8). After washing, the column was eluted using 20 m*M* Tris·HCl–3 m*M* EDTA–1 *M* NaCl–3 *M* KSCN (pH 7.8). The purity of the material eluted from each run was determined by SDS-PAGE.

2.7. Washing the column with detergent to reduce endotoxin (ET) levels

Semi-purified r-HBsAg was contaminated with various amounts of bacterial lysate (*Escherichia coli*) to evaluate the ability of the affinity column to remove endotoxins (ETs).

The protocol for the adsorption and elution of the r-HBsAg was similar to that described for previous experiments. Two washing procedures, each involving three consecutive steps, were compared: procedure (a), 1 *M* NaCl + buffer + 1 *M* NaCl; procedure (b), 1 *M* NaCl + 0.1% sodium deoxycholate + 1 *M* NaCl. All buffers contained 20 m*M* Tris·HCl–3 m*M* EDTA (pH 7.8). Samples were analysed for ET content with the Toxicolor LAL test (Seikagaku Kogyo, Tokyo, Japan).

2.8. Influence of ligand density on adsorption capacity

Different amounts of mAb were coupled to 1 ml of activated CL-Sepharose 4B gel. The exact amounts of coupled mAb were calculated from the difference between protein concentrations before and after the coupling procedure. Five columns were prepared with 8.6, 7.1, 4.9, 2.5 and 1.0 mg of mAb/ml of immunogel. Runs were performed by overloading the column with semi-purified r-HBsAg equilibrated in 20 m*M* Tris·HCl–3 m*M* EDTA (pH 7.8), washed with 1 *M* NaCl and eluted with 3 *M* KSCN–1 *M* NaCl in the same buffer.

2.9. Influence of flow-rate and bed height on recovery and productivity of the affinity chromatographic step

Studies were performed on a K 16/20 column (10 cm × 1.6 cm I.D.) packed with the immunogel at linear flow-rates of 10, 20, 50, 70 and 100 cm/h. Three runs were carried out for each condition.

For all experiments, the column was first equilibrated with 20 m*M* Tris·HCl–3 m*M* EDTA (pH 7.8). A semi-purified r-HBsAg sample (about 85% of maximum gel capacity) equilibrated in the starting buffer was applied and the column washed with 1 *M* NaCl in the same buffer. After the washing step, elution was performed using 3 *M* KSCN–1 *M* NaCl in the same buffer.

In order to assess the influence of bed height on the recovery of r-HBsAg, a K 16/20 column was packed with different amounts of immunogel to give bed heights of 20, 10, 5 and 2 cm. Three runs were carried out for each condition, loading the immunogel with 85% of its maximum loading capacity for HBsAg. The linear flow-rate was 20 cm/h. The adsorption, washing and elution steps were carried out as described in previous experiments.

2.10. Determination of r-HBsAg concentration

The concentration of r-HBsAg was determined by a sandwich ELISA using sheep polyclonal antibodies against HBsAg both in the capture antibody and the horseradish peroxidase conjugate. The HBsAg secondary standard was calibrated against an international HBsAg stan-

dard preparation obtained from the Paul Erlich Institute (Frankfurt/Main, Germany).

2.11. Determination of protein concentration

Protein concentration was determined by the Bradford method [25] using bovine serum albumin (BSA) as a standard.

2.12. Electrophoresis

SDS-PAGE of reduced samples was performed according to Laemmli [26]. The gels were stained with Coomassie Brilliant Blue R-250.

3. Results and discussion

3.1. Elution of bound antigen with different agents

The screening for appropriate elution agents using 96-well plates showed that urea, $MgCl_2$, KSCN and GuSCn had the highest elution efficiency, recovering between 65 to 75% of bound antigen (Fig. 1). In contrast, extreme pH buffers and 10% dioxane had a low elution effect. According to these results CB-HEP.1 belongs to the group of antibodies whose interaction with the antigen is better disrupted by chaotropic agents than by extreme pH values.

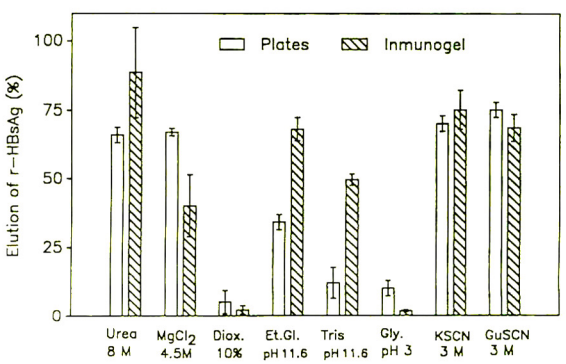

Fig. 1. Elution of r-HBsAg from microplates and Sepharose 4B immobilized mAb using different elution agents. Elution is expressed as % of adsorbed antigen. Diox. = Dioxane; Et. Gl. = ethylene glycol; Gly. = glycine.

In addition, a good correlation of the elution profiles of the different agents using plates and packed immunogel was obtained for most of them (Fig. 1). Only for basic pH buffers was the antigen recovery higher [about twice as much with 50% ethyleneglycol (pH 11.6) and four times as much with Tris adjusted to pH 11.6 with NaOH] on the immunogel than in plates.

In spite of these differences, the results demonstrate that the microplate assay can be very useful for the initial evaluation of a large number of solutions.

Among the solutions tested, 3 *M* KSCN was chosen as the elution buffer, mainly because KSCN is a well known HBsAg particle stabilizer [1].

3.2. Optimization of washing step

Results from the comparison of the different washing procedures are summarized in Table 1. Only with procedures H and I were purity levels higher than 90% achieved. In both instances the washing agent (sodium deoxycholate in H and NaCl in I) was added to the sample before loading it into the column. It is remarkable that the use of NaCl and sodium deoxycholate in other protocols, even at higher concentration, did not produce similar results. This outcome underlines the importance of avoiding the non-specific adsorption of contaminant proteins to the matrix by previously mixing the washing agent with the sample.

The recovery of r-HBsAg in the eluted fraction was adequate for variants A, B and I. On the other hand, variants D and F showed a significant loss of r-HBsAg (41 and 33%, respectively) in the washing fraction, probably owing to the presence of detergents (0.5% of sodium deoxycholate and 1% Tween 20). Variant H showed a low recovery (26%) and only 60% of the applied sample was found in the other fractions.

The same happened with variant E, but in this instance the elution of r-HBsAg was due to the presence of 1 *M* KSCN. The purity of r-HBsAg

Table 1
Washing of the immunoaffinity column using different protocols and solutions

Washing protocol	Amount (mg)				r-HBsAg yield (%)	SDS-PAGE[a] purity (%)
	Applied	Non-bound	Washing	Elution		
A	1.9	0.2	0.1	1.2	63	70–80
B	2.4	0.2	0.2	2.2	91	70–80
C	1.9	0.3	0.1	0.1	5	70–80
D	3.4	0.7	1.4	0.5	14	70–80
E	3.1	1.0	1.4	0.9	29	80–90
F	3.6	0.5	1.2	1.9	52	70–80
G	3.5	0.7	0.6	0.7	20	70–80
H	3.5	0.7	0.5	0.9	26	>90
I	2.9	0.7	0.03	1.9	65	>90

[a] Purity was estimated visually from SDS-PAGE of eluates.

obtained with this variant was higher, but the yield was very low.

With washing protocols C and G, the bound antigen was recovered neither in the washed nor in the eluted fraction. In further studies, GuHCl was found to interfere in the r-HBsAg determination test, so the missing antigen may have been, in fact, in the washed fraction.

Further analysis on a TSK-2000 SW HPLC gel-filtration chromatographic column of the eluted r-HBsAg from protocols H and I showed that some molecule population of the antigen coming from H (0.1% sodium deoxycholate) is overaggregated, judging by the retention time of a peak that eluted before the mean peak of well particulated antigen. The degree of aggregation of r-HBsAg particles was corroborated by electron microscopy (not shown). Changes in the morphology (aspect and size) of the natural HBsAg particles submitted to heat treatment has been described previously [27]. This HBsAg overaggregation is probably induced by the action of sodium deoxycholate on the lipid moieties of the particle.

On the other hand, antigen coming from protocol I had a homogeneous molecule population, showing the expected particle size of about 22 nm, determined by electron microscopy. Fig. 2 shows the SDS-PAGE of purified antigen using washing protocol I.

3.3. Ability of the immunoaffinity column to remove ETs

The use of 0.1% sodium deoxycholate in the washing buffer reduced the ET levels about 25-fold, whereas the washing procedure without detergent reduced ETs only about 1.5-fold (Fig.

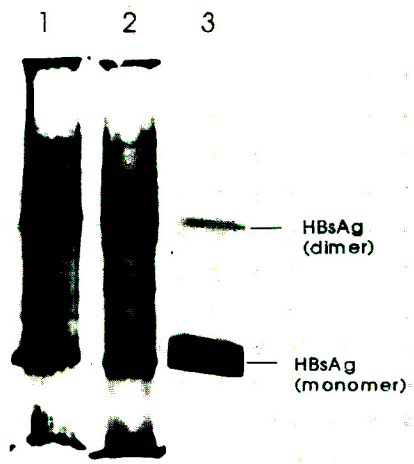

Fig. 2. SDS-PAGE of reduced samples from the immunoaffinity purification using washing protocol I (15% polyacrylamide gel). 1 = Starting material; 2 = non-bound fraction; 3 = eluted fraction. 20 μg of protein were applied per sample.

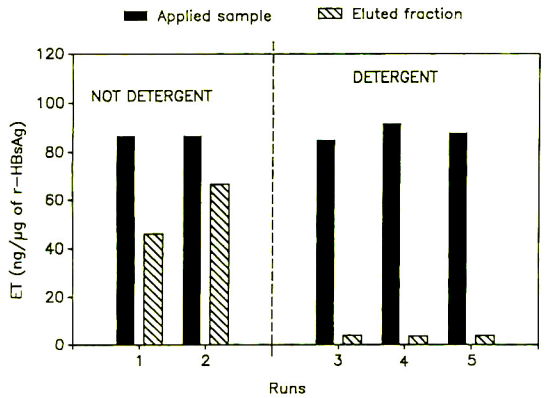

Fig. 3. Effect of detergent on the removal of endotoxins (ETs) from r-HBsAg in the immunoaffinity column. Bars represent the level of Ets in applied and eluted fractions.

3). The recoveries of r-HBsAg in the eluted fraction of runs 1–5 were 57, 65, 62, 57 and 68%, respectively. As can be seen, detergent treatment was able to wash away non-specifically bound lipopolysaccharides (LPSs) without significant losses of adsorbed antigen. This result was predictable, considering the highly hydrophobic nature of LPSs. The use of a washing solution with a high ionic strength must enhance the hydrophobic interactions between LPSs and the matrix or with hydrophobic patches of the adsorbed proteins. Detergents lower this interaction, causing the elution of the contaminating LPSs.

3.4. Effect of ligand density in the productivity per milligram of mAb in the gel

Table 2 shows the results of the adsorption and elution of r-HBsAg from gels prepared with a different ligand density. Although the total adsorbed antigen increased with increasing amount of coupled mAb, this increment was not linear. As a result, the amount of antigen adsorbed per milligram of coupled mAb decreased drastically (fivefold). Consequently, the purification cost per unit of r-HBsAg increased. In this instance, for practical purposes, the use of 1 or 2 mg of mAb/ml of gel can be recommended.

Table 2
Adsorption capacity of the immunoadsorbent at different ligand densities

Ligand coupling density (mg mAb/ml gel)	r-HBsAg eluted (μg)	Antigen purified per mg of coupled mAb (μg r-HBsAg/mg mAb)
8.6	217	25.2
7.1	212	29.8
4.9	196	40.0
2.5	153	61.2
1.0	131	131.0

3.5. Effect of flow-rate on the performance of the immunoadsorbent

Within the range of linear flow-rates studied, high recoveries were obtained up to 25 cm/h (Fig. 4), but the recovery began to decrease almost linearly as the flow-rate increased from 50 to 100 cm/h. Although the gel itself (Sepharose CL-4B) can resist such elevated flow-rates, a diffusion mechanism limits the antigen accessibility to the mAb molecules in the beads, considerably lowering the functionality of the

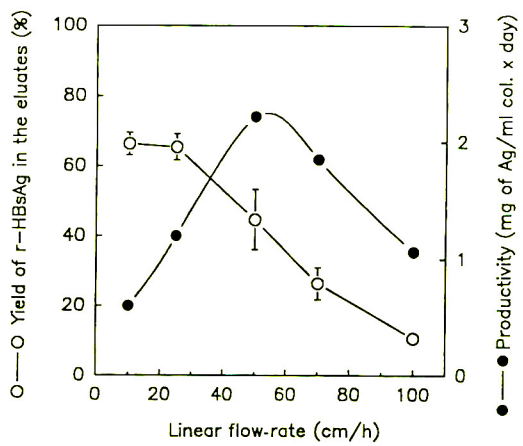

Fig. 4. Influence of linear flow-rate on recovery of r-HBsAg in the eluted fraction. Yield of antigen is expressed as a percentage of the initial r-HBsAg applied to the column. Productivity was calculated on the basis of the average recovery obtained for each linear flow-rate and the time required for completion of a single run.

coupled ligand. Flow-rate is also limited by the slow process of antigen–antibody complex formation. In Fig. 4 the estimated productivity is also shown, based on the average recovery obtained for each linear flow-rate and the time required for completion of a single run. When a high productivity (mg of purified antigen per volume of immunogel per day) is required, 50 cm/h could be used to achieve the highest productivity values, although a recovery of only 44% should be expected at this flow-rate.

3.6. Effect of bed height on adsorption capacity

An unexpected result was obtained when two different bed lengths were compared. When the length/diameter ratio (L/D) of the immunogel column was decreased from 12.5 to 1.25, the amount of antigen that escaped in the non-bound fraction increased proportionally. For a 12.5 ratio $27 \pm 4\%$ of antigen was not retained in the column (found in the non-bound fraction), for a 6.25 ratio $39 \pm 6\%$, for a 3.12 ratio $48 \pm 5\%$ and for a 1.25 ratio $65 \pm 7\%$. This result does not agree with the normal behaviour of affinity chromatography when short and wide columns are used to improve productivity. The observed phenomenon seems to be the result of an inefficient mass transfer of the r-HBsAg particle into the CL-Sepharose 4B gel. The fractionation range reported for Sepharose 4B extends up to M_r $2.0 \cdot 10^7$ and the average molecular mass of the r-HBsAg particle is about $2.4 \cdot 10^6$. The ratio between these values is less than 10, which indicates that some restriction to the free diffusion of the r-HBsAg molecules exists in this system. Other gels with a larger pore diameter could be more suitable for the immunopurification of high-molecular-mass particulate antigens.

3.7. Stability of the immunoadsorbent

Using the optimum running parameters, that is, washing with 1 M NaCl and eluting the bounded antigen with 3 M KSCN, at a linear flow-rate of 25 cm/h, the column was stable for up to 30 runs (with an insignificant decrease in recovery). With further runs the recovery was rapidly affected. Leakage of ligand was measured in the wash and eluates fractions among the runs, using an ELISA for detecting murine IgG. Negligible amounts of IgG were found in such fractions, as compared with the coupled one. From this result it is thought that the cause of inactivation of the immunoadsorbent could be produced by the action of proteases present in the starting material.

4. Acknowledgements

The authors thank the Monoclonal Antibodies Production Unit of CIGB for supplying the mAb CB-HIP.1 and the Hepatitis B Vaccine Production Unit of CIGB for providing the r-HBsAg semi-purified material and performing the r-HBsAg determinations.

5. References

[1] D.E. Wampler, E.D. Lehman, J. Boger, W.J. McAleer and E.M. Scolnick, *Proc. Natl. Acad. Sci. U.S.A.*, 82 (1985) 6830.
[2] F. Gavillanes, J. Gomez-Gutierrez, M. Aracil, J.M. Gonzales-Roz, J.A. Ferragut, E. Guerrero and D.L. Peterson, *Biochem. J.*, 265 (1990) 857.
[3] J.C. Edman, R.A. Halleweli, P. Valenzuela, H.M. Goodman and W.J. Rutter, *Nature*, 291 (1981) 503.
[4] C.J. Burrel, P. Mackay, P.J. Greenaway, P.H. Hofschneider and K. Murray, *Nature*, 279 (1979) 43.
[5] J.D. Christman, M. Gerber, P.M. Price, C. Flordellis, J. Edelman and G. Acs. *Proc. Natl. Acad. Sci. U.S.A. (Biochem.)*, 79 (1982) 1815.
[6] N. Hsiung, R. Fitts, S. Wilson, A. Milne and D. Hamer, *J. Mol. Appl. Genet.*, 2 (1984) 479.
[7] A.M. Moriarty, B.H. Hoyer, J.W.-K. Shih, J.L. Gerin and D.H. Hamer, *Proc. Natl. Acad. Sci. U.S.A.*, 78 (1981) 2606.
[8] E.J. Patzer, C.C. Simonsen, G.R. Nakamora, R.D. Hershberg, T.J. Gregory and A.D. Levinson, in G.N. Vyas, J.L. Dienstag and J.H. Hoofnagle (Editors), *Viral Hepatitis and Liver Disease*, Grune & Stratton, New York, 1984, p. 477.
[9] B. Moss, G.L. Smith, J.L. Gerin and R.H. Purcel, in G.N. Vyas, J.L. Dienstag and J.H. Hoofnagle (Editors), *Viral Hepatitis and Liver Disease*, Grune & Stratton, New York, 1984, p. 294.
[10] M.R. Hilleman, R.E. Weibel and E.M. Scolnick, *J. Hong Kong Med. Assoc.*, 37 (1985) 75.

[11] E.A. Emini, R.W. Ellis, W.J. Miller, W.J. McAleer, E.M. Scolnick and R.J. Gerety, *J. Infect.*, 13, Suppl. A (1986) 3.
[12] N. Harford, T. Cabezon, B. Colau, A.M. Delisse, T. Rutgers and M. De Wilde, *Postgrad Med. J.*, 63, Suppl. 2 (1987) 65.
[13] J.M. Cregg, J.F. Tschopp, C. Stillman, R. Siegel, M. Akong, W.S. Craig, R.G. Buckholz, K.R. Madden, P.A. Kellaris, G.R. Davis, B.L. Smiley, J. Cruze, R. Torregrossa, G. Velicelebi and G.P. Thill, *Biotechnology*, 5 (1987) 479.
[14] W.J. McAleer, E.B. Buynak, R.Z. Maigetter, D.E. Wampler, W.J. Miller and M.R. Hilleman, *Nature*, 307 (1984) 178.
[15] A. Miyanohara, A. Toh-E, C. Nozaki, F. Hamada, N. Ohtomo and K. Matsubara, *Proc. Natl. Acad. Sci. U.S.A.*, 80 (1983) 1.
[16] J. Petre, F. Van Wijnendaele, B. De Neys, K. Conrath, O. Van Opstal, P. Hauser, T. Rutger, T. Cabezon, C. Capiau, N. Harford, M. De Wilde, J. Stephen, S. Carr, H. Hemling and J. Swadesh, *Postgrad. Med. J.*, 63, Suppl. 2 (1987) 73.
[17] P. Valenzuela, A. Medina, W.J. Rutter, G. Ammerer and B.D. Hall, *Nature*, 298 (1982) 347.
[18] F.V. Wijnendaele and G. Simonet, *US Pat.*, 4 649 192 (1987).
[19] F. Hamada, K. Sungahara, K. Shiosaki, S. Adachi and H. Mizokami, *US Pat.*, 4 738 926 (1988).
[20] W.S. Craig and R.S. Siegel, *Eur. Pat. Appl.*, 89 106 753.0 (1989).
[21] E. Pentón, L. Herrera, V. Muzio, V. Ramirez, A. García, C. Duarte, C. Ruiz, M. Izquierdo, L. Perez, G. Fontirrochi, M. Gonzales, M. Nazabal, A. Beldarrain, G. Padrón, J. García, G. De la Riva, A. Santiago, F. Ayan, R. Páez, A. Agraz, R. Díaz and Y. Quiñones, *Eur. Pat. Apl.*, 480 525 (1992).
[22] M.R. Hilleman, *Eur. J. Clin. Study Treat. Infect.*, 15 (1987) 3.
[23] J. Stephene, *Vaccine*, 8, Suppl. (1990) 69.
[24] G. Fontirrochi, M. Dueñas, M.E. Fernández de Cossio, P. Fuentes, M. Pérez, D. Mainet, M. Ayala, J.V. Gavilondo and C.A. Duarte, *Biotecnol. Appl.*, 10 (1993) 24.
[25] M.M. Bradford, *Anal. Biochem.*, 72 (1976) 248.
[26] U.K. Laemmli, *Nature*, 227 (1970) 680.
[27] A.M. Prince and K.S. Kim, *US Pat.*, 4 695 454 (1987).

ELSEVIER

Journal of Chromatography A, 672 (1994) 35–49

JOURNAL OF CHROMATOGRAPHY A

Silica-based metal chelate affinity sorbents I. Preparation and characterization of iminodiacetic acid affinity sorbents prepared via different immobilization techniques

Friedrich Birger Anspach

GBF-National Research Centre for Biotechnology, Biochemical Engineering, Mascheroder Weg 1, D-38124 Braunschweig, Germany

(First received October 12th, 1993; revised manuscript received March 1st, 1994)

Abstract

Iminodiacetic Acid (IDA) was immobilised on silica supports using either activated chromatographic supports or silanes carrying IDA in ω-position to silicium. Through reaction of IDA with glycidoxypropyltrimethoxysilane (GLYMO) before immobilization, a new and simple method is introduced which provides a metal chelate affinity sorbent of both high capacity for Cu(II) (28 μmol/ml) and almost identical chromatographic characteristics to soft gel metal chelate affinity sorbents.

By immobilization of IDA through n-alkyl spacers exclusive of an epoxy group a different chemical neighborhood to the chelator is obtained. These metal chelate sorbents demonstrated higher capacities for Cu(II) (39 μmol/ml). The selectivity for lysine was higher, for histidine lower, compared to epoxy-immobilized IDA chelates. It is concluded that the β-hydroxyl group, evolved during reaction with epoxy groups, is integrated with the metal chelate, thus forming a N-(hydroxyethyl)iminodiacetic acid (HEIDA).

The most distinct chromatographic behaviour was observed with CDI-immobilised IDA chelates, which displayed higher selectivity for acidic amino acids than common IDA chelates.

1. Introduction

Immobilised metal chelates are employed as affinity chromatographic sorbents due to their interaction with some proteins. Metal chelate interactions take place with functional groups of amino acids located at the surface of these proteins [1], such as imidazole of histidine, but also tryptophan and cysteine. Following the pioneering work of Porath *et al.*, considering metal chelate-interaction chromatography (MCIC) with proteins, primarily metal chelates based on carboxymethylated amines were investigated, such as iminodiacetic acid (IDA) [2,3] or triscarboxyethylenediamine (TED) [4,5]; recently also nitrilotriacetic acid (NTA) [6] was considered. Particularly IDA is used as a general tool for the purification of proteins from complex mixtures and is introduced today in many laboratories. It has been demonstrated that the replacement of one metal chelator by another, for example IDA with TED, is of great significance for the selectivity of the metal chelate sorbent [4].

0021-9673/94/$07.00
SSDI 0021-9673(94)00210-Z

Changes on selectivity of metal chelate sorbents are also observed by exchanging metal ions, such as Cu(II) against Ni(II) or Zn(II) [7,8,9,10]. Usually, Cu(II) is preferred as metal ion in separation protocols, followed by Zn(II) and Ni(II), in that order. The preference for Cu(II) is due to the high stability of the IDA:Cu(II) chelate and a stronger interaction of this chelate with histidine, compared to most of the other metal ions used in MCIC. The utilization of metal ions, such as Fe(III) [11], Al(III) [12] or Tl(III) [13] is described; however, their use is limited in practice.

The introduction of high-performance immobilized metal chelate sorbents allows a much higher resolution of biopolymers [14]. These high-performance sorbents are intended to display almost identical elution characteristics compared to soft gel sorbents, in order to employ analogous chromatographic protocols. Therefore, immobilization of IDA onto silicas should be accomplished through an epoxy group, as with most soft gels. Unfortunately, this immobilization technique results in low ligand densities when aliphatic amines are bound below pH 8, as required with silica-based matrices [15]. This is a disadvantage, since the interaction strength in MCIC is related to the ligand density [16,17], as is the capacity for proteins.

The object of this study was the introduction of a chemical procedure which allows the synthesis of a silica-immobilised IDA representing almost identical chromatographic characteristics compared to commercial metal chelate sorbents based on soft gels. Apart from that, immobilization techniques involving alkyl-silanes of IDA, were employed on silicas for comparison. Both avenues led to metal chelate affinity sorbents demonstrating high capacities for Cu(II) and good resolution for the amino acids employed. However, immobilization techniques, which either changed the structure or the chemical neighborhood of the chelator IDA, affected significantly the selectivity of the immobilised metal chelates for amino acids, especially histidine.

2. Experimental

2.1. Chemicals and chromatographic materials

Polygosil 500-1525 was obtained from Macherey Nagel, Düren, Germany. Glycine, L-histidine, L-lysine, L-cysteine, L-serine, and L-phenylalanine were obtained from Sigma, München, Germany. L-Arginine, malonic acid, L-tryptophan and L-glutamic acid were obtained from Serva, Heidelberg, Germany. 3-Aminopropyltriethoxysilane, 1,1′-carbonyldiimidazole (CDI), bromoacetic acid, chloroacetic acid, iminodiacetic acid (IDA), epibromohydrin (Epi) and all salts were obtained from E. Merck, Darmstadt, Germany. 3-Glycidoxypropyltrimethoxysilane (GLYMO) was obtained from Aldrich, Steinheim, Germany. 3-Bromopropyltrimethoxysilane and 4-aminobutyltriethoxysilane were obtained from ABCR, Germany. 3-Chloropropyltrimethoxysilane, Sepharose 4B and lanthanum nitrate hexahydrate were obtained from Fluka, Neu-Ulm, Germany. Chelating Sepharose FF (CS) was purchased from Pharmacia, Freiburg, Germany. The adduct of IDA-di-*tert*-butylester and GLYMO was a generous gift from H.-J. Wirth [18] and K.K. Unger of the University of Mainz, Germany.

2.2. Instruments

The liquid chromatographic system used for all chromatographic experiments was the Pharmacia 500 system assembled for zonal and frontal chromatography, respectively. IR analysis was performed on a Perkin-Elmer 881 IR spectrophotometer using potassium bromide pellets. Specific surface area (BET) was determined by N_2-sorption using the micromeritics ASAP 2000 system.

2.3. Elemental analysis

The coverage of the silica surface with silanes was determined with elemental analysis for carbon, nitrogen and hydrogen. The concentration

of immobilised groups was calculated on the basis of the surface area of the native silica support, as described by Kováts *et al.* [19].

2.4. Preparation of activated supports

Polygosil 500-1525 was chemically modified with GLYMO in acetate buffer at pH 5.5, as described by Bogart *et al.* [20]. Either GLYMO-activated silica was employed directly for the immobilization of IDA via method 4 (see below) or converted to diol-silica. To this end the GLYMO-activated silica was suspended in 0.01 *M* HCl at 323 K for 3 h. Lastly activation of the diol-silica with 1,1′-Carbonyldiimidazole (CDI) was performed, as described by Hearn *et al.* [21]. It is essential to use anhydrous acetone, in order to secure the capacity for Cu(II) described in this study.

Sepharose 4B was activated with epibromohydrin in 0.5 *M* NaOH, as described by Hochuli *et al.* [6].

2.5. Preparation of N-(3-Trisodiumsilanolate-propyl)-N,N-diacetic acid (IDA-propyl-silane)

Procedure A

The silane was synthesised according to a procedure described by Gimpel *et al.* for the chromatography of α-amino acids [22]. Briefly, 22.6 ml 6 *M* NaOH were added to 10 g of aminopropyltriethoxysilane at 273 K. 8.5 g of chloroacetic acid were dissolved in 45 ml 2 *M* NaOH and subsequently added to the silane. The reaction was carried out for one h at 333 K, then the solution was adjusted to pH 12 with 6 *M* HCl and finally the product was precipitated by addition of 9.4 g of barium chloride dissolved in 45 ml of water. The precipitate was filtered, washed with water, suspended in 90 ml 0.5 *M* potassium sulfate and stirred overnight to obtain the potassium salt of the silane. After centrifugation, the supernatant was collected and stored for further use. IR analysis was in concordance with the published data. IR: 3430(–OH); 2920 ($-CH_2-$); 1580($-COO^-$); 1390($-CH_2-$); 1100 ($-Si-O^-$) cm^{-1}.

Procedure B

In a similar reaction 50 ml 3 *M* NaOH and 3.34 g of IDA were added successively to 5 g of 3-chloropropyltrimethoxysilane at 273 K. Reaction conditions and treatment of the product were the same as described for procedure A.

Using 3-bromopropyltrimethoxysilane instead of chlorosilane caused development of bubbles during reaction and did not result in a useful product.

2.6. Preparation of N-(4-trisodiumsilanolate-butyl)-N,N-diacetic acid (IDA-butyl-silane)

This silane was synthesised analogously to IDA-propyl-silane. 6.4 ml 6 *M* NaOH were added to 3 g of 4-aminobutyltriethoxysilane at 273 K. 2.4 g of chloroacetic acid were dissolved in 12.7 ml 2 *M* NaOH and added to the silane. After reaction for 1 h at 333 K and adjusting to pH 12 with 6 *M* HCl, the product was precipitated by addition of 3.1 g of $BaCl_2$ dissolved in 14 ml of water. The filtered cake was suspended in 25.5 ml 0.5 *M* K_2SO_4 and stirred overnight, in order to recrystallize. The supernatant contained the potassium salt of the silane. IR analysis yielded nearly identical results compared to IDA-propyl-silane. IR: 3430(–OH); 2900 ($-CH_2-$); 1620($-COO^-$); 1390($-CH_2-$); 1110 ($-Si-O^-$) cm^{-1}.

2.7. Preparation of GLYMO-IDA-silane

This silane was synthesised as described by Anspach [23] for the immobilization of aliphatic amines. Briefly, 4.24 g of NaOH and 2.82 g of IDA were dissolved in water at 273 K. Then 5 g of GLYMO were slowly added whilst stirring. The reaction mixture was allowed to warm up to room temperature and maintained at this temperature for 4 h. Finally the temperature was raised to 338 K and the reaction mixture stirred

overnight. The reaction mixture forms a stable solution; no precipitation or polymerization of the silane was apparent at the high pH chosen during reaction. It can be stored at room temperature for at least 1 month under these conditions. IR: 3430(–OH); 2930($-CH_2-$); 1570 ($-COO^-$); 1430($-CH_2-$); 1100 ($-Si-O^-$); 1000 (–C–O–) cm^{-1}.

2.8. Preparation of metal chelating sorbents

For the sake of clarity, the different methods for preparation of metal chelate sorbents are differentiated as method 1 to 8.

Method 1: Polygosil 500-1525 propyl-IDA

3 ml of the IDA-propyl-silane solution, as synthesised through procedure B, were adjusted to pH 3.5 with 1 *M* HCl. After adjusting the volume to 10 ml with water, 2 g of Polygosil 500-1525 were added and the suspension evacuated 3 times at 2000 Pa, in order to ensure complete wetting of the pores of the silica with the reaction mixture. The temperature was raised to 368 K over 2 h, while stirring. The chelating sorbent was filtered and resuspended once in water and again filtered. The filtered sorbent was dried overnight in a desiccator and consequently heated to 423 K at 3 Pa, in order to ensure formation of siloxane groups of most of remaining ethoxysilane groups [24]. This procedure improves the stability of the functionalised sorbent in water.

Method 2: Polygosil 500-1525 propyl-IDA

12 ml of the N-(3-trisodiumsilanolatepropyl)-N,N-diacetic acid solution (procedure A) were adjusted to pH 3.5 with 1 *M* HCl. Subsequently, 4 g of Polygosil 500 were added. Reaction conditions and treatment of the modified silica were the same as described in method 1.

Method 3: Polygosil 500-1525 butyl-IDA

20 ml of the IDA-butyl-silane supernatant were adjusted to pH 3.5 and 5 g of Polygosil 500 were added. Reaction conditions and treatment of the sorbent afterwards were exactly the same as described in method 1.

2.9. Epoxy-derived metal chelating sorbents

Method 4: immobilization of IDA onto GLYMO-activated Polygosil 500-1525

0.6 g of NaOH and 2 g of IDA were dissolved in 15 ml of water in that order and adjusted to pH 8.3 with 2.5 *M* NaOH. Then 3 g of GLYMO-activated Polygosil 500 were added to the solution and degassed 3 times, in order to ensure complete wetting of the porous system of the silica. The reaction mixture was heated to 333 K for 24 h with stirring and the product isolated by filtration. The modified silica was washed several times with water. Remaining epoxy groups were converted to diol groups by suspending the sorbent in 0.01 *M* HCl as described above. After washing with water the gel was dried and stored. This product is referred to as GLYMO::IDA to distinguish it from the metal chelate sorbent obtained from GLYMO-IDA-silane (method 6).

Method 5: immobilization of IDA-di-tert-butylester-silane

The immobilization of IDA comprising protected carboxyl groups was carried out according to Wirth *et al.* [17]. In brief, 5 g of Polygosil 500-1525 were heated to 418 K at 3 Pa overnight. This silica was suspended in 30 ml of anhydrous toluene and 0.34 g of IDA-di-*tert*-butylester-silane were consequently added. The suspension was stirred at 383 K for 24 h. Then the sorbent was washed with toluene, 2-propanol, and water. *Tert*-butanol was cleaved from the IDA sorbent by addition of 10 m*M* HCl.

In addition to the reported procedure, the remaining hydroxyl groups at the silica surface were endcapped in 20 ml of a 5% GLYMO solution at pH 3. Reaction conditions were 368 K for 3 h with stirring, as described by Regnier *et al.* [25].

Method 6: preparation of Polygosil 500 GLYMO-IDA

3.3 ml of the GLYMO-IDA-silane solution were adjusted to pH 3.5 with 6 *M* HCl and to 10 ml with water. 3 g of Polygosil 500 were added and the temperature raised to 368 K for 3 h with stirring. The chelating gel was treated as de-

scribed in method 1. This product is referred as to GLYMO-IDA.

Method 7: binding of IDA onto epibromohydrin-activated Sepharose supports

1.5 g of NaOH, 2.5 g of Na_2CO_3 and 3 g of IDA were dissolved in 25 ml of water. Finally, 20 g of suction dried epibromohydrin-activated Sepharose 4B was added and adjusted to pH 11.5. The suspension was shaken overnight at 323 K and the chelating gel filtrated and washed several times with water until the supernatant was neutral. The gel was stored in 0.05% sodium azide solution. It is referred as Epi::IDA.

Method 8: immobilization of IDA onto CDI-activated Polygosil-Diol 500-1525.

2 g of CDI-activated Polygosil-Diol 500-1525 were suspended in 70 ml of phosphate buffer, pH 8.3, containing 0.35 g of IDA. The suspension was shaken for 48 h at 328 K. The resulting sorbent was filtered, washed with water and stored in 0.05% sodium azide until used. It is referred to as CDI::IDA.

2.10. Chromatographic conditions

Sepharose 4B based chelating gels were packed in water. Silica based chelating sorbents were dry-packed. All experiments were carried out with 5 mm I.D. columns with bed heights between 20 and 30 mm.

2.11. Zonal chromatography

Chromatographic tests were performed using standard FPLC equipment operating automatically. The columns were washed first with 30 m*M* EDTA + 0.5 *M* NaCl, pH 6, in order to remove any bound metal ion or contaminant, then water, then 15 m*M* metal ion solution and again water. The columns were equilibrated with 20–25 column volumes of the starting buffer. All experiments were carried out at 298 K and a flow-rate of 0.5 ml/min.

2.12. Retention of amino acids

Investigation of the retention behaviour of 7 α-amino acids and malonic acid was performed using 25 m*M* phosphate buffer, pH 6.0. Sample concentrations of 0.2–0.3 mg/ml for serine, glycine, lysine, malonic acid and 0.1 mg/ml for cysteine, tryptophan, phenylalanine and histidine were injected using a 20-μl sample loop. A 206 nm filter was used to monitor the column effluent. Each run was terminated after 10 min.

2.13. Frontal chromatography of Cu(II)

Frontal chromatography was performed with automated adsorption, elution and equilibration. Each run was terminated by the integrator after reaching the plateau region of the frontal breakthrough. Before each run the columns were equilibrated as described for zonal chromatography. To allow adsorption at defined conditions, the metal ion was dissolved in 50 m*M* acetate buffer, pH 5.0. Acetate forms a complex with the metal ion allowing up to 20 m*M* $CuCl_2$ to be dissolved without precipitation of copper hydroxide. Seven concentrations between 0.1 m*M* and 20 m*M* of the metal ion were found adequate to describe the adsorption behaviour.

3. Results

3.1. Chromatography of amino acids

The metal chelators employed in this study are cation exchangers at the chosen pH. For example, the p*K* of one carboxyl group of iminodiacetic acid is reported as 2.65 [26]. Therefore, basic amino acids, such as histidine and lysine, displayed mainly ionic interactions with the carboxylic groups of the chelator. Fig. 1 displays the typical elution behaviour of amino acids on the silica-based GLYMO-IDA chelator under isocratic conditions at pH 6. Charging the chelators with Ca(II) or La(III) did not lead to significant changes of the retention behaviour. Ba(II) displayed almost identical results as Ca(II); therefore, these results are not included

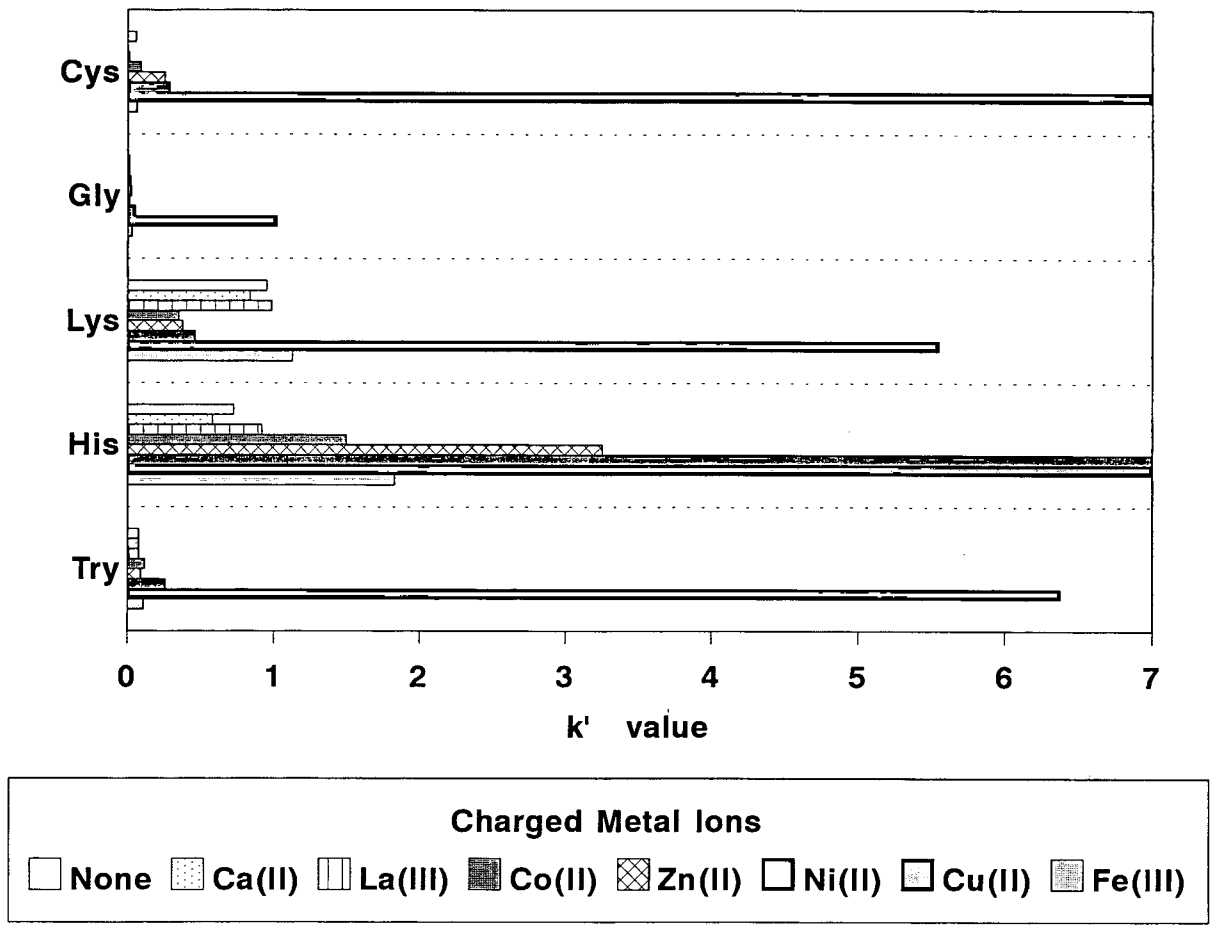

Fig. 1. Retention factors of amino acids on Polygosil 500 GLYMO-IDA charged with hard and borderline metal ions. Column, 30 × 5 mm I.D.; flow-rate, 1.0 ml/min; temperature, 298 K; buffer, 25 m*M* phosphate buffer, pH 6.0. Cys and His were not eluted on the Cu(II)-charged chelate. His eluted at the Ni(II)-chelate at $k' \sim 16$.

in Fig. 1. Co(II)-chelates displayed weak interactions with amino acids. Ionic interactions with carboxylic groups were suppressed after formation of this chelate. The retention time for lysine decreased and evolved closer to other amino acids. The k' value of histidine increased significantly, whereas all other amino acids displayed only small increases in retention time. A further increase in retention was observed when charged with Zn(II) and Ni(II), in that order. Interaction with all amino acids, except lysine, increased. Histidine eluted rather late on high-capacity Ni(II)-charged IDA chelates ($k' \approx 16$ on GLYMO-IDA, $k' > 4$ on butyl-IDA). These results are in concordance with data published by Horváth *et al.* [27].

The most interacting metal chelates were obtained when charged with Cu(II). Then histidine and cysteine were not eluted on any metal chelate, except CDI::IDA, under the chosen chromatographic conditions. In contrast to histidine, cysteine was not as strongly retained on Ni(II)-charged chelators, indicating a deviate interaction of the Cu(II)-charged IDA chelate with cysteine. In fact, if larger volumes of cysteine- or other mercapto-containing solutions

were passed through the column, a dark precipitate of copper mercaptide formed, insoluble in 15 m*M* EDTA or 1 *M* HCl.

The interaction with amino acids increased with the sequence Ca(II) ≈ Ba(II) ≈ La(III) < Co(II) < Fe(III) < Zn(II) < Ni(II) < Cu(II) when charged onto all IDA chelators and follows the order described elsewhere [28]. The retention factor of amino acids increased with the sequence Glu < Gly < Ser < Phe < Trp < Cys < His for Ni(II)- and Cu(II)-charged IDA.

Non-specific interactions originating from remaining hydroxyl groups of the silica matrix were not apparent in most cases. The main interactions with the IDA chelator and Ca(II)-, La(III)- or Ba(II)-charged IDA were caused by ionic interactions with the carboxylic groups of IDA.

3.2. Capacity of immobilised metal chelators

The equilibrium adsorption isotherms obtained from frontal chromatography of Cu(II) are demonstrated in Fig. 2. The interaction with Cu(II) is nearly irreversible with all chelators examined. Thus, almost rectangular shaped isotherms were obtained. The incline of the curve at elevated Cu(II) concentrations is attributed to interactions of Cu(II) with the Sepharose and silica matrix. Securer data from the rising part of the isotherm were not collected, since lower metal ion concentrations were not detected with the UV spectrophotometer employed in this study.

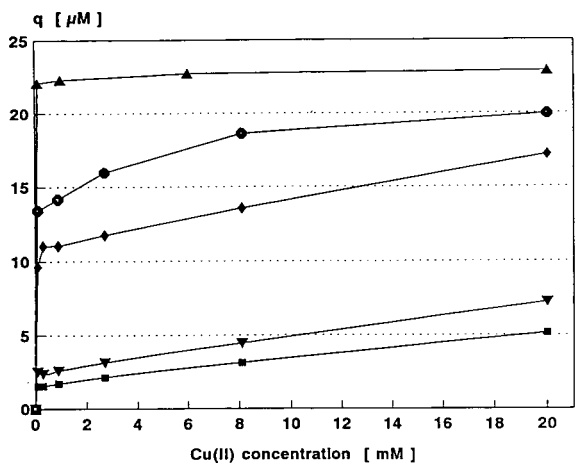

Fig. 2. Equilibrium adsorption isotherms of Cu(II) on metal chelators immobilised on Polygosil 500-1525. Columns, 20-30 × 5 mm I.D.; ■ = CDI::IDA (method 8), ▼ = propyl-IDA (method 1), ◆ = GLYMO-IDA (method 6), ○ = Butyl-IDA (method 3), ▲ = propyl-IDA (method 2). Rectangular shaped isotherms indicate strong interactions of Cu(II) with all metal chelators.

The lowest capacity for Cu(II) was determined for IDA-sorbents synthesised by method 1 (Table 1). Probably side products developed to a large extent under the chosen reaction conditions. This was confirmed by the application of-3-bromo- instead of 3-chloropropyltriethoxysilane. The reaction did not lead to the product of interest under otherwise identical reaction conditions. Instead, the evolution of a gas of undetermined origin was experienced.

Metal chelate sorbents obtained by immobilization of IDA onto activated silica supports (methods 4 and 8) displayed generally lower capacities for Cu(II) compared to sorbents obtained by immobilization of the silanes of the same chelators, employing methods 2, 3 or 6 (Table 1). The low capacities for Cu(II) indicate low ligand densities of the sorbents. This is due to the low pH employed during binding of chelators onto GLYMO- and CDI-activated silicas. Above pH 8.3 considerable amounts of siloxane bonds between silane and silica matrix would be hydrolysed [29]. However, the optimum reaction conditions for the immobilization

Table 1
Capacity of metal chelating sorbents for Cu(II)

Metal chelating sorbent	Method	q_m (μmol/ml)
Chelating Sepharose FF		39
Propyl-IDA	1	4.6
Propyl-IDA	2	39 [a]
Butyl-IDA	3	39.3
GLYMO::IDA	4	7.5
GLYMO-IDA	6	28
CDI::IDA	8	5.1

[a] Capacity decreased with time.

of aliphatic amines onto epoxy-activated supports equals pH 10–12 [4,15]. For CDI-activated matrices contradictory results are reported leading either to highest ligand densities at pH 5–6 [30] or at pH 10–12 [31].

Data from adsorption of Cu(II) and from elemental analysis are compared in Table 2 for sorbents obtained by methods 2, 4 and 6. Although activation of silica with subsequent immobilization of IDA (method 4) led to a higher carbon content compared to the immobilization of the GLYMO-IDA-silane (method 6), a considerably lower capacity was achieved for Cu(II). This result indicates that less than 20% of the epoxy groups of the activated silica react with IDA due to the unfavorable reaction conditions (low pH). The sorbent based on the reaction procedure described by Gimpel *et al.* [32] (procedure A) displayed a higher capacity for Cu(II) at the beginning of the test; however, capacity decreased with time. The instability of this metal chelate sorbent is consistent with the results described by Gimpel. In addition, only 38% of the theoretical capacity of this sorbent was accessible for Cu(II), as calculated from elemental analysis. This is explained by polymerization of silane at the silica surface, occurring either during the immobilization or the preparation of the silane. Consequently, very dense crosslinked structures may develop, not accessible for metal ions. The butyl-IDA sorbent displayed similar capacity for Cu(II) as the propyl-IDA sorbent. The stability of the butyl-IDA sorbent was higher, demonstrating no apparent loss of capacity with time.

A very high accessibility for Cu(II) was obtained through method 6 which displayed a ratio of 0.93 of Cu(II) binding to carbon content. This was the highest ratio obtained in this study, indicating a rather homogeneous metal chelate sorbent. This sorbent displayed also high stability of the linkage between silica surface and IDA. No decrease of ligand density was observed during frontal chromatography of Cu(II).

3.3. Selectivity of immobilised metal chelators

The immobilization methods employed in this study led to different chemical structures in the neighborhood of the metal chelator, as displayed in Table 3. This is due to the type and length of spacers containing at least 3 carbon atoms in case of silica bound IDA (propyl spacer) and either 10 or 12 atoms in case of the bisoxirane spacer, depending on whether the hydroxyl group evolved after formation of the covalent linkage to IDA is considered as part of the chelator or not.

Results from previous investigations indicated that the chemical neighborhood of immobilised chelators affects the elution behaviour of amino acids [33]. The deviation in selectivity is a result of changes of the recognition mechanism. In Fig. 3a and 3b the separation factors of some amino acids for glycine of sorbents obtained through methods 4, 6 and 7 are compared against Chelating Sepharose FF (CS). For clarity the logarithms of the separation factors are considered as

$$\Delta \lg\alpha = \lg\alpha_2 - \lg\alpha_1$$

at which, for example, α_1 and α_2 are the separation factors of CS and other metal chelate sorbents, respectively. $\Delta \lg\alpha$ has no direct link to

Table 2
Comparison of ligand densities from elemental analysis and adsorption of Cu(II) for silica-based metal chelating sorbents

Method	Sorbent	Carbon content (%C)	Ligand density ($\mu M/m^2$)	Capacity for Cu(II) ($\mu M/m^2$)	Ratio
4	GLYMO::IDA	1.84	3.1	0.38	0.12
2	Propyl-IDA	2.33	5.73	2.2	0.38
6	GLYMO-IDA	1.18	1.95	1.82	0.93

The ratio is calculated as capacity:ligand density. A low ratio displays an non-homogeneous sorbent.

Table 3
Chemical structure of metal chelators. The distinct structures are a result of the chemistry employed during immobilization onto silicas and soft gels

Method	Chemistry	Spacer	Structure of metal chelator
1	Propyl-Cl	$-(CH_2)_3-$	$-N(CH_2-COOH)(CH_2-COOH)$
2	Propyl-NH_2	$-(CH_2)_3-$	
3	Butyl-NH_2	$-(CH_2)_4-$	
4,5,6	GLYMO	$-(CH_2)_3-O-CH_2-$	$-CH(OH)-CH_2-N(CH_2-COOH)(CH_2-COOH)$
7	Epibromohydrin	$-CH_2-$	
CS	Bisoxirane	$-CH_2-CHOH-CH_2-O(CH_2)_4-O-CH_2-$	
8,9	CDI	$-(CH_2)_3-O-CH_2-CHOH-CH_2-$	$-O-C(=O)-N(CH_2-COOH)(CH_2-COOH)$

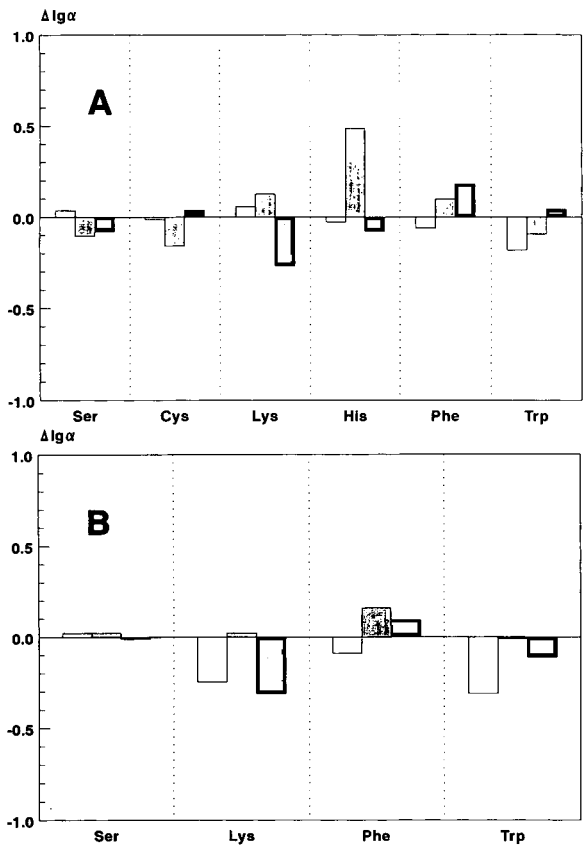

Fig. 3. Variation of selectivity for amino acids of metal chelates depending on chromatographic support and ligand density in comparison to CS. (A) Ni(II)-chelates, (B) Cu(II)-chelates; for each amino acid the left bar represents Sepharose 4B Epi::IDA, the centre bar Polygosil 500 GLYMO-IDA and the right bar Polygosil 500 GLYMO::IDA.

physicochemical parameters. It is utilised for graphic demonstration of selectivity differences. Positive and negative values indicate higher or lower selectivity for amino acids under consideration, respectively.

The separation factors are obtained from the capacity factors (k') of the amino acid under consideration and glycine. The hold-up time (t_0) was determined from solvent peaks.

$$\alpha = \frac{k'(\text{aminoacid})}{k'(\text{glycine})}$$

Histidine and cysteine were not included in figures of Cu(II)-charged chelators due to irreversible adsorption of these amino acids under the chosen chromatographic conditions.

$\Delta\lg\alpha$ values close to zero are considered not significant in this study due to data fluctuations caused by the short columns and dispersion effects. High-performance columns should have been used instead to confirm such small $\Delta\lg\alpha$ values. For the same reason Zn(II)- or Co(II)-charged chelators were not considered for comparison in this study. However, large differences are significant as observed for histidine on the Ni(II)-charged sorbent obtained through method 6. The higher selectivity of this high capacity silica-based metal chelate for histidine might be due to the interaction of neighboring chelates with imidazole and α-aminocarboxylic acid of the same histidine molecule leading to a tempor-

ary bridge between both metal chelate molecules. Sorbents with lower ligand densities, such as the GLYMO::IDA or the Epi::IDA, demonstrated lower selectivity for histidine.

Hydrophobic interactions with the spacer of the Epi::IDA sorbent are low; thus lower selectivities for tryptophan and phenylalanine were observed with this sorbent. The different $\Delta \lg \alpha$ values of lysine for GLYMO-IDA and GLYMO::IDA are due to the contribution of ionic charges, originating from the chelator and/or the chromatographic matrix. Apparently, remaining hydroxyl groups of the silica matrix are more effectively shielded by application of method 4, which led to a higher carbon content. Unfortunately, this method led to a low coverage with IDA and consequently low capacity for Cu(II), as described above.

In Fig. 4 the differences in selectivity for chelators obtained through method 5 is compared against Polygosil 500-1525 GLYMO-IDA. After removal of the large *tert*-butyl protection groups from the sorbent obtained through method 5, some charged hydroxyl groups were exposed at the silica surface, leading to additional ionic interactions with lysine. The higher retention of hydrophobic amino acids might be due to non-specific interactions with uncleaved protection groups. After this sorbent was endcapped with GLYMO, it displayed only minor differences in selectivity compared to the sorbent obtained by method 6. Endcapping seems to cleave remaining protection groups, as is evident from the decrease of selectivity for hydrophobic amino acids.

Changing the linkage between metal chelator and the chromatographic matrix led to large differences in selectivity of silica based sorbents for amino acids (Fig. 5). The immobilization of IDA onto CDI-activated silica was associated with a loss of selectivity for lysine when charged

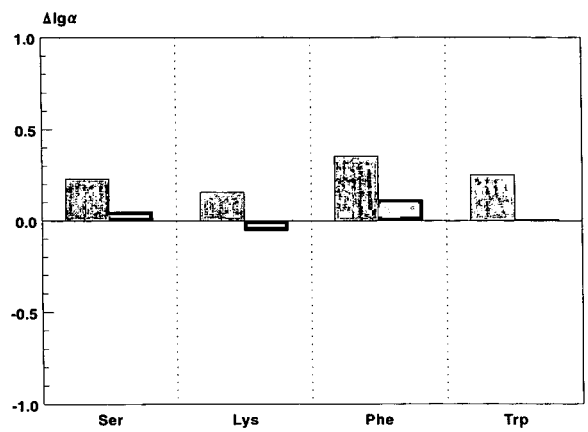

Fig. 4. Variation of selectivity for amino acids of Cu(II)-chelate sorbents obtained through method 5, before and after endcapping in comparison to GLYMO-IDA (method 6); left bars without endcapping, right bars endcapped with GLYMO.

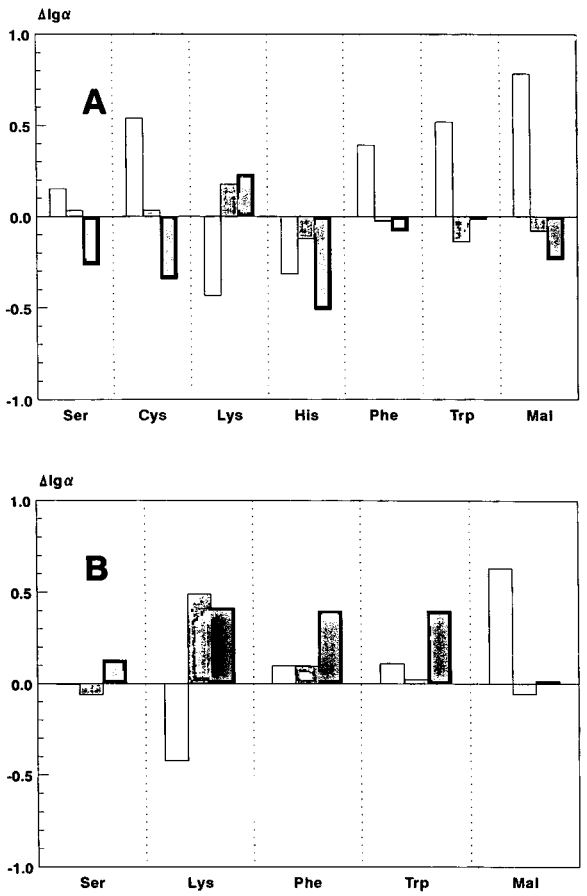

Fig. 5. Variation in selectivity for amino acids of silica-based metal chelates depending on immobilization chemistry in comparison to GLYMO-IDA (method 6). (A) Ni(II)-chelates, (B) Cu(II)-chelates; for each amino acid the left bar represents CDI::IDA, the centre bar propyl-IDA and the right bar butyl-IDA.

with Ni(II) or Cu(II). The selectivity for hydrophobic amino acids, cysteine and malonic acid increased. In contrast to epoxy- and alkyl-bound IDA, cysteine eluted from the Cu(II)-charged CDI::IDA sorbent.

It is remarkable that interactions of amino acids with CDI::IDA chelates followed the same sequence of metal ions observed with other chelators. Hence, the type of interaction is probably mainly chelating and not ionic. Unfortunately, the capacity of this type of metal chelate was low compared to the other chelates (Table 1).

IDA-sorbents bound via propyl or butyl spacers (methods 2 and 3) displayed significantly higher selectivities for lysine but lower selectivities for histidine and cysteine (Fig. 5a). Zn(II)- or Co(II)-charged chelators of this type as well as the chelator itself did not show higher selectivity for lysine (data not shown). Therefore, the higher retention of lysine cannot be explained on the basis of ionic interactions with remaining silanol groups only. Cu(II)-charged butyl-IDA displayed higher selectivities for tryptophan and phenylalanine (Fig. 5b). Probably synergistic interactions took place of both the chelate and the hydrophobic spacer. Such effects were found with chiral ligand exchangers on the basis of amino acid derivatives as well [34].

4. Discussion

4.1. Properties of metal chelates

Metal chelates are characterised by the interaction of a metal ion with a polydentate ligand, such as IDA or EDTA. Metal ions, belonging to the 3d-block elements, may reach the noble gas shell through attachment of ligands. The stabilization of transition metal chelates is enhanced by inductive charge compensation of the central metal ion by the ligands. This compensation ensues a dispersion of any charge, either localised at the metal ion or the chelator, over the entire structure of the metal chelate, the extent depending on the electronegativity of central metal ion and ligands. With Ca(II), Ba(II) and La(III) such a charge compensation is not possible. As a consequence, these metal chelates displayed different characteristics compared to metal chelates involving transition metal ions. For example, although adsorption of Ca(II) onto IDA-sorbents was confirmed by AAS measurements (data not shown), the IDA:Ca(II)-complex displayed almost identical elution behaviour as IDA without metal ions.

At strong metal chelates the retention of amino acids is explained as follows. Metal ions form chelates with different structures, depending on oxidation state and position in the periodic system. All transition metal ions employed form distorted octahedral structures in water. The distortion depends on both the type of metal ion and the chelator. For example, Cu(II) exhibits quadratic planar structure in a symmetric ligand field, such as plain water; however, it changes to a distorted octahedral structure when complexed by a chelator (Fig. 6), such as IDA (Jahn–Teller distortion [35]). The coordination sites of the metal chelate octaeder are occupied by the polydentate chelator and water molecules. Since water is a weak ligand it can be exchanged by stronger ligands, such as α-amino or carboxyl groups of amino acids and their functional

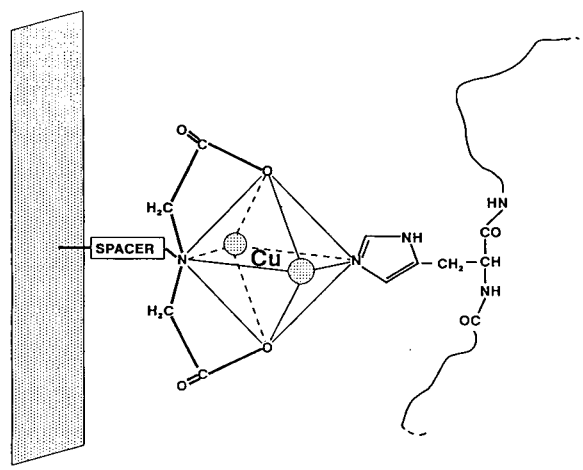

Fig. 6. Octahedral structure of immobilised IDA:Cu(II). Spheres symbolise water ligands. Binding of proteins occurs by exchange of water against imidazole of protein surface located histidines.

groups, ensuing further stabilization of the metal chelate.

After charging with the metal ion a charge might be left at the chelate (Fig. 7), depending on the type of chelator, the oxidation state of the metal ion, and the environment the metal ion is solved in (pH, buffer ions, etc.). Water molecules can be exchanged by OH^- with increasing pH. Therefore, at high pH a neutral or negative charge may develop with IDA when charged with a metal ion. This negative charge might be the reason for stronger interaction with lysine at Cu(II)-charged butyl-IDA and propyl-IDA chelates.

4.2. Immobilization methods

Various methods for the immobilization of IDA and other chelators onto silicas are described in literature [27,36]. Most methods proceed from glymo-activated silicas which allow the binding of IDA through an epoxy group in a similar reaction as described for soft gels [4,37]. Since commonly used silicas are hydrolysed at ph >8, either excess of aliphatic amines are required due to their high pK value or special reaction conditions [36] are employed for reaction with the epoxy group of glymo. However, such reaction conditions may not be disadvantageous from an economic point of view only, but also ecologically, if large quantities of used reagents have to be disposed of. In addition, results from this work demonstrated that even with a large excess of iminodiacetic acid only low ligand densities were obtained, attributed to low reaction rates at the chosen pH (method 4).

On silica-based supports highest ligand densities of low molecular weight ligands are obtained by utilising the silanes of these ligands [38]; but often the chemistry is time consuming employing protection groups [17], as described in this study for the sake of comparison (method 5). In contrast to this, method 6 allows synthesis of the IDA-silane and successive binding onto silica without any further step of isolation. At the chosen pH no condensation of silanol groups takes place in water due to the three negative charges left at the silanol molecule [24]. Accordingly, reactions of primary or secondary amines to the epoxy group of GLYMO can be performed in water under these conditions, as described for other silanes as well [32]. The resulting ligand-silane may be stored in the reaction solution, whereby the time scale depends mainly on the stability of the ligand at high pH. This chemistry is (i) simple and cheap, since no activation of the silica is needed and hydrophilic or ionic silanes are obtained without complicated derivatisation chemistry of the silane, (ii) it is ecologically feasible since very few by-products are obtained which do not need to be separated, (iii) no organic solvents are used, and (iv) high capacities and stable affinity sorbents are obtained by carefully choosing reaction conditions, such as concentration of the silane and pH. This reaction is particularly important for the immobilization of aliphatic amines, demanding high pH during reaction with epoxy groups due to their high pK values. The method allows the formation of homogeneous affinity sorbents as evident from elemental analysis and capacity for Cu(II) on immobilised IDA (Table 2). In addition, silica based metal chelate sorbents displayed negligible non-specific ionic

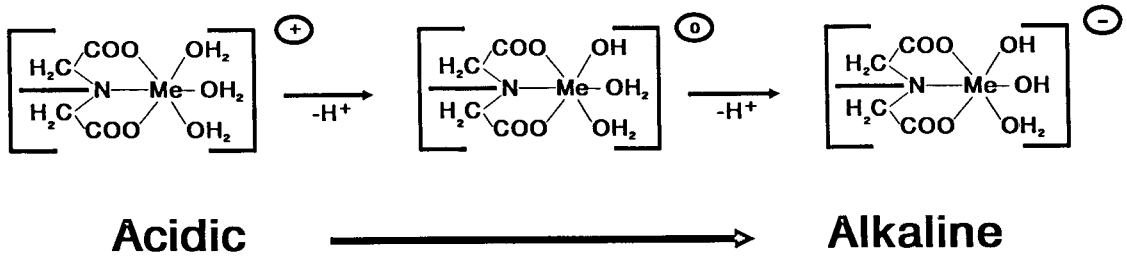

Fig. 7. Appearance of positive and negative charges at metal chelates depending on oxidation state of metal ions and pH. The character of the metal chelate sorbent may shift from an anion exchanger to a cation exchanger.

interaction, comparable to sorbents based on soft gels.

4.3. Chemical neighborhood

The application of GLYMO, epibromohydrin and bisoxirane for the immobilization of IDA involves the reaction of the nitrogen of IDA with the epoxy group of these reagents. As a consequence a hydroxyl group in β position to the tertiary amine evolves at the spacer (Table 3). This β-hydroxyl group is in proper distance to the nitrogen atom to be integrated with the metal chelator (method 4–7 and CS). A similar compound, N-(hydroxymethyl)iminodiacetic acid comprising α-hydroxyl group, is described in literature [2]. The stability constant (lg K) of the Cu(II) complex of this compound is 11.7, compared to 11.1 for the IDA:Cu(II) complex. The integration of a β-hydroxyl group in the chelating complex should be more likely than with α-hydroxyl group, because the distance between the nitrogen and oxygen of the β-hydroxyl group is almost identical to the distance between nitrogen and oxygen of the carboxyl group. The influence of a hydroxyl group located in close proximity to iminodiacetic acid (α-, β- or γ-position to nitrogen) in solution was investigated by Chabarek *et al.* [39]. They concluded that the hydroxyl group is incorporated in the metal chelate, consequently leading to stronger interaction with metal ions. If the β-hydroxyl group of the immobilised IDA is part of the Cu(II) chelate also, the spacer length of epoxy-derived metal chelates is 2 carbon atoms shorter than the immobilized chelator itself. This implies that the spacer of the metal chelate obtained from epibromohydrin-activated Sepharose 4B may contain one carbon atom only. The proposed chemical structure of the Cu(II)-charged chelate is illustrated in Fig. 8. Thus, the name of this type of immobilised chelator should be N-(hydroxyethyl)iminodiacetic acid (HEIDA) rather than iminodiacetic acid (IDA). In contrast, the chelator consists of the immobilised IDA only, when methods 2 and 3 are employed for the immobilization on silicas.

The largest differences in the retention be-

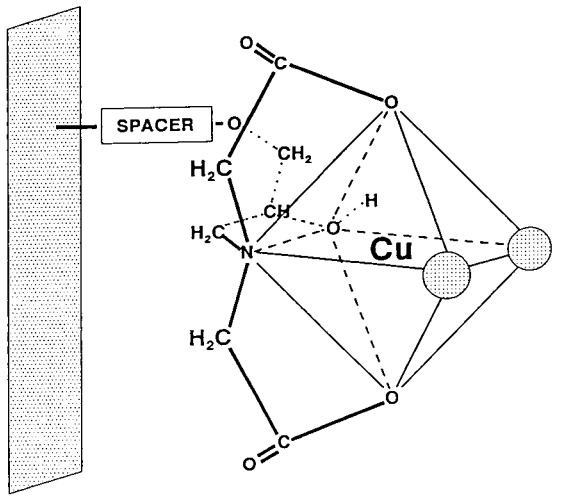

Fig. 8. Proposed octahedral structure of Cu(II)-charged N-(hydroxyethyl)iminodiacetic acid (HEIDA). The β-hydroxyl group at the spacer is in proper distance to the nitrogen for integration in the metal chelate.

haviour were observed on the CDI::IDA sorbent. Especially the high selectivity for malonic acid should be considered. It appears that Cu(II) and Ni(II) ions are harder with CDI::IDA than with other chelates, therefore demonstrating higher interactions with carboxylic groups. Probably, the remaining hydroxyl group of the diol spacer is to far away to get involved into the metal chelate. Moreover, through the reaction of the amine with CDI-activated supports a carbamate group is formed. The nitrogen gets amidic character and consequently less nucleophilic than the amine. Due the decrease in electron density at the nitrogen atom the stability constant of the metal chelate should be affected. The structure of this metal chelate cannot be determined from these experiments; therefore, the presumed structure in Fig. 9 should be considered with care.

5. Conclusions

The different chemistries employed for the immobilization of IDA led to distinct chemical structures in the neighborhood of IDA. As a consequence, the selectivity of formed metal

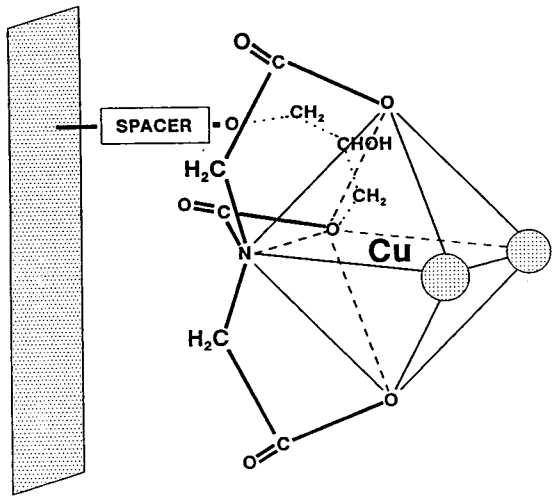

Fig. 9. Presumed structure of Cu(II)-charged CDI::IDA. Maybe other oxygen atoms take part with the metal chelate instead of or in addition to the carbamate oxygen.

chelates for amino acids was influenced. Probably, the changes in selectivity are related to a different structure of these IDA chelates, as proposed in Fig. 8 and Fig. 9.

The different chemical methods yielded the following:

(i) The introduction of reaction method 6 resulted in immobilised metal chelates with high capacity and almost identical chromatographic characteristics compared to soft gel metal chelate sorbents.

(ii) Reaction method 3 results in a butyl-IDA chelator demonstrating high capacity for Cu(II). The Cu(II) chelate demonstrated less selectivity for histidine but increased selectivity for lysine compared to the GLYMO-IDA chelate. Thus, the butyl-IDA chelate may show higher interaction with proteins rich in lysine than common epoxy-derived IDA chelates.

(iii) Reaction method 8 yields a CDI::IDA chelator demonstrating the largest deviation in selectivity compared to CS or GLYMO-IDA. The Cu(II) chelate displayed increased selectivity for acidic amino acids; thus it might be useful for the purification of proteins rich in acidic amino acids.

Most chromatographic protocols obtained from soft gel metal chelate sorbents should be applicable for the silica-based GLYMO-IDA sorbent. The butyl-IDA and CDI::IDA chelates may address specific properties of certain proteins; however, practical chromatographic protocols for the purification of those proteins need to be developed.

Acknowledgments

Financial support was provided by the "Hochschulnachwuchsförderungsprogramm" of the German federal ministry of education and research (Möllemann II).

References

[1] E. Sulkowski, *Trends Biotechnol.*, 3 (1985) 1.
[2] L. Kågedal, in J.-C. Janson and L. Rydén (Editors), *Protein Purification*, VCH Publishers, New York, NY, 1989, p. 231.
[3] G. Lindeberg, H. Bennich and Å. Engström, *Int. J. Peptide Protein Res.*, 38 (1991) 253.
[4] J. Porath and B. Olin, *Biochemistry*, 22 (1983) 1621.
[5] P. Samaraweera, J. Porath and J.H. Law, *Arch. Insect Biochem. Physiol.*, 20 (1992) 243.
[6] E. Hochuli, H. Döbeli and A. Schacher, *J. Chromatogr.*, 411 (1987) 177.
[7] P. Jungblut, H. Baumeister and J. Klose, *Electrophoresis*, 14 (1993) 638.
[8] L. Andersson, E. Sulkowski and J. Porath, *J. Chromatogr.*, 421 (1987) 141.
[9] B.-L. Yang and S. Goto, *Sep. Sci. Technol.*, 26 (1991) 637.
[10] O. Rossetto, G. Schiavo, P.P. Delaureto, S. Fabbiani and C. Montecucco, *Biochem. J.*, 285 (1992) 9.
[11] P. Scanff, M. Yvon and J.P. Pelissier, *J. Chromatogr.*, 539 (1991) 425.
[12] L. Andersson, *J. Chromatogr.*, 539 (1991) 327.
[13] J. Porath, B. Olin and B. Granstrand, *Arch. Biochem. Biophys.*, 225 (1983), 543.
[14] Y. Nakagawa, T.T. Yip, M. Belew and J. Porath, *Anal. Biochem.*, 168 (1988) 75.
[15] P.-O. Larsson, M. Glad, L. Hansson, M.-O. Mansson and K. Mosbach, *Adv. Chromatogr.*, 21 (1982) 41.
[16] M. Belew and J. Porath, *J. Chromatogr.*, 516 (1990) 333.
[17] H.-J. Wirth, K.K. Unger and M.T.W. Hearn, *Anal. Biochem.*, 208 (1993) 16.
[18] H.-J. Wirth, *PhD Thesis*, University of Mainz, Mainz, 1990.

[19] J. Gobet and E.sz. Kováts, *Adv. Sci. Technol.*, 1 (1984) 77.
[20] G.R. Bogart, D.E. Leyden, T.M. Wade, W. Schafer and P.W. Carr, *J. Chromatogr.*, 483 (1989) 209.
[21] G.S. Bethell, J.S. Ayers, M.T.W. Hearn and W.S. Hancock, *J. Chromatogr.*, 219 (1981) 361.
[22] M. Gimpel and K. Unger, *Chromatographia*, 17 (1983) 200.
[23] GBF, *Deutsche Patentanmeldung*, 1993, DE 4217101A1.
[24] C.J. Brinker and G.W. Scherer, *Sol-Gel Science*, Academic Press, London, 1990, pp. 97.
[25] S.H. Chang, K.M. Gooding and F.E. Regnier, *J. Chromatogr.*, 125 (1976) 103.
[26] A.E. Martell and R.M. Smith, *Critical Stability Constants*, Vol. 1, Plenum Press, New York, NY, 1974, p. 1.
[27] Z. El Rassi and Cs. Horváth, *J. Chromatogr.*, 359 (1986) 241.
[28] Cs. Horváth and G. Nagydiosi, *J. Inorg. Nucl. Chem.*, 37 (1975) 767.
[29] B. Anspach, K.K. Unger, P. Stanton and M.T.W. Hearn, *Anal. Biochem.*, 179 (1989) 171.
[30] K. Ernst-Cabrera and M. Wilchek, *J. Chromatogr.*, 397 (1987) 187.
[31] G.S. Bethell, J.S. Ayers, W.S. Hancock and M.T.W. Hearn, *J. Biol. Chem.*, 254 (1979) 2572.
[32] M. Gimpel and K. Unger, *Chromatographia*, 16 (1982) 117.
[33] F.B. Anspach and J. Klein, *X. International Symposium on HPLC of Proteins, Peptides, and Polynucleotides, 1990*, Poster No. 119.
[34] P. Roumeliotis, K.K. Unger, A.A. Kurganov and V.A. Davankov, *J. Chromatogr.*, 255 (1983) 51.
[35] H.L. Schläfer and G. Gliemann, *Einführung in die Ligandenfeldtheorie*, Akademische Verlagsgesellschaft, Frankfurt, 1967.
[36] L. Fanou-Ayi and M. Vijayalakshmi, *Ann. N.Y. Acad. Sci.*, 413 (1983) 300.
[37] P.D.G. Dean, W.S. Johnson and F.A. Middle, *Affinity Chromatography: A practical approach*, IRL Press, Oxford, 1985, p. 34.
[38] J.N. Kinkel, B. Anspach, K.K. Unger, R. Wieser and G. Brunner, *J. Chromatogr.*, 297 (1984) 167.
[39] S. Chaberek and A.E. Martell, *J. Am. Chem. Soc.*, 76 (1954), 215.

ELSEVIER

Journal of Chromatography A, 672 (1994) 51–57

JOURNAL OF CHROMATOGRAPHY A

Synthesis of polymer-coated mixed-functional packing materials for direct analysis of drug-containing serum and plasma by high-performance liquid chromatography

Taketoshi Kanda*, Hiroshi Kutsuna, Yutaka Ohtsu, Michihiro Yamaguchi

Shiseido Research Centre, 1050 Nippacho, Kouhoku-ku, Yokohama 223, Japan

(First received September 30th, 1993; revised manuscript received February 15th, 1994)

Abstract

Silicone polymer-coated mixed-functional (PCMF) silica packing materials were developed for the direct determination of drugs contained in serum or plasma. The new stationary phases were prepared by the following three-step procedure: (1) coating porous silica with a silicone polymer; (2) partial introduction of hydrophobic groups; and (3) introduction of hydrophilic groups. Two PCMFs were synthesized, one having polyoxyethylene groups as hydrophilic groups (PCMF-POE) and the other having oligoglyceryl groups (PCMF-OG). PCMF-POE showed higher recoveries for injected proteins and a greater overall retention for drug molecules than PCMF-OG. PCMF-POE did not show any column deterioration in 500 serum sample injections (10 ml in total).

1. Introduction

The determination of drugs in serum and plasma using high-performance liquid chromatography (HPLC) normally requires several sample preparation processes, such as filtration, deproteinization, solvent extraction and concentration. Although these steps are essential to prevent column clogging or other negative effects on separation efficiency, they are time consuming, and also generate possibilities of experimental errors in the final determination results.

Recently, packing materials that make it possible to inject directly serum and plasma containing drugs and their metabolites were developed in order to alleviate these problems. All of these packing materials are designed so that large protein molecules are quickly eluted from the system, and relatively small molecules, such as drug molecules, are retained longer. Hagestam and Pinkerton [1–3] designed a so-called "internal-surface reversed phase (ISRP)", which had hydrophobic tripeptide parts (glycyl-L-phenylalanyl-L-phenylalanine) on the internal surface of porous silica and hydrophilic diol–glycine residues on the external surface. Haginaka *et al.* [4] prepared another ISRP, having N-octanoylaminopropyl and N-(2,3-dihydroxypropyl)aminopropyl groups as internal and external groups, respectively. Kimata and co-workers [5,6] reported a simple method to prepare a "superficially hydrophilic reversed phase", which includes decomposition of alkylsilylated silica with aqueous acid, followed by introduction of diol groups. Gish *et al.* [7]

* Corresponding author.

0021-9673/94/$07.00
SSDI 0021-9673(94)00197-H

prepared a "shield hydrophobic phase", which consists of a polymeric bonded phase containing hydrophobic phenyl groups enclosed by hydrophilic polyoxyethylene networks. Gluntz *et al.* [8] prepared a semipermeable surface, which has a hydrophilic polyoxyethylene polymer on external surface and hydrophobic phase on internal surface. Haginaka and co-workers [9–13] reported the use of another type of mixed-functional packing materials which possess hydrophobic groups and hydrophilic groups on both the external and internal surfaces, which showed advantageous features for direct analysis of serum.

A novel polymer-coating technique to form reactive polymethylsiloxane films on metal oxides by chemical vapour deposition of 1,3,5,7-tetramethylcyclotetrasiloxane (H4) was developed by Fukui *et al.* [14]. Ohtsu and co-workers [15,16] utilized this polymer coating technique to prepare a polymer-coated C_{18} silica packing.

Polymer-coated C_{18} silica seems to have a more homogeneous surface than another type of polymer-coated silica phase prepared with silicone oligomers [17]. Polymer-coated C_{18} showed an excellent performance in the determination of protonated amine and chelating compounds, which are normally considered difficult to determine owing to their undesirable secondary interactions with the silica surface [18].

In this paper, an attempt to combine the polymer coating technology mentioned above and the idea of a mixed-functional (MF) stationary phase is described. The MF phases here contain styrene groups as hydrophobic groups and oligoglycerol (OG) or polyoxyethylene (POE) moieties as hydrophilic groups, both of which are attached to the polymer-coated silica. The performance of the new stationary phases was evaluated by the direct analysis of serum and plasma containing drugs.

2. Experimental

2.1. Reagents and materials

High-purity silica (Shiseido, Tokyo, Japan) (particle diameter, 5 μm; pore size, 90 Å; specific surface area, 410 m^2/g; metal impurities, <5 ppm) was used as a starting material for polymer-coated mixed-functional (PCMF) packing materials. 1,3,5,7-Tetramethylcyclotetrasiloxane (H4), a silicone monomer used for the polymer coating, was purchased from Toshiba Silicone (Tokyo, Japan), calf bovine serum from Dainippon Pharmaceutical (Osaka, Japan), trimethoprim and chrolamphenicol from Nacalai Tesque (Kyoto, Japan), human serum, phenobarbital, carbamazepine, phenytoin, theophylline and indomethacin from Wako (Osaka, Japan), allyloligoglycerol (OG, degree of polymerization 3) from Nagase Chemicals (Hyogo, Japan) and polyoxyethylene allyl ether (POE, average degree of polymerization 16) from Nihonyushi (Tokyo, Japan). Other reagents and solvents used in the synthetic procedure were of special grade from Wako and were used as received. Acetonitrile used for mobile phases was of HPLC grade from Nacalai Tesque. Water was purified with a Milli-Q system (Nihon Millipore Kogyo, Tokyo, Japan).

2.2. Preparation of polymer-coated mixed-functional packing material

Preparation of polymer-coated silica

The H4-coated silica was prepared according to the method of Fukui *et al.* [14]. The H4 molecules were deposited on the silica surface, where they polymerized. The measured thickness of the homogeneous polymer layer was *ca.* 7 Å, which corresponds to that of a monolayer. The silicone polymer formed in this step had many reactive Si–H groups (2.15 mmol/g), which were to be utilized for the subsequent modifications.

Introduction of hydrophobic groups

H4-coated silica gels (30 g) were heated at 120°C for 2 h and then dispersed into 150 ml of dry toluene and well stirred. Portions of styrene (0.3359, 0.6718 or 1.3435 g), which are equivalent to 5, 10 or 20% of Si–H groups in the silicone polymer, respectively, were added to the mixture, in the presence of hexachloroplatinic acid (3 mg). After the mixture had been heated at refluxing temperature for 7 h, it was cooled at

room temperature. The solvent was filtered off and the silica was rinsed with toluene and acetone. The silica obtained here was heated for 2 h at 80°C. The silicas treated in this way were named 5Ph, 10Ph or 20Ph, according to the amount of styrene added.

Introduction of hydrophilic groups

The 5Ph, 10Ph and 20Ph materials (15 g) were dispersed into water (150 ml). Allyloligoglycerol (20 g) or polyoxyethylene allyl ether (25 g) was added to the dispersion. The mixture was refluxed for 3 h in the presence of hexachloroplatinic acid (1.5 mg) under a nitrogen atmosphere, then cooled at room temperature. The phases obtained here were named 5Ph-OG, 10Ph-OG, 20Ph-OG, or 5Ph-POE, 10Ph-POE and 20Ph-POE, according to the reagent used. The amounts of groups reacted were determined by elemental analysis (C,H,N) using a Model 2400 CHN elemental analyser (Perkin-Elmer). The micropore distribution, micropore volume and mean pore radius (surface area) were measured by the nitrogen adsorption method using Autosorb-1 (Quantachrom).

2.3. Instrumentation

The HPLC system consisted of an LC-6A pump, an SPD-6A UV detector, a CTO-6A column oven, a SIL-6B injector and a C-R3A data processor (Shimadzu, Kyoto, Japan). The column temperature was maintained at 40°C. The PCMF was packed into a stainless-steel column (100 or 150 mm × 4.6 mm I.D.). The flow-rate was maintained at 1.0 ml/min except for the determination of theophylline, for which it was 0.6 ml/min. The mobile phase conditions are given in the figure captions.

2.4. Preparation of human serum

The drugs were dissolved in human serum at known concentrations and 20 μl of human serum sample were passed through a 0.22-μm membrane filter (Nippon Millipore, Tokyo, Japan) before being injected into the column.

2.5. Recovery of serum proteins from polymer-coated mixed-functional packing materials

The recovery of human serum proteins from a column packed with the PCMF packing material was examined as follows. A 20-μl portion of a control human serum sample was injected into the column (100 mm × 4.6 mm I.D.) packed with the PCMF packing material using 100 m*M* phosphate buffer (pH 6.9)–acetonitrile (9:1, v/v) as the mobile phase. The eluate was collected for 9 min and diluted to 10 ml with the mobile phase. A 1.0-ml portion of the liquid was mixed with 5 ml of Coomassie Brilliant Blue G-250 reagent, and kept for 10 min. The absorbance of the mixture was measured at 595 nm with the mobile phase as a standard. The recovery was calculated as the absorbance ratio with and without the column.

3. Results and discussion

3.1. Preparation of polymer-coated mixed-functional packing material

The PCMF packing materials were prepared in three steps: (1) coating porous silica with a silicone polymer, (2) partial introduction of hydrophobic groups and (3) introduction of hydrophilic groups. Table 1 shows the carbon contents of the PCMF materials, surface coverage of hydrophobic and hydrophilic groups and the capacity factors (k') of naphthalene under the HPLC conditions given.

The capacity factor (k') of naphthalene increased as the amount of hydrophobic groups increased. The k' values with Ph-POEs are generally larger than those with Ph-OGs with the same amount of surface coverage. With introduction of OG groups, the group density remained constant even when the surface coverage of hydrophobic groups was altered, whereas the group density decreased slightly with increasing amount of the hydrophobic groups on introduction of POE groups. These results suggest that the final density of hydrophilic groups is not greatly affected by the amount of hydrophobic groups within the tested range (5Ph to 20Ph),

Table 1
Carbon content and surface coverage of packing materials and capacity factor of naphthalene

Packing material	Carbon content (%)	Surface coverage (μmol/m^2)		k' [a]
		Hydrophobic phase	Hydrophilic phase	
5Ph-OG	10.29	0.22	1.03	3.38
10Ph-OG	10.65	0.31	1.03	3.61
20Ph-OG	10.78	0.37	1.01	3.89
5Ph-POE	14.40	0.22	0.57	5.42
10Ph-POE	14.34	0.31	0.55	5.71
20Ph-POE	14.33	0.37	0.53	5.93

[a] Capacity factors were measured under the following HPLC conditions: column size, 100 mm × 4.6 mm I.D.; mobile phase, acetonitrile–water (30:70, v/v); detection, 254 nm.

but rather is determined by the steric hindrance of the hydrophilic groups themselves, which are assumed to occupy significant parts of micropores.

Fig. 1 shows the pore distribution in each preparation step of 10Ph stationary phases. The pore radius decreased from 91.6 to 83.8 Å during the initial polymer coating and then from 83.8 to 82.0 Å on introduction of styrene groups. The final introduction of OG or POE groups further lowered the pore radius to 76.4 or 76.2 Å, respectively. The shifts of the distribution curves, which were not accompanied by major changes in their shapes, indicate that the introductions of hydrophobic and hydrophilic groups were performed highly homogeneously, not only on the external but also on the internal surface. It should be noted that the amount of phenyl groups hardly affected the pore radius and distribution curve.

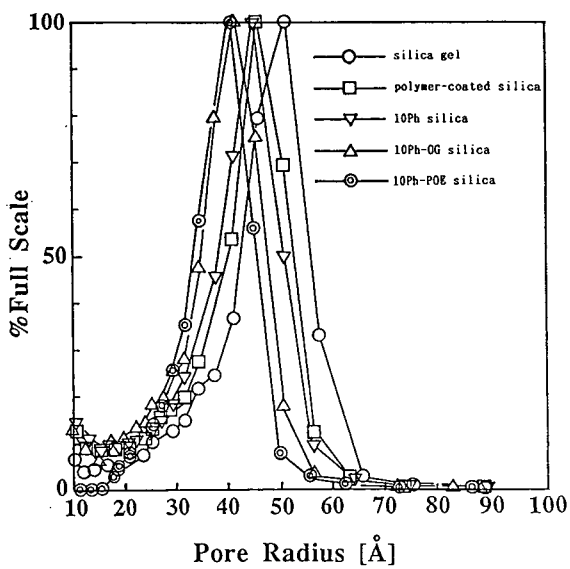

Fig. 1. Pore distribution at each step of the prepared 10Ph-OG and 10Ph-POE packing materials.

3.2. Recovery of serum proteins in first injection and column efficiency

Table 2 shows the recoveries of human serum proteins in the first injection and the plate

Table 2
Recovery of proteins in first injection and efficiency of PCMF packing material

Packing material	Recovery of proteins in first injection[a] (%)	Column efficiency[b] (plates per 100 mm)
5Ph-OG	35	3600
10Ph-OG	30	3900
20Ph-OG	20	3900
5Ph-POE	100	4300
10Ph-POE	100	4400
20Ph-POE	100	4600

[a] The recovery of serum proteins was measured using Coomassie Brilliant Blue G-250 reagent under the following HPLC conditions: column size, 100 mm × 4.6 mm I.D.; mobile phase, 100 m*M* phosphate buffer (pH 6.9)–acetonitrile (90:10, v/v); injection volume, 20 μl.

[b] Number of theoretical plates for carbamazepine under the following HPLC conditions: column size, 100 mm × 4.6 mm I.D.; mobile phase, 100 m*M* phosphate buffer (pH 6.9)–acetonitrile (85:15, v/v); detection, 254 nm.

number for each PCMF packing material. The recovery of human serum proteins with Ph-OGs decreased with increasing density of hydrophobic groups, whereas those measured with Ph-POEs were almost 100% in spite of the low density of hydrophilic groups. It is suggested that OG groups do not hinder the interaction between the hydrophobic groups and proteins, whereas POE groups are more effective in limiting the contact between them owing to their bulky structure. Ph-POEs also showed a better column efficiency than Ph-OGs for small molecules, probably because the molar-based density of hydrophilic groups is lower in Ph-POEs than in Ph-OGs, and mass transfer of small molecules is expected to be easier in Ph-POEs.

3.3. Direct injection analysis of serum containing drugs

Fig. 2 shows the results of direct injection analysis of human serum containing antiepileptics drugs (phenobarbital, carbamazepine and phenytoin) at therapeutic levels. Although these drugs were eluted after the serum proteins in the void volume, 20Ph-OG could not separate phenobarbital and serum proteins sufficiently. In contrast, 20Ph-POE showed a complete separation for phenobarbirtal and also carbamazepine and phenytoin. Figs. 3–5 show chromatograms for the direct injection analysis of human serum containing chloramphenicol, an antibacterial drug, indomethacin, an anti-inflamatory, and theophylline, a xanthine derivative, at therapeutic levels. These drugs were well separated from serum proteins. Thus, the prepared PCMF packing material having POE groups as hydrophilic phase seems to have advantageous features as a stationary phase for the direct injection analysis.

Table 3 gives the relative standard deviation (R.S.D.) values in the determination of the drugs in serum samples and the recoveries of these small drug molecules. The recovery of the

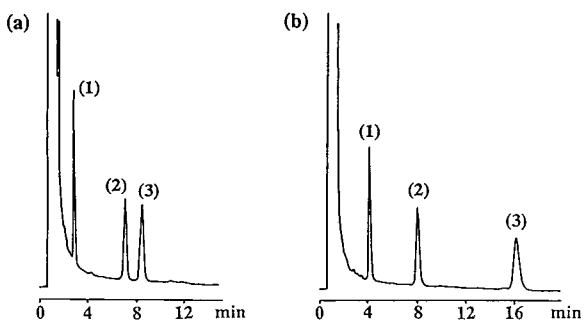

Fig. 2. Chromatograms of human serum spiked with (1) phenobarbital (20 μg/ml), (2) carbamazepine (5 μg/ml) and (3) phenytoin (40 μg/ml) on (a) 20Ph-OG and (b) 20Ph-POE packing materials. HPLC conditions: column size, 150 mm × 4.6 mm I.D.; mobile phase, 100 m*M* phosphate buffer (pH 6.9)–acetonitrile (80:20, v/v); detection, 254 nm; injection volume, 20 μl.

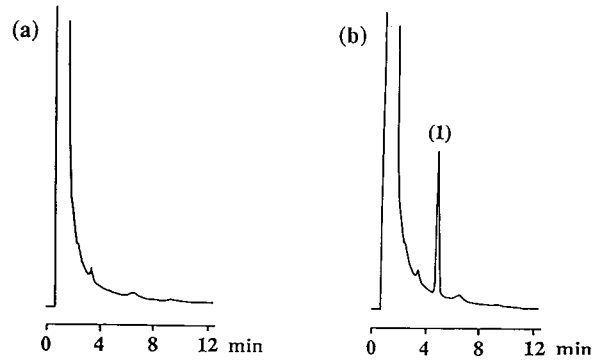

Fig. 3. Chromatograms of (a) human serum and (b) human serum spiked with (1) chloramphenicol (10 μg/ml) on 20Ph-POE packing material. HPLC conditions: column size, 100 mm × 4.6 mm I.D.; mobile phase, 100 m*M* phosphate buffer (pH 6.9)–acetonitrile (90:10, v/v); detection, 280 nm; injection volume, 20 μl.

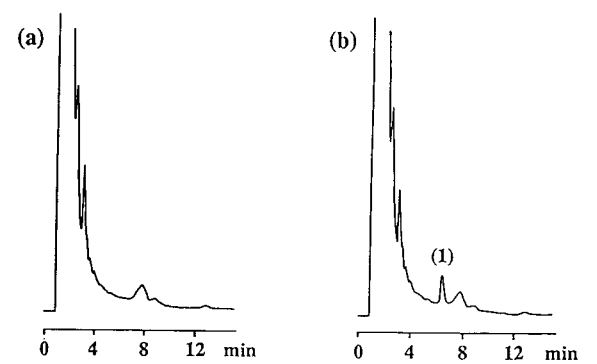

Fig. 4. Chromatograms of (a) human serum and (b) human serum spiked with (1) indomethacin (500 ng/ml) on 20Ph-POE packing material. HPLC conditions: column size, 150 mm × 4.6 mm I.D.; mobile phase, 100 m*M* phosphate buffer (pH 6.9)–acetonitrile (80:20, v/v); detection, 254 nm; injection volume, 20 μl.

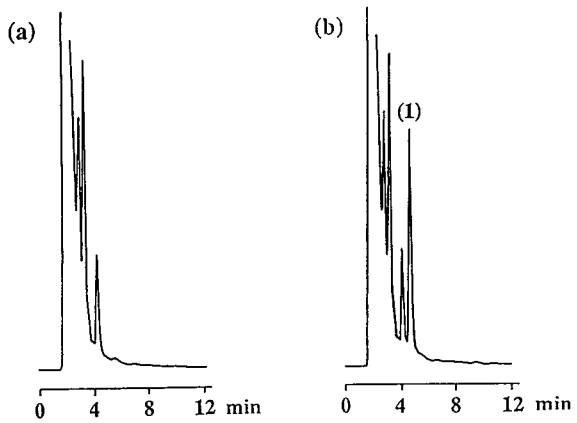

Fig. 5. Chromatograms of (a) human serum and (b) human serum spiked with (1) theophylline (10 μg/ml) on 20Ph-POE packing material. HPLC conditions: column size, 150 mm × 4.6 mm I.D.; mobile phase, 200 m*M* phosphate buffer (pH 6.9)–acetonitrile (98:2, v/v); detection, 254 nm; injection volume, 10 μl.

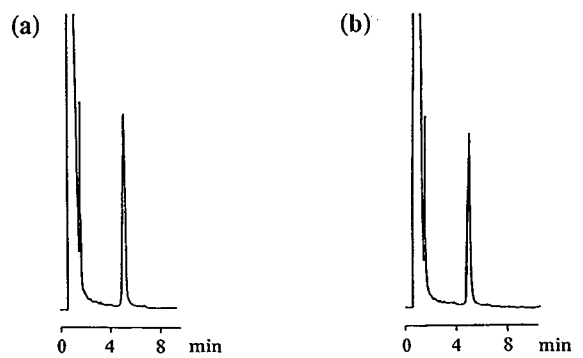

Fig. 6. Chromatograms for (a) the first and (b) the 500th repetitive injection of calf bovine serum spiked with trimethoprim (25 μg/ml) on 20Ph-POE packing material. HPLC conditions: column size, 100 mm × 4.6 mm I.D.; mobile phase, 100 m*M* phosphate buffer (pH 6.9)–acetonitrile (90:10, v/v); detection, 254 nm; injection volume, 20 μl.

drugs in human serum was almost 100% with good reproducibility. This was to be expected from a previous report [19], where drug molecules were found to be released from binding proteins in an organic-containing mobile phase.

3.4. Durability of polymer-coated mixed-functional packing material

Fig. 6 shows chromatograms of (a) the first and (b) the 500th injection of 20 μl (total 10ml) of calf bovine serum spiked with trimethoprim (25 μg/ml) and using 20Ph-POE. The capacity factors of trimethoprim for the first and 500th injection were 5.19 and 5.20, respectively. There was no noticeable decrease in peak efficiency. These results suggest that 20Ph-POE is highly stable at least during 500 analyses. The durability under alkaline conditions (pH 9) was also examined. The initial capacity factor ($k' = 5.21$) of lidocaine on 20Ph-POE, which was injected together with human serum (10 μg/ml), was slightly decreased to 5.01 after 50 h. The 20Ph-POE seems to be less stable against alkaline conditions than more hydrophobic C_{18} polymer-coated phases are [20].

Table 3
Recovery of drug molecules and reproducibility of analysis

Drug	Concentration (μg/ml)	Recovery[a] (%)	R.S.D.[b] (%)
Phenobarbital	20	97.9	1.06
Carbamazepine	5	101.6	0.69
Phenytoin	40	98.8	0.80
Chloramphenicol	5	96.5	0.14
Indomethacin	0.5	97.3	0.65
Theophylline	10	98.5	0.13

[a] The recovery was calculated from the peak-area ratio for a given concentration of the drug dissolved in human serum and mobile phase.
[b] Relative standard deviation of five analyses.

Acknowledgement

We thank Dr. Osamu Shirota for his critical reading of the manuscript.

References

[1] I.H. Hagestam and T.C. Pinkerton, *Anal. Chem.*, 57 (1985) 1757.
[2] I.H. Hagestam and T.C. Pinkerton, *J. Chromatogr.*, 351 (1986) 239.
[3] T.C. Pinkerton, *J. Chromatogr.*, 554 (1991) 13.
[4] J. Haginaka, J. Wakai, N. Yasuda and Y. Kimura, *J. Chromatogr.*, 515 (1990) 59.
[5] K. Kimata, R. Tsuboi, K. Hosoya, N. Tanaka and T. Araki, *J. Chromatogr.*, 515 (1990) 73.
[6] K. Kimata, K. Hosoya, N. Tanaka, T. Arai, R. Tsuboi and J. Haginaka, *J. Chromatogr.*, 558 (1991) 19.
[7] D.J. Gish, B.T. Hunter and B. Feibush, *J. Chromatogr.*, 433 (1988) 264.
[8] L.J. Gluntz, J.A. Perry, B. Invergo, H. Wagner, T.J. Szczerba, J.D. Rateike and P.W. Gluntz, *J. Liq. Chromatogr.*, 15 (1992) 1361.
[9] J. Haginaka and J. Wakai, *Chromatographia*, 29 (1990) 223.
[10] J. Haginaka, J. Wakai and H. Yasuda, *J. Chromatogr.*, 535 (1990) 163.
[11] J. Haginaka and J. Wakai, *Anal. Chem.*, 62 (1990) 997.
[12] J. Haginaka and J. Wakai, *J. Chromatogr.*, 596 (1992) 151.
[13] J. Haginaka and J. Wakai, *Anal. Sci.*, 8 (1992) 137 and 141.
[14] H. Fukui, T. Ogawa, M. Nakano, M. Yamaguchi and Y. Kanda, *Controlled Interphases in Composite Materials*, Elsevier, New York, 1990, pp. 469–478.
[15] Y. Ohtsu, H. Fukui, T. Kanda, K. Nakamura, M. Nakano, O. Nakata and Y. Fujiyama, *Chromatographia*, 24 (1987) 380.
[16] Y. Ohtsu, O. Shirota, T. Ogawa, I. Tanaka, T. Ohta, O. Nakata and Y. Fujiyama, *Chromatographia*, 24 (1987) 351.
[17] O. Shirota, Y. Ohtsu and O. Nakata, *J. Chromatogr. Sci.*, 28 (1990) 553.
[18] Y. Ohtsu, Y. Shiojima, T. Okumura, J. Koyama, K. Nakamura, O. Nakata, K. Kimata and N. Tanaka, *J. Chromatogr.*, 481 (1989) 147.
[19] T. Nakagawa, A. Shibukawa, N. Shimono, T. Kawashima, H. Tanaka and J. Haginaka, *J. Chromatogr.*, 420 (1987) 297.
[20] T. Kanda, J. Koyama, K. Nakamura, Y. Ohtsu and T. Ohta, *Nippon Kagaku Kaishi*, 4 (1989) 702.

ELSEVIER

Journal of Chromatography A, 672 (1994) 59–65

JOURNAL OF CHROMATOGRAPHY A

Comparison between silica-bonded chiral stationary phases derived from 3,5-disubstituted N-benzoyl-(*S*)-phenylalanine and (*S*)-cyclohexylalanine in the resolution of racemic compounds by liquid chromatography

Laureano Oliveros[a], Cristina Minguillón*[,b], Teresa González[b]

[a]*Conservatoire National des Arts et Métiers, Laboratoire de Chimie Générale, 292 Rue Saint-Martin, 75141 Paris Cédex 03, France*

[b]*Laboratorio de Química Farmacéutica, Facultad de Farmacia, Universidad de Barcelona, Avd. Diagonal s/n, 08028 Barcelona, Spain*

(Received January 26th, 1994)

Abstract

A study was made of the role of the phenylalanine phenyl ring in the enantioselectivity of several chiral stationary phases (CSPs) whose chiral selectors consist of several N-(3,5-disubstituted)benzoyl derivatives of this amino acid covalently bonded to silica gel. Racemic compounds with π-acceptor, π-donor or both characters were resolved on two series of CSPs derived from N-(3,5-dimethyl)benzoyl, N-(3,5-dimethoxy)benzoyl and N-(3,5-dinitro)benzoyl-(*S*)-phenylalanine and (*S*)-cyclohexylalanine. In all instances the best enantioselectivities were obtained with CSPs derived from (*S*)-cyclohexylalanine. The results show that the phenyl ring in the phenylalanine moiety does not have an electronic role in the recognition of the racemic compound by the chiral selector on the CSP, a non-classical $\pi-\pi$ interaction between the 3,5-dinitrobenzoyl group in the racemic compound and in the CSP acts in the resolution of N-(3,5-dinitro)benzoyl derivatives of amino acids on CSPs with the same group and the change in the arrangement of solutes in the diastereomeric solute–stationary phase complexes can take place without an inversion of the elution order of enantiomers.

1. Introduction

The 3,5-dinitrobenzamides and particularly the N-(3,5-dinitro)benzoyl derivatives of racemic amino acids are generally well resolved on chiral stationary phases (CSPs) whose chiral selectors are N-(3,5-dinitro)benzoyl derivatives of amino acids [1–4]. That is, racemic compounds with a π-acceptor character are resolved on CSPs with the same π-acceptor character. This cannot be explained by the three-point interaction chiral recognition model in which one of the interactions is of π-acceptor–π-donor character [5–7]. The amino acids in the chiral selectors of these CSPs often have aromatic groups (phenylglycine, phenylalanine and tyrosine). The presence of a 3,5-dinitrobenzoyl group and an additional phenyl ring on the chiral selector of the CSP could give rise, *a priori*, to several modes of electronic interaction between the solute and the chiral entity in the CSP. The most important one in this kind of CSP is a classical π-acceptor–π-

* Corresponding author.

0021-9673/94/$07.00
SSDI 0021-9673(94)00178-C

donor interaction between the 3,5-dinitrobenzoyl group in the CSP and the aryl group in the racemic compound. However, a $\pi-\pi$ interaction between the phenyl ring of the CSP and the analytes [8], or a non-classical π-acceptor–π-acceptor interaction between the 3,5-dinitrobenzoyl groups in the racemic compounds and those in the CSPs, or even a classical π-donor–π-acceptor interaction between the 3,5-dinitrobenzoyl group in the racemic compound and the phenyl ring in the CSP could be considered.

On the other hand, it has been shown [9] that there is no inversion of the elution order of the enantiomers of the methyl esters of N-(3,5-dinitro)benzoyl derivatives of racemic amino acids when these are resolved on CSPs whose chiral selectors are N-(3,5-dimethyl)- or N-(3,5-dimethoxy)benzoylphenylalanine and 3,5-dimethylanilidophenylalanine. If the $\pi-\pi$ interaction were the driving force in the chiral recognition in this kind of CSP and analytes [10], the inversion of the fixation direction of the phenylalanine between the π-donor group and the spacer, which binds the chiral selector to the silica gel, would produce an inversion in the elution order of enantiomers. However, this order would be maintained if the π-acceptor–π-donor interaction were established between the 3,5-dinitrobenzoyl group in the racemic compound and the phenyl ring in the phenylalanine moiety in the CSPs based on N-(3,5-dimethyl)- or N-(3,5-dimethoxy)benzoylphenylalanine. In this instance, the dipole stacking would be orientated in the same direction as in the case in which the chiral selector is 3,5-dimethylanilidophenylalanine and the maintenance of the elution order of enantiomers could be explained [11,12].

The aim of this study was to elucidate the role of the phenyl group of the phenylalanine in the enantioselectivity of the CSP in which the chiral selector is derived from this amino acid. The chromatographic behaviour of two series of CSPs whose chiral selectors are derived from either (*S*)-phenylalanine or (*S*)-cyclohexylalanine was studied by means of the resolution of racemic compounds with π-acceptor, π-donor or both kinds of aromatic groups (Fig. 1). The CSPs also

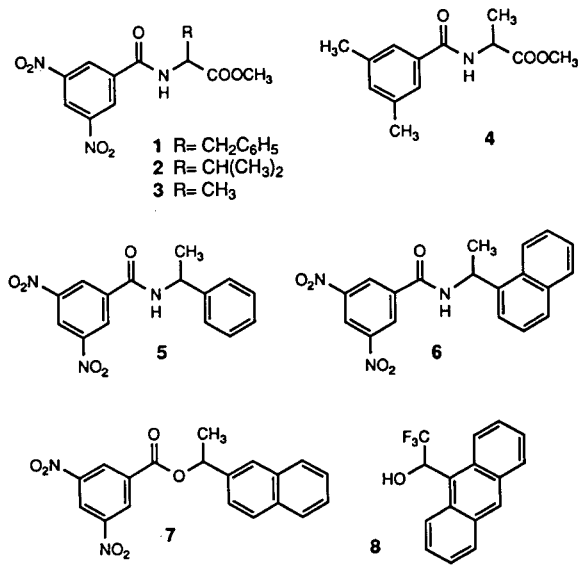

Fig. 1. Structures of racemic test compounds.

have either π-acceptor or π-donor character. An additional CSP whose chiral selector is N-(3,5-dinitrobenzoyl)alanine was prepared and tested to compare the steric effect of the methyl, the benzyl and the cyclohexylmethyl groups on the chiral centre of the CSPs (Fig. 2).

2. *Experimental*

NMR spectra were measured using a Varian Gemini-200 spectrometer. Tetramethylsilane (TMS) was used as the internal standard and the chemical shift, δ, is measured in ppm. Rotatory power was measured with a Perkin-Elmer (Überlingen, Germany) Model 241 polarimeter. Elemental analyses were performed at the Institut de Química Bioorgànica de Catalunya (Barcelona, Spain). The chromatographic experiments were carried out on an HPLC system consisting of a Waters Model 600E pump and a Waters Model 717 autosampler (Millipore, Milford, MA, USA) and equipped with a Waters Model 996 pohotodiode-array detector and a Perkin-Elmer Model 241LC polarimetric detector. The chiral stationary phases were packed into stainless-steel tubes (100 × 4.6 mm I.D.) by the slurry method by Interchim (Montluçon,

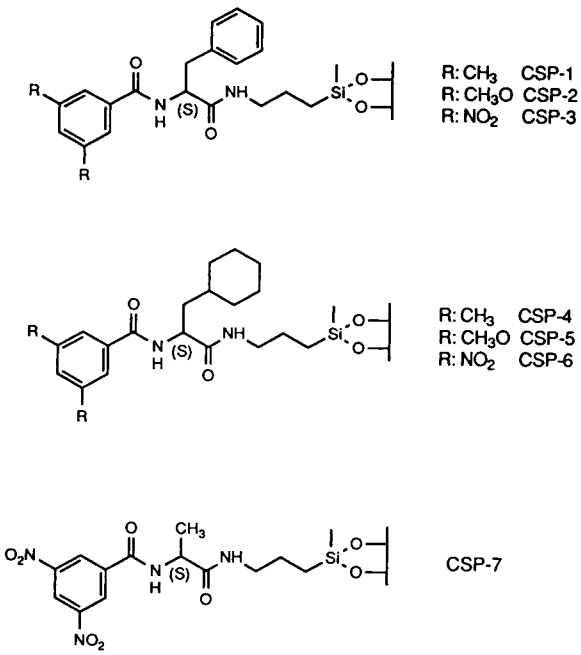

Fig. 2. Structures of chiral stationary phases.

France). The volume of sample injected was 1 μl, the flow-rate of the pump was 1 ml/min and the detection wavelength was 254 nm. The mobile phases consisted of various mixtures of *n*-heptane, chloroform and methanol. The void volume was determined using tri-*tert.*-butylbenzene [13].

2.1. Chemicals and reagents

Chiral selectors of CSPs 1–3 were prepared by the method described previously [9]. Compounds **1–3** (Fig. 1) were obtained by treating the methyl ester of each racemic amino acid with 3,5-dinitrobenzoyl chloride. Compound **4** (Fig. 1) was obtained by treating the methyl ester of racemic alanine with 3,5-dimethylbenzoyl chloride. Compounds **5–7** were obtained by treating the corresponding amines or alcohol with 3,5-dinitrobenzoyl chloride. Compounds **8** (Fig. 1) and 3-aminopropyltriethoxysilane were purchased from Aldrich.

3,5-Disubstituted N-benzoyl derivatives of (*S*)-cyclohexylalanine, chiral selectors of CSP 4–6, were prepared as follows. To a solution of 2.26 g (11 mmol) of (*S*)-cyclohexylalanine hydrochloride, obtained by catalytic reduction of (*S*)-phenylalanine [14], in 1 *M* NaOH, 11 mmol of the appropriate acyl chloride was added following the same method as for N-benzoyl derivatives of (*S*)-phenylalanine [9].

N-(3,5-Dimethylbenzoyl)-(S)-cyclohexylalanine (yield 51%)

^{1}H NMR (200 MHz): δ (C^2HCl_3) 0.7–2.0 (m, 13H, C_6H_{11} and CH_2), 2.35 (s, 6H, CH_3Ar), 4.84 (m, 1H, CH), 6.57 (d, 1H, NH), 7.15 (s, 1H, C^4H), 7.39 (s, 2H, C^2H and C^6H), 8.63 (ba, 1H, COOH). ^{13}C NMR (50.3 MHz): δ (C^2HCl_3) 20.9 (CH_3Ar), 25.7, 25.9 and 26.1 ($C^{3'}H_2$, $C^{4'}H_2$ and $C^{5'}H_2$), 32.3 and 33.2 ($C^{2'}H_2$ and $C^{6'}H_2$), 33.9 ($C^{1'}H$), 39.7 (CH_2), 50.5 (CH), 125.0 ($C^{2,6}H$), 133.5 (C^1), 133.6 (C^4H), 138.4 ($C^{3,5}$), 168.6 (CONH), 177.3 (COOH). $[\alpha]_D^{20} = -19.5°$ (c = 1.4, pyridine). M.p.: 97–98°C (diethyl ether–hexane). Analysis: calculated for $C_{18}H_{25}NO_3$, C 71.26, H 8.31, N 4.62; found, C 71.23, H 8.27, N 4.62%.

N-(3,5-Dimethoxybenzoyl)-(S)-cyclohexylalanine (yield 52%)

^{1}H NMR (200 MHz): δ ($C^2HCl_3/C^2H_3O^2H$) 0.7–2.0 (m, 13H, C_6H_{11} and CH_2), 3.84 (s, 6H, CH_3O), 4.84 (m, 1H, CH), 6.53 (d, 1H, NH), 6.61 (m, 1H, C^4H), 6.93 (d, 2H, $C^{2,6}H$). ^{13}C NMR (50.3 MHz): δ ($C^2HCl_3/C^2H_3O^2H$) 25.6, 25.8 and 26.0 ($C^{3'}H_2$, $C^{4'}H_2$ and $C^{5'}H_2$), 32.0 and 33.2 ($C^{2'}H_2$ and $C^{6'}H_2$), 33.9 ($C^{1'}H$), 39.3 (CH_2), 50.3 (CH), 55.2 (CH_3O), 103.7 (C^4H), 105.0 ($C^{2,6}H$), 135.8 (C^1), 160.8 ($C^{3,5}$), 167.7 (CONH), 175.6 (COOH). $[\alpha]_D^{20} = -7.0°$ (c = 1.6, pyridine). M.p.: 127–129°C (diethyl ether–hexane). Analysis: calculated for $C_{18}H_{25}NO_5$, C 64.46, H 7.51, N 4.18; found, C 64.47, H 7.48, N 4.20%.

N-(3,5-Dinitrobenzoyl)-(S)-cyclohexylalanine (yield 33%)

^{1}H NMR (200 MHz): δ ($C^2HCl_3/C^2H_3O^2H$) 0.8–2.2 (m, 13H, C_6H_{11} and CH_2), 4.80 (m, 1H, CH), 8.53 (d, 1H, NH), 9.11 (d, 2H, C^2H and

C^6H), 9.15 (d, 1H, C^4H). ^{13}C NMR (50.3 MHz): δ ($C^2HCl_3/C^2H_3O^2H$) 25.9, 26.1 and 26.2 ($C^{3'}H_2$, $C^{4'}H_2$ and $C^{5'}H_2$), 32.1 and 33.5 ($C^{2'}H_2$ and $C^{6'}H_2$), 34.2 ($C^{1'}H$), 39.1 (CH_2), 51.0 (CH), 121.0 ($C^{4'}H$), 127.8 ($C^{2',6'}H$), 137.3 ($C^{1'}$), 148.5 ($C^{3',5'}$), 163.3 (CONH), 175.1 (COOH). $[\alpha]_D^{20} = -11.5°$ ($c = 1.4$, pyridine). M.p.: 173–174°C (diethyl ether). Analysis: calculated for $C_{16}H_{19}N_3O_7$, C 52.60, H 5.24, N 11.50; found, C 52.95, H 5.32, N 11.40%.

N-(3,5-Dinitrobenzoyl)-(S)-alanine

Following the same procedure, from 11.2 mmol of (*S*)-alanine and 3,5-dinitrobenzoyl chloride, the title compound was obtained in 85% yield. ^1H NMR (200 MHz): δ ($C^2HCl_3/C^2H_3O^2H$) 1.58 (d, 3H, CH_3), 4.73 (m, 1H, CH), 9.13 (d, 2H, C^2H and C^6H), 9.18 (d, 1H, C^4H). ^{13}C NMR (50.3 MHz): δ ($C^2HCl_3/C^2H_3O^2H$) 17.3 (CH_3), 48.9 (CH), 120.9 (C^4H), 127.7 ($C^{2,6}H$), 137.3 (C^1), 148.4 ($C^{3,5}$), 162.9 (CONH), 174.7 (COOH). $[\alpha]_D^{20} = +15.6°$ ($c = 1.4$, pyridine). M.p.: 156–157°C (diethyl ether). Analysis: calculated for $C_{10}H_9N_3O_7$, C 42.41, H 3.20, N 14.84; found, C 42.32, H 3.16, N 14.73%.

2.2. Chiral stationary phases

Following the described procedure [15], to a solution of 6 mmol of the appropriate chiral acidic compound in 18 ml of pyridine, 1.7 ml (7.2 mmol) of 3-aminopropyltriethoxysilane in 12 ml of pyridine was added. The mixture was stirred under reflux for 1.5 h. The solvent and the excess of 3-aminopropyltriethoxysilane were removed under reduced pressure (0.1 mmHg) and the residue was used in the following step without further purification. A 6-g mass of spherical silica (5 μm, 100 Å, Nucleosil 100-5; Macherey–Nagel) was slurried with toluene and the water was then removed azeotropically using a Dean–Stark trap. After complete removal of water, toluene was removed by distillation and a solution of 6 mmol of the appropriate chiral silane freshly prepared in 50 ml of pyridine was added. The mixture was stirred under reflux for 1.5 h and 3 ml of hexamethyldisilazane were added, and the mixture was left to react for a further 1 h at reflux temperature. The resulting bonded silica was collected by filtration and washed exhaustively in pyridine, ethanol, water, ethanol, acetone and diethyl ether, and dried *in vacuo* at room temperature.

The elemental analyses and the surface concentration of surface-bonded chiral entities (μmol/m^2) according to Unger *et al.* [16] of the stationary phases are given in Table 1.

3. Results and discussion

Chromatographic parameters for the separation of the test compounds are given in Table 2.

The racemic compounds **1**, **2** and **3**, with π-acceptor character, are resolved on all CSPs tested. However, the selectivity is higher when they are resolved on CSPs with π-donor character (CSPs 1, 2, 4 and 5). Conversely, **4**, with π-donor character, is better resolved on π-acceptor CSPs (CSPs 3, 6 and 7) than on π-donor CSPs (CSPs 1, 2, 4 and 5). On the other hand, when **4** is resolved on CSPs 6 and 7 the only $\pi-\pi$ interaction that could be established is of π-acceptor–π-donor type. Moreover, **8** is only resolved on CSPs with π-acceptor character. All these observations are as expected: a π-acceptor–π-donor interaction could favour the chiral recognition of solutes by the CSP considerably.

Compounds **2** and **3** are well resolved on CSPs 6 and 7 even if the only aromatic group present on these racemic compounds and on the CSPs is a 3,5-dinitrobenzoyl ring. In such a case, if a $\pi-\pi$ interaction takes part in the recognition of those solutes by the CSPs, it could only be established between both 3,5-dinitrobenzoyl rings. Some facts seem to indicate this possibility. In all instances the α values are of the same order. This seems to indicate that the difference in stability of solute–CSP adsorbates in all CSPs tested is similar, and therefore a similar recognition mechanism could be expected. Moreover, the elution order of the enantiomers of **2** and **3** on CSPs 6 and 7 is the same as on π-donor CSPs, where a reasonable

Table 1
Elemental analyses of chiral stationary phases

Stationary phase	Elemental analysis (%)			Ratio of carbon atoms per nitrogen atom		mmol of chiral moiety per g of stationary phase (from % N)	α_{exp} [b] (μmol/m^2)
	C	H	N	Analytical	Theoretical[a]		
CSP 1	8.42	1.44	1.10	8.93	10.5	0.39	1.16
CSP 2	8.01	1.33	0.95	9.84	10.5	0.34	1.11
CSP 3	10.36	1.36	2.11	5.73	4.75	0.38	1.26
CSP 4	8.55	1.64	1.03	9.68	10.5	0.38	1.20
CSP 5	10.05	1.59	1.10	10.66	10.5	0.39	1.31
CSP 6	9.47	1.71	2.02	5.47	4.75	0.36	1.21
CSP 7	8.34	1.66	1.96	4.96	3.25	0.35	1.13

[a] Methyl groups coming from the "end-capping" treatment were not taken into account.

[b] Surface concentration of surface-bonded chiral entities, $\alpha_{exp} = \frac{m}{M} \cdot \frac{10^6}{S_{BET}(1-m)}$, where m = mass of functional group (grams per gram of adsorbent), M = molar mass of the bonded functional group (g/mol) and S_{BET} = specific surface area of the starting support (m^2/g) [16].

π-donor–π-acceptor interaction could be established. That is, in both situations the arrangement of the diastereomeric adsorbates could be the same. The 3,5-dinitrobenzoyl group on **2** and **3** may establish a $\pi-\pi$ interaction with the 3,5-disubstituted benzoyl ring on the CSP (π-acceptor–π-donor interaction in the case of CSP 1, 2, 4 and 5 and π-acceptor–π-acceptor interaction in the case of CSPs 6 and 7). Moreover, **1** and **2** are not resolved and $\alpha = 1.02$ in the case of **3**, on a CSP whose chiral selector is N-acetylphenylalanine [3], where the 3,5-dinitrobenzoyl group present on CSP 3 has been replaced by an acetyl group.

From the comparative study of data obtained with CSPs derived from (*S*)-cyclohexylalanine (CSPs 4, 5 and 6), and those obtained with CSPs derived from (*S*)-phenylalanine (CSPs 1, 2 and 3), it can be deduced that the phenyl ring in the phenylalanine moiety does not establish a $\pi-\pi$ interaction with the aryl group in racemic compounds. In all instances, the selectivity values of cyclohexylalanine-derived CSPs are higher than those of phenylalanine-derived CSPs. This lack of $\pi-\pi$ interaction is confirmed by the comparison of the performances of CSPs 3, 6 and 7. The selectivity values of CSP 6 are higher than those of CSPs 3 and 7 and those of CSP 7 are the lowest. These differences seem to have a steric origin. In fact, there are results in the literature in which the presence of hindering groups near the chiral centre, either on the CSP or on the racemic compound, enhances the separation.

The racemic compounds **5–7**, which simultaneously bear a π-donor and a π-acceptor group, are not resolved on π-donor CSPs, in spite of the presence of a 3,5-dinitrobenzoyl group in their structures. This is unexpected if the similarity in the structures of **1–3** (better resolved on π-donor than on π-acceptor CSPs) and **5** and **6** (resolved only on π-acceptor CSPs) is taken into account. In this case the π-donor aryl group on racemic compounds **5–7** seems to interact with the 3,5-dinitrobenzoyl group on the CSPs, as is supposed to happen in compound **8**. It should be noted that, in this instance, the chiral recognition involves the formation of diastereomeric solute–CSP complexes with different arrangements of groups to that of compounds **1–3**. However, in all instances the first enantiomer eluted has the same configuration at the chiral centre (if the absolute configuration of **8** changes, it is because of the inversion in the priority order of substituents on the chiral centre). This is possible even if the diastereomeric solute–CSP complexes were those proposed. In fact, a rotation of 180° could change one arrangement into the other [12].

Table 2
Chromatographic parameters (capacity factor, k_1, selectivity factor, α, and resolution, R_s) for the separation of test compounds

Racemic compound	CSP-1			CSP-2			CSP-3			CSP-4			CSP-5			CSP-6			CSP-7			Mobile phase: $CHCl_3$[b]–heptane
	k_1'	α	R_s	k_1'	α	R_s	k_1'	α	R_s	k_1'	α	R_s	k_1'	α	R_s	k_1'	α	R_s	k_1'	α	R_s	
1	0.36	2.06	4.13	0.48	2.35	4.98	0.43	1.52	1.94	0.29	2.61	3.66	0.38	2.94	5.38	0.51	1.64	2.51	0.52	1.41	1.76	75:25
	R/−[a]			*R*/−			*R*/−			*R*/−			*R*/−			*R*/−			*R*/−			
2	0.29	1.94	3.13	0.40	2.01	3.32	0.42	1.46	1.79	0.25	2.25	3.03	0.33	2.35	3.49	0.52	1.49	2.13	0.48	1.37	1.56	75:25
	R/−			*R*/−			*R*/−			*R*/−			*R*/−			*R*/−			*R*/−			
3	0.83	1.74	4.44	1.05	1.96	5.44	0.62	1.56	2.66	0.74	2.08	4.38	0.87	2.63	5.88	0.90	1.61	3.21	0.82	1.36	1.78	75:25
	R/−			*R*/−			*R*/−			*R*/−			*R*/−			*R*/−			*R*/−			
4	6.53	1.07	–	7.51	1.07	–	7.02	1.51	2.30	5.09	1.09	–	4.26	1.12	–	7.63	1.52	2.73	6.71	1.44	3.25	10:90
	–			–			–			–			–			–			–			
5	2.41	1.00	–	2.88	1.00	–	1.73	1.13	1.01	1.92	1.00	–	2.50	1.00	–	2.41	1.28	2.12	2.95	1.06	–	50:50
							R/−			[c]						*R*/−			*R*/−			
6	1.94	1.00	–	2.40	1.00	–	2.53	1.13	1.11	1.51	1.00	–	1.97	1.00	–	3.10	1.44	3.02	3.52	1.13	1.30	50:50
							R/−									*R*/−			*R*/−			
7	1.29	1.00	–	1.94	1.00	–	5.84	1.10	1.03	0.86	1.00	–	1.32	1.00	–	3.51	1.18	1.85	3.83	1.05	–	10:90
							R/−									*R*/−			*R*/−			
8	0.96	1.00	–	1.21	1.00	–	1.39	1.58	3.98	1.13	1.00	–	1.18	1.00	–	1.86	1.60	4.17	2.17	1.25	2.27	75:25
							S/+									*S*/+			*S*/+			

[a] Absolute configuration/optical rotation sign of the first-eluted enantiomer in the solvent used as eluent.
[b] $CHCl_3$ to which 0.5% of MeOH was added.
[c] Using $CHCl_3$–heptane (25:75) as the mobile phase: $k_1' = 11.79$ (*R*/−), $\alpha = 1.05$.

4. Conclusions

In bonded-silica CSPs whose chiral selector is a phenylalanine derivative, the phenyl ring belonging to this moiety seems to have a steric role instead of acting as a π-interacting group in the chiral recognition mechanism.

According to the results obtained, racemic compounds belonging to different structural series, even if they are similar, could interact with CSPs following different patterns, *i.e.*, they could be recognized at different interacting groups.

Acknowledgements

Financial support from the Comisión Interministerial de Ciencia y Tecnologia and from the Generalitat de Catalunya (Project No. QFN91-4201) is acknowledged. T.G. thanks the Comissió Interdepartamental de Recerca i Innovació Technològica (Generalitat de Catalunya) for a doctoral fellowship.

References

[1] P. Macaudière, M. Lienne, M. Caude, R. Rosset and A. Tambuté, *J. Chromatogr.*, 467 (1989) 357.
[2] M. Caude, A. Tambuté and L. Siret, *J. Chromatogr.*, 550 (1991) 357.
[3] L. Oliveros, C. Minguillón, B. Desmazières and P.-L. Desbène, *J. Chromatogr.*, 543 (1991) 277.
[4] W.H. Pirkle and J.A. Burke, *J. Chromatogr.*, 598 (1992) 159.
[5] W.H. Pirkle, T.C. Pochapsky, G.S. Mahler, D.E. Corey, D.S. Reno and D.M. Alessi, *J. Org. Chem.*, 51 (1986) 4991.
[6] J.M. Finn, in M. Zief and L.J. Crane (Editors), *Chromatographic Chiral Separations (Chromatographic Science Series*, Vol. 40), Marcel Dekker, New York, 1987, Ch. 3, p. 53.
[7] P. Macaudière, M. Lienne, M. Caude and A. Tambuté, in A.M. Krstulovic (Editor), *Chiral Separations by HPLC, Applications to Pharmaceutical Compounds*, Ellis Horwood, Chichester, Ch. 3.
[8] T.D. Doyle, W.M. Adams, F.S. Fry and I.W. Wainer, *J. Liq. Chromatogr.*, 9 (1986) 455.
[9] L. Oliveros, C. Minguillón, B. Desmazières and P.-L. Desbène, *J. Chromatogr.*, 589 (1992) 53.
[10] L. Siret, A. Tambuté, M. Caude and R. Rosset, *J. Chromatogr.*, 540 (1991) 129.
[11] I.W. Wainer and T.D. Doyle, *J. Chromatogr.*, 284 (1984) 117.
[12] W.H. Pirkle and J.E. McCune, *J. Chromatogr.*, 469 (1989) 67.
[13] W.H. Pirkle and C.J. Welch, *J. Liq. Chromatogr.*, 14 (1991) 173.
[14] E. Peggion, L. Strasorier and A. Cosani, *J. Am. Chem. Soc.*, 92 (1970) 381.
[15] L. Oliveros, C. Minguillón, B. Desmazières and P.-L. Desbène, *J. Chromatogr.*, 606 (1992) 9.
[16] K.K. Unger, N. Becker and P. Roumeliotis, *J. Chromatogr.*, 125 (1976) 115.

ELSEVIER

Journal of Chromatography A, 672 (1994) 67–85

JOURNAL OF CHROMATOGRAPHY A

Computational strategy for solvent strength optimization in reversed-phase liquid chromatography

P. Chaminade*, A. Baillet, D. Ferrier

Laboratoire de Chimie Analytique III, Faculté de Pharmacie, 1 Avenue Jean-Baptiste Clément, F-92296 Chatenay-Malabry Cedex, France

(First received November 23rd, 1993; revised manuscript received January 28th, 1994)

Abstract

Computer algorithms for iterative solvent strength optimization are presented together with a practical development strategy consistent with other widely accepted schemes. This optimization strategy appears to be flexible enough to make use of all the experiments realized during the mobile phase development. The computer algorithm accepts any case of solute elution, during or after the gradient rise for linear or multi-linear gradients, as input or output parameters. The computer routine is able to compute solute retention from two gradients differing in their slopes and also slight changes in solvent composition. The iterative computation of the linear model allows a further minimization of the error in prediction. If some additional experiments are provided, the retention model can be extended to a more accurate quadratic form. From its computation, which uses the Nedler and Mead simplex controlled by an error reduction criterion, this model allows a further improvement in retention time prediction. This permits low prediction errors in the case of difficult developments that need several chromatographic runs.

1. Introduction

In the last 10 years, particular attention has been paid to the use of computer-assisted method development in liquid chromatography. Numerous approaches of great help for chromatographers have been published, recently summarized by Tchapla [1]. However, some drawbacks have been pointed out, particularly the rigidity of the procedure and the possible "overkilling" of easy separations.

In reversed-phase high-performance liquid chromatography (RP-HPLC), the primary goal is to optimize the solvent strength in order to achieve a good elution within a reasonable analysis time. When the technique is to be used routinely and one or more compounds are to be determined, isocratic elution is the preferred method as column equilibration between each run is not needed. In this case, if the required analysis time and/or resolution are not met, the mobile phase development can be followed by a selectivity optimization with a change of the organic modifier and, further, the use of ternary and quaternay mobile phases.

The use of a particular organic modifier may be preferred to improve solute detection (hyperchromic effect in UV detection or organic modifier limit of oxidation in electrochemical detection) or to ensure solute stability (peptides

* Corresponding author.

0021-9673/94/$07.00
SSDI 0021-9673(94)00099-U

analysis). In those cases, the only method is to perform a gradient elution to achieve the elution of both polar and non-polar solutes within a reasonable analysis time. The development of binary isocratic mobile phases is advantageous as only one parameter (the organic content of the mobile phase) is to be set and the solute retention *vs.* mobile phase composition can be conveniently depicted by a graphical procedure. The advantages of computer-aided development become clear for gradient profile optimization as the chromatographer must simultaneously consider at least three parameters: the initial and final composition and the gradient slope.

However, the common drawback of the software involved is that it only solves the retention equations which depict a particular kind of initial experiment (*e.g.*, unique gradient, pair of linear gradients, pair of isocratic experiments). Further, the software is unable to take advantage of subsequent experiments if their corresponding experimental conditions do not match the required input.

Our purpose was to write an adaptable computer program usable as a specific tool designed for the chromatographer. This program is based on the two main strategies proceeding from linear gradients but may also use isocratic experiments and/or multilinear gradients.

2. Theoretical background

In RP-HPLC with binary mobile phases, the solute capacity factor (k') is accurately described by a quadratic relationship involving the volume fraction (ϕ) of organic modifier [2]:

$$\ln k' = A\phi^2 + B\phi + C \quad (1)$$

As three experiments are needed to compute the parameters A, B and C of the model, a simplified equation is widely preferred:

$$\ln k' = \ln k_w - S\phi \quad (2)$$

where k_w is the hypothetical value of the solute capacity factor for an aqueous mobile phase and S is the slope of the relationship. However, this model often fails to describe the solute retention for wide variations of the organic content of the mobile phase.

In the specific case of linear gradient elution, this last relationship allows the algebraic development of the fundamental equation of gradient elution [3]:

$$\int_0^{V_g} \frac{\delta V}{V_a} = 1 \quad (3)$$

where V_g is the retention volume under gradient conditions and V_a is the retention volume under isocratic elution. This equation can be expressed as a function of time and solute capacity factor:

$$\int_0^{t'_g} \frac{\delta t}{k'_{(\phi)}} = t_0 \quad (4)$$

where t_0 is the column dead time, t'_g is the net retention time under gradient conditions and $k'_{(\phi)}$ is the solute capacity factor expressed as a function of the volume fraction of organic modifier ϕ and therefore as a function of time since ϕ varies with time under gradient conditions. Consequently, by solving Eq. 4 for S and $\ln k_w$, it becomes possible to obtain the solute retention time for any composition of the mobile phase [4–8].

Many workers have pointed out the usefulness of gradient-based development procedures [9–11]: first, as the sample is subjected to wide variations of mobile phase composition, the polar and less polar compounds of the sample can be measured on the same chromatogram; and moreover, linear gradients allow the solute band width to remain nearly constant for the overall chromatogram [9,12].

From a general point of view, the initial gradient experiment is designed to appreciate the sample complexity. Consequently, this first gradient will preferably cover a wide range of elution strength. However, gradients which meet these requirements are also subjected to "non-ideal" processes generated by the gradient equipment or the retention mechanism in gradient elution itself. An extensive review of these phenomena was published by Quarry *et al.* [13,14].

An important equipment-related cause of non-ideality that contributes greatly to the error in prediction is the gradient delay time, t_D. The delay time is generated by the time needed by the mobile phase to flow through the gradient mixer and tubing. However, t_D can be easily accounted for by considering an isocratic elution step before the actual start of the gradient (see Section 2.1). The gradient mixer also generates gradient profile distortions due to dispersion of the mobile phase in the mixer itself [13].

Chromatographic-related causes of error are quantitatively more important: the flow-rate during the gradient run can vary by as much as 5% [15,16], mainly because of volume contraction generated by the mixing of the aqueous and organic fractions of the mobile phase [17]; the column dead volume also varies during the gradient, owing to changes in spatial conformation of the alkyl chains [18] and uptake of the organic component of the mobile phase by the stationary phase [19]; this last phenomenon (solvent uptake) was also implicated in solute retention by Quarry *et al.* [14]; and non-equilibrium between the stationary and mobile phases during the gradient run is encountered with short gradients, which limits the calculation of isocratic retention times from gradient elution as this equilibrium is the basis of isocratic elution.

Two main strategies have been suggested for gradient-based mobile phase development: (1) the calculation of parameters S and $\ln k_w$ from two gradient runs with different slopes proposed by Quarry *et al.* [5] and Heinish and co-workers [6–8] permits one to solve the two equation–two unknowns system only in the specific case where the solute elution occurs before the end of the gradient rise; and (2) the strategy put forward by Schoenmakers *et al.* [4] based on a further correlation which links together the parameters S and $\ln k_w$ [2]:

$$S = p + q \ln k_w \quad (5)$$

where p (intercept) and q (slope) were obtained by regression analysis based on isocratic measurements. As Eq. 2 can be expressed as a function of only one parameter, both S and $\ln k_w$ can be computed from a single gradient run.

The application fields and the accuracy of these two methods are different:

(i) The simultaneous estimate of S and $\ln k_w$ requires a prior knowledge of the p and q constants from Eq. 5. These two constants depend on the organic modifier, the stationary phase [2] and also the chemical structure of the solute [20]. As these constants are the result of a linear regression, these reflect the average behaviour of a set of solutes. Consequently, even in the most favourable case where all the solutes to be separated are structurally related, it is possible that at least one of them will exhibit a particular retention behaviour. This limits the present strategy to be a rapid procedure designed to provide a rough estimate of the first- and last-eluting peak retention times.

(ii) In the case of the dual gradients-based strategy, the necessity for solute elution before the end of the gradient rise may require several experiments to be performed before this condition is met. Nevertheless, this calculation method is independent of the organic modifier in use, the stationary phase and the solute structure and, therefore, is suitable for a simultaneous estimate of analysis time and resolution.

The common drawback of the preceding methods is that they are non-iterative. After the initial gradient or pair of gradients has been applied, the proposed mobile phase or gradient profile must be adjusted without any assistance from the computer program. The computer program we propose was designed to perform an iterative solvent strength optimization. The basic requirement was to accept data from any kind of experiment, *i.e.*, including both isocratic and linear and multi-linear gradients, although a linear gradient is the preferred initial experiment. Consequently, a numerical integration of Eq. 4 is used to facilitate the calculation of retention times both in isocratic and gradient conditions. The algorithm used to compute the values of S and $\ln k_w$ from one experiment consists in a classical bisection method [21]. The bisection method is a simple and robust algorithm for root finding. When solving a function

such as $y = f(x)$ the principle of this algorithm is to bracket the zero value of $f(x)$ using lower and upper values of x, x_a and x_b, that lead to $f(x_a) < 0$ and $f(x_b) > 0$. The next step, that will be repeated until completion, will be to test the value of $x_c = (x_a + x_b)/2$. If, for example, $f(x_c) < 0$, the value of x_a will be replaced by x_c until the zero value of $f(x)$ is approximated with sufficient precision The linear model (2) and Eq. (5) allow one to express the capacity factor as a function of only one parameter:

$$\ln k' = \frac{S(1 - q\phi) - p}{q} \tag{6}$$

As soon as two experiments are available, the values of parameters S and $\ln k_w$ are computed using a numerical method. A Monte Carlo-based algorithm permits one to take into account gradients with differences in initial and/or final compositions and also in gradient slope. When more than two experiments are performed, the Nedler and Mead simplex [22] is used to compute the linear model by χ^2 fitting. Further, when a sufficient number of experiments are performed, the linear model is extended to a quadratic relationship by adding the term $A\phi^2$ to Eq. 2. The parameters A, S and $\ln k_w$ are fitted to data using the same Nedler and Mead simplex algorithm [22].

2.1. Calculation of retention times

Retention times under isocratic or gradient conditions are calculated by numerical integration of a rearranged form of Eq. 4:

$$\frac{1}{t_0}\int_0^{t_g} \frac{\delta t}{k'_{(\phi_{i,i+1})}} = 1 \tag{7}$$

This calculation method assumes that a gradient step is similar to a sequence of short isocratic steps of increasing solvent strength. This calculation is similar to the algorithm proposed by Tomellini *et al.* [23] but uses a dynamic calculation of the step duration.

Typically three cases must be taken into account in a linear gradient: solute elution can occur during (1) the gradient delay time, this case being identical with isocratic elution arising in the initial mobile phase of the gradient; (2) the gradient rise, where the contribution of the previous isocratic step must also be accounted for, especially for polar solutes; and (3) after the gradient end, corresponding to a late isocratic elution in the final mobile phase after the two preceding steps.

Isocratic elution

An isocratic step between times t_i and t_{i+1} contributes to the integration of the fundamental equation for a quantity x given by

$$\frac{1}{t_0}\int_{t_i}^{t_{i+1}} \frac{\delta t}{k'_{(\phi_{i,i+1})}} = x$$

$$\frac{1}{t_0}\cdot\frac{t_{i+1} - t_i}{k'_{(\phi_{i,i+1})}} = x \tag{8}$$

Gradient elution

A gradient step is considered as a sequence of short isocratic steps. The number of isocratic steps n is calculated as a function of the gradient slope b to be $n = 100b$. Consequently, n is greater for a short gradient than for a gradient with a low slope. The contribution of each short isocratic step is calculated using Eq. 8. The instantaneous capacity factor is averaged between its value in the current and the next step. The whole equation for a complete gradient step is

$$\frac{1}{t_0}\sum_{j=1}^{j=n-1} \frac{t_{j+1} - t_j}{\dfrac{k'_{(\phi_j)} + k'_{(\phi_{j+1})}}{2}} = x \tag{9}$$

The contributions of each isocratic (and therefore gradient) step are summed in addition to the time intervals of each step. The integration is complete when the sum of contributions (denoted Σx) exceeds unity. The excess time Δt can then be calculated according to the following equation derived from Eq. (8):

$$\Delta t = \left[\left(\sum x\right) - 1\right] k'_{(\phi_{i,i+1})} t_0 \tag{10}$$

This excess time must then be subtracted from

the sum of the time intervals to obtain the net retention time.

In all the preceding equations, the capacity factor can be expressed as a log–linear (Eq. 2) or log–quadratic (Eq. 1) function of the volume fraction of organic modifier ϕ.

2.2. Numerical solution for a pair of gradients

The algorithm used to compute the two equations describing the two experiments is based on a Monte Carlo simulation [21]. The basis of this technique is to submit an equation to a set of random numbers until the solution is reached with reasonable precision. In our case, the two experimental runs are described by the numerical integration of Eq. 4 that uses Eq. 2 to express the solute capacity factor for a given composition of the mobile phase. Solving this system of two equations that include two parameters (S and $\ln k_w$) by searching for which pair of random numbers satisfies both equations would be easy to program, but would also lead to excessive calculation times.

Our algorithm consists in a few steps designed to minimize the calculation time:

(i) Rather than solving the two equations simultaneously, each of them is solved separately and the common solutions of S and $\ln k_w$ are then computed. For each equation, the result of the Monte Carlo simulation is a set of S and $\ln k_w$ values. By plotting S as a function of $\ln k_w$, the two sets of solutions lead to two straight lines. The common solution, *i.e.*, the values of S and $\ln k_w$ which satisfy both equations, are at the intersection point of these two lines.

(ii) The random values of S and $\ln k_w$ are enclosed within boundaries to avoid testing the lowest or highest values of S and $\ln k_w$. The algorithm assumes that the "true" values of S and $\ln k_w$ are near by the values of the estimate S_e and $\ln k_{w_e}$ computed for each run using the correlation $S = p + q \ln k_w$ (Eq. 5). Consequently, for each equation, the variation interval is:

(1) run 1:

$S : [0.50S_{e1} \ldots 1.50S_{e1}]$

$\ln k_w : [0.50 \ln k_{w_{e1}} \ldots 1.50 \ln kw_{e1}]$

(2) run 2:

$S : [0.50S_{e2} \ldots 1.50S_{e2}]$

$\ln k_w : [0.50 \ln k_{w_{e2}} \ldots 1.50 \ln k_{w_{e2}}]$

Once the values of S and $\ln k_w$ satisfying the two equations have been calculated, the validity of the solution is checked as follows:

(i) As considered previously, the values of the estimate S_e and $\ln k_{w_e}$ are assumed to be close to the true solution. For example, if the value of S lies outside the interval $[0.50S_{e1} \ldots 1.50S_{e1}]$ and $[0.50S_{e2} \ldots 1.50S_{e2}]$, this solution is rejected. In this case, it is considered that the two experiments are incompatible and do not admit a common solution. This last point will be discussed later.

(ii) A second Monte Carlo simulation computes which variation of the parameters S and $\ln k_w$ still lets them verify the two equations with a 1% precision. This last step allows one to appreciate the precision of the calculation of S and $\ln k_w$ for each solute.

2.3. Iterative calculation and linear model extension

The simplex algorithm [21,22] is used to perform the iterative calculation of S and $\ln k_w$ and to extend the linear model to a quadratic form. The simplex rules will not be discussed as this algorithm, first designed for non-linear regression, is a well known and widely used optimization procedure [24–27].

Although its convergence is slow, this algorithm is a powerful means of iterative calculation as the criterion used to fit the model (noted χ^2) is based on the reduction of the squared difference between experimental and calculated values. Starting from the values of S and $\ln k_w$ obtained by Monte Carlo simulation, this algorithm is used to compute the linear model from more than two experiments.

When three or more experiments are available, the linear model can be extended to Eq. 2. The quadratic extension is given by

$$\ln k' = A\phi^2 - S\phi + \ln k_w \qquad (11)$$

Considering Eq. (11), we prefer to call this model "extended linear" to avoid confusion with the true quadratic model. In the case of Eq. 1, the three parameters A, B and C are computed simultaneously from three or more isocratic measurements. In the case of the extended linear model, the starting equation is Eq. 2: S and $\ln k_w$ are equal to the values calculated in the preceding step and the parameter A is initially set to zero. The use of the simplex algorithm allows one to perform smooth variations of A, S and $\ln k_w$ enclosed within boundaries. These boundaries are of particular importance as they ensure that the simplex will smoothly extend the linear model to approach the flexibility of the quadratic model and to improve the calculation accuracy by the mean of the χ^2 reduction. It should be noted that the values of the linear model are kept by the program if the calculation accuracy cannot be improved by adding this $A\phi^2$ term.

3. Experimental

The programming and calculations were carried out with a Chronosoft 486-33 IBM-AT compatible microcomputer with built-in math coprocessor. The computer program is written in Pascal using Borland's Turbo Pascal. The cluster analysis was performed using the MVSP statistical package from W.L. Kovach (Kovach Computing Services, Pentraeth, UK).

Measurements were carried out with a Spectra-Physics XR 8700 ternary gradient liquid chromatograph equipped with a Rheodyne injection valve with a 10-μl sample loop (Spectra-Physics, Les Ulis, France). Detection was performed with a Shimadzu SPD-2A UV detector (Touzat et Matignon, Vitry sur Seine, France). The chromatograms were recorded with a Spectra-Physics ChromJet integrator or a Kontron PC-Integration pack Rev. 3.90 (Kontron Instruments, St. Quentin Yvelines, France). The flow-rate was set at 1 ml min^{-1}. The column dead time was measured by injection of a 50 mg l^{-1} solution of sodium nitrate (Merck, Nogent sur Marne, France) diluted in the mobile phase. The gradient delay time (t_D) was measured by the observation of the rise in the baseline while running a gradient from a 100% methanol to a methanol–0.2% dimethyl ketone mobile phase. The experimental value of t_D was 2.90 min for a flow-rate set at 1 ml min^{-1} for the part of the study concerning phenolic antioxidants and 3.40 min (flow-rate 1 ml min^{-1}) for benzodiazepines as an on-line filter was added to the pumping device.

Benzodiazepine standards were obtained by courtesy of Professor Farinotti from the toxicological department of X. Bichat C. Bernard Hospital (Paris, France). The hydrolysis procedure was adapted from the method of Maurer and Pfleger [28] used to identify 1,4- and 1,5-benzodiazepines in urine by gas chromatography–mass spectrometry: 1.0 ml of a stock solution of each compound at a concentration of 1 mg ml^{-1} in methanol was evaporated under a stream of nitrogen at ambient temperature. The residue was then refluxed with 10 ml of 37% hydrochloric acid (Merck) for 30 min and then neutralized with 90 ml of 1 M Na_2CO_3 (Merck) solution in acetonitrile–water (50:50). The volume was adjusted at 100 ml with acetonitrile–water (50:50) after the excess of CO_2 had been removed. The resulting solution containing 10 mg l^{-1} of each standard was injected directly into the chromatograph. Peak identification was done using solutions of each hydrolysed benzodiazepine prepared at the same level of 10 mg l^{-1}. UV detection was performed at 230 nm. The column was Sup.Rs (250 × 4.6 mm I.D.) packed with LiChrospher C_{18} with a particle size of 5 μm (Prolabo, Paris, France). The experimental value of the column dead time was 2.10 min for a flow-rate set at 1 ml min^{-1}. Acetonitrile (Merck) and water (Baker) were of HPLC quality.

Phenolic antioxidants were obtained as pure compounds from Merck. Standard solutions of approximately 0.1 mg ml^{-1} of each compound were prepared in the mobile phase (or initial mobile phase in the case of gradient elution). Methanol of HPLC gradient quality was purchased from Prolabo. Water was glass-distilled. Acetic acid of analytical-reagent grade was obtained from Prolabo. UV detection was per-

formed at 230 nm. The column was SFCC Spherisorb ODS-2 (150 × 4.6 mm I.D.) with a particle size of 3 μm (SFCC–Shandon, Eragny, France). The experimental value of the column dead time was 1.12 min for a flow-rate set at 1 ml min^{-1}.

4. Results and discussion

4.1. Iterative solvent strength optimization

The two main strategies for solvent strength optimization were described in section 2. They are summarized and compared with the methodology we propose in Fig. 1. Our strategy is consistent with both of the two preceding approaches but uses an iterative calculation algorithm. This feature is illustrated hereafter by the separation of a complex mixture of a hydrolysis product of benzodiazepines presented in Table 1. The aim of this separation was to investigate how HPLC could be used as a screening procedure before a gas chromatographic–mass spectrometric analysis.

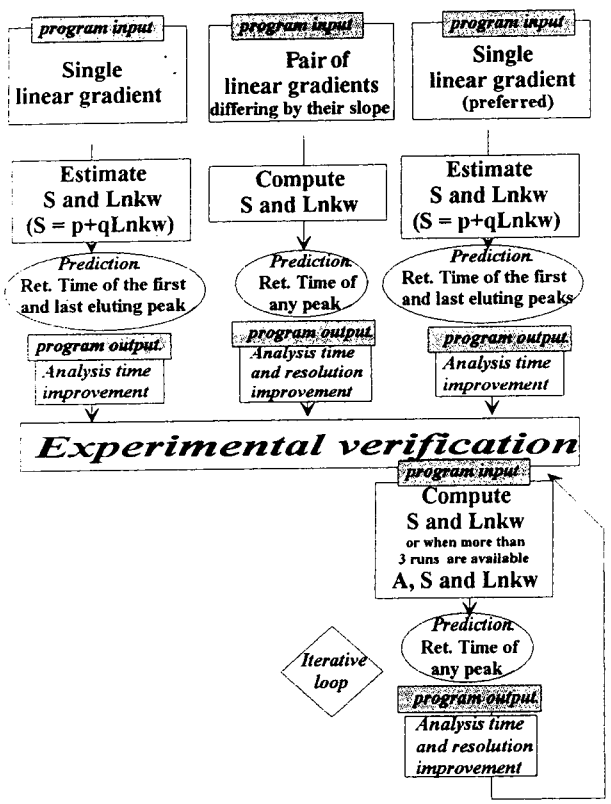

Fig. 1. Schematic representation of the optimization procedure.

Iterative solvent strength optimization using the linear model

The methodology used by Schoenmakers *et al.* [4] uses only one gradient to compute an estimate of the S and $\ln k_w$. The two gradients-based method uses a pair of gradient runs with the same initial and final compositions but a difference in slope to calculate S and $\ln k_w$. In our approach, we use the results from the first gradient to estimate S and $\ln k_w$ and then to compute the conditions of the second gradient. The aim of this step is to try to adjust the gradient profile in order to maximize the peak separation. To illustrate this step, two gradient pairs were designed in order to compare the mean (accuracy) and the standard deviation (precision), σ, of the error in prediction obtained with these two data sets: two gradients A and B, ranging from 10 to 100% of acetonitrile with a gradient duration of 30 and 90 min, respectively, that are consistent with the experiments needed with the two gradient based method; the gradient A and a gradient B′ computed from gradient A, using the one gradient-based estimation of S and $\ln k_w$ (gradient B′ = 30–70% acetonitrile in 40 min).

The retention times of benzodiazepines are summarized for the different gradient profiles in Table 1. The accuracy and precision of the calculated retention times for a further gradient denoted C are presented in Table 2. The elution parameters S and $\ln k_w$ were computed by the Monte Carlo simulation algorithm using either the AB or AB′ pair of gradients. Both the gradient pairs AB and AB′ lead to an overestimate of the solute retention times. The average error ($\bar{m}$) induced by the computation based on gradients A and B is 9.16% with a standard deviation of 8.48%. This average error was found to be significantly higher than that observed for gradients A and B′ ($\bar{m}$ = 3.36%, σ =

Table 1
Retention times and gradient profiles for the hydrolysis products of benzodiazepines

No.	Parent compound	t_R (min)					
		A	B	B′	C	D	E
1	Tetrazepam	19.33	36.24	17.16	11.66	17.32	14.86
2	Triazolam	19.93	38.10	18.39	12.10	19.70	16.26
3	Tofisopam (1)	20.20	38.56	18.93	13.01	20.36	16.98
4	Medazepam	20.85	39.97	20.27	14.91	22.13	18.93
5	Tofisopam (2)	21.03	40.77	20.97	15.87	23.15	20.20
6	Bromazepam	22.31	42.70	23.16	20.08	25.25	23.07
7	Tofisopam (3)	22.95	45.84	25.89	26.49	28.72	26.13
8	Nitrazepam	23.32	46.65	26.70	28.55	29.42	26.65
9	Clonazepam (2)	24.04	49.04	28.97	33.23	31.82	28.59
10	Midazolam	24.75	48.23	28.23	30.59	30.76	27.73
11	Flunitrazepam	25.38	52.32	32.22	37.20	34.97	31.14
12	Flurazepam	25.93	53.57	33.49	38.42	36.11	32.04
13	Nordazepam	26.54	54.71	34.60	39.44	37.18	32.86
14	Tetrazepam	27.80	62.03	41.87	45.69	43.83	37.99
15	Medazepam	29.58	63.15	43.12	46.35	44.73	38.79
16	Diazepam	30.13	64.22	44.04	47.61	45.80	39.66
Initial % and duration		10% to 100% at 30 min	10% to 100% at 90 min	30% to 70% at 40 min	40% for 22 min to 70% at 40 min	35% for 10 min to 70% at 40 min	30% to 40% at 10 min to 40% at 15 min to 70% at 30 min

Table 2
Percentage error in retention time prediction for gradients C, D and E using the linear (L) or extended-linear (EL) model

No.[a]	Data set and target									
	AB C	ABC D	ABCD E	ABC D	ABCD E	AB′ C	AB′C D	AB′CD E	AB′C D	AB′CD E
1	10.98	−0.12	0.94	−0.12	2.56	7.29	−0.12	0.87	−0.29	0.94
2	22.81	−8.38	4.12	−8.63	4.12	15.87	−8.38	1.48	−8.38	1.48
3	19.83	−5.84	2.00	−16.80	3.83	13.37	−5.84	1.47	−7.17	−0.47
4	20.59	−4.52	−2.43	−5.11	−2.43	11.40	−4.52	1.80	−6.37	1.43
5	20.04	−5.36	−3.81	−5.36	−3.86	10.14	−6.00	1.24	−10.45	0.69
6	16.88	−3.41	−0.69	−4.87	−1.30	5.38	−7.68	−0.26	−4.75	−0.74
7	11.10	−3.24	−0.80	−3.17	−0.80	0.60	−3.24	−0.80	−3.24	−0.80
8	8.06	−2.21	0.41	−1.90	0.26	−0.56	−2.21	0.41	−2.21	0.38
9	3.04	−1.10	1.61	−1.16	1.47	−1.81	−1.10	0.80	−1.10	0.77
10	8.47	−1.72	2.88	−1.66	2.13	−1.67	−1.72	1.55	−1.72	1.55
11	1.45	−0.63	0.71	−0.66	0.67	−1.56	−0.63	0.29	−1.06	0.29
12	1.28	−0.47	0.47	−0.55	0.44	−1.33	−0.47	0.19	−0.50	0.16
13	1.24	−0.40	0.43	−0.75	0.33	−1.39	−0.40	0.18	−1.40	0.18
14	−0.33	−0.55	−3.13	−0.52	−3.13	−0.72	−1.05	−3.13	−1.05	−3.13
15	0.82	0.18	−0.46	0.40	−0.46	−0.09	−0.40	−0.72	−0.40	−0.77
16	0.25	0.20	0.38	0.33	0.38	−1.09	−0.90	0.20	−0.87	−1.94
$\bar{m}$	9.16	−2.35	0.16	−3.16	0.26	3.37	−2.79	0.35	−3.19	0.00
σ	8.48	2.55	2.08	4.44	2.28	6.21	2.80	1.22	3.23	1.28
Model	L	L	L	EL	EL	L	L	L	EL	EL

[a] See Table 1 for compound names.

6.21%) while the difference between the two standard deviations was not significant.

From these two pairs of gradients, it appears that by reducing the polarity range of the second gradient, the accuracy of retention time calculation increases while the precision remains about the same.

When computing a new gradient (D) on the basis of gradients ABC and AB'C, by Monte Carlo simulation followed by a simplex refinement of S and $\ln k_w$, the average error in prediction and the standard deviation are lowered to: $\bar{m} = -2.35\%$ and $\sigma = 2.55\%$ for ABC and $\bar{m} = -2.79\%$ and $\sigma = 2.80\%$ for AB'C. Considering the error in prediction obtained from AB and ABC, both the mean and the standard deviation were found to be significantly different. The same result is observed using AB' and AB'C. This shows the increase in accuracy and precision obtained with the iterative procedure when the results from a third solvent programme are entered as data. It is also noticeable that the two data sets ABC and AB'C now induce the same accuracy and precision.

Further, when computing the last gradient E (Fig. 2), on the basis of the previous four, the mean calculation error is lowered to 0.16% with a standard deviation of 2.1% for ABCD and 0.35% with a standard deviation of 1.20% for the AB'CD set.

This illustrates the need for an iterative strategy in solvent strength optimization: the use of two gradient programmes that differ in the slope and the initial and final compositions leads to a more efficient calculation of S and $\ln k_w$; and the iterative procedure allows the accuracy and precision of the calculated retention times to be increased.

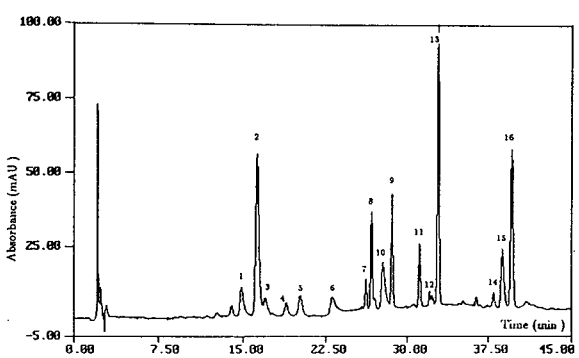

Fig. 2. Chromatogram of the hydrolysis products of benzodiazepines. See Table 1 for peak identification and gradient (E) conditions.

Linear model extension

All the preceding calculations were made using the linear model (Eq. 2). When at least three experiments are available, it appears possible to extended this linear model by adding an $A\phi^2$ term that allows a more adequate description of the solute retention behaviour. The results obtained with the model we call "extended linear" are presented in Table 2.

Calculation from four chromatographic runs. When performing the calculations using the four preceding experiments (data sets ABCD and AB'CD), the accuracy and precision of the extended linear model are now comparable to those obtained from the linear model.

Using the ABCD data set, the mean error and standard deviation of the predicted retention times obtained with the extended linear model are not significantly different from those computed with the linear model. The results obtained with the AB'CD data set show that the error in prediction tend to zero using the extended linear model, with a precision that is comparable to that for the linear model (linear model, $\bar{m} = 0.35$, $\sigma = 1.22$; extended linear model, $\bar{m} = 0.01$, $\sigma = 1.28$).

Two main conclusions can be drawn on comparing the results obtained from the two models: (i) Four experiments are needed for an effective computation of this model. Consequently, one must be conscious that we do not recommend performing four initial experiments to allow the computation of the extended linear model, but rather we recommend this computational method in iterative solvent strength optimization when four experiments are available. (ii) The differences in accuracy and precision observed between the two original data sets AB and AB' tend to vanish on adding some additional experiments. This shows that, even if one experiment

does not provide some adequate data, and leads to the adoption of an erroneous mobile phase composition and/or gradient profile for the following experiment, this inaccuracy may be corrected by the results of this last experiment itself. Considering this point, this method appears more rugged than non-iterative procedures.

Factors influencing retention time prediction

In our example, the error in prediction, initially high, decreases with increasing number of experiments involved in the data set. Two points must be considered to try to explain this initial error and to verify the influence of the input gradient profile on accuracy improvement: the experimentally determined gradient delay may not agree with its actual value; and the prediction accuracy may proceed from the similarity between experiments rather than from the iterative calculation procedure.

Prediction accuracy and experiments. Marengo *et al.* [29] reported that, when calculating retention times under gradient conditions from isocratic data, the gradient steepness directly influences the error in prediction. For a series of simulations recorded with the same column and organic modifier, the rate of variation of the mobile phase composition is mainly responsible for the error in prediction. In our example, gradients C, D and E look similar as the optimization process tends to lead to a multilinear gradient. Considering this point, one may believe that this similarity between the input and calculated conditions is mainly responsible for the improvement in accuracy and precision when supplementary runs are added. To elucidate this point, we decided to compare results obtained with the data sets ABC and AB'C with those obtained with ABB', ABD and AB'D for the calculation of gradient E using the linear model (Eq. 2). Among these gradients, B' and D are the more closely related to gradient E. Consequently, if this hypothesis of similarity of gradients is true, a set of experiments containing those two gradients (B' and D) would be assumed to lead to superior calculation accuracy and precision. Despite this, the AB'D data set did not provide better calculation results than the other four. The mean errors in prediction ranged from −1.28 and 2.16 for all these sets and the standard deviation ranged from 1.69 to 2.91. Significant differences in accuracy were found for data sets ABD and AB'D with respect to ABC and AB'C. The most accurate and precise results were obtained with the set ABB' ($\bar{m} = 0.37$, $\sigma = 1.69$), but significant differences in standard deviation were observed only for ABD ($\bar{m} = 2.16$, $\sigma = 2.67$) and AB'D ($\bar{m} = 1.94$, $\sigma = 2.91$). The mean errors in prediction for these two sets were also found to be significantly different from those for sets ABC ($\bar{m} = -0.99$, $\sigma = 1.98$) and AB'C ($\bar{m} = -1.28$, $\sigma = 2.13$), as the retention times are underestimated using ABC and AB'C and overestimated with ABD or AB'D. As stated previously, the best accuracy and precision observed with data set ABB' tend to confirm that the prediction accuracy and precision of this computational method are more closely related to differences in gradient profiles than to similarity between the input and predicted values.

Gradient delay time. The technique used to determine the gradient delay influences the calculation accuracy. In this study, the system dwell time is determined experimentally by adding a UV tracer (dimethyl ketone) to the mobile phase. However, according to some workers [8,30] and despite of the reliability of this method, a calculated value of t_D leads to superior accuracy in the prediction of retention times. This calculation [8] uses the results from three gradients of decreasing slope. The system dwell time is calculated by comparing the solute retention time recorded with the gradient of intermediate slope with the values predicted from the calculations based on the two remaining gradients. From the data provided [8], values of t_D calculated in this way are about 17–25% higher than those determined by the use of a UV tracer. In our study, the gradient delay was estimated to be 3.40 min. If we consider Fig. 3, which depicts the average error in prediction as a function of the gradient delay, the most appropriate value for t_D is 4.0 min. The use of this value, which is about 20% higher than the experimental t_D,

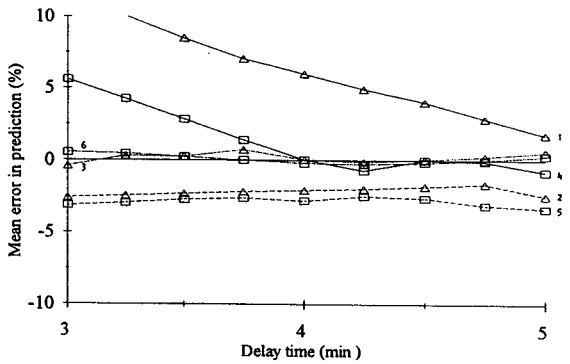

Fig. 3. Percentage error in retention time prediction as a function of the gradient delay time. 1 = AB; 2 = ABC; 3 = ABCD; 4 = AB′; 5 = AB′C; 6 = AB′CD.

lowers the error in prediction from 3.37% to nearly 0% for the AB′ pair and 9.16 to 6% for AB. The influence of the t_D value is less important when three or more experiments are included in the calculations of the linear model. Concerning the sets ABC, AB′C, ABCD and AB′CD, the prediction accuracy remains nearly constant for a large range of t_D values.

This illustrates the importance of using an iterative procedure in solvent strength optimization. The error-minimization algorithm, used for the calculation of elution parameters, is necessary as it allows one to compensate for the effect of partially accounted for parameters such as gradient delay.

4.2. Choice of initial gradient programmes

If we consider the error in prediction at each step of the preceding example, the most critical step is the computation of the retention times from a pair of gradients (the one run-based calculation is only used to compute a rough estimate of the retention times of the first- and last-eluting peaks in order to obtain the second gradient profile). It has been found that the use of a second gradient differing in slope and solvent composition may lead to a threefold decrease in the error in prediction compared with a gradient programme that differs only in the slope. The actual problem is to appreciate which, and which kind of, difference is allowable, that is, should the main difference preferably concern the gradient slope or the solvent composition? To investigate this point, we designed five gradient programmes denoted A–E that differ in slope and/or composition. The calculation results from each pair of gradients were compared with isocratic data. Six isocratic runs were performed with volume fractions of organic modifier ranging from 0.65 to 0.90. All these gradients were chosen with a high slope in order to maximize the errors in prediction and thus to obtain significant differences between the different pairs of gradients.

The compounds used for this part of the study were eight phenolic antioxidants or preservatives of pharmaceutical and/or cosmetic interest (Table 3). These compounds were chosen as the

Table 3
List of phenolic solutes

Compound	Common name	Abbreviation
2-Butyl-4-hydroxyanisole		BHA
2-*tert.*-butylphenol		TBP
2-*tert.*-butyl-4-methylphenol		TBMP
2,6-Di-*tert.*-butyl-4-methylphenol	Butylated hydroxytolene	BHT
3,4,5-Trihydroxybenzoic acid propyl ester	Propyl gallate	PG
3,4,5-Trihydroxybenzoic acid octyl ester	Octyl gallate	OG
3,4,5-Trihydroxybenzoic acid dodecyl ester	Dodecyl gallate	DG
p-Hydroxybenzoic acid propyl ester		PHBP

resulting set of solutes exhibit a wide range of polarity, as seen from their isocratic retention times (see Table 4). Methanol was used as organic modifier and 1% of acetic acid was added to the aqueous fraction of the mobile phase to improve peak shape.

The results obtained with the Monte Carlo-based method of resolution show that of the ten possible pairs that could be constituted with the five gradients, only seven pairs of experiments led to acceptable values of S and $\ln k_w$. The incompatible pairs are AE, BE and CE, *i.e.*, gradients in which the greatest differences in initial mobile phase composition are encountered (10% methanol for A, B and C and 50% for E).

Calculation precision for S and ln k_w

For the seven remaining pairs of gradients, the best calculation precision for S and $\ln k_w$ is encountered with gradient pairs AC and AD, as depicted in Figs. 4 and 5. These two gradient pairs exhibit the maximum difference in slope. Gradient AC has the same initial and final compositions. The initial and final compositions of gradients A and D differ by 10% of the organic modifier.

As noted previously, if the gradient slopes are too similar, the set of two experiments describes nearly the same equations. Only a reasonable change in mobile phase composition may be allowed. An important difference in mobile phase composition will cause the two equations not to admit a single solution (the case of gradient A, B or C coupled with E), or a single solution with a low calculation precision (gradient pair DE). This can be explained as the parameter $\ln k_w$, *i.e.*, the logarithm of the hypothetical value of the capacity factor in the fully aqueous mobile phase, is extrapolated from the presumed value of the capacity factor in the initial mobile phase of the gradient elution.

Retention time prediction

The mean error and standard deviation (σ) of the error on retention time prediction for each isocratic mobile phase, presented in Table 5, were examined through cluster analysis to individualize similarities between gradient pairs. From the dendrogram presented in Fig. 6, it appears that the pairs of gradients can be associated in two main clusters: gradient pairs BC and CD in a first cluster and gradient pairs AB, AC, AD, BD and DE in a second cluster.

According to Table 5, gradient pairs BC and CD both lead to more inaccurate and less precise predictions. As expected, this cluster contains the gradient pairs with the most comparable conditions: gradients B and C share the same solvent composition and differ slightly in their slopes; gradients C and D share the same slope and differs by 10% in the initial and final organic modifier compositions.

The second cluster may be divided into smaller structures with an increasing inaccuracy and poorer precision from the centre of the cluster towards its boundaries. (i) The inner cluster is constituted by the gradient pairs AB and AD, which lead to the best compromise between accuracy and precision. As shown previously, these gradient pairs also induce the best calculation precision for the parameters S and $\ln k_w$. (ii) The next cluster is surrounded by a larger one corresponding to the gradient pair BD, that leads to more accurate but also less precise retention time prediction than the previous two. This gradient pair is similar to AD, except that the difference in gradient slope is less important. (iii) The following cluster includes the gradient AC, which is the gradient pair with the same initial and final compositions that exhibits the maximum difference in slope. (iv) The outer cluster involves the gradient pair DE, which differs only in the initial and final compositions and yields a large underestimate of the solute retention times associated with a poor precision.

From this analysis, the most accurate results are obtained with gradients differing at least in their slope, and also by a limited difference in their solvent compositions. When comparing two pairs of gradients with the same difference in slopes, the pair of gradients that also differ in a limited difference in composition yield the best results. The most inaccurate results were obtained with gradients with similar slopes or too large differences in solvent compositions.

Table 4
Retention times of phenolic compounds under gradient and isocratic elution (average column dead time 1.12 min)

Compound[a]	A	B	C	D	E	$\phi = 0.65$	$\phi = 0.70$	$\phi = 0.75$	$\phi = 0.80$	$\phi = 0.85$	$\phi = 0.90$
PG	15.39	18.75	20.94	17.30	4.04	2.22	2.03	1.88	1.76	2.04	1.90
PHBP	19.16	24.66	28.74	24.73	9.03	3.81	3.05	2.60	2.26	2.30	1.90
BHA	20.63	27.05	32.65	27.93	11.98	5.66	4.19	3.33	2.70	2.53	2.05
TBP	21.45	28.31	34.57	29.67	13.78	7.40	5.26	4.00	3.09	2.72	2.17
TBMP	22.10	29.77	36.66	31.70	15.94	10.37	6.94	4.98	3.65	2.74	2.17
OG	22.36	30.28	37.58	32.64	17.00	14.26	9.36	5.75	3.76	2.84	2.35
BHT	25.56	34.78	43.47	40.35	23.26	–	31.62	18.02	10.18	6.12	3.77
DG	25.78	35.09	44.07	42.55	23.92	–	–	–	13.18	6.59	3.95
Composition											
Initial (%)	10.0	10.0	10.0	20.0	50.0						
Final (%)	90.0	90.0	90.0	80.0	90.0						
Duration (min)	20.0	30.0	40.0	30.0	20.0						
Slope (% min^{-1})	4.0	2.67	2.0	2.0	2.0						

[a] See Table 3 for compound names.

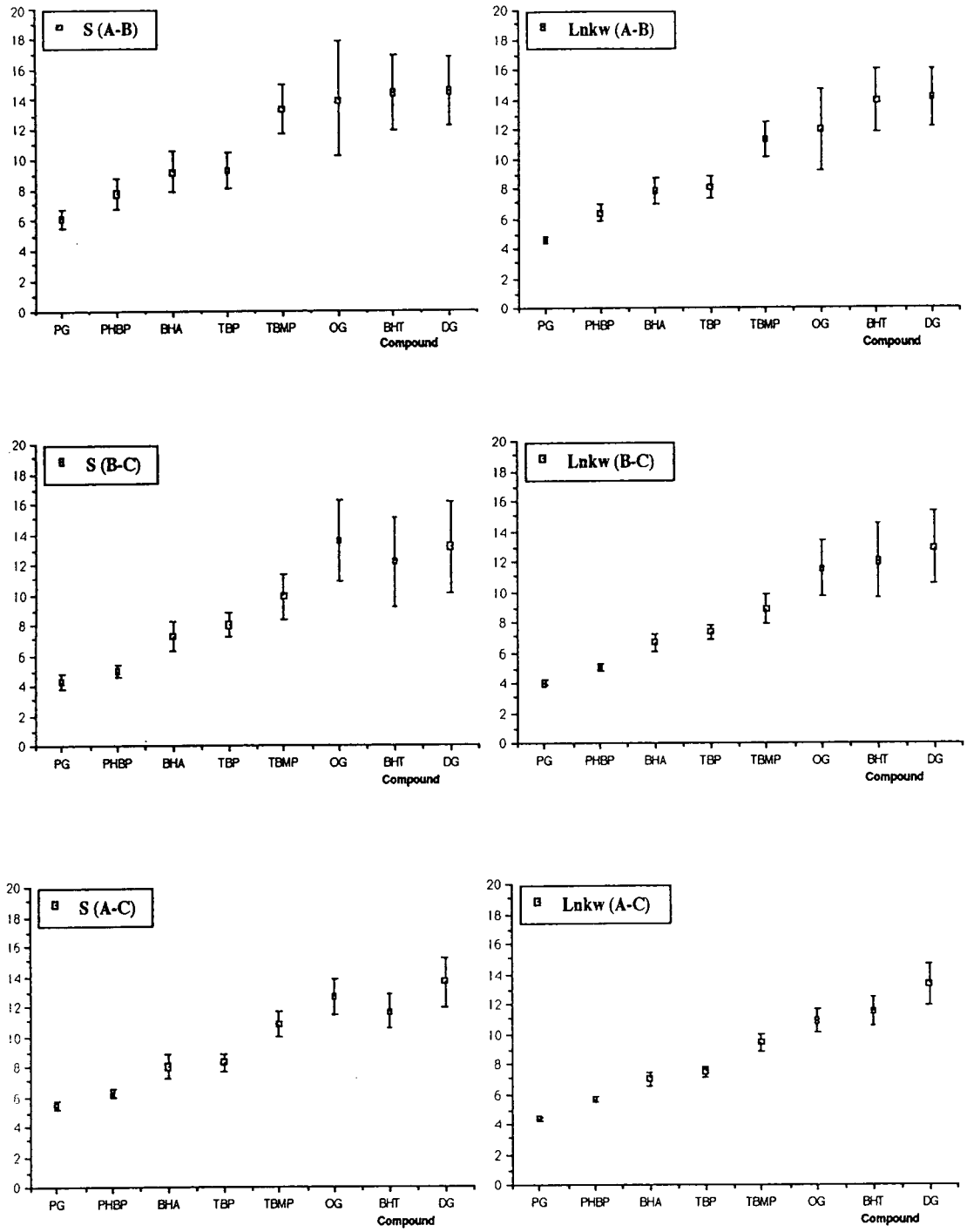

Fig. 4. Plots of S and $\ln k_w$ with calculated standard errors. Gradients of various initial and final composition. For abbreviations, see Table 3.

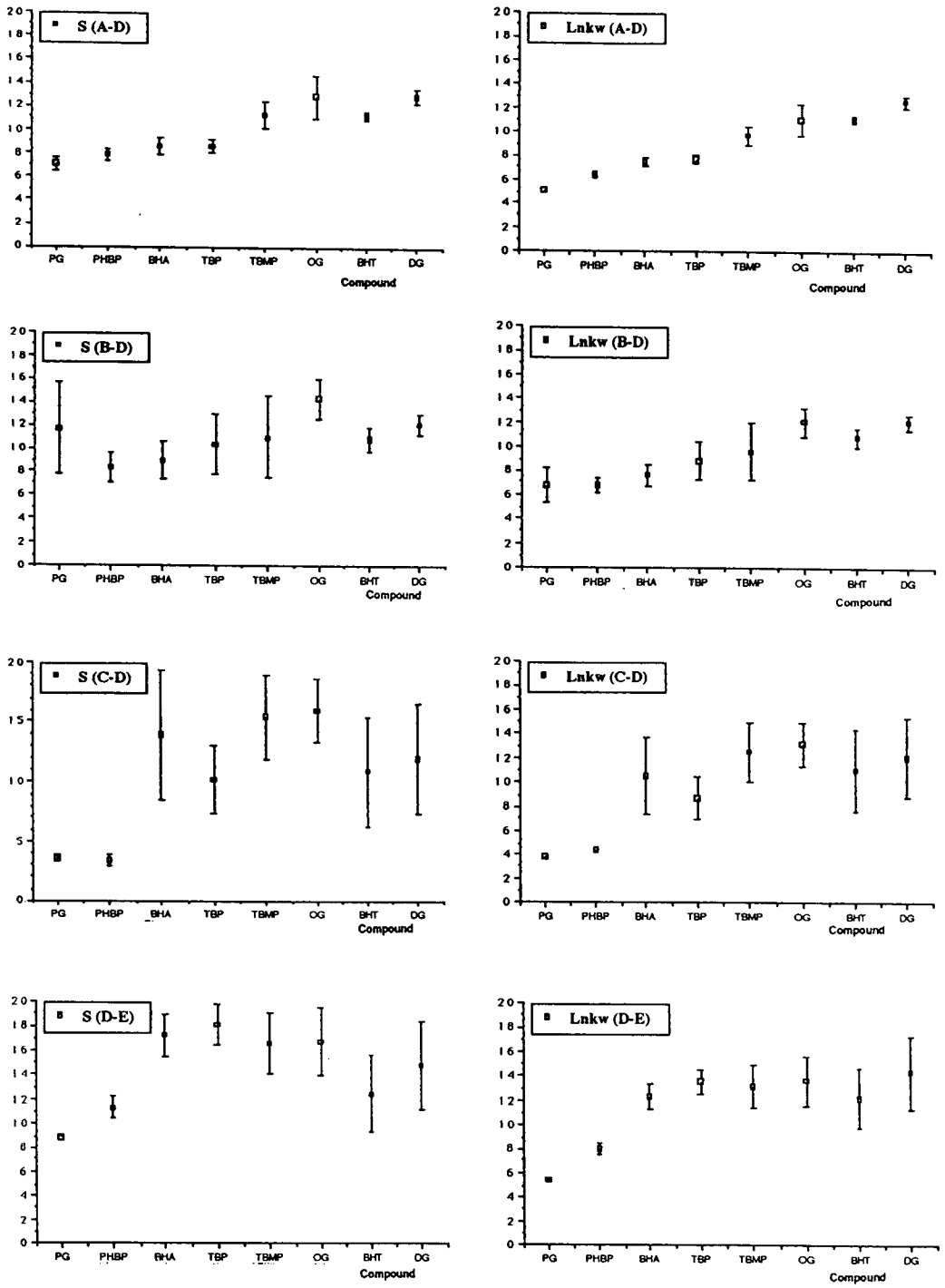

Fig. 5. Plots of S and $\ln k_w$ with calculated standard errors. Gradients of various initial and final composition. For abbreviations, see Table 3.

Table 5
Percentage error in isocratic retention times prediction using the Monte Carlo-based calculation of the parameters S and $\ln k_w$ from a pair of gradients

Gradient	$\phi = 0.65$		$\phi = 0.70$		$\phi = 0.75$		$\phi = 0.80$		$\phi = 0.85$		$\phi = 0.90$		$\bar{m}$	σ		
	$\bar{m}$	σ	$\bar{m}$	σ	$\bar{m}$	σ	$\bar{m}$	σ	$\bar{m}$	σ	$\bar{m}$	σ			$\bar{m}$	σ
AB	36.6		27.4		16.8		8.4		−4.0		−6.7		13.6	17.2		
		10.0		11.8		9.9		9.2		10.5		10.4			10.3	0.9
AC	40.4		28.8		21.8		13.9		2.8		1.7		18.3	15.1		
		20.3		22.7		18.0		14.9		7.9		11.6			15.9	5.5
AD	31.2		18.6		10.6		3.9		−5.3		−5.8		8.9	14.4		
		11.3		15.2		10.6		8.6		12.3		14.3			12.1	2.4
BC	59.9		47.6		43.7		34.8		23.2		23.6		38.8	14.4		
		44.5		47.2		40.3		34.7		18.8		22.3			34.6	11.8
BD	22.8		13.5		7.1		2.2		−5.3		−5.5		5.8	11.1		
		21.2		20.2		16.3		12.9		17.6		17.5			17.6	2.9
CD	72.2		62.0		59.1		48.4		33.5		31.8		51.2	16.2		
		58.3		56.1		48.6		43.7		23.3		22.7			42.1	15.7
DE	−9.9		−22.3		−28.2		−25.4		−25.6		−21.1		−22.1	6.5		
		21.1		16.7		18.7		22.6		30.3		31.2			23.4	6.0
$\bar{m}$	36.2		25.1		18.7		12.3		2.7		2.6					
σ	26.5		26.8		27.9		23.9		19.8		18.6					
$\bar{m}$		27.6		28.9		24.0		20.7		15.1		16.4				
σ		19.5		18.3		16.4		14.8		5.8		5.2				

$\bar{m}$ = mean of the percentage error; σ = corresponding standard deviation.

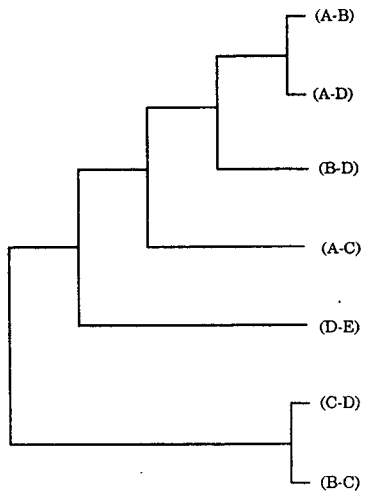

Fig. 6. Cluster analysis of results in Table 5.

5. Conclusions

A schematic presentation of our iterative algorithm is depicted in Fig. 1. This optimization strategy appears flexible enough to make use of all the experiments realized during the mobile phase development. The computer algorithm accepts any case of solute elution, during or after the gradient rise for linear or multi-linear gradients. The initial experiments must be selected with care to ensure the maximum accuracy from the beginning of the development process. As with previously reported algorithms, the computer routine discussed in this study is able to compute solute retention from two gradients differing in their slopes. However, from our examples, an improvement in the accuracy of retention time prediction is observed when the two gradients also vary by a limited difference in solvent composition. In this case, this improvement may be attributed to the greater independence between the parameters of the two gradients leading to a more pertinent solution. This may be explained by the meaning of the linear model, which, in turn, is a tangent to the quadratic relationship that links the solute capacity factor and the volume fraction of the organic modifier. Consequently, for the same solute, the linear model will lead to different values of S and $\ln k_w$ depending on the investigated solvent compositions. In the case of gradient experiments, this difference will also exist depending on the starting and ending mobile phases. Computing the common solution of two gradient runs with slight differences in solvent composition led to averaged values of S and $\ln k_w$. Nevertheless, as a limit, if the two experiments are carried out with a large difference in solvent composition, the two tangents to the quadratic relationship will concern two distinct regions of the quadratic curve. Consequently, the values of the slope and the intercept will be different for the two tangents. In this case, the two equations that describe the two gradients runs will not admit a common solution. In this step, the accuracy will depend heavily on the non-ideal process generated by the solvent delivery system and the gradient delay. The iterative computation of the linear model allows one to minimize the error in prediction generated by a partial account of this parameter. Hence, if some additional experiments are needed, the retention model can be extended to a more accurate quadratic form. From its computation, which uses the Nedler and Mead simplex controlled by an error-reduction criterion, this model allows a further improvement in retention time prediction. This permits a low prediction error in the case of difficult developments that require several chromatographic runs.

References

[1] A. Tchapla, *Analusis*, 20, No. 7 (1992) 71.
[2] P.J. Schoenmakers, H.A.H. Billiet and L. de Galan, *J. Chromatogr.*, 185 (1979) 179.
[3] L.R. Snyder, *J. Chromatogr.*, 13 (1964) 415.
[4] P.J. Schoenmakers, H.A.H. Billiet and L. de Galan, *J. Chromatogr.*, 205 (1981) 13.
[5] M.A. Quarry, R.L. Grob and L.R. Snyder, *Anal. Chem.*, 58 (1986) 907.
[6] S. Heinisch, P. Rivière and J.L. Rocca, *Chromatographia*, 32 (1991) 559.
[7] S. Heinisch and J.L. Rocca, *Analusis*, 18 (1990) 83.
[8] S. Heinish, J.L. Rocca and M. Kolosky, *Chromatographia*, 29 (1990) 482.
[9] L.R. Snyder, J.W. Dolan and J.R. Gant, *J. Chromatogr.*, 165 (1979) 3.
[10] J.W. Dolan, J.R. Gant and L.R. Snyder, *J. Chromatogr.*, 165 (1979) 32.

[11] M.A. Quarry, R.L. Grob, L.R. Snyder, J.W. Dolan and M.P. Rigney, *J. Chromatogr.*, 384 (1987) 163.
[12] H. Poppe, J. Paanakker and M. Bronckorst, *J. Chromatogr.*, 204 (1981) 77.
[13] M.A. Quarry, R.L. Grob and L.R. Snyder, *J. Chromatogr.*, 285 (1984) 1.
[14] M.A. Quarry, R.L. Grob and L.R. Snyder, *J. Chromatogr.*, 285 (1984) 19.
[15] J.P. Foley, J.A. Crow, B.A. Thomas and M. Zamora, *J. Chromatogr.*, 478 (1989) 287.
[16] D.P. Herman, H.A.H. Billet and L. de Galan, *J. Chromatogr.*, 463 (1989) 1.
[17] E.D. Katz, K. Ogan and R.P.W. Scott, *J. Chromatogr.*, 352 (1986) 67.
[18] R. Rosset, M. Caude and A. Jardy, *Chromatographies en Phases Liquide et Supercritique*, Masson, Paris, 1991, pp. 327–346.
[19] R.M. McCormick and B.L. Karger, *Anal. Chem.*, 52 (1980) 2249.
[20] J.D. Baty and S. Sharp, *J. Chromatogr.*, 432 (1988) 13.
[21] W.H. Press, B.P. Flannery, S.A. Teukolsky and W.T. Vetterling, *Numerical Recipes in Pascal*, Cambridge University Press, Cambridge, 1989, pp. 274–279; 212–253; 326–330.
[22] J.A. Nedler and R. Mead, *Comput. J.*, 7 (1965) 308.
[23] S.A. Tomellini, R.A. Hartwick and H.B. Woodruff, *Anal. Chem.*, 57 (1985) 811.
[24] C. Ortigosa, *Lyon Pharm.*, 40 (1989) 315.
[25] M.W. Routh, P.A. Swartz and M.B. Denton, *Anal. Chem.*, 49 (1977) 1422.
[26] S.N. Deming and S.L. Morgan, *Anal. Chem.*, 45 (1973) 278A.
[27] F.H. Walters and S.N. Deming, *Anal. Chim. Acta*, 167 (1985) 361.
[28] H. Maurer and K. Pfleger, *J. Chromatogr.*, 222 (1981) 409.
[29] E. Marengo, C. Baiocchi, M.C. Gennaro and P. Bertolo, *Chromatographia*, 27 (1989) 19.
[30] N. Lundell, *Ph.D. Thesis*, Uppsala University, Uppsala, 1992.

ELSEVIER

Journal of Chromatography A, 672 (1994) 87–99

JOURNAL OF CHROMATOGRAPHY A

Reversed-phase liquid chromatography–mass spectrometry of the uncommon triacylglycerol structures generated by randomization of butteroil

L. Marai, A. Kuksis*, J.J. Myher

Banting and Best Department of Medical Research, University of Toronto, 112 College Street, Toronto M5G 1L6, Canada

(First received November 16th, 1993; revised manuscript received March 1st, 1994)

Abstract

The test triacylglycerols were prepared by randomization of natural butterfat followed by silver ion TLC segregation of the saturates, monoenes and dienes. The molecular species were identified by on-line positive chemical ionization mass spectrometry. Within a series of isologous triacylglycerols, those containing the shortest fatty acid chain were eluted last from a reversed-phase column (XX10 > XX8 > XX6 > XX4, where X = long-chain acid), although common experience would have predicted that the shorter and more polar species would be eluted first. A comparable order of elution was obtained for isologous triacylglycerols containing two short- and one long-chain (X88 > X86 > X66 > X84 > X64 > X44) or three short-chain fatty acids per molecule, when compared to triacylglycerols containing medium or long-chain fatty acids in combination with short-chain acids. Since this resolution is similar to that achieved on adsorption chromatography, it is suggested that the C_{18} reversed-phase column possesses residual adsorptive activity. No discernible separation was seen among the corresponding positional or reverse isomers of short-chain triacylglycerols with the present reversed-phase system.

1. Introduction

The presence of high proportions of the short-chain (C_4–C_8) fatty acids in butterfat has been long known [1] as has been their overall positional distribution and molecular association. Early studies by high-temperature gas chromatography (GC) [2] and silver ion thin-layer chromatography ($AgNO_3$-TLC) [3] showed that the bulk of these acids occurred with the frequency of one short-chain fatty acid per triacylglycerol molecule. Furthermore, evidence was obtained that the short-chain fatty acids were confined largely to the *sn*-3 position [4,5]. More recently butterfat composition has been analyzed by capillary GC on polarizable liquid phases [6,7], reversed-phase high-performace liquid chromatography (HPLC) [8,9] and GC and HPLC with mass spectrometry (MS) [10], as well as by MS–MS [11]. These studies have led to an extensive resolution of butterfat triacylglycerols, but the possible presence of small amounts of positional and reverse isomers as well as of species containing two or three short-chain acids per molecule has not been addressed.

As an aid in the identification of such triacylglycerols in butterfat, we have investigated the reversed-phase LC–MS behavior of randomized butterfat, which contains the various isomeric triacylglycerols in known and sufficient amounts

* Corresponding author.

0021-9673/94/$07.00
SSDI 0021-9673(94)00207-P

for analysis. The results show that conventional C_{18} reversed-phase columns would not resolve the positional and reverse isomers of mixed acid triacylglycerols, but that the resolution of isologous triacylglycerols is retained also when two or three short-chain fatty acids occur per molecule.

2. Materials and methods

2.1. Butterfat samples

The rearranged butteroil sample had been prepared by Distillation Products Industries, Rochester, NY, USA, and had been stored in solid form in a sealed container at 7°C and −20°C. The natural butterfat sample was from a local Canadian creamery and also had been stored at −20°C. Synthetic triacylglycerols of short, medium and long chain length were available in the laboratory from previous studies [7,12].

2.2. Reagents and solvents

All reagents and solvents were of analytical or chromatographic grade and were obtained from reputable laboratory supply houses. Acetonitrile was from Caledon (Canada), while propionitrile was from Romil (UK) or Fluka (Switzerland).

2.3. Gas chromatography

GC analyses of fatty acid butyl esters and intact triacylglycerols by carbon number were performed on non-polar capillary columns [7] while the separations based on both carbon and double bond number of the fatty acids were done on polar capillary columns as previously described in detail [7].

2.4. High-performance liquid chromatography

The triacylglycerols were resolved by reversed-phase HPLC with a Supelcosil LC-18 reversed-phase column (5 μm, 25 cm × 0.46 cm I.D.; Supelco, Mississauga, Canada) using a linear gradient of 0–90% propionitrile in acetonitrile or 10–90% propionitrile in acetonitrile (2.2 ml/min). The column was installed in a Hewlett-Packard Model 1084B liquid chromatograph connected via a direct liquid inlet interface to a mass spectrometer as previously described [10]. Alternatively, these analyses were performed with a Hewlett-Packard Model 1050 liquid chromatograph equipped with the reversed-phase HPLC column coupled to a Varex ELSD II light-scattering detector (Varex, Burtonsville, MD, USA). This column was operated at a flow-rate of 1 ml/min (90 min) using a linear gradient of 10–90% isopropanol in acetonitrile.

2.5. $AgNO_3$-TLC

The rearranged butteroil was segregated on basis of degree of unsaturation by TLC on silica gel G impregnated with 15% $AgNO_3$ (20 × 20 cm, 250 μm thick layer) using chloroform containing 0.75% ethanol as the developing solvent. The resolved triacylglycerols were located by spraying the plate with a 0.05% solution of 2,7-dichlorofluorescein in methanol–water (50:50) and viewing the plates under UV light. A total of five fractions were collected [3,5] by eluting with chloroform–methanol (2:1) the silica gel scraped from areas corresponding to the following R_F values: 0.70–0.85 (band 1); 0.55–0.70 (band 2); 0.35–0.55 (band 3); 0.25–0.37 (band 4); and 0.06–0.25 (Band 5).

2.6. Mass spectrometry

On-line LC–MS was performed with a Hewlett-Packard Model 5985B quadrupole mass spectrometer coupled to a Hewlett-Packard 1084B liquid chromatograph via a direct liquid inlet interface [10] as previously described. For LC–MS analysis about 1% of the column effluent was admitted to the mass spectrometer. The LC–MS analyses were made in both positive and negative chemical ionization mode as previously described [7,10], with the HPLC solvent providing the reagent gas. Specifically, full mass spectra were taken every 7 s in the mass range 200–900 over the entire elution profile and were stored in the computer. Subsequently single-ion

profiles were recalled from the data stored in the computer for both molecular and fragment ions.

2.7. Calculations

The 1,2,3-random calculation of the molecular association of fatty acids in the rearranged butteroil was performed as described elsewhere [13]. The triacylglycerol peaks were summed by carbon and by partition number and compared to the distributions determined experimentally by polar capillary GC and reversed-phase HPLC.

3. Results

3.1. General characteristics of rearranged butteroil

Table 1 gives the fatty acid composition of the rearranged in relation to natural butterfat triacylglycerols as obtained by polar capillary GC. There are close similarities between these two samples in the quantitative composition of the fatty acids, except for a reversal in the proportions of the stearic and oleic acids. The overall composition of the natural fat is not unlike that reported previously for blended bovine milk fats [14].

Table 2 compares the carbon number distribution in the two butterfat samples as obtained by GC on a non-polar capillary column. This column gives an essentially quantitative recovery for all triacylglycerols in the C_{20}–C_{56} range and the peak areas provide a true account of the carbon number proportions, as evidenced from a comparison of the experimentally determined and calculated proportions of the rearranged triacylglycerols. The triacylglycerol peak proportions are similar to those reported previously from analyses on packed columns containing a non-polar liquid phase [14], except for the estimates of the odd-carbon-number triacylglycerols, which were not very well resolved in the earlier work. It is seen that the rearranged fat is increased in the proportion of both short- and long-chain triacylglycerols and decreased in the proportion of the medium-chain triacylglycerols.

Table 1
Fatty acid composition of randomized and reference butterfat

Fatty acid	Butterfat (mol%)[a]	
	Reference	Randomized
4:0	8.76	6.21
6:0	4.79	3.34
8:0	2.44	1.84
10:0	4.80	3.37
10:1	0.47	0.39
11:0	0.10	0.10
12:0	5.11	3.90
12:1		
13:0	0.16	0.13
14:0 *iso*	0.21	0.02
14:0 *n*	13.39	13.89
14:1	1.02	0.39
15:0 *iso*	0.36	0.41
15:0 *anteiso*	0.60	0.65
15:0 *n*	1.34	1.46
16:0 *iso*	0.23	0.42
16:0	32.36	34.51
16:1	1.58	0.54
17:0 *iso*	0.23	0.53
17:0 *anteiso*	0.43	0.62
17:0 *n*	0.58	0.97
18:0 *iso*	0.06	0.30
18:0 *n*	7.35	5.23
18:1 *trans*	1.01	1.35
18:1 *cis*-9	11.40	8.86
18:2	0.95	0.07
18:3	0.29	0.00

[a] Determined by polar capillary GC as the *n*-butyl esters following acid transesterification. The relative standard deviations for repeat analyses were $<1\%$ for components making up more than 1% of total, and $<5\%$ for components making up less than 1% of total.

Fig. 1 shows the separation of the natural and rearranged butterfat triacylglycerols by reversed-phase HPLC using a linear gradient of 10–90% isopropanol in acetonitrile and light-scattering detection. Comparable elution profiles were obtained with a linear gradient of 10–90% [10] or 30–90% [15] propionitrile in acetonitrile. The natural triacylglycerol distribution differs from the rearranged one mainly in the molecular

Table 2
Carbon number distribution of butterfat triacylglycerols

Carbon No.	Butterfat (mol%)[a]		
	Reference	Randomized	Calculated[b]
18	0.00	0.13	0.07
20	0.00	0.19	0.10
22	0.04	0.49	0.25
24	0.13	1.21	0.66
25	0.00	0.12	0.06
26	0.39	1.75	0.97
27	0.03	0.09	0.06
28	0.89	1.53	1.00
29	0.07	0.00	0.08
30	1.50	1.60	1.26
31	0.12	0.01	0.12
32	2.83	2.29	1.83
33	0.39	0.26	0.25
34	6.13	3.75	3.17
35	1.11	0.70	0.60
36	11.13	6.46	5.57
37	1.64	0.97	0.89
38	12.84	8.11	6.88
39	1.17	0.72	0.78
40	9.96	6.84	6.04
41	0.71	0.42	0.71
42	6.61	5.12	5.61
43	0.76	0.69	0.93
44	5.72	5.93	6.93
45	0.87	0.60	1.47
46	5.82	8.35	9.83
47	1.09	1.83	2.40
48	6.62	11.58	13.32
49	1.42	2.34	2.77
50	7.77	12.51	13.14
51	1.41	1.80	1.77
52	6.72	8.39	7.62
53	0.62	0.29	0.48
54	2.99	2.64	2.03
55	0.15	0.01	0.02
56	0.28	0.23	0.10

[a] Determined by non-polar capillary GC. The relative standard deviations for repeat determinations were $<1\%$ for components making up more than 2% of total and $<2\%$ for components making up less than 2% of total.

[b] 1,2,3-Random calculation based on the fatty acid composition of the randomized butteroil.

association of the fatty acids, although discrepancies are also present in the proportions of the 18:0 and 18:1 fatty acids (Table 1).

3.2. Peak identification in total oil

The individual triacylglycerols in the various HPLC peaks were identified by on-line LC–MS using a variety of strategies [10,16]. Single-ion profiles for the diacylglycerol type of fragments were systematically matched against those recorded for the total ion current and the partition number and elution order established for all triacylglycerols by reference to the fatty acid moiety lost during fragmentation. The identification of individual molecular species was confirmed by examining the full mass spectra taken from the ascending and descending limbs or the heart section of each peak for the presence of characteristic diacylglycerol fragment ions and the molecular ions, if any.

Fig. 2A gives the LC–MS profile for the saturated diacylglycerol moieties of the triacylglycerol peaks in the randomized butteroil. The major saturated even-carbon-number diacylglycerols determined as the $[MH - RCOOH]^+$ ions range from 8:0 to 36:0 and are combined randomly with all the fatty acids present in the rearranged oil. The relative proportions of the various diacylglycerols are indicated by the ion counts given in the left hand corner of each ion plot, while the nature of the fatty acid lost during fragmentation is indicated by its carbon and double bond number attached to each diacylglycerol peak. The splittings in the partition numbers of the triacylglycerols correspond to the splittings in the peaks for the diacylglycerol fragment ions and are due to differences in elution times of the species containing fatty acids of different chain length within isologous triacylglycerols. There is a clear indication of the separation of various critical pairs of species, *e.g.* the palmitates from oleates and the myristates from palmitoleates. Among the triacylglycerols containing short-chain fatty acids, *e.g.* butyrates, caproates and caprylates, there is a clear-cut resolution of a triplet, with the butyrates being preceded by caproates, which are preceded by caprylates and higher chain lengths within each isologous series of triacylglycerols. Thus, the triacylglycerols yielding a diacylglycerol (DG) fragment DG22:0 were made up of a triplet of peaks within the

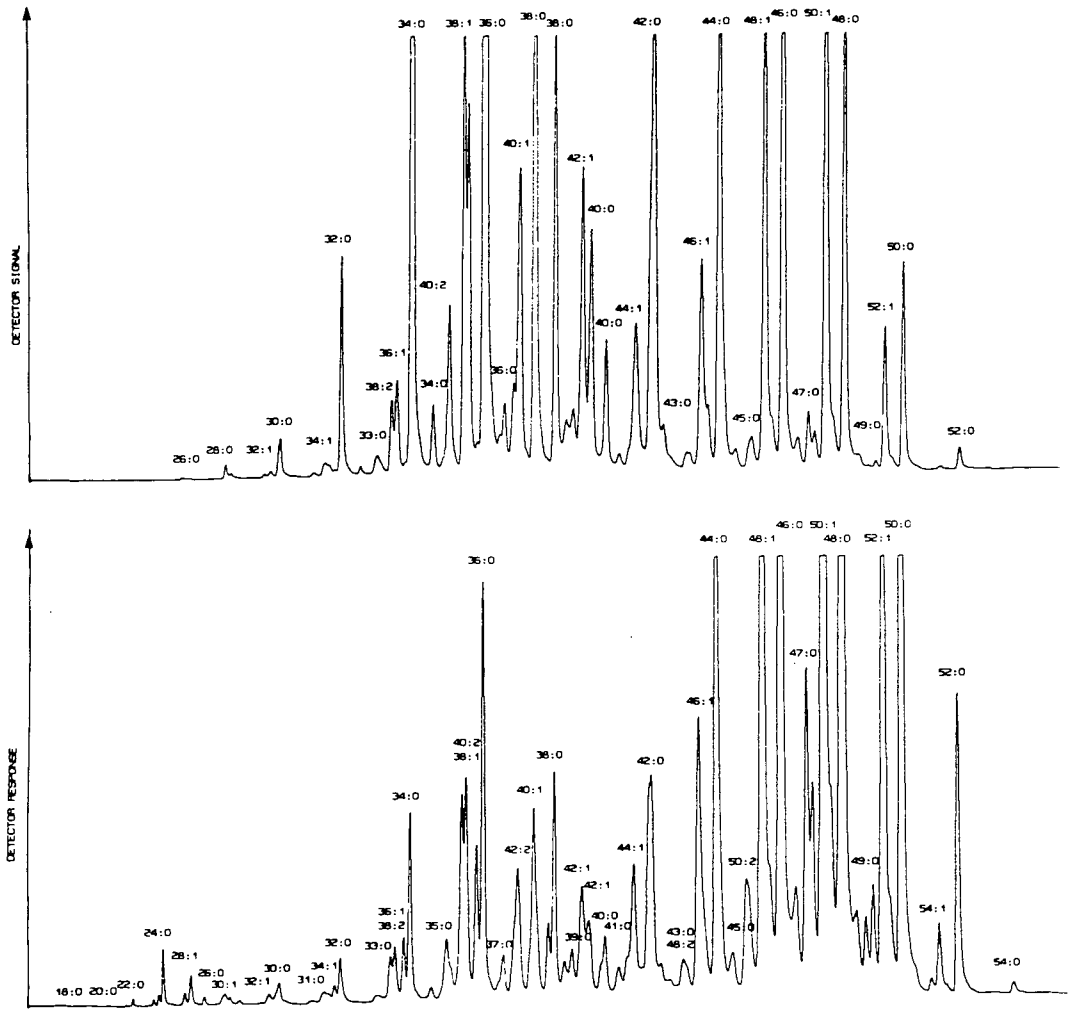

Fig. 1. Reversed-phase HPLC profiles of natural (top) and rearranged (bottom) butterfat triacylglycerols as obtained with light-scattering detector. HPLC conditions: Hewlett-Packard Model 1050 liquid chromatograph equipped with a Supelcosil LC-18 column (25 cm × 0.46 cm I.D.) coupled to a Varex ELSD II light-scattering detector. Solvent: linear gradient of 10–90% isopropanol in acetonitrile at 25°C over a period of 90 min (1 ml/min); recording stopped at 70 min. Peak identification by carbon and double bond number of triacylglycerols.

partition numbers 26–40. This was due to the presence of diacylglycerols containing such combinations of saturated fatty acids as 18:0–4:0, 16:0–6:0, 14:0–8:0 and 12:0–10:0, which are well resolved when combined with 4:0 to 18:0 saturated fatty acids and the corresponding unsaturated fatty acids in the original triacylglycerols. Likewise, there is resolution among isologous triacylglycerols containing two short-chain fatty acids. Thus, DG8:0, mainly 4:0–4:0, when combined with 18:0, is retained longer than DG10:0, mainly 6:0–4:0, when combined with 16:0, which is retained slightly longer than DG12:0, mainly 6:0–6:0 and 8:0–4:0, when combined with 14:0. The shouldering is due to the earlier elution of 14:0–6:0–6:0 when com-

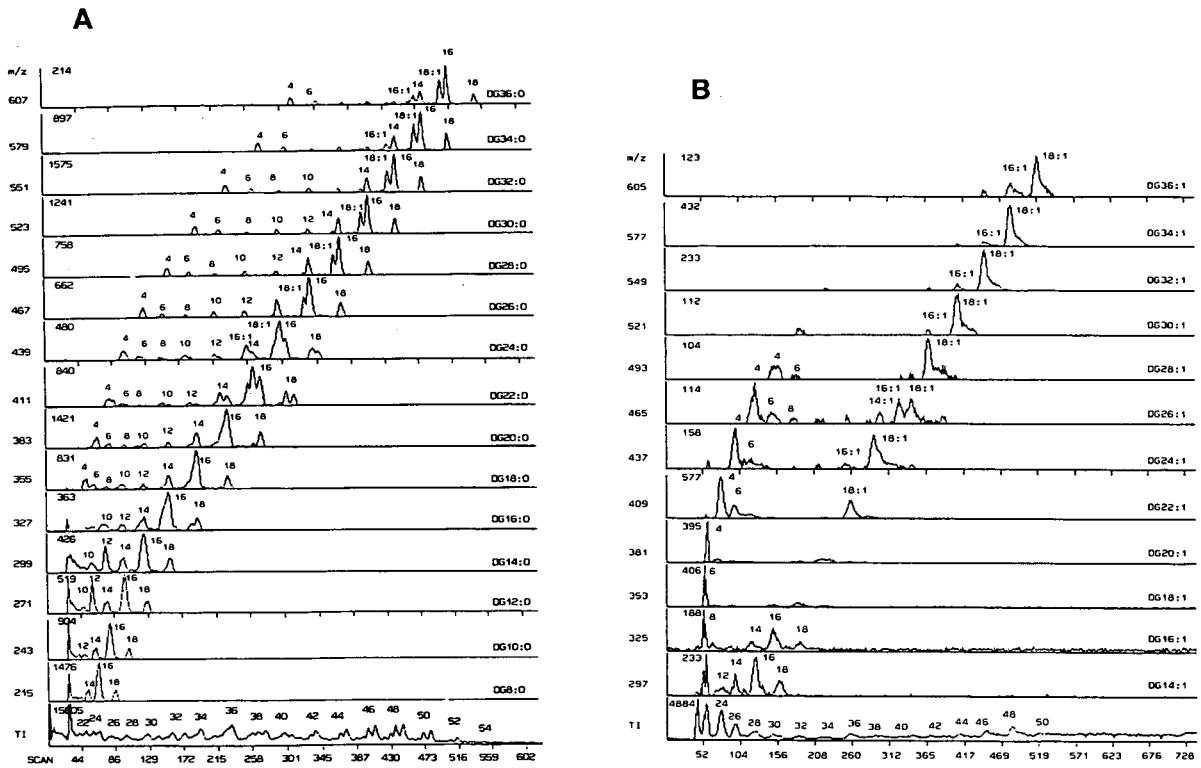

Fig. 2. (A) Mass chromatograms of the saturated diacylglycerol fragment ions, $[MH - RCOOH]^+$, as obtained for rearranged butterfat triacylglycerols by LC–MS. DG36:0–DG8:0 = Diacylglycerols corresponding to the fragment ions (m/z 607-215); FA4–FA18 = fatty acids lost from triacylglycerols during formation of diacylglycerol fragment ions; TI = total positive chemical ionization current. Numbers in upper left hand corner of individual ion plots indicate the ion counts for the most intense peak. LC–MS conditions: Hewlett-Packard Model 1048B liquid chromatograph equipped with a Supelcosil LC-18 column (25 cm × 0.46 cm I.D., Supelco). Solvent: linear gradient of 10–90% propionitrile in acetonitrile (2.2 ml/min) at 30°C over a period of 60 min. Sample: 25 μl of a 0.01% solution in tetrahydrofuran. (B) Mass chromatograms of the monounsaturated and diunsaturated diacylglycerol fragment ions, $[MH - RCOOH]^+$, as obtained for rearranged butterfat triacylglycerols by LC–MS using a linear gradient of 0–90% propionitrile in acetonitrile. Other details and peak identification as in (A).

pared to that of the isologous 14:0–8:0–4:0. Similar orders of elution can be recognized among other short-chain triacylglycerols.

The split in the partition number 50 is due to the presence of two major triacylglycerols, 18:0–18:1–16:0 and 18:0–16:0–16:0, with the 18:1-containing species being eluted ahead of the 16:0-containing species. In addition, the front part of this triacylglycerol peak contained also 18:0–18:0–16:1 and the rear part 18:0–14:0–18:0 as major species. The composition of the diacylglycerol moieties derived from the rear peak of partition number 48 revealed the presence of 18:0–16:0, 14:0–16:0 and 14:0–18:0 diacylglycerol species in nearly equal proportions, corresponding to 14:0–16:0–18:0. The front of partition peak 48 yielded diacylglycerol ions for 16:1–18:1, 18:1–18:1, 16:0–18:1, 18:0–18:1 and 18:0–16:1, corresponding to triacylglycerols 16:1–18:0–18:1 and 16:0–18:1–18:1. The triacylglycerols eluted between the even partition number peaks were due to odd-carbon number species.

Fig. 2B shows the single-ion plots for the fragment ions corresponding to the even-carbon-number monounsaturated diacylglycerols. Again the diacylglycerol moieties can be readily matched to the triacylglycerol parent molecules from which the various saturated fatty acids have been

lost in proportion to their content in the total randomized oil. The plots confirm further the effective resolution of the critical pairs, and of the isologous triacylglycerols containing one or two short-chain fatty acids. Due to low 18:2 content, it was not possible to obtain reliable plots for the 22:2 due to 18:2–4:0, and 24:2 due to 18:2–6:0. However, the combinations of 18:1–18:1 and 18:1–16:1 with 4:0 and 6:0 were clearly recognized and could be traced to the front limb of the corresponding triacylglycerol triplet within the appropriate partition number of the parent triacylglycerols. The above resolution of the critical pairs and isologous triplets in the even series was faithfully reproduced in the odd-carbon-number series. Furthermore, separate series were apparent for the normal- and branched-chain odd-carbon-number species, the *iso* and *anteiso* isomers not being resolved (results not shown).

3.3. Peak identification in subfractions

Fig. 3 shows the LC–MS profiles of the five major triacylglycerol bands resulting from randomization of butteroil. TLC band 1 contained the long-chain saturates, TLC band 2 the short-chain saturates and long-chain *trans*-monoenes,

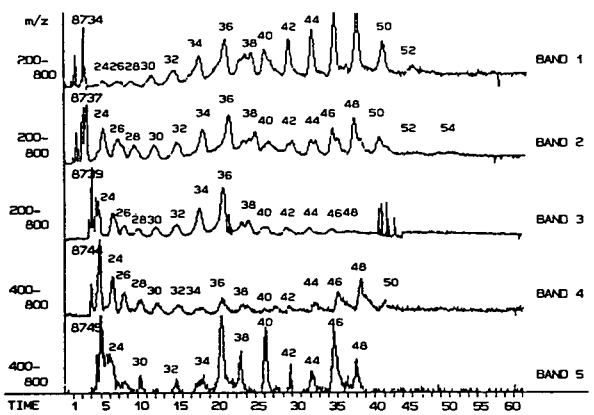

Fig. 3. Total ion current profiles of selected mass ranges as obtained by reversed-phase LC–MS for rearranged butterfat triacylglycerols recovered in $AgNO_3$-TLC bands 1–5. Peaks are identified by triacylglycerol partition numbers. LC–MS conditions as in Fig. 2A. Time in min.

TLC band 3 the short-chain *trans*-monoenes and long-chain *cis*-monoenes, TLC band 4 the short-chain *cis*-monoenes and the long-chain *trans*-dienes, while TLC band 5 contained long-chain *cis*-dienes, short-chain *cis*-dienes and both *cis*- and *trans*-trienes of both long and short chain length. Such an overlap of natural butterfat triacylglycerols had been recognized previously during $AgNO_3$-TLC [3] as had been the separation of *cis*- and *trans*-monounsaturated triacylglycerols.

The single-ion plots for the diacylglycerol moieties of the saturated long-chain triacylglycerols in TLC band 1 (results not shown) indicated the presence of diacylglycerols ranging from DG10:0 to DG36:0. The single-ion plots obtained for the saturated diacylglycerol moieties of the short-chain saturated and the long-chain *trans*-monounsaturated triacylglycerols recovered from TLC band 2 (results not shown) indicated that the short-chain triacylglycerols were largely butyrates, caproates and caprylates. TLC band 2 contained a high proportion of the saturated medium-chain triacylglycerols that possessed the same composition of molecular species in both TLC band 1 and TLC band 2. The small amounts of long-chain monoenoic triacylglycerols found in TLC band 2 were characterized largely by the presence of 16:1 and *trans*-18:1t and to a lesser extent 14:1. Characteristically, these triacylglycerols were eluted from the HPLC column between the fully saturated and the *cis*-monounsaturated triacylglycerols of the same partition number. The *trans*-monoenoic and the *cis*-monoenoic triacylglycerols were resolved into long- and short-chain species, which facilitated their identification and determination of elution order. These conclusions were confirmed by the single-ion plots for the monounsaturated diacylglycerol moieties derived from the *trans*-monounsaturated long-chain triacylglycerols in relation to the parent molecules in the total ion current profile of TLC band 2 (results not shown). Interestingly, the single-ion plots for the monounsaturated diacylglycerols showed a symmetrical repetitive pattern representing the combination of *trans*-18:1- with two saturated fatty acids, which were seen in the

proportions in which they occur in the total mixture (see also Fig. 2B). The combinations of the *trans*-monoenoic acids with the shorter-chain saturated acids were found in TLC band 3.

Fig. 4A shows the single-ion plots for the saturated diacylglycerol moieties derived from the short-chain *trans*-monoenoic and the long-chain *cis*-monoenoic triacylglycerols recovered from TLC band 3. The short-chain triacylglycerols are characterized by the exclusive association of the *trans*-18:1 (elaidic) acid with the short-chain saturated diacylglycerols, which is consistent with a high proportion of butterfat *trans*-monoenes contributed by elaidic acid [17]. In contrast, the *cis*-monounsaturated triacylglycerols were made up of the saturated diacylglycerols in combination with a variety of monounsaturated fatty acids ranging from 10:1 to 18:1. The monounsaturated fatty acids were combined with each diacylglycerol moiety in proportion to the content of the fatty acids and the proportion of the specific diacylglycerols in the randomized butteroil. Fig. 4B shows the single-ion plots for the monounsaturated diacylglycerol moieties of the short-chain *trans*-monoenoic and the long-chain *cis*-monoenoic triacylglycerols from TLC band 3. Perpendicular lines dropped from the various monoenoic-diacylglycerol-like fragment ion peaks to the corresponding triacylglycerol peaks reveals them to be of two types. One being retained somewhat longer (*trans*) than the other (*cis*), when compared within the same partition number, both being eluted ahead of the fully saturated triacylglycerols of same partition number.

Single-ion plots for the saturated diacylglycer-

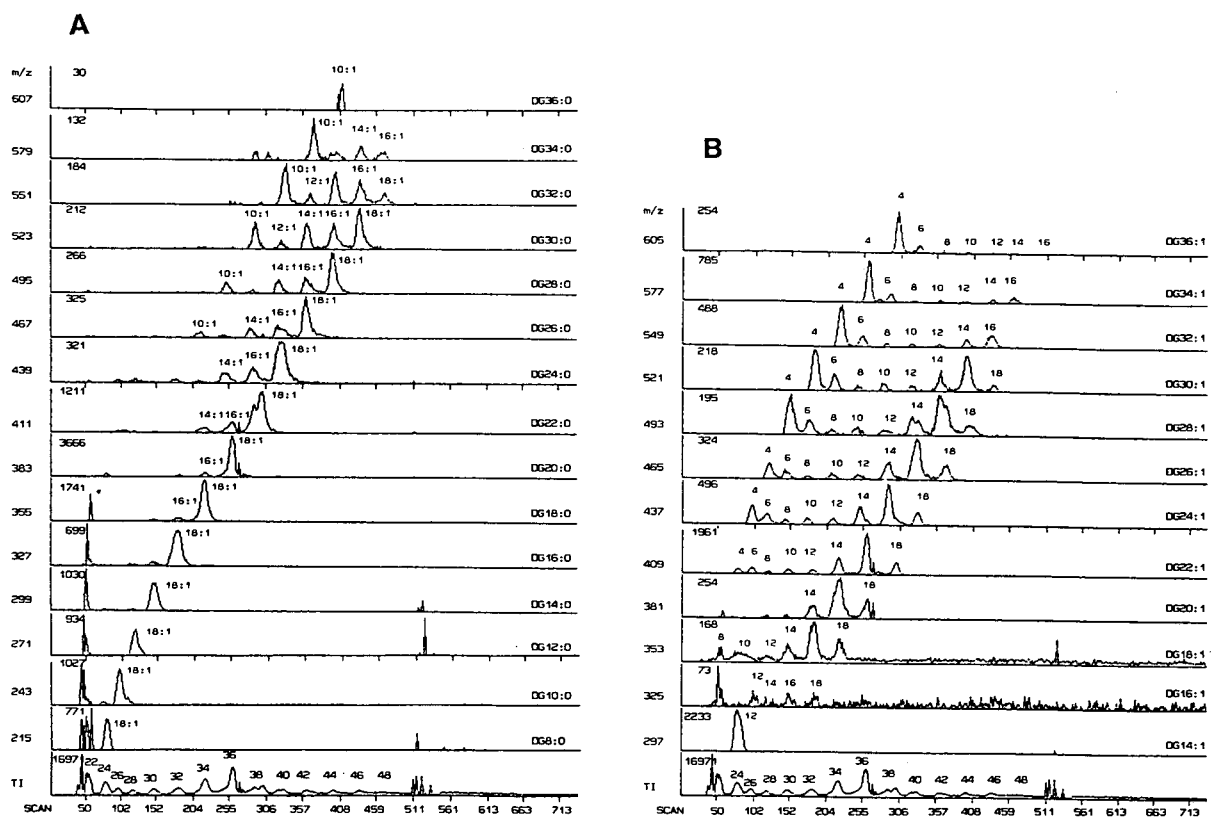

Fig. 4. (A) Mass chromatograms of saturated diacylglycerol fragment ions, $[MH - RCOOH]^+$, as obtained for TLC band 3 by LC–MS. LC–MS conditions and peak identification as in Fig. 2. (B) Mass chromatograms of monounsaturated diacylglycerol fragment ions, $[MH–RCOOH]^+$, as obtained for TLC band 3 by LC–MS. LC–MS conditions and peak identification as in Fig. 2.

ol moieties of the short-chain *cis*-monoenoic and the long-chain *trans*-dienoic triacylglycerols from TLC band 4 (results not shown) indicated that the long-chain *trans*-dienes were minor components. The short-chain *cis*-monoenoic triacylglycerols corresponded to the *trans*-monoenoic triacylglycerols in an apparent near-exclusive combination of the short-chain saturated diacylglycerols with *cis*-18:1 acid. In addition, TLC band 4 contained long-chain dienoic triacylglycerols. Single-ion plots for the dienoic diacylglycerol moieties showed that they are combined with the major long-chain saturated fatty acids. The dienoic diacylglycerols were made up largely of two monounsaturated fatty acids, *e.g.* 18:1–18:1, 16:1–18:1, 16:1–16:1, 14:1–16:1 and 14:1–18:1, presumably mainly *trans* isomers. The single-ion plots for the monoenoic diacylglycerols derived from the short-chain *cis*-monoenoic and the long-chain *trans*-dienoic triacylglycerols in TLC band 4 (results not shown) led to the finding that the 26:1 monoenoic diacylglycerol occurred in two peaks due to a resolution of the species containing the 6:0–18:1 and the 8:0–16:1 diacylglycerol moieties in the triacylglycerols of the same partition number. A similar doubling of several other triacylglycerol peaks was seen because of a resolution of other isologous monoenoic triacylglycerols.

Fig. 5 shows the single-ion plots for the saturated, monounsaturated and some diunsaturated diacylglycerol moieties derived from the long-chain *trans*-dienoic and the short- and long-chain *cis*-dienoic triacylglycerols and traces of trienoic triacylglycerols in TLC band 5. All of these separations are also highly regular based on the principles recognized earlier in the resolution of the saturated and monoenoic triacylglycerols. It should be noted, however, that in several instances the monounsaturated and diunsaturated diacylglycerol peaks coincide fully with the corresponding peak for the parent triacylglycerol, when previous discussion would suggest doubling or tripling of the triacylglycerol peak as well as differences in the elution times for the diacylglycerol moieties. This is not an exception, but a result of the origin of all these diacylglycerol moieties from a single triacylglycerol species.

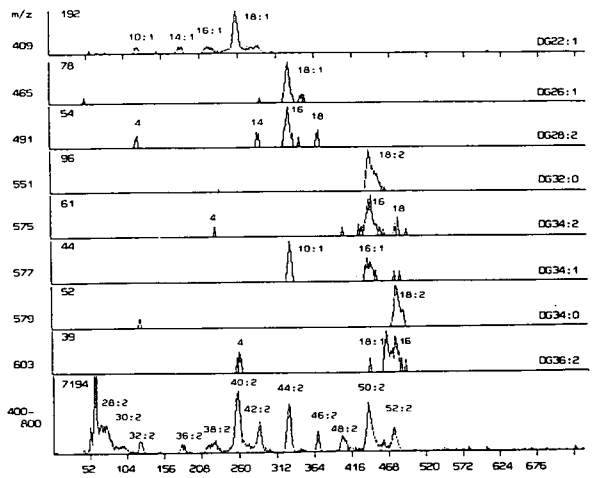

Fig. 5. Mass chromatograms of selected saturated, monounsaturated and diunsaturated diacylglycerol fragment ions, $[MH - RCOOH]^+$, as obtained for TLC band 5 by LC–MS. LC–MS conditions and peak identification as in Fig. 2.

Thus, the 18:1–DG26:1 combination overlapped with the 16:0–DG28:2 combination and the combination of 10:1–DG34:1, all of which corresponded to the triacylglycerol (TG) TG44:2. The simple explanation for this observation was the presence of a single triacylglycerol, 10:1–18:1–16:0, in this chromatographic peak.

No evidence was obtained for the resolution of enantiomers or reverse isomers of unsaturated triacylglycerols of the type 16:0–18:1–18:1 and 18:1–16:0–18:1, which had been observed on $AgNO_3$-TLC [18]. Also, the 15% $AgNO_3$-TLC system employed here did not permit this delicate resolution of the molecular species.

3.4. Quantitation

The quantitative estimates of the various triacylglycerol species are given in Table 3 as obtained by HPLC–light-scattering detection, LC–MS and by calculation. The uncorrected estimates show considerable divergence from the calculated values, which, however, do not indicate non-randomness of fatty acid association. This is due to a variable response of the different molecular species in the two different detector types, none of which shows a true mass or mole composition. A more accurate quantitation

Table 3
Composition of randomized butteroil as estimated by reversed-phase HPLC–light-scattering detection and reversed-phase LC–MS

Molecular species	Determined (%, w/w)		Calculated (%, w/w)[b]
	HPLC–LSD[a]	LC–MS	
10:0 (4–4–2)		0.08	
12:0 (4–4–4)		0.14	0.02
14:0 (4–4–6)		0.32	0.04
16:0 (4–4–8; 4–6–6)		0.12	0.04
18:0 (4–4–10; 4–6–8)		0.30	0.07
20:0 (4–4–12; 4–6–10)		0.36	0.10
22:0 (4–4–14; 4–6–12)	0.16	0.73	0.24
26:1 (4–4–18:1)	0.17	0.62	0.13
24:0 (4–4–16; 4–6–14)	0.50	1.17	0.64
28:1 (4–6–18:1)	0.26	0.75	0.16
26:0 (4–6–16; 4–4–18)	0.42	1.63	0.83
30:1 (4–8–18:1)	0.32	0.61	0.18
28:0 (4–8–16; 4–6–18)	0.20	1.80	0.80
32:1 (4–10–18:1)	0.30	0.40	0.25
30:0 (4–10–16; 4–12–14)	0.50	2.20	1.07
31:0 (4–15–12)	0.31	0.25	0.12
34:1 (4–12–18:1)	0.32	0.75	0.33
32:0 (4–12–16; 4–14–14)	0.64	3.90	1.55
33:0 (4–15–14)	0.59	0.61	0.24
36:1 (4–14–18:1)	0.68	1.39	0.73
38:2 (4–16–18:2)	0.70		0.03
34:0 (4–14–16; 6–12–16)	1.48	5.13	2.80
35:0 (4–15–16)	1.10	0.53	0.58
40:2 (4–18:1–18:1)	1.68	0.19	0.23
38:1 (4–16–18:1; 6–14–18:1)	1.76	1.09	1.82
36:0 (4–16–16; 6–14–16)	2.63	7.84	4.72
37:0 (4–15–18; 4–17–16)	0.60	0.33	0.77
42:2 (6–18:1–18:1)	1.73	0.04	0.16
40:1 (4–18–18:1; 6–16–18:1)	2.05	2.90	1.73
38:0 (4–16–18; 6–16–16)	1.78	6.75	4.92
39:0 (4–17–18)	0.67	0.50	0.62
42:1 (6–18–18:1; 8–16–18:1)	1.33	0.76	1.33
40:0 (6–16–18; 10–14–16)	1.07	6.29	4.01
41:0 (6–17–18)	0.90	0.87	0.59
44:1 (10–16–18:1)	1.76	1.54	1.51
42:0 (10–16–16; 12–14–16)	2.68	3.25	4.04
43:0 (16–12–15)	0.68	0.41	0.78
48:2 (12–18:1–18:1)	0.66	0.21	0.23
46:1 (12–16–18:1	2.79	2.03	1.95
44:0 (12–16–16; 10–16–18)	4.56	3.74	5.15
45:0 (16–14–15)	0.66	0.38	1.27
50:2 (14–18:1–18:1)	1.51	0.88	0.49
48:1 (14–16–18:1)	5.90	3.85	3.43
46:0 (14–16–16; 12–16–18)	7.90	5.03	7.47
47:0 (16–16–15)	2.47	0.98	2.02
52:2 (16–18:1–18:1)	n.d.	1.57	1.17
50:1 (16–16–18:1)	9.04	5.42	5.26
48:0 (14–16–18; 16–16–16)	10.14	5.66	9.32

Table 3. (*Continued*)

Molecular species	Determined (%, w/w)		Calculated (%, w/w)[b]
	HPLC–LSD[a]	LC–MS	
49:0 (16–16–17)	0.82	1.02	1.95
54:2 (18–18:1–18:1)	n.d.	1.07	0.51
52:1 (16–18–18:1)	5.26	3.07	3.48
50:0 (16–16–18)	7.03	3.54	7.05
54:1 (18–18–18:1)	0.88	0.64	0.86
52:0 (16–18–18)	2.25	1.28	2.83
54:0 (18–18–18)	0.27	0.29	0.54
55:0 (18–17–20)			0.01
56:0 (18–18–20)		Trace	0.01
Total	92.05	97.21	93.18

[a] Reversed-phase HPLC with light-scattering detection. The relative standard deviations for repeat analyses were >2% for components making up more than 5% of total and <10% for components making up less than 5% of total.
[b] 1,2,3-Random calculation followed by appropriate summation of corresponding molecular species.

would require much more extensive calibration of the detector response which was not possible in the absence of pure reference compounds.

4. Discussion

The purpose of this investigation was to determine the relative order of elution of the molecular species of rearranged butterfat triacylglycerols for which the exact quantitative composition can be calculated by statistical considerations. The initial part of the study was concerned with the verification that a random distribution of the fatty acids had indeed been obtained, which was established by detailed GC and HPLC resolution and MS identification of the species.

Previous work had shown that the short- and long-chain triacylglycerols of butterfat undergo extensive resolution within the isologous series and within a given calculated partition number due to a longer retention of the molecular species containing short-chain fatty acids [7,12]. In order to simplify the LC–MS resolution and identification, we used $AgNO_3$-TLC for a preliminary segregation and isolation of triacylglycerol molecules differing in the number and geometric configuration of double bonds [3,5]. $AgNO_3$-TLC also permitted a separation of the short- and long-chain triacylglycerols within each degree of unsaturation and type of geometric configuration of the double bond.

The present study confirms the separation of isologous short-chain triacylglycerols based on the presence of butyric, caproic or caprylic and longer-chain fatty acids. The order of peak elution within an isologous series of saturated triacylglycerols can be summarized as follows: XX10 < XX8 < XX6 < XX4, where X stands for any other saturated fatty acid. A similar order of resolution was observed for the monoenoic and dienoic species within isologous series. A similar order of elution was obtained for isologous triacylglycerols containing two short-chain fatty acids: X88 < X86 < X66 < X84 < X64 < X44. The acetates were eluted last in each isologous series of triacylglycerols. Since this resolution is similar to that achieved on adsorption chromatography, it is possible that adsorptive sites remaining on the support of the conventional reversed-phase columns are responsible for the longer retention of the short-chain species.

Reverse isomers of triacylglycerols may be defined as isologous series of triacylglycerols of opposite fatty acid distribution in the primary and secondary positions of the glycerol molecule. Normally reverse isomers of triacylglycerols are not resolved by chromatographic methods, ex-

cept for certain unsaturated reverse isomers of triacylglycerols by $AgNO_3$-TLC [18]. Despite much attention to detail, no evidence was obtained for a resolution of the reverse isomers of short-chain triacylglycerols under the present experimental conditions. Specifically, the anticipated double peaks were not observed for such triacylglycerol pairs as 1,3-dibutyryl-2-palmitoylglycerol and its reverse isomer, 1,2-dibutyryl-3-palmitoylglycerol, and 1,3-dibutyryl-2-oleoylglycerol and its reverse isomer, 1,2-dibutyryl-3-oleoylglycerol.

There was also no evidence for an effect of the placement of the *cis*- and *trans*-monoenoic fatty acids in the primary and secondary positions of the glycerol molecules, although the *cis*- and *trans*-monoenoic species were partially resolved. Butterfat contains up to 20% of the 18:1 as elaidic (*trans*-9) and over 80% as oleic (*cis*-9) acids, while the other monoenoic fatty acids are believed to contain a somewhat smaller proportion of the *trans*-isomer, except 10:1, which contains none because of the terminal double bond [17]. Specifically, separation was obtained for such medium-chain triacylglycerols as 16:0–18:1t–4:0 (t = *trans*) and 16:0–18:1c–4:0, (c = *cis*) as well as the long-chain 16:0–18:1t–16:0 and 16:0–18:1c–16:0 isomers. Since conventional chromatographic liquid phases do not resolve enantiomers, there was no need to distinguish between the fatty acid compositions of the *sn*-1 and *sn*-3 positions.

The utilization of the rearranged butteroil for the chromatographic separations allowed the identification and characterization of the elution times of several unusual triacylglycerol species. Thus, the lowest-molecular-mass triacylglycerol that we identified in the rearranged oil was 4:0–4:0–2:0, followed by 4:0–4:0–4:0, 4:0–4:0–6:0, 4:0–4:0–8:0, etc. These triacylglycerols were found to conform to the order of elution of mixed saturated fatty acid isologous triacylglycerols of their higher-molecular-mass homologues. Acetic acid had been previously found to be present in butterfat triacylglycerols, where it had been reported to occur in combination with long-chain fatty acids [7,19].

This investigation establishes the empirical chromatographic elution order of all major mixed acid triacylglycerols found in butterfats. In parallel studies Myher *et al.* [20] have derived retention factors for each of the fatty acids, which can be used to determine the order of elution of one triacylglycerol species relative to any other. A comparison of the observed and predicted order of elution for a variety of molecular species showed good agreement.

5. Acknowledgement

These studies were performed with funds from the Heart and Stroke Foundation of Ontario, Toronto, Canada and the Medical Research Council of Canada, Ottawa, Canada.

6. References

[1] R.G. Jensen, A.M. Ferris and C.J. Lammi-Keefe, *J. Dairy Sci.*, 74 (1991) 3228.
[2] A. Kuksis and J.M. McCarthy, *Can. J. Biochem.*, 40 (1962) 679.
[3] W.C. Breckenridge and A. Kuksis, *Lipids*, 3 (1968) 291.
[4] R.G. Jensen, R.E. Pitas and J. Sampugna, *J. Dairy Sci.*, 50 (1967) 1332.
[5] W.C. Breckenridge and A. Kuksis, *J. Lipid Res.*, 9 (1968) 388.
[6] E. Geeraert and P. Sandra, *J. Am. Oil Chem. Soc.*, 64 (1987) 100.
[7] J.J. Myher, A. Kuksis, L. Marai and P. Sandra, *J. Chromatogr.*, 452 (1988) 93.
[8] C. Maniongui, J. Gresti, M. Bugaut, S. Gauthier and J. Bezard, *J. Chromatogr.*, 543 (1991) 81.
[9] S. Bornaz, G. Novak and M. Parmentier, *J. Am Oil Chem. Soc.*, 69 (1992) 1131.
[10] A. Kuksis, L. Marai, J.J. Myher, Y. Itabashi and S. Pind, in E.G. Perkins (Editor), *Analysis of Fats, Oils and Lipoproteins*, American Oil Chemists' Society, Champaign, IL, 1991, pp. 464–495.
[11] H. Kallio and G. Currie, in *Short Course on HPLC of Lipids*, American Oil Chemists' Society, Bloomingdale, IL, 1991.
[12] A. Kuksis, L. Marai and J.J. Myher, *J. Am. Oil Chem. Soc.*, 50 (1973) 193.
[13] F. Manganaro, J.J. Myher, A. Kuksis and D. Kritchevsky, *Lipids*, 16 (1981) 508.
[14] A. Kuksis, M.J. McCarthy and J.M.R. Beveridge, *J. Am. Oil Chem. Soc.*, 41 (1964) 201.

[15] A. Kuksis, L. Marai, J.J. Myher and Y. Itabashi, in V.K.S. Shukla and G. Holmer (Editors), *Proceedings of the 15th Scandinavian Symposium on Lipids*, Lipidforum Publ., Rebild Bakker, Skorping, Denmark, 1989, pp. 336–370.
[16] A. Kuksis, L. Marai and J.J. Myher, *J. Chromatogr.*, 588 (1991) 73.
[17] P. Laakso and H. Kallio, *J. Am. Oil Chem. Soc.*, 70 (1993) 1161.
[18] B. Nikolova-Damyanova, in W.W. Christie (Editor), *Advances in Lipid Methodology —1*, Oily Press, Ayr, UK, 1992, pp. 181–237.
[19] P.W. Parodi, *J. Chromatogr.*, 111 (1975) 223.
[20] Myher, J.J., A. Kuksis and L. Marai, *J. Am. Oil Chem. Soc.*, 70 (1993) 1183.

ELSEVIER

Journal of Chromatography A, 672 (1994) 101–108

JOURNAL OF CHROMATOGRAPHY A

pH-Zone-refining counter-current chromatography: a displacement mode applied to separation of dinitrophenyl amino acids

Yoichiro Ito*, Ying Ma

Laboratory of Biophysical Chemistry, National Heart, Lung, and Blood Institute, National Institutes of Health, Bethesda, MD 20892, USA

(First received December 30th, 1993; revised manuscript received February 15th, 1994)

Abstract

A new mode of pH-zone-refining counter-current chromatography operates in a manner analogous to displacement chromatography. The method uses a retainer base (acid) in the stationary phase to retain analytes in the column and a displacer acid (base) to elute the analytes in the decreasing order of pK_a and hydrophobicity. The elution produces a train of highly concentrated rectangular solute peaks with minimum overlap. Utility of the method is demonstrated in the separation of dinitrophenyl amino acids in a two-phase solvent system composed of methyl *tert.*-butyl ether and water. Compared with the original mode of pH-zone-refining counter-current chromatography, the present mode is more amenable to ligand-affinity separation which may cover a broader range of analytes including non-ionizable compounds.

1. Introduction

pH-Zone-refining counter-current chromatography (CCC) is a recently developed preparative separation method using a retainer acid (base) to retain acidic analytes and an eluent base (acid) to elute analytes in the order of their pK_a and hydrophobicity [1–5]. The method has been applied to various ionizable compounds such as amino acid derivatives [1–5] and hydroxyxanthene dyes [2–10].

Comparison of this technique to displacement chromatography [11] reveals that the key reagents in these two methods, *i.e.*, retainer in pH-zone-refining CCC and displacer in displacement chromatography, act in an opposite manner: the retainer transfers the solute from the mobile phase to the stationary phase at the front end of the solute bands, whereas the displacer transfers the solute from the stationary phase to the mobile phase at the back of the solute bands. Nevertheless, these two actions produce similar results such as formation of successive rectangular solute peaks and concentration of minor impurities at their boundaries. From this point of view, the "pH-zone-refining CCC" technique reported earlier may be more properly considered as "reverse displacement mode pH-zone-refining CCC".

In this work, pH-zone-refining CCC is carried out in a displacement mode directly comparable to displacement chromatography simply by interchanging the action of the mobile and the stationary phases. Thus, the original eluent base

* Corresponding author.

0021-9673/94/$07.00
SSDI 0021-9673(94)00209-R

becomes a retainer for analytes in the stationary phase, and the original retainer acid becomes a displacer to displace the analytes from the stationary phase to the mobile phase at the back of the solute bands. The results are demonstrated in separations of a set of dinitrophenyl (DNP) amino acids on a two-phase solvent system composed of methyl *tert.*-butyl ether and water using trifluoroacetic acid (TFA) as a displacer and ammonia as a retainer. The preparative capability of the present method is also demonstrated in the separation of gram quantity of samples.

2. Mechanism of displacement pH-zone-refining CCC

A model experiment is initiated by filling the entire column with the stationary aqueous phase which contains a retainer, NH_3. This is followed by injection of a sample solution containing three major components (solutes S_1, S_2 and S_3). The column is then eluted with an organic mobile phase containing a displacer, TFA. As the mobile phase moves through the column by partially displacing the stationary phase, it distributes TFA anions to the stationary phase retained in the column according to its partition coefficient as determined by the pH at a given point in the column. This partition process depletes the TFA from the flowing mobile phase front resulting in formation of a sharp TFA front border due to the concentration-dependent partition behavior of TFA based on its non-linear isotherm. After equilibrium is established, this sharp TFA border travels through the column at a uniform rate lower than that of the mobile phase front.

Fig. 1A schematically illustrates a portion of the separation column which contains the stationary aqueous phase in the lower half (shaded) and the mobile organic phase in the upper half. The sharp TFA border is indicated by a thick line across the column.

In the early stage of the experiment, all solutes present on the right side of the TFA border are exposed to a high pH, mostly deprotonated to

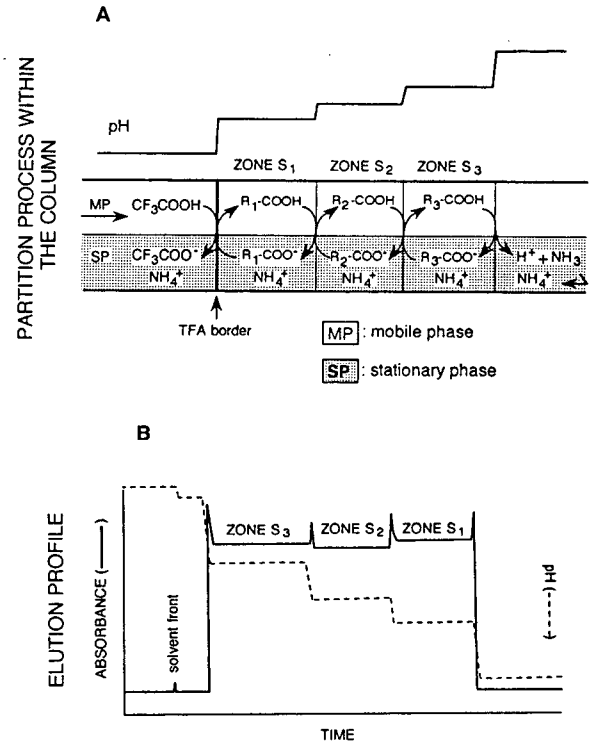

Fig. 1. Mechanism of displacement mode of pH-zone-refining CCC. (A) Partition process within the separation column, (B) elution profile.

become a hydrophilic form ($R–COO^-$) and partitioned into the aqueous stationary phase. As the TFA front advances, these compounds are exposed to a low pH, protonated into a hydrophobic form (R–COOH) and transferred into the flowing organic phase, *i.e.*, TFA in the mobile phase gradually displaces all solute molecules present in the stationary phase in a manner analogous to the action of the displacer in displacement chromatography.

As this process continues, the solute concentration at the front of the TFA border increases causing the pH to fall. In this situation, solute S_1 with the lowest pK_a and hydrophobicity among the three components will act as a displacer of the other two solutes to occupy the column space immediately after the sharp TFA border. It forms the first zone (zone S_1) by making a sharp front border. The competition continues among other two solutes in which solute S_2 with a lower

pK_a and hydrophobicity will form the second zone (zone S_2) which is in turn preceded by the third zone (zone S_3) consisting of solute S_3.

When this partition process is completed, a train of solute zones is formed in front of the TFA border as shown in Fig. 1A. As in displacement chromatography, each zone consists of a single species, is equipped with self-sharpening boundaries, and has the solute partition coefficient (K_s) (the solute concentration in the stationary phase divided by that in the mobile phase) equal to that of TFA (K) in the succeeding zone. As indicated earlier, all zones are arranged in a decreasing order of pK_a and hydrophobicity and move together at the same rate determined by that of the succeeding TFA border.

As indicated by curved arrows, proton transfer and displacement of the solute molecule takes place between the two neighboring species at each zone boundary. Ammonium ion created at the far front border (solute S_3) remains permanently in the stationary phase and serves as the counterion for all species. Charged impurities present in each solute zone are quickly eliminated toward the zone boundaries of either side where they accumulate to form narrow bands as seen in displacement chromatography. Consequently the solutes are eluted as successive rectangular peaks with minimum overlap and with sharp impurity peaks at their boundaries as shown in Fig. 1B. Each zone shows a distinct pH plateau in a downward staircase fashion as indicated by a dotted line. As described elsewhere [3,5], net pH values of these plateaus may be predicted from three parameters, *i.e.*, pK_a, δ (intrinsic partition coefficient) and K_s (apparent partition coefficient) of each solute.

3. Experimental

3.1. CCC apparatus

A commercial model (Ito Multilayer Coil Separator/Extractor, Potomac, MD, USA) of the high-speed CCC centrifuge was used throughout the present studies. The detailed design of the apparatus was given elsewhere [12]. Briefly, the apparatus holds a multilayer coil separation column and a counterweight symmetrically at a distance of 10 cm from the central axis of the centrifuge. The column holder is equipped with a plastic gear which is engaged to an identical stationary gear mounted around the central axis of the apparatus. This gear arrangement produces the desired planetary motion to the column holder, *i.e.*, rotation and revolution of the holder in the same direction at the same rate. This planetary motion also prevents the flow tubes from twisting during revolution, thus permitting the elution of the mobile phase through the rotating column without the use of rotary seals.

The separation column consists of a single piece of 160 m × 1.6 mm I.D. polytetrafluoroethylene (PTFE) tubing (Zeus, Raritan, NJ, USA) wound around the column holder hub with 16 layers and 325 ml capacity. Both terminals of the column were connected to a flow tube (0.85 mm I.D. PTFE) (Zeus) by the aid of a set of tube connectors (Upchurch Scientific, Oak Harbor, WA, USA) rigidly mounted on the holder flange. A narrow-bore PTFE tube (5 m × 0.3 mm I.D.) (Zeus) was placed at the outlet of the column to restrict the flow, thus preventing formation of negative pressure at the inlet of the column which may cause suction of excess solvent from the reservoir through the check valves of the pump.

The speed of the apparatus was regulated with a speed controller (Bodine Electric Co., North Chicago, IL, USA). An optimum speed of 600 rpm was used throughout the present studies.

3.2. Reagents

Methyl *tert.*-butyl ether, methanol and TFA were glass-distilled chromatographic grade (Burdick & Jackson, Muskegon, MI, USA). Ammonium hydroxide, hydrochloric acid, acetic acid, propionic acid and *n*-butyric acid were of reagent grade (Fisher Scientific, Fair Lawn, NJ, USA). DNP-Amino acids used in the present studies include N-2,4-DNP-L-aspartic acid (DNP-Asp), N-2,4-DNP-DL-glutamic acid (DNP-Glu),

N,N′-2,4-diDNP-L-cystine [diDNP-$(Cys)_2$], N-2,4-DNP-L-alanine (DNP-Ala), N-2,4-DNP-L-proline (DNP-Pro), N-2,4-DNP-L-valine (DNP-Val) and N-2,4-DNP-L-leucine (DNP-Leu) (Sigma, St. Louis, MO, USA).

3.3. Preparation of solvent phases and sample solutions

The solvent pairs were prepared as follows: methyl *tert.*-butyl ether and distilled water were thoroughly equilibrated in a separatory funnel at room temperature and the two phases separated. The upper organic phase was acidified with TFA (displacer) at 5–20 m*M* and used as the mobile phase. Spacer acids such as propionic acid and *n*-butyric acid were sometimes added to the stationary phase in arbitrary amounts. Aqueous ammonia (retainer) was added to the lower aqueous phase used as the stationary phase.

Solutions were prepared by dissolving 2,4-DNP derivatives in 5–40 ml of stationary upper phase. A small amount of methyl *tert.*-butyl ether was added to form two phases and spacer acids were occasionally added directly to the sample solution. The 2,4-DNP derivatives were only partially soluble and it was necessary to sonicat the solution for several minutes to disperse undissolved particles before injection into the column.

3.4. Separation procedure

In each separation, the column was first entirely filled with the aqueous ammoniacal stationary phase. The sample solution was injected through the sample port and the organic mobile phase eluted through the column in the tail to head elution mode at a flow-rate of 3.3 ml/min (metering pump: Rainin, Emeryville, CA, USA) while the apparatus rotated at 600 rpm. The effluent from the column was continuously monitored by absorbance at 206 nm (Uvicord S: LKB, Bromma/Stockholm, Sweden) and collected at 3.3 ml/tube or 1 min/tube (Ultrorac fraction collector: LKB). After the peaks eluted, the apparatus was stopped and the column contents collected into a graduated cylinder by connecting the inlet of the column to a nitrogen line at 80 p.s.i. (1 p.s.i. = 6894.76 Pa). The retention of the stationary phase relative to the total column capacity was computed from the volume of the stationary phase collected from the column.

3.5. Studies on concentrations of displacer and retainer

Series of experiments were carried out with a set of three components, DNP-Leu, DNP-Ala and DNP-Asp to study the effects of the displacer (TFA) and retainer (NH_3) on the separation. In the first series, the effect of the displacer (TFA) was studied by varying its concentration in the organic mobile phase from 0.02% (2.6 m*M*) to 0.16% (20.5 m*M*) while the concentration of the retainer (NH_3) in the aqueous stationary phase was kept constant at 0.1% (11 m*M*). In the second series, the effect of the retainer (NH_3) was investigated by varying its concentration in the aqueous stationary phase from 5.5 to 44 m*M* while the displacer (TFA) concentration in the mobile phase was fixed at 0.4% (10.8 m*M*).

In each separation, the column was first filled with the aqueous stationary phase followed by injection of a sample mixture consisting of 100 mg each component in 5 ml solvent (4 ml lower phase and 1 ml methyl *tert.*-butyl ether). Then, the column was rotated and eluted with an acidified organic phase at a flow-rate of 3.3 ml/min. The effluent from the column was continuously monitored with a UV monitor at 206 nm. From the resulting chromatogram, the average solute concentration was estimated from the width of each peak. The partition coefficient of the displacer TFA was also computed from its retention volume and the volume of the stationary phase retained in the column.

3.6. Analysis of fractions

The pH value of each fraction was manually determined with a portable pH meter (Accumet Portable Laboratory, Fisher Scientific, Pittsburgh, PA, USA).

DNP-Amino acids were identified by their partition coefficients K_{std} (U/L) in a standard two-phase system composed of chloroform–acetic acid–0.1 *M* HCl (2:2:1); U and L stand for upper and lower phase, respectively. An aliquot of each fraction (usually 1 ml) was delivered into a test tube and dried under vacuum (Speed Vac Concentrator; Savant Instruments, Hicksville, NJ, USA). Then, 2 ml of the standard solvent system (1 ml of each phase) were added to each tube and the contents vigorously shaken to equilibrate the solute. An aliquot of each phase (usually 100–200 μl) was then diluted with 2 ml of methanol and the absorbance determined at 430 nm.

4. Results and discussion

Fig. 2 shows a typical chromatogram of DNP-amino acids obtained by the present method. A 100-mg amount of each of seven DNP-amino acids was eluted as a broad rectangular peak.

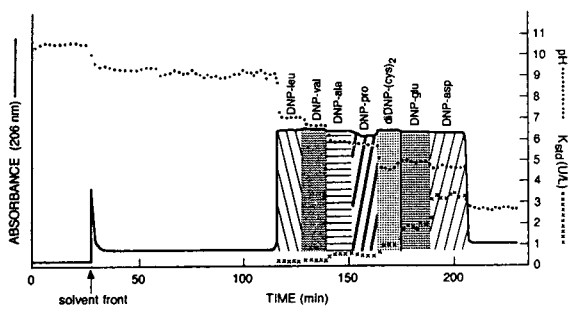

Fig. 2. Separation of seven DNP-amino acids by the present method. An abrupt change of the pH at each peak boundary suggests minimum overlap between neighboring zones while the partition coefficient values (K_{std}) indicate that each mixing zone is no more then several milliliters. Experimental conditions: apparatus: multilayer coil high-speed CCC centrifuge with a semipreparative column of 1.6 mm I.D. and 325 ml capacity; sample: seven DNP-amino acids as indicated in the chromatogram, each 100 mg dissolved in 10 ml of solvent consisting of 8 ml lower phase and 2 ml methyl *tert.*-butyl ether; solvent system: methyl *tert.*-butyl ether–water, 22 m*M* NH_3 in aqueous stationary phase (pH 10.53) and 10.8 m*M* TFA in organic mobile phase (pH 2.68); flow: 3.3 ml/min, tail to head elution mode; revolution: 600 rpm; stationary phase retention: 76.2% of total column capacity.

Partition coefficients of each fraction, however, revealed that it consisted of a series of narrow rectangular peaks with minimum overlap as observed in the reverse mode pH-zone-refining CCC [1–4]. Each component formed a pH plateau in a downward staircase fashion. Some irregularity of the pH level at the diDNP-$(Cys)_2$ peak may be due to its significantly lower pH in the organic mobile phase than that in the aqueous stationary phase.

A series of experiments has been performed to investigate effects of concentrations of displacer acid and retainer base on those of the eluted analytes. The effects of the TFA (displacer) concentration are shown in Fig. 3A where concentrations of three analytes (DNP-Leu, DNP-Ala and DNP-Asp) are plotted against those of the displacer acid (TFA) in the mobile phase. Concentrations of all analytes increase rather sharply as the TFA concentration increases. Concentrations of DNP-Leu and DNP-Ala are

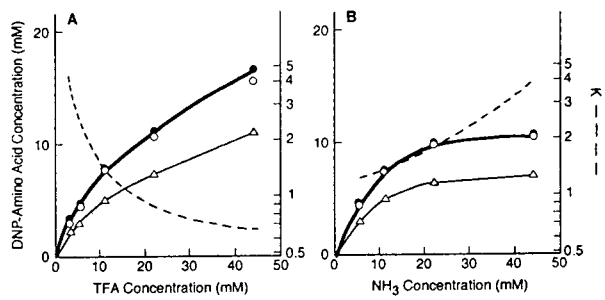

Fig. 3. Effects of displacer (TFA) (A) and retainer (NH_3) (B) on the concentration of DNP-amino acids and the partition coefficient (K) for TFA. Experimental conditions: apparatus: multilayer coil high-speed CCC centrifuge; column: 1.6 mm I.D. PTFE multilayer coil with 325 ml capacity; sample: DNP-Leu (○), DNP-Ala (●) and DNP-Asp (△), each 100 mg in 5 ml solvent consisting of 4 ml aqueous stationary phase and 1 ml methyl *tert.*-butyl ether; solvent system: methyl *tert.*-butyl ether–water, (A): NH_3 11 m*M* in aqueous stationary phase and TFA 2.7–43 m*M* in organic mobile phase; (B) TFA 10.8 m*M* in organic mobile phase and NH_3 5.5–44 m*M* in aqueous stationary phase; flow: 3.3 ml/min in tail to head elution mode; revolution: 600 rpm. K was determined from each chromatogram using the conventional formula: $K = (V - V_m)/V_s$ where V is the retention volume of the TFA border and V_m and V_s are the the volumes of the mobile and stationary phases in the column, respectively. Note that K values are equal for TFA and all solutes in each experiment (see text for more details).

almost identical while that of the divalent DNP-Asp is much less than those of the above monovalent acids. Fig. 3B similarly shows the effects of NH_3 (retainer) concentration in the stationary phase. Concentrations of all analytes sharply rise with the increased NH_3 concentration up to 22 m*M* where they show a tendency to saturate. Here again, concentrations of divalent DNP-Asp are much lower than those of other two monovalent acids.

In each diagram, concentrations of the monovalent acids (DNP-Leu and DNP-Ala) are approximated by a thick solid line which represents the ratio of the NH_3 concentration in the stationary phase to the partition coefficient of TFA (*K*) indicated by a dotted line. Since the partition coefficient of each analyte (K_s) is equal to that of the retainer TFA (*K*) as described elsewhere [3,4], the above result indicates that the concentration of each analyte in the retained stationary phase is mainly determined by the concentration of its ammonium counterion. The above result suggests that the concentration of a divalent acid may become one half the concentration of the monovalent acids to yield the 1:1 charge ratio to the ammonium counterion. The actual plots of the divalent acid (DNP-Asp), however, fall at about 2/3 times those of the monovalent acids as shown by thin solid lines. Similar results were also obtained in other divalent amino acids such as DNP-Glu and diDNP-$(Cys)_2$ indicating that the concentration of these divalent acids in the stationary phase can significantly exceed the 1:1 charge ratio to that of the ammonium counterion due to their relatively high polarities.

As in displacement chromatography and isotachophoresis, the spacers may be used to isolate particular components in pH-zone-refining CCC. In the present method, spacers can be introduced either in the sample solution or in the mobile phase. In the examples shown below, the two spacer organic acids, propionic acid and *n*-butyric acid, were chosen for separating DNP-Leu, DNP-Ala and DNP-Asp. Selection of the spacer acids was based on the results of preliminary experiments where various organic acids and DNP-amino acids were cochromatographed to investigate the order of their elution.

Fig. 4 shows separations of the three DNP-

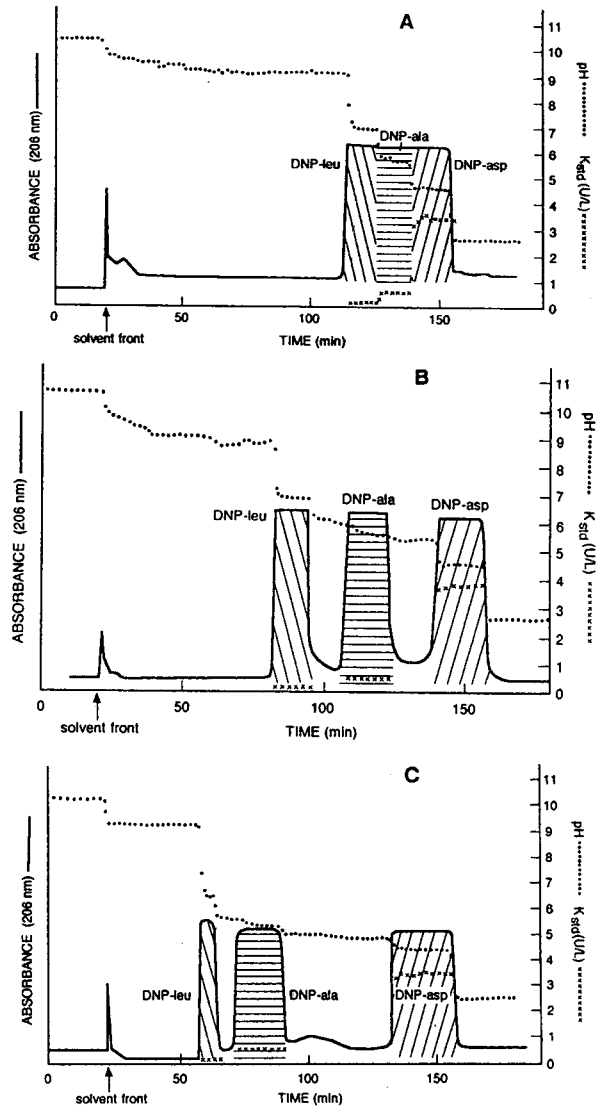

Fig. 4. Separation of DNP-amino acids with spacer acids. (A) Chromatogram obtained from the control run without spacer acids, (B) chromatogram obtained by adding the spacer acids in the sample solution, (C) chromatogram obtained by adding the spacer acid in the mobile phase. Experimental conditions: apparatus: multilayer coil high-speed CCC centrifuge; separation column: 1.6 mm I.D., 325 ml capacity; sample: DNP-Leu, DNP-Ala and DNP-Asp each 100 mg in 5 ml solvent (4 ml aqueous stationary phase and 1 ml methyl *tert.*-butyl ether); spacer acid: (A) none, (B) propionic acid and *n*-butyric acid each 50 μl in the sample solution, (C) propionic acid and *n*-butyric acid each 0.08% in the organic mobile phase; solvent system: methyl *tert.*-butyl ether, NH_3 22 m*M* in aqueous stationary phase, TFA 10.8 m*M* in organic mobile phase; flow: 3.3 ml/min, tail to head elution mode; revolution: 600 rpm.

amino acids without spacer acids (Fig. 4A), with the spacer acids in the sample solution (Fig. 4B) and with the spacer acids in the mobile phase (Fig. 4C). In Fig. 4A, three components were eluted as a single rectangular peak as shown in Fig. 2. When the spacer acids (each 50 μl) were introduced into the sample solution, DNP-amino acids were completely resolved into three rectangular peaks each corresponding to the single species as labeled in the chromatogram (Fig. 4B). In this case, the two spacers show similar widths and the original peak width for each component is preserved. When the same spacer acids were introduced into the mobile phase (each 0.08%), however, the width and the retention time of each peak were altered in such a way that the first peak became narrower and eluted much earlier while the third peak became much broader compared with those in Fig. 4A. The peak spacing also became different: the width between the first and the second peaks is much narrower than that between the second and the third peaks. These changes were mainly produced by a steady supply of the spacer acids through the mobile phase which increased the traveling rate of the front border of each spacer acid and the preceding solute band.

The above results indicate that for uniform spacing and preservation of the original peak width of each component the spacers should be introduced locally in the sample solution.

Fig. 5 shows the separation of three DNP-amino acids, each 0.5 g, obtained by the present method. The experiment was performed by methyl *tert.*-butyl ether–water system by adding NH_3 at 0.4% (44 m*M*) to the aqueous stationary phase and TFA at 0.8% (10.8 m*M*) to the organic mobile phase. The sample volume was 40 ml consisting of 30 ml acidified aqueous phase and 10 ml methyl *tert.*-butyl ether. A solution containing undissolved sample was thoroughly sonicated into a uniform suspension and introduced into the column without filtration. Under a flow-rate of 3.3 ml/min and a revolution speed of 600 rpm, the separation was completed in about 4 h. Three components were eluted as broad rectangular peaks with sharp boundaries as indicated by the abrupt transition of the

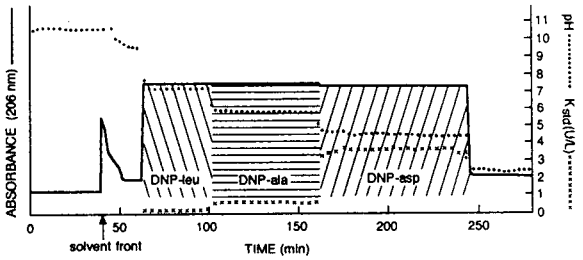

Fig. 5. Preparative separation of DNP-amino acids by the present method. Experimental conditions: apparatus: multilayer coil high-speed CCC centrifuge; column: 1.6 mm I.D. multilayer coil with 325 ml capacity; sample: DNP-Leu, DNP-Ala and DNP-Asp, each 0.5 g in 25 ml of solvent (20 ml aqueous stationary phase and 5 ml methyl *tert.*-butyl ether); solvent system: methyl *tert.*-butyl ether, NH_3 44 m*M* in aqueous mobile phase (pH 10.68), TFA 10.8 m*M* in organic stationary phase (pH 2.62); flow: 3.3 ml/min, tail to head elution mode; revolution: 600 rpm; retention of stationary phase: 51.3%.

partition coefficient (K) and pH levels plotted in the diagram.

5. Conclusions

The technique of pH-zone-refining CCC can be efficiently performed in the displacement mode to separate gram quantities of DNP-amino acids in a few hours. As in the reverse displacement mode, the method produces concentrated rectangular elution peaks with minimum overlap. As observed in displacement chromatography, a better yield and purity is realized as the sample size is increased [2]. The method can be used for separation of organic bases by adding a retainer acid such as HCl to the aqueous stationary phase and a displacer base such as triethylamine to the organic mobile phase.

Compared to the original reverse displacement mode of pH-zone-refining CCC, the displacement mode of operation results in salt-free organic fractions which are easily evaporated. The most important advantage of the displacement mode, however, derives from the fact that the retainer is permanently located within the column instead of being eluted. Consequently, the displacement mode is better adapted to a ligand-affinity separation. In this way, applica-

tions may be extended to cover the separation of non-ionizable compounds.

We believe that the displacement mode of the pH-zone-refining CCC technique will open a rich domain of applications in the preparative-scale separation.

6. Acknowledgement

The authors are indebted to Dr. Henry M. Fales for editing the manuscript with valuable suggestions.

7. References

[1] Y. Ito, K. Shinomiya, H.M. Fales, A. Weisz and A.L. Scher, presented at the *1993 Pittsburgh Conference and Exposition on Analytical Chemistry and Applied Spectroscopy, Atlanta, GA, March 8–12, 1993*, abstract 054P.

[2] A. Weisz, A.L. Scher, K. Shinomiya, H.M. Fales and Y. Ito, *J. Am. Chem. Soc.*, 116 (1994) 704.

[3] Y. Ito, K. Shinomiya, H.M. Fales, A. Weisz and A.L. Scher, *Countercurrent Chromatography (ACS Monographs)*, American Chemical Society, Washington, DC, submitted for publication.

[4] A.L. Scher and Y. Ito, *Countercurrent Chromatography (ACS Monographs)*, American Chemical Society, Washington, DC, submitted for publication.

[5] Y. Ito, in Y. Ito and W.D. Conway (Editors), *High-Speed Countercurrent Chromatography*, Wiley-Interscience, New York, in press.

[6] A. Weisz, K. Shinomiya and Y. Ito, presented at the *1993 Pittsburgh Conference and Exposition on Analytical Chemistry and Applied Spectroscopy, Atlanta, GA, March 8–12, 1993*, abstract 865.

[7] A. Weisz, D. Andrzejewski and Y. Ito, *J. Chromatogr. A.*, 658 (199) 505.

[8] A. Weisz, A.L. Scher, D. Andrzejewski, and Y. Ito, presented at the *10th International Symposium on Preparative Chromatography, Arlington, VA, June 14–16, 1993.*

[9] A. Weisz, D. Andrzejewski, R.J. Highet, and Y. Ito, *J. Chromatogr.*, 658 (1994) 505.

[10] A. Weisz, in Y. Ito and W.D. Conway (Editors), *High-Speed Countercurrent Chromatography*, Wiley-Interscience, New York, in press.

[11] Cs. Horváth, A. Nahum and J.H. Frenz, *J. Chromatogr.*, 218 (1981) 365.

[12] Y. Ito, in N.B. Mandava and Y. Ito (Editors), *Countercurrent Chromatography: Theory and Practice*, Marcel Dekker, New York, 1988, pp. 79–442.

ELSEVIER

Journal of Chromatography A, 672 (1994) 109–115

JOURNAL OF CHROMATOGRAPHY A

Comparison of the recovery of amino acids in vapour-phase hydrolysates of proteins performed in a Pico Tag work station and in a microwave hydrolysis system ☆

Enikö Tatár, Mohamed Khalifa, Gyula Záray, Ibolya Molnár-Perl*

Institute of Inorganic and Analytical Chemistry, L. Eötvös University, P.O. Box 32, H-1518 Budapest 112, Hungary

(First received August 23rd, 1993; revised manuscript received February 22nd, 1994)

Abstract

An exhaustive study was made to determine the amino acid composition of lysozyme in hydroysates performed in a CEM microwave oven under various conditions [0.621–0.827 MPa (90–120 p.s.i.g.) for 5, 10, 20 and 40 min], determined by HPLC as their phenylthiocarbamyl derivatives. The results showed that the CEM microwave hydrolysis system works reproducibly up to 0.689 MPa (100 p.s.i.g.) pressure only. Uniformly optimum parameters for all components present in hydrolysates were not found. The recoveries of the components at 0.621 MPa (90 p.s.i.g.) (after 20 and 40 min) and at 0.689 MPa (100 p.s.i.g.) (after 10 20 and 40 min) varied from 63 to 111%. The reproducibility of the measurements was <8.0% (relative standard deviation).

1. Introduction

Pioneering microwave hydrolyses have been achieved in cooking apparatus [1–4] and proved to be very promising; *e.g.*, for native and oxidized ribonuclease A and insulin B [1], after 5 min of microwave hydrolysis the recoveries of amino acids were the same as or higher than those obtained by the conventional method (6 *M* HCl, 110°C, 24 h).

Outstandingly high recoveries have been reported for microwave hydrolysed N-*tert.*-butoxycarbonyl (N-t-Boc) amino acid resin esters [2], with the only exception being N-t-Boc-leucine (97.6%). All the other amino acids provided 99.7–113.8% recoveries, with the exception of the serine derivative, the recovery of which was repeatedly 343%. However, pressure and temperature conditions were not reported [1,2]. Subsequently [3,4], hydrolyses of lysozyme performed with methanesulphonic acid + tryptamine [3-(2-aminoethyl)indole] and with hydrochloric acid provided favourable results, in both instances applying optimum conditions, *i.e.*, 160°C for 45 min for methanesulphonic acid + tryptamine [3] and 178–180°C for 4 min for 6 *M* HCl (the optimum temperature was tentatively estimated by the "indirect method" [4], conducting preliminary calibration of the microwave oven by use of several organic compounds with known melting points).

A special "microwave hydrolysis system" supplied with a capping station, a manifold, a

* Corresponding author.

☆ Presented at the *9th Danube Symposium on Chromatography, Budapest, August 23–27, 1993.* The proceedings of the symposium were published in *J. Chromatogr. A*, Vol. 668, No. 2 (1994).

0021-9673/94/$07.00
SSDI 0021-9673(94)00184-B

turntable with vials and a fibre-optic thermometer (for details see Experimental) was introduced by CEM in 1989 [5]. Originally [5], the vapour-phase microwave hydrolysis of methionyl human growth hormone was performed in the CEM apparatus at 178°C and 0.910 MPa (132 p.s.i.g.) for 8, 10 and 12 min. The results obtained [6] were poorer than those published previously [1–4]. Identical optimized hydrolysis conditions for all sixteen amino acids tested were not found. The maximum recoveries of the single components varied between 93 and 145%, depending on the experimental conditions used, with the exceptions of threonine and serine (93% and 77%, respectively).

On the other hand, the microwave technique showed beneficial effects in the hydrolysis of hydrophobic contact-containing peptides [7], although the recoveries of amino acids not involved in the hydrophobic linkages of the same peptides were not presented.

Special applications of microwave irradiation [8–10], such as its utilization in protein detection [8], in proline determination [9] and in the determination of the components of tripeptides [10] have been reported.

An increased hydrolysis time (2 and 4 h at 125°C) for a bovine serum albumin sample provided nearly theoretical amino acid yields [11]. However, such a large increase in hydrolysis time makes the application of the very expensive microwave technique questionable. In Hewlett-Packard application note [6], the traditional gas-phase hydrolysis (24 h at 110°C) was compared with fast gas-phase hydrolysis (90 min at 150°C) and microwave heating gas-phase hydrolysis (20–25 min at 150°C). The data obtained by the three methods for eleven peptides and proteins were in an excellent agreement, but reproducibility data were not reported.

Recently, a review has been published [12] outlining the possibilities of the microwave technique in analytical chemistry. It was stated that because of the few references available, researchers are hesitating to purchase this expensive apparatus.

Continuing our earlier studies (performed in order to optimize the determination of amino acids in protein hydrolysates as their phenylthiocarbamyl [PTC] derivatives by HPLC [13–18]), in this work we surveyed the diverse literature data with respect to the recovery of amino acids from microwave-hydrolysed proteins [1–2] and examined the impact of microwave hydrolysis on the composition of lysozyme as an example in comparison with what was obtained from hydrolyses [13–18] carried out in a Pico Tag work station system.

2. Experimental

2.1. Materials

Triethylamine (TEA), phenyl isothiocyanate (PITC), amino acids and proteins were obtained from Sigma (St. Louis, MO, USA) and Serva (Heidelberg, Germany). HPLC-grade acetonitrile and methanol were purchased from Reanal (Budapest, Hungary). All other reagents were of the highest purity available.

2.2. Apparatus

Hydrolyses were performed both in a Pico-Tag work station (Waters, Milford, MA, USA) (henceforth, work station) and in a CEM (Matthews, NC, USA) MDS-2000 microwave hydrolysis system, consisting of three major components, the vessel capping station, the vapour- and liquid-phase hydrolysis vessels and the turntable and valve panel for vacuum evacuation and nitrogen purging (henceforth, CEM hydrolysis system). The same hydrolysis and derivatization tubes (Waters) were used for both types of hydrolysis apparatus.

2.3. Hydrolysis of proteins

Lysozyme (0.014–0.016 g, weighed with analytical precision) was dissolved in 10 ml of 0.1 *M* HCl. Standards of free amino acids in a mixture containing 5 μmol/ml of each were prepared in 0.1 *M* HCl. Tryptamine was dissolved in distilled water (2 μg/μl). Into a 50 × 6 mm I.D. tube, 5 μl of amino acid solution or 20 μl of lysozyme

solution were injected and 15 μl of tryptamine stock solution were added to each. Twelve tubes were placed in a Waters vacuum vial. The vial was then attached to the work station manifold and the solvent removed under vacuum. After drying, the vacuum was released and the samples were ready for hydrolyses.

Hydrolyses which serve as the basis of comparison were carried out in the work station at 145°C for 4 h, as described previously [16,17]. In the microwave hydrolyses, four tubes were hydrolysed simultaneously in three vessels, using the same procedure (at the same pressure and temperature). Of the four vessels available (in order to have four parallel hydrolysis tests), two tubes were placed in one vessel and 1-1 tube in the two others. The fourth vessel was reserved for the fibre-optic thermometer. Hydrolyses were performed in the presence of 5 and 10 ml of distilled HCl, poured into all four vessels. After sealing the vessels by means of the electronic capping station and connecting them with the turntable to the apparatus (both to the fibre-optic thermometer and to the valve panel), the vessels were evacuated and purged with nitrogen five times in succession.

Microwave hydrolyses were carried out at 0.621 MPa (90 p.s.i.g.) and 0.689 MPa (100 p.s.i.g.) for 5, 10, 20 and 40 min, and at 0.758 MPa (110 p.s.i.g.) and 0.827 MPa (120 p.s.i.g.) for various reaction times (0–20 min). The hydrolysed sample-containing tubes (after releasing the caps of the vessels with the help of the capping station) were wiped from the outside and were transferred into reaction vials of the work station. The vials were attached to the manifold and dried to a constant minimum reading [*ca.* 65 mTorr (8.65 Pa)]. The hydrolysed samples were then ready for derivatization.

2.4. Derivatization of amino acids with PITC

Free amino acids and hydrolysed proteins, previously dried under vacuum, were re-dried after adding 10 μl of ethanol–water–TEA (2:2:1) to each tube. Thereafter, to each re-dried sample, 20 μl of derivatization reagent [ethanol–TEA–H_2O–PITC (7:1:1:1)] were added and vortex mixed. The test-tubes containing derivatized samples were then transferred to the reaction vials, installed in the work station, evaporated to a minimum reading of *ca.* 65 mTorr and held at this constant reading for 20 min.

The derivatized standards were dissolved by stepped addition of 50 μl of acetonitrile, 50 μl of H_2O and 500 μl of 0.05 *M* sodium acetate solution (pH 7.2); 20-μl aliquots of standards contained *ca.* 1700 pmol of each amino acid.

2.5. Chromatography

The system used was a Liquochrom Model 2010 liquid chromatograph (Labor MIM, Budapest, Hungary) which consisted of a two-Liquopump 312/1 solvent-delivery system and a Type OE-308 UV detector with a wavelength range of 195–440 nm. Samples were injected in 20-μl volumes using an injector supplied by Labor MIM. The 150 mm × 4.0 mm I.D. columns (BST, Budapest, Hungary) contained Hypersil ODS bonded phase (5 μm) (Shandon, Runcorn, UK). Eluents we kept under a blanket of nitrogen. The solvent system consisted of two eluents: (A) 0.05 *M* sodium acetate (pH 7.2) and (B) 0.1 *M* sodium acetate–acetonitrile–methanol (46:44:10, v/v/v) titrated with glacial acetic acid or 50% sodium hydroxide to pH 7.2. The gradient, which was optimized for the separation, was from 0 to 100% B in 22 min, then 5 min with 100% B, followed by 2 min with 100% A. After an additional 3 min, elution with solvent A was performed. Thereafter the system was ready for the next injection.

3. Results and discussion

3.1. Microwave parameters

Advances in the HPLC determination of amino acids in protein hydrolysates now ensure rapid derivatization and elution procedures and the rate-limiting step in amino acid analysis remains the hydrolysis. Therefore, a need exists to speed up the hydrolysis step in protein analysis.

A shortened time (4 h at 160°C) for liquid-phase hydrolyses was introduced by Gehrke *et al.* [19], and a useful vapour-phase technique (4 h at 145°C) is offered by Waters (work station) [20]. Both of these possibilities provided the same values for amino acid components as the classical liquid-phase procedure (6 *M* HCl, 24 h, 110°C). Recently we demonstrated [17] that by means of the work station the same recovery can be obtained for all essential amino acids, also under milder conditions (145°C for 2 h and 125°C for 5 h).

From our detailed experience with the work station [13–17], we intended to start with probably the most advantageous microwave conditions proposed for the CEM hydrolysis system, *i.e.*, with the shortest hydrolysis time, which means also with the highest pressure [0.827 MPa (120 p.s.i.g.)], as advised in the manual [21]. The power applied was 650 W throughout.

At the beginning of our experiments with the CEM station, we attempted to work with the shortest possible time and at the highest pressure [0.827 MPa (120 p.s.i.g.)] However, of the four hydrolysis flasks supplied with the apparatus, only one was tight enough to withstand this pressure. The producer states [22] that it is not possible to operate the CEM station at maximum pressure, *i.e.*, above 0.621 MPa (91 p.s.i.g.). Therefore, remaining on the safe side, our investigations were performed at constant pressures, *i.e.*, at 0.621 and 0.689 MPa (90 and 100 p.s.i.g.) for different hydrolysis times (under the latter conditions the CEM hydrolysis system works excellently).

3.2. Microwave hydrolysis and recovery study

Lysozyme (see also refs. 15–17) was used as a standard protein. The results obtained were compared with the data provided by the work station applying vapour-phase hydrolysis for 4 h at 145°C (Table 1, values in braces). The following conclusions can be drawn.

(1) General optimum conditions applicable to all amino acids apparently cannot be established and the laboratory routine will always be some sort of compromise.

(2) In accordance also with literature data [4,11], the yields of threonine, cyst(e)ine, isoleucine, valine and tryptophan were lower than the values of the reference methods under all conditions tested.

(3) Nearly the theoretical recovery could be obtained for serine, in order of listing, at 0.621 and 0.689 MPa (90 and 100 p.s.i.g.) for 10 and 5 min, similar to that reported at 180°C for 4 min (pressure not given) [4]. After longer hydrolysis times (40, 40 and 20 min), even under mild conditions at 0.621, 0.689 and 0.379 MPa (90, 100 and 55 p.s.i.g.), considerable losess of serine were observed, 15, 27 and 10% [17], respectively.

(4) The recovery of histidine is usually high, being 175% at 180°C after 4 min [4]. According to our data, the histidine recovery increases with increasing pressure and hydrolysis time at 0.621 MPa (90 p.s.i.g.) (55, 86, 83 and 100%) and at 0.621 MPa (100 p.s.i.g.) (90, 96, 100 and 104%), respectively (see Table 1).

(5) Tyrosine proved to be very sensitive to the hydrolysis conditions: (i) at 180°C after 4 min only an 80% recovery was reported [10], whereas (ii) according to our results at 0.621 MPa (90 p.s.i.g.) the cleavage of its peptide bond needed at least 10 min.

(6) Regarding the expected amount of lysine, the cleavage of its peptide bond needs stronger conditions: at 0.621 MPa (90 p.s.i.g.) after only 40 min and at 0.689 MPa (100 p.s.i.g) after any hydrolysis time the amount of lysine proved to be satisfactory. The reported [10] 119% yield at 180°C after 4 min is unlikely, to our knowledge.

(7) The recoveries of the rest of amino acids, are within acceptable experimental error.

3.3. Reproducibility

The microwave parameters proved to be highly reproducible: working at constant pressures the chosen values were reached in 2.0–2.5 min, and during the period of the hydrolyses the temperature at 0.621 ± 0.02 MPa (90 ± 3 p.s.i.g.) varied between 152 and 157°C (Fig. 1a), and at 0.689 ± 0.02 MPa (100 ± 3 p.s.i.g.) between 154 and 157°C (Fig. 1b). In our system, at 0.379 MPa

Table 1
Recovery of amino acids from microwave hydrolysate of lysozyme obtained under different conditions

Conditions			Amino acid (%)[a]																	
Pressure (MPa) (p.s.i.g.)	Time (min)	Reproducibility	Aspartic acid	Glutamic acid	Serine	Glycine	Histidine	Threonine	Alanine	Proline	Arginine	Tyrosine	Valine	Methionine	Cyst(e)ine	Isoleucine	Leucine	Phenylalanine	Tryptophan	Lysine
			(20) {18.0}	(5) {5.0}	(18) {6.6}	(12) {10.1}	(1) {1.0}	(7) {5.2}	(12) {12.6}	(2) {2.0}	(11) {9.0}	(3) {2.9}	(6) {4.9}	(2) {1.9}	(8) {8.9}	(6) {4.7}	(8) {7.5}	(3) {2.5}	(6) {5.1}	(6) {6.6}
0.621	5	*A*	79	84	84	92	55	53	73	73	60	69	39	83	53	70	82	43	53	66
(90)		S.D.	1.2	6.3	1.5	2.7	3.2	2.0	3.6	6.1	4.3	5.0	3.6	4.0	4.5	2.7	1.3	4.9	2.5	3.9
		R.S.D. (%)	1.5	7.6	1.8	2.9	5.8	3.7	4.3	8.4	7.2	7.2	9.2	4.8	8.5	3.9	1.6	11.4	4.7	5.9
0.621	10	*A*	95	82	103	105	86	88	104	105	93	95	70	98	66	86	97	68	83	87
(90)		S.D.	0.73	5.5	1.8	3.0	5.7	2.1	1.0	7.8	1.7	1.1	3.5	10.3	10.8	2.6	1.4	9.8	10.7	13.9
		R.S.D. (%)	0.8	6.7	1.7	2.9	6.6	2.3	1.0	7.4	1.8	1.2	5.0	10.5	16.4	3.0	1.4	14.4	12.9	16
0.621	20	*A*	108	75	96	110	83	93	99	98	98	100	68	102	90	92	94	63	92	86
(90)		S.D.	0.5	4.7	1.6	1.9	5.8	2.1	1.9	0.3	1.3	6.0	6.1	2.6	6.3	1.8	2.4	12.6	3.0	1.0
		R.S.D. (%)	0.5	6.7	1.7	1.7	7.0	2.3	1.9	3.3	1.3	6.0	8.9	2.5	7.0	2.0	2.5	2.0	3.3	1.2
0.621	40	*A*	80	105	85	105	100	78	97	96	101	94	82	96	81	97	100	76	79	100
(90)		S.D.	2.6	4.7	2.4	1.4	1.1	8.6	0.4	1.1	0.6	4.1	6.2	6.0	5.8	1.5	0.3	4.6	4.8	3.4
		R.S.D. (%)	3.2	4.7	2.8	1.3	1.1	1.1	0.4	1.1	0.6	4.4	7.5	7.3	7.2	1.5	0.3	6.0	6.1	3.4
0.689	5	*A*	84	85	106	87	94	86	85	85	86	115	60	105	71	64	82	95	85	100
(100)		S.D.	13.9	6.5	14.8	4.0	1.4	12.2	2.0	5.9	5.1	7.9	0.5	5.7	15.2	1.3	1.2	5.5	12.2	4.8
		R.S.D. (%)	16.6	7.7	14.0	4.6	1.5	14.2	2.4	6.9	5.9	6.9	0.9	5.4	21.4	0.2	1.5	5.8	14.4	4.8
0.689	10	*A*	86	90	95	98	96	77	106	100	85	97	75	92	73	78	89	111	80	101
(100)		S.D.	0.39	2.0	2.1	0.7	4.0	1.2	0.8	2.0	1.5	3.9	3.2	5.3	2.9	2.3	1.3	5.9	5.8	2.2
		R.S.D. (%)	0.45	2.2	2.2	0.7	4.2	1.5	0.8	2.0	1.8	3.9	4.2	5.8	4.0	3.0	1.5	5.3	7.3	2.2
0.689	20	*A*	92	95	84	98	100	77	108	100	89	93	88	93	95	85	105	110	67	99
(100)		S.D.	2.6	5.6	3.4	1.4	2.0	4.2	5.2	3.7	1.2	5.9	4.8	6.7	5.5	4.8	2.5	4.6	5.4	3.2
		R.S.D. (%)	2.8	5.9	4.0	1.4	2.0	0.54	4.8	3.7	1.4	6.3	5.4	7.2	5.8	5.7	2.4	4.2	8.0	3.2
0.689	40	*A*	95	101	73	101	104	76	108	100	96	95	98	92	88	94	104	112	63	102
(100)		S.D.	4.7	3.6	2.3	4.2	4.4	1.6	4.3	7.7	2.8	3.8	4.5	6.9	4.6	4.5	3.3	3.6	4.7	4.7
		R.S.D. (%)	4.9	3.6	3.1	4.2	4.2	2.2	4.0	7.7	2.9	4.0	4.6	7.5	5.2	4.8	3.2	3.2	7.4	4.6
Literature values		Ref.																		
n.m.	4	10	92	88	102	94	175	100	100	n.m.	91	80	98	105	92	104	89	104	n.m.	119
0.379(55)	20	17	100	102	90	93	100	90	100	91	93	110	87	95	93	93	99	97	n.m.	87

[a] Expressed as percentages of data obtained from hydrolyses performed in the work station values, in parentheses, literature values given in ref. 19; values in braces, values of lysozyme components expressed in pmol; these serve as the basis of comparison. *A* = Averages of four separate hydrolyses performed in three vials; S.D. = standard deviation; R.S.D. = relative standard deviation; n.m. = not measured.

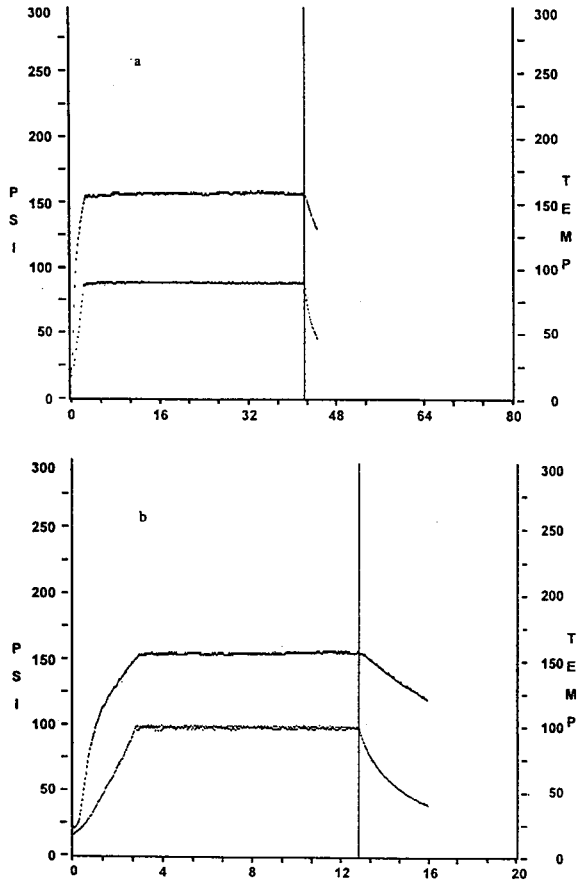

Fig. 1. Variation of temperature (upper curve) and pressure (lower curve) for a microwave hydrolysis system operating at (a) 0.621 MPa (90 p.s.i.g.) and (b) 0.689 MPa (100 p.s.i.g.). The traces are the original curves given by the CEM apparatus, *i.e.*, values on the abscissa are the hydrolysis time in minutes, and on the ordinate both the temperature (in °C) and the pressure (in p.s.i.) are presented.

(55 p.s.i.g.) the temperature did not exceed 125°C (Fig. 1a and b), in spite of the fact that strictly the same parameters as reported in ref. 11 were followed.

Generally, the reproducibility, characterized by the relative standard deviation (R.S.D.) (Table 1), is higher than in previous experiments [13–17]. In the case of microwave-hydrolysed lysozyme, the highest error can be attributed mainly to incomplete hydrolysis [tests performed at 0.621 MPa (90 p.s.i.g.) for 5 and 10 min and at 0.689 MPa (100 p.s.i.g.) for 5 min, and also for all values for phenylalanine]. Regarding the other data, the reproducibility of these measurements proved to be <8.0% (R.S.D.).

4. Conclusions

The microwave irradiation procedure shortened the hydrolysis time of lysozyme considerably. As optimum hydrolysis conditions could not be defined uniformly for all essential amino acids, we suggest its use in the following cases: (1) the sample to be hydrolysed contains a limited and known number of peptide bonds (mainly synthetic short-chain peptides); the optimization of the conditions seems to be easier than for natural proteins and/or protein matrices; and (2) the microwave apparatus is needed also for other purposes, or the samples to be hydrolysed require the entire capacity of the apparatus.

Acknowledgement

This work was supported by the Hungarian Academy of Sciences (Project Numbers OTKA I/3 2284 and I/4 T5053).

References

[1] S.T. Chen, S.H. Chiou, Y.H. Chu and K.T. Wang, *Int. J. Pept. Protein Res.*, 30 (1987) 572.
[2] H.M. Yu, S.T. Chen, S.H. Chiou and K.T. Wang, *J. Chromatogr.*, 456 (1988) 357.
[3] S.H. Chiou and K.T. Wang, *J. Chromatogr.*, 448 (1988) 404.
[4] S.H. Chiou and K.T. Wang, *J. Chromatogr.*, 491 (1989) 424.
[5] C. Woodward, L.B. Gilman and W.G. Englehart, *Int. Lab.*, 20 (1990) 40.
[6] R. Grimm, *Hewlett-Packard Publication Number 1-5091-4585E*, Hewlett-Packard, Avondale, PA, 1992.
[7] L.B. Gilman and C. Woodward, in *Current Research in Protein Chemistry*, Vol. 23, Academic Press, New York, 1990, p. 13.
[8] H. Engelhardt, M. Kramer and H. Waldhoff, *Chromatographia*, 30 (1990) 523.

[9] K. Kolar and H. Berg, in *Meat and Meat Products*; *Publication 1990-04-17 KK Ba K 0924a*, Swedish Meat Research Institute, 1990.
[10] A. Pecavar, M. Prosek, D.F. Temeljotov and J. Marsel, *Chromatographia*, 30 (1990) 159.
[11] S.A. Margolis, L. Jassie and H.M. Kingston, *J. Autom. Chem.*, 13 (1991) 93.
[12] A. Sinquin, T. Görner and E. Dellacherie, *Analusis*, 21 (1993) 1.
[13] M. Morvai, V. Fábián and I. Molnár-Perl, *J. Chromatogr.*, 600 (1992) 87.
[14] I. Molnár-Perl and M. Morvai, *Chromatographia*, 34 (1992) 132.
[15] I. Molnár-Perl, M. Pintér-Szakács, M. Morvai and V. Fábián, in I. Ishiguro, R. Kido, T. Nagatsu, Y. Nagamura and Y. Ohta (Editors), *Advances in Tryptophan Research 1992*, Fujita Health University Press, Toyoake, 1993, pp. 195–198.
[16] I. Molnár-Perl, M. Pintér-Szakács and M. Khalifa, *J. Chromatogr.*, 632 (1993) 57.
[17] I. Molnár-Perl and M. Khalifa, *Chromatographia*, 36 (1993) 43.
[18] I. Molnár-Perl, *J. Chromatogr.*, 661 (1994) 43.
[19] C.W. Gehrke, L.L. Wall, J.S. Absheer, F.E. Kaiser and R.W. Zumwalt, *J. Assoc. Off. Anal. Chem.*, 68 (1985) 811.
[20] *Pico Tag Work Station Operator's Manual*, Manual Number 86746, Revision C, Waters, Milford, MA, 1988.
[21] W.G. Engelhart, personal communication.
[22] *Installation and Operation Manual: Microwave Sample Preparation System MD-S 2100*, CEM, Matthews, NC, 1991, p. IV-14-24.

ELSEVIER

Journal of Chromatography A, 672 (1994) 117–124

JOURNAL OF CHROMATOGRAPHY A

High-performance liquid chromatographic method for the analysis of aminocarb, mexacarbate and some of their N-methylcarbamate metabolites by post-column derivatization with fluorescence detection

K.M.S. Sundaram*, J. Curry

Forestry Canada, Forest Pest Management Institute, P.O. Box 490, 1219 Queen Street East, Sault Ste. Marie, Ontario P6A 5M7, Canada

(First received July 13th, 1993; revised manuscript received February 3rd, 1994)

Abstract

A sensitive and selective high-performance liquid chromatographic method with post-column derivatization, using *o*-phthalaldehyde and 2-mercaptoethanol, is described for the analysis of aminocarb, mexacarbate and some of their carbamate metabolites. The separation system consisted of an RP-8 OS (10 μm) 20 cm × 4.6 mm I.D. column, an acetonitrile–water mobile system and a reactor for the hydrolysis of analytes from column effluents and fluorophore formation. The fluorophores were detected at 230 nm (excitation) and 418 nm (emission). The recoveries of the carbamates in spiked natural water at 2 and 20 ng/ml fortification levels ranged from 72.0 to 98.4% with relative standard deviations of 5.0 to 11.5%. The recoveries for spiked forest soil at 20 and 200 ng/g fortification levels ranged from 74.1 to 97.6% with relative standard deviations of 5.8 to 10.7%. Limits of detection and quantification for all the analytes were 0.1 and 0.4 ng in water and soil, respectively.

1. Introduction

Aminocarb (4-dimethylamino-3-methylphenyl N-methylcarbamate, trade name Matacil; Mobay, Kansas City, MO, USA) and mexacarbate (4-dimethylamino-3,5-xylyl N-methylcarbamate, trade name Zectran; Union Carbide Agricultural Products, Research Triangle Park, NC, USA) are highly effective broad-spectrum commercial insecticides derived from carbamic acid. Aminocarb has been one of the principal insecticides used aerially in eastern Canada since 1975 against the spruce budworm, *Choristoneura fumiferana* (Clemens), a destructive defoliator of conifers. Mexacarbate has been used off and on in experimental aerial spray programs since 1969. The two carbamates degrade initially with the carbamate moiety intact when applied to foliar surfaces [1]. Some of these degradation products, such as 4-methylamino, 4-methylformamido, 4-amino and 4-formamido analogues, like the parent materials, are toxic [1–3] causing concern to regulatory and scientific communities.

To evaluate the potential hazard from the use of aminocarb and mexacarbate, it is necessary to know their fate in different forest matrices. This requires sensitive, efficient and reliable analytical methods to determine the parent materials and

* Corresponding author.

0021-9673/94/$07.00
SSDI 0021-9673(94)00151-X

their degradation products. Numerous gas–liquid (GLC) and high-pressure liquid chromatographic (HPLC) methods have been described for the analysis of carbamate residues in a variety of agricultural matrices [4–6]. However, the preferred method for the analysis of aminocarb and mexacarbate from forestry matrices is by GLC [7] and for mexacarbate and its metabolites by HPLC–UV detection [8]. Drawbacks of the GLC method are the laborious cleanup and partition procedures involved, while disadvantages of the HPLC method include its insensitivity for all the analyte–matrix combinations studied. Moye *et al.* [9] introduced HPLC–fluorescence for the detection of fluorophores following post-column derivatization (PCD). Krause [10–14] refined the method and Engelhardt and Lillig [15] optimized the procedure, making it a sensitive and selective approach with widespread acceptance for the analysis of N-methylcarbamate residues.

The purpose of this study was to extend these techniques to develop an expeditious and sensitive method to quantify aminocarb, mexacarbate and their carbamate metabolites that are likely to be formed (Table 1) in natural waters and forest soil, which are the major receptors of aerially sprayed insecticides. The analytes, after elution through the HPLC system, were hydrolysed by aqueous sodium hydroxide, then the primary amines were derivatized forming the highly fluorescent isoindole derivative (Fig. 1), using *o*-phthalaldehyde (OPA) and 2-mercaptoethanol (MCE), and their fluorescence was measured by the on-line detector (Fig. 2). The method was used to examine its applicability to quantify the analytes in natural water and forest soil after necessary fortification, extraction, cleanup and derivatization steps.

2. Experimental

2.1. Reagents

Analytical-grade standards of aminocarb and four of its metabolites were supplied by Mobay, while mexacarbate and four of its metabolites were supplied by Union Carbide Agricultural Products. The common and chemical names

Table 1
List of aminocarb and mexacarbate and their carbamate metabolites used in the study

Designation	Chemical name	Abbreviation
Aminocarb	4-Dimethylamino-3-methylphenyl N-methylcarbamate	A
Methylformamido aminocarb	4-Methylformamido-3-methylphenyl N-methylcarbamate	MFA
Methylamino aminocarb	4-Methylamino-3-methylphenyl N-methylcarbamate	MA
Formamido aminocarb	4-Formamido-3-methylphenyl N-methylcarbamate	FA
Amino aminocarb	4-Amino-3-methylphenyl N-methylcarbamate	AA
Mexacarbate	4-Dimethylamino-3,5-xylyl N-methylcarbamate	M
Methylformamido mexacarbate	4-Methylformamido-3,5-xylyl N-methylcarbamate	MFM
Methylamino mexacarbate	4-Methylamino-3,5-xylyl N-methylcarbamate	MAM
Formamido mexacarbate	4-Formamido-3,5-xylyl N-methylcarbamate	FM
Amino mexacarbate	4-Amino-3,5-xylyl N-methylcarbamate	AM

HYDROLYSIS

$$RO\text{-}CO\text{-}NH\text{-}CH_3 \xrightarrow[95°C]{NaOH} R\text{-}OH + CH_3\text{-}NH_2 + CO_3^{2-}$$

Monomethylcarbamate

FLUOROPHORE

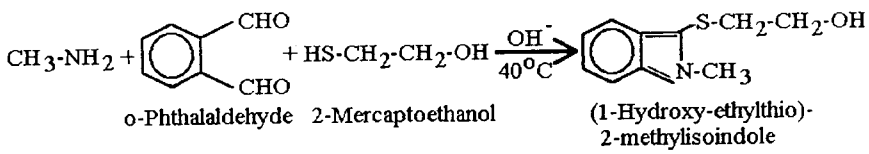

o-Phthalaldehyde 2-Mercaptoethanol (1-Hydroxy-ethylthio)-2-methylisoindole

Fig. 1. Reaction scheme of post-column derivatization.

(IUPAC) and the abbreviations used for each are listed in Table 1. All analytical standards were greater than 98.5% pure and stored at −20°C in sealed vials until use.

Methanol, ethyl acetate, *n*-hexane, acetonitrile and water were HPLC grade and obtained from J.T. Baker, through Baxter (Canlab Division), Mississauga, Canada. Alumina (activity 1, type WN-6 neutral) was from Sigma, Mississauga, Canada. OPA and MCE were obtained from BDH, Toronto, Canada. Analytical-grade sodium hydroxide, sodium sulphate (anhydrous, granular) and boric acid were obtained from Fisher Scientific, Don Mills, Canada.

Borate buffer (pH 10.4) was prepared by dissolving 12.4 g of boric acid in 1 l of water and adjusting the pH to 10.4 by adding 2 *M* NaOH. The derivatization reagent was prepared first by dissolving 160 mg OPA in 2 ml methanol and then adding 0.10 ml of MCE followed by 200 ml of borate buffer. The solution was mixed well and filtered through a 0.45-μm membrane filter (product No. 66068, Gelman Sciences, Rexdale, Canada) and stored at 4°C. The hydrolysis reagent (0.05 *M* NaOH) was prepared by dissolving 2.0 g of sodium hydroxide in 1 l of solution, filtering through a 0.45-μm membrane filter and degassing with helium. Natural stream water (pH 6.2, hardness 16 μg $CaCO_3$/ml, alkalinity 10.2 μg $CaCO_3$/ml, conductivity 2.7 μS) was col-

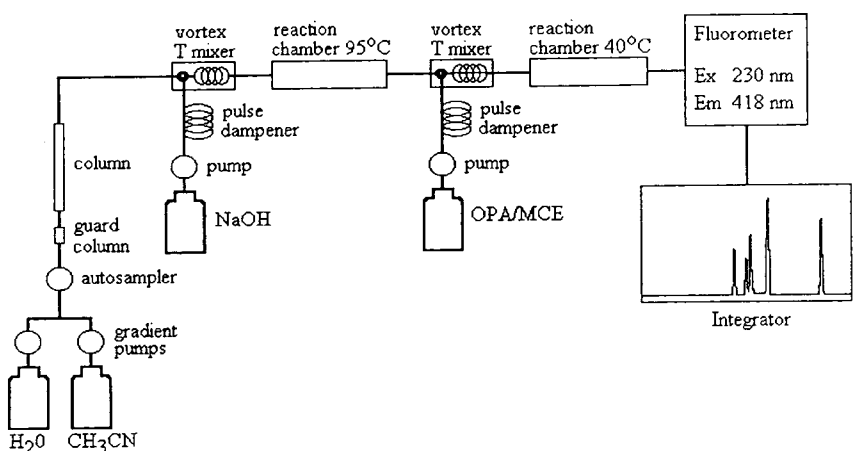

Fig. 2. HPLC post-column fluorometric system.

lected from the Icewater Creek near Searchmont, Ontario, Canada, filtered through a 5-μm filter and stored at 4°C until use. Forest soil (organic matter 3.9%, sand 51%, silt 42%, clay 7% and pH 5.91) was collected from the same area. It was sieved (2 mm opening) to remove stones, root pieces, etc., and stored in glass jars at −20°C until use.

Standard stock solutions (50 ml) of each analyte noted in Table 1 were prepared separately in amber-coloured volumetric flasks by dissolving 10 mg of the material in acetonitrile. Standard working solutions were prepared by diluting aliquots of each stock solution with acetonitrile to give concentrations ranging from 0.5 to 500 ng/ml. Similarly, mixed standards of the parent compounds, aminocarb and mexacarbate, together with their four respective metabolites, were prepared separately by mixing aliquot quantities of the individual standard stock solutions, so that the concentrations of each analyte in the mixed standards ranged from 0.5 to 500 ng/ml. Unless used immediately, the solutions were stored at −20°C.

2.2. Apparatus

A Hewlett-Packard (HP) 1084B HPLC system was interfaced with a HP 79842A variable-volume injector and autosampler (Model 79842). The instrument also incorporated an automatic degassing system and two dual-head reciprocating solvent-delivery systems controlled by a solvent flow programmer to give stable, reproducible flows. A prepacked HP RP-8 OS (10 μm) stainless-steel separation column (20 cm × 4.6 mm I.D.) was used in conjunction with a HP RP-8 guard column (3 cm × 4.6 mm I.D., 10 μm). The column temperature was kept at 30°C to maintain retention time reproducibility. The fluorescence detector was a Kratos (Ramsey, NJ, USA) FS970 LC fluorometer equipped with a 10-μl flow-cell and automatic overload reset (FSA 986) with variable excitation wavelengths (GM 970 monochromator) and fixed-wavelength emission filters. The derivatization was done in a Kratos URS 051 post-column reaction system (PCRS) equipped with two reagent pumps, hydrolysis and reaction coils and a URA 200 temperature controller. The detector signal was recorded and processed with a HP data module (Model 79850B), which provided the chromatogram, area, retention time, etc., for each peak. Additional operating parameters were: mobile phase: acetonitrile–water; flow-rate: 1.0 ml/min; injection volume: 100 μl; run time: 60 min; gradient [% (v/v) acetonitrile]: 0 min 0%, 25 min 30%, 35 min 50%, 45 min 50%, 55 min 0%; derivatization: hydrolysis: 0.5 ml NaOH/min, hydrolysis coil 1 ml, temperature 95°C, fluorophore: 0.3 ml OPA–MCE/min, reaction coil 0.5 ml, temperature 40°C; detection: excitation 230 nm, emission 418 nm.

2.3. Evaluation

To evaluate sensitivity, standard solutions of aminocarb and mexacarbate containing their respective metabolites were injected separately several times ($n > 6$) to obtain reproducible peak area measurements under the PCD conditions mentioned previously. Individual standards were used for the FA and AA metabolites of aminocarb, because of poor chromatographic separation (see section 3). The relative standard deviation (R.S.D.) between injections ranged from 1.1 to 4.1% depending on the type of analyte. Similarly, replicate analysis of mixed standards (except FA and AA) at four-day intervals gave good reproducibility (average R.S.D. < 4%).

2.4. Recovery studies from natural water

To study the recovery of the analytes, 100-ml aliquots of natural stream water were fortified in triplicate with mixed standards of aminocarb and mexacarbate, and their respective metabolites, to yield concentrations of 2 and 20 ng/ml of each analyte. Due to co-elution of FA and AA on the HPLC column, water samples were fortified with these metabolites separately to assess the recovery efficiencies for these compounds. Each fortified water sample was serially extracted

using 3 × 40 ml of dichloromethane. The organic layer was dried with anhydrous sodium sulphate and flash-evaporated to dryness at 30°C. The residue, after flash-evaporation, was dissolved in 30 ml of acetonitrile and partitioned twice with 10 ml of hexane each time. The polar layer was flash-evaporated to dryness, dissolved in ethyl acetate, transferred to a graduated centrifuge tube and the volume was adjusted to 10 ml by evaporation under a stream of pure, dry nitrogen. A 1-ml volume of the crude extract was loaded onto an alumina minicolumn (1 g Al_2O_3 sandwiched between 0.5-cm thick layers of anhydrous sodium sulphate in a glass wool-plugged disposable Pasteur pipette, 14.5 cm × 7.5 mm I.D., preconditioned with 10 ml of ethyl acetate). Commercially available solid-phase extraction cartridges containing Al_2O_3 (PrepSep extraction columns, Fisher Scientific, Unionville, Canada) were found to be equally suitable for the cleanup, except for the high cost involved in analyzing large numbers of samples, normally expected following a spray application. The analytes were eluted with 15 ml of ethyl acetate, with the exception of the aldehyde moieties (MFA, FA, MFM and FM), which required an additional 10 ml of polar-modified eluent containing 10% (v/v) methanol. The eluates were evaporated to dryness and recovered in 1 ml of acetonitrile for HPLC analysis. Recovery levels of the analytes in water were determined by injecting aliquots of analytical solutions and comparing the peak areas with those of the standard solutions.

2.5. Recovery studies from forest soil

To study the recoveries of the analytes in soil, 10-g aliquots were fortified in triplicate to give 20 and 200 ng/g of each analyte. Each sample was extracted (Sorval Omni-Mixer; Ivan Sorval, Norwalk, CT, USA) thrice using 50 ml ethyl acetate each time. After passing through a column of anhydrous sodium sulfate (3 × 2.5 cm), the ethyl acetate was flash-evaporated to dryness at 30°C. The remaining cleanup and recovery determinations were similar to water.

3. Results and discussion

3.1. Optimization of chromatographic response

Attempts to alter the excitation and emission wavelengths to optimize sensitivity were not successful. In particular, longer excitation wavelengths resulted in considerable sensitivity reductions for all of the analytes. The use of a methanol–water gradient system did not distinctly resolve all of the peaks and the sensitivity was lower compared to the acetonitrile–water mobile phase. Also, efforts to optimize the post-column reaction conditions by adjusting the molarity of sodium hydroxide used in hydrolysis, temperature of the reactor etc. did not enhance sensitivity or resolution of the compounds.

3.2. Linearity of the detector and detection limit

Linearity of the fluorescence detector was determined by 100-μl injections of serially diluted standards of both insecticides and their metabolites in the range of 0.5 to 500 ng/ml. Peak areas were integrated electronically and plotted against concentration. Regression analysis of the data indicated linearity of the detector from 0.1 to 50 ng for all the analytes and correlation coefficients ranged from 0.981 to 1.00 depending on the type of analyte. These results illustrate that PCD with fluorescence detection is a very sensitive technique and can be used to detect and quantify the analytes in Table 1.

3.3. Chromatograms of the mixed standards

Figs. 3 and 4 illustrate the chromatographic separations obtained respectively for the mixed standards of aminocarb and its four metabolites and mexacarbate and its four metabolites. Mean retention times (min) of each individual compound (six determinations) are given in the caption of each figure. The variation in retention time was less than 2% for all the analytes. The separation of FA and AA (Fig. 3) was not possible under any of the experimental conditions tested. Altering experimental variables, such as mobile phase composition, solvent sys-

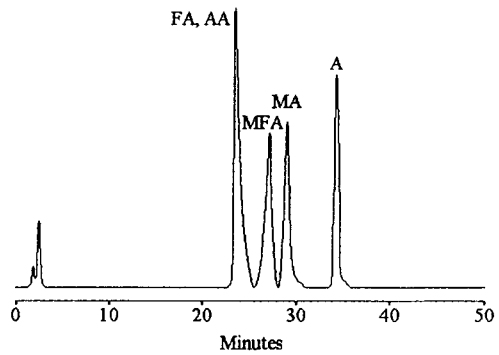

Fig. 3. Sample chromatogram of aminocarb and its four metabolites (5 ng/injection) with retention times (min): A = 34.34; MFA = 27.06; MA = 29.07; FA, AA = 23.43.

tems with varying solvent strength, column type, length and packing, flow-rates, etc., did not result in the disengagement of FA and AA bands. It is likely that the use of different fluorophore systems could result in improved resolution. The chromatographic separation of mexacarbate and its metabolites (Fig. 4) is satisfactory, the peaks are sharp and well defined. The peaks of AM and MFM are not fully resolved, but good integration parameters (properly set peak width and peak threshold values) allowed satisfactory quantitation of the two analytes.

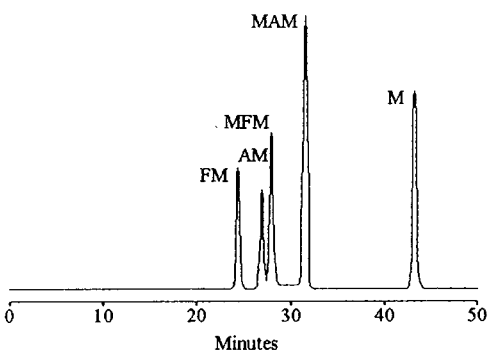

Fig. 4. Sample chromatogram of mexacarbate and its four metabolites (5 ng/injection) with retention times (min): M = 43.31; MFM = 28.04; MAM = 31.62; FM = 24.43; AM = 27.01.

3.4. Recoveries of carbamates from water and soil

Recoveries of the carbamates obtained from natural water at 2 and 20 ng/ml fortification levels and forest soil at 20 and 200 ng/g are given in Table 2 along with their S.D. and R.S.D. values. Corresponding chromatograms are given in Figs. 5 (water blank after cleanup), 6 (aminocarb and its metabolites in water at 20 ng/ml fortification level), 7 (mexacarbate and its metabolites in water at 20 ng/ml), 8 (soil blank after cleanup), 9 (aminocarb and its metabolites in soil at 200 ng/g) and 10 (mexacarbate and its metabolites in soil at 200 ng/g). Recoveries of the two parent insecticides, A and M, were above 93% at both fortification levels with R.S.D.s less than 6.5% (Table 2). However, compared to other analytes, the recoveries of the four aldehydes at both fortification levels in water and soil were low, especially the FA and FM which averaged only $77.8 \pm 5.6\%$. The low recoveries in water could be due to their high polarity and enhanced water solubility, preventing quantitative partition from aqueous to organic phase. Generally, from the data in Table 2, it is apparent that the recoveries of the analytes from water and soil are slightly higher at the higher fortification level, but the ranges in R.S.D. (5.0 to 11.5%) were nearly the same in both cases. The limit of detection (LOD) for each analyte, calculated as three times the S.D. of the blank response [16], was in the order of 0.1 ng. Limit of quantification (LOQ) ($10 \times$ S.D.) was determined to be 0.4 ng for all the analytes.

The Al_2O_3 minicolumn method provided adequate cleanup for natural water and forest soil by removing the bulk of the coextracted impurities. The chromatograms of the blank water and soil samples (Figs. 5 and 8) exhibit no peaks which would interfere with the analysis of the carbamate analytes. Figs. 6 and 9 show the typical chromatograms obtained for aminocarb and its metabolites in fortified samples of water and soil respectively. Similar chromatograms for mexacarbate and its metabolites are given in Figs. 7 and 10. Like the blanks, they are clean

Table 2
Average recoveries ($n = 3$) of aminocarb and mexacarbate and their carbamate metabolites[a] from natural water and forest soil

Carbamate	Recovery ± S.D. (R.S.D., %)			
	Fortification			
	Natural water		Forest soil	
	2 ng/ml	20 ng/ml	20 ng/g	200 ng/g
A	95.1 ± 5.9 (6.2)	98.4 ± 5.2 (5.3)	95.7 ± 6.1 (6.4)	97.6 ± 5.7 (5.8)
MFA	87.8 ± 6.7 (7.6)	91.2 ± 6.4 (7.0)	85.2 ± 7.1 (8.3)	89.9 ± 6.8 (7.6)
MA	91.4 ± 6.1 (6.7)	93.7 ± 5.7 (6.1)	93.6 ± 6.9 (7.4)	95.3 ± 6.1 (6.4)
FA	73.2 ± 8.4 (11.5)	77.6 ± 8.3 (10.7)	81.1 ± 8.7 (10.7)	84.7 ± 7.9 (9.3)
AA	83.6 ± 7.8 (9.3)	87.2 ± 7.7 (8.8)	78.3 ± 8.2 (10.5)	84.8 ± 7.8 (9.2)
M	94.2 ± 5.3 (5.6)	98.2 ± 4.9 (5.0)	93.6 ± 6.0 (6.4)	96.2 ± 5.7 (5.9)
MFM	82.7 ± 6.6 (8.0)	85.6 ± 6.6 (7.7)	81.4 ± 7.8 (9.6)	85.1 ± 7.2 (8.5)
MAM	92.8 ± 6.3 (6.8)	94.6 ± 6.1 (6.4)	93.3 ± 6.5 (7.0)	94.9 ± 6.3 (6.6)
FM	72.0 ± 7.9 (11.0)	75.1 ± 8.2 (10.9)	77.6 ± 8.3 (10.7)	81.0 ± 7.5 (9.3)
AM	74.7 ± 7.5 (10.0)	84.6 ± 7.1 (8.4)	74.1 ± 7.2 (9.7)	82.4 ± 6.3 (7.6)

[a] FA and AA were fortified separately.

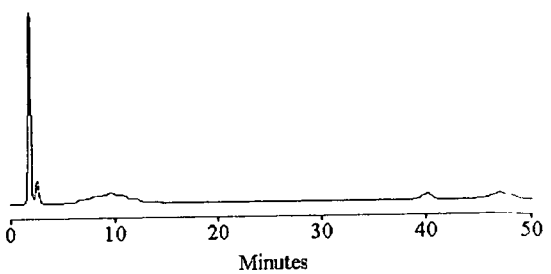

Fig. 5. Chromatogram of natural water blank after column cleanup.

and free from interfering compounds. Any minor matrix interference did not affect the analysis. The Nuchar–Celite mixture used by others [4,12] in the column cleanup was tried for the water and soil samples and found to be unsatisfactory, due to low recovery levels, especially for the aldehydes, and also because of interference peaks due to coextractive impurities.

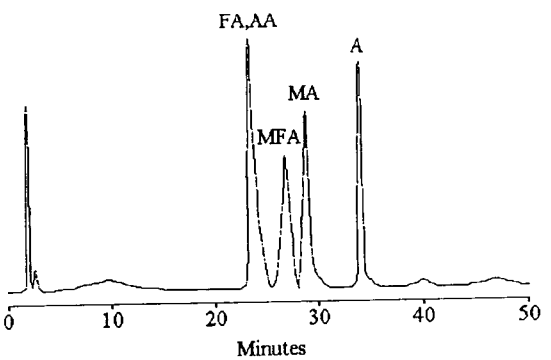

Fig. 6. Chromatogram of water fortified with aminocarb and its metabolites each at 20 ng/ml (100 μl/injection).

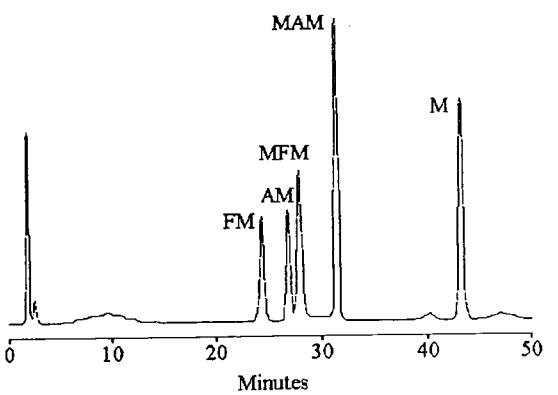

Fig. 7. Chromatogram of water fortified with mexacarbate and its metabolites each at 20 ng/ml (100 μl/injection).

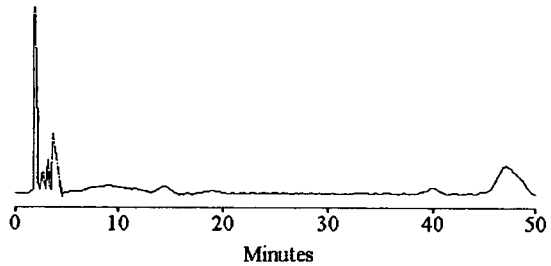

Fig. 8. Chromatogram of soil blank after column cleanup.

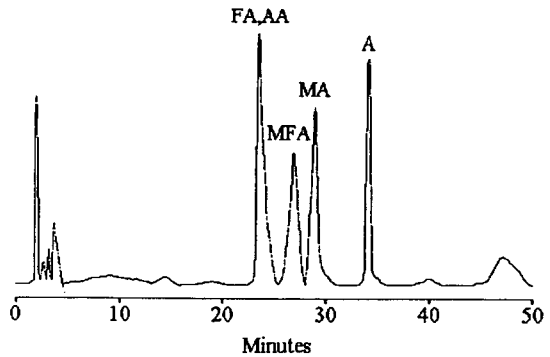

Fig. 9. Chromatogram of soil fortified with aminocarb and its metabolites each at 200 ng/g (100 μl/injection).

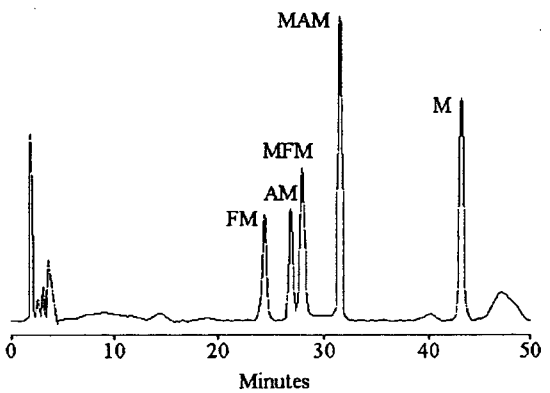

Fig. 10. Chromatogram of soil fortified with mexacarbate and its metabolites each at 200 ng/g (100 μl/injection).

4. Conclusions

The HPLC–PCRS method reported in this paper is suitable for isolating and quantifying low levels of aminocarb and mexacarbate and their carbamate metabolites in natural water and forest soil with good reproducibility. The method is straightforward and combines high selectivity due to pre-run chromatographic separation and high sensitivity of fluorometric detection. The on-line coupling of separation, derivatization and detection simplifies the analytical scheme thus making the method effective for routine use in situations where a lot of samples will be analyzed. With the development of suitable extraction and cleanup techniques, the method could be extended to analyze the residues of monoalkyl carbamates in different environmental matrices, such as conifer needles, forest litter, etc.

5. References

[1] A.M. Abdel-Wahab, R.J. Kuhr and J.E. Casida, *J. Agric. Food Chem.*, 14 (1966) 290.
[2] A.M. Abdel-Wahab and J.E. Casida, *J. Agric. Food Chem.*, 15 (1967) 479.
[3] B.V. Helson and K.M.S. Sundaram, *Pestic. Sci.*, 39 (1993) 13.
[4] D. Chaput, *J. Assoc. Off. Anal. Chem.*, 71 (1988) 542.
[5] M.J. Page and M. French, *J. AOAC Int.*, 75 (1992) 1073.
[6] E. Ballesteros, M. Gallego and M. Valcarcel, *J. Chromatogr.*, 633 (1993) 169.
[7] S.Y. Szeto and K.M.S. Sundaram, *J. Chromatogr.*, 200 (1980) 179.
[8] K.M.S. Sundaram, C. Feng and J. Broks, *J. Liq. Chromatogr.*, 8 (1985) 2579.
[9] H.A. Moye, S.J. Scherer and P.A. St. John, *Anal. Lett.*, 10 (1977) 1049.
[10] R.T. Krause, *J. Chromatogr. Sci.*, 16 (1978) 281.
[11] R.T. Krause, *J. Chromatogr.*, 185 (1979) 615.
[12] R.T. Krause, *J. Assoc. Off. Anal. Chem.*, 63 (1980) 1114.
[13] R.T. Krause, *J. Assoc. Off. Anal. Chem.*, 68 (1985) 726.
[14] R.T. Krause, *J. Assoc. Off. Anal. Chem.*, 68 (1985) 734.
[15] H. Engelhardt and B. Lillig, *Chromatographia*, 21 (1986) 136.
[16] L.H. Keith, in *Environmental Sampling and Analysis: A Practical Guide*, Lewis Publishers, Chelsea, MI, 1991, p. 143.

ELSEVIER

Journal of Chromatography A, 672 (1994) 125–133

JOURNAL OF CHROMATOGRAPHY A

Optical resolution of imidapril hydrochloride by high-performance liquid chromatography and application to the optical purity testing of drugs

Hiroyuki Nishi*, Kazuya Yamasaki, Yoshio Kokusenya, Tadashi Sato

Analytical Chemistry Research Laboratory, Tanabe Seiyaku Co. Ltd., 16–89, Kashima 3-chome, Yodogawa-ku, Osaka 532 (Japan)

(First received December 30th, 1993; revised manuscript received February 11th, 1994)

Abstract

Imidapril hydrochloride, a newly synthesized angiotensin-converting enzyme (ACE) inhibitor, is administered as a single enantiomer (*SSS*-form) because it is the most active of the eight possible optical isomers. Three different approaches to applying high-performance liquid chromatography (HPLC) were developed for the resolution of optical isomers of imidapril hydrochloride. One is the reversed-phase HPLC method for the separation of diastereomers from the enantiomeric pairs of imidapril. The second method involves the derivatization of imidapril with a chiral reagent and separation on a silica gel column (normal-phase HPLC). The last method is the direct separation of enantiomers of imidapril hydrochloride by using chiral stationary phases (CSPs). These three methods were successfully applied to the optical purity testing of drug substances and those in tablets. The methods were also used in a stability study of imidapril hydrochloride, including its stability in aqueous solutions, and imidapril tablets.

1. Introduction

Imidapril hydrochloride is a recently developed prodrug-type angiotensin-converting enzyme (ACE) inhibitor [1,2]. Imidapril, having an ethyl ester structure, is converted into a dicarboxy-type compound (imidaprilat) in the body (Fig. 1). Imidaprilat shows about a 500 times higher activity than the ester form, imidapril.

Imidapril hydrochloride was developed as a single enantiomer (*SSS*-form) because it shows the strongest activity of the eight optical isomers [2]. It is therefore important to determine the

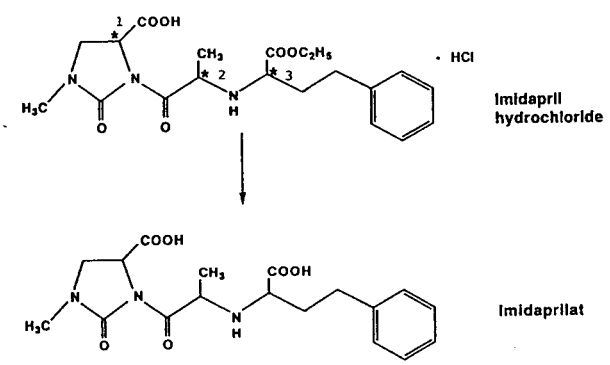

Fig. 1. Structures of imidapril hydrochloride and imidaprilat. Asymmetric carbons are indicated with asterisks. Absolute configuration of imidapril ($*^1$, $*^2$, $*^3$) is (*S*, *S*, *S*).

* Corresponding author.

0021-9673/94/$07.00
SSDI 0021-9673(94)00179-D

optical purity of the single *SSS*-form isomer. The aim of the work was to develop a method for determining the optical purity of the drug.

Chromatographic methods, especially HPLC, have been widely accepted for the separation of optical isomers. Diastereomers can be separated by the usual HPLC modes, although the separation of enantiomers requires some special techniques such as a chiral derivatization method or chiral stationary phases (CSPs). In other words, six diastereomers of imidapril hydrochloride (*SSR*, *RRS*, *SRS*, *RSR*, *RSS* and *SRR*) can be separated from the other diastereomers, *RRR* or *SSS* (imidapril), by reversed- or normal-phase HPLC. The separation of the *RRR*- and *SSS*-forms (enantiomers of imidapril hydrochloride) can be achieved by two methods. One is a chiral derivatization method using a chiral reagent having an amino group such as L-alanine-β-naphthylamide (L-ANA), because imidapril hydrochloride has a carboxy group in the molecule. The other is a direct chiral separation method using CSPs. Among many commercially available CSPs [3,4], the ligand-exchange type may offer sufficient enantiomeric separation of imidapril hydrochloride considering that the imidapril structure is like an amino acid.

This paper describes the HPLC separation of optical isomers of imidapril hydrochloride by using three methods: the first is for the separation of diastereomers from the enantiomers of imidapril hydrochloride; the second is for the separation of enantiomers by a chiral derivatization method; and the third is a direct chiral separation method. Applications to the quality control of drug substances (single *SSS*-form) and those in tablets by these methods are reported. Stability studies of the drug substances and those in tablets and of imidapril hydrochloride in aqueous solutions were also performed by the methods developed.

2. Experimental

2.1. Apparatus

The HPLC system consisted of an LC-6A high-pressure pump, a CTO-6A column oven and an SPD-6A variable-wavelength UV detector (Shimadzu, Kyoto, Japan). Samples were applied to the column with a Rheodyne Model 7125 loop injector (20 μl) or a Shimadzu SIL-6B autoinjector. Peak integration was carried out with a Shimadzu Chromatopac C-R5A data processor. An M-80A mass spectrometer (Hitachi, Ibaragi, Japan) was operated in the beam electron impact mode at 70 eV.

2.2. Chemicals

Imidapril hydrochloride ($C_{20}H_{27}N_3O_6 \cdot HCl$), (4*S*)-3-[(2*S*)-2-[N-((1*S*)-1-ethoxycarbonyl-3-phenylpropyl)amino] propionyl]-1-methyl-2-oxoimidazolidine-4-carboxylic acid hydrochloride, with molecular mass (M_r) 441.91 (M_r of base = 405), and its seven optical isomers were obtained from Tanabe Seiyaku (Osaka, Japan). Potassium dihydrogenphosphate, phosphoric acid, copper(II) sulphate pentahydrate, diethylamine, pyridine, hydrochloric acid and ethanol were of analytical-reagent grade from Katayama Kagaku Kogyo (Osaka, Japan). Analytical-reagent grade N,N′-dicyclohexylcarbodiimide (DCC) was purchased from Tokyo Kasei Kogyo (Tokyo, Japan). HPLC-grade chloroform, acetonitrile and methanol were obtained from Katayama Kagaku Kogyo. Water was purified with a Millipore RO-60 water system (Millipore Japan, Tokyo, Japan). Ethyl *p*-hydroxybenzoate of analytical-reagent grade from Nacalai Tesque (Kyoto, Japan) was used as an internal standard in the assays. The chiral derivatization reagent, L-alanine-β-naphthylamide hydrobromide (L-ANA) (M_r of base = 214), was obtained from United States Biochemical (Cleveland, OH, USA). The structure of L-ANA is shown in Fig. 2. A Sep-Pak C_{18} cartridge column from Millipore was used for sample pretreatment.

2.3. HPLC columns

A Nucleosil 5C_8 (5 μm) reversed-phase col-

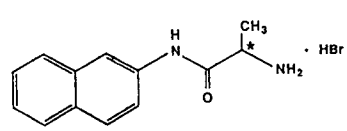

Fig. 2. Structure of L-alanine-β-naphthylamide hydrobromide (L-ANA).

umn (150 mm × 4.6 mm I.D.) from Macherey–Nagel (Düren, Germany) and a Zorbax Sil (5 μm) normal-phase column (150 mm × 4.6 mm I.D.) from DuPont (Wilmington, DE, USA) were used. A Chiralpak WH column (250 mm × 4.6 mm I.D.) from Daicel Chemical Industries (Osaka, Japan) was used for the direct separation of enantiomers of imidapril hydrochloride.

2.4. Sample preparation for reversed-phase HPLC

About 5 mg of imidapril hydrochloride were weighed and dissolved in 10 ml of the mobile phase for the Nucleosil $5C_8$ column and 20 μl of this solution were injected into the HPLC system. For the tablets, more than 20 tablets were weighed and ground. The resulting powder, equivalent to 25 mg of the drug substance according to the labelled amount, was weighed into a 50-ml volumetric flask and 40 ml of 40% methanol were added for extraction. The flask was shaken vigorously for 10 min and finally the contents were diluted to volume with 40% methanol. The solution was filtered through a membrane filter (0.45 μm) and 20 μl of the filtrate were injected into the HPLC system.

2.5. Chiral derivatization procedure

About 5 mg of imidapril hydrochloride and 15 mg of L-ANA were weighed into a glass-stoppered test-tube and 100 μl of chloroform, 50 μl of pyridine and 2 ml of a chloroform solution of DCC (0.45 g of DCC in 100 ml of chloroform) were added. The mixture was shaken vigorously and allowed to stand at room temperature for 1 h. After reaction, the mixture was washed with 2 ml of 1 *M* hydrochloric acid and continuously with 2 ml of water twice. A 1-ml volume of the chloroform layer was pipetted into a test-tube and diluted to 5 ml with chloroform. A 20-μl volume of the solution was injected into the HPLC system.

A blank solution was prepared by using the same procedure as described above but in the absence of the drug substance.

2.6. Sample preparation for direct chiral separation

About 20 mg of imidapril hydrochloride were weighed and dissolved in 10 ml of the mobile phase for the Chiralpak WH column and 2 μl of this solution were injected into the HPLC system. For imidapril tablets, more than 20 tablets were weighed and ground. The resulting powder, equivalent to 20 mg of the drug substance according to the labelled amount, was weighed and 20 ml of water was added for extraction. The solution was sonicated for 5 min and filtered through a membrane filter (0.45 μm). A 2-ml volume of the filtrate was charged to a previously activated Sep-Pak C_{18} column. The column was washed with 2 ml of water twice and dried with a stream of nitrogen. The sample adsorbed on the column was then eluted with 1 ml of methanol and the eluate was dried *in vacuo*. Finally, 1 ml of the mobile phase for the Chiralpak WH column was added to the residue (if necessary, the solution was filtered with a 0.45-μm membrane filter) and used as the sample solution of tablets. A 2-ml volume of each pH solution (containing 2 mg of the drug substance) for the stability testing of the drug substance in aqueous solutions (see below) was charged to a previously activated Sep-Pak C_{18} column. The column was treated continuously with the same procedure as for tablets described above. A 2-μl volume of the sample solution was injected into the HPLC system.

2.7. Stability study of drug substance in aqueous solutions

About 0.1 g of imidapril hydrochloride was weighed and dissolved in 100 ml of each buffer solution (pH range 2–11, ionic strength *ca.* 0.1). The solution was warmed on a water-bath at 90°C for 1 h. After cooling the solution with ice–water, 5 ml of the solution were diluted to 10 ml with 80% methanol and used as the sample solution for purity testing in reversed-phase HPLC. For assay, 2 ml of the internal standard solution (0.1 g of ethyl *p*-hydroxybenzoate in 200 ml of the mobile phase for the Nucleosil $5C_8$ column) and 2 ml of the buffer solution prepared above (0.1 g of drug substance in 100 ml of each

buffer solution) were pipetted into a 10-ml volumetric flask and diluted to volume with 80% methanol. A 20-μl volume of the sample solution was injected into the reversed-phase HPLC system.

3. Results and discussion

3.1. Separation of diastereomers by reversed-phase HPLC

There are eight optical isomers of imidapril hydrochloride because it has three asymmetric carbons in the molecule (Fig. 1). Six of them are diastereomers to imidapril, and these were successfully separated from imidapril (*SSS*-form) by reversed-phase HPLC employing a C_8 column, as shown in Fig. 3, although each enantiomeric pair of the diastereomer (*SRR* and *RSS*, *SSR* and *RRS*, *SRS* and *RSR*) was not resolved. Good linearity for each diastereomer over the concentration range 0.03–5% (w/w) was obtained. The limit of detection of each diastereomer at a signal-to-noise ratio of 3 was *ca.* 0.05%.

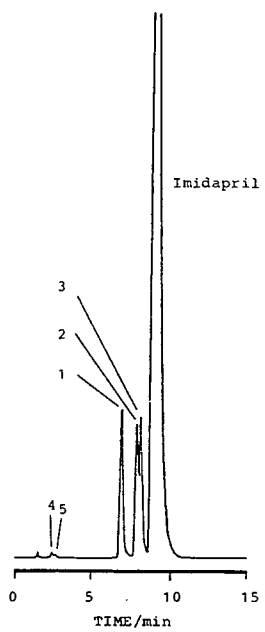

Fig. 3. Separation of imidapril, its diastereomers and the degradation products by reversed-phase HPLC. Peaks: 1 = *SRR*-form and *RSS*-form; 2 = *SSR*-form and *RRS*-form; 3 = *SRS*-form and *RSR*-form; 4 = degradation product; 5 = imidaprilat. Conditions: column, Nucleosil $5C_8$ (150 mm × 4.6 mm I.D.); column temperature, 40°C; mobile phase, 0.01 *M* phosphate buffer (pH 2.7)–methanol (3:2); flow-rate, 1.0 ml/min; detection, 215 nm.

The determination of diastereomers in drug substances (single *SSS*-form) and those in tablets was performed using the proposed method. Six diastereomers were not found in six batches each of imidapril hydrochloride and imidapril tablets, which were produced for the investigation of the physico-chemical properties, testing specifications, etc. Three batches were also used in the long-term stability studying. The results of the determination of the diastereomers in the drug substances and tablets that had been stored for 3 years at room temperature are summarized in Table 1. Under these conditions, no epimerization was observed. It was found that imidapril is optically stable in the solid state.

The reversed-phase HPLC conditions mentioned above also offered a sufficient separation of related substances of imidapril hydrochloride such as metabolites and degradation products, other than the diastereomers. Fig. 3 shows the separation of imidapril and two degradation products, including imidaprilat. Imidaprilat is one of the major degradation products and also a major metabolite. The other degradation product was produced through hydrolysis of the ethyl ester and amide bond. The determination of related substances in the drug substances and in tablets was performed by the proposed method and the results are summarized in Table 1. Small amounts of the related substances (0.2–0.4%) were detected.

3.2. Separation of enantiomers by chiral derivatization method

Chiral amino compounds can be applied as derivatization reagents for imidapril hydrochloride having a carboxy group in the molecule. From the investigation of several chiral reagents, L-ANA, which is commercially available, was selected. Enantiomers of several drugs having a carboxyl group, such as naproxen (non-steroidal anti-inflammatory drug), have been successfully

Table 1
Optical purity and impurity of the drug substances and those in tablets after storage for 3 years at room temperature

Sample	Lot No.	Impurity[a] (%)	Diastereomer[a] (%)	Enantiomer (*RRR* %)		Enantiomeric purity (*SSS* %)
				Direct[b]	Derivatization[c]	
Drug substance	040	0.20	N.D.[d]	N.D.	N.D.	100.0
	050	0.20	N.D.	N.D.	N.D.	100.0
	060	0.21	N.D.	N.D.	N.D.	100.0
Tablets	040	0.37	N.D.	N.D.	–	100.0
	050	0.34	N.D.	N.D.	–	100.0
	060	0.34	N.D.	N.D.	–	100.0

[a] By reversed-phase HPLC and area-percentage method. Detection limit *ca.* 0.05%.
[b] Direct separation by using Chiralpak WH. Detection limit *c.a.* 0.2%.
[c] Derivatization method using L-ANA. Detection limit *c.a.* 0.05%.
[d] N.D. = not detected.

resolved using the chiral reagent L-ANA and normal-phase HPLC [5].

The derivatization procedure for imidapril hydrochloride was optimized by varying the amounts of the chiral reagent, DCC and pyridine by reference to the procedure for naproxen described in ref. 5. It turned out that pyridine is essential for the reaction of imidapril hydrochloride, although it was unnecessary in the derivatization of naproxen. It was also found that more than four or five times the molar amounts of both the chiral reagent and DCC with respect to the sample are required for complete reaction. The optimized conditions are described under Experimental. By-products in the reaction were efficiently removed by washing the reaction mixture with 1 *M* hydrochloride acid.

A typical chromatogram of enantiomers of imidapril hydrochloride after derivatization with L-ANA is shown in Fig. 4, with a chromatogram of a blank solution. The resolution (R_s) between two derivatized enantiomers was 10.5. Each of the derivatized enantiomers was collected and identified by mass spectrometry. The molecular ion peak M^+ of m/z 601, which is equal to the M_r of derivatized imidapril (405 + 214 − 18), was observed for both compounds. Both mass spectra were also identical.

For the separation of the other six diastereomers, the chiral derivatization method was also successful except for the *SSR*-form, as shown in Fig. 5. We can determine six kinds of optical isomers by the proposed method. The separation between the *SSR*- and *SSS*-forms may be successful by changing of the mobile phase, although in this case (Fig. 5) they eluted in one peak. It is not clear why the peak of the L-ANA-derivatized *RSS*-form was broad compared with the others.

The linearity of response of the *RRR*-form was investigated by derivatizing samples containing 0.05–0.5% (w/w) of the *RRR*-form in the stan-

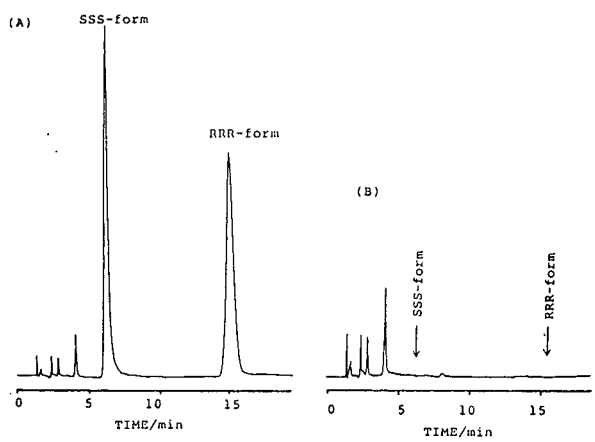

Fig. 4. (A) Separation of enantiomers of imidapril hydrochloride by the chiral derivatization method and (B) a blank chromatogram. Conditions: column, Zorbax Sil (5 μm; 150 mm × 4.6 mm I.D.); column temperature, 40°C; mobile phase, chloroform–methanol–ethanol–diethylamine (600:10:2:0.1); flow-rate, 1.0 ml/min; detection, 254 nm.

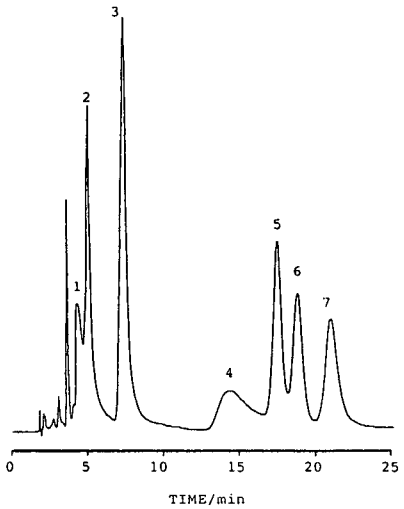

Fig. 5. Separation of eight optical isomers by the chiral derivatization method. Peaks: 1 = *SRS*-form; 2 = *SRR*-form; 3 = *SSS*-form and *SSR*-form; 4 = *RSS*-form; 5 = *RRR*-form, 6 = *RRS*-form, 7 = *RSS*-form. Conditions as in Fig. 4.

dard *SSS*-form. The results are shown in Fig. 6. The graph passed through the origin with r = 0.999 and the detection limit of the *RRR*-form in Fig. 7 at a signal-to-noise ratio of 3 was *ca.* 0.05%.

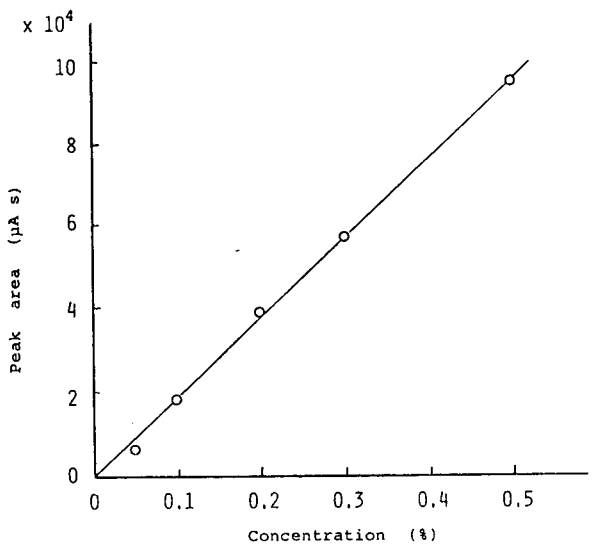

Fig. 6. Linearity of response of *RRR*-form in the chiral derivatization method.

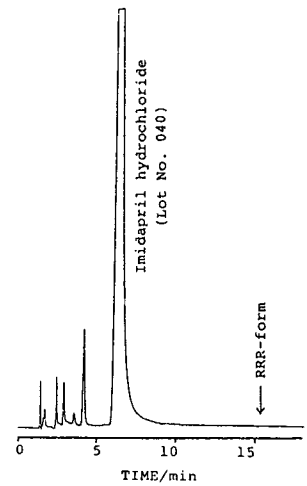

Fig. 7. Enantiomeric purity testing of imidapril hydrochloride by the chiral derivatization method. Conditions as in Fig. 4.

According to the derivatization procedure, three batches of the drug substances that had been stored at room temperature for 3 years were reacted with L-ANA and chromatographed under the conditions described in Fig. 4. The results are summarized in Table 1 and a typical chromatogram is shown in Fig. 7. The *RRR*-enantiomer was not detected in all batches.

3.3. Direct separation of enantiomers

It is well known that DL-amino acids have been successfully resolved by using ligand-exchange type CSPs [6–8], employing a solution of copper(II) sulphate as the mobile phase. Resolution of the enantiomers of imidapril hydrochloride, which can be regarded as an amino acid derivative, was achieved by employing ligand-exchange type CSPs. Among several commercially available CSPs, only Chiralpak WH offered the enantiomeric separation of imidapril. The optimization of the composition of the mobile phase was carried out by varying the concentration of copper(II) ion and the column temperature and adding some additives such as an organic solvent, by reference to ref. 8.

The effects of the concentration of copper(II) ion and the column temperature on R_s and the

Table 2
Effect of the concentration of copper(II) sulphate on the resolution of enantiomers of imidapril hydrochloride

$CuSO_4$ concentration (m*M*)	Retention time (min)		Theoretical plate number		R_s
	SSS-form	*RRR*-form	*SSS*-form	*RRR*-form	
2	12.66	14.57	1094	733	0.98
3	12.42	14.26	1084	703	0.94
4	12.18	14.15	1036	638	0.95
8	11.17	13.04	808	531	0.92

Flow-rate, 1.5 ml/min; column temperature, 40°C; detection, 230 nm.

retention times of the enantiomers are summarized in Tables 2 and 3. The higher the copper ion concentration or the column temperature, the faster the compound is eluted. The R_s values showed no noticeable change in the copper(II) concentration range 2–8 m*M*. However, it was advantageous to use a higher column temperature for improving the theoretical plate number (*N*), leading to a higher R_s. The effects of acetonitrile addition on R_s values and retention times are summarized in Table 4. The peak shape was markedly improved, that is, *N* increased with increase in the acetonitrile content, resulting in an improvement in R_s values (from 1 to 2.5).

The selected mobile phase composition and a typical chromatogram of the enantiomers are shown in Fig. 8A. Other optical isomers were also successfully separated from imidapril hydrochloride (*SSS*-form), except for the *SSR*-form, as

Table 3
Effect of column temperature on the resolution of enantiomers of imidapril hydrochloride

Temperature (°C)	Retention time (min)		Theoretical plate number		R_s
	SSS-form	*RRR*-form	*SSS*-form	*RRR*-form	
40	12.42	14.26	1084	703	0.94
45	11.87	13.64	1202	792	1.00
50	11.39	13.12	1360	1019	1.12

Concentration of $CuSO_4$, 3 m*M*; flow-rate, 1.5 ml/min; detection, 230 nm.

Table 4
Effect of acetonitrile addition on the resolution of enantiomers of imidapril hydrochloride

Acetonitrile (%)	Retention time (min)		Theoretical plate number		R_s
	SSS-form	*RRR*-form	*SSS*-form	*RRR*-form	
0	12.08	13.94	1100	752	1.00
10	8.82	10.80	1558	1370	1.80
20	6.42	8.14	2158	1847	2.46
30	4.80	6.15	1980	1782	2.49

Concentration of $CuSo_4$, 3 m*M*; flow-rate, 1.5 ml/min; detection, 230 nm; column temperature, 40°C.

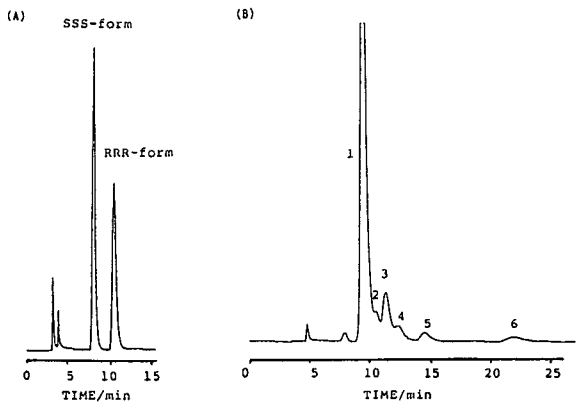

Fig. 8. Direct chiral separation of imidapril hydrochloride: (A) separation of enantiomers; (B) separation of eight optical isomers. Peaks: 1 = *SSR*-form and *SSS*-form; 2 = *RSS*-form; 3 = *SRR*-form and *RRR*-form; 4 = *RRS*-form; 5 = *RSR*-form; 6 = *SRS*-form. Conditions: column, Chiralpak WH (250 mm × 4.6 mm I.D.); column temperature, 40°C; mobile phase, 3 m*M* aqueous solution of copper(II) sulphate–acetonitrile (3:1); flow-rate, 1.0 ml/min; detection, 230 nm.

shown in Fig. 8B, where *ca.* 2% of each isomer was added to the *SSS*-isomer. Related substances of imidapril hydrochloride such as imidaprilat did not disturb the peaks of the eight optical isomers of imidapril under the conditions used in Fig. 8.

The linearity of response for the *RRR*-form was investigated over the range 0.25–3% (w/w). The graph passed through the origin with $r = 0.997$. The detection limit of the *RRR*-form at a signal-to-noise ratio of 3 was *ca.* 0.2% (see Fig. 9C). The detection limit of the antidope in the direct separation method (*ca.* 0.2%) was higher than that in the chiral derivatization method (*ca.* 0.05%). This can be interpreted by the low sample load capacity of the Chiralpak WH column and the low detection sensitivity at 230 nm.

The sample load capacity is one of the important parameters in ligand-exchange type CSPs, because it is not large compared with other common stationary phases such as an ODS column. A large sample loading affects the resolution [7]. It is necessary and recommended to decrease the sample loading in order to achieve good resolution. The results of the investigation of sample loading (1–5 μg) are summarized in Table 5. There was no significant decrease in N values when up to 5 μg of the compound were injected.

Table 5
Effect of sample load on the theoretical plate number of enantiomers of imidapril hydrochloride

Sample load (μg)	Theoretical plate number		R_s
	SSS-form	*RRR*-form	
1	3083	2450	3.05
2	2106	2860	2.99
3	3497	2471	3.00
5	3301	2846	2.81

Concentration of $CuSO_4$, 3 m*M*; concentration of acetonitrile, 30%; flow-rate, 1.0 ml/min; column temperature, 40°C; detection, 230 nm.

The enantiomeric purity of imidapril hydrochloride and its tablets that had both been stored for 3 years at room temperature was determined using the proposed method. Typical chromatograms are shown in Fig. 9A and B, with a chromatogram of imidapril standard spiked with

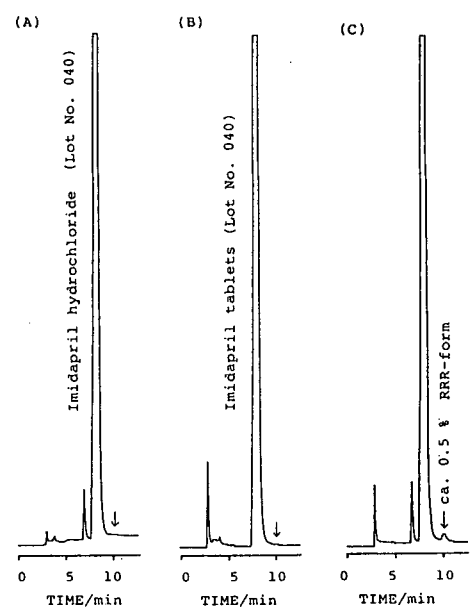

Fig. 9. Enantiomeric purity testing of (A) imidapril hydrochloride and (B) its tablet by the direct method. (C) Chromatogram of standard imidapril spiked with *ca.* 0.5% of the *RRR*-form. Conditions as in Fig. 8.

ca. 0.5% of the *RRR*-form (Fig. 9C). The *RRR*-form was not detected in all samples, as indicated in Table 1.

The method was also applied to the enantiomeric purity testing of the drug substance in aqueous solutions (pH 2–11). The results are summarized in Table 6, with the results of assay and diastereomer determination. Imidapril was found to be stable under acidic (pH 2) and neutral (pH 7) conditions. The *RRR*-form was not detected over the whole pH range investigated, although epimerization of imidapril occured at the asymmetric carbon 3 (see Fig. 1) and small amounts of *SSR*-form (*ca.* 0.5%) were detected in the pH range 5–9. The *SSR*-form was determined by using reversed-phase HPLC, considering the result in this direct separation, that is, no *RRS*-form was observed. At high pH (9–11), larger amounts of imidapril were degraded into imidaprilat and the degradation product as shown in Fig. 3.

In conclusion, the enantiomeric separation of imidapril hydrochloride was achieved by both the direct and indirect methods (derivatization method). Eight optical isomers of imidapril hydrochloride were successfully determined by the combined use of three chromatographic methods. First, reversed-phase HPLC should be performed to determine the six diastereomers because the *SSR*-isomer was not separated from the *SSS*-isomer by the succeeding enantiomeric separation method. After checking the diastereomers, enantiomeric purity testing according to the derivatization method or the direct method should be performed. It was found that no racemization of imidapril hydrochyloride occurs on long-term storage and in aqueous solutions of various pH.

References

[1] K. Hayashi, K. Nunami, J. Kato, N. Yoneda, M. Kubo, T. Ochiai and R. Ishida, *J. Med. Chem.*, 32 (1989) 289.
[2] H. Kubota, K. Numani, K. Hayashi, Y. Hashimoto, N. Ogiku, Y. Matsuoka and R. Ishida, *Chem. Pharm. Bull.*, 40(6) (1992) 1619.
[3] W. Lindner, *Chromatographia*, 24 (1987) 97.
[4] D. Armstrong, *Anal. Chem.*, 59 (1987) 84A.
[5] Y. Fujumoto, K. Ishii, H. Nishi, N. Tsumagari, T. Kakimoto and R. Shimizu, *J. Chromatogr.*, 402 (1987) 344.
[6] H. Kiniwa, Y. Baba, T. Ishida and H. Katoh, *J. Chromatogr.*, 461 (1989) 397.
[7] H. Katoh, T. Ishida, Y. Baba and H. Kiniwa, *J. Chromatogr.*, 473 (1989) 241.
[8] *Chiralcel and Chiralpak No. 4 Technical Brochure*, Daicel, Osaka, 1989.

Table 6
Assay and enantiomeric purity of imidapril hydrochloride in solutions of various pH

Sample pH	Residual imidapril[a] (%)	Diastereomer[b] (%)	*RRR*-form[c] (%)
2	93.2	N.D.[d]	N.D.
3	85.9	N.D.	N.D.
5	88.7	0.48 (*SSR*)	N.D.
7	92.1	0.55 (*SSR*)	N.D.
9	75.6	0.44 (*SSR*)	N.D.
11	12.1	N.D.	N.D.

Sample solutions were heated at 90°C for 1 h.
[a] HPLC assay using internal standard method.
[b] By reversed-phase HPLC and area-percentage method. Detection limit *ca.* 0.05%.
[c] By direct chiral separation method. Detection limit *ca.* 0.2%.
[d] N.D. = not detected.

ELSEVIER

Journal of Chromatography A, 672 (1994) 135–140

JOURNAL OF CHROMATOGRAPHY A

Analysis of forensic samples using precolumn derivatization with (+)-1-(9-fluorenyl)ethyl chloroformate and liquid chromatography with fluorimetric detection

Yu-Pen Chen, Mei-Chich Hsu*, Chun Sheng Chien

National Laboratories of Foods and Drugs, Department of Health, Executive Yuan, 161–2 Kuen-Yang St., Nankang, Taipei 11513, Taiwan

(First received July 29th, 1993; revised manuscript received January 18th, 1994)

Abstract

An indirect chiral separation of forensic methamphetamine samples by liquid chromatography with fluorescence detection was developed. Carbamate derivatives of the methamphethamine enantiomers were formed by using (+)-1-(9-fluorenyl)ethyl chloroformate. The response appeared to be linear from 16.7 to 1674.0 ng/ml ($r = 0.9999$) for each enantiomer. The relative standard deviations in the within-day and between-day assays for (*S*)-(+)-methamphetamine and (*R*)-(−)-methamphetamine are reported. As the developed procedure can also be used to determine ephedrine and pseudoephedrine, it will provide valuable information concerning the method of synthesis and the purity of the product.

1. Introduction

In recent years, the number of methamphetamine forensic samples obtained from police courts has increased strikingly. Methamphetamine, which is known to cause addiction and to have intense psychostimulant actions, has two optical isomers, the (*S*)-(+)- and (*R*)-(−)-isomers. The latter isomer has greater sympathomimetic properties whereas the former has greater anorexic and stimulant properties [1]. The abuse of this drug is a serious social problem. Hence it is necessary to develop a method with good sensitivity and selectivity for investigating methamphetamine enantiomers.

The purity of methamphetamine can be attributed in part to its route of synthesis, based on the reduction of ephedrine or pseudoephedrine. The advantage of ephedrine as the starting material is that side-products are limited. Also, because ephedrine is a stereochemically pure natural product, the process generates the more potent dextrorotatory enantiomer of methamphetamine, not a racemic mixture (Fig. 1). The absolute configurations of the α-carbon of (1*R*,2*S*)-ephedrine and (1*S*,2*S*)-pseudoephedrine are the same, so that (*S*)-(+)-methamphetamine could be prepared from either compound. Another approach for methamphetamine synthesis has been reported involving reaction between phenylacetone and methylamine (Leuc-

* Corresponding author. Present address: Graduate Institute of Sports Sciences, National College of Physical Education and Sports, 250 Wen Hua 1st Road, Kweishan, Taoyuan 33333, Taiwan.

0021-9673/94/$07.00
SSDI 0021-9673(94)00078-N

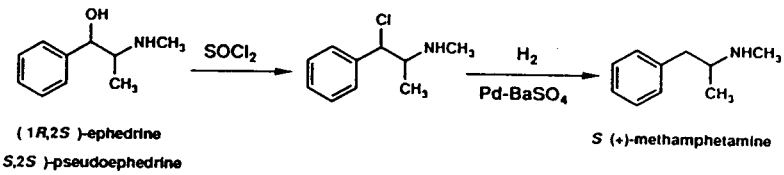

Fig. 1. Conversion of ephedrine and pseudoephedrine into (*S*)-(+)-methamphetamine.

kart procedure). This procedure generates the racemic mixture and, unless carefully purified, a higher proportion of contaminants. The purity of these illicit drugs is highly variable.

It has long been recognized that chromatographic methods can offer distinct advantages over classical techniques in the separation of stereoisomers. Several liquid chromatographic methods for the determination of amphetamine-related compounds have been reported [2–14]. Relatively fewer methods based on an indirect separation of enantiomers by precolumn derivatization with chiral reagents have been published [15–19]. Some of the commonly used reagents for amines give UV-sensitive derivatives for both primary and secondary amines. However, UV detection is hampered by the low molar absorptivities of these compounds in the UV region. We decided to use fluorescence detection, an intrinsically more sensitive method. This paper describes an approach for the derivatization of enantiomeric drugs using (+)-1-(9-fluorenyl)ethyl chloroformate reagent under optimized conditions using fluorimetric detection (Fig. 2). The detectability of enantiomers is enhanced and the chromatographic behaviour of basic compounds is improved as a result of such derivatization. This method was evaluated in terms of linearity, selectivity and detection limit. Further, we applied the method to the analysis of forensic samples that consisted of mixtures of methamphetamine product and its semi-products from clandestine laboratories. The results show that the method can simultaneously determine ephedrine, pseudoephedrine and methamphetamine enantiomers.

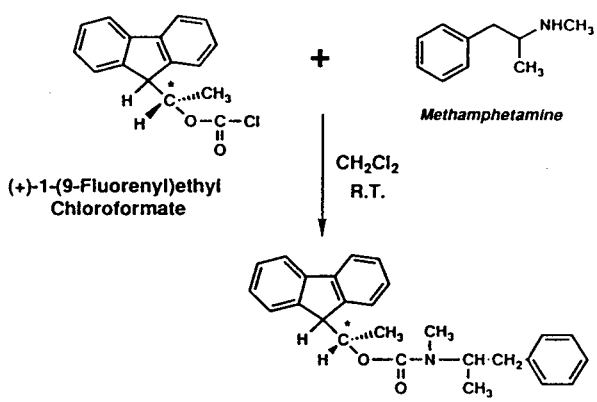

Fig. 2. Formation of carbamate derivatives from methamphetamine with (+)-FLEC.

2. Experimental

2.1. Reagents and chemicals

(1*R*,2*S*)-Ephedrine hydrochloride, (1*S*,2*S*)-pseudoephedrine hydrochloride, (*R*)-(−)-methamphetamine, (*S*)-(+)-methamphetamine hydrochloride and racemic methamphetamine hydrochloride were purchased from Sigma (St. Louis, MO, USA). (+)-1-(9-Fluorenyl)ethyl chloroformate [(+)-FLEC] ($[\alpha]_D^{25} = +70.0°$; $c = 1$ in $CHCl_3$; optical purity >99.5%) was obtained from Fluka (Buchs, Switzerland). All organic solvents and reagents were of either LC or analytical-reagent grade and used as received. Triply distilled water with an electric conductance 18.3 MΩ was used (obtained with a Millipore Milli-Q reagent water system).

2.2. Apparatus

The high-performance liquid chromatographic (HPLC) system consisted of a Model 600E system controller (Waters Chromatography Division, Millipore, Milford, MA, USA), a Waters Model 510 pump, a Waters Model 745B data module and a Shimadzu Model RF-535 spectrofluorimeter operated with excitation at 295 nm and emission at 315 nm. The mobile phase was

pumped through a $5C_{18}$-AR (5 μm) (Waters) reversed-phase column (25 cm × 3.9 mm I.D.) (Nacalai Tesque) with an isocratic flow-rate of 1.0 ml/min. Chromatography was performed at room temperature. Samples were injected automatically with a WISP-712 injector (Waters). Injections of 25 μl of all solutions were made.

2.3. Mobile phase

The mobile phase was acetonitrile–0.05 *M* phosphate buffer (65:35, v/v). It was filtered (0.45-μm Millipore filter) and degassed with an ultrasonic bath prior to use.

2.4. Standard solutions

An accurately weighed amount of (*S*)-(+)-methamphetamine or (*R*)-(−)-methamphetamine was dissolved in distilled water to give a concentration of 1674 ng/ml. For derivatization, the amine solution to be studied was placed in a 10-ml screw-capped glass tube, 0.5 ml of distilled water was added and the pH was made alkaline (about pH 12) with 1 *M* NaOH. The solution was reacted with 0.2 ml of (+)-FLEC–dichloromethane (0.1:10, v/v), 0.5 ml of dichloromethane was added and the solution was shaken for 30 min. The aqueous phase was discarded and the organic phase was washed twice with 0.5-ml portions of distilled water. The organic phase was evaporated to dryness under nitrogen and the residue was dissolved in 3 ml of methanol and mixed. This solution was passed through a 0.45-μm filter. The filtrate was then ready for injection into the chromatographic system.

2.5. Sample solution

A weighed aliquot (about 1 mg) of an illicit methamphetamine sample was dissolved in 1 ml of distilled water and the solution was derivatized in the same manner as the reference material.

2.6. Solution for linearity response

Calibration graphs were constructed. Solutions of seven concentrations of (*S*)-(+)- or (*R*)-(−)-methamphetamine, 16.74, 33.48, 100.44, 167.4, 334.8, 1004.4 and 1674.0 ng/ml, were prepared and each solution was derivatized through the whole procedure as described in Section 2.4. Each concentration was chromatographed six times.

3. Results and discussion

The effect of the (+)-FLEC concentration on derivatization was examined by varying the molar ratio of methamphetamine to (+)-FLEC from 1:1 to 1:7. The results indicated that ratios greater than 1:2 gave the maximum fluorescence intensity for these amines. In order to minimize chromatographic difficulties associated with excess of reagent, a molar ratio of 1:2 was adopted. The effect of reaction time was examined by allowing the derivatization to proceed for times ranging from 1 to 60 min. The results showed that maximum fluorescence intensity was observed at reaction times over 20 min, hence 20 min were used in all subsequent work. In order to establish the stabilities of the derivatized amines, derivatizations with concentrations of 167.4 ng/ml of (*S*)-(+) and (*R*)-(−)-methamphetamine were studied. The results showed that more than 99.5% of the amine in the original solution remained for 1 month.

Mobile phase conditions such as acetonitrile content, pH and salt concentration were investigated to determine their effects on the separation of the methamphetamine enantiomers and related compounds. Of these, the most critical factor was found to be pH. A pH of 6.0 was chosen because it produced the best combinations of separation and speed of analysis of the combined product. A buffer molarity of 0.05 was necessary to maintain the optimum pH of 6.0. A mobile phase concentration of acetonitrile of 65% was found to be the optimum for separating the enantiomers of methamphetamine (Table 1). Good selectivity with $\alpha = 1.04$ and capacity factors (k') of 17.0 and 17.7 for the (*S*)-(+)- and (*R*)-(−)-isomers, respectively, were found. The sensitivity of fluorescence detection was *ca.* 200 times higher than that of UV absorbance detection at 254 nm.

Table 1
Effect of organic solvent content in the mobile phase

Acetonitrile–0.05 *M* phosphate buffer (pH 6.0)	$k'_{(S)-(+)}$	$k'_{(R)-(-)}$	α
70:30	13.1	13.5	1.033
65:35	17.0	17.7	1.040
60:40	39.3	41.1	1.047

The calibration graphs passed through or near the origin. The linearity of the relationships between peak area (y) and each enantiomer concentration (x, ng/ml) was verified by injection of seven concentrations ranging from 16.7 to 1674.0 ng/ml. For typical calibration graphs, the regression equations and their correlation coefficients were calculated as follows: (*S*)-(+)-methamphetamine, $y = 1.0126x - 0.0392$ ($r = 0.9999$); (*R*)-(−)-methamphetamine, $y = 0.9974x - 0.0537$ ($r = 0.9999$). The detection limit for each enantiomer was down to 145.2 pg at signal-to-noise ratios higher than 3 (Fig. 3).

Reproducibilities (R.S.D.s) for both within-day and between-day assays were evaluated. A new calibration graph was prepared each day with a new series of samples. Each enantiomer was assayed in triplicate on five separate days. The within-day and between-day variabilities are shown in Table 2. The R.S.D.s in the within-day assay were between 0.11 and 0.80% for (*S*)-(+)-methamphetamine and between 0.22 and 1.50% for (*R*)-(−)-methamphetamine and those in the between-day assay were 1.00% for (*S*)-(+)-methamphetamine and 0.68% for (*R*)-(−)-methamphetamine.

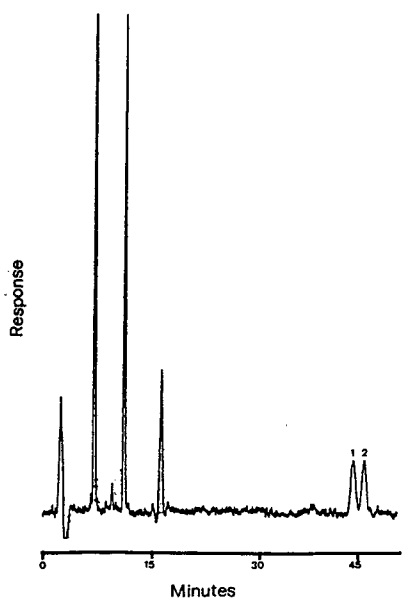

Fig. 3. Chromatogram showing detection limit of racemic methamphetamine derivative (290.4 pg). Peaks: 1 = 145.2 pg; 2 = 145.2 pg.

Typical chromatograms of carbamate derivatives of the (*S*)-(+)- and (*R*)-(−)-methamphetamine are shown in Fig. 4. The method can also separate carbamate derivatives of compounds related to methamphetamine, *e.g.*, ephedrine and pseudoephedrine, which are eluted prior to methamphetamine (Fig. 4). The first two peaks (retention times *ca.* 7 and 11 min) in each chromatogram are solvent peaks. The third peak (retention time *ca.* 16.7 min) in each chromatogram is from the (+)-FLEC reagent. The separation parameters of these enantiomeric compounds are given in Table 3.

The utility of enantiomeric composition determinations using the (+)-FLEC derivatization method is best illustrated with the analysis of some forensic samples. We analysed 50 illicit methamphetamine powder samples and two liquid samples seized in Taiwan. Only (*S*)-(+)-methamphetamine was detected in the powder samples (Fig. 4). (1*R*,2*S*)-Ephedrine, (1*S*,2*S*)-pseudoephedrine and (*S*)-(+)-methamphetamine were detected in the liquid samples. These observations showed that these forensic samples of (*S*)-(+)-methamphetamine had been synthesized from (1*R*,2*S*)-ephedrine and/or (1*S*,2*S*)-pseudoephedrine.

4. Acknowledgements

The authors thank Miss Hsiou-Chuan Chung for her assistance with the preparation of the manuscript. This work was supported by the Division of Drug Chemistry, National Laboratories of Foods and Drugs, Department of Health.

Table 2
Accuracy and reproducibility data

Isomer	Initial concentration (ng/ml)	Within-day variability			Between-day variability		
		Mean measured concentration (ng/ml)[a]	S.D. (ng/ml)	R.S.D. (%)	Mean measured concentration (ng/ml)[b]	S.D. (ng/ml)	R.S.D. (%)
(*S*)-(+)-Methamphetamine	1674.0	1674.0	5.00	0.29	–	–	–
	502.2	490.0	1.04	0.21	500.2	0.50	1.00
	50.2	54.0	0.08	0.15	–	–	–
(*R*)-(−)-Methamphetamine	1674.0	1673.0	3.61	0.22	–	–	–
	502.2	488.7	1.13	0.23	497.9	0.34	0.68
	50.2	54.7	0.41	0.70	–	–	–

[a] $n = 3$.
[b] $n = 5$. The between-day studies included 15 samples at each concentration level.

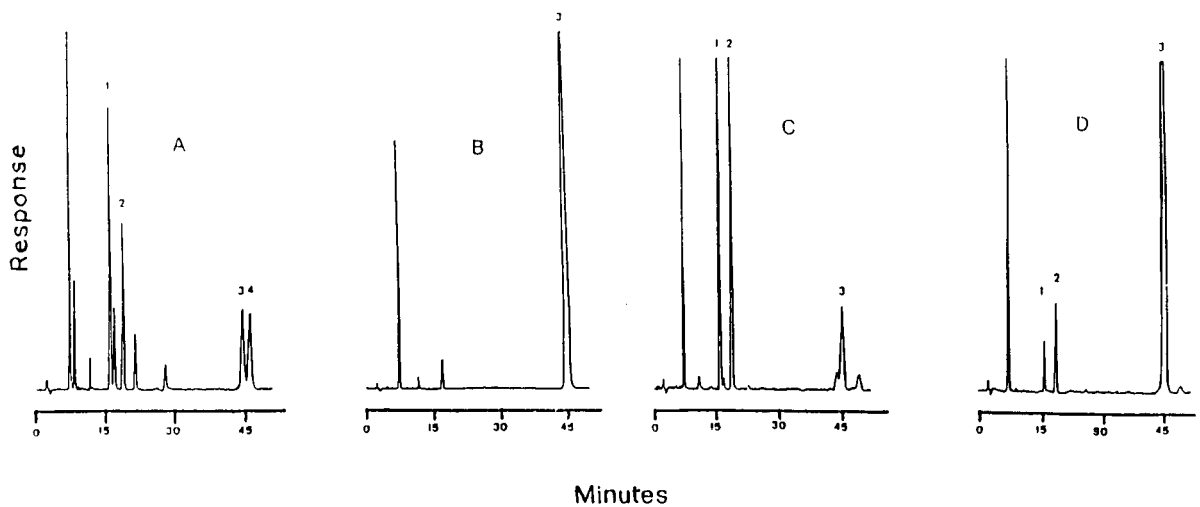

Fig. 4. Chromatograms of (A) standard amine compounds, (B) powder forensic sample, (C) liquid forensic sample 1 and (D) liquid forensic sample 2. Peaks: 1 = (1*R*,2*S*)-ephedrine–(+)-FLEC; 2 = (1*S*,2*S*)-pseudoephedrine–(+)-FLEC; 3 = (*S*)-(+)-methamphetamine–(+)-FLEC; 4 = (*R*)-(−)methamphetamine–(+)-FLEC.

Table 3
Separation parameters of enantiomeric drugs

Drug	$k'_{(S)-(+)}$	$k'_{(R)-(-)}$	α
Methamphetamine	17.00	17.70	1.04
Ephedrine	6.11	5.53	1.10
Pseudoephedrine	7.82	7.23	1.08

References

[1] A.K. Cho, *Science*, 249 (1990) 631.
[2] T.H. Jupille, *Am. Lab.*, 8 (1976) 85.
[3] I.S. Lurie and J.M. Weber, *J. Liq. Chromatogr.*, 1 (1978) 587.
[4] M. Moriyasu, M. Endo, Y. Hashimoto and T. Koeda, *Chem. Pharm. Bull.*, 32 (1984) 600.
[5] E.D. Lee, J.D. Henion, C.A. Brunner, I.W. Wainer, T.D. Doyle and J. Gal, *Anal. Chem.*, 58 (1986) 1349.
[6] D.M. Demorest, J.C. Fetzer, I.S. Lurie, S.M. Carr and K.B. Chatson, *LC·GC*, 5 (1987) 128.
[7] R.W. Roos and C.A. Lau-Cam, *J. Chromatogr.*, 370 (1986) 403.
[8] S.M. Sottolano, *J. Forensic Sci.*, 33 (1988) 1415.
[9] K. Hayakawa, K. Hasegawa, N. Imaizumi, O.S. Wong and M. Miyazaki, *J. Chromatogr.*, 464 (1989) 343.
[10] Y. Nakahara, A. Ishigami and Y. Takeda, *J. Chromatogr.*, 489 (1990) 371.
[11] T.L. Ascah and B. Feibush, *J. Chromatogr.*, 506 (1990) 357.
[12] D.W. Hill, *J. Liq. Chromatogr.*, 13 (1990) 3147.
[13] M. Boqusz and M. Wu, *J. Anal. Toxicol.*, 15 (1991) 188.
[14] N. Beaulieu, T.D. Cry, S.J. Graham and E.G. Lovering, *J. Assoc. Off. Anal. Chem.*, 74 (1991) 453.
[15] J.M. Barksdale and C.R. Clark, *J. Chromatogr. Sci.*, 23 (1985) 176.
[16] F.T.J. Noggle, J. DeRuiter and C.R. Clark, *Anal. Chem.*, 58 (1986) 1643.
[17] S.M. Hayes, R.H. Liu, W.S. Tsang, M.G. Legendre, R.J. Berni, D.J. Pillion, S. Barnes and M.H. Ho, *J. Chromatogr.*, 398 (1987) 239.
[18] T. Nagai, M. Sato, T. Nagai, S. Kamiyama and Y. Miura, *Clin. Biochem.*, 22 (1989) 439.
[19] F.T.J. Noggle, J. DeRuiter and C.R. Clark, *J. Chromatogr. Sci.*, 28 (1990) 529.

ELSEVIER

Journal of Chromatography A, 672 (1994) 141–148

JOURNAL OF CHROMATOGRAPHY A

Determination of the liquid vapour pressure of low-volatility compounds from the Kováts retention index

Walter Spieksma, Ronald Luijk, Harrie A.J. Govers*

Department of Environmental and Toxicological Chemistry, Amsterdam Research Institute for Substances in Ecosystems, University of Amsterdam, Nieuwe Achtergracht 166, 1018 WV Amsterdam, Netherlands

(First received November 3rd, 1993; revised manuscript received February 17th, 1994)

Abstract

The isothermal gas–liquid chromatographic Kováts retention index and an infinite dilution equilibrium fugacity model are combined to arrive at an expression relating the Kováts indices and the McReynolds numbers of a series of compounds to their isothermal pure liquid vapour pressures. This novel expression is the basis for ultra-low vapour pressure determination at environmentally relevant temperatures of pure organic (sub-cooled) liquids by routine gas–liquid chromatography on a non-polar stationary phase. Examples of the potential of the method are given for chlorobenzenes and chlorophenols.

1. Introduction

The vapour pressure of a compound is a physico-chemical property important for, *e.g.*, the assessment of its fate in the environment [1]. The latter demands (sub-cooled) liquid vapour pressure data at environmentally relevant temperatures, often lying below the compound's melting point. Experimental data on vapour pressures for series of compounds are required for the development of quantitative structure–activity relationships (QSARs) for vapour pressure, heat of vaporization and Henry's law constants [2].

In order to measure vapour pressure, gas saturation, effusion and gas–liquid chromatographic (GLC) methods can be used. GLC methods have several advantages over the other methods [3]. They are not sensitive to volatile impurities, can be carried out with only small amounts of compound, are fast and require less care in obtaining accurate and reproducible results.

GLC can separate compounds with different volatilities in the liquid stationary phase. The volatility or retention of a solute depends on both its activity coefficient in the stationary phase and its vapour pressure in the pure liquid state [4]. The measurement of a single GLC retention parameter produces only one data point, which therefore is insufficient for the purpose of vapour pressure determination. In addition, the value of the activity coefficient (measured or estimated) is required.

Several attempts have been made in order to solve this fundamental problem [3,5–7]. In all instances relatively non-polar stationary phases and one or more reference compounds with known vapour pressures have been employed.

* Corresponding author.

0021-9673/94/$07.00
SSDI 0021-9673(94)00173-7

The basic expression for most of these determinations is the Hamilton equation [7]:

$$\ln P_1 = (\Delta H_1/\Delta H_2) \ln P_2 + C$$

where 1 refers to the compound under investigation and 2 to the reference compound, P and ΔH are the vapour pressure and heat of vaporization, respectively, and C is a constant. The ratio of specific retention volumes V_{R1}/V_{R2} is equated to the ratio of the vapour pressures P_1/P_2, which is equivalent to equating the activity coefficients of compounds 1 and 2. After substitution into the Hamilton equation, the final expression is obtained:

$$\ln (V_{R1}/V_{R2}) = (1 - \Delta H_1/\Delta H_2) \ln P_2 - C$$

Plotting the measured specific retention volumes against known vapour pressures P_2 at different temperatures thus yields the assumed temperature-independent $\Delta H_1/\Delta H_2$ and C and, via the Hamilton equation, also P_1 at different temperatures.

In addition, a direct correlation equation of the type

$$-\log P = B_0 + B_1 I$$

has been used to express the relationship between the vapour pressure at 25°C and the Kováts GLC retention index (I) at 200°C for a series of compounds [8]. Once the I and P values of a number of compounds in a series have been measured, B_0 and B_1 can be found through linear regression. After measurement of the I values of other members of the series, their vapour pressures at 25°C can be calculated from this correlation equation. The Kováts index used in this method expresses the specific retention time or volume of a compound i relative to two n-alkanes with z and $z + 1$ carbon atoms, eluting before and after the compound, respectively [9]:

$$I_i = 100(\log V_{Ri} - \log V_{Rz})/(\log V_{Rz+1} - \log V_{Rz}) + 100z \quad (1)$$

The authors [8] did not explain how the pertinent correlation equation can be derived from this definition. However, it will be shown here that a constant ratio of the activity coefficients of i and z forms part of a larger number of necessary assumptions.

It should be pointed out that the physical chemistry behind the Kováts index allows one to measure (sub-cooled) liquid vapour pressures at environmentally relevant temperatures on a non-polar GLC column. The McReynolds number [10] of a model compound in the GLC liquid phase is used for quantification of its activity coefficient. Vapour pressure data for liquid n-alkanes [11] are used as reference pressures. Only isothermal Kováts indices at two or more temperatures need to be measured on a non-polar GLC column. As a first validation of this method, the (sub-cooled) liquid vapour pressures of chlorobenzenes and chlorophenols were determined at 25 and 160°C, respectively. Kováts indices measured by Haken and co-workers [12,13] were applied. The specific advantages with respect to other GLC methods are discussed below.

2. Method and results

2.1. Description of the method

The method includes main assumptions on the combination of the Kováts index and an infinite dilution equilibrium fugacity model, ratios of activity coefficients of solute/n-alkane (γ_i/γ_z) and subsequent n-alkanes (γ_{z+1}/γ_z) and the temperature dependence of the Kováts index. These assumptions will be described below along with a summary of the procedure in order to obtain vapour pressures.

2.2. Kováts index and infinite dilution equilibrium fugacity

The Kováts index of a compound i is defined according to Eq. 1. By definition the term $100z$ is the Kováts index I_z of an n-alkane with z carbon atoms. Instead of the specific retention volume, one may use other retention parameters in this equation such as the net retention times $t_i - t_0$, $t_z - t_0$ and $t_{z+1} - t_0$ or the capacity factors $(t_i - t_0)/t_0$, etc., provided that a constant carrier gas

flow-rate is applied [4]; t_0 is the dead retention time of a non-sorbed compound, representing the passage of this compound through the column, including extra-column inlet and outlet spaces.

The equilibrium fugacity model states that the ratio of the mole fraction y_i and x_i in the carrier gas and stationary phase, respectively, is proportional to the activity coefficient γ_i and the vapour pressure P_i of the incompressible pure liquid compound i [4]:

$$y_i/x_i = \gamma_i P_i/P_t \quad (2)$$

where P_t is the (mean) carrier gas pressure; $\gamma_i = 1$ for pure liquids and ideal solutions. It is assumed that the pure vapour and the vapour–carrier gas mixture both exhibit ideal behaviour or both exhibit identical non-ideal behaviour.

In order to derive an expression for the Kováts index as a function of activity coefficients and vapour pressures, we proceed as follows. It can be shown that at infinite dilution the capacity factor is inversely proportional to the ratio y_i/x_i (or volatility) of compound i in Eq. 2 [4]. The same holds true for the n-alkanes z and $z+1$. Substitution of these relationships between volatility and capacity factor into Eq. 2 yields relationships between capacity factor and activity coefficient plus vapour pressure. After subsequent substitution of the latter relationships into Eq. 1, one ultimately arrives at

$$I_i = I_z + 100(\log \gamma_z P_z - \log \gamma_i P_i)/(\log \gamma_z P_z - \log \gamma_{z+1} P_{z+1}) \quad (3)$$

In Eq. 3, both the vapour pressures and the activity coefficients are temperature dependent. In addition, the activity coefficients depend on the nature of the stationary phase. Thus the Kováts index is dependent on both temperature and the nature of the stationary phase.

2.3. Ratios of activity coefficients for homologous series

Eq. 3 does not solve the fundamental problem described in the Introduction. This problem will be approached here through the assumption that ratios between activity coefficients (γ_i/γ_z and γ_{z+1}/γ_z) are constants for (homologous) series of related compounds.

First, a simple and accurate log–linear regression relationship, $\log P_z = \log P_{H_2} + (\mathrm{d} \log P_z/\mathrm{d}z)z$, exists between the liquid vapour pressure and carbon number z of an n-alkane [$H(CH_2)_zH$] [13] that can be written in terms of its Kováts index:

$$\log P_z = (\mathrm{d} \log P_z/\mathrm{d}I_z)I_z + \log P_{H_2} \quad (4)$$

where P_{H_2} is the vapour pressure of liquid hydrogen ($z = 0$). Application of Eq. 4 to both n-alkanes z and $z+1$ yields a simple expression for $\log (P_z/P_{z+1})$. In Table 1 values of the regression coefficients and vapour pressure ratios for n-alkanes at different temperatures are given, based on Antoine constants derived from experimental vapour pressure data [11]. The lower the temperature, the larger is the decrease in vapour pressure with increase in carbon number and the higher is the vapour pressure ratio between two subsequent n-alkanes. The maximum errors in the slope and intercept of Eq. 4 amount to 1% and 0.5%, respectively.

Second, an evaluation of the ratio γ_z/γ_{z+1} at 120°C reveals that this ratio can be approximated by 1 ($\gamma_z = \gamma_{z+1}$) within an overestimation error of 2–18% depending on the nature of the stationary phase. The results of this evaluation are given in Table 2. They were obtained by evaluating net retention data for n-alkanes at 120°C [10] using the relationship $(t_i - t_0)/(t_z - t_0) = (\gamma_z P_z)/(\gamma_i P_i)$

Table 1
Calculated regression coefficients of Eq. 4 and vapour pressure ratios of n-alkanes at different temperatures (T) using Antoine constants [11] with 95% confidence limits in parentheses

T (°C)	$\mathrm{d} \log P_z/\mathrm{d}I_z \cdot 10^{-3}$	$\log P_{H_2}$ [a]	z	P_z/P_{z+1}
180	−2.257 (0.021)	5.181 (0.016)	10–18	1.681
160	−2.454 (0.023)	5.151 (0.018)	10–18	1.759
140	−2.684 (0.027)	5.129 (0.021)	10–18	1.855
120	−2.985 (0.035)	5.119 (0.027)	10–18	1.976
25	−5.213 (0.009)	5.315 (0.008)	5–14	3.322

[a] Log P values based on P in Torr (1 Torr = 133.322 Pa).

Table 2
Ratios of experimental net retention times taken from the literature [10] and ratios of activity coefficients of subsequent *n*-alkanes on different stationary phases at 120°C, calculated from these and from the vapour pressure ratios in Table 1 (see text)

Stationary phase	$(t_{z+1} - t_0)/(t_z - t_0)$	γ_z/γ_{z+1}
Squalane	1.945	1.016
SE-30, DB1	1.776	1.113
OV-101	1.771	1.116
OV-3, DB5	1.797	1.100
OV-17	1.799	1.098
Carbowax 20M	1.673	1.181

also used in the derivation of Eq. 3 and applying the vapour pressure ratios in Table 1.

After insertion of Eq. 4 and $\gamma_z = \gamma_{z+1}$ into Eq. 3 and some rearrangements, the isothermal pure liquid vapour pressure P_i can be written as a function of the isothermal Kováts index I_i of component i:

$$\log P_i = (\mathrm{d} \log P_z / \mathrm{d}I_z) I_i + \log P_{H_2} + \log(\gamma_z/\gamma_i) \quad (5)$$

Finally, an assumption has to be introduced regarding the ratio γ_z/γ_i in Eq. 5. This can be expressed in the ΔI values of McReynolds [10]. ΔI of a compound on a stationary phase is its shift in Kováts index compared with the most non-polar stationary phase squalane (Sq). It follows from Eq. 5, with $\Delta I = I_i - I_i(\mathrm{Sq})$, written explicitly in terms of the ratio of the activity coefficients, that

$$\log(\gamma_z/\gamma_i) = \log[\gamma_z(\mathrm{Sq})/\gamma_i(\mathrm{Sq})] - (\mathrm{d} \log P_z / \mathrm{d}I_z)\, \Delta I \quad (6)$$

The activity coefficient ratios at 120°C of compounds containing typical functional groups can be evaluated using data from McReynolds [10] and Eqs. 5 and 6 (see Table 3). McReynolds measured the Kováts indices of 68 compounds on 25 liquid phases and selected the ten most characteristic compounds to give the best prediction of the Kováts index on different stationary phases. For these ten compounds the Kováts index was measured on more than 200 liquid phases. For chlorinated compounds (*e.g.*, chlorobenzenes) 1-iodobutane is the best compound to predict Kováts indices, whereas for alcohols (*e.g.*, phenols) 2-methyl-2-pentanol is the better predictor [9]. In addition, ΔI and γ_z/γ_i values are considered to be temperature independent. As

Table 3
Calculated activity coefficient ratios at 120°C of compounds with different functional groups on SE-30 and Carbowax 20M (CW-20) stationary phases, calculated with Eqs. 5 and 6, and auxiliary data from the literature

Compound	$I_i(\mathrm{Sq})$ [a]	P_i [b] (Torr)	$\mathrm{Log}\,\gamma_z/\gamma_i(\mathrm{Sq})$ [c]	ΔI [a]		$\mathrm{Log}\,(\gamma_z/\gamma_i)$ [d]	
				SE-30	CW-20	SE-30	CW-20
Benzene	653	2297	0.191	15	322	0.236	1.153
1-Butanol	590	823	−0.442	53	536	−0.284	1.158
2-Pentanone	627	1260	−0.147	44	368	−0.016	0.952
Nitropropane	652	546	−0.436	64	572	−0.245	1.272
Pyridine	699	871	−0.093	41	510	0.030	1.430
2-Methyl-2-pentanol	690	739	−0.191	31	387	−0.098	0.964
1-Iodobutane	818	575[e]	0.083	3	282	0.092	0.924
2-Octyne	841	466[e]	0.060	22	221	0.126	0.720
1,4-Dioxane	654	1310	−0.049	44	434	0.082	1.246

[a] Data from ref. 9.
[b] Data from ref. 11.
[c] Calculated using Eq. 5.
[d] Calculated using Eq. 6.
[e] Using the Clausius–Clapeyron equation and the enthalpies of vaporization and boiling points from ref. 16.

far as γ_z/γ_i is concerned, the same assumption is made in the well known Flory–Huggins athermal approximation for polymer solutions [4].

2.4. Kováts index and temperature

From Eq. 3, it follows that the Kováts index will be a complicated function of temperature. However, a simple linear relationship was given by Kováts [9]:

$$I_i = (dI_i/dT)T + I_{i0} \quad (7)$$

In Eq. 7, the intercept I_{i0} is the Kováts index at $T = 0$°C. In Table 4, Eq. 7 is evaluated using Kováts indices for chlorobenzenes at 140, 160 and 180°C on non-polar SE-30 and polar Carbowax 20M stationary phases.

The difference in temperature dependence of the Kováts index (*i.e.*, the difference in the slope dI_i/dT; see Table 4) on two stationary phases can only originate from different temperature dependences of the activity coefficients in Eqs. 3 and 5. The Kováts index on the non-polar SE-30 stationary phase shows the best linear behaviour (lowest errors in slope and intercept).

According to Kováts [9], an inversion of the elution sequence of compounds when extrapolating from $I_i(T)$ to I_{i0} normally does not occur.

Table 4
Regression coefficients of Eq. 7 on SE-30 and Carbowax 20M stationary phases using Kováts indices at 140, 160 and 180°C [12] with 95% confidence limits in parentheses

Chlorobenzene congener	SE-30		Carbowax 20M	
	I_{i0}	dI_i/dT (°C^{-1})	I_{i0}	dI_i/dT (°C^{-1})
Mono-	815 (1)	0.15 (0.03)	1144 (2)	0.80 (0.09)
1,2-Di-	972 (2)	0.48 (0.07)	1000 (2)	3.20 (0.09)
1,3-Di-	985 (1)	0.20 (0.03)	1077 (23)	2.35 (0.81)
1,4-Di-	993 (3)	0.15 (0.06)	1155 (10)	2.28 (0.36)
1,2,3-Tri-	1111 (3)	0.75 (0.12)	1458 (4)	1.75 (0.14)
1,2,4-Tri-	1098 (2)	0.60 (0.06)	1388 (9)	1.70 (0.32)
1,3,5-Tri-	1091 (1)	0.38 (0.04)	1250 (6)	1.88 (0.22)
1,2,3,4-Tetra-	1209 (1)	1.13 (0.04)	1627 (2)	1.75 (0.06)
1,2,3,5-Tetra-	1195 (3)	0.95 (0.12)	1532 (2)	1.75 (0.09)
1,2,4,5-Tetra-	1195 (3)	0.95 (0.12)	1508 (3)	1.65 (0.12)
Penta-	1339 (3)	1.18 (0.10)	1710 (6)	1.78 (0.22)
Hexa-	1497 (2)	1.25 (0.09)	1849 11)	2.00 (0.40)

dI_i/dT values are small for most compounds and constant over a wide range of temperatures. Errors resulting from extrapolation over 100°C amount to a few I units at the maximum. From Fig. 1, it can be inferred that inversion occurs only for 1,2-dichlorobenzene with respect to the 1,3-plus 1,4-isomers.

2.5. Determination of pure liquid vapour pressure using the Kováts index

On the basis of Eq. 5, a general procedure can be described for the determination of the vapour pressure of compound i (P_i) or of a series of related compounds at a particular temperature (T').

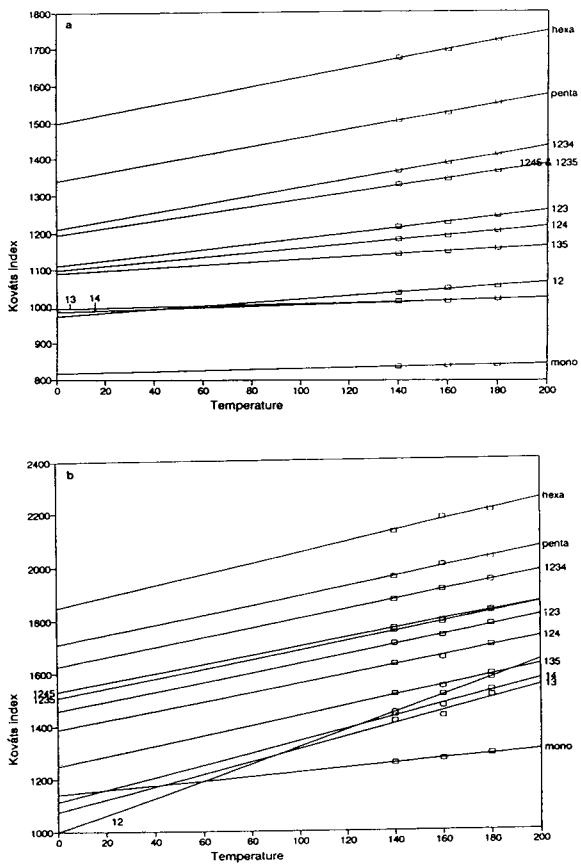

Fig. 1. Kováts indices (I) of chlorobenzenes on (a) non-polar SE-30 and (b) polar Carbowax 20M GLC stationary phases as a function of temperature (T, °C).

The first step is the routine measurement of the isothermal Kováts index (I_i) of compound i at two or more temperatures on a non-polar column (*e.g.*, SE-30 or DB1). These temperatures have to be as close as possible to T' in order to minimize extrapolation errors.

The second step is the calculation of I_i at T' with the help of Eq. 7 by extrapolation from the experimental temperatures to T'.

The third step is the calculation of the regression coefficients $\mathrm{d}\log P_z/\mathrm{d}I_z$ and $\log P_{H_2}$ at T' using data from Ohé [11] for liquid *n*-alkanes in Eq. 4. Table 1 already provides regression coefficients at some specified temperatures.

The fourth step is the calculation of $\log \gamma_z/\gamma_i$ from Eq. 6, using ΔI values from McReynolds [10] for the pertinent stationary phase and the compound with the proper functional group or using data from Table 3.

The final step is the calculation of the vapour pressure at the desired temperature inserting I_i, $\log P_{H_2}$, $\mathrm{d}\log P_z/\mathrm{d}I_z$ and $\log(\gamma_i/\gamma_z)$ in Eq. 5.

2.6. Determination of the vapour pressures of chlorobenzenes and chlorophenols

Validation of the method

The procedure described in the previous section can be validated by comparison of vapour pressure values obtained in this way with vapour pressure data obtained independently via other methods. Especially the fourth step in our procedure is associated with several uncertainties with respect to the choice of the proper model chemical and the availability of data at only one temperature (120°C). Experimental vapour pressure data suitable for this purpose are available for chlorobenzenes and chlorophenols [14]. For these compounds we can use Kováts indices already available in the literature [12,13] in order to obtain vapour pressure values determined via our method.

Vapour pressure and heat of vaporization of chlorobenzenes at 25°C

The vapour pressures of (sub-cooled) liquid chlorobenzenes at 25°C were determined according to our method with the help of Eq. 5. Experimental Kováts indices on an SE-30 stationary phase [12] were extrapolated to 25°C using the data in Table 4. (Mean) values of the regression coefficients $\mathrm{d}\log P_z/\mathrm{d}I_z$ and $\log P_{H_2}$ at 25°C were available from Table 1. The $\log(\gamma_z/\gamma_i)$ value of 1-iodobutane at 120°C on SE-30 from Table 3 was used. With the help of the same data and additional calculations of the regression coefficients of Eq. 4, the vapour pressures at 0, 5, 10, 15 and 20°C were calculated and from these, using the Clausius–Clapeyron equation, the heats of vaporization (ΔH) in the temperature range 0–25°C. The results are given in Table 5. Deviations from current data are considered to be acceptable in view of the known errors of other methods. However, it remains uncertain to what extent the results are sufficiently accurate in order to determine the differences between isomeric compounds in the proper way. Inversion of the retention sequence might have been caused by the large extrapolation step from Kováts indices at 140–180°C to 25°C, in addition to the uncertainties in the $\log(\gamma_z/\gamma_i)$ value from Table 3.

Vapour pressure of chlorophenols at 160°C

The (sub-cooled) liquid vapour pressures of phenol and nine chlorophenols at 160°C were determined according to our method with the help of Eq. 5. Experimental Kováts indices on SE-30 stationary phase at 160°C were available in the literature [13] and no extrapolation was required or possible. Values of the regression coefficients $\mathrm{d}\log P_z/\mathrm{d}I_z$ and $\log P_{H_2}$ at 160°C were taken from Table 1. The $\log(\gamma_z/\gamma_i)$ value of 2-methyl-2-pentanol at 120°C on SE-30 from Table 3 was used. The results are given in Table 6. With respect to isomer sequences, the results are better than those for the chlorobenzenes. The reason is probably the smaller extent to which temperature effects are present. Apparently the ΔI and γ_z/γ_i values are temperature independent. Except for the inversion for phenol and 2-monochlorophenol, and to a lesser extent also for the two trichlorophenols, the isomer values show a sequence similar to that of the literature data.

Table 5
Comparison of vapour pressure (P_i, in Pa) and heat of vaporization (ΔH, in kJ/mol) data for chlorobenzenes at *ca.* 25°C derived from Kováts indices on SE-30 using Eq. 5 and using other methods

Chlorobenzene congener	P_i [a]	P_i [b]	ΔH [a] (0–25°C)	ΔH [c] (25°C)
Mono-	1828	1560	43.91	41.55 (40.97)[d]
1,2-Di-	252	185	50.90	49.87
1,3-Di-	236	299	53.89	48.55
1,4-Di-	216	257	54.83	48.74
1,2,3-Tri-	44.1	56.9	57.16	56.64
1,2,4-Tri-	53.4	60.1	57.62	55.74
1,3,5-Tri-	62.4	74.9	59.00	54.82
1,2,3,4-Tetra-	12.1	8.0	60.14	63.19
1,2,3,5-Tetra-	15.1	16.3	60.69	61.69
1,2,4,5-Tetra-	15.1	12.5	60.69	61.42
Penta-	2.49	2.19[e]	67.74	67.54
Hexa-	0.367	0.344[e]	76.80	73.82

[a] Derived using Eq. 5.
[b] Data from ref. 14.
[c] Values calculated from experimental boiling point data according to the Hildebrand rule [2].
[d] Ref. 16.
[e] Extrapolated value from ref. 15.

3. Discussion and conclusions

A method was developed for the determination of the (sub-cooled) liquid vapour pressures of low-volatility compounds or series of compounds at environmentally relevant temperatures. The results obtained for chlorobenzenes and chlorophenols according to this method are within 3–51% of values obtained by other methods with an average deviation of only 19%. These deviations are considered to be acceptable in view of the available data on the accuracy and reproducibility of other methods [3,15]. Remaining uncertainties are associated with the extrapolation of Kováts indices from the temperature region of their measurement to environmentally relevant temperatures and with the selection of McReynolds model compounds for log (γ_z/γ_i) values at suitable temperatures. The method can be improved with respect to these uncertainties. After these improvements it will probably be sufficiently accurate to distinguish between isomers in a completely reliable way.

Table 6
Comparison of vapour pressure (P_i, in Pa) data for chlorophenols at 160°C derived from Kováts indices on SE-30 using Eq. 5 and using other methods

Chlorophenol congener	P_i [a]	P_i [b]
Phenol	79	53
2-Mono-	56	70
3-Mono-	22	18
4-Mono-	22	18
2,4-Di-	20	22
2,6-Di-	17	16
2,4,5-Tri-	7.1	7.3
2,4,6-Tri-	7.5	7.1
2,3,4,6-Tetra-	2.5	2.6
Penta-	0.91	0.72

[a] Derived using Eq. 5.
[b] Data from ref. 14.

The uncertainties associated with the current method are present in other GLC methods to an even greater extent. In GLC methods based on the Hamilton equation [3,5–7] (see Introduction), C and $(1-\Delta H_1/\Delta H_2)$ values are obtained at the temperatures of measurement of the relative retention times. Only if these values

are assumed to be temperature independent and if a value of the vapour pressure of the reference compound is available at the environmentally relevant temperature can vapour pressures at the latter temperature be found. In addition, the Hamilton equation assumes a constant value of 1 for the ratio γ_1/γ_2 of the activity coefficients of compound 1 and its reference compound 2. The reference compound may have a retention time differing considerably from that of the compound. This assumption has not yet been validated and is only treated implicitly in this method. In the present method a constant value, different from 1, is assumed for the ratio γ_i/γ_z of the activity coefficient of compound i and the reference n-alkane z, *eluting close to compound* i. Moreover, this value is treated explicitly and therefore is open to improvement. It is interesting to note an example of the use of the Hamilton method with two reference n-alkanes (octadecane and eicosane) [3]. The present method, using an extensive series of n-alkanes, can be considered as a further development of this idea.

Finally, the present method can be compared with the use of a direct correlation equation relating the Kováts index at 200°C to the vapour pressure at 25°C as mentioned in the Introduction [8]. One may ask which further assumptions have to be introduced into Eq. 5 in order to arrive at a simple direct correlation equation. After application of Eq. 5 at 25°C and substitution of Eq. 7 $[I_i(25°C) = I_i(200°C) - (dI_i/dT)(200 - 25)]$, it follows that in addition to the independence of d log P_z/dI_z of z and γ_i/γ_z of z and i, dI_i/dT also has to be independent of i. The first two requirements are also included in our method, whereas the last is not. From Table 4, it can be seen that large differences between dI_i/dT values for different congeners exist and that, as a consequence, this requirement cannot be fulfilled. This may lead to erroneous predictions if isomer sequences of vapour pressures in the case of inversion of $I_i(T)$ values within the pertinent temperature range. Non-linear correlation equations are currently in use that apply much less drastic assumptions [2]. In addition, the direct correlation equation can be used only when several vapour pressure values of compounds belonging to the series are already known.

Acknowledgement

We acknowledge the critical reading of the manuscript by Dr. Pim de Voogt.

References

[1] D. Mackay and S. Paterson, in W. Karcher and J. Devillers (Editors), *Practical Applications of Quantitative Structure Activity Relationships (QSAR) in Environmental Chemistry and Toxicology*, Kluwer, Dordrecht, 1990, pp. 433–460.
[2] H.A.J. Govers, *J. Chem. Soc., Faraday Trans.*, 89 (1993) 3751–3759.
[3] T.F. Bidleman, *Anal. Chem.*, 56 (1984) 2490–2496.
[4] J. Novak, in J.A. Jonsson (Editor), *Chromatographic Theory and Basic Principles*, Marcel Dekker, New York, 1987, pp. 103–156.
[5] J.W. Westcott and T.F. Bidleman, *J. Chromatogr.*, 210 (1981) 331–336.
[6] B.D. Eitzer and R.A. Hites, *Environ. Sci. Technol.*, 22 (1988) 1362–1364.
[7] D.J. Hamilton, *J. Chromatogr.*, 195 (1980) 75–83.
[8] W.T. Foreman and T.F. Bidleman, *J. Chromatogr.*, 330 (1985) 203–216.
[9] E. Kováts, *Helv. Chim. Acta*, 41 (1958) 1915–1932.
[10] W.O. McReynolds, *J. Chromatogr. Sci.*, 8 (1970) 685–691.
[11] S. Ohé, *Computer Aided Data Book of Vapour Pressure*, Data Publ. Book Co., Tokyo, 1976.
[12] J.K. Haken and I.O.O. Korhonen, *J. Chromatogr.*, 265 (1983) 323–327.
[13] M.B. Evans and J.K. Haken, *J. Chromatogr.*, 468 (1989) 373–382.
[14] D.R. Stull, *Ind. Eng. Chem.*, 39 (1947) 517–540.
[15] D. Mackay and W.Y. Shiu, *J. Phys. Chem. Ref. Data*, 10 (1981) 1175–1199.
[16] D.R. Lide (Editor), *Handbook of Chemistry and Physics*, CRC Press, Boca Raton, FL, 72nd ed., 1991.

ELSEVIER

Journal of Chromatography A, 672 (1994) 149–158

JOURNAL OF CHROMATOGRAPHY A

Retention of halocarbons on a hexafluoropropylene epoxide modified graphitized carbon black I. Methane-based compounds☆

Thomas J. Bruno *, Michael Caciari☆☆

Thermophysics Division, National Institute of Standards and Technology, Boulder, CO 80303, USA

(Received December 14th, 1993)

Abstract

The retention characteristics of eight methane-based chlorofluorocarbon and fluorocarbon fluids have been studied as a function of temperature on a stationary phase consisting of a 5% (w/w) coating of a low-molecular-mass polymer of hexafluoropropylene epoxide on a graphitized carbon black. The fluids that were studied include chlorotrifluoromethane (R-13), tetrafluoromethane (R-14), dichlorofluoromethane (R-21), chlorodifluoromethane (R-22), trifluoromethane (R-23), difluoromethane (R-32), chloromethane (R-40), and fluoromethane (R-41). Measurements were made at −20, 0, 20 and 40°C for all fluids except dichlorofluoromethane, which was measured at 40, 60, 80 and 100°C. Net retention volumes, corrected to a column temperature of 0°C, were calculated from retention time measurements, the logarithms of which were fitted against reciprocal thermodynamic temperature. The relative retentions, also as a function of temperature, were calculated with respect to the retention of tetrafluoromethane. Qualitative features of the data are examined, and trends are identified. In addition, the data were fit to linear models for the purpose of predicting retention behavior of these compounds to facilitate chromatographic analysis.

1. Introduction

Many laboratories are engaged in a comprehensive research program geared toward the development of new fluids for use as refrigerants, blowing and foaming agents, and propellants. These new materials are needed to replace the fully halogenated materials that are believed to contribute to atmospheric ozone depletion, and which will be phased out of production by law. The research that comprises this large scale effort includes thermophysical properties measurements and correlation, materials compatibility testing, chemical stability measurement, and cycle suitability studies [1,2]. An important part of all of these research programs is the chemical analysis of new fluids that are tested [3–6].

Gas chromatography is one of the major chemical analysis methods that is applied to the study of alternative refrigerants for several important reasons, not the least of which are simplicity and economics of operation [7,8]. It is used both as a qualitative identification tool and for quantitative analysis of impurities that are

* Corresponding author.

☆Contribution of the United States Government.

☆☆Permanent address: Fort Lupton High School, Fort Lupton, CO 80621, USA.

0021-9673/94/$07.00
SSDI 0021-9673(94)00192-C

known to be present in a sample [7,9]. A knowledge of the retention characteristics of important fluids on the more useful stationary phases is an important component in the design of effective qualitative and quantitative chromatographic analyses. Such information would fill two very important analytical needs. First, we would like to identify unknown or unfamiliar peaks that appear on a chromatogram obtained from, for example, the analysis of a field sample of a new refrigerant fluid. Second, we would like to optimize chromatographic separations by being able to predict the response of elution times and separation factors to controllable instrumental parameters.

It is well known that the use of chromatographic retention characteristics as a means of compound identification must be approached with extreme caution, since the results are indirect [7,9]. For example, the equality of retention times of two materials (measured under the same conditions of column temperature, carrier gas flow-rate and stationary phase identity and quantity) does not constitute absolute proof that the materials are in fact the same. One must consider (1) the possibility of coincidence, and (2) the possibility of a chromatographic peak being caused by multiple compounds that co-elute. The coincidence of retention times of two or more peaks, in the absence of any other data, must therefore be viewed as supporting evidence only. The "other data" to which we refer may be the results from other analytical tests, or simply a knowledge of the sample history or synthetic route. One can generally make the contrary statement about retention time coincidence, however. In this respect, if the retention times of two materials are different under the same instrumental conditions (and the instrument is functioning properly), then the materials are indeed very likely different.

There are a number of measures that one can take to significantly increase the utility and reliability of retention data as a qualitative identification tool. The first method we shall mention involves the measurement of retention times on two different columns having stationary phases of different polarity. A close match of the two retention times with the retention times of a standard compound provides much more confidence in identification. One may also route the effluent of a single column to different but appropriate detectors. For example, the consistency of the response ratio from a thermal conductivity detector and a flame ionization detector for a standard and an unknown is good evidence of identity. Both of these methods are somewhat difficult to implement, however. The first suffers from inconvenience and from being very time-consuming. The second approach suffers from difficulty in reproducibly controlling the split pneumatics. The need for two detectors instead of one increases both the complexity and implementation cost. Moreover, it is sometimes difficult to select two distinct yet appropriate detectors for a given analyte.

Corrected retention parameters, although indirect, provide a very useful and well known method to overcome some of the difficulties and complexities of peak identification in chromatographic analysis. The use of such parameters (which have been corrected for controllable instrumental variables) will minimize many of the pitfalls caused by the day-to-day variation in chromatographic performance. An example of this is the use of net retention volumes (which themselves may be further corrected for column temperature). The calculation of relative retention volumes is a useful way to minimize instrument to instrument (or column to column) variations. This is important when multiple instruments operating at somewhat different conditions and using separate columns (but the same stationary phase and column type) are to be compared. It is then possible to rationally compare the retentions obtained from an unknown sample with retentions measured from pure materials. When one further measures the temperature dependence of these parameters for unknown peaks and compares these results with such data measured on pure materials, a far greater level of confidence is achieved. This is especially true if more than one compound elutes under a single peak at a given temperature, since changing column temperature will often resolve such species.

In this paper, we present temperature-depen-

dent measurements of the net retention volume, corrected to a column temperature of 0°C, of eight methane-based fluids that are commonly encountered in alternative refrigerant research and testing. The fluids we have studied are all gaseous at room temperature and pressure. To facilitate the data analysis and comparison, one measurement each (at 40°C) is also provided for trichlorofluoromethane (R-11), dichlorofluoromethane, (R-12) and methane (R-50). A listing of all the fluids studied is provided in the left-hand column of Table 2, along with the accepted code numbers. An explanation of the numbering system for these compounds is provided in the appendix. The measurements were made on the packed-column stationary phase that is most commonly used for refrigerant analysis; a 5% coating of a low-molecular-mass polymer of hexafluoropropylene epoxide (HPE) on a graphitized carbon black [10]. Other stationary phases have been used for these types of analyses [11–13], but the HPE has proven to be the most chemically stable. This modifier has a usable temperature range of −35 to 290°C. The relative retentions were then calculated with respect to tetrafluoromethane. In addition to the discussion of qualitative trends in the data, fits to simple linear models are presented of the logarithms of the net retention volumes and the relative retentions against thermodynamic temperature. These fits provide a predictive capability.

2. Theory

The typical chromatographic integrator (or chromatographic software package for a computer) will report, among many possible analytical parameters, the retention time of each peak. If the volumetric carrier gas flow-rate (at the column exit) is measured and multiplied by the retention time, the retention volume, V_R, is obtained. The adjusted retention volume, V'_R, is the retention volume corrected for the void volume (or mobile phase holdup) of the column. It is obtained by simply subtracting the retention volume of an unretained solute (V_M) such as air:

$$V'_R = V_R - V_M \tag{1}$$

The net retention volume, V_N, is obtained by applying a factor, j, to account for the pressure drop across the column:

$$V_N = jV'_R \tag{2}$$

where j is usually[a] the Martin–James compressibility factor:

$$j = \frac{3}{2}\left[\frac{\left(\frac{P_i}{P_0}\right)^2 - 1}{\left(\frac{P_i}{P_0}\right)^3 - 1}\right] \tag{3}$$

where P_i is the inlet pressure (absolute) and P_0 is the outlet pressure (usually atmospheric pressure). The specific retention volume, V^0_g, corrects the net retention volume for the amount of stationary phase, and the column temperature is adjusted to 0°C:

$$V^0_g = (273.15)\frac{V_N}{(W_s T_{col})} \tag{4}$$

where T_{col} is the column temperature, and W_s is the mass of stationary phase in the column. This value is a characteristic for a particular solute on a particular stationary phase in a particular carrier gas, and is instrument independent. This is a quantity that may be compared from instrument to instrument, and laboratory to laboratory with a high level of confidence provided the stationary phase used is a single, pure compound. If the mass of stationary phase is not known, or is not meaningful, it is still of value to correct the net retention volume to a column temperature of 0°C (represented by V^0_N) by simply not including the term for W_s (that is, setting it equal to unity). In the present study, the stationary phase is a solid sorbent modified with a liquid coating. Since the retention in this case is not caused exclusively by either adsorption or absorption processes, we will use the net retention volume, V^0_N, corrected to 0°C (that is, V^0_g, with $W_s = 1$).

[a] Other expressions or approximations have been used as well. One of the most reliable approximations to the Martin–James compressibility factor is due to Halasz and Heine: $j_{approx.} = 3/[2(P_i/P_0) + 1]$.

It is also extremely valuable to calculate a relative retention, $r_{a/b}$:

$$r_{a/b} = \left(\frac{V_g^b}{V_g^a}\right) = \left(\frac{V_N^b}{V_N^a}\right) \quad (5)$$

where the numerical superscripts refer to the retention volumes of solutes a and b. In this case, solute a is a reference. The relative retention is dependent only on the column temperature and the type of stationary phase. For reasons of operational simplicity, this parameter is usually one of the best to use for qualitative analysis [7,9]. It can account for small differences in column temperature, stationary phase considerations, column history, and minor disturbances in carrier gas flow-rate. Some of the stationary phase considerations for packed columns include differences in liquid loadings, purities and packing density, coiling effects, and residual activity of the solid support. The last concern is very important when the stationary phase is an adsorbent or an adsorbent modified by a coating. For capillary columns, these considerations include differences in coating thicknesses, purity, and irregularities in split ratios. When measurements are performed carefully, the relative retention varies only with column temperature and stationary phase, and thus forms a reasonable basis for qualitative identification.

To extend the applicability of relative retention data, it is possible to account for temperature by plotting $\ln(r_{a/b})$ against $1/T$, where T is the thermodynamic temperature. Such plots are approximately linear (especially in gas–liquid chromatography), and allow comparisons at many column temperatures. The plots can become very non-linear when measured with unmodified solid sorbents as the stationary phase, depending upon the detailed characteristics of the adsorption isotherms. The use of a surface modifier (as was done in the present study) on a solid phase will often increase the linearity of the plots, and shorten retention times.

Although it is not generally considered good practice to extrapolate the plot beyond the temperature range for which experimental data are available, we have found with this class of compounds that extrapolation to temperatures 50°C higher than that used in the correlation can provide acceptable predictions. Naturally, interpolation within the region covered by the experimental data provides very good predictions of both the relative retentions and the net retention volumes. These data can even provide the basis for scaling isothermal analyses to temperature-programmed analyses.

3. Experimental

The measurements presented in this paper were performed on a commercial gas chromatograph that had been modified to provide high-precision retention data. The column oven was modified by the addition of 1.9 cm thick, 10 × 10 cm square aluminum plates surrounding the column to provide additional thermal mass for stability, and also to integrate out temperature variations in different locations within the oven. Additional insulation (in the form of mineral wool board and bubble-wrap) was placed in appropriate locations around the oven compartment. The oven temperature was measured with a quartz-crystal oscillator thermometer (calibrated against a NIST-standard platinum resistance thermometer) that was accurate to within ± 0.01°C. Injection was done with a valve containing a sample loop of 0.1 ml volume. The valve was pneumatically actuated with pilot valves using helium as the actuation gas to inject very rapidly and thereby minimize the injection pressure pulse. The injection valve and loop were maintained at 50°C for all measurements. The carrier gas line to the injection valve was modified to allow the column head pressure to be measured with a calibrated Bourdon tube gauge. This gauge was calibrated with an electronic Bourdon tube transfer standard that was itself calibrated against a NIST-standard dead mass pressure balance. The column outlet pressure was measured with an electronic barometer that had a resolution of 1.3 Pa (approximately 0.01 mm Hg). This barometer was calibrated against a dead mass pressure balance. The col-

umn carrier gas flow-rate was measured with an electronic soap-bubble flow meter, the temperature of which was referenced to the oven temperature with a pair of type-j thermocouple junctions operated in differential mode. The electromotive force of the pair was measured with a nanovoltmeter. This measurement allowed the flow-rate to be corrected for the vapor pressure of water. Retention times were measured by a commercial integrator. A Ranque–Hilsch vortex tube was used to provide cooling in the column oven for the subambient temperature measurements [13]. Thermal conductivity detection (TCD) was used with a carrier gas of research-grade helium. The TCD was maintained at 50°C for all measurements.

The stationary phase was a commercially prepared packing consisting of a 5% (mass/mass) coating of a low-molecular-mass polymer of hexafluoropropylene epoxide modifier on a 60/80 mesh (250–177 μm) graphitized carbon black [10]. Some representative properties of this modifier are presented in Table 1. A column was prepared by packing the phase into a cleaned, 2 m long section of copper tubing (0.65 cm O.D.). The column was conditioned for 4 h in the chromatograph by equilibration at 100°C with a gentle flow of helium carrier gas.

For each retention time measurement, five fluid injections were performed at each column temperature. Each series of injections was preceded and followed by five measurements of the carrier gas flow-rate, and the injection of five aliquots of air. The air was injected separately, before and after the injection of fluid, to measure the void volume of the column without introducing air as an impurity into the fluid containers. The corrected retention time was simply obtained by subtracting the average air retention time. At the start of each of these fifteen injections (five air, five fluid, five air), the requisite temperatures (column, flowmeter, and barometer) and pressures (column head and column exit) were recorded. These replicate measurements furnished the uncertainties used for the error propagation that provided the overall experimental uncertainties that are reported. The column head pressure was maintained uniformly at 137.9 ± 0.3 kPa (approximately 20 p.s.i.g.) for the measurements, although measurements were initially performed at several other pressures to verify consistency in the operation of the chromatograph. The carrier gas flow-rate at the column exit was maintained at 45 ± 0.3 ml/min.

Measurements were performed on four isotherms for each fluid. Most of the fluids were measured at −20, 0, 20 and 40°C, but the less volatile fluids were measured at 40, 60, 80 and 100°C.

The chlorofluorocarbon samples used for these measurements were all obtained from commercial sources in the highest purity available, and were used without any further purification.

Table 1
Properties of hexafluoropropylene epoxide modifier

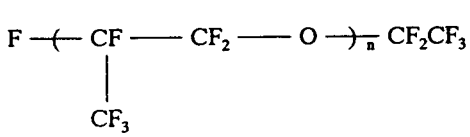

n = 10 - 60

Number average molecular mass	6250
Vapor pressure	$1 \cdot 10^{-8}$ kPa (38°C) $1 \cdot 10^{-4}$ kPa (260°C)
Density (24°C)	1.86–1.91 g/ml
Refractive index (n_D^{25})	1.296–1.301

4. Results and discussion

The corrected net retention volumes, V_N^0, for each fluid are presented in Table 2. The reported uncertainties are the result of an error propagation performed with the standard deviations obtained from replicate measurements of each experimental parameter. The errors were added in quadrature since all variables are essentially uncorrelated (as determined by examination of Spearman's ρ and Kendall's τ), and the deviations were found to fit a normal distribution and were therefore treated as being random. In addition to the uncertainty, the coefficient of

Table 2
The net retention volume, V_N^0 (ml), and their logarithms, of the fluids measured in this study

Name	V_N^0 (ml)				log (V_N^0)			
	−20°C (253.15 K)	0°C (273.15 K)	20°C (293.15 K)	40°C (313.15 K)	−20°C (253.15 K)	0°C (273.15 K)	20°C (293.15 K)	40°C (313.15 K)
Chlorotrifluoromethane, R-13	243.5 ± 2.84 1.17%	108.9 ± 1.42 1.30%	57.3 ± 0.53 0.92%	30.9 ± 0.54 1.76%	2.39	2.04	1.76	1.49
Tetrafluoromethane, R-14	18.4 ± 0.16 0.87%	9.9 ± 0.10 1.04%	6.5 ± 0.06 0.87%	4.0 ± 0.06 1.49%	1.27	1.00	0.81	0.60
Chlorodifluoromethane, R-22	474.2 ± 3.78 0.86%	201.6 ± 2.16 1.07%	101.3 ± 0.89 0.88%	52.4 ± 0.62 1.48%	2.68	2.31	2.01	1.72
Trifluoromethane, R-23	38.5 ± 0.41 1.05%	20.5 ± 0.32 1.55%	12.1 ± 0.11 0.88%	7.4 ± 0.11 1.49%	1.59	1.31	1.08	0.87
Difluoromethane, R-32	46.5 ± 0.63 0.74%	23.6 ± 0.26 1.11%	12.5 ± 0.16 1.31%	8.3 ± 0.06 0.77%	1.67	1.37	1.10	0.92
Chloromethane, R-40	413.8 ± 4.16 1.00%	179.7 ± 2.20 1.22%	91.0 ± 0.79 0.86	47.3 ± 0.14 0.70%	2.62	2.26	1.96	1.68
Fluoromethane, R-41	30.1 ± 0.15 0.51%	16.6 ± 0.24 1.42%	10.0 ± 0.08 0.85%	6.3 ± 0.09 1.48%	1.48	1.22	1.00	0.80
	V_N^0 (ml)				log (V_N^0)			
	40°C (313.15 K)	60°C (333.15 K)	80°C (353.15 K)	100°C (373.15 K)	40°C (313.15 K)	60°C (333.15 K)	80°C (353.15 K)	100°C (373.15 K)
Trichlorofluoromethane, R-11	774.3 ± 2.3 0.30%				2.89			
Dichlorodifluoromethane, R-12	149.2 ± 1.3 0.86%				2.17			
Dichlorofluoromethane, R-21	309.8 ± 4.72 1.52%	156.9 ± 1.18 0.75%	87.6 ± 0.57 0.65%	51.3 ± 0.82 1.60%	2.49	2.20	1.94	1.71
Methane, R-50	17.54 ± 0.01 0.05%				1.24			

The uncertainties cited are propagated from replicate measurements of the experimental parameters.

variation in percent is provided. The uncertainty of the measurements is generally between 0.5 and 1.5%, with the average precision of all the measurements being 1.04%. This figure compares very well with the precision of typical measured retention parameters (generally between 1 and 2%) obtained in other physicochemical gas chromatographic studies [15]. A plot of log (V_N^0) against ($1/T$) is provided in Fig. 1. These temperature-dependent data were then fit with the best linear model (simple linear, logarithmic, power or exponential) [16]. The results of these fits are provided in Table 3. Included with each fluid are the coefficients, the Pearson correlation coefficient of the fit, and the temperature range over which the fit was taken.

Most of the measurements are represented very well (within experimental error) with the simple linear model:

$$\log (V_N^0) = m/T + b \quad (6)$$

where m is the slope and b is the intercept. In one instance, with difluoromethane (R-32), the power model was slightly better able to account for all of the structure in the data, and therefore provides a somewhat more accurate representation of the measurements. The form of this model is:

$$\log^2(V_N^0) = m[\log (1/T)] + b \quad (7)$$

where m is the slope and b is the intercept. To

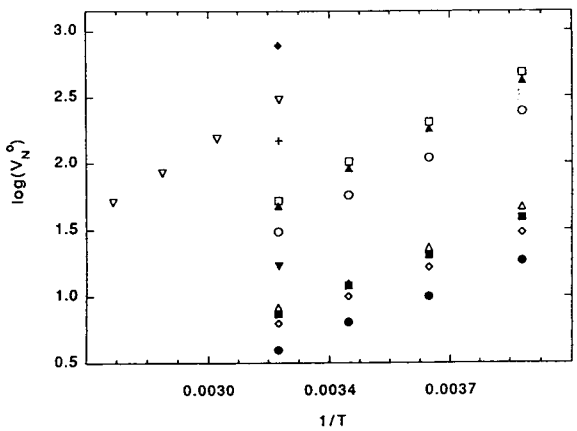

Fig. 1. A plot of the logarithm of the net retention volume, $\log(V_N^0)$, against $1/T$, for each fluid. ○ = R-13, ● = R-14, □ = R-22, ■ = R-23, △ = R-32, ▲ = R-40, ◇ = R-41, ◆ = R-11, + = R-12, ▽ = R-21, ▼ = R-50.

recover the V_N^0 value from this model, one must take the antilogarithm (that is, 10^x) twice.

The relative retentions, $r_{a/b}$, were calculated with tetrafluoromethane (R-14) as the reference. This fluid was chosen because it is the least retained of all the fluids examined. These results are summarized in Table 4, along with their respective common logarithms. A plot of $\log(r_{a/b})$ against $1/T$ is provided in Fig. 2. The expected trend with temperature is observed, and the plot and fits can be used for prediction of retention behavior on other columns containing the same stationary phase.

In addition to the quantitative relationships and correlations presented above, the retention parameters we have measured appear to fit an important qualitative scheme that is useful in understanding the behavior of chlorofluorocarbons and fluorocarbons. One can construct a kind of "periodic chart" or property diagram for these types of compounds. The chart has a triangular format that groups the fluids according to their molecular structures and properties. We present in Fig. 3 such a chart for one-carbon fluids. The top of the chart represents compounds rich in hydrogen (with methane the extreme member); the right-hand side represents compounds rich in fluorine (with tetrafluoromethane being the extreme member); and the left-hand side represents compounds rich in chlorine (with carbon tetrachloride being the extreme member). Such charts have been successful in systematizing, in a semiquantitative manner, properties such as normal boiling point, atmospheric lifetime, flammability, and toxicity [2]. The retention parameters measured in this study fit this scheme qualitatively, with expected minima in the fluorine-rich section, and expected

Table 3
Coefficients of the fits of $\log(V_N^0)$ against $1/T$, with the respective correlation coefficients

Name	m	b	r	Temperature range
Chlorotrifluoromethane, R-13	1176.28	−2.26	0.99981	−20–40°C
Tetrafluoromethane, R-14	860.50	−2.14	0.99919	−20–40°C
Dichlorofluoromethane, R-21	1518.77	−2.36	0.99998	40–100°C
Chlorodifluoromethane, R-22	1256.10	−2.29	0.99986	−20–40°C
Trifluoromethane, R-23	948.39	−2.16	0.99995	−20–40°C
Difluoromethane, R-32	2.83	7.04	0.99932	−20–40°C
Chloromethane, R-40	1243.33	−2.29	0.99979	−20–40°C
Fluoromethane, R-41	896.44	−2.06	0.99998	−20–40°C

Note that for difluoromethane, R-32, the coefficients are for the power model rather than the simple linear model.

Table 4
Relative retentions, $r_{a/b}$, of each fluid with respect to tetrafluoromethane, R-14

Name	$r_{a/b}$				log ($r_{a/b}$)			
	−20°C (253.15 K)	0°C (273.15 K)	20°C (293.15 K)	40°C (313.15 K)	−20°C (253.15 K)	0°C (273.15 K)	20°C (293.15 K)	40°C (313.15 K)
Chlorotrifluoromethane, R-13	13.23	11.00	8.82	7.73	1.12	1.04	0.95	0.89
Dichlorofluoromethane, R-21	*281.94*	*183.53*	*97.90*	77.45	2.45	2.26	1.99	1.89
Chlorodifluoromethane, R-22	25.77	20.36	15.58	13.10	1.41	1.31	1.19	1.12
Trifluoromethane, R-23	2.09	2.07	1.86	1.85	0.32	0.32	0.27	0.27
Difluoromethane, R-32	2.53	2.38	1.92	2.08	0.40	0.38	0.28	0.32
Chloromethane, R-40	22.49	18.15	14.00	11.83	1.35	1.26	1.15	1.07
Fluoromethane, R-41	1.64	1.68	1.54	1.58	0.21	0.23	0.19	0.20

The values in italics were calculated from the fit from 40–100°C data.

maxima predicted to occur in the chlorine-rich section. This chart can provide guidance in the design of analyses of (1) compounds not measured in this study, and (2) analyses done with somewhat different modifier concentration on the stationary phase.

5. Conclusions

Measurements of the corrected net retention volume and relative retentions of eight halocarbons relevant to research on alternative refrigerants have been presented. The logarithms of these data were fitted against reciprocal thermodynamic temperature to several linear models. In most cases, a simple linear relationship accounts for all structure in the data; in one case, a power model is slightly better. These derived equations can be used for the prediction of the retention behavior of these fluids on this important stationary phase (hexafluoropropylene epoxide modified graphitized carbon black), and therefore can be used for solute identification and analytical

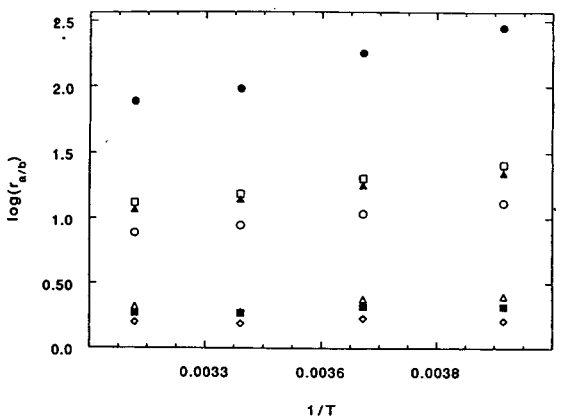

Fig. 2. A plot of the logarithm of the relative retention, log ($r_{a/b}$), with respect to tetrafluoromethane, against $1/T$. ○ = R-13, ● = R-21, □ = R-22, ■ = R-23, △ = R-32, ▲ = R-40, ◇ = R-41.

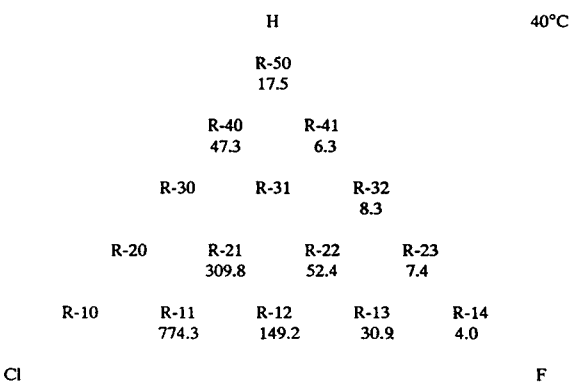

Fig. 3. A triangular diagram that provides a semiquantitative representation of refrigerant properties correlated with molecular structure. In this diagram, we have listed the net retention volumes (ml), V_N^0, for each of the indicated fluids measured at 40°C (313.15 K).

separation design. In addition, we note that the retention parameters also fit the triangular diagram scheme that successfully describes the normal boiling point, flammability, atmospheric lifetime and toxicity of these compounds.

6. Acknowledgements

The financial support of the Colorado Alliance for Science is gratefully acknowledged.

7. Appendix

The code numbering system used for the systematic designation of refrigerant fluids and related products follows the appropriate ANSI/ASHRAE standard [17]. The code number is built up from the right-hand side of the designation.

Refrigerant numbering:

$$j\ X\ Y\ Z\ i$$

Z: number of fluorines

Y: number of hydrogens + 1

X: number of carbons − 1, or omitted.

where X = number of carbons − 1, or omitted; Y = number of hydrogens + 1; Z = number of fluorines. Number of chlorines = [2 + 2(number of carbon bonds)] − (F + H) − 2(number of double bonds); i = isomer designation: a, b . . . ; j = cyclic designation, C; ether designation, E; or else it is omitted.

For example, R-152a:

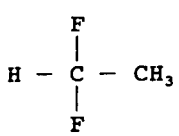

1. The first digit on the right is the number of fluorine atoms on the molecule. When there are no fluorines on the molecule, such as in methylene chloride, a zero is assigned to this position as a place-holder.
2. The second digit from the right is one more than the number of hydrogen atoms on the molecule.
3. The third number from the right is one less than the number of carbon atoms in the compound. When this digit is zero, as in the case of methane-based fluids, it is omitted.
4. The number of chlorines is found by subtracting the sum of the number of fluorine and hydrogen atoms from the total of the number of atoms that can be connected to the carbon atoms. 5. For cyclic compounds, an upper case C is placed before the identifying number.
6. In those instances where bromine is present, the same rules apply except that the upper case letter B after the number for the parent refrigerant shows the presence of bromine. The number to the right of the B indicates the number of bromine atoms present. When isomers of brominated compounds exist, the position of the bromine atoms are indicated by the Greek letters α and β. The Greek letters indicate the carbon atoms of the backbone chain, starting from the end carbon having the largest sum of atomic masses bonded to it. If more than one bromine is bonded to the same carbon, the Greek letter identifying that carbon is repeated for each bromine atom. It should be noted that the isomerization of brominated compounds is not explicitly addressed in the ANSI/ASHRAE standard 34-1992. The extension of this system of nomenclature to include bromine isomers according to the format presented here is very commonly used, however.
7. In the case of ethane-based isomers, each isomer carries the same number. The different isomers are then indicated by appending lower case a, b, c, *etc.*, to the extreme right-hand side of the code. The most symmetrical isomer does not have a letter appended. The letters are appended to the isomers as they become more and more unsymmetrical. The symmetry is determined by adding the atomic masses of the atoms bonded to each carbon, and subtracting one sum from another.
8. Unsaturated compounds are indicated by a

the fourth number from the right, which indicates the number of double bonds.

9. The code number generated by rules 1–8 is prefixed with a letter or name. The preferred prefix in the standard is R (or R- or Refrigerant) (*e.g.*, R134a, R-134a, or Refrigerant 134a). The use of composition-designating prefixes is also allowed (*e.g.*, CFC-12, HCFC-22, HFC-134a).
10. For compounds that contain an ether linkage (–O–), rules 1–8 are applied as they would be in the absence of oxygen. The presence of the ether linkage is then indicated by the code number being preceded by an upper case E. For example, bis(difluoromethyl) ether, E-134:

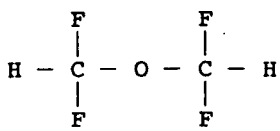

The extension to ethers is not part of the ANSI/ASHRAE standards; at present there is no standard (or even unofficial method) for designating isomers with more than two carbons.

8. References

[1] E.J. Lizardos, *Maint. Tech.*, 6(8) (1993)17–19.
[2] M.O. McLinden and D.A. Didion, *ASHRAE J.*, 29(12) (1987) 32–42.
[3] T.J. Bruno, *Spectroscopic Library for Alternative Refrigerant Analysis*, National Institute of Standards and Technology, Boulder, CO, Special Publication 794, 1990, 192 pp.
[4] T.J. Bruno, *Strategy of Chemical Analysis of Alternative Refrigerants*, National Institute of Standards and Technology, Boulder, CO, Technical Note 1340, 1990, 104 pp.
[5] T.J. Bruno, *ASHRAE Trans.*, 98(2) (1992) 204–208.
[6] T.J. Bruno, *ASHRAE Trans.*, 98(2) (1992) 210–215.
[7] R.L. Grob (Editor), *Modern Practice of Gas Chromatography*, John Wiley and Sons, New York, 2nd ed., 1985.
[8] T.J. Bruno, *Chromatographic and Electrophoretic Methods*, Prentice-Hall, Englewood Cliffs, NJ, 1991.
[9] J.E. Willett, *Gas Chromatography (Analytical Chemistry by Open Learning)*, John Wiley and Sons, Chichester, 1987.
[10] J.L. Glajch and W.G. Schindel, *LC–GC*, 4 (1986) 574.
[11] G. Crescentini and F. Bruner, *Ann. Chim. (Rome)*, 68 (1978) 343.
[12] D. Krockenberger, H. Lorkowski and L. Rohrsneider, *Chromatographia*, 12 (1979) 787.
[13] J.D. Gibbons and Chakraborti, Nonparametic Statistical Inference, Marcel Dekker, New York, 1992.
[14] T.J. Bruno, *Anal. Chem.*, 58 (1986) 1596.
[15] T.J. Bruno and D.E. Martire, *J. Phys. Chem.*, 87 (1986) 2430.
[16] T.J. Bruno (Editor), *CRC Handbook for the Analysis and Identification of Alternative Refrigerants*, CRC Press, Boca Raton, 1994.
[17] *Number Designation and Safety Classification of Refrigerants, ASHRAE Standard, ANSI/ASHRAE 34-1992*, American Society of Heating, Refrigerating, and Air-Conditioning Engineers, Atlanta, GA, 1992.

ELSEVIER

Journal of Chromatography A, 672 (1994) 159–165

JOURNAL OF CHROMATOGRAPHY A

Some observations on the standard addition procedure in gas chromatographic analysis

C. Nerín*, J. Cacho, A.R. Tornés, I. Echarri

Dept. Química Analítica, Centro Politécnico Superior, Universidad de Zaragoza, 50015 Zaragoza, Spain

(First received December 8th, 1993; revised manuscript received February 17th, 1994)

Abstract

A critical study was made of the standard addition procedure as applied in gas chromatography. The general procedure when an electron-capture detector is used in gas chromatography is discussed with the example of the determination of organochlorine compounds in a certified reference material of animal diet.

1. Introduction

The gas chromatographic (GC) determination of organochlorine compounds in real samples often shows strong matrix effects. Usually these matrix effects are attributed to the interaction between the detector and other unidentified organic compounds contained in the sample. When these problems appear, the use of the standard addition procedure is suggested as a good alternative to avoid the matrix influence. However, the problems cannot always be eliminated in practice.

Analysis with different gas chromatographic detectors has been considered by some workers in an additional attempt to compare the responses obtained with various compounds, so that the interferences can be identified and eliminated.

Further, numerous theoretical and practical problems can be identified when the standard addition procedure is applied. The linear range and the slope of the straight line obtained can vary depending on the concentration level of the analytes. In addition, the treatment of the data obtained and the final plot selected, *i.e.*, response obtained *versus* concentration added or measured concentration *versus* concentration added, can modify the final results.

This paper presents a critical study of the standard addition procedure as applied to a certified sample (CRM 115) of organochlorine pesticides in animal diet. Several limitations of the standard addition procedure applied to real samples when using gas chromatography with electron-capture detection (ECD) are discussed.

2. Experimental

2.1. Apparatus and reagents

A Hewlett-Packard 57980 Series II gas chromatograph equipped with an electron-capture detector, a Selecta vibrator, a Heidolph rotary evaporator and Selecta ultrasonic bath were used.

α-Hexachlorocyclohexane, β-hexachloro-

* Corresponding author.

0021-9673/94/$07.00
SSDI 0021-9673(94)00174-8

cyclohexane, δ-hexachlorocyclohexane, hexachlorobenzene, γ-chlordane, heptachlor, heptachlor epoxide, aldrin, dieldrin, endrin, α-endosulfan, *p,p'*-DDE, *p-p'*-TDE, *o,p'*-DDT and *p,p'*-DDT were obtained from Riedel-de Häen. Dichloromethane, light petroleum, hexane and cyclohexane (residue analysis quality) were purchased from Merck. Florisil and silica gel for residue analysis were supplied by Fluka and anhydrous sodium sulphate by Panreac.

2.2. Procedure

A 2.5-g amount of a certified sample (CRM 115) of animal diet was weighed exactly. This sample was placed in a 125-ml Soxhlet apparatus with dichloromethane–light petroleum (1:4). After 6 h of extraction at 35°C, the organic extract was transfered to a glass column containing a combined solid bed of 2.5 g of Florisil (7% deactivated) and 2.5 g of silica gel (7% deactivated). A 2-cm layer of anhydrous sodium sulphate was placed on the top of this column to keep the extract dried. After passing through the clean-up column, the organic extract was evaporated to 2 g and then analysed by GC–ECD.

2.3. Chromatographic conditions

The GC analysis was carried out with a fused-silica column (60 m × 0.25 mm I.D.) containing DB 1701 bonded phase with a 0.25-μm film thickness. The column oven temperature programme was as follows: 60°C for 2 min, increased at 20°C/min to 185°C, held for 10 min at 185°C, then increased at 5°C/min to 250°C and held for 20 min at 250°C. The injector temperature was 250°C. Hydrogen was used as the carrier gas at a flow-rate of 1.45 ml/min and nitrogen as the make-up gas at a flow-rate of 60 ml/min.

3. Results and discussion

3.1. Linear range

It is well known that the response of detectors used in gas chromatography is non-linear over the whole range of concentration. The limitations of the linear range when using ECD are well known [1,2], and most workers have attempted to calibrate the detector using the most linear portion of the response curve. In order to establish the non-linear range in each instance, several standard solutions were injected into the GC column. The response obtained, height or area counts per unit mass injected, was plotted against the mass injected in each instance. Fig. 1 shows the curves obtained. From these curves, the lower limits of linear range were obtained for each compound. It can be seen that in all instances the ECD response at very low concentrations is non-linear. This behaviour is especially important in the determination of organochlorine compounds in which the concentration level is very low and the lower and upper limits of this linear range can be very critical [3–6]. This linear range can vary according to the state of the detector, clean-up, make-up gas used [7,8], gas flow-rate, etc., and it also depends on the detector design. The presence of such a non-linear range is one of the major limitations of the standard addition procedure.

The standard addition procedure is widely applied in atomic absorption and emission spectrometry and has also found application in electrochemical analysis and other areas [9,10]. Equal volumes of the sample solution are taken, all but one are separately spiked with known, different amounts of the analyte and all are then diluted to the same volume. The instrument signals are then determined for all these solutions and the results plotted as shown in Fig. 2. As usual, the signal is plotted on the ordinate; in this instance the abscissa is graduated in terms of the amounts of analyte added (either as an absolute mass or as a concentration). The unweighted regression line is calculated in the normal way, but space is provided for it to be extrapolated back to the point on the abscissa at which $y = 0$. It is clear that this negative intercept on the abscissa corresponds to the amount of analyte in the test sample.

However, if the detector response is non-linear over the whole concentration range, such extrapolation can produce an erroneous value. This is especially true when organochlorine com-

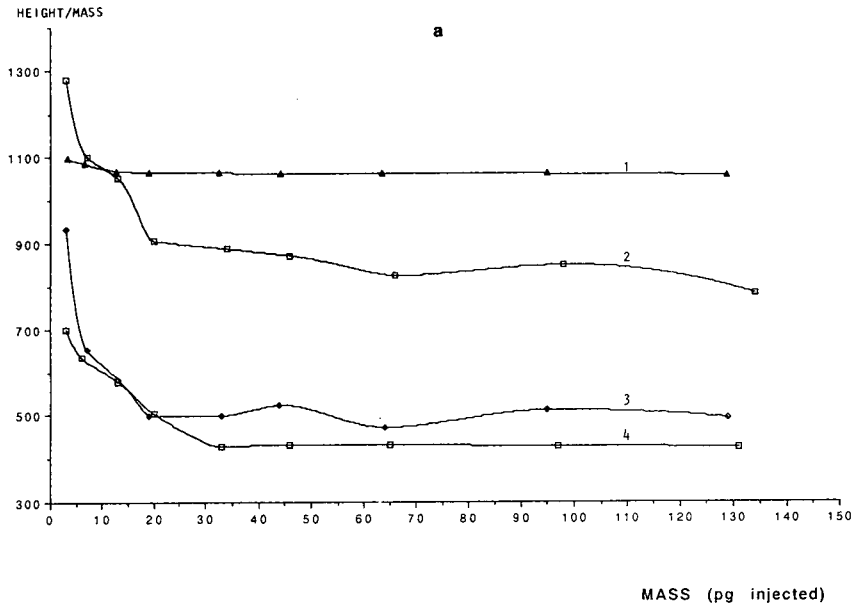

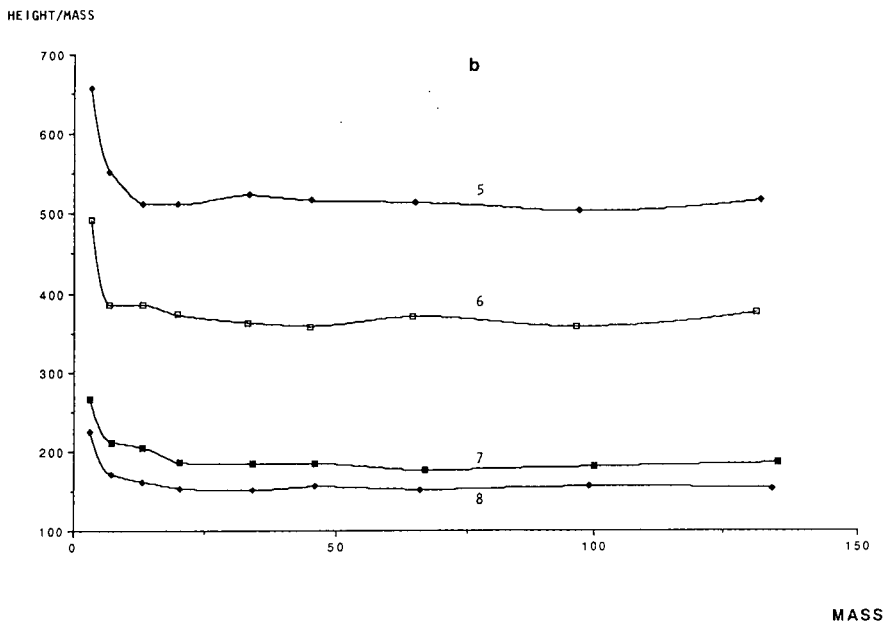

Fig. 1.

(Continued on p. 162)

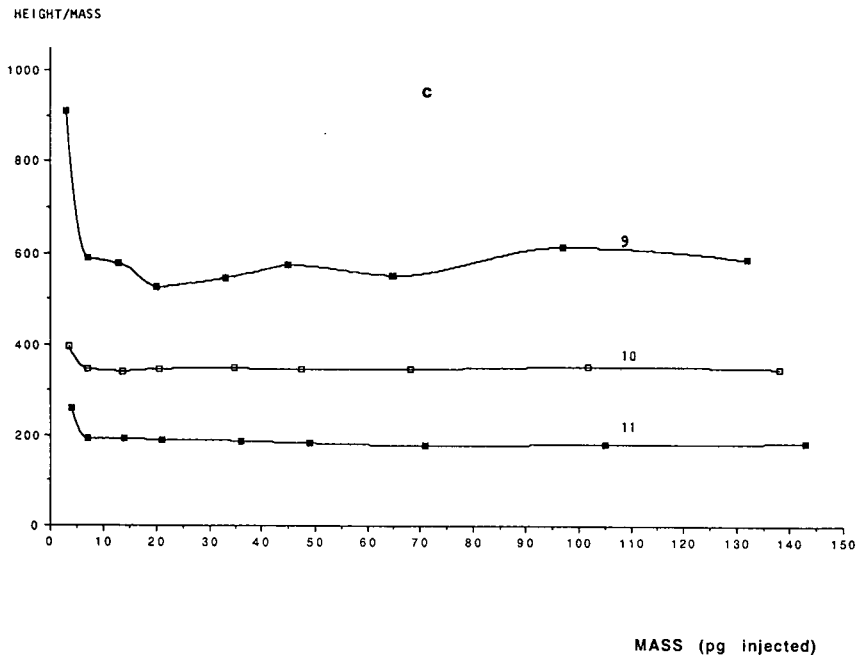

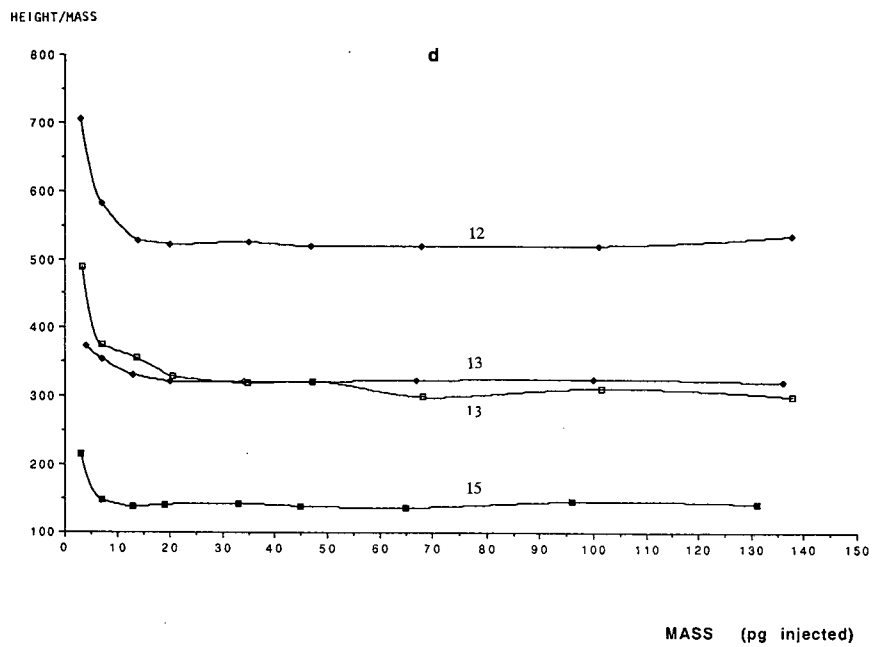

Fig. 1. ECD response *versus* the mass injected into the column. Curves: 1 = α-HCH; 2 = HCB; 3 = heptachlor; 4 = γ-chlordane; 5 = aldrin; 6 = α-endosulfan; 7 = endrin; 8 = *o,p'*-DDT; 9 = γ-HCH; 10 = dieldrin; 11 = *p,p'*-TDE; 12 = heptachlor epoxide; 13 = *p,p'*-DDE; 14 = β-HCH; 15 = *p,p'*-DDT.

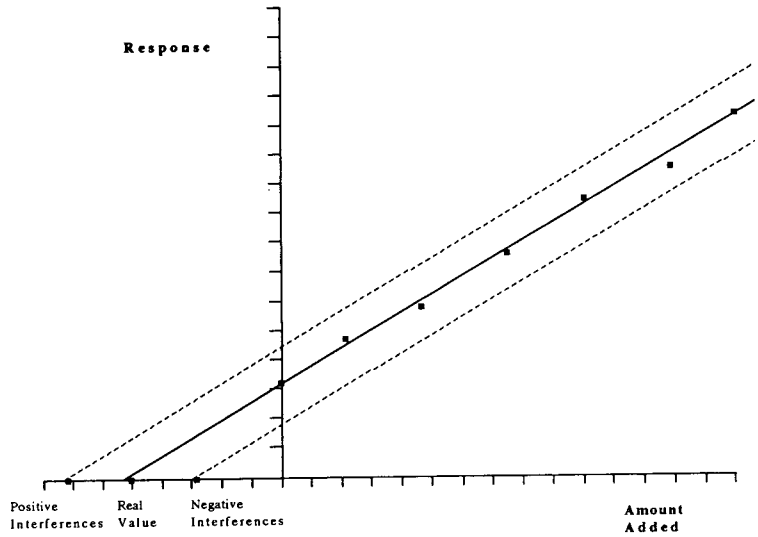

Fig. 2. Plot of a general standard addition procedure (—) and influence of matrix interferences in the standard addition procedure applied to GC–ECD (---).

pounds in real samples are determined by GC–ECD because of their low concentrations.

In order to check this theory, the standard addition procedure was applied to the determination of a series of organochlorine compounds in the certified reference material BCR CRN 115. The sample was simultaneously analysed by the normal procedure, using a calibration plot and an internal standard. The results obtained, together with the certified values and the lower limits of the linear range of the detector, are given in Table 1. It can be seen that the values

Table 1
Determination of organochlorine pesticides in BCR CRM 115 using different procedures

Compound	Lower linearity limit (ng/g)	Observed values (ng/g)	Certified values (ng/g)	Standard addition results (ng/g)[b]
α-HCH	19.15	22.26	18.47[a]	9.46 ± 2.66
β-HCH	20.50	17.74	24.20[a]	26.02 ± 1.49
γ-HCH	6.67	21.90	19.53[a]	24.56 ± 1.44
HCB	19.88	23.60	17.01	23.65 ± 8.30
Aldrin	13.01	17.36	17.42	11.92 ± 0.62
Heptachlor epoxide	6.95	68.33	17.63	7.68 ± 1.46
γ-Chlordane	33.01	55.34	53.00	48.16 ± 9.39
α-Endosulfan	6.61	48.12	44.57	45.23 ± 7.09
p,p'-DDE	20.23	53.70	47.99	51.39 ± 0.69
Dieldrin	6.98	22.10	19.00	22.06 ± 2.14
Endrin	20.10	56.96	47.92	55.31 ± 33.07
p,p'-TDE	7.24	68.29	62.94	53.14 ± 12.45
o,p'-DDT	19.98	44.15	47.40	55.92 ± 2.37

[a] Values given as indicative values in CRM report.
[b] Mean ± S.D. × *f*, where *f* is the multiplication factor according to the statistical requirements.

for α-HCH, aldrin and heptachlor epoxide obtained with the standard addition procedure differ from those obtained with the direct procedure and also from the certified values. This error could be attributed to the fact that the final concentration of the compound is near the lower limit of the linear range.

The extrapolation to zero implies that the range included is linear. When this is not the case, the standard addition procedure cannot be recommended for quantitative analysis.

It could be argued whether a larger amount of original sample could have been taken in order to obtain a more concentrated final extract containing the compounds. In such a case, the mass injected into the chromatographic column would be higher than the lower limit of the linear range. This is true when the direct interpolation procedure is applied, but with the standard addition procedure this approach only serves to move the working range to an upper part of the same straight line which has the same slope and obviously the same problems with extrapolation to zero. This effect is shown in Fig. 2.

The concentration effect is only valid when directed analysis through a calibration plot is used, and it does not work with the standard addition procedure.

3.2. Matrix effect

One of the major advantages of the standard addition procedure is that it avoids the matrix interference effects. However, this is only acceptable when the technique to which the standard addition procedure is applied is a relative technique. GC is an absolute technique, which means that the detector gives the total response to all the mass injected into the column instead of the response to the relative concentration (mass per unit volume). If a different compound, an interferent, is co-eluted with the analyte, the detector gives the total response of the sum of both compounds. Under these conditions, when the standard addition procedure is applied, the presence of positive or negative interferents affects the position of the straight line but the slope is not affected. Only a parallel line is obtained. This can be seen in Fig. 2. In such a case, the extrapolation to zero gives very different values, only one being the true value.

Consequently, the standard addition procedure does not avoid matrix interference effects, as can be established, for example, with spectroscopic methods.

3.3. Accuracy

In the analysis of real samples by GC, small or no significant differences are obtained between several independent aliquots of the sample. On applying the standard addition procedure these differences result in little variation of the slope of the straight line. Nevertheless, the extrapolation to zero amplifies the differences, and erroneous values could be obtained. The relative standard deviations are higher than those obtained by the direct interpolation procedure through a calibration plot applied to the same compounds in the analysis of the same sample, as can be seen in Table 1. From a statistical point of view, extrapolation methods are always less precise than interpolation techniques [4].

3.4. Recovery experiments

The addition of increasing and known amounts of a standard solution to a sample can be used to calculate the recovery of the analytes through the whole process, including extraction, clean-up, concentration and final analysis.

In this case, the final values have to be obtained by direct analysis using the calibration plot. When the obtained concentration values (quantified concentration) are plotted against the concentration added to the sample, a linear plot results. The slope of this straight line represents the recovery of each compound. This can be seen in Fig. 3.

Often this procedure is erroneously named "standard addition", but the quantification is achieved from a normal calibration plot using calibration solutions. In this instance, no extrapolation is used and the procedure is not affected by the aforementioned problems.

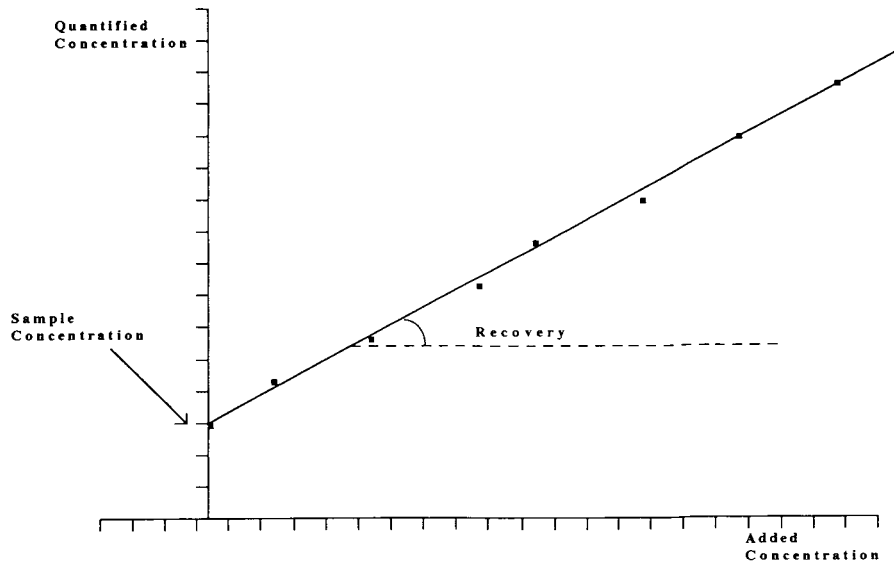

Fig. 3. Plot of quantified concentration *versus* added concentration of each compound.

4. Conclusions

The standard addition procedure cannot be applied in GC–ECD to samples containing very low concentrations of compounds that have a non-linear detector response when the final value is very near the lower limit of this linear range. The standard addition procedure does not eliminate the matrix effects in GC.

The relative standard deviations obtained by the application of standard addition procedure are higher than those obtained using the normal procedure of direct analysis using a calibration plot with calibrating solutions. When the final quantification of the samples after adding the standard is achieved by direct analysis with a normal calibration plot, the data obtained can be used to obtain the recovery of the compound.

References

[1] M. Dressler, *Selective Gas Chromatographic Detectors* (*Journal of Chromatography Library*, Vol. 36), Elsevier, Amsterdam, 1986.

[2] C. Litenau and I. Rice, *Statistical Theory and Methodology of Trace Analysis*, Ellis Horwood, Chichester, 1980.

[3] D.E. Wells, in D. Barceló, *Environmental Analysis. Techniques, Applications and Quality Assurance*, Elsevier, Amsterdam, 1993, Ch. 3, pp. 80–109.

[4] T.A. Bellar and J.J. Lichtenberg, *J. Am. Water Works Assoc.*, 66 (1974) 739.

[5] M.E. Comba and K.L.E. Kaiser, *Int. J. Environ. Anal. Chem.*, 16 (1983) 17.

[6] M.L. Langhorst, *J. Chromatogr. Sci.*, 19 (1981) 98.

[7] D.E. Wells, J.N. Robson and A.G. Kelly, *The ECD and NICI-MS detector for the determination of organochlorine residues in environmental samples*, Internal Report, Scottish Office Agriculture and Fisheries Department, Aberdeen, 1992.

[8] B.K. Afghan and A.S.Y. Chau, *Analysis of Trace Organics in the Aquatic Environment*, CRC Press, Boca Raton, FL, 1989.

[9] J.C. Miller and J.N. Miller, *Statistics for Analytical Chemistry*, Ellis Horwood, Chichester, 2nd ed, 1987.

[10] D.T.E. Hunt and A.L. Wilson, *The Chemical Analysis of Water. General Principles and Techniques*, Royal Society of Chemistry, London, 2nd ed., 1986.

ELSEVIER

Journal of Chromatography A, 672 (1994) 167–175

JOURNAL OF CHROMATOGRAPHY A

Mini-round-robin study of a supercritical fluid extraction method for polynuclear aromatic hydrocarbons in soils with dichloromethane as a static modifier

Viorica Lopez-Avila*[,a], Richard Young[a], Joe Tehrani[b], Jess Damian[b], Steve Hawthorne[c], Jan Dankers[d], Cees van der Heiden[d]

[a]*Midwest Research Institute, California Operations, 625-B Clyde Avenue, Mountain View, CA 94043, USA*
[b]*Isco, Inc., P.O. Box 5347, Lincoln, NE 68605, USA*
[c]*University of North Dakota, Grand Forks, ND 58202, USA*
[d]*BCO Centre for Research BV, Bergschot 71, 4817 PA Breda, Netherlands*

(First received January 25th, 1994; revised manuscript received February 11th, 1994)

Abstract

A mini-round-robin study of a supercritical fluid extraction (SFE) method for polynuclear aromatic hydrocarbons (PAHs) from soil samples was conducted. Three laboratories participated in the study, and each laboratory extracted three real-world samples in triplicate. The cryogenically milled samples were extracted at 350 atm (1 atm = 101 325 Pa) and 90°C for 20 min in the dynamic mode using supercritical carbon dioxide at a flow-rate of 1 to 1.5 ml/min and the extracted material was collected in 10 ml dichloromethane, which was then subjected to silica chromatography. The SFE method accuracy (percent recovery) was determined relative to the sonication extraction since the true levels of PAHs in these samples are not known. The PAHs were recovered quantitatively (recovery > 80%) by SFE when present at concentrations of 1 mg/kg or higher. The interlaboratory method precisions (overall R.S.D.s) appear to be concentration-dependent; at concentrations above 1 mg/kg, they were 27% or lower; at concentrations below 1 mg/kg, they ranged from 19 to 80%. From these results, we concluded that the method appears quite rugged, and the interlaboratory data compare well with other SFE interlaboratory studies.

1. Introduction

The extraction of organic pollutants from environmental matrices is a crucial step in their determination. The technique chosen for sample extraction should, to the extent possible, yield quantitative recoveries of the target analyte(s), be selective, not generate large volumes of waste solvents, require few steps in sample and extract handling, and be inexpensive. One such technique that has generated much interest in the last few years is supercritical fluid extraction (SFE).

The purpose of our study was to select one of the SFE methods that were published in the literature, which appears promising to work on all commercial SFE systems, and to evaluate it. Of the 10 literature references that deal specifically with the extraction of polynuclear aromatic

* Corresponding author.

0021-9673/94/$07.00
SSDI 0021-9673(94)00243-3

hydrocarbons (PAHs) by SFE [1–10], we selected four promising methods [1–4] for closer scrutiny. A brief description of each method follows.

In the method by Dankers *et al.* [1], which we evaluated in this mini-round-robin study, a cryogenically milled sample (5 g) is extracted with supercritical carbon dioxide at 350 atm (1 atm = 101 325 Pa) and 90°C for 20 min (dynamic). Dichloromethane (2 ml) is added as a static modifier to the sample immediately prior to extraction, and the extracted material is collected in dichloromethane and is then analyzed by GC–MS.

The procedure by Lee *et al.* [2] uses three consecutive extractions. The sample (1 g plus 0.5 ml water), to which has been added 500 μl of methanol–dichloromethane (1:1), is first extracted with supercritical carbon dioxide at 336 atm for 7 min (2 min static, 5 min dynamic) at 120°C, and a flow-rate of 4 ml/min (as liquid). The PAHs are collected on a C_{18}-bonded silica trap held at 15°C and are rinsed from the trap with either 1.5 ml isooctane–dichloromethane (1:3) for GC–MS analysis or with 1.5 ml tetrahydrofuran–acetonitrile (1:1) for HPLC analysis. The extraction is continued at 336 atm and 120°C with carbon dioxide modified with 1% methanol and 4% dichloromethane at 2 ml/min for 31 min (1 min static, 30 min dynamic), and then with carbon dioxide alone for 2.5 min at 4 ml/min. After extraction, the trap is rinsed with an additional 1.5 ml and then 1.2 ml of the solvent (indicated above) for GC–MS or HPLC analysis.

The method reported by Gere *et al.* [3] also uses three steps. In step 1, extraction is performed with supercritical carbon dioxide at 119 atm and 120°C (2 min static, 10 min dynamic) at a flow-rate of 2 ml/min; the extracted material is collected on a C_{18}-bonded silica trap held at 5°C and is subsequently rinsed from the trap with 0.8 ml of tetrahydrofuran–acetonitrile (1:1). The extraction is then continued at 333 atm and 120°C with carbon dioxide–methanol–water (95:1:4) (1 min static, 30 min dynamic) at a flow-rate of 4 ml/min. During step 2 of the extraction, the trap temperature is 80°C (to prevent modifier from condensing onto the trap), and the nozzle temperature is kept at 45°C. In step 3 of the extraction, pressure and temperature remain the same as in step 2, but the fluid used is carbon dioxide. The material collected on the trap is rinsed off with 0.8 ml of tetrahydrofuran–acetonitrile (1:1) and analyzed by HPLC. To make the SFE method compatible with GC analysis, Gere *et al.* recommend using carbon dioxide–methanol–dichloromethane (95:1:4) in step 2 and rinsing the extracted material from the trap with methanol–dichloromethane (50:50).

Levy *et al.* [4] reported experiments performed at 75°C and three pressures (250, 350 and 450 atm) and at 475 atm and three temperatures (40, 100 and 150°C) and concluded that the highest extraction efficiencies for PAHs were achieved at 450 atm and 150°C. However, this method has not yet been sufficiently validated with real-world samples and, thus, was not considered in our study.

Refs. 5–10 discuss applications that deal with extraction of PAHs from various environmental matrices by SFE, but because they have not been fully optimized or validated, they did not appear to be relevant to this study.

Following the literature review, we concluded that the method of Dankers *et al.* would work on any of the commercial SFE systems and, thus, we subjected it to the mini-round-robin study.

2. Experimental

2.1. Materials

Analytical reference standards of the 16 PAHs were obtained as a composite solution in dichloromethane–benzene (50:50) (concentration 2 mg/ml per compound) from Supelco (Bellefonte, PA, USA). Purities were stated to be higher than 98.2%. Working calibration standards at 1, 5, 10, 25, 50 and 100 ng/μl were prepared by dilution of the composite stock solution with dichloromethane. Five deuterated compounds ([$^2H_8$]naphthalene, [$^2H_{10}$]acenaphthene, [$^2H_{10}$]phenanthrene, [$^2H_{12}$]chrysene and [$^2H_{12}$]perylene) were used as internal standards; they were also obtained as a composite stock solution in dichloromethane (concentration 2

mg/ml per compound, purity > 99%). Of this composite stock solution, 20 μl were spiked into every standard, and 10 μl of the composite stock solution were spiked into every sample extract immediately prior to GC–MS analysis (note that the sample extracts were concentrated to 0.5 ml).

The three samples used in this study, identified as samples A, B and C, were non-spiked, real-world soil samples, randomly chosen from samples analyzed at the BCO Centre for Research, Breda, Netherlands. Sample A was a sandy material from a polluted industrial site with 85% dry residue, sample B was a non-polluted soil with 87% dry residue and sample C was a highly contaminated soil sample from a polluted industrial site with 94% dry residue. Each sample was subjected to cryogenic milling before extraction (done at laboratory 1) as follows: 100 g anhydrous sodium sulfate, cooled to 4°C and contained in a 500-ml polyethylene bottle, and 100 g sample were mixed in this bottle with a spatula. The polyethylene bottle was then placed in a Dewar flask filled with liquid nitrogen; after 10 min the contents of the bottle were transferred to a stainless-steel cryogenic homogenizer (Model 300A; ProScientific, Monroe, CT, USA) and mixed for approximately 30 s. After a brief shake, the grinding was repeated for an additional 30 s. The milled sample was sieved through a 1-mm mesh size sieve and was then split into two 20-g portions and one 60-g portion. One 20-g portion was kept by laboratory 1, the other 20-g portion was sent to laboratory 3 and the 60-g portion was sent to laboratory 2 (this laboratory extracted the three samples in parallel by SFE and sonication extraction).

SFE-grade carbon dioxide (Air Products, Allentown, PA, USA) was used for extraction by laboratories 1 and 2. Laboratory 3 used supercritical fluid chromatography-grade carbon dioxide (Scott Specialty Gases, Plumsteadville, PA, USA).

2.2. SFE procedure

All extractions were performed with an Isco (Lincoln, NE, USA) dual-chamber extraction module (Model SFX 2-10) and Isco Model 260D pump operated in the constant-pressure mode. The extraction conditions were 350 atm, 90°C, 20 min dynamic. For laboratories 1 and 2, the flow-rate of the carbon dioxide was controlled by a stainless-steel capillary (37 cm × 50 μm I.D.) and was approximately 1.5 ml/min (as liquid). Laboratory 3 used a variable restrictor (prototype from Isco) and reported a flow-rate of approximately 1 ml/min. To prevent plugging during extraction, the restrictor was heated at 100°C (except laboratory 3 at 60°C), and the collection vial (initially filled with 10 ml dichloromethane) was kept in a small beaker with water at 30°C. A 10-ml disposable extraction cartridge was used to extract a 5-g milled sample. Immediately prior to extraction, 2 ml dichloromethane were added to the sample directly in the extraction vessel. The cartridge was first pressurized to 350 atm before the outlet valve of the extractor was opened to avoid immediate removal of dichloromethane by the extraction fluid. The reader is cautioned that if full pressurization of the extraction cartridge is not reached before the outlet valve is opened, recoveries could be much lower that those reported here since the modifier does not contact the sample at full pressure.

2.3. Sonication extraction

Extractions using a sonic probe (Sonifier 450; Branson Ultrasonics, Danbury, CT, USA) were performed with 30-g portions of each milled sample mixed with 60 g anhydrous sodium sulfate. The resulting mixtures were sonicated for 3 min at 50% power (output setting 10) with 100 ml dichloromethane–acetone (1:1) and then decanted; the extraction was repeated twice with 100 ml fresh solvent. The decanted extracts were filtered through Whatman 31 filter paper and combined, the solvent was exchanged to hexane, and the hexane solution was concentrated to 1 ml. A silica gel procedure using 1.8 g silica gel (80–150 μm mesh; EM Science, Gibbstown, NJ, USA), activated for 16 h at 130°C prior to use, was used to clean up the extracts. The first fraction that was eluted with 10 ml hexane was discarded. PAHs were then eluted from the silica gel column with 10 ml hexane–dichloromethane

(60:40). This fraction was concentrated to 0.5 ml. The silica procedure was verified prior to use to ensure that quantitative recoveries (>90%) of the target compounds were obtained under these conditions.

2.4. GC–MS analyses

All GC–MS analyses were performed by laboratory 2 on a Hewlett-Packard (Wilmington, DE, USA) 5890 Series II gas chromatograph interfaced to a 5971A mass-selective detector and a Hewlett-Packard DOS Chemstation. The column used was a Supelco PTE-5 fused-silica capillary column (30 m × 0.25 mm I.D. × 0.25 μm film thickness). The column temperature was held at 75°C for 3 min, then programmed at 12°C/min to a final temperature of 300°C. Helium at a linear velocity of 39 cm/s was used as carrier gas. The injector temperature was held at 250°C, the transfer line temperature at 280°C and the ion source at 188°C. The mass spectrometer was scanned from 40 to 500 u at a rate of 1.6 s/scan. All 1-μl injections were performed in the splitless mode (splitless time 1 min). Quantitation was performed using internal standard calibration.

2.5. Quality control procedures

The GC–MS analyses were performed according to method 8270 of the US Environmental Protection Agency (EPA) [11] for semivolatile organics. To ensure the quality of the data generated, the following quality control procedures were implemented: (1) all extracts were analyzed by one laboratory (laboratory 2); (2) SFE system blanks were performed by each laboratory; no PAHs were detected in these blanks; (3) the GC–MS system was tuned to meet the decafluorotriphenylphosphine (DFTPP) specifications; (4) a six-level calibration (using standards at 1, 5, 10, 25, 50 and 100 ng/μl) was performed daily, during sample analysis; when the response factors did not meet the criteria specified in EPA Method 8270, then either the multilevel calibration was repeated or fresh standards were prepared; (5) five internal standards ([$^2H_8$]naphthalene, [$^2H_{10}$]acenaphthene, [$^2H_{10}$]phenanthrene, [$^2H_{12}$]chrysene and [$^2H_{12}$]perylene) were spiked into every sample extract immediately prior to GC–MS analysis; the areas of the quantitation ions of the five internal standards were monitored during every 12-h period to ensure that they were within −50/ + 100% of the corresponding areas established for the mid-level calibration standard; any sample extracts for which the internal standards fell outside the quality control criteria were reanalyzed; (6) a GC–MS column blank was performed before any batch of sample extracts was analyzed to ensure the cleanliness of the system; (7) sample extracts that were found to contain concentrations in excess of 100 ng/μl were diluted and reanalyzed; and (8) compounds known to be present in the sample extracts (from previous data acquired on that particular sample) but not detected by the automated processing routines were searched for manually.

3. Results and discussion

3.1. Method accuracy

Tables 1–3 present the concentrations of the 16 compounds found in the three soils by sonication extraction–GC–MS and the recoveries using SFE–GC–MS. The SFE data are presented by laboratory as the individual average recoveries (method accuracy) and R.S.D.s (method precision), and the overall method accuracy and precision. The SFE recoveries were determined relative to the sonication data since the sonication method is an approved EPA procedure (EPA method 3550 [12]).

For sample A (Table 1), which was known to be highly polluted, the SFE recoveries looked almost as good as one might expect from a freshly spiked sample. From the 45 values (3 laboratories × 15 compounds) reported in Table 1 as average recoveries for the three laboratories, there was one value below 80% (for benzo[*ghi*]perylene), and three values were exceeding 120% (for naphthalene); the remainder of

Table 1
SFE method performance for sample A

Compound	Concentration by sonication (mg/kg)[a]	Laboratory 1[b]		Laboratory 2[b]		Laboratory 3[b]		Overall average recovery (%)	Overall R.S.D. (%)
		Average recovery (%)	R.S.D (%)	Average recovery (%)	R.S.D. (%)	Average recovery (%)	R.S.D. (%)		
Naphthalene	0.16	158	61	131	50	125	30	138	48
Acenaphthylene	1.79	93.1	6.0	93.8	0.6	86.4	5.9	91.1	5.8
Acenaphthene	0.42	103	16	94.0	33	79.9	11	92.4	23
Fluorene	2.00	103	7.4	98.4	8.0	87.3	4.2	96.4	9.6
Phenanthrene	28.8	102	15	103	11	96.8	7.6	101	11
Anthracene	4.33	105	6.4	97.6	8.5	94.5	1.1	98.9	7.2
Fluoranthene	44.7	102	16	101	11	96.5	8.5	99.9	11
Pyrene	35.4	103	16	98.6	9.5	94.4	8.6	98.8	12
Benzo[*a*]anthracene	13.2	107	2.6	98.5	1.3	99.5	4.3	102	4.7
Chrysene	15.4	105	2.6	96.6	1.7	97.3	3.1	99.5	4.5
Benzo[*b* + *k*]fluoranthene[c]	22.6	108	1.1	97.1	2.0	104	3.8	103	5.0
Benzo[*a*]pyrene	13.2	107	1.2	98.2	1.3	101	4.2	102	4.5
Indeno[1,2,3-*cd*]pyrene	8.44	99.7	3.7	103	2.7	82.1	5.5	94.9	11
Dibenzo[*a*,*h*]anthracene	2.59	95.0	2.1	97.1	5.1	86.7	5.8	92.9	6.5
Benzo[*ghi*]perylene	9.06	81.2	5.0	100	3.3	74.9	6.3	85.4	14

[a] Single determination.
[b] The number of replicates was four. The SFE recoveries were determined relative to the sonication data.
[c] Benzo[*b*]fluoranthene and benzo[*k*]fluoranthene could not be chromatographically resolved, so the results reported are the sums of the concentrations of both compounds or the total recoveries for both compounds.

Table 2
SFE method performance for sample B

Compound	Concentration by sonication (mg/kg)[a]	Laboratory 1[b]		Laboratory 2[b]		Laboratory 3[b]		Overall average recovery (%)	Overall R.S.D. (%)
		Average recovery (%)	R.S.D (%)	Average recovery (%)	R.S.D. (%)	Average recovery (%)	R.S.D. (%)		
Phenanthrene	0.22	56.6	31	49.8	10	52.7	8.1	53.0	19
Anthracene	0.04	50.1	37	43.0	18	50.0	13	47.7	24
Fluoranthene	0.36	69.8	31	48.7	10	50.7	8.0	56.4	27
Pyrene	0.23	72.7	40	46.5	15	52.0	13	57.1	35
Benzo[*a*]anthracene	0.09	80.1	47	49.8	19	57.0	18	62.3	40
Chrysene	0.15	62.1	37	48.5	13	45.7	18	52.1	29
Benzo[*b* + *k*]fluoranthene[c]	0.13	87.8	58	47.5	25	55.7	24	63.7	53
Benzo[*a*]pyrene	0.04	170	69	61.6	28	84.2	40	105	77

[a] Single determination. The other PAH compounds reported in Tables 1 and 3 were not detected in this sample.
[b] The number of replicates was four. The SFE recoveries were determined relative to the sonication data.
[c] Benzo[*b*]fluoranthene and benzo[*k*]fluoranthene could not be chromatographically resolved, so the results reported are the sums of the concentrations of both compounds or the total recoveries for both compounds.

Table 3
SFE method performance for sample C

Compound	Concentration by sonication (mg/kg)[a]	Laboratory 1[b]		Laboratory 2[b]		Laboratory 3[b]		Overall average recovery (%)	Overall R.S.D. (%)
		Average recovery (%)	R.S.D (%)	Average recovery (%)	R.S.D. (%)	Average recovery (%)	R.S.D. (%)		
Naphthalene	6.49	106	32	126	22	89.1	18	107	27
Acenaphthylene	2.33	75.7	10	90.1	5.3	84.7	6.9	83.5	10
Acenaphthene	0.77	106	7.2	94.2	8.4	92.9	5.9	97.7	9.2
Fluorene	3.39	106	14	98.9	6.6	100	10	102	10
Phenanthrene	23.7	97.4	15	121	7.3	131	23	117	20
Anthracene	5.08	88.8	14	93.2	6.4	92.0	7.8	91.3	9.1
Fluoranthene	31.2	98.1	11	122	10	122	25	114	19
Pyrene	21.9	104	11	121	8.2	124	24	116	17
Benzo[*a*]anthracene	10.7	95.9	8.9	88.1	3.7	87.3	7.6	90.4	7.9
Chrysene	13.9	100	8.7	92.5	6.5	89.1	9.0	94.0	9.0
Benzo[*b* + *k*]fluoranthene[c]	24.2	96.0	11	90.6	6.1	99.5	12	95.4	10
Benzo[*a*]pyrene	10.0	98.3	9.0	93.1	5.9	88.0	9.1	93.1	8.8
Indeno[1,2,3-*cd*]pyrene	5.29	73.2	2.2	85.3	8.0	60.5	11	73.0	16
Dibenzo[*a*,*h*]anthracene	1.83	71.9	4.6	90.0	4.7	64.3	11	75.4	16
Benzo[*ghi*]perylene	5.18	55.0	5.1	82.0	8.2	54.7	13	63.9	22

[a] Single determination.
[b] The number of replicates was four. The SFE recoveries were determined relative to the sonication data.
[c] Benzo[*b*]fluoranthene and benzo[*k*]fluoranthene could not be chromatographically resolved, so the results reported are the sums of the concentrations of both compounds or the total recoveries for both compounds.

the individual average recoveries ranged from 80 to 108%. The overall average recoveries ranged from 85.4 to 138%. The high recovery of naphthalene by SFE may be a consequence of the higher losses during sonication extraction because of the heat released during the 3-min sonication in an open vessel.

For sample B (Table 2), which was known to be relatively clean, the individual average recoveries were low, ranging from 43.0 to 87.8% (excluding two values over 100% for benzo[*a*]pyrene); the overall average recoveries ranged from 47.7 to 105%. This is not surprising since the levels that we detected by GC–MS were at or below 1 ng/μl, where the precision of the measurement was approximately ± 20%.

For sample C (Table 3), which was also a highly polluted soil, the individual average recoveries ranged from 54.7 to 131%. From the 45 values given in Table 3 for the individual average recoveries, seven values were below 80% and seven were above 120%. The overall average recoveries ranged from 63.9 to 117%, with three values being below 80%. The three compounds for which we had low but still reasonable recoveries were indeno[1,2,3-*cd*]pyrene, dibenzo[*a,h*]anthracene and benzo[*ghi*]perylene.

3.2. Method precision

Method precision is reported (Tables 1–3) for each compound as the R.S.D. for each laboratory and also as the overall R.S.D. for the three laboratories. In general, as expected, the R.S.D.s for the individual laboratories were lower than the overall R.S.D.s, and the lower the concentration of the target analyte was in the sample, the higher was the R.S.D. For example, for sample A, the individual R.S.D.s were below 10% for most compounds (specifically, from the 45 values reported in Table 2 for R.S.D., 34 values were below 10%), whereas only half of the overall R.S.D.s were below 10%. In the case of naphthalene, which had the lowest concentration in this sample, the individual R.S.D.s were 61, 50 and 30% for laboratories 1, 2 and 3, respectively; these values were significantly higher than the R.S.D.s for the other compounds. Acenaphthene also exhibits a high R.S.D., and its concentration is almost two orders of magnitude lower than some of the other compounds present in that sample.

4. Conclusions

The results of this mini-round-robin study, in which three laboratories participated, indicate that PAHs can be extracted with better than 80% recoveries by SFE when present at concentrations of 1 mg/kg or higher. At lower concentrations (<0.2 mg/kg), average recoveries ranged from 48 to 105%, with most values in the range of 50 to 60%. The interlaboratory method precisions (overall R.S.D.s) also appear to be concentration dependent; at concentrations above 1 mg/kg, they were 27% or lower; at concentrations below 1 mg/kg, they ranged from 19 to 80%. We correlated the results obtained by SFE for samples A and C with those obtained by sonication extraction with dichloromethane–acetone (1:1) (the SFE data were plotted on the *y*-axis) and found excellent correlation between SFE and sonication extraction (the slopes of the regression lines were 1.01 for sample A and 1.16 for sample C; the correlation coefficients were 0.999 and 0.991).

This study addressed the performance of the method of Dankers *et al.* [1] with a very limited number of samples and only three laboratories using the same type of SFE system. Nonetheless, the method appears to be quite rugged, and the interlaboratory data compare well with those from the interlaboratory study of the SFE method for petroleum hydrocarbons [13].

Acknowledgement

The authors wish to thank Werner Beckert of the US Environmental Protection Agency for reviewing the manuscript before publication and providing constructive comments.

References

[1] J. Dankers, M. Groenenboom, L.H.A. Scholtis and C. van der Heiden, *J. Chromatogr.*, 641 (1993) 357.

[2] H.-B. Lee, T.E. Peart, R.L. Hong-You and D.L. Gere, *J. Chromatogr.*, 653 (1993) 83.

[3] D.R. Gere, C.R. Knipe, P. Castelli, L.G. Randall Frank, H. Schulenberg-Schell, R. Schuster, L. Doherty, J. Orolin and H.-B. Lee, *J. Chromatogr. Sci.*, 31 (1993) 246.

[4] J.M. Levy, L.A. Dolata and R.M. Ravey, *J. Chromatogr. Sci.*, in press (1993).

[5] M.M. Schantz and S.N. Chester, *J. Chromatogr.*, 363 (1986) 397.

[6] S.B. Hawthorne and D.J. Miller, *J. Chromatogr. Sci.*, 24 (1986) 258.

[7] S.B. Hawthorne and D.J. Miller, *Anal. Chem.*, 59 (1987) 1705.

[8] B.W. Wright, C.W. Wright, R.W. Gale and R.D. Smith, *Anal. Chem.*, 59 (1987) 38.

[9] S.B. Hawthorne, D.J. Miller and J.J. Langenfeld, *J. Chromatogr. Sci.*, 28 (1990) 2.

[10] V. Lopez-Avila, N.S. Dodhiwala and W.F. Beckert, *J. Chromatogr. Sci.*, 28 (1990) 468.

[11] *Test Methods for Evaluating Solid Waste, Physical/ Chemical Methods, SW-846*, US Environmental Protection Agency, Office of Solid Waste, Washington, D.C., 3rd ed., 1991, method 8270.

[12] *Test Methods for Evaluating Solid Waste, Physical/ Chemical Methods, SW-846*, US Environmental Protection Agency, Office of Solid Waste, Washington, D.C., 3rd ed., 1991, method 3550.

[13] V. Lopez-Avila, R. Young, R. Kim and W.F. Beckert, *J. AOAC Int.*, 76 (1993) 555.

ELSEVIER

Journal of Chromatography A, 672 (1994) 177–183

JOURNAL OF CHROMATOGRAPHY A

Rapid identification of some coumarin derivatives in deterpenated citrus peel oil by gas chromatography

Dalida Chouchi, Danielle Barth*

Laboratoire de Thermodynamique et Chimique Appliquée, Équipe Fluides Supercritiques, École Nationale Supérieure des Industries Chimiques, 1 Rue Grandville, B.P. 451, F54001 Nancy Cedex, France

(First received August 9th, 1993; revised manuscript received November 22nd, 1993)

Abstract

Generally on the gas chromatogram of a volatile essential oil, terpenes, oxygenated compounds and sesquiterpenes appear. With temperature programming, it was shown that some non-volatiles are present with the volatiles. They are simple coumarin (2*H*-1-benzopyran-2-one) derivatives such as citropten (5,7-dimethoxycoumarin) and furocoumarins (psoralen, 7*H*-furo[3,2-*g*][1]benzopyran-7-one) such as bergapten (5-methoxypsoralen), some of which are phototoxic. Terpeneless oils are used in perfumes and cosmetics, so it is important to be able to establish rapidly if they contain phototoxic compounds.

1. Introduction

Furocoumarins have been used empirically for centuries in the treatment of depigmentations, especially in Egypt (a papyrus mentions the use against vitiligo of a plant nowadays named *Psoralea caryfolia*).

It has been reported that lemon oil elicits a phototoxic reaction in animal skin [1,2]. Various coumarin and furocoumarin derivatives found in several plants of the Umbelliferae, Rutaceae and Moraceae families are potent photosensitizing agents, and are known to have lethal and mutagenic effects [3,4]. Several coumarin derivatives have been reported to impart a variety of biological manifestations, ranging from antibiotic, anti-inflamatory activity [5], phytotoxic activity, inhibition of seed germination and inhibition of growth of plants and microorganisms [6] to those causing skin dermatitis, liver damage and carcinogenisis.

Some psoralens, such as bergapten, are used in the therapeutic treatment (buvatherapia) of psoriasis and mycosis fungoides [7], but they induce skin dermatitis at high concentrations [8,9].

Lemon oil is an essential oil of considerable commercial importance [10]. Citrus oils are used in the formulation of perfumes and cosmetics and coumarins are used for their flavour quality and are added to sunscreen formulations to enhance tanning induced by ultraviolet radiation [5,11]. Coumarin derivatives are photosensitizing, so the International Fragrance Association [12] guideline limits the lemon oil content in fragrances to 4%.

Coumarin derivatives are separated by extraction and liquid chromatography before the identification [13,14]. HPLC with spectrofluorimetric detection is the most generally used

* Corresponding author.

0021-9673/94/$07.00
SSDI 0021-9673(94)0117-R

method to determine coumarin derivatives [11,15–17] after their separation from the volatiles. In this paper, we report the identification of some coumarin derivatives on the same chomatogram as the volatile compounds of a deterpenated citrus peel oil.

2. Experimental

2.1. Materials

This study was carried out on a lemon essential oil (*Citrus limon* L. var. Eureka) from the Ivory Coast, kindly supplied by Chauvet (Seillans, France). The oil was obtained by cold-pressing of the fruit peel and was "purified" by chilling. The volatile fraction contained 94% (percentage area) of terpenes, 3–4% of oxygenated compounds and 2% of sesquiterpens. The non-volatile fraction was estimated to be 2.5% [18].

2.2. Chromatography and spectroscopy

GC analyses were performed in a Carlo Erba Fractovap 2900 instrument equipped with a flame ionization detector. A fused-silica column (25 m × 0.32 mm I.D.) coated with SE-54 was utilized. The initial temperature was 100°C for 3 min after injection, then increased to 230°C at 3°C/min, with a final hold at 230°C for 20 min. The injector and detector were maintained at 200 and 260°C, respectively. Helium was used as the carrier gas at a flow-rate of 30 ml/min (splitting ratio 1:100) and the auxiliary gases were air (100 ml/min) and hydrogen (1 ml/min).

On the chromatogram, terpene compounds have retention times from 7 to 13 min, oxygenated compounds from 13.5 to 26 min, sesquiterpenes from 26.5 to 40 min and non-volatiles from 40 min to the end of the analyses.

A Finnigan ITD ion trap detector coupled to a gas chromatograph was used to analyse samples, the GC temperature programme was the same as above for GC alone. We compared mass spectra from three databanks: National Institute of Standards and Technology, General Purpose and Toxicology and Terpenes.

Samples were run in ethanol (1:7, v/v) and the retention times and mass spectra were compared with those of pure products: coumarin, 7-methoxycoumarin (herniarin), 5,7-dimethoxycoumarin (limettin, citropten), psoralen, 5-methoxypsoralen (bergapten) and 2,3-dihydroflavone (flavanone).

The samples were obtained by supercritical carbon dioxide fractionation. The description of the experimental procedure will be the subject of another paper.

3. Results and discussion

The chromatogram in Fig. 1 shows a classical representation [19] of the volatile compounds of cold-pressed lemon oil variety Eureka obtained using an SE-54 column with temperature programming from 100 to 190°C. The components are 94% terpenes, 3% oxygenated compounds and 2% sesquiterpenes. Fifty-one constituents accounting for 99.7% of the total volatiles have been identified and quantified in commercial lemon peel oil [20].

Fig. 2 shows the GC analysis of whole peel oil (the same sample as for Fig. 1), with temperature programming from 100 to 230°C. It can be seen that there are two small peaks at 52 and 56 min. The chromatogram in Fig. 3 shows the analysis with temperature programming of a terpeneless fraction. After 40 min many unidentified compounds with volatile can be seen; they represent 0.5–15.0% of the terpeneless oil. Examination of several such chromatograms shows that their content increases with increase in oxygenated compounds in the fractions. This fact is important if we want to separate flavour compounds from non-volatiles.

For preliminary identification, the samples of essential oil were analysed and compared with several coumarins by GC and GC–MS using some pure compounds. Table 1 gives the retention times with temperature programming for the pure products used. The results of the GC–

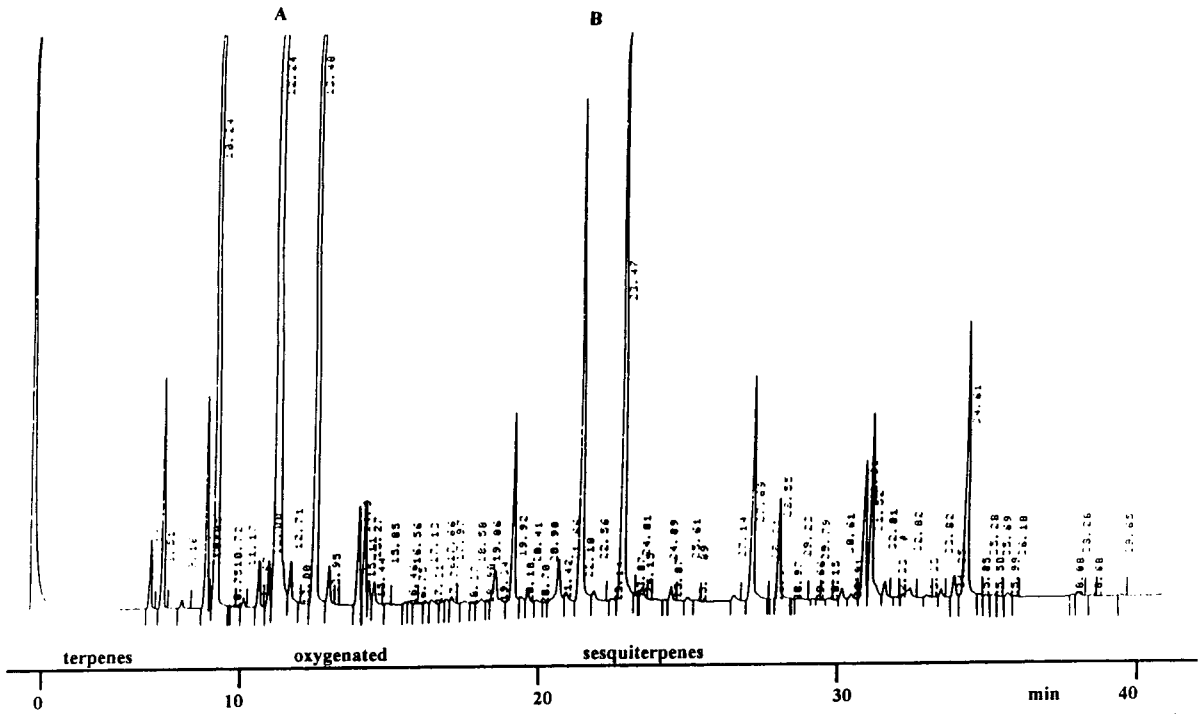

Fig. 1. Classical GC analysis of whole peel oil with a temperature gradient from 100 to 190°C. A = Limonene; B = citral.

MS analysis, reported in Table 2, show that there are sesquiterpenes, oxygenated compounds, three coumarins, three psoralens (Fig. 4) and two fatty acid methyl esters. Our interest is mainly in the identification of the coumarin derivatives, because they play an important role

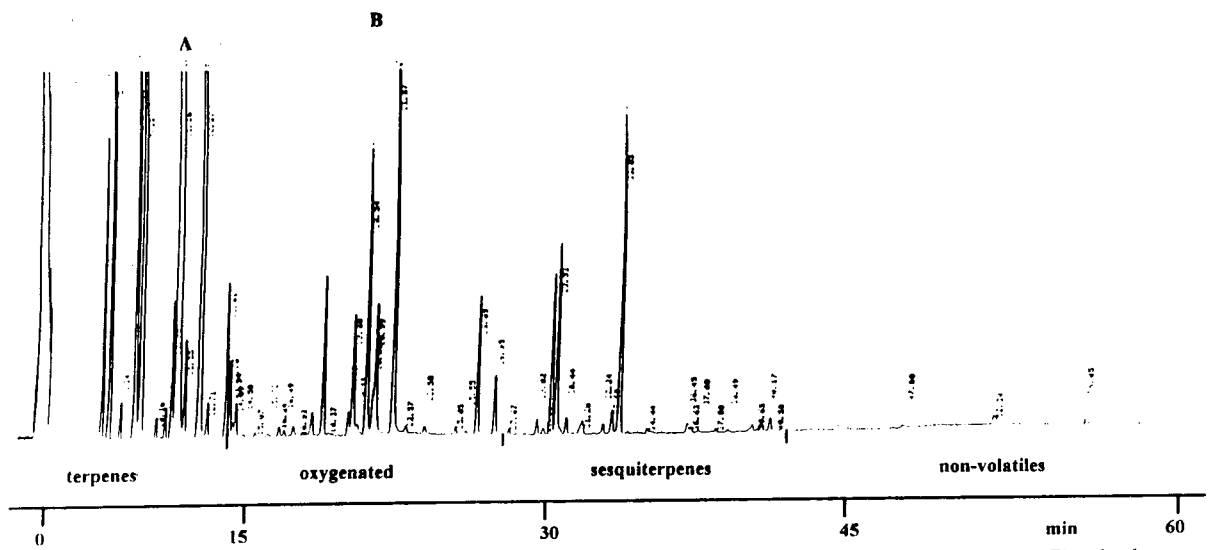

Fig. 2. GC analysis of whole peel oil with a temperature gradient from 100 to 230°C. A = Limonene; B = citral.

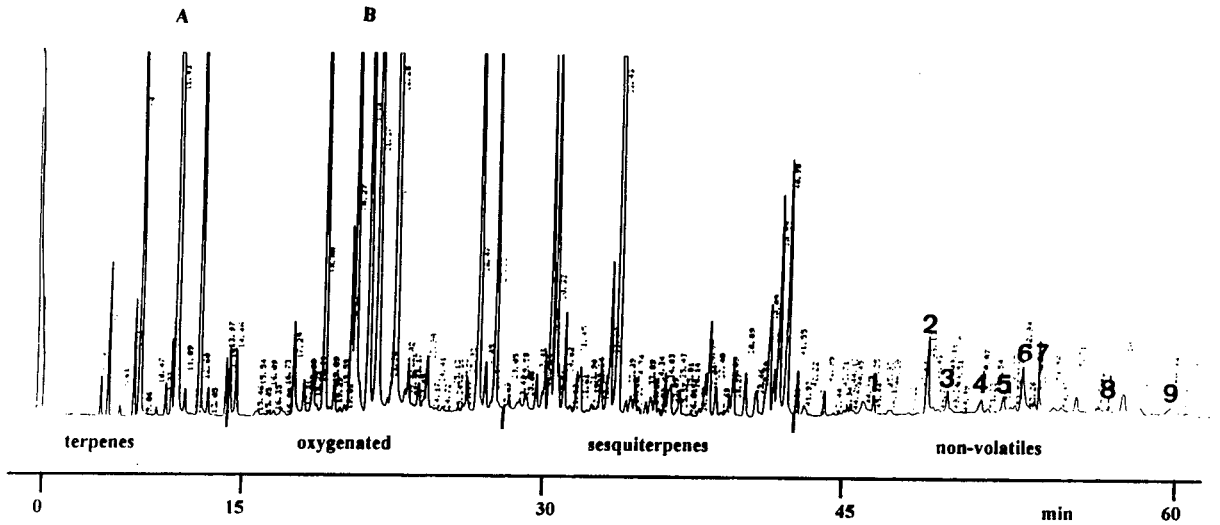

Fig. 3. GC analysis of terpeneless citrus oil with a temperature gradient from 100 to 230°C. See Table 2 for products identified.

Table 1
Retention times of pure compounds

Compound	t_R (min)[a]	M_r
Limonene (A)	11	136
Citral (B)	19–21	154
Coumarin	30	146
Herniarin	46	176
Citropten	51	206
Bergapten	55	216
Flavanone	61	224

[a] Retention time ±1 min.

in the fragrance and flavour quality of the treated oil.

From Fig. 3 and Tables 1 and 2, it can be seen that the retention time increases with increasing molecular mass for coumarin derivatives and with increasing number of methoxyl groups [21]. With our technique we can identify only the compounds that have molecular masses up to about 300; polymethoxyflavones [22], carotenoids and other pigments should be analysed with more appropriate conditions (*e.g.*, SE-30 column and higher temperatures) [23,24]. An

Table 2
Compounds identified on the same chromatogram of volatiles

No.	Compound	M_r	Retention time (min)
1	7-Methoxycoumarin (herniarin)	176	46
2	Bicyclic sesquiterpen	208	48
3	5-Methoxy-8-(3′-methylbut-2′-enyloxy)psoralen (phellopterin)	300	49
4	Methylpentadecanoate	256	50
5	6,7-Dimethoxycoumarin (scoparone)	206	51
6	5,7-Dimethoxycoumarin (citropten)	206	52
7	Methylhexadecanoate	286	55
8	5-Methoxypsoralen (bergapten)	216	56
9	5-(2′,3′-Epoxy-3′-methylbutyloxy)psoralen (oxypeucedanin)	286	59

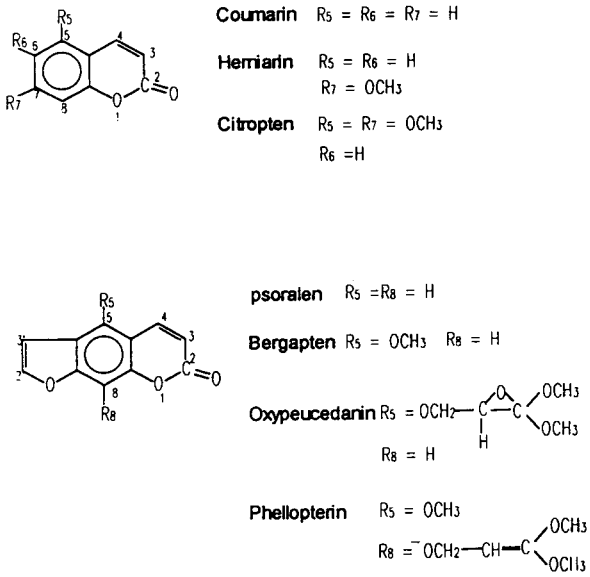

Fig. 4. Formulae of coumarins and psoralens identified by GC analysis.

increase in oxygenated sesquiterpenes in the terpeneless fractions occurs. However, we did not analyse them because terpenoids generally have a complex skeleton, making them difficult to identify, and in addition they have several isomers. Some thermal degradation during the GC analysis was observed [25]. Some compounds such as furanone or pyranone and lactone derivatives resulting from the oxidation of linalool and linalool ester have been found only in old essential oils [26].

Using GC–MS, some compounds were identified with volatile compounds as shown in Table 2. For preliminary identification, the samples of essential oil were analysed and compared with some pure compounds by GC and GC–MS. We used also a comprehensive databank that contains 40 000 reference spectra for identification, and we compared the mass spectra with those in the literature.

About fifteen coumarin derivatives have been found in different citrus oils [3]. A study of the volatile compositions of several citrus species showed that the qualitative and quantitative composition of the product depends on the climatic and geographical origin, the harvesting season and the isolation procedure [27–29]. We may draw the same conclusions for the Eureka lemon, but data are scarce.

In the literature, these compounds are considered as non-volatiles, and are normally analysed separately from volatiles, as it is assumed that they are not present in the volatile fractions, *e.g.*, after a vacuum distillation. However, Shu *et al.* [16] reported that the content of bergapten was 11–88 ppm in a lemon cold-pressed oil from the Ivory Coast, and Naganuma et al. [30] gave 69–87 ppm for the natural oil of the same origin and 5–17 ppm for oil from Sicily.

It is generally accepted that psoralens are more important than coumarins in the phototoxicity of lemon oil. Of the psoralens, oxypeucedanin [30] is said to be 2–100 times more important than bergapten in citrus oils. The content of bergapten in citrus oils is difficult to specify with any certainty because its content depends on the origin of the oil and the way in which it is identified. The highest concentration of bergapten is found in bergamot and lime oils (0.3–0.4% and 0.21%, respectively) [31], and it must be purified when it is employed in perfumes and in the fragrance and flavour industry.

We can identify six coumarin derivatives, herniarin, scoparone, citropten, bergapten, phellopterin and oxypeucedanin, of those mentioned in the literature [17]; for the other compounds we do not have enough data because of their very low concentration. We can say that some of them are coumarin derivatives because their mass spectra show a fragmentation pattern characteristic of the psoralen nucleus [32–34].

We identified by GC–MS as phellopterin a compound for which other workers [35] gave the same mass spectrum but were not sure of its structure (*m/z* 217 and 232). We found herniarin (7-methoxycoumarin) and a dimethoxycoumarin, which we tentatively identify as 6,7-dimethoxycoumarin because of its retention time (50–51 min), differing by about 1 min from that of citropten (51–52 min) (*cf.*, Furuya and Kojima [18]), whereas 4,7-dimethoxycoumarin appears 3 min later. The major coumarin in this oil is citropten, which is not phototoxic for human skin [7]. It precipitates as a white powder in terpeneless samples, suggesting the presence of

other coumarins. After treatment with hexane and ethanol it gives white, filamentous crystals.

In addition to the six coumarins that we report, Rouzet *et al.* [17] identified in the non-volatile fraction of lemon oil 5-geranoxypsoralen (bergamottin), 5-geranoxy-7-methoxycoumarin (Same), 5-isopentenoxy-7-methoxycoumarin, 8-geranoxypsoralen, 5-methoxy-8-(2′,3′-epoxy-3′-methylbutyloxy)psoralen (byakangelicol), 5-(2′,3′-dihydroxy-3′-methylbutyloxy)psoralen (oxypeucedaninehydrate) and 5-methoxy-8-(2′,3′-dihydro-3′-methylbutyloxy)psoralen (byakangelicin). He estimated their concentration to be 0.91% [36]. Only traces of other compounds have been found by TLC, so it makes them difficult to identify.

Glandian [36] analysed extracts of non-chilled Eureka lemon oil to determine the coumarin and psoralen compounds. There are differences between our results and his, which may be explained by the different extraction methods used (solvent extraction and steam distillation by Glandian and supercritical fractionation in this work). The chilling step is used to precipitate some non-volatile compounds [10].

4. Conclusions

We have demonstrated the possibility of the qualitative and rapid analysis of lemon peel oil by a single capillary GC run to obtain data rapidly on components, principally coumarins, important for the fragrance and phototoxicity quality of the sample. The major important coumarin (citropten) could be used as a marker of the other non-volatile components of the oil. The presence of coumarins in chilled oils shows that the process is not sufficient to remove all coumarin compounds from cold-pressed lemon oil.

5. Acknowledgements

We thank Chauvet for kindly supplying the essential oil and M. M. Dzierzinsky (DCPR–ENSIC Nancy) for use of the mass spectrometer.

6. References

[1] P.D. Forbes, F. Urbach and R.E. Davies, *Food Cosmet. Toxicol.*, (1976) 303.
[2] A.R. Young, S.L. Walker, J.S. Kinley, D. Averbeck, P. Morlière and L. Dubertret, *J. Photochem. Photobiol. B: Biol.*, 7 (1990) 231.
[3] J.F. Kefford and V.B. Chandler, *The Chemical Constituents of Citrus Fruits*, Academic Press, New York, 1970.
[4] U.R. Cieri, *J. Assoc. Off. Anal. Chem.*, 52 (1969) 719.
[5] T.J. Mabry and A. Ulubelen, *J. Agric. Food Chem.*, 28 (1980) 188.
[6] P.M. Dey and J.B. Harborne, *Methods in Plant Biochemistry, Vol. 1, Plant Phenolics*, Academic Press, New York, 1989, p. 29.
[7] D.A. Averbeck and E. Moustacchi, *Phytochem. Phytobiol.*, 31 (1980) 475.
[8] S.T. Zaynoun, B.E. Johnson and W. Frain-Bell, *Br. J. Dermatol.*, 96 (1976) 475.
[9] J. Girard, J. Unkovic, J. Delahayes and C. Lafille, *Dermatologica*, 158 (1979) 229.
[10] D. Moyler, *Chem. Ind. (London)*, (1991) 11.
[11] G. Verger, *Parfums Cosmet. Aromes*, 51 (1983) 63.
[12] International Fragrance Association, Geneva.
[13] M. Benincasa, F. Buirelli, G.P. Cartoni and F. Coccioli, *Chromatographia*, 30 (1990) 271.
[14] A. Bettero and C.A. Benassi, *J. Chromatogr.*, 280 (1983) 167.
[15] M. Herpol-Borremans, M.O. Masse and R. Grimée, *J. Pharmacol. Belg.*, 40 (1985) 147.
[16] C.K. Shu, J.P. Walradt and W.I. Taylor, *J. Chromatogr.*, 106 (1975) 271.
[17] M. Rouzet, R. Glandian, F. Pouchus and H. Corneteau, presented at *Symposium, Recherches et Techniques en Cosmétologie; Les Substances Naturelles, Orléans, 21–23 April, 1980.*
[18] T. Furuya and H. Kojima, *J. Chromatogr.*, 29 (1967) 382.
[19] G.P. Cartoni, G. Goretti, B. Monticelli and M.V. Russo, *J. Chromatogr.*, 370 (1986) 93.
[20] T.S. Chamblee, B.C. Clark, Jr., G.B. Brewster, T. Radford and G. Iacobucci, *J. Agric. Food Chem.*, 39 (1991) 162.
[21] H.J. Thompson and S.A. Brown, *J. Chromatogr.*, 314 (1984) 323.
[22] E. Gaydou, T. Berahia, J.C. Wallet and J.P. Bianchini, *J. Chromatogr.*, 549 (1991) 440.
[23] G. Micali, F. Lanuzza, P.A Currô and G. Calabrô, *J. Chromatogr.*, 514 (1990) 317.
[24] S. Nagy and H.E. Nordby, *Lipids*, 6 (1971) 826.
[25] H. Maarse, *J. Chromatogr.*, 106 (1975) 369.
[26] G. Mazza, *J. Chromatogr.*, 362 (1986) 87.
[27] M.H. Boelens and R. Jimenez, *J. Essent. Oil Res.*, 1 (1989) 151.
[28] B.M. Lawrence, *Perfum. Flavorist*, 17 (1992) 45.
[29] M.H. Boelens, *Perfum. Flavorist*, 16 (1991) 17.

[30] M. Naganuma, S. Hirose, Y. Nakajima and T. Someya, *Arch. Dermatol. Res.*, 278 (1985) 31.
[31] M. Poiana, F. Crispo, E. Manziu, V. Sicari and B. Mincione, in E. Reverchon and A. Schiraldi (Editors), *Atti del II Congresso i Fluidi Supercritici e le Loro Applicazioni, Ravello, 20–22 June 1993*, p. 113.
[32] G.R. Waller and O.C. Dermer, *Biochemical Applications of Mass Spectrometry*, Wiley, New York, First Supplementary Volume, 1980, pp. 1150–1156.
[33] Q.N. Porter, in E.C. Taylor and A. Weissberg (Editors), *Mass Spectrometry of Heterocyclic Compounds*, Wiley, 1985.
[34] H. Ziegler, *Doctoral Thesis*, University of Bayreuth, 1992.
[35] H.W. Latz and B.C. Madsen, *Anal. Chem.*, 41 (1969) 1180.
[36] R. Glandian, *Doctoral Thesis*, University of Nantes, 1979.

ELSEVIER

Journal of Chromatography A, 672 (1994) 185–201

JOURNAL OF CHROMATOGRAPHY A

Some thermodynamic aspects of packed column supercritical fluid chromatography

D.Y. Shang, J.L. Grandmaison, S. Kaliaguine*

Department of Chemical Engineering, Laval University, Sainte-Foy, Québec G1K 7P4, Canada

(First received October 18th, 1993; revised manuscript received February 1st, 1994)

Abstract

Packed column supercritical fluid chromatography (SFC) was employed in the investigation of the effects of density and packing surface silanol groups on the enthalpy and entropy of transfer of the solute between the mobile and stationary phases using CO_2 as the mobile phase and solutes of various polarity. The solutes were aromatics, phenols and amines and the stationary phases were untreated silica gel Partisil-10, thermally treated Partisil-10 and Partisil-10 bonded with octadecylsilane. In the density range 0.3–0.9 g ml^{-1}, the enthalpies decrease as the mobile phase fluid density increases while the entropies remain constant for well coated packings. A moderate pressure drop does not change this trend. The thermodynamic value obtained from a Van 't Hoff plot suggests a strong influence of the retention of polar solutes by surface silanol groups in the low-density region of SFC separation. In addition, a characteristic line of intersection points may be obtained from the extrapolated line of the Van 't Hoff plots. Tested with solutes and packings of various polarity, the characteristic line reveals the nature of the packing materials.

1. Introduction

The place of supercritical fluid chromatography (SFC) and supercritical fluid extraction (SFE) in chemical analysis is being established with the arrival of new and better SFC systems and some cases of acceptance of SFE methods as standard analytical procedures [1]. With simple control of the density of the mobile phase or addition of modifiers or additives, SFC and SFE offer chromatographers a wide range of choices of methods to tackle the ever demanding analytical problems. However, to achieve the same status as is enjoyed by GC or HPLC, SFC must not only have more validated application methods but also solve the problem of lack of suitable kinetic models to describe fully the retention process in SFC. The lack of a kinetic model is partly due to too many complex factors being involved, such as temperature, pressure drop, density, solutes, the nature of the mobile and stationary phases used and partly the paucity of fundamental data. Nevertheless, as supercritical fluids have the properties of both liquids and gases, depending on temperature and pressure, SFC also provides an ideal tool for the study of retention behaviour in chromatographic processes.

To take advantage of the liquid-phase-like and gas-phase-like properties of supercritical fluids, a number of papers have been published on a thermodynamic approach to retention behaviour

* Corresponding author.

0021-9673/94/$07.00
SSDI 0021-9673(94)00113-N

in SFC [2–4]. Nevertheless, the application of the Van 't Hoff equation in chromatographic studies was proposed and studied in the early stages of the development of chromatography [5]. Meyer [6] proposed a simple thermodynamic model and the concept of unit concentration to define the standard state for studying solute retention as a function of temperature at constant pressure. Later, Yonker and co-workers [7–9] studied the effects of density on the enthalpy and entropy of transfer for SFC and they developed a simple thermodynamic model to describe the retention process in capillary SFC systems. Chester and Innis [10] established an empirical thermodynamic model relating SFC retention to GC and HPLC retention. Combining the models of Yonker and co-workers and Chester and Innis, Berger [3] proposed an empirical equation based on experimental results and the Van 't Hoff equation. This empirical equation was quickly adapted by Grandmaison and Kaliaguine [4] in their study of phenols under capillary column SFC conditions. The density range was narrow, however, owing to the limitations of the capillary column system. So far the relationship between enthalpy and the contribution of surface silanol groups and solutes of various polarity in packed column SFC systems has not been fully explored.

In recent years, packed column SFC has been experiencing renewed interest among the researchers working on SFC [11–13]. For example, Bartle *et al.* [14] used the Peng–Robinson equation of state (EOS) to develop a simple thermodynamic equation describing solute retention as a function of density and pressure in packed column SFC. Although open-tubular wall-coated capillary column SFC is much more popular because it offers more efficient separations of polar compounds owing to the large number of theoretical plates achievable, many reasons exist for developing packed column SFC technology, such as ease of transferring chromatographic data to preparative SFC, short analysis times and the choice of a wide range of packing materials developed for HPLC.

Packing surface activity creates a major obstacle to the wider use of packed column SFC, because in many instances the surface activity of silica packing materials presents a serious limitation for packed column SFC when mobile phases of low polarity (*e.g.*, CO_2) are used to elute polar analytes. An unmodified silica gel surface exhibits reversible adsorption of polar compounds owing to the presence of silanol groups, resulting in tailing peak shapes and extended retention times. Our test results show that many polar compounds were not eluted from an unmodified silica gel packed column, whereas nonpolar compounds such as alkanes and aromatics eluted easily under similar experimental conditions [15]. To deal with this problem, polar organic modifiers such as methanol are often needed in both capillary and packed column SFC systems. These modifiers usually have dual functions, *i.e.*, to increase the solubility of polar solutes and to provide a dynamic coating of surface silanol groups. However, most of the modifiers are not compatible with flame ionization detection (FID), the most widely used universal detection method in SFC. In addition, the introduction of polar organic modifiers will also create many problems for SFC processes, *e.g.*, the toxicity of some modifiers and the complexity of the pumping and recovery systems. Therefore, much attention has been focused on improving surface modification methods in order to allow the elution of polar compounds when using CO_2 as the sole mobile phase [11–13].

Essentially, SFC is a water-free process and it is therefore possible to adopt different approaches other than the conventional HPLC column packing deactivation methods. A new deactivation method should produce not just well deactivated but also stable packing materials under SFC conditions. In this regard, thermal treatment of silica gel might yield useful information for the development of new chromatographic packing materials [16]. The method of preparation and the thermal treatment decide the composition of the silica gel surface. Scott and Kucera [17] studied the thermal treatment of silica gel and they concluded that at about 650°C the primary layer of strongly hydrogen-bound water is completely removed. They also reported

that at still higher temperatures (>900°C) sintering of the silica particles starts and the dehydration of silanol groups is complete, forming a hydrophobic surface covered with siloxane groups. Other researchers [16] have disputed the temperature range of dehydration and the existence of a hydrophobic surface, presenting evidence for the existence of free silanols that are hardly affected by thermal treatment at 600°C and below. Nevertheless, it is fairly obvious that thermal treatment of silica gel over a wide range of temperatures will provide silica gel surfaces with distinctly different characteristics in SFC studies.

Presumably, the retention time of polar solutes such as phenols is caused not only by the remaining silanol groups on the silica surface (silanophilic effects), but also by the long alkyl functional groups (solvophobic effects) introduced through reaction with chlorosilanes, which also play an important role in the adsorption and desorption in the separation process [18]. The thermal deactivation method, therefore, would provide some insight into the interaction of surface silanols with a particular fluid mobile phase–solute combination, as the method avoids using long alkyl groups and gives controlled concentrations of silanol groups on the silica gel surface. As the chromatographic process is closely associated with the free energy of transfer of the solute from the mobile to the stationary phase, any modification of the stationary phase should be reflected in the measurement of thermodynamic data. Hence a thermally treated surface free of silane groups and having a controlled amount of silanol groups provides an ideal material to study the correlation between silanol groups on a silica gel stationary phase and the solute in the mobile phase. The data obtained from the study of thermally modified silica gel surfaces would be useful in developing an accurate quantitative thermodynamic model, which is essential for extracting the maximum amount of information about the SFC systems and helping to make SFC become a mature and viable analytical technique. However, so far the thermal treatment of silica gel packings in SFC has not been reported.

As an integral part of the study of the pyrolysis of lignocellulosic materials [4], the purpose of this work was to investigate the retention behaviour of thermally treated silica gel under SFC conditions and to compare it with commercial silane-modified packings. An attempt was also made to measure the enthalpy and entropy of interaction between the mobile phase and the stationary phase as a function of density, in order to introduce quantitative aspects in the investigation of thermally treated silica gel and other packings being developed in our laboratory. It is also intended to demonstrate that the Van 't Hoff plot can be further explored for characterizing packed columns in SFC systems.

2. Theoretical

The effect of density on retention in SFC has been well studied [3,9,19]. The adsorption and desorption processes between the mobile and stationary phases are associated with enthalpic and entropic effects. The free energy of transfer of the solute from the mobile to the stationary phase is considered to be the major factor governing retention [5]. Yonker and Smith [9] have shown that the enthalpy of solute transfer between the stationary and mobile phase at infinite dilution (ΔH_T^0) is a basic thermochemical parameter which can be used to understand and predict solute retention behaviour in SFC. Grandmaison and Kaliaguine [4] obtained the enthalpy and entropy of transfer of five phenols in their investigation of behaviour of phenols under SFC conditions, further demonstrating the usefulness of this approach in SFC studies.

The principle of this thermodynamic approach is to compare the enthalpy and entropy changes of different chromatography systems. These enthalpy and entropy data can be obtained from the well known Van 't Hoff plot, which expresses the dependence of the capacity factor, k', on temperature, T, as

$$\ln k' = -\frac{\Delta H_T^0}{RT} + \frac{\Delta S_T^0}{R} - \ln \beta \quad (1)$$

where k' is related to the retention times of the

solute, t_R, and of an unretained solute, t_0, according to the equation

$$k' = \frac{t_R - t_0}{t_0} \quad (2)$$

ΔH_T^0 and ΔS_T^0 are the enthalpy and entropy, respectively, associated with the transfer of the solute from the mobile to the stationary phase, R is the gas constant and β is defined as the phase ratio and is often considered to be constant [4].

The relationship between ln k' and T^{-1} at constant density (ρ) is linear whenever ΔS_T^0 and β are considered to be independent of temperature. If this is the case, from Eq. 1 we can write

$$\left[\frac{d \ln k'}{d(1/T)}\right]_\rho = -\frac{\Delta H_T^0}{R} \quad (3)$$

Thus, when ln k' is plotted against $1/T$ at constant ρ, the slope of the linear part of the experimental curves yields estimated values for the enthalpy of transfer. Once the value of enthalpy has been obtained, we can calculate the entropy of transfer from the intercept of the plot of Eq. 3 provided that phase ratio β can be estimated. The standard state for both ΔH_T^0 and ΔS_T^0, based on the concept of concentration units for the distribution coefficient [6], is 1 g ml^{-1} [3].

Chester and Innis [10] applied the Van 't Hoff equation to study the solute retention behaviour of a capillary SFC system. From the observation of GC data in the literature and limited experimental results, they suggested that for SFC systems the retention mechanism can be divided into GC-like (adsorption-like) and LC-like (partition-like) regions. This model is very interesting because it provides a clear picture of the solute retention mechanism in SFC and bridges the thermodynamic study of GC and LC through SFC. Nevertheless, tested only with a capillary column and over a narrow range of density, this model may not be applicable to packed-column SFC as the behaviour of packed column SFC is different from that of capillary column SFC in many ways, such as the presence on the packing surface of long alkyl groups, usually a larger amount of surface silanol groups and a high pressure drop.

Yonker and Smith [9] used the Van 't Hoff plots (ln k' *vs.* $1/T$) to determine the overall enthalpy of transfer between the mobile and stationary phase for *n*-alkanes and *n*-alkanols with two capillary columns of different polarity. Their experimental results of the enthalpy and entropy of transfer showed significant differences between two columns tested with the same solutes under identical experimental conditions, reflecting the important role played by the nature of stationary phase in determining ΔH_T^0 and ΔS_T^0.

Based on the work of Chester and Innis [10] and Yonker and Smith [9], Berger [3] noted that in capillary SFC, the natural logarithm of the retention factor (ln k') decreases linearly with increasing density at constant temperature. He also assumed that the stationary phase does not change much with the introduction of a supercritical carrier gas, and solute–stationary phase (s–sp) interaction should be the same in GC or SFC. Berger proposed the following empirical equation:

$$\Delta H_T^0 = \Delta H_{s-sp}^0 - \rho(\Delta H_{s-mp}^0) \quad (4)$$

where ΔH_{s-sp}^0 is obtained from ln k' *vs.* $1/T$ plots under GC conditions or by extrapolation of ΔH_T^0 at zero density, and ΔH_T^0 is obtained from Van 't Hoff plots in SFC at various fixed densities. This equation has been employed to study the behaviour of phenols in a capillary column SFC system [4], and seems to work very well at low densities and for capillary column SFC. The applicability of this equation to packed column SFC has not been tested. Here it must be noted that the assumptions made for this equation, *i.e.*, ΔH_{s-sp}^0 is constant (or changes negligibly) regardless of the mobile phase density and ΔH_{s-mp}^0 depends only on density, may not hold in packed column SFC as long as they are not tested experimentally. The simplified approach of this equation necessitates a prudent attitude when applying it under packed column SFC conditions, as packed column SFC usually employs much higher pressures than in capillary SFC and exhibits a higher surface polarity. In addition, the interactions of the solute with the mobile

phase depend not only on the density of the mobile phase but also on the nature of the solutes and the mobile phase. Hence, the ΔH^0_{s-mp} value should be decided accordingly. We believe that testing this simple thermodynamic model in packed column SFC warrants its applicability and would be useful in establishing a realistic model that takes the differences of packed column SFC into account.

3. Experimental

3.1. Instrumentation

The SFC system (Lee Scientific 600) has been described elsewhere [4]. For packed column SFC experiments, some minor modifications were made to this SFC system. At the packed column outlet end, a tee column end-fitting (Valco TCET 441) is attached. One end of this tee is connected to a capillary restrictor (25 cm × 15 μm I.D.) leading to a flame ionization detector, which gave a flow-rate of 1 ml s^{-1} at 300 atm (1 atm = 101 325 Pa) and 80°C with SFC-grade CO_2 (Scott, Plumsteadville, PA, USA) as the mobile phase; the other end of the tee (at right-angles to the normal flow path) is used to accept the capillary splitter, which is a 15 or 25 μm I.D. capillary tube having a length from 1 to 4 cm to adjust the splitting ratio. The column was packed at our laboratory using the supercritical fluid displacement method developed by Dean and Poole [12].

Taking the oven configuration and optimum operating parameters into consideration, we chose a 15 cm × 2.1 mm I.D. × 1/4 in. O.D. (1 in. = 2.54 cm) stainless-steel tube as a blank column for our SFC system. Standard Valco fittings (Valco Instruments, Houston, TX, USA), 2-μm screens and precut, smooth-bore tubing from Anspec (Ann Arbor, MI, USA) were used for all columns. The packing materials were unmodified silica gel (Partisil 10, 10-μm irregular particles) and modified silica gel ODS-1, ODS-2 and ODS-3 (Partisil-10 particles surface-bonded with octadecylsilane groups) from Whatman (Clifton, NJ, USA). In total six columns were packed for this investigation. Packings of columns B and C were thermally treated at 660 and 900°C for 2 h, respectively. To avoid the drastic changes in the physical properties of the packings that may occur during sudden temperature changes, the packings were cooled gradually in a muffle furnace after heat treatment. Descriptions of these columns are given in Table 1 and the properties of the packing materials are given in Table 2.

3.2. Chemicals

Naphthalene was obtained from BDH Chemicals (Ville St.-Laurent, Quebec, Canada). Dichloromethane (HPLC purity) was purchased from Aldrich (Milwaukee, WI, USA) and used for dead-time (t_0) measurements. Eugenol (4-allyl-2-methoxyphenol) with a purity of 99%, pyridine, vanillin and 2,4-dimethylphenol with a purity of 97% were also bought from Aldrich.

Phenols were chosen as probes in this work because they have medium polarity, providing a means to observe interactions between active sites and solutes with a reasonable retention time and peak shape. Another probe in this work was pyridine, which is a very sensitive probe for silanol activity as observed by De Weerdt *et al.* [20]. However, pyridine can only be used for very well coated packing materials, which limits its usefulness as a probe for packings of various polarity. Each probe was dissolved in HPLC-

Table 1
Descriptions of packed columns

Column	Packing material	Treatment
A	Partisil-10	Unmodified
B	Partisil-10, thermally treated	Calcined at 660°C for 2 h
C	Partisil-10, thermally treated	Calcined at 900°C for 2 h
D	ODS-1	Silane treated, C_{18}, 5% C[a]
E	ODS-2	Silane treated, C_{18}, 15% C[a]
F	ODS-3	Silane treated and end-capped, C_{18}, 10% C[a]

[a] Manufacturer's specification.

Table 2
Properties of packing materials

Column	Stationary phase	Pore volume ($ml\ g^{-1}$)[a]	Surface area ($m^2\ g^{-1}$)[a]	C (%)[b]	OH/nm^2 [c]
A	Partisil-10	0.897	373.5	0.44	3.61
B	T-660	0.926	304.1	N/A	2.52
C	T-900	0.559	159.3	N/A	1.92
D	ODS-1	0.774	300.0	4.75	2.73
E	ODS-2	0.485	212.5	17.32	1.75
F	ODS-3	0.559	267.7	10.75	1.05

[a] Measured by the BET technique.
[b] CHN analysis results.
[c] OH analysis results.

grade dichloromethane prior to introduction on to the column. Sample size plays an important role in SFC [21]. In this work the concentration of samples per component was about 1–3 $\mu g\ \mu l^{-1}$.

3.3. Surface hydroxyl groups

The concentration of hydroxyl groups on the surface of a silica gel packing has long been a research subject and many measurement techniques have been explored [22]. The general consensus is that there exist about 4–5 hydroxyl groups per nm^2 [23,24]. In this investigation the measurement was based on the work of Sato *et al.* [25] and Marcinkowska [24]. The basis of this method is the reaction of an organometallic reagent with the surface hydroxyl groups on silica gel. In this work, triethylaluminium was chosen as an organometallic reagent as it does not produce secondary reactions. Sato *et al.* [25] showed that one molecule of triethylaluminium reacts with one surface OH group and releases one molecule of ethane:

$$-Si-OH + Al(C_2H_5)_3 \rightarrow Si-O-Al(C_2H_5)_2 + C_2H_6$$

By measuring the volume of ethane released, one can calculate the concentration of surface hydroxyl groups of the silica gel. Duplicate measurements were performed for all samples and the results were averaged. The precision of the hydroxyl group measurements for these samples was usually within the 5–10% (R.S.D.) range.

3.4. CHN elemental analysis

Elemental analysis data on unbonded and bonded-phase packings were obtained with a Model 1106 elemental analyser (Carlo Erba, Milan, Italy). Duplicate analyses for carbon, hydrogen and nitrogen were normally performed for all the samples. To verify the accuracy of the measurement, some of the bonded samples were sent to an independent analytical laboratory (INRS, Ste.-Foy, Quebec, Canada). The precision of the measurement was usually within the 4–5% range.

3.5. Nitrogen BET measurement

Surface areas, pore size distributions and pore volumes of the silica gels were measured by the BET method [26] using an Omnisorp 100 instrument from Omicron (Berkeley Heights, NJ, USA). The sample pretreatment involved heating the sample at 220°C for 8 h under a vacuum of 10^{-5} mbar. Duplicate measurements were performed for selected samples. The precision of the surface area measurements for these samples was usually within the 4–5% range.

3.6. Experimental procedures

For each chromatographic experiment, approximately 10 μl of a solution containing naphthalene in dichloromethane were injected. Eugenol, pyridine, vanillin and 2,4-dimethylphenol solution were prepared similarly. For fear of dynamic masking effects, a single solute solution was used in this study. The experiments were normally performed at CO_2 densities ranging from 0.4 to 0.9 g ml^{-1} and infrequently from 0.3 to 0.9 g ml^{-1}. The density of carbon dioxide at different temperatures and pressures was calculated using the Peng–Robinson equation of state and checked against values given by a density calculation program of Lee Scientific.

All experimental measurements were made twice and averaged. In the event of divergence of the results, triplicate measurements were made and averaged. Although in column SFC systems the calculated ΔH_T^0 is a convenient approach for providing some chromatographic insight, it also has definite restrictions. The precision of ΔH_T^0 values is compromised by the working density range in both capillary and packed columns. With packed columns, our own laboratory results [15] and those of Lauer *et al.* [27] show that heavy peak tailing appeared with densities less than 0.5 g ml^{-1}. In addition, the applicable density range of capillary columns can hardly exceed 0.5 g ml^{-1} without a serious decrease in resolution. To overcome this limitation, three measurements instead of two were made and averaged for chromatograms taken when the density was less than 0.5 g ml^{-1} in this work.

4. Results and discussion

4.1. Thermally treated silica gel

The retention of naphthalene and eugenol on columns A, D and F, three columns with different properties, was first studied under carefully controlled constant-density conditions and the results were plotted as ln k' *vs.* $1/T$ at each of a number of constant densities. Selected plots of ln k' *vs.* $1/T$ are shown in Figs. 1, 2 and 3 for columns A, D and F, respectively. Generally, in Figs. 1–3 all the Van 't Hoff plots yield straight lines (with some slight indication of "roll-over" at low temperatures for columns A and F) over the temperature range 40–160°C, the pressure range 148–415 atm or the CO_2 density range 0.3–0.9 g cm^{-3}.

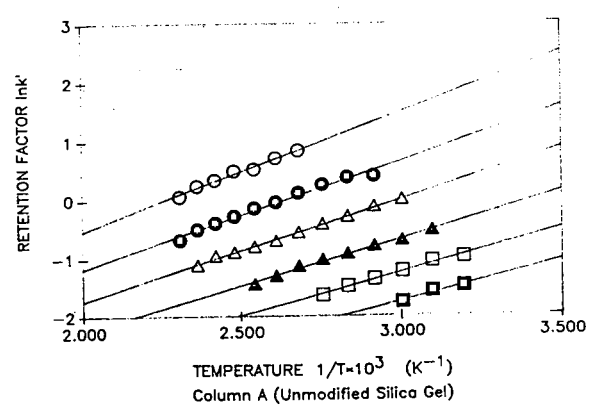

Fig. 1. Logarithm of capacity factor, k', of naphthalene as a function of reciprocal temperature (K^{-1}) for different densities of the mobile phase. Stationary phase, unmodified Partisil-10; mobile phase, CO_2. Density: ○ = 0.4; ● = 0.5; △ = 0.6; ▲ = 0.7; □ = 0.8; ■ = 0.9 g ml^{-1}.

The slopes of the lines in Figs. 1–3 yield

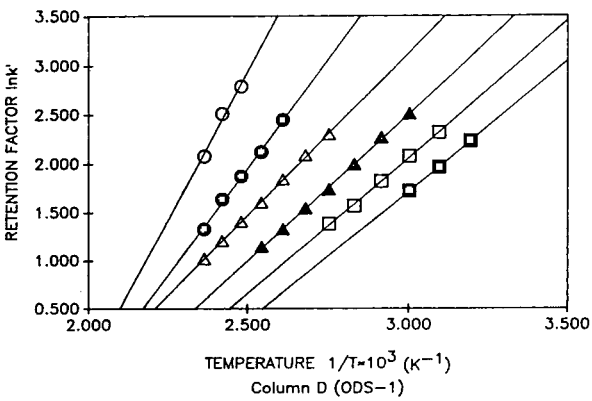

Fig. 2. Logarithm of capacity factor, k', of eugenol as a function of reciprocal temperature (K^{-1}) for different densities of the mobile phase. Stationary phase, Partisil-10 ODS-1; mobile phase, CO_2. Symbols as in Fig. 1.

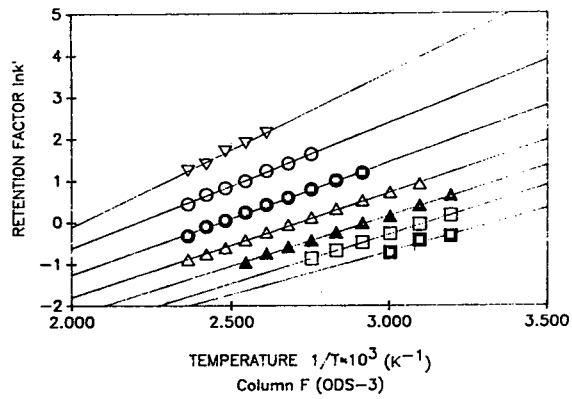

Fig. 3. Logarithm of capacity factor, k', of eugenol as a function of reciprocal temperature (K^{-1}) for different densities of the mobile phase. Stationary phase, Partisil-10 ODS-3; mobile phase, CO_2. Symbols as in Fig. 1; $\nabla = 0.3$ g ml^{-1}.

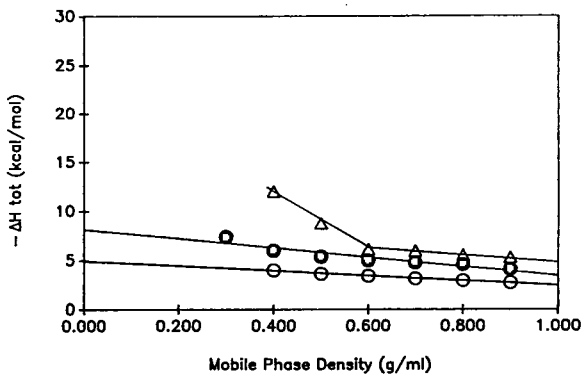

Fig. 4. Total enthalpies of transfer as a function of CO_2 density of the mobile phase. Stationary phase: ○ = unmodified Partisil-10; △ = Partisil ODS-1; ● = ODS-3. Mobile phase, CO_2. Solute: △, ● = eugenol; ○ = naphthalene.

calculated values of enthalpy, which are plotted against density in Fig. 4. It is noted that the enthalpy values obtained from the curves in Fig. 4 (naphthalene line for column A and eugenol line for ODS-3) form nearly straight lines, while the eugenol curve for ODS-1 first follows a similar trend in the density range 0.6–0.9 g ml^{-1} but diverges in the low-density region. Similar data treatment was applied to all columns and the data obtained are presented in Tables 3–8.

The ΔH_T^0 values for naphthalene and 2,4-dimethylphenol on columns A, B and C are between 2 and 13 kcal mol^{-1} (1 kcal = 4.184 kJ), similar values having been reported for naphthalene, *n*-pentane and propane as mobile phases [14,28], and for 2,4-dimethylphenol in pure CO_2 as eluent [4]. The ΔH_T^0 and ΔS_T^0 values reported for these solutes are also of similar magnitude to published results [3,8,9,29].

For all the solutes tested in this work, the data in Tables 3–5 show that the retention increases with decrease in density and ΔH_T^0 tends to become more negative. Grandmaison and Kaliaguine [4] reported that ΔH_T^0 also reflects the elution order of the polycyclic aromatics tested in their capillary SFC system, which is in agreement with the results of packed column SFC in this work [15]. As shown in Table 2, the surface geometry of the silica is also altered during the thermal treatment. The untreated silica gel has a large surface area, which generates low phase ratios, leading to high retention. The thermal treatment process decreased the surface areas and hence decreased the retention

Table 3
Enthalpy and entropy of transfer for column A (unmodified Partisil-10) from Van 't Hoff plot

Solute	Parameter[a]	Mobile phase density (g ml^{-1})					
		0.4	0.5	0.6	0.7	0.8	0.9
Naphthalene	$-\Delta H_T^0$	4.00	3.64	3.44	3.16	2.95	2.73
	$-\Delta S_T^0$	4.26	4.85	5.52	6.00	6.51	6.85
2,4-Dimethyl-phenol	$-\Delta H_T^0$	12.90	7.31	4.71	4.17	3.21	2.99
	$-\Delta S_T^0$	21.62	9.21	3.11	2.53	0.91	0.55

[a] Enthalpies are in kcal mol^{-1} and entropies in cal mol^{-1} K^{-1} ($R = 1.98$ cal mol^{-1} K^{-1}). The volume phase ratio β was estimated to be 11.2.

Table 4
Enthalpy and entropy of transfer for column B (thermally treated at 660°C) from Van 't Hoff plot

Solute	Parameter[a]	Mobile phase density (g ml^{-1})					
		0.4	0.5	0.6	0.7	0.8	0.9
Naphthalene	$-\Delta H_T^0$	4.99	3.99	3.65	3.05	2.79	2.75
	$-\Delta S_T^0$	6.44	5.31	5.64	5.05	5.31	6.18
2,4-Dimethyl-phenol	$-\Delta H_T^0$	13.10	8.91	7.33	7.11	6.96	6.10
	$-\Delta S_T^0$	22.12	13.15	10.38	11.76	12.26	10.89

[a] See Table 3.

Table 5
Enthalpy and entropy of transfer for column C (thermally treated at 900°C) from Van 't Hoff plot

Solute	Parameter[a]	Mobile phase density (g ml^{-1})					
		0.4	0.5	0.6	0.7	0.8	0.9
Naphthalene	$-\Delta H_T^0$	4.37	3.57	3.61	3.05	2.71	2.23
	$-\Delta S_T^0$	3.86	4.55	5.76	5.33	5.37	4.89
2,4-Dimethyl-phenol	$-\Delta H_T^0$	11.79	8.70	7.70	6.58	5.97	4.39
	$-\Delta S_T^0$	19.09	12.71	10.93	10.24	10.08	6.18

[a] See Table 3.

factors of polar compounds such as phenols. Therefore, the role of the physical properties of thermally treated silica gel should be taken into account. However, comparing the ΔH_T^0 data for columns A, B and C, we note that the ΔH_T^0 values for naphthalene are of similar magnitude. In addition, the thermally treated packings produced almost identical chromatograms for naphthalene although their physical properties were altered during thermal treatment, especially in the case of column C. As naphthalene is a non-polar solute, the main retention mechanism with naphthalene in these three columns is predominantly physical adsorption and desorption. Small differences in ΔH_T^0 and ΔS_T^0 among these columns could mean that the column packing surface geometry plays a minor role in the SFC process.

The OH concentration measurement (Table 2) shows that the thermal treatment produced a

Table 6
Enthalphy and entropy of transfer for column D (ODS-1) from Van 't Hoff plot

Solute	Parameter[a]	Mobile phase density (g ml^{-1})					
		0.4	0.5	0.6	0.7	0.8	0.9
2,4-Dimethyl-phenol	$-\Delta H_T^0$	11.65	9.25	8.02	7.69	7.36	7.36
	$-\Delta S_T^0$	18.71	14.26	11.84	12.32	12.51	14.32
Eugenol	$-\Delta H_T^0$	12.03	8.75	6.12	5.97	5.54	5.29
	$-\Delta S_T^0$	19.46	13.23	7.62	8.16	7.76	7.70

[a] See Table 3.

Table 7
Enthalpy and entropy of transfer for column E (ODS-2) from Van 't Hoff plot

Solute	Parameter[a]	Mobile phase density (g ml^{-1})					
		0.4	0.5	0.6	0.7	0.8	0.9
2,4-Dimethyl-phenol	$-\Delta H_T^0$	10.46	9.90	9.57	7.69	6.71	6.45
	$-\Delta S_T^0$	15.09	15.74	15.88	12.32	11.17	11.46
Eugenol	$-\Delta H_T^0$	9.23	8.48	7.80	7.66	7.03	7.04
	$-\Delta S_T^0$	12.81	12.43	12.89	13.48	12.57	13.37

[a] See Table 3.

silica gel with less surface silanol groups in columns B and C, which would in turn yield less negative ΔH_T^0 values and a shorter retention time and peak shape improvement for 2,4-dimethylphenol compared with column A. In addition, in comparison with chromatographic data for column A packed with untreated silica gel, the retention time of a polar solute such as 2,4-dimethylphenol is much shorter and peak tailing is decreased to a certain extent for both columns B and C packed with silica gel thermally treated at 660 and 900°C, respectively. The most probable explanation is that the heat treatment produced an inert silica gel by removing the silanol groups from the packing surface, forming a more hydrophobic surface as expected. This improvement, however, cannot match that of a well coated packing such as ODS-3.

Nevertheless, the enthalpy values for 2,4-dimethylphenol indicate that other factors exist that contribute to ΔH_T^0 besides the amount of surface silanol groups. For example, there are different kinds of sites on the surface of a silica particle. According to Colin and Guiochon [30], five main types of sites are present: free or isolated silanol, silanol with physically adsorbed water, dehydrated oxide, germinal silanol and bound silanols. Of these sites, two different types of surface silanols, *i.e.* bound and isolated silanols, are predominantly responsible for the retention of hydroxyl-containing solutes. Solutes with hydroxyl groups are able to interact with the bonded silanols and are adsorbed on these sites. The retention of these solutes decreases with the removal of these hydroxyl groups or bonded silanols. It is generally accepted that

Table 8
Enthalpy and entropy of transfer for column F (ODS-3) from Van 't Hoff plot

Solute	Parameter[a]	Mobile phase density (g ml^{-1})						
		0.3	0.4	0.5	0.6	0.7	0.8	0.9
2,4-Dimethyl-phenol	$-\Delta H_T^0$		7.82	7.75	6.94	5.84	5.50	5.24
	$-\Delta S_T^0$		14.30	13.29	13.17	11.19	11.13	11.01
Eugenol	$-\Delta H_T^0$	7.37	5.97	5.38	5.00	4.78	4.59	4.10
	$-\Delta S_T^0$	9.80	8.38	8.46	8.77	9.23	9.50	9.80
Pyridine	$-\Delta H_T^0$		7.41	6.37	6.30	6.17	6.12	6.28
	$-\Delta S_T^0$		11.37	9.46	9.60	9.94	10.16	11.04
Vanillin	$-\Delta H_T^0$		7.61	6.96	6.04	5.66	5.73	5.57
	$-\Delta S_T^0$		11.80	11.54	10.40	10.42	11.60	11.98

[a] See Table 3.

after heating silica gel over 600°C, only isolated OH groups still exist on the silica gel surface and that these isolated (free) OH groups are, nevertheless, very active [24]. Mauss and Engelhardt [16] pointed out that the reaction of silica with chlorosilanes takes place mainly at these isolated silanols, which may explain the significant differences in capacity factor for columns C and E for these two column packings having similar amounts of silanols on the silica gel surface. Other possible causes are impurities on the surface of the silica gel [31] and rehydration of the packing material [32].

Concerning the problem of rehydration of thermally treated silica gel, according to the competition model, the solutes must be able to displace these eluent molecules from the surface in order to be adsorbed. The selective adsorption of solutes on silica gel has been attributed exclusively to the surface silanols [20]. In this case, chromatographic retention and selectivity should be correlated with the surface silanol concentration. Therefore, rehydration of thermally treated silica gel would alter the retention time of a polar probe solute after a certain period of time under the chromatographic conditions. In fact, one of the thermally treated columns, column B, was in use for 3 months during one experimental run to elute 2,4-dimethylphenol without appreciable changes in the retention time, showing stable chromatographic characteristics. Rehydration of thermally treated silica gel can be preformed by boiling in water [16]. However, under pure CO_2 SFC conditions, the thermally treated packing would not be rapidly rehydrated.

It is *a priori* possible that a difference in k' might be caused by the differences in pressure drop due to the laboratory packing procedure. Although the outlet pressure of the columns at each mobile phase density was not measured, the retention factors of polycyclic aromatics on the three columns were carefully measured and found to be very similar under identical conditions, indicating that the pressure drop of the three columns does not affect the retention time of 2,4-dimethylphenol. In addition, the reproducibility of the packing procedure has been

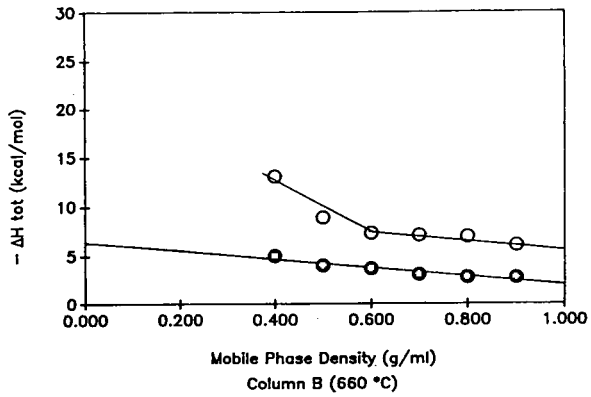

Fig. 5. Total enthalpies of transfer as a function of CO_2 density of the mobile phase. Stationary phase, thermally treated Partisil-10. Solute: ○ = 2,4-dimethylphenol; ● = naphthalene.

examined with unmodified Partisil-10 silica gel and polycyclic aromatics and found to be very good [15].

For both thermally treated and octadecylsilane (ODS)-treated silica gel, the study of ΔS_T^0 at constant density as a function of temperature provides another means of elucidating the retention mechanism of SFC. Figs. 5 and 6 give ΔH_T^0 and ΔS_T^0, respectively, *versus* CO_2 density for column B. The ΔH_T^0 values of naphthalene in column B at different CO_2 densities lie on a straight line from 0.4 to 0.9 g ml^{-1}, as do the ΔS_T^0 values, indicating a simple adsorption-like retention mechanism. However, the ΔH_T^0 values

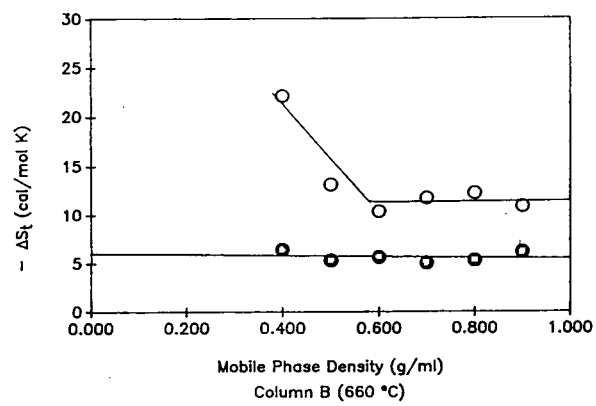

Fig. 6. Total entropies of transfer as a function of CO_2 density of the mobile phase. Stationary phase and solutes as in Fig. 5.

of 2,4-dimethylphenol follow a trend similar to that of naphthalene from 0.9 to 0.6 g ml^{-1}, then diverge from 0.6 to 0.4 g ml^{-1}, showing increasing interactions between surface silanol groups and hydroxyl groups of the solute. As shown in Fig. 6, the entropy values of 2,4-dimethylphenol change more dramatically than the enthalpy values, giving a clear indication of the silanophilic effects at low density. Similarly to the entropy study for thermally treated samples, ΔS_T^0 provides a useful tool in studying the nature of the packings.

4.2. Octadecylsilane-bonded packings

ODS-1 and ODS-2 are octadecyl-bonded columns prepared without end-capping, and thus still have accessible hydroxyl groups on their surface (see Table 2). Employing pure CO_2 as the mobile phase, the ODS columns permitted phenols such as 2,4-dimethylphenol and eugenol to elute. However, the chromatographic peak shapes suggest in all instances strong interactions between the analyte and the stationary phase, as the phenols eluted with strong tailing. It was originally believed that the ODS-2 would exhibit little affinity for the phenols and fewer silanol groups on its surface, as the material had been extensively treated with silane as shown by its high hydrocarbon content (17.3% carbon). However, silanol group concentration measurement, poor chromatographic peak shape and failure to elute pyridine all indicate that maximum coverage of surface hydroxyl groups is not reached for the ODS-2 packing. For silica-based supports, Berendsen and De Galan [33] employed a geometrical model to demonstrate that unreacted hydroxyl groups still exist at the surface of silica gel even at maximum coverage of silane owing to steric constraints. Many workers have shown that conventional end-capping is not totally effective in that all silanol sites are not reacted [33,34]. However, our test results show that the ODS-3 column eluted pyridine with relative ease, indicating that end-capping is very effective in masking unreacted silanols. As the exact commercial silylation treatment process is not known, it would be pure speculation to state that

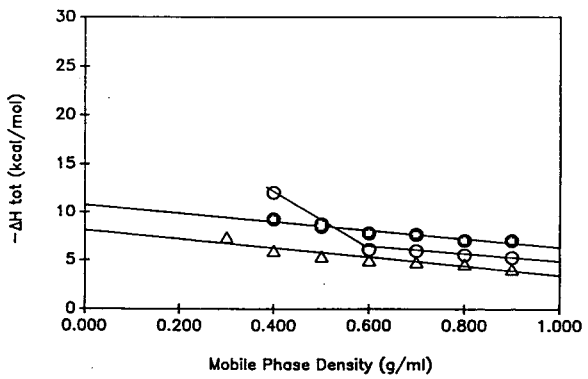

Fig. 7. Total enthalpies of transfer as a function of CO_2 density of the mobile phase. Stationary phase: ○ = Partisil ODS-1; ● = ODS-2; △ = ODS-3. Solute: eugenol.

the end-capping of ODS-3 is more successful in masking silanols than other similar packings used by other workers [20], as different ways exist to perform end-capping [35].

Using eugenol as a probe, characteristic plots of enthalpy and entropy as functions of density for low- and high-polarity packings can be established, as shown in Figs. 7 and 8. The well coated ODS-3 produces a linear plot and has the smallest enthalpy values, whereas ODS-1 shows a sudden increase in enthalpy and entropy values at low density. For the ODS-3 packing, this characteristic plot shows a typical adsorption and desorption process in a chromatographic column over a wide density region. For example, Fig. 9 shows the enthalpy of interaction between

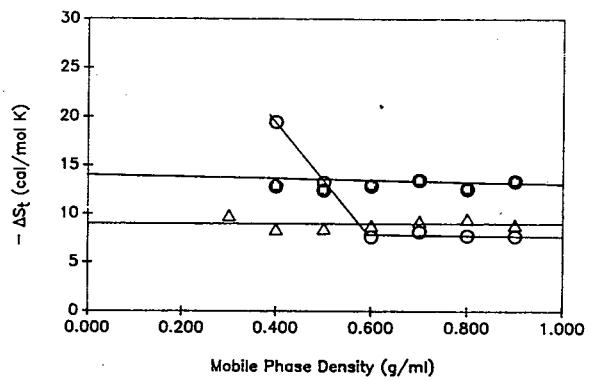

Fig. 8. Total enthalpies of transfer as a function of CO_2 density of the mobile phase. Stationary phases and solute as in Fig. 7.

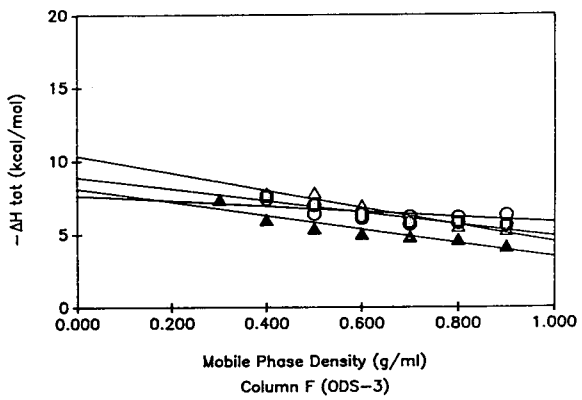

Fig. 9. Total enthalpies of transfer as a function of CO_2 density of the mobile phase. Stationary phase: Partisil-10 ODS-3. Solute: ▲ = eugenol; ● = vanillin; △ = 2,4-dimethylphenol; ○ = pyridine.

pyridine, carbon dioxide and the octadecylsilane-coated stationary phase ODS-3. Unlike phenols, pyridine interacts with the surface silanol groups mainly through dipole–dipole effects. Nevertheless, the pyridine enthalpy curve for ODS-3 demonstrates the same linear characteristic as for eugenol, which interacts with surface silanol groups mainly through hydrogen bonds. The linear characteristic of a well coated column is also supported by the vanillin enthalphy measurement results (see Table 8 and Fig. 9). As expected, changes in pressure drop or flow-rate have little impact on the linear characteristic of the ODS-3 packing [15]. Therefore, the retention behaviour in packed column SFC involves two different types of mechanisms. As shown in Figs. 7 and 8, with polar compounds low-polarity columns such as ODS-2 and ODS-3 show minor variations in ΔH_T^0 and no variation in ΔS_T^0 over the whole CO_2 density range. The same behaviour is observed for high-polarity columns such as ODS-1 at high CO_2 densities. Similar variations were also found for non-polar compounds such as naphthalene interacting with highly polar columns such as A and B (see Figs. 4, 5 and 6). As the CO_2 density decreases, silanophilic effects begin to play a more important role, as illustrated by the significant contribution of interactions of eugenol with the residual silanols of ODS-1 (Figs. 7 and 8).

The difference in ΔH_T^0 and ΔS_T^0 between ODS-2 and ODS-3, as shown by Figs. 7 and 8, is probably caused by long alkyl chains on the densely coated ODS-2 packing surface, which make the elution of solutes with large alkyl groups difficult and thus increase the energy required. Horváth [36] and Schoenmakers *et al.* [21] proposed a dual retention mechanism, in which the bonded silane groups and the silanol groups contribute independently. The contribution of the silanol groups to retention is assumed to follow a Langmuir isotherm, whereas the chemically bonded alkyl groups on the surface are assumed to give rise to a linear isotherm. Our experimental results seem to be in good agreement with the dual retention mechanism. In addition to the silanol contribution, the ODS-2 packing has more densely bonded groups on the surface and thus has more contributions of aliphatic groups to the retention of solute. In the high-density region, the linear isotherm of bonded groups is predominant. This may explain why when packings without a bonded phase such as column C are tested with 2,4-dimethylphenol, the enthalpy of transfer is smaller at high density when compared with that of column E (compare Tables 5 and 7), even if both have very similar surface silanol concentrations. The reason is that there is no solvophobic effect for column C owing to the lack of a bonded hydrocarbonaceous surface.

In the low-density region, the situation is different as other factors are playing more and more important roles. Although supercritical carbon dioxide is usually considered to be a non-polar solvent, it has been shown to possess hydrogen bonding capabilities and some dipole selectivity. In fact, Phillips and Robey [37] compared the solvent strength and selectivity of supercritical carbon dioxide with those of liquid hexane. They found that CO_2 is a Lewis base readily pairing with the Lewis acid phenol, making the solute, to a certain extent, unavailable for hydrogen bonding with the silanol groups. As the interaction of solute and solvent is closely related to the density of the mobile phase, a density decrease will lead to a decrease in solute–solvent interactions and a progressive

dominance of stationary phase–solute interactions in the retention process. However, for a well coated column packing material such as ODS-3, the stationary phase–solute interactions are limited even in the low-density region owing to the small concentration of reactive silanols left at the surface of silica gel prepared by reaction with organosilane. In addition, for packings such as ODS-1, increased stationary phase–solute interactions and easy access to active sites give the silanol groups at the surface of the silica gel more chances to absorb the solute and, thus, more energy is required to desorb the solute, which in turn is reflected in the absolute increase in enthalpy values. In other words, the lower the density, the greater is the role for silanol groups on the surface of the packing support.

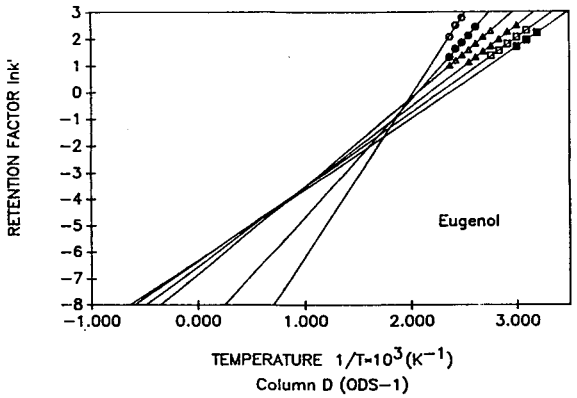

Fig. 11. Van 't Hoff plots (ln k' *vs.* $1/T$) for eugenol at different CO_2 densities of the mobile phase. The plots are extrapolated to show the intersection point. Stationary phase: Partisil-10 ODS-1. Symbols as in Fig. 1.

4.3. *Intersection points of Van 't Hoff plots*

The calculation of enthalpy of solute transfer from the slope of ln k' *vs.* T^{-1} at constant density is well known. However, the data in Fig. 10 for eugenol eluted from a silane-modified silica gel (ODS-3) system demonstrate another interesting point, that may not have been previously studied. It is noted that when the linear relationships between ln k' and T^{-1} are extrapolated, these lines seem to intersect at a common point around $(-0.30 \pm 0.2, -7.50 \pm 0.5)$. In fact, similar intersection points were observed for all other solute–stationary combinations investigated in this work, as exemplified by eugenol eluted from ODS-1 (high-density region in Fig. 11) and naphthalene eluted from the unmodified silica gel Partisil-10 (Fig. 12). Capillary column SFC also exhibits similar phenomena. For example, the plots of ln k' *vs.* $1/T$ for octadecane in the density range 0.3–0.4 g ml^{-1} in the work of Yonker and Smith [9] show a perfect converging point. Similar cases can be found in many other works [3,4]. Nevertheless, each column system shows some specific characteristics. For example, for more polar columns such as ODS-1, only in the high-density region (0.6–0.9 g ml^{-1}) is this kind of intersection point observed, as shown in

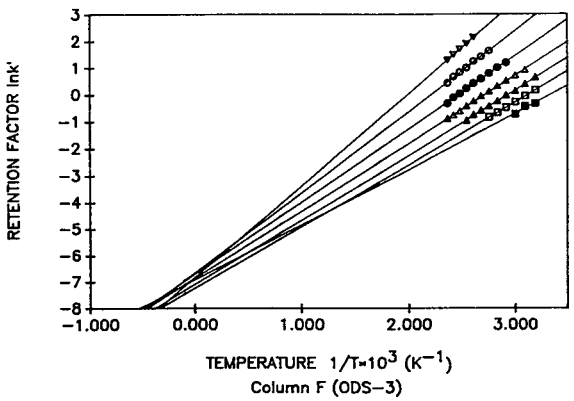

Fig. 10. Van 't Hoff plots as in Fig. 3, except the plots are extrapolated to show the intersection point.

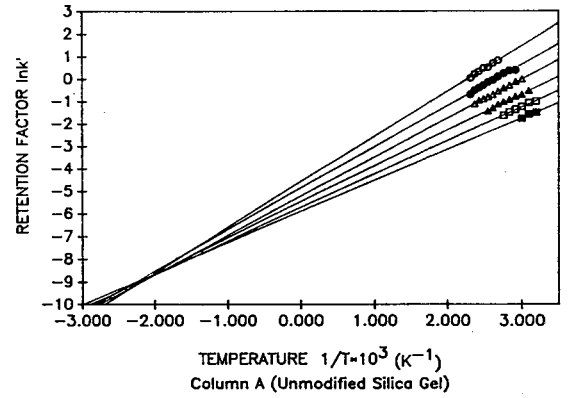

Fig. 12. Van 't Hoff plots as in Fig. 1, except the plots are extrapolated to show the intersection point.

Fig. 11. In the low-density region, the slope of ln k' *vs.* $1/T$ becomes very steep and the lines would not converge as they do when non-polar solutes elute from unmodified silica gel as shown in Fig. 12.

Table 9 lists our estimates of the values of ln k'_{LP} and $1/T_{LP}$ obtained at this intersection point for various solutes eluting from the six columns tested in this work. Note that as the values are extrapolated in the ln k' *vs.* $1/T$ diagram, negative values of $1/T_{LP}$ are possible. These estimated values are plotted in Fig. 13, which shows some correlation between ln k'_{LP} and $1/T_{LP}$. One line is obtained for 2,4-dimethylphenol eluting from the six columns and when two columns have similar OH concentrations their points are close to each other on this line (compare columns B and D or columns C and E). Large differences in intersection point positions are observed when different solutes are eluting from the same column. Note, for example, the points pertaining to naphthalene and 2,4-dimethylphenol in column A. This difference seems to be larger for more polar columns (compare naphthalene and 2,4-dimethylphenol for columns A, B and C).

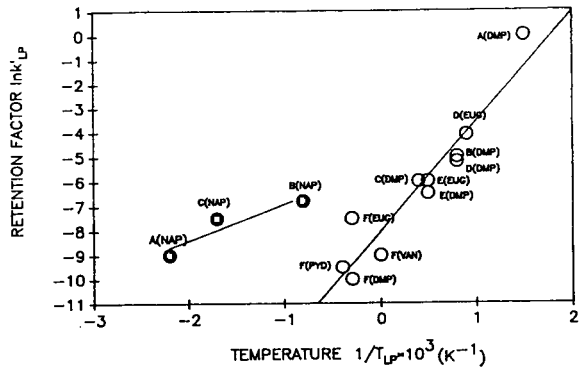

Fig. 13. Variation of the intersection points from extrapolated Van 't Hoff plots. For abbreviations, see Table 9.

The values of ln k'_{LP} obtained with 2,4-dimethylphenol and the six columns under study are plotted against OH surface concentration in Fig. 14. A linear correlation is observed, indicating that for one polar solute the coordinates of this intersection point on Van 't Hoff plot are strongly depending on OH concentration.

From Eq. 1, these coordinates must satisfy

$$\ln k'_{LP} = -\frac{\Delta H^0_T}{RT_{LP}} + \frac{\Delta S^0_T}{R} - \ln \beta \qquad (5)$$

Table 9
Converging points from Van 't Hoff plot for treated and untreated packing materials

Column	Stationary phase	Solute	Retention factor, ln k'_{LP}	Temperature $1/T_{LP} \cdot 10^3$, (K^{-1})	Code
A	Partisil-10	2,4-Dimethylphenol	0.0	1.5	A(DMP)
		Naphthalene	−9.0	−2.2	A(NAP)
B	T-660	2,4-Dimethylphenol	−5.0	0.8	B(DMP)
		Naphthalene	−6.8	−0.8	B(NAP)
C	T-900	2,4-Dimethylphenol	−6.0	0.4	C(DMP)
		Naphthalene	−7.5	−1.7	C(NAP)
D	ODS-1	Eugenol	−4.1	0.9	D(EUG)
		2,4-Dimethylphenol	−5.2	0.8	D(DMP)
E	ODS-2	Eugenol	−6.0	0.5	E(EUG)
		2,4-Dimethylphenol	−6.5	0.5	E(DMP)
F	ODS-3	Eugenol	−7.5	−0.3	F(EUG)
		2,4-Dimethylphenol	−10.0	−0.3	F(DMP)
		Vanillin	−9.0	0.0	F(VAN)
		Pyridine	−9.5	−0.4	F(PYD)

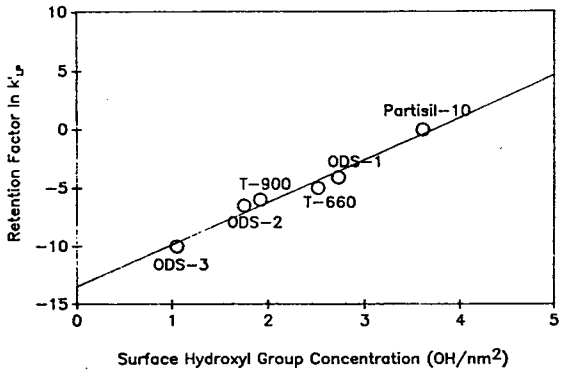

Fig. 14. Values of ln k'_{LP} of the six columns for 2,4-dimethylphenol *versus* stationary phase surface OH concentration.

Because, as shown in Figs. 6 and 8, the $\Delta S^0_T/R$ values are almost independent of CO_2 density in instances where intersection points are found, Eq. 5 indicates that an intersection point of Van 't Hoff plots is obtained whenever the variations of $\Delta H^0_T/RT_{LP}$ in the density range of interest are negligible compared with $\Delta S^0_T/R - \ln \beta$. Fig. 15, in which the data points correspond to ΔH^0_T and ΔS^0_T of the various solutes used in this investigation eluting through the six columns under study at high CO_2 density, shows that this is indeed the case and that Eq. 5 is roughly satisfied in this instance.

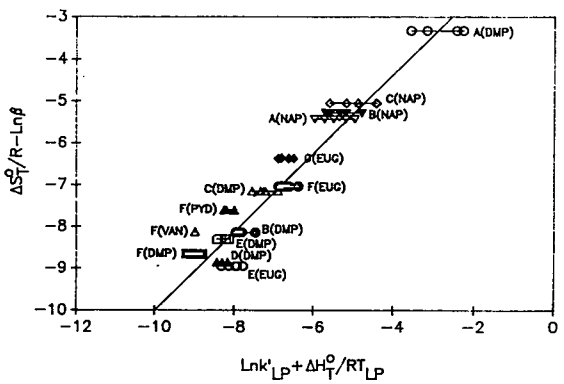

Fig. 15. $(\Delta S^0_T/R) - \ln \beta$ *versus* $\ln k'_{LP} + \Delta H^0_T/RT_{LP}$. For abbreviations, see Table 9.

5. Conclusions

Retention in SFC is a complex function of temperature, pressure, density and surface chemical characteristics of the stationary phase. Therefore, a multi-dimensional approach was adopted, including thermodynamic parameters, BET and surface silanol OH group concentration measurements in the study of silica gel packing materials used in packed column SFC. This allowed us to establish certain relationships between the thermodynamic values and the number of silanol groups on the silica gel surface. The results can be summarized as follows:

(1) Enthalpy and entropy values obtained from Van 't Hoff plots can be utilized as thermodynamic criteria to determine the polarity and to extract other information on stationary phases in packed column SFC.

(2) A characteristic slope of enthalpy *vs.* density for each category of packing may be obtained with certain low-polarity phenols such as eugenol and 2,4-dimethylphenol.

(3) The characteristic slope depends mainly on the nature of the packing. For a well coated packing such as ODS-3, moderate pressure drops and solutes of different polarity have little impact on the slope.

(4) At low CO_2 density, interactions with silanol groups on the stationary phase surface become more significant as a result of the decrease in solute–solvent interactions.

(5) Extrapolated Van 't Hoff plots have common intersection points. When plotted, these points produce a straight line. The coordinates of these points are correlated with the OH surface concentration and also with the ΔH^0_T and ΔS^0_T values.

6. Acknowledgements

The authors thank the Natural Science and Engineering Research Council (NSERC) of Canada for a strategic grant and Whatman (Clifton, NJ, USA) for kindly providing some of the packing materials used in this work.

7. References

[1] V. Lopez-Avila, J. Benedicto, N.S. Dodhiwala, R. Young and F.W. Becket, *J. Chromatogr. Sci.*, 30 (1992) 335–345.

[2] C.R. Yonker and R.D. Smith, *J. Phys. Chem.*, 92 (1988) 1664–1667.

[3] T.A. Berger, *J. Chromatogr.*, 478 (1989) 311–324.

[4] J.L. Grandmaison and S. Kaliaguine, *J. Chromatogr.*, 540 (1991) 225–238.

[5] H. Purnell, *Gas Chromatography*, Wiley, New York, 1962.

[6] E. Meyer, *J. Chem. Educ.*, 57 (1973) 120–124.

[7] C.R. Yonker, R.W. Gale and R.D. Smith, *J. Phys. Chem.*, 91 (1987) 3 336–3341.

[8] C.R. Yonker, B.W. Wright, R.C. Petersen and R.D. Smith, *J. Phys. Chem.*, 89 (1985) 5526–5530.

[9] C.R. Yonker and R.D. Smith, *J. Chromatogr.*, 351 (1986) 211–216.

[10] T.L. Chester and D.P. Innis, *J. High Resolut. Chromatogr. Chromatogr. Commun.*, 8 (1985) 561–566.

[11] M. Ashraf-Khorassani, L.Y. Taylor and R.A. Henry, *Anal. Chem.*, 60 (1988) 1529–1533.

[12] T.A. Dean and C.F. Poole, *J. Chromatogr.*, 468 (1989) 127–144.

[13] K.M. Payne, B.J. Tarbet, J.S. Bradshaw, K.E. Markides and M.L. Lee, *Anal. Chem.*, 62 (1990) 1379–1384.

[14] K.D. Bartle, A.A. Clifford, J.P. Kithinji and G.F. Shilstone, *J. Chem. Soc., Faraday Trans.* 1, 84 (1988) 4487–4493.

[15] D.Y. Shang and S. Kaliaguine, to be published.

[16] M. Mauss and H. Engelhardt, *J. Chromatogr.*, 351 (1986) 393–401.

[17] R.P.W. Scott and P. Kucera, *J. Chromatogr. Sci.*, 13 (1975) 337–346.

[18] H. Figge, A. Deege, J. Köhler and G. Schomburg, *J. Chromatogr.*, 351 (1986) 393–401.

[19] D.R. Luffer, W. Ecknig and M. Novotny, *J. Chromatogr.*, 505 (1990) 79–97.

[20] M. De Weerdt, C. Dewaele, M. Verzele and P. Sandra, *J. High Resolut. Chromatogr.*, 13 (1990) 40–46.

[21] P.J. Schoenmakers, L.G.M. Uunk and P.K. Bokx, *J. Chromatogr.*, 459 (1988) 201–213.

[22] H. Rotzsche, *Stationary Phases in Gas Chromatography* (*Journal of Chromatography Library*, Vol. 48), Elsevier, Amsterdam, 1991.

[23] C.G. Armistead, A.J. Tyler, F.H. Hambleton, S.A. Mitchell and J.A. Hockey, *J. Phys. Chem.*, 73 (1969) 3974–3980.

[24] K. Marcinkowska, *Ph.D. Thesis*, Laval University Sainte-Foy, Québec, 1990.

[25] M. Sato, T. Kanbayashi, N. Kobayashi and Y. Shima, *J. Catal.*, 7 (1967) 342–351.

[26] S. Brunauer, P.H. Emmett and E. Teller, *J. Am. Chem. Soc.*, 60 (1938) 309–319.

[27] H.H. Lauer, D. McManigill and R.D. Board, *Anal. Chem.*, 55 (1983) 1370–1375.

[28] D. Leyendecker, D. Leyendecker, B. Lorenschat, F.P. Schmitz and E. Klesper, *J. Chromatogr.*, 398 (1987) 89–103.

[29] B.P. Semonian and L.B. Rogers, *J. Chromatogr. Sci.*, 16 (1978) 49–60.

[30] H. Colin and G. Guiochon, *J. Chromatogr.*, 289 (1977) 289–312.

[31] K. Kimata, N. Tanaka and M. Araki, *J. Chromatogr.*, 594 (1992) 87–96.

[32] A.J. Roosmalen and J.C. Mol, *J. Phys. Chem*, 83 (1979) 2485–2488.

[33] G.E. Berendsen and L. de Galan, *J. Liq. Chromatogr.*, 1 (1978) 403–426.

[34] T.A. Berger and J.F. Deye, *J. Chromatogr. Sci.*, 29 (1991) 54–56.

[35] B.D. Marshall and K.A. Stutier, *J. Chromatogr. Sci.*, 22 (1984) 217–220.

[36] C. Horváth, in C.F. Simpson (Editor), *Techniques in Liquid Chromatography*, Wiley, New York, 1982, pp. 229–301.

[37] J.H. Phillips and R.J. Robey, *J. Chromatogr.*, 465 (1989) 177–188.

ELSEVIER

Journal of Chromatography A, 672 (1994) 203–211

JOURNAL OF CHROMATOGRAPHY A

Calculation of chromatographic parameters by molecular topology: sulphamides

G.M. Antón-Fos*, F.J. García-March, F. Pérez-Giménez, M.T. Salabert-Salvador, R.A. Cercós-del-Pozo

Unit of Drug Design and Molecular Connectivity Investigation, Department of Physical Chemistry, Faculty of Pharmacy, University of Valencia, 46100 Valencia, Spain

(First received May 14th, 1993; revised manuscript received February 16th, 1994)

Abstract

This investigation was undertaken to test the ability of the molecular connectivity model to predict R_F values in thin-layer chromatography (TLC) for a group of sulphamides using multi-variable regression equations with multiple correlation coefficients, standard error of estimate, *F*-Snedecor function values and Student's *t*-test as criteria of fit. Regression analyses showed that the molecular connectivity model predicts the values for this property in different silica gel stationary phases and different polar mobile phases. Corresponding stability and random studies were made on the selected prediction models which confirmed their goodness of fit. The results also demonstrated that different structural features determine the R_F values in TLC of sulphamides.

1. Introduction

Molecular topology has been shown to be a very important structural model for describing the chromatographic [1–4] and environmental [5,6] behaviour of chemicals. This method transcribes molecular structure into a topological graph from which a number is derived, the topological index. Topological parameters, such as molecular connectivity indices [7], can be used to quantify these properties.

In quantitative structure–activity relationship (QSAR) studies, the kind of descriptor parameters mentioned above are used to explain or predict the pharmacological behaviour of drug molecules. During the last 5 years, molecular connectivity indices have been used to predict several parameters related to the biological activities of drugs [8]. It was concluded that the direct correlation of molecular topology with biological activity is possible [9]. Therefore, it might be possible that the chromatographic behaviour of drugs in phases of different polarity contains information that is useful in describing their pharmacological behaviour, *e.g.*, for barbiturates [10] and neuroleptics [11].

In a previous paper [12] it was demonstrated that the molecular connectivity model [13,14] successfully predicts retention parameters of benzodiazepines in gas–liquid chromatography (GLC) and thin-layer chromatography (TLC) on polar and low-polarity eluents. In this study, we examined the relationship between R_F values in

* Corresponding author.

0021-9673/94/$07.00
SSDI 0021-9673(94)00165-6

TLC and the connectivity indices of a group of sulphamides.

2. Method of calculation

Several extensive reviews have been published [8,15–18] which give detailed descriptions of the theory and method of calculation of all-valence and non-valence molecular connectivity indices used in this investigation.

Connectivity indices are calculated from a hydrogen-supressed formula or graph of the molecule, following the method of Kier and Hall [7]. Thus, for a graph of m edges and s subgraphs (binding between $m+1$ atoms), the general form of the indices, ${}^{m}\chi_t$, is calculated according to the equation

$$ {}^{m}\chi_t = \sum_{s=1}^{n_m} \prod_{i=1}^{m+1} (\delta_i)_s^{-1/2} \qquad (1) $$

where n_m is the number of paths. Connectivity indices describing non-linear arrangements of bonds, such as clusters of three bonds, ${}^{3}\chi_c$, and path-clusters of four bonds, ${}^{4}\chi_{pc}$, are calculated in the same way.

Each non-hydrogen atom is described by its valence delta value, δ^v, which is calculated by the expression $\delta^v = Z^v - N_H$, where Z^v is the number of valence electrons in the atom and N_H is the number of hydrogen atoms attached to it [8].

Single and multiple regression analyses were used to find the relationship between the TLC properties and the connectivity indices, and were calculated from the equation

$$ P = A_0 + \sum_{m,t} A_{m,t}\, {}^{m}\chi_t \qquad (2) $$

where P is a property, and A_0 and $A_{m,t}$ represent the regression coefficients of the equation obtained.

Eq. 2 was obtained by multilinear regression with program 9R of the biostatistic package BMD (Biomedical Computer Programs) [19]. To test the quality of the regression equations, the following statistical parameters were used: multiple correlation coefficient (r), standard error of estimate (s), F-Snedecor function values (F) and Student's t-test (statistical significance).

Random and stability studies were performed on the selected equations as follows. (a) Randomness was achieved by randomly modifying the value of the independent variables which intervene in the equation, subsequently modifying the value of the dependent (property), also done randomly; after each modification the BMDP 9R was executed, passing on to compare the calculated correlation coefficient with the one obtained for the selected equation [20]. (b) Stability: using the jack-knife method [21], the elimination of n observations was effected, by means of a random process, and a regression program was executed, repeating the process as many times as necessary until all the observations had been eliminated a minimum of once a maximum of 5 times. The correlation coefficients, standard deviations and the residuals with those obtained are subsequently compared with those of the selected equation.

The different experimental R_F values in TLC were obtained with precoated silica gel 60 F_{254} plates, 20 cm × 20 cm with a 0.25-mm layer thickness, activated for 1 h in a saturated chamber, as the ascending method with a length of run of 12 cm at 20°C with different stationary and mobile phases (Table 1). Development was achieved with a 0.1% solution of p-dimethylaminobenzaldehyde in 0.5% HCl. The sulphamide solutions were prepared at a 0.2% concentration in ethanol–water (70:30, v/v). Six chromatograms were obtained for each of the molecules studied in each of the systems employed, calculating the mean and error standard (see Table 2).

3. Results and discussion

The experimental R_F values and molecular connectivity indices of the eighteen sulphamides examined are given in Tables 2 and 3, respectively. Essentially, the R_F value represents the degree of affinity between the solute considered and the stationary and mobile phases. This

Table 1
Stationary and mobile phases used in the study of experimental R_F values

TLC	Stationary phase	Mobile phase
A	Toluene–castor oil (92:8, v/v)	Sörensen solution (pH 6.2)
B	Toluene–castor oil (92:8, v/v)	Sörensen solution–acetone (80:20, v/v) (pH 6.2)
C	Toluene–silicone DC-200 (95:5, v/v)	Sörensen solution (pH 6.2)
D	Toluene–silicone DC-200 (95:5, v/v)	1% sodium chloride Sörensen solution (pH 6.2)

affinity is quantified by the distribution coefficient for the solute in the two phases.

Multi-variable regression equations were screened to find the simplest equation that generated the experimental elution sequence. Both the order and number of connectivity indices were varied.

The selected equations for R_{F_A}, R_{F_B}, R_{F_C} and R_{F_D} of the compounds studied were as follows:

$$R_{F_A} = 0.299\ {}^1\chi^v - 1.110\ {}^3\chi_p - 1.647\ {}^3\chi_c^v + 1.698\ {}^4\chi_{pc} + 0.380 \quad (3)$$
$$n = 18;\quad r = 0.939;\quad s = 0.046;\quad F = 24.16$$

$$R_{F_B} = 0.303\ {}^0\chi^v - 1.380\ {}^3\chi_p - 1.275\ {}^3\chi_c + 1.331\ {}^4\chi_{pc} + 1.841 \quad (4)$$
$$n = 18;\quad r = 0.924;\quad s = 0.074;\quad F = 18.96$$

Table 2
Experimental R_F values (mean ± standard error) of sulphamides

Compound	R_{F_A}	R_{F_B}	R_{F_C}	R_{F_D}
Sulphasomidine	0.391 ± 0.003	0.699 ± 0.003	0.408 ± 0.010	0.522 ± 0.013
Sulphafurazole	0.503 ± 0.014	0.396 ± 0.013	0.316 ± 0.016	0.535 ± 0.018
Sulphadiazine	0.465 ± 0.011	0.612 ± 0.001	0.486 ± 0.017	0.497 ± 0.030
Sulphasimazine	0.323 ± 0.017	0.326 ± 0.012	0.169 ± 0.012	0.342 ± 0.013
Sulphamerazine	0.320 ± 0.014	0.552 ± 0.005	0.334 ± 0.013	0.402 ± 0.013
Sulphamethazine	0.241 ± 0.008	0.514 ± 0.005	0.239 ± 0.007	0.327 ± 0.008
Sulphadoxine	0.298 ± 0.016	0.398 ± 0.007	0.201 ± 0.009	0.362 ± 0.010
Sulphamethoxypyridazine	0.240 ± 0.006	0.499 ± 0.010	0.219 ± 0.005	0.331 ± 0.008
Sulphamethoxazole	0.308 ± 0.013	0.337 ± 0.008	0.307 ± 0.023	0.433 ± 0.012
Sulphalene	0.278 ± 0.016	0.410 ± 0.017	0.278 ± 0.014	0.416 ± 0.013
Sulphametomidina	0.232 ± 0.008	0.438 ± 0.008	0.203 ± 0.008	0.343 ± 0.011
Sulphamonomethoxine	0.260 ± 0.014	0.340 ± 0.007	0.231 ± 0.009	0.386 ± 0.014
Sulphaethoxypyridazine	0.160 ± 0.011	0.363 ± 0.010	0.111 ± 0.006	0.203 ± 0.007
Sulphenazole	0.158 ± 0.012	0.164 ± 0.006	0.086 ± 0.005	0.209 ± 0.017
Sulphadimethoxine	0.129 ± 0.006	0.178 ± 0.006	0.078 ± 0.005	0.185 ± 0.017
Sulphazamet	0.124 ± 0.005	0.137 ± 0.004	0.056 ± 0.004	0.153 ± 0.017
Sulphaquinoxaline	0.121 ± 0.005	0.118 ± 0.006	0.072 ± 0.006	0.172 ± 0.017
Sulphamoprine	0.087 ± 0.004	0.158 ± 0.008	0.076 ± 0.004	0.149 ± 0.017

Table 3
Connectivity indices used in the correlations of a group of sulphamides

Compound	$^{0}\chi^{v}$	$^{1}\chi^{v}$	$^{2}\chi$	$^{3}\chi_{p}$	$^{3}\chi_{c}$	$^{3}\chi_{c}^{v}$	$^{4}\chi_{p}$	$^{4}\chi_{p}^{v}$	$^{4}\chi_{pc}$
Sulphasomidine	10.787	5.943	6.423	3.761	1.658	0.719	2.788	1.860	2.075
Sulphafurazole	10.171	5.582	6.247	4.265	1.601	0.713	2.451	1.486	2.579
Sulphadiazine	8.942	2.102	5.412	3.322	1.325	0.475	2.213	1.417	1.760
Sulphasimazine	12.071	6.934	6.792	4.408	1.561	0.617	2.967	1.892	2.213
Sulphamerazine	9.864	5.523	5.916	3.562	1.492	0.604	2.439	1.561	1.930
Sulphamethazine	10.787	5.943	6.423	3.761	1.658	0.733	2.788	1.833	2.075
Sulphadoxine	11.734	6.300	6.689	4.570	1.500	0.591	3.222	1.947	2.398
Sulphamethoxypyridazine	10.273	5.642	6.097	3.910	1.443	0.542	2.510	1.576	2.014
Sulphamethoxazole	9.248	5.159	5.901	3.597	1.529	0.608	2.172	1.372	1.986
Sulphalene	10.273	5.631	6.216	4.072	1.437	0.527	2.735	1.629	2.128
Sulphametomidine	11.195	6.056	6.607	4.084	1.609	0.642	2.871	1.788	2.144
Sulphamonomethoxine	10.325	5.682	6.264	4.012	1.469	0.550	2.748	1.643	2.037
Sulphaethoxypyridazine	10.980	6.230	6.493	4.041	1.443	0.542	2.730	1.692	1.979
Sulphenazole	11.751	6.910	6.942	4.651	1.505	0.614	3.011	2.093	2.285
Sulphadimethoxine	11.604	6.168	6.792	4.408	1.561	0.583	2.967	1.743	2.213
Sulphazamet	12.674	7.331	7.445	4.880	1.671	0.743	3.308	2.295	2.449
Sulphaquinoxaline	11.096	6.517	6.608	4.293	1.492	0.619	2.966	2.096	2.129
Sulphamoprine	11.604	3.168	6.792	4.408	1.561	0.581	2.967	1.720	2.213

$$R_{F_C} = -0.482\ ^{2}\chi + 0.838\ ^{3}\chi_{c} + 0.254\ ^{4}\chi_{p} + 1.347 \quad (5)$$

$$n = 18; \quad r = 0.927; \quad s = 0.053; \quad F = 28.52$$

and

$$R_{F_D} = -0.750\ ^{3}\chi_{p} - 0.884\ ^{3}\chi_{c}^{v} + 0.290\ ^{4}\chi_{p}^{v} + 1.168\ ^{4}\chi_{pc} + 0.943 \quad (6)$$

$$n = 18; \quad r = 0.915; \quad s = 0.059; \quad F = 16.79$$

Statistically, all the equations are significant above the 99.9% level. All the variables are statistically significant above the 99.9% level, except $^{1}\chi^{v}$ in Eq. 3 and $^{3}\chi_{c}$ in Eqs. 4 and 5, which are significant above the 99% level, $^{3}\chi_{c}^{v}$ in Eq. 6 above the 95% level and $^{4}\chi_{p}$ in Eq. 5 and $^{4}\chi_{p}^{v}$ in Eq. 6 above the 90% level.

The study of randomness of these equations (Table 4) demonstrates their non-randomness.

For R_{F_A}, four correlation coefficients >0.7 are obtained when the independent variable is studied and three correlation coefficients >0.7 when the dependent variable is studied; therefore, the probability (p) that a correlation coefficient >0.9 can be obtained is considerably less than 0.04 and 0.03, respectively. For R_{F_B}, two correlation coefficients >0.8 are obtained when the independent variable is studied and one correlation coefficient >0.8 when the dependent variable is studied; therefore, the probability that a correlation coefficient >0.9 can be obtained is less than 0.02 and 0.01, respectively. For R_{F_C}, two correlation coefficients >0.7 are obtained when the independent variable is studied and one correlation coefficient >0.7 when the dependent variable is studied; therefore, the probability that a correlation coefficient >0.9 can be obtained is considerably less than 0.02 and 0.01, respectively. For R_{F_D}, one correlation coefficient >0.8 is obtained when the independent variable is studied and eight correlation coefficients >0.7 when the dependent variable is studied; therefore, the probability that a correlation coefficient >0.9 can be obtained is less than 0.01 and 0.08, respectively.

The stability study of the equations was carried out by varying the number of eliminations done (between one and five) and the number of runs (eighteen runs in the case of one elimination or twenty runs with the rest), observing that by raising the number of eliminations the model was made more unstable, which was expected because the degrees of freedom were consider-

Table 4
Correlation coefficients computed from random number variables for a four-variable model of R_{F_A}, R_{F_B}, R_{F_C} and R_{F_D} value data for sulphamides

Modification variable								
Range of r	Independent (100 runs)				Dependent (100 runs)			
	Number of values				Number of values			
	R_{F_A}	R_{F_B}	R_{F_C}	R_{F_D}	R_{F_A}	R_{F_B}	R_{F_C}	R_{F_D}
<0.1	0	0	0	0	1	0	2	1
0.1–0.2	1	6	6	2	1	3	10	4
0.2–0.3	9	8	24	10	8	10	14	16
0.3–0.4	27	21	25	14	23	26	30	13
0.4–0.5	26	20	21	19	26	18	22	26
0.5–0.6	21	22	18	29	25	28	13	21
0.6–0.7	11	19	4	12	14	13	8	11
0.7–0.8	4	2	2	13	3	1	1	8
0.8–0.9	0	2	0	1	0	1	0	0
>0.9	0	0	0	0	0	0	0	0

ably diminished. In all instances the corresponding stability was chosen at two eliminations (twenty runs), which corresponds approximately to 10% of eliminated observations, the value recommended by some workers [8] (Tables 5–8). Comparison of the results between the obtained values for the selected model and the model of two eliminations shows that the selected equations are more stable, as is clear from the equality of the terms obtained and from the low standard deviations of each of these terms. The analysis of the residuals obtained for the selected model and for the model of two eliminations shows minimum discrepancies for the means and

Table 5
Statistical stability test information for the regression model of R_{F_A} values for sulphamides

Parameter	Original model (no deletions)		Two deletions per run (20 runs)	
	Regression value	Standard deviation	Regression value	Standard deviation
Correlation coefficient	0.939		0.939	0.009
Standard deviation	0.046		0.047	0.003
Coefficient of $^1\chi^v$	0.299	0.069	0.298	0.014
Coefficient of $^3\chi_p$	−1.110	0.161	−1.110	0.036
Coefficient of $^3\chi_c^v$	−1.647	0.339	−1.642	0.115
Coefficient of $^4\chi_{pc}$	1.698	0.239	1.693	0.062
Constant	0.380	0.144	0.392	0.038
Average residual	0.031		0.037	0.003
Residuals less than one standard deviation	77.8%		76.3%	
Residuals between one and two standard deviations	22.2%		23.7%	
Residuals greater than two standard deviations	0%		0%	

Table 6
Statistical stability test information for the regression model of R_{F_B} values for sulphamides

Parameter	Original model (no deletions)		Two deletions per run (20 runs)	
	Regression value	Standard deviation	Regression value	Standard deviation
Correlation coefficient	0.924		0.925	0.008
Standard deviation	0.074		0.075	0.005
Coefficient of $^0\chi^v$	0.303	0.073	0.297	0.033
Coefficient of $^3\chi_p$	−1.380	0.234	−1.364	0.110
Coefficient of $^3\chi_c$	−1.275	0.413	−1.244	0.205
Coefficient of $^4\chi_{pc}$	1.331	0.300	1.312	0.156
Constant	1.841	0.336	1.866	0.147
Average residual	0.057		0.058	0.005
Residuals less than one standard deviation	77.8%		77.5%	
Residuals between one and two standard deviations	22.2%		22.5%	
Residuals greater than two standard deviations	0%		0%	

for their standard deviations, an aspect of the study which strengthens the predictive quality of the model.

The regression analyses show that the most significant structural factor influencing the R_F values is the substitution pattern and typically the branching parameter, given by the $^4\chi_{pc}$ index (Eqs. 3, 4 and 6). In a previous paper [12] we suggested that this index is a measure of the eluent's polar character: more polar eluents (*e.g.*, Sörensen solution, pH 6.2) will make a higher contribution (higher regression coefficient for the $^4\chi_{pc}$ index) to the property studied than other less polar eluents [Sörensen solution–ace-

Table 7
Statistical stability test information for the regression model of R_{F_C} values for sulphamides

Parameter	Original model (no deletions)		Two deletions per run (20 runs)	
	Regression value	Standard deviation	Regression value	Standard deviation
Correlation coefficient	0.927		0.929	0.007
Standard deviation	0.053		0.052	0.004
Coefficient of $^2\chi$	−0.482	0.056	−0.485	0.045
Coefficient of $^3\chi_c$	0.838	0.188	0.849	0.091
Coefficient of $^4\chi_p$	0.254	0.339	0.252	0.047
Constant	1.347	0.241	1.349	0.136
Average residual	0.040		0.042	0.003
Residuals less than one standard deviation	61.1%		69.4%	
Residuals between one and two standard deviations	38.9%		30.6%	
Residuals greater than two standard deviations	0%		0%	

Table 8
Statistical stability test information for the regression model of R_{F_D} values for sulphamides

Parameter	Original model (no deletions)		Two deletions per run (20 runs)	
	Regression value	Standard deviation	Regression value	Standard deviation
Correlation coefficient	0.915		0.914	0.012
Standard deviation	0.059		0.061	0.004
Coefficient of $^3\chi_p$	−0.750	0.148	−0.750	0.050
Coefficient of $^3\chi_c^v$	−0.884	0.415	−0.894	0.119
Coefficient of $^4\chi_p^v$	0.290	0.155	0.289	0.064
Coefficient of $^4\chi_{pc}$	1.168	0.261	1.169	0.085
Constant	0.943	0.169	0.952	0.034
Average residual	0.037		0.048	0.004
Residuals less than one standard deviation	72.2%		76.3%	
Residuals between one and two standard deviations	27.8%		23.7%	
Residuals greater than two standard deviations	0%		0%	

tone (80:20, v/v), pH 6.2]. The size of the sulphamides, described and quantified by the $^1\chi^v$ and $^0\chi$ indices, whose numerical value is directly proportional to the number of ties, also contributes to the increase in the value of the property. The other factors that control the magnitude of the R_F values are $^3\chi_p$ (Eqs. 3, 4 and 6), $^3\chi_c$ (Eqs. 4 and 5) and $^3\chi_c^v$ (Eqs. 3 and 6). A measure of the molecular symmetry is given by the index $^3\chi_p$ [8]: sulphamides are non-symmetrical molecules, which explains why this index has a negative influence on the R_F values for this group of molecules. The indices $^3\chi_c$ and $^3\chi_c^v$ take into account the solvation effects, closely related to steric aspects. In Eqs. 5 and 6 other indices such as $^4\chi_p$, $^4\chi_p^v$ and $^4\chi_{pc}$ appear, characteristic of the presence of branchings. These results suggest that these indices, particularly $^4\chi_{pc}$, appear with more polar eluents [12].

Comparisons between experimental and theoretical R_F values following Eqs. 3, 4, 5 and 6 are given in Figs. 1, 2, 3 and 4, respectively.

This investigation has demonstrated that a relationship exists between molecular connectivity and R_F values for a group of sulphamides; with a three- or four-variable model a good degree of correlation can be obtained.

4. Conclusions

The molecular connectivity method has been used for the prediction of different R_F values in TLC using mobile phases of different polarity. The statistical studies of randomness show that the predictive models selected are not random, and the stability studies suggest that they are good statistical models because of their stability and predictive capacity. It is necessary to highlight the presence of the $^3\chi_p$ index, which in a

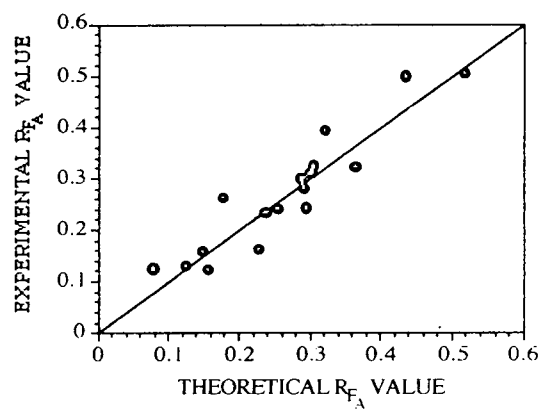

Fig. 1. Correlation between experimental and calculated (Eq. 3) R_{F_A} values of eighteen sulfamides.

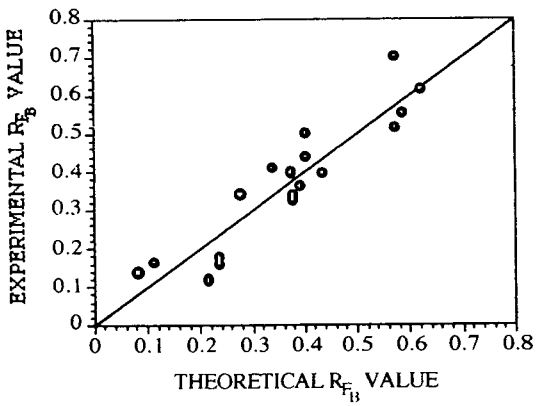

Fig. 2. Correlation between experimental and calculated (Eq. 4) R_{F_B} values of eighteen sulphamides.

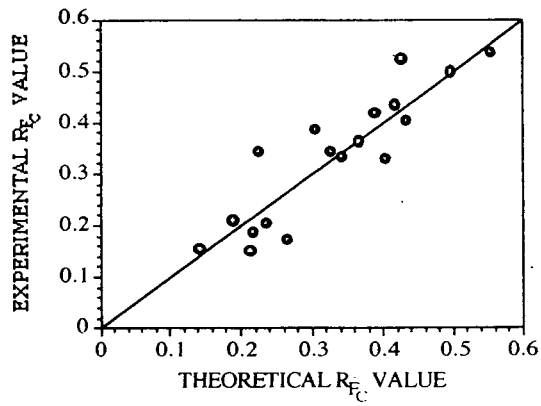

Fig. 3. Correlation between experimental and calculated (Eq. 5) R_{F_C} values of eighteen sulphamides.

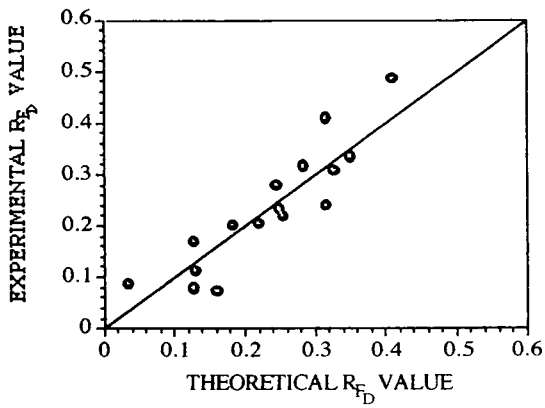

Fig. 4. Correlation between experimental and calculated (Eq. 6) R_{F_D} values of eighteen sulphamides.

certain way evaluates the molecular symmetry [12], because of which non-symmetrical molecules such as sulphamides will have a negative influence on this index. In all the equations the indices $^3\chi_c$ and $^3\chi_c^v$ are indicative of the solvent's solvation effects on the molecules and are also accompanied by $^4\chi_{pc}$, a parameter that gives information about the polar character of the eluents [12] and for $^2\chi$ index. All of this leads us to conclude that the selected equations predict the R_F values correctly, as was expected by the presence in the connectivity indices of information on factors that directly influence the studied property.

5. Acknowledgement

The authors thank CICYT, SAF92-0684 (Spanish Ministry of Science and Education), for financial support of this work.

6. References

[1] A. Sabljic, *J. Chromatogr.*, 314 (1984) 1.
[2] M. Gassiot-Matas and G. Firpo-Panies, *J. Chromatogr.*, 187 (1980) 1.
[3] Gy. Szász, O. Papp, J. Vámos, K. Hanko-Novák and L.B. Kier, *J. Chromatogr.*, 269 (1983) 91.
[4] J.K. Haken and I.O.O. Korhonen, *J. Chromatogr.*, 265 (1983) 323.
[5] A. Sabljic and M. Protic, *Bull. Environ. Contam. Toxicol.*, 28 (1982) 162.
[6] R. Koch, *Toxicol. Environ. Chem.*, 6 (1983) 87.
[7] L.B. Kier and L.H. Hall, *Molecular Connectivity in Chemistry and Drug Research*, Academic Press, New York, 1976.
[8] L.B. Kier and L.H. Hall, *Molecular Connectivity in Structure–Activity Analysis*, Research Studies Press, Letchworth, 1986.
[9] B.W. Blake, K. Enslein, V.K. Gombar and H.H. Borgstedt, *Mutat. Res.*, 241 (1990) 261.
[10] R. Kaliszan, *J. Chromatogr.*, 220 (1981) 71.
[11] L. Buydens, D.L. Massart and P. Geerlings, *J. Chromatogr. Sci.*, 23 (1985) 304.
[12] R.M. Soler, F.J. García, G.M. Antón, R. García, F. Pérez and J. Gálvez, *J. Chromatogr.*, 607 (1992) 91.
[13] L.B. Kier and L.H. Hall, *J. Pharm. Sci.*, 68 (1979) 120.
[14] D. Hadzi and B. Jerman-Blazic, *Q.S.A.R. in Drug Design and Toxicology*, Elsevier, Amsterdam, 1987.

[15] R. García, J. Gálvez, R. Moliner and F.J. García, *Drug. Invest.*, 3 (1991) 344.
[16] N. Trinasjstic, *Chemical Graph Theory*, CRC Press, Boca Raton, FL, 1983.
[17] R. Wilson, *Introduction to Graph Theory*, Academic Press, New York, 1972.
[18] J. Ciudad, R. García and J. Gálvez, *An. Quim.*, 83 (1987) 385.
[19] W.J. Dixon, *BMD Manual: Biomedical Computer Programs*, University of California Press, Los Angeles, 1982.
[20] J. Topliss and R. Costello, *J. Med. Chem.*, 15 (1972) 1066.
[21] H.L. Gray and W.R. Shucany, *The Generalized Jackknife Statistic*, Marcel Dekker, New York, 1972.

ELSEVIER

Journal of Chromatography A, 672 (1994) 213–218

JOURNAL OF CHROMATOGRAPHY A

High-performance capillary electrophoresis of SDS-proteins using pullulan solution as separation matrix

Manabu Nakatani*,[a], Akimasa Shibukawa[b], Terumichi Nakagawa[b]

[a]*Pharmaceutical Research Department, Nippon Boehringer Ingelheim Co. Ltd., 3-10-1, Yato Kawanishi, Hyogo 666-01, Japan*
[b]*Faculty of Pharmaceutical Sciences, Kyoto University, Sakyo-ku, Kyoto 606, Japan*

(First received November 11th, 1993; revised manuscript received March 9th, 1994)

Abstract

Sodium dodecyl sulphate (SDS) capillary electrophoresis using pullulan solution as a separation matrix was developed for the separation and molecular mass determination of proteins. The silanol functions on the inner surface of a fused-silica capillary were deactivated by coating with linear polyacrylamide through Si–C linkages, into which the pullulan solution was filled. The stability of the coating was examined by exposure to an alkaline buffer solution (pH 9.2) for up to 30 days. Compared with conventional coatings with linear polyacrylamide through siloxane linkages, the present capillary was more stable even under alkaline conditions and markedly reduced electroosmotic flow. Thus, polymer solutions of low viscosity such as pullulan solution could be stabilized in the capillary, resulting in a prolonged life-span of the capillary and improved reproducibility of separations. An excellent linear relationship was obtained between the mobility and the logarithm of the molecular mass of SDS-proteins. The relative standard deviation of migration times was below 0.5% when the pullulan solution was refilled in each analysis ($n = 10$). The calibration plots of the integrated peak areas at 214 nm *vs.* concentration of standard proteins were linear in the range 5 μg/ml–0.1 mg/ml.

1. Introduction

Sodium dodecyl sulphate–polyacrylamide gel electrophoresis (SDS-PAGE) has been used for the separation and molecular mass determination of polypeptides and proteins [1]. However, it is time consuming, detection is tedious and there are difficulties in quantification. SDS capillary gel electrophoresis (SDS-CGE) has several advantages over slab gel electrophoresis in that a high-intensity electric field can be applied, resulting in high resolution, and on-column detection can be employed, thus permitting high-speed separations and real-time detection.

SDS-CGE has been achieved using cross-linked polyacrylamide [2,3], linear polyacrylamide [4–7] and other polymers [8–10]. Although proteins can be detected at a wavelength of 200 nm where they have strong UV absorption, cross-linked and/or linear polyacrylamide also has strong UV absorption below 230 nm. Therefore, UV-transparent polymer matrices such as dextran and poly(ethylene glycol) have been used [9]. In addition, these water-soluble polymer solutions can be easily refilled into the capillary because of the low viscosity. However, the low viscosity causes gradual extrusion of the matrices out of the capillary by the electroosmotic pressure generated on the untreated capillary surface. To overcome these difficulties, efforts

* Corresponding author.

0021-9673/94/$07.00
SSDI 0021-9673(94)00244-4

have been made to inactivate silanol functions by coating the capillary with hydrophilic polymers, which were covalently bonded to silanol groups through siloxane linkages (Si–O–Si–C) [11–17]. This treatment was effective in reducing the zeta potential and in preventing the adsorption of proteins. However, the siloxane linkages are prone to hydrolysis under alkaline conditions [19]. This paper describes the durability of coatings under alkaline conditions, and demonstrates the separation of SDS-proteins in a hydrolytically stable capillary using pullulan solution as a sieving matrix.

2. Experimental

2.1. Materials

Acrylamide, N,N,N′,N′-tetramethylethylenediamine (TEMED), ammonium peroxodisulphate (APS), tris(hydroxymethyl)aminomethane (Tris) of electrophoretic grade, thionyl chloride, tetrahydrofuran (THF), pullulan (claimed molecular mass $M_r = 50\,000$–$100\,000$), which is a branched polysaccharide composed of α-(1–6)-linked maltotriose (Fig. 1), 2-(cyclohexylamino)ethanesulphonic acid (CHES), 2-(N-morpholino)ethanesulphonic acid (MES), sodium dodecyl sulphate (SDS) and 2-mercaptoethanol of analytical-reagent grade were obtained from Wako (Osaka, Japan). Mesityl chloride and vinylmagnesium bromide (1 *M* solution in THF) were obtained from Tokyo Kasei (Tokyo, Japan). 3-Methacryloxypropyltrimethoxysilane (MAPS) was purchased from Shin-etsu Chemicals (Tokyo, Japan). The buffer solution for SDS-CGE consisted of 0.1 *M* Tris–CHES and 0.1% (w/v) SDS (pH 8.7). Standard proteins were obtained from Sigma (St. Louis, MO, USA).

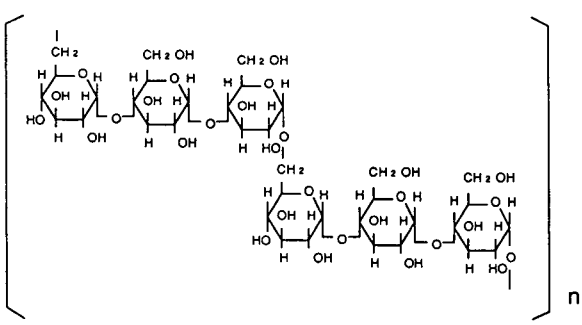

Fig. 1. Structure of pullulan.

2.2. Apparatus

A CE-800 capillary electrophoresis instrument (Jasco, Tokyo, Japan) was used with a fused-silica capillary of 50 μm I.D. for assessment of the durability of coatings and a fused-silica capillary of 75 μm I.D. for SDS-CGE (GL Sciences, Tokyo, Japan). Capillary electrophoresis was performed at room temperature without temperature control. The UV absorbance of polymer solutions was measured on a Shimadzu (Kyoto, Japan) UV-160A spectrophotometer.

2.3. Procedures

Preparation of linear polyacrylamide-coated capillary through siloxane linkage

A detection window was first opened by burning off about a 2 mm length of polyimide coating on a fused-silica capillary at an appropriate position, and the window was protected by covering it with a small plastic tube.

The inner surface of the capillary was treated with 1 *M* NaOH for 1 h at room temperature followed by washing with distilled water for 1 h, then reacted with MAPS as described by Hjertén [15]. After reaction, the capillary was washed with distilled water, filled with an aqueous solution containing 3% acrylamide, 0.1% (w/v) APS and 0.1% (v/v) TEMED, and kept at 28 ± 2°C for 1 h for polymerization. Water was then passed through the capillary by suction until only water came out.

Preparation of linear polyacrylamide-coated capillary through Si–C linkage

The capillary with the detection window was coated with linear polyacrylamide through Si–C linkages by four-step reactions according to the following procedure, which was a simplified version of that employed by Cobb *et al.* [18].

The capillary was first treated with 1 *M* NaOH at room temperature for 1 h, rinsed with distilled water and dried at 110°C by flushing with nitrogen for 6 h. Thionyl chloride was passed through the dried capillary for several minutes using a suction pump. The capillary was sealed at both ends using a small propane torch and kept at 70°C for 6 h. After reaction, the seal was opened, and nitrogen was passed through the capillary for 5 min to remove excess thionyl chloride.

A 0.25 *M* vinylmagnesium bromide solution in THF was introduced into the capillary by suction, and the capillary was sealed again to complete the Grignard reaction. After the reaction at 70°C for 6 h, the seal was opened and the capillary was rinsed with THF for several minutes, then with distilled water. An aqueous solution containing 3% (w/v) acrylamide, 0.1% (w/v) APS and 0.1% (v/v) TEMED was filled into the capillary by suction and kept at 28 ± 2°C for polymerization. After 1 h, distilled water was passed through the capillary in the manner described above.

Preparation of pullulan matrix-filled capillary

A stock standard solution of pullulan was prepared by dissolving a weighed amount of pullulan in the running buffer containing 0.1 *M* Tris–CHES and 0.1% (w/v) SDS (pH 8.7). The solution was degassed by aspiration for 5 min and then filled into the capillary coated with linear polyacrylamide through Si–C linkages by means of suction or with a micro-syringe.

Assessment of durability of coated capillaries under alkaline conditions

The capillaries (50 μm I.D. × 50 cm, effective length to the detector 30 cm) coated with linear polyacrylamide through Si–O–Si–C linkages or Si–C linkages were filled with 50 m*M* sodium tetraborate buffer (pH 9.2) and kept at room temperature for up to 30 days. After exposure to alkaline conditions for a given number of days, the electroosmotic flow-rates were measured in a running buffer of 20 m*M* sodium tetraborate (pH 9.2) using mesityl oxide as a neutral marker with an applied potential of 400 V/cm.

Protein samples for SDS electrophoresis

A mixture of standard proteins, containing *ca.* 0.1 mg/ml of the individual proteins, was dissolved in an aqueous solution containing 1% (w/v) SDS and 1% (v/v) 2-mercaptoethanol. The sample solution was incubated at 80°C for 15 min in a water-bath and submitted to analysis.

3. Results and discussion

3.1. Durability of coating under alkaline conditions

Fig. 2 illustrates the time courses of electroosmotic mobilities measured in the uncoated capillary and in the capillaries bonded with linear polyacrylamide through Si–O–Si–C linkages and through Si–C linkages, all of which had been kept under alkaline conditions (50 m*M* sodium tetraborate, pH 9.2). The coated capillary involving Si–C linkages showed a very low electroosmotic mobility even after exposure to alkaline conditions for 30 days, indicating high stability against hydrolysis. In contrast, the capillary

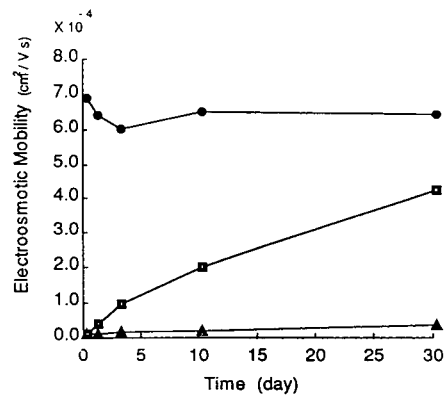

Fig. 2. Time course of electroosmotic mobility as a function of number of days of exposure under alkaline conditions [50 m*M* sodium tetraborate (pH 9.2)]. ○ = Uncoated capillary; □ = capillary coated with linear polyacrylamide through Si–O–Si–C linkages; ▲ = capillary coated with linear polyacrylamide through Si–C linkages. Capillary, 50 μm I.D. × 50 cm (30 cm to the detector); running buffer, 20 m*M* sodium tetraborate (pH 9.2); electric field, 20 kV 25 μA; injection, syphonic, 5 cm, 15 s; detection, UV at 250 nm; neutral marker, mesityl oxide (0.1%, v/v).

involving Si–O–Si–C linkages resulted in an increased electroosmotic mobility, although the initial value of the mobility was as low as that observed with the capillary involving Si–C linkages. After alkaline treatment for 30 days, the electroosmotic mobilities became $0.25 \cdot 10^{-4}$ $cm^2/V \cdot s$ (Si–C) and $4.13 \cdot 10^{-4}$ $cm^2/V \cdot s$ (Si–O–Si–C), while the mobility in the uncoated capillary remained as high as $6 \cdot 10^{-4}$–$7 \cdot 10^{-4}$ $cm^2/V \cdot s$ for 30 days. These results indicate that polyacrylamide coatings markedly decreased the zeta potential on the inner surface of the fused-silica capillary and that Si–C linkages are more stable than Si–O–Si–C linkages against hydrolysis. It is also suggested that the polyacrylamide network bonded through Si–C linkages can protect the siloxane bondings of the capillary wall itself from attack by hydroxyl anions. It is important in capillary gel electrophoresis to reduce the electroosmotic flow in order to stabilize the gel. Therefore, the use of a coated capillary involving Si–C linkages is advantageous in optimizing separation conditions, because it widens the selection of separation media to soft gel or polymer solutions of low viscosity, and allows the use of running buffer solutions with a wide range pH.

3.2. UV absorbance of pullulan matrix

The UV absorbances of pullulan solution and linear polyacrylamide solution were measured using a spectrophotometer with a 1-cm light path length. The absorbance for 7% (w/v) pullulan in water was 0.399 at 214 nm and 0.136 at 280 nm, whereas the absorbance for the 3% (w/v) linear polyacrylamide in water was over 2.5 at 214 nm and 0.509 at 280 nm. These results indicate that pullulan is advantageous over linear polyacrylamide with detection in the lower wavelength region (below 230 nm), which gives a 20–50 times higher sensitivity for proteins than that at 280 nm [20]. Therefore, the use of a low wavelength is advantageous for the detection of low-concentration proteins, especially for the detection of small peptides lacking tyrosine and tryptophan residues.

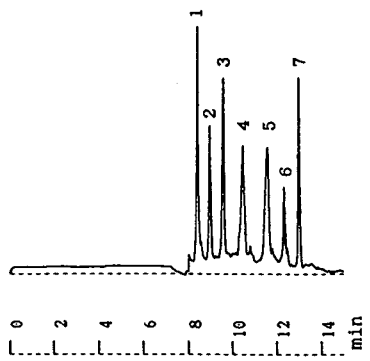

Fig. 3. Electropherograms of SDS-proteins on a 7% (w/v) pullulan solution-filled capillary. The inner wall of the capillary was coated with linear polyacrylamide through Si–C linkages. Capillary, 75 μm I.D. × 50 cm (30 cm to the detector); running buffer, 0.1 *M* Tris–CHES–0.1% (w/v) SDS (pH 8.7); electric field, −15 kV, 15 μA; injection, −5 kV, 5 μA, 5 s; detection, UV at 214 nm. Peaks: 1 = α-lactalbumin; 2 = trypsin inhibitor; 3 = carbonic anhydrase; 4 = ovalbumin; 5 = bovine serum albumin; 6 = phosphorylase b; 7 = β-galactosidase.

3.3. Separation of SDS-proteins

Fig. 3 shows the electropherogram of standard proteins separated in the 7% (w/v) pullulan solution-filled capillary which was coated with linear polyacrylamide through Si–C linkages, where the applied intensity of the electric field was −300 V/cm and UV detection at 214 nm was used. The proteins with molecular masses ranging from 14 400 to 116 000 were completely separated within 13 min with high efficiency; the theoretical plate number for peak 7 in Fig. 3, for example, was *ca.* 150 000. In contrast, no proteins were detected at the anodic end of the uncoated capillary filled with pullulan solution of the same concentration. This means that the electroosmotic flow overwhelmed the electrophoretic movement of SDS-proteins, which should be directed towards the anodic (detection) end. In fact, the peaks of proteins were observed when the polarity of the power supply was reversed, while the pullulan solution was gradually extruded because of electroosmotic flow.

Table 1 gives the statistical data for the run-to-run reproducibility of migration times deter-

Table 1
Reproducibility of migration times using 7% (w/v) pullulan

Peak No.	Protein	Molecular mass	Migration time (min)[a] (mean ± S.D., $n = 10$)
1	α-Lactalbumin	14 400	8.54 ± 0.031
2	Trypsin inhibitor	20 100	9.16 ± 0.024
3	Carbonic anhydrase	30 000	9.83 ± 0.023
4	Ovalbumin	43 000	10.70 ± 0.024
5	Bovine serum albumin	67 000	11.88 ± 0.041
6	Phosphorylase b	94 000	12.63 ± 0.036
7	β-Galactosidase	116 000	13.31 ± 0.035

[a] Separation conditions: the inner wall of the capillary was coated with linear polyacrylamide through Si–C linkages; capillary, 75 μm I.D. × 50 cm (30 cm to the detector); running buffer, 0.1 *M* Tris–CHES–0.1% (w/v) SDS (pH 8.7); electric field, −15 kV, 15 μA; injection, −5 kV, 5 μA, 5 s; detection, UV at 214 nm.

mined by the repeated injection of an SDS-protein into a 7% (w/v) pullulan solution-filled capillary which we had coated with linear polyacrylamide through Si–C linkages.

Ten consecutive injections were performed by refilling the capillary with the matrix after every analysis. As a result, the relative standard deviations of the migration times averaged over seven proteins were less than 0.5%. This excellent reproducibility was obviously attributable to the suppression of electroosmotic flow and the stabilization of the separation matrix. Even after the coated capillary had been used for more than 100 injections during 1 month (the pullulan solution was replaced with water overnight), the electroosmotic mobility measured using 50 m*M* Tris–MES buffer (pH 7.0) remained constant at $1.04 \cdot 10^{-5}$ cm^2/V·s. This value is considerably lower than that measured with the uncoated capillary ($3.13 \cdot 10^{-4}$ cm^2/V·s).

The column-to-column reproducibility of migration times of seven proteins ($n = 3$) was below 1.3% (R.S.D.).

Fig. 4 shows the relationship between the electrophoretic mobility and the logarithm of the molecular mass of standard proteins on the coated capillary involving Si–C linkages at five different concentrations (1, 3, 5, 7 and 10%, w/v) of pullulan solutions. Excellent linearity (correlation coefficient $r^2 > 0.995$) was obtained in each relationship and the lines were almost parallel to each other in the range of pullulan concentrations examined. Ferguson plots [21] exhibited linear relationships ($r^2 > 0.993$) for each of seven proteins between log (mobility) and pullulan concentration. The slopes of the plots were found to be proportional to the molecular mass of the proteins ($r^2 = 0.960$). These results indicated that the separation was achieved by the difference in size or molecular mass of the proteins based on the sieving effect.

The linear range of the calibration lines for α-lactalbumin and carbonic anhydrase was examined using a 5% (w/v) pullulan solution-filled capillary which was coated with linear poly-

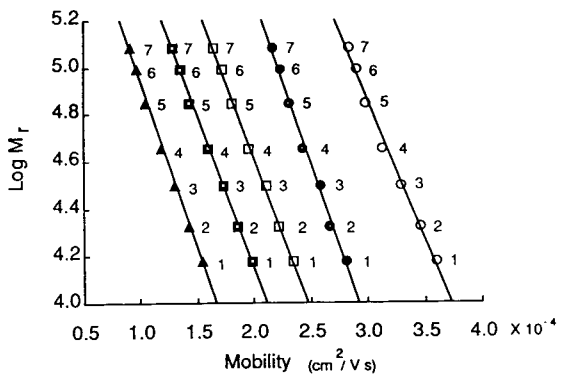

Fig. 4. Plots of log (molecular mass) *vs.* mobility of proteins measured in the capillary containing (○) 1, (●) 3, (□) 5, (■) 7 and (▲) 10% (w/v) pullulan solution. The capillary was coated with linear polyacrylamide through Si–C linkages. 1 = α-Lactalbumin; 2 = trypsin inhibitor; 3 = carbonic anhydrase; 4 = ovalbumin; 5 = bovine serum albumin; 6 = phosphorylase b; 7 = β-galactosidase.

acrylamide through Si–C linkages, the applied intensity of the electric field being −300 V/cm, the length of capillary 50 cm (30 cm to the detector) and UV detection at 214 nm was used. The concentration of the proteins in the buffer solution was varied, while electrokinetic injection was achieved at a constant electric field of −100 V/cm for 15 s. The plot of peak area *vs.* sample concentration was linear ($r > 0.999$) up to at least 5 μg/ml and passed through the origin. The precision for the integrated peak area was examined by repeated injection ($n = 3$). The R.S.D. of the peak area was less than 2.5% for α-lactalbumin ranging over 25 μg/ml and less than 5% for carbonic anhydrase ranging over 5 μg/ml. The minimum detectable concentration (signal-to-noise ratio = 4) for both proteins was 1 μg/ml under the given injection conditions.

4. Conclusions

The Si–C bondings which link linear polyacrylamide to silanol groups on a fused-silica capillary are more effective than siloxane bondings in stabilizing the inner surface of a fused-silica capillary. The capillary generated essentially no electroosmotic flow even under alkaline conditions, and hence the soft gel or a solution of pullulan can be used as a separation medium for the capillary electrophoresis of SDS-proteins. This serves to extend the applicability to the separation of a wider range of macromolecules.

References

[1] K. Weber and M. Osborn, *J. Biol. Chem.*, 244 (1969) 4406.
[2] A.S. Cohen and B.L. Karger, *J. Chromatogr.*, 397 (1987) 409.
[3] K. Tsuji, *J. Chromatogr.*, 550 (1991) 823.
[4] A. Widhalm, C. Schwer, D. Blaas and E. Kenndler, *J. Chromatogr.*, 549 (1991) 446.
[5] D. Wu and F.E. Regnier, *J. Chromatogr.*, 608 (1992) 349.
[6] M. Nakatani, A. Shibukawa and T. Nakagawa, *Biol. Pharm. Bull.*, 16 (1993) 1185.
[7] W.E. Werner, D.M. Demorest, J. Stevens and J.E. Wiktorowicz, *Anal. Biochem.*, 212 (1993) 235.
[8] M. Zhu, D.L. Hansen, S. Burd and F. Gannon, *J. Chromatogr.*, 480 (1989) 311.
[9] K. Ganzler, K.S. Greve, A.S. Cohen, B.L. Karger, A. Guttman and N.C. Cooke, *Anal. Chem.*, 64 (1992) 2665.
[10] A. Guttman, J.A. Nolan and N. Cooke, *J. Chromatogr.*, 632 (1993) 171.
[11] A.S. Cohen, A. Paulus and B.L. Karger, *Chromatographia*, 24 (1987) 15.
[12] A. Guttman, A. Paulus, A.S. Cohen, N. Grinberg and B.L. Karger, *J. Chromatogr.*, 448 (1988) 41.
[13] A. Guttman, A.S. Cohen, D.N. Heiger and B.L. Karger, *Anal. Chem.*, 62 (1990) 137.
[14] J.W. Jorgenson and K.D. Lukacs, *Science*, 222 (1983) 266.
[15] S. Hjertén, *J. Chromatogr.*, 347 (1985) 191.
[16] R.M. McCormick, *Anal. Chem.*, 60 (1988) 2322.
[17] G.J.M. Bruin, J.P. Chang, R.H. Kuhlman, K. Zegers, K.J.C. Kraak and H. Poppe, *J. Chromatogr.*, 471 (1989) 429.
[18] K.A. Cobb, V. Dolnik and M. Novotny, *Anal. Chem.*, 62 (1990) 2478.
[19] K.K. Unger, *Porous Silica*, Elsevier, Amsterdam, 1979, Ch. 3.
[20] P.D. Grossman and J.C. Colburn, *Capillary Electrophoresis; Theory and Practice*, Academic Press, San Diego, CA, 1992, Ch. 5, p. 145.
[21] K.A. Ferguson, *Metabolism*, 13 (1964) 1985.

ELSEVIER

Journal of Chromatography A, 672 (1994) 219–229

JOURNAL OF CHROMATOGRAPHY A

Comparison of the utility of capillary zone electrophoresis and high-performance liquid chromatography in peptide mapping and separation

Suzanne E. Rudnick[a], Vincent J. Hilser, Jr.[b], Gregory D. Worosila*[,c]

[a]*Department of Chemistry, Manhattan College, Riverdale, NY, USA*

[b]*Graduate Program in Biology, Johns Hopkins University, Baltimore, MD, USA*

[c]*Analytical Development Department, Ciba Pharmaceuticals Division, Ciba-Geigy Corporation, Suffern, NY 10901, USA*

(First received October 18th, 1993; revised manuscript received March 2nd, 1994)

Abstract

Capillary zone electrophoresis (CZE) and high-performance liquid chromatography (HPLC) have been used in the analysis of the primary structure of recombinant human insulin-like growth factor I (rhIGF-I). CZE both complements and supplements HPLC separations. CZE has been used to resolve peaks which co-elute on HPLC, as well as to help establish the identity of tryptic fragments in peptide mapping experiments.

1. Introduction

Capillary zone electrophoresis (CZE) has become a major new analytical tool in chemistry and biochemistry laboratories. CZE separations are performed in free solution with no solid-phase matrix, facilitated by use of a capillary tube (100 cm × 100 μm) and conditions of high voltage (30 kV) and low current (50 μA). CZE has allowed separations previously unattainable and improved separations in already existing systems [1]. In addition, certain characteristics intrinsic only to CZE separations allow this technique to be used in situations where other separation techniques are not applicable [2].

We report here that CZE can both complement and supplement HPLC, particularly in peptide mapping experiments. Specifically, we have performed peptide mapping experiments on recombinant human insulin-like growth factor I (rhIGF-I), using both HPLC and CZE. Consequently, we have compared HPLC analysis of tryptic fragments of rhIGF-I with CZE analysis of the same peptides. This comparison has helped to elucidate the relative applicability of these two techniques.

As a complementary method, CZE is useful in ensuring the integrity of peptide fragments collected from HPLC analysis of enzymatic digests. Reversed-phase (RP) HPLC separation of proteins and peptides is generally achieved via interactions between specific non-polar amino acid residues and the column stationary phase, so that factors other than the side-chain residues may affect the separation [3]. CZE separations depend on peptide solvent interactions [4], where physical characteristics such as charge-to-

* Corresponding author.

0021-9673/94/$07.00
SSDI 0021-9673(94)00212-R

mass ratios are important [5]. CZE may thus separate closely related peptides which may coelute in the RP-HPLC mode. As a supplemental method, we demonstrate here the use of CZE for the positive identification of peptide peaks on an electropherogram.

2. Experimental

rhIGF-I was obtained from Ciba Pharmaceuticals. A single batch of rhIGF-I, which was >98% chromatographically pure by protein mass, was used to generate peptide fragments. HPLC-grade acetonitrile (Fisher, Pittsburgh, PA, USA) was used for HPLC analysis of tryptic fragments, optima-grade acetonitrile (Fisher) was utilized for all amino acid analysis experiments, and certified trifluoroacetic acid (TFA) (Fisher) was used for all HPLC analyses. In addition, reagent grade iodoacetamide (Sigma, St. Louis, MO, USA), gold-label triethylamine (Aldrich, Milwaukee, WI, USA), and sequanal-grade phenylisothiocyanate (PITC) and constant-boiling HCl (Pierce, Rockford, IL, USA) were used. All other chemicals were analytical grade and not further purified. Distilled, deionized Milli-Q water (Millipore, Bedford, MA, USA) was used for all experiments. Trypsin, in various treated forms, was purchased from three sources (Sigma, Pierce and ICN, Cleveland, OH, USA) and used without further purification.

2.1. Microdialysis

A Pierce Model 500 micro dialyzer with a molecular mass cutoff of 1000 was used.

2.2. RP-HPLC apparatus

Chromatographic separations were performed with a system composed of a Waters (Milford, MA, USA) Model 600E gradient pump and WISP Model 712 autosampler with temperature control, a Kratos (Foster City, CA, USA) Spectroflow 783 UV detector at 214 nm, and a Dionex (Sunnyvale, CA, USA) eluent degas module. Data collection and peak processing were performed with a Nelson 760 Series interface and a modified version of Nelson analytical software. A Gilson (Model 201) programmable fraction collector was used to isolate HPLC fractions. Well resolved peaks were collected by time programming, while closely eluting peaks were collected manually to avoid contamination due to small shifts in migration times.

2.3. Capillary electrophoresis apparatus

CZE was performed on an Applied Biosystems 270A capillary electrophoresis system with a fused-silica capillary (122 cm × 100 μm). Ultraviolet detection at 200 nm was used for peak analysis. Data collection and peak processing were performed as described for the HPLC analysis.

2.4. Amino acid analysis

Peptides were identified by amino acid analysis. The Waters Pico-Tag work station was utilized for the gas-phase hydrolysis of each peptide fragment and subsequent generation of PITC-derivatized amino acids [6]. Separation of derivatized amino acids, data collection and peak processing were performed by HPLC, as described below.

2.5. Carboxymethylation

Iodoacetamide was used for the carboxymethylation of rhIGF-I according to standard methods [7]. After derivatization, microdialysis was used for buffer exchange.

2.6. Trypsin digestion of rhIGF-I

The hydrolysis conditions utilized were a modification of those described by Worosila [8]. A 10-μl volume of trypsin solution (10 mg/ml in 0.1 m*M* HCl) was added to a solution of carboxymethylated rhIGF-I (250 μl of a 10 mg/ml solution in water) initially and, again, after 3 h (trypsin–rhIGF-I 1:25). After an 18-h incubation at 37°C, the reaction was quenched by the addition of 100 μl of 10% (v/v) TFA in water.

2.7. RP-HPLC method

Reversed-phase chromatographic analyses of rhIGF-I tryptic digests were performed on a Vydac Protein and Peptide C_{18} column (15.0 cm × 4.6 mm I.D.) (Vydac, Hesperia, CA, USA) at ambient temperature. The flow-rate was 0.8 ml/min. Mobile phases consisted of (A) 0.1% TFA in water and (B) 0.08% TFA in acetonitrile–water (80:20). A gradient was employed which ran according to the following program: 100% A at 3 min, 65% A at 38 min, 0% A at 55 min. Final gradient conditions were kept for 5 min before being returned to the initial conditions. A 15-min equilibration time was utilized between each run. The injection volume was 20 μl for optimum resolution and 30 μl for fraction collection.

2.8. Peak identification

Peptides were identified using amino acid analysis by comparison with a standard mixture. HPLC fractions were pooled from ten runs and lyophilized in acid-washed vials. Peak purity was determined by rechromatographing collected peaks using the gradient elution described above. The lyophilisate was then redissolved in 200 μl of distilled water and 30 μl used for amino acid analysis using a modification of the Waters Pico-Tag PITC method. Samples were dried under vacuum, subjected to gas-phase hydrolysis for 18 h at 105°C, and again dried under vacuum and made alkaline with a redrying solution [ethanol–triethylamine–water (40:20:40, v/v/v)]. Redrying was repeated and the samples were combined with 20 μl of derivatizing solution [ethanol–PITC–triethylamine–water (70:10:10:10, v/v)]. Solutions were allowed to react for 20 min at ambient temperature, again dried under vacuum, diluted in 200 μl of sample diluent [0.05 *M* disodium hydrogenphosphate, pH 7.4 in acetonitrile–water (5:95, v/v)] and analyzed chromatographically. RP-HPLC analyses of amino acid derivatives were performed using a Waters Pico-Tag amino acid analysis column maintained at 38°C. The flow-rate was kept at 1.0 ml/min for 12 min and changed linearly to 1.5 ml/min over a 30-s period. Mobile phases consisted of (A) 0.13 *M* sodium acetate trihydrate in triethylamine, pH 6.4–acetonitrile–water (0.05:6:93.95, v/v/v) and (B) acetonitrile–water (60:40, v/v). A concave gradient was employed which ran according to the following program: 100% A to 54% A at 10.0 min, 0% A at 10.5 min.. Final mobile phase conditions were kept for 1 min and the flow gradient listed above was overlaid on the mobile phase gradient. The column was equilibrated at a flow of 1.5 ml/min for 8 min between injections. The injection volume was varied to optimize peak response and the amino acid derivatives were detected at 254 nm.

2.9. CZE method

CZE was performed on all peptide peaks isolated from RP-HPLC. After lyophilization, the samples were dissolved in 10 m*M* sodium citrate, pH 2.5 at a concentration of approximately 0.5 mg/ml. The CZE mobile phase was 20 m*M* sodium citrate, pH 2.5. CZE was performed at 30°C with a constant voltage of 30 kV. Samples were introduced by a 1-s vacuum injection onto a 122-cm capillary (99.7 cm to the detector). A proprietary mobility standard was utilized to calculate peptide mobilities, thereby eliminating drift in the elution times. Electrophoretic mobilities (μ) of samples were calculated according to Eq. 1.

$$\mu = \frac{(L_d L_t)}{V} \cdot \left(\frac{1}{t} - \frac{1}{t_s}\right) + \mu_s \quad (1)$$

where L_d = length of capillary to detector (cm), L_t = total length of capillary (cm), V = system voltage (V), t = migration time of sample peak (s), t_s = migration time of standard peak (s) and μ_s = mobility value for standard peak.

2.10. Charge calculation

All peptide charges were calculated using the Henderson–Hasselbach equation using the pK_a values in ref. 9.

3. Results

3.1. Peptide fragment identification

The primary sequence of rhIGF-I is shown in Fig. 1 along with the nine theoretical tryptic cleavage sites. The ten resulting tryptic fragments are labelled T1–T10. Table 1 shows the amino acid molar ratios of all of the peptide fragments isolated by HPLC (see Fig. 3), which were used to identify the corresponding peptide stretches. Residual chymotryptic activity, which is often seen in tryptic digests, was evident by the appearance of some non-tryptic fragments. These fragments were used in the calculations described in this paper. Since the primary structure of the current batch of rhIGF-I had previously been determined by fast-atom bombardment mass spectrometry, the amino acid ratios were sufficient to identify the peaks [10].

In addition to amino acid analysis, aliquots of all fractions were analyzed by CZE. Comparison of the retention behavior in the two methods formed the basis for peak assignment in all comparative chromatograms. In all but one case, fractions which eluted as one peak on HPLC also proved to be homogenous by CZE analysis. In the case of coeluting peaks on RP-HPLC, positive identification was accomplished through the use of amino acid analysis and electrophoretic mobility on CZE.

3.2. Method development

Trypsin digestions are routinely performed in urea-containing solutions to minimize precipitation; however, the desire to analyze the resultant fragments by CZE limited the amount and type of buffer used. Although buffer com-

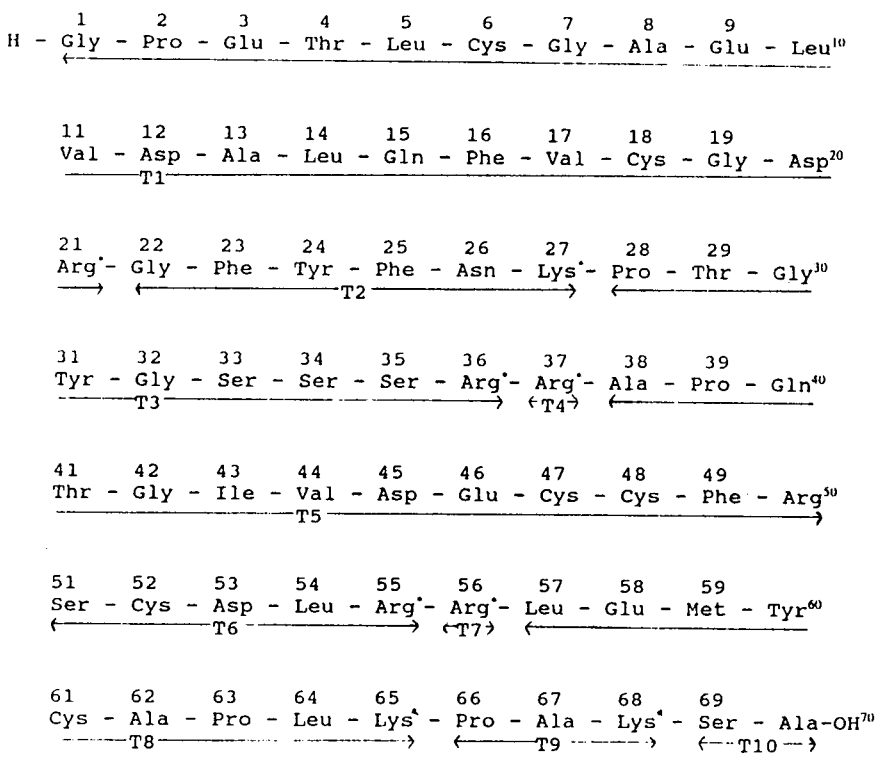

Fig. 1. The nine theoretical tryptic cleavage sites of rhIGF-I. Arrows in combination with an asterisk represent cleavage sites at the carboxyl terminal of Arg and Lys residues. Tryptic fragments are labeled T1 through T10.

Table 1
The amino acid analysis of rhIGF-I

Amino acid	Molar ratio														
	Gly1–Leu14	Gly1–Arg21	Gln15–Phe16	Val17–Arg21	Gly22–Tyr24	Gly22–Phe25	Phe25–Tyr31	Phe25–Arg36	Arg37–Arg50	Ser51–Arg55	Arg56–Tyr60	Arg56–Ala70	Leu57–Tyr60	Cys61–Lys65	Pro66–Lys68
Asx	1.0	1.8		1.0			0.8	1.2	1.0	1.1					
Glx	2.2	3.3	1.0						2.0		1.0	1.0	1.3		
CM-Cys	P[a]	P		P			P		P	P				P	
Ser								2.7		1.0		0.3			
Gly	2.3	3.2		0.9	1.1	1.3	1.2	1.9	1.2						
Arg		0.9		1.0			1.3	1.8	1.0	1.2	1.3				
Thr	1.0	1.0					1.1		1.0						
Ala	1.9	1.8						0.8	0.9			2.4		1.0	1.0
Pro	1.1	1.0					1.4	0.6	1.0			2.4		1.2	1.0
Tyr					0.7	1.0	0.9				0.9	0.6	0.9		
Val	1.0	2.5		0.8					0.6						
Met											0.8	0.5	0.9		
Ile									0.6						
Leu	2.8	3.4								0.9	0.9	1.9	1.0	0.5	
Phe		1.1	0.8		1.0	1.8	1.1	1.0	0.9						
Lys							1.4	0.8				2.3		1.2	1.2
Fragments		T1			T2A			T2BT3	T4T5	T6		T8			T9

The amino acid analysis was performed as described in ref. 5. PITC-labelled amino acids were quantified by comparison with a standard mixture of the 20 common amino acids, after separation by HPLC.
[a] P = peak present, but not quantified.

ponents elute early and consequently do not interfere with sample peaks in HPLC, many buffer ions exhibit mobilities similar to samples in CZE and must therefore be used in minimal quantities. In order to increase the solubility of intermediate-sized fragments, and at the same time eliminate buffer additives, the cysteine residues were carboxymethylated with iodoacetamide. The ability to irreversibly reduce disulfide bonds and dialyze reagents out of the sample buffer allows for minimal baseline noise in CZE.

A standard for the carboxymethylated cysteine was not prepared, and the location of the PITC carboxymethyl-cysteine was determined by comparison of the total amino acid hydrolysates for the reacted and unreacted protein (Fig. 2). The extent of the carboxymethylation reaction was determined by amino acid analysis through the concomitant appearance of a peak thought to be the carboxymethylated cysteine with the disappearance of peaks corresponding to unreacted cysteine and cystine residues (Fig. 2). The predicted trypsin cleavage sites within the amino acid sequence of rhIGF-I are indicated in Fig. 1. Of the nine potential cleavage sites, six are arginine and three are lysine residues. Analysis of the sequence reveals two points of arginine tandem repeats (Arg-36,37 and Arg-55,56). The poor exoproteolytic ability of trypsin results in a mix of peptide fragments in these regions.

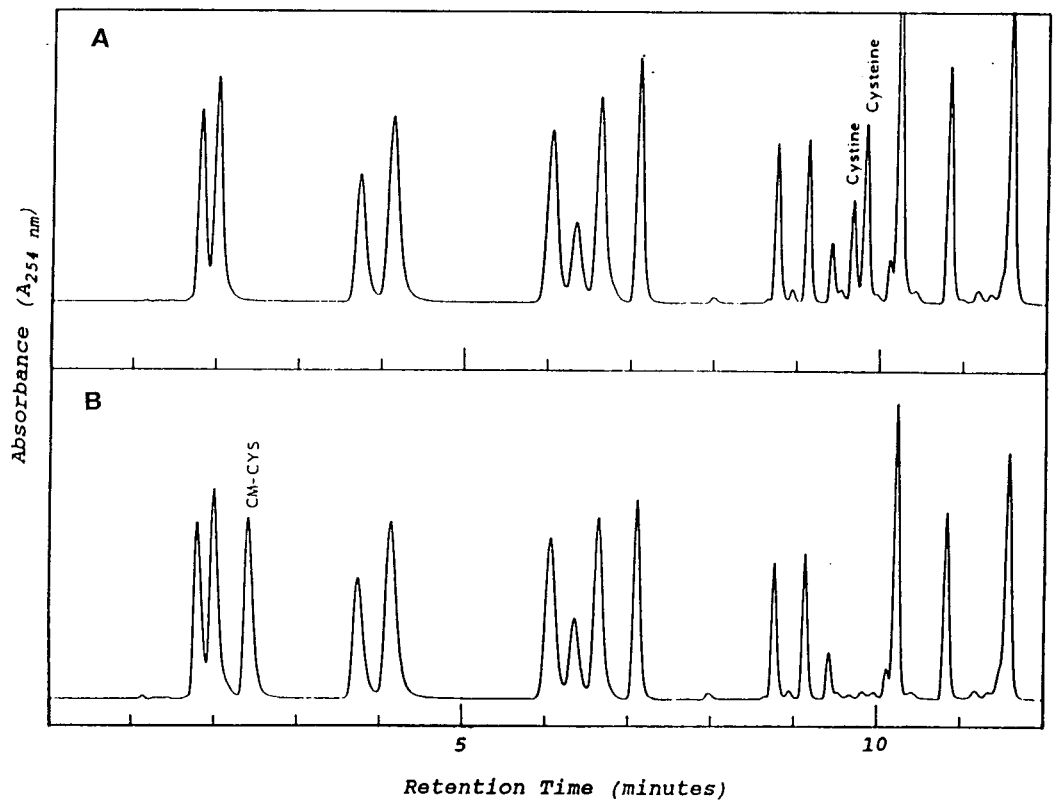

Fig. 2. Comparison of amino acid analysis results of unreacted (A) and derivatized rhIGF-I (B). The figure shows HPLC chromatograms of component amino acids. The disappearance of the cysteine and cystine peaks in (B) is concomitant with the appearance of the peak corresponding to the carboxymethylated cysteine (CM-CYS). Absorbance range in both chromatograms is 65 mAU.

3.3. Analysis of tryptic map of rhIGF-I

Tryptic hydrolysis yielded the HPLC map shown in Fig. 3. Amino acid analysis results indicated that the peaks corresponding to fragments T8, T7T8, T7T8T9 and T8T9T10 coelute on the HPLC system at 34 min, and result from the tandem arginine repeats. The coelution of the four fragments indicates that retention on the reversed-phase medium of the HPLC column is heavily influenced by the hydrophobic stretches of the T8 fragment since this sequence is common to all four fragments. CZE analysis of the HPLC fraction collected at 34 min showed four major peaks of the following area percentages: peak 1, 59%; peak 2, 22%; peak 3, 11%; peak 4, 6% (Fig. 4A). This observation was investigated in an attempt to further delineate the differences in HPLC and CZE as laboratory techniques for peptide separation. Degradation and cross-contamination were not the cause of the impurity profile demonstrated on CZE as the fraction was subsequently reanalyzed by HPLC and found to be >98% chromatographically pure (Fig. 4B).

3.4. Selectivity of CZE and HPLC separations

That the separation mechanisms of CZE and HPLC are different is seen by the behavior of the T8-containing fragments (T8, T7T8, T7T8T9 and T8T9T10). HPLC separations involve a mass transfer which is energetically determined by the hydrophobic character of the sample. Since most

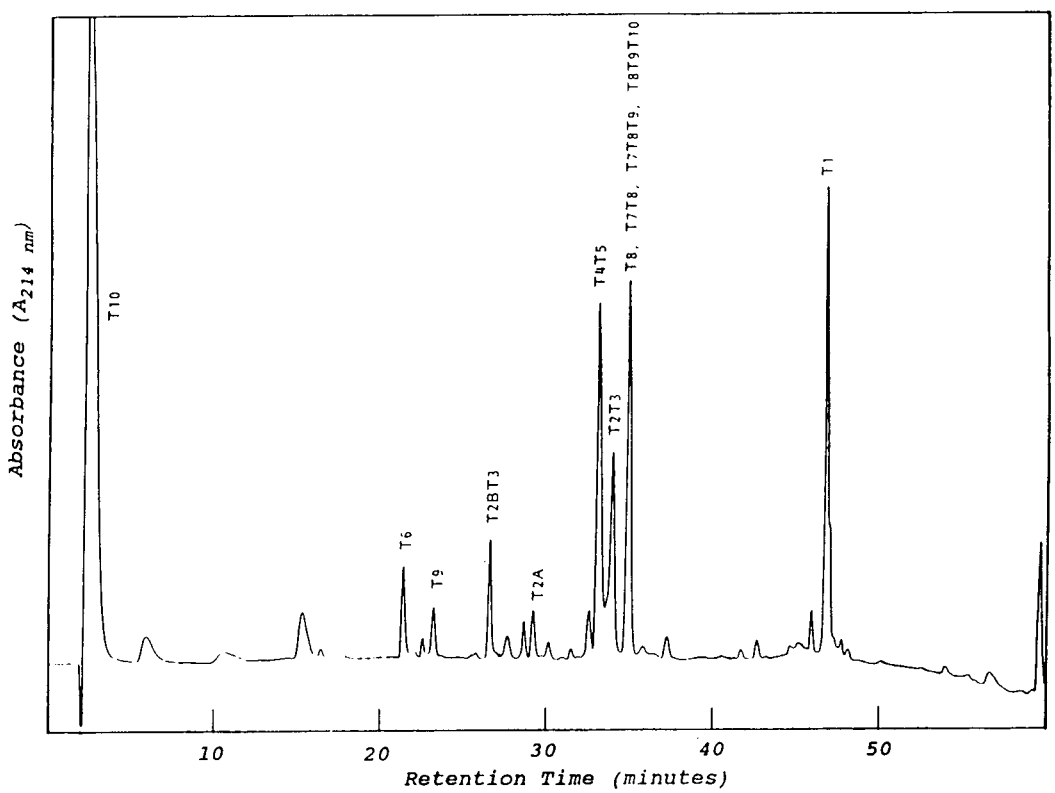

Fig. 3. Final HPLC tryptic map of rhIGF-I. Incomplete digestion products are indicated by continuous fragment labels (*e.g.* T3T4). Multiple coeluting peaks are separated by commas. A and B are used to indicate two parts of a tryptic fragment which were cleaved at a non-tryptic cleavage site (*e.g.* T2A and T2BT3). The absorbance range is 500 mAU.

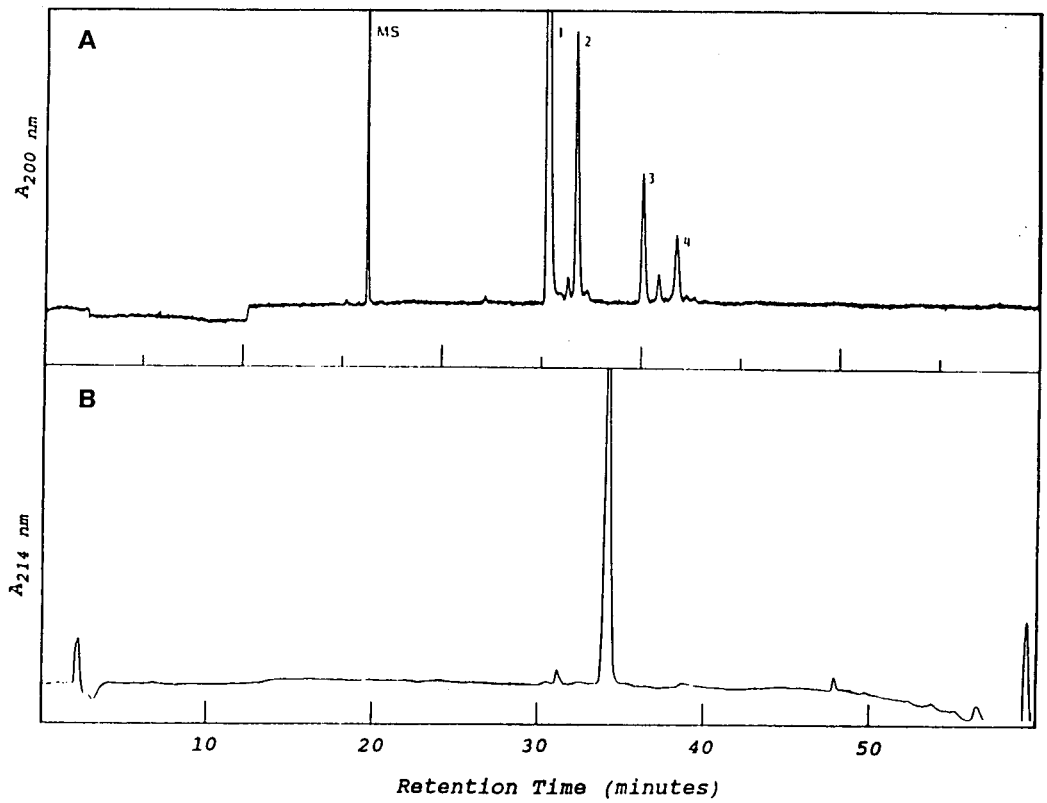

Fig. 4. Comparison of the CZE (A) and HPLC (B) analysis of the T8-containing fragments. The identities of these fragments are: peak 1 = T7T8; peak 2 = T7T8T9; peak 3 = T8T9T10; peak 4 = T8. MS = Mobility standard. The absorbance range is 7 mAU for CZE and 500 mAU for HPLC.

peptides are intrinsically amphipathic, separation is most often a function of a limited region of a peptide. CZE separations depend on the sample charge and size. Because mass transfer does not occur in CZE, mobility should be influenced by each residue in the peptide. If all chemical moieties contribute to mobility, it should be possible to separate very similar peptides. Further resolution by CZE of the fraction containing the T8 fragments illustrates this point.

A comparison of the tryptic map of rhIGF-I was performed to elucidate the differences in selectivity between CZE and HPLC. Fig. 5 indicates a large difference in the selectivity of both methods, where lines are used to connect identical peaks and to demonstrate reversals in the elution order between the two separation mechanisms.

Amino acid analysis of reversed-phase separated T8-containing fragments showed molar ratios suggestive of the expected fragments; however, two anomalies in the amino acid analysis rendered the ratios inconclusive —the molar ratios calculated for alanine, proline, lysine and arginine were not stoichiometric (Table 1), and a low recovery was calculated for serine (0.3 molar ratio). Through a systematic analysis of possible peptide cleavages, it was determined that the CZE peaks in Fig. 4A should have the following amino acid sequences. However, these data alone were insufficient to predict the relative elution order of these fragments.

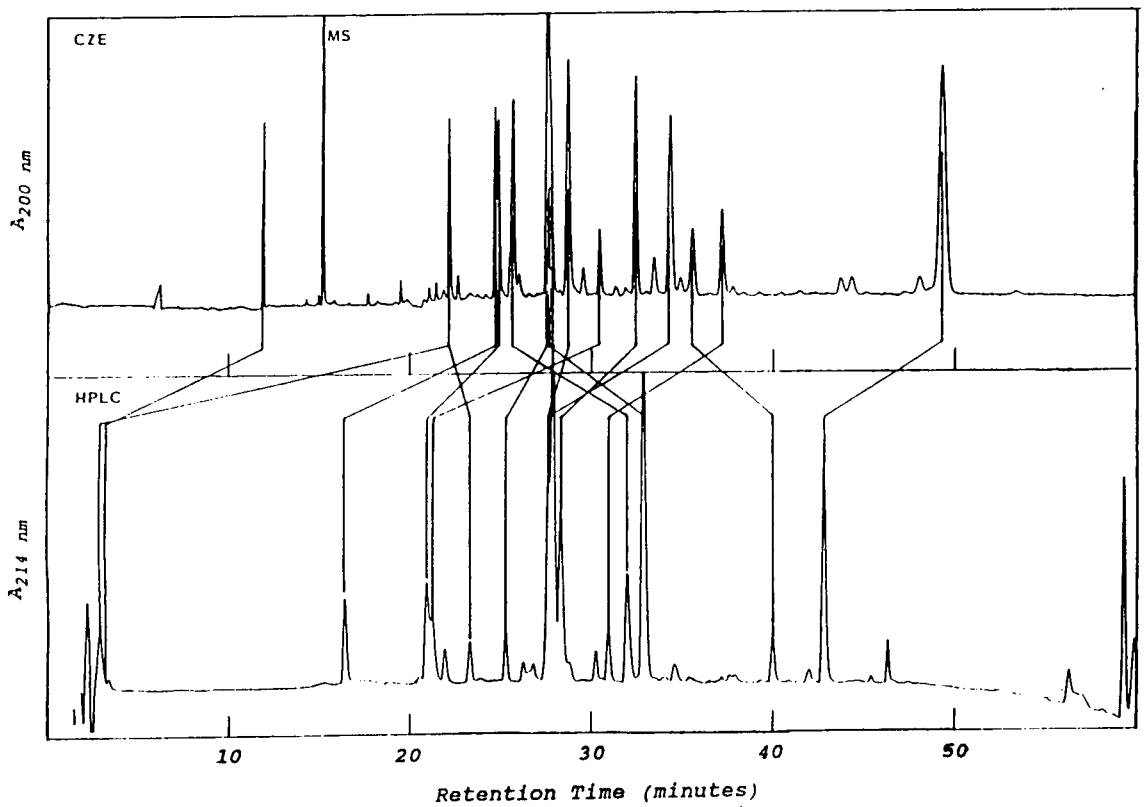

Fig. 5. Comparison of selectivity between CZE and HPLC. Lines are used to connect identical peaks and emphasize changes in elution order. MS = Mobility standard. The absorbance range is 7 mAU for CZE and 500 mAU for HPLC.

Peak	*T7*	*T8*	*T9*	*T10*
1	Arg-	Leu-Glu-Met-Tyr-Cys-Ala-Pro-Leu-Lys		
2	Arg-	Leu-Glu-Met-Tyr-Cys-Ala-Pro-Leu-Lys-Pro-Ala-Lys		
3		Leu-Glu-Met-Tyr-Cys-Ala-Pro-Leu-Lys-Pro-Ala-Lys-	Ser-Ala	
4		Leu-Glu-Met-Tyr-Cys-Ala-Pro-Leu-Lys		

Since the T8-containing fragments could not be unequivocally identified through routine amino acid analysis, it was decided to calculate the CZE electrophoretic mobilities using the polymer function (Eq. 2) proposed by Grossman *et al.* [11].

$$\mu \propto \ln \frac{(q+1)}{N^{0.43}} \qquad (2)$$

Table 2 shows the values used in Eq. 2, as well as experimental mobilities for each of the peptide fragments. In order to identify the elution order of the four T8-containing fragments, the polymer function in Eq. 2 was plotted against the experimental mobility values for each of the identified tryptic fragments (Fig. 6). The slope and intercept values from this plot were determined and then used to calculate the theoretical mobility value for each of the T8-containing fragments. The theoretical mobilities were then compared to the experimentally determined mo-

Table 2
Data for tryptic fragments of rhIGF-I

Peptide fragment	Charge (q)	Polymer number (N)	Molecular mass	Mobility (μ) ($\times 10^4$)
Leu57–Tyr60	0.31	4	554.7	1.31
Gly22–Tyr24	0.33	3	385.4	1.58
Gly1–Leu14	0.31	14	1443.6	0.90
Gln15–Phe16	0.43	2	293.3	1.74
Gly22–Phe25	0.43	4	532.6	1.41
Gly1–Arg21	1.06	21	2305.6	1.18
Val17–Arg21	1.16	5	604.6	2.25
Ser51–Arg55	1.16	5	648.7	2.23
Leu57–Lys65*	1.30	9	1123.4	1.91
Arg56–Tyr60	1.31	5	710.9	2.14
Pro66–Lys68	1.32	3	314.4	2.60
Cys61–Lys65	1.32	5	586.7	1.86
Phe25–Tyr31	1.33	7	825.9	1.97
Arg37–Arg50	2.13	14	1706.9	1.94
Arg56–Lys65*	2.31	10	1279.9	2.31
Leu57–Ala70*	2.39	14	1577.9	2.03
Phe25–Arg36	2.20	12	1300.4	2.21
Arg56–Lys68*	3.30	13	1576.0	2.46

Calculations of charge, polymer number, molecular mass and electrophoretic mobility for each of the peptide fragments obtained after tryptic digestion of rhIGF-I are summarized in the table. These data were subsequently used to obtain the plots in Figs. 6–8. Asterisks refer to T8-containing fragments.

bilities to establish the fragment identities. Once the peaks were identified, the polymer functions for the peptides were plotted against the actual mobility values (Fig. 7). The slope of the line derived from the four peptides correlated within 4% of that plotted for the identified tryptic fragments (Fig. 6). An overlay of Fig. 6 with Fig. 7 reveals a good correlation (Fig. 8) in which all

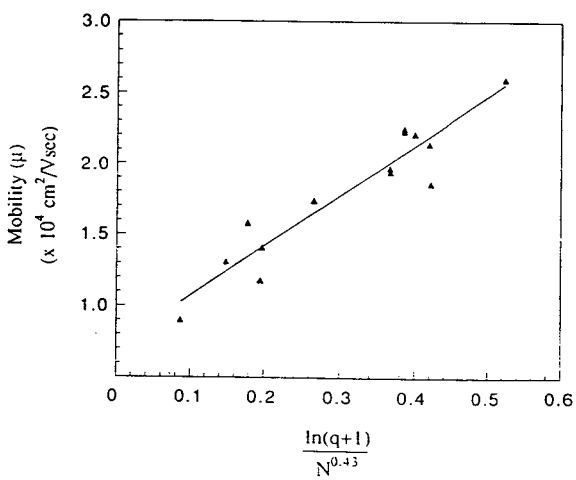

Fig. 6. Plot of the polymer function (Eq. 2) for all the peptides in Table 2 except the T8-containing fragment *versus* the mobility values.

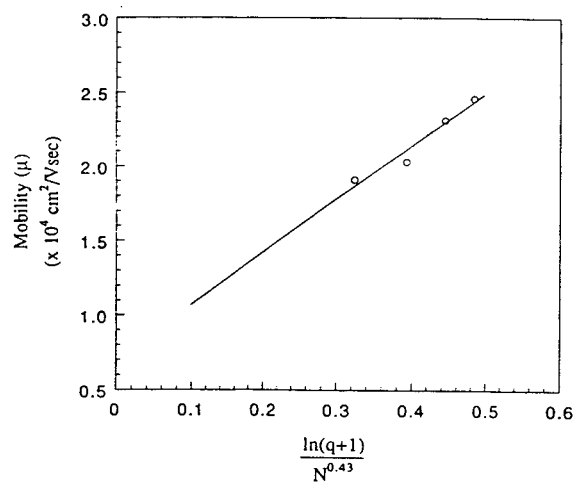

Fig. 7. Plot of the polymer function (Eq. 2) for the T8-containing fragments *versus* the experimental mobility values.

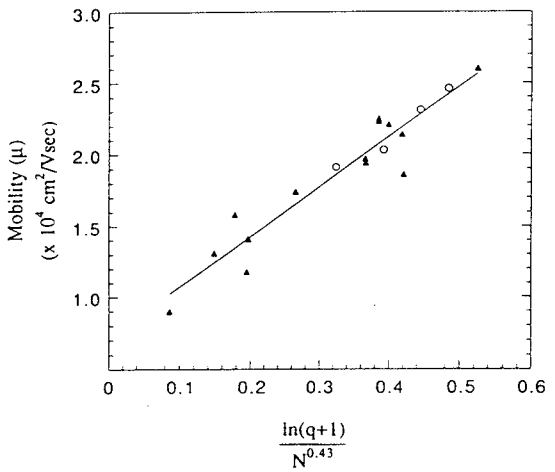

Fig. 8. Comparison of plots from Figs. 6 and 7.

four calculated points fall inside of the 95% confidence limits of the line. Validation of fragment assignment was derived by iteration of the assignments of the T8-containing fragments. The above peak assignments represent the only relationship in which all of the peaks fall within the 95% confidence limits of the line.

4. Discussion

Our analysis shows that CZE is a useful tool for both structural identification and purity confirmation in peptide mapping experiments. Although it is unlikely that CZE will take the place of HPLC for routine separation, its potential as a complementary method has been shown. The difference in the selectivity of CZE demonstrated has resulted in a peptide map which differs significantly from the HPLC map. In addition to the difference in selectivity, CZE offers the unique predictive ability associated with mobility correlations. The added potential, resulting from the mobility correlations, indicates a powerful supplemental role for CZE in peptide mapping experiments.

Acknowledgement

We thank Dr. Frank Gasparini for helpful discussions and critical assessment of this manuscript.

References

[1] R.G. Nielsen, R.M. Riggin and E.C. Rickard, *J. Chromatogr.*, 480 (1989) 393–401.
[2] P.D. Grossman, H.H. Lauer, S.E. Moring, D.E. Mead, M.F. Oldham, J.H. Nickel, J.R.P. Goudberg, A. Krever, D.H. Ransom, and J.C. Colburn, *Am. Biotechnol. Lab.*, 8 (1990) 35–43.
[3] B.L. Karger, L.R. Snyder and Cs. Horváth, *An Introduction to Separation Science*, Wiley, New York, 1973.
[4] J.W. Jorgensen and K.D. Lukacs, *Science*, 222 (1983) 266–272.
[5] V.J. Hilser, Jr., G.D. Worosila and S.E. Rudnick, *J. Chromatogr.*, 630 (1993) 329–336.
[6] B.A. Bidlingmeyer, S.A. Cohen and T.L. Tarvin, *J. Chromatogr.*, 336 (1984) 93.
[7] M.J. Waxdal, W.H. Konigsberg, W.L. Henley and G.M. Edelman, *Biochemistry*, 7 (1968) 1959–1966.
[8] G. Worosila, *Ph.D. Thesis*, Rutgers, State University of New Jersey, New Brunswick, NJ, 1985, p. 45.
[9] B. Skoog and A. Wichman, *Trends Anal. Chem.*, 5 (1986) 82.
[10] F. Raschdorf, R. Dahinden, W. Maerki and W.J. Richter, *Biomed. Environ. Mass Spectrom.*, 16 (1988) 3.
[11] P.D. Grossman, J.C. Colburn and H. Lauer, *Anal. Biochem.*, 179 (1989) 28.

ELSEVIER

Journal of Chromatography A, 672 (1994) 231–236

JOURNAL OF CHROMATOGRAPHY A

Separation of pig liver esterase isoenzymes and subunits by capillary zone electrophoresis in the presence of fluorinated surfactants

Å. Emmer, M. Jansson, J. Roeraade*

Department of Analytical Chemistry, Royal Institute of Technology, S-100 44 Stockholm, Sweden

(First received November 23rd, 1993; revised manuscript received February 23rd, 1994)

Abstract

An attempt was made to separate the isoenzymes and subunits of pig liver esterase by capillary zone electrophoresis. This enzyme is a complex mixture and is strongly adsorbed on a fused-silica capillary. However, by simply adding a cationic fluorosurfactant to the running buffer, adsorption was significantly reduced. The effects of adding a zwitterionic and a neutral fluorosurfactant were also investigated. Large changes in the elution pattern were observed when using different combinations of these additives. Mixtures of different fluorosurfactants added to the running buffer can therefore be utilized in strategies for optimization of the separation selectivity.

1. Introduction

Pig liver esterase (PLE) is an enzyme of considerable interest as a chiral catalyst in asymmetric organic synthesis. Even though studies of PLE have been reported by several workers [1,2], the exact molecular structure has remained unknown. This is mainly due to the extreme complexity of this enzyme, which consists of several isoenzymes and subunits [3].

It is highly desirable to be able to improve the catalytic performance of PLE in organic synthesis. This could be achieved by means of protein engineering. However, this has not yet been possible because of the uncertainties regarding the molecular structure and the difficulties in separating the different isoenzymes [3].

Capillary zone electrophoresis (CZE) is rapidly advancing as a powerful technique for the separation of proteins. However, wall adsorption is a basic problem associated with such separations and it frequently leads to broadened and distorted peaks. Several ways of improving this situation have been proposed [4–12]. However, the efficiency of these suggestions has mostly been demonstrated for molecules such as peptides and small model proteins and very little has been reported on free-flow CZE separations of large proteins.

Even a molecule such as lysozyme, which is often used as a model compound and is considered "difficult" in terms of wall adsorption owing to its high p*I*, is a relatively small and compact protein. Large proteins usually have a more complex tertiary (three-dimensional) and quarternary structure (combinations of different subunits) and therefore a more complex charge distribution. Consequently, the mechanisms of

* Corresponding author.

0021-9673/94/$07.00
SSDI 0021-9673(94)00186-D

wall adsorption become unpredictable. For example, regional charge heterogeneities within the molecule can cause adsorption of solutes under conditions where these have the same net charge as the wall [13]. Large proteins also have more charged sites that can cause electrostatic interactions and, once such proteins have been adsorbed, desorption will be very difficult.

Previously, we proposed a new concept in which a cationic fluorosurfactant was added to the running buffer. Strongly reduced protein adsorption, high efficiencies and excellent reproducibility were observed for smaller model proteins [14,15]. Other workers have also been able successfully to confirm our findings [16]. The unique properties of the fluorosurfactant prompted us to extend our studies to larger, more complex proteins. Apart from the cationic surfactant, this work also included studies with a zwitterionic and a neutral fluorosurfactant. Pig liver esterase was chosen as a model for these studies.

2. Experimental

A laboratory-made CZE apparatus was utilized. A UV detector (Linear Instruments, Reno, NV, USA) was employed at 230 nm for on-column detection. Injections were carried out by timer-controlled electromigration. New capillaries (fused silica, 100 cm × 50 μm I.D.) were flushed with 0.4 *M* NaOH for 30–60 min and then to neutrality with water and finally with running buffer for 20–30 min. The surfactants FC134 [$C_8F_{17}O_2NH(CH_2)_3N^+(CH_3)_3I^-$], FC430 (non-ionic fluoroaliphatic polymeric esters) (3M, St Paul, MN, USA) and a zwitterionic fluorosurfactant [$F(CF_2CF_2)_{3-8}CH_2CH(OCOCH_3)CH_2N^+(CH_3)_2CH_2CO_2^-$] (DuPont, Wilmington, DE, USA) were added to the running buffer, either separate or in various combinations at concentrations ranging between 50 and 400 μg/ml.

The experiments were carried out with a crude sample of PLE (Sigma, St. Louis, MO, USA) with a total protein concentration of 0.5 mg/ml. The enzymatic activity of PLE in presence of fluorosurfactants was assayed at pH 7 in 0.05 *M* phosphate buffer. After desalting on a PD-10 gel filtration column (Pharmacia, Uppsala, Sweden), spectrophotometric measurement at 405 nm was carried out. The conditions used were 2 m*M* *p*-nitrophenyl acetate, 5% dimethyl sulphoxide and PLE (1.4 μg/ml) dissolved in phosphate buffer.

3. Results and discussion

PLE is an acidic protein and is a complex mixture of at least six isoenzymes (M_r *ca.* 180 000, p*I* = 4.7–5.6), each consisting of trimers of different combinations of at least seven subunits (M_r *ca.* 60 000). PLE is strongly adsorbed on an untreated fused-silica capillary. Our initial attempts to operate at a pH of 7, according to the concept of Lauer and McManigill [4], failed. This method uses the fact that proteins are amphoteric and are repelled from the negatively charged silica surface if the pH of the buffer medium is above the p*I* of the protein. At pH 7, PLE has a net negative charge and should therefore not interact with the silica wall. However, the adsorption of PLE is severe. In fact, no relevant peaks are recognized in the electropherogram. This suggests that there are positively charged local domains in the molecule, which are attracted to the wall. A remedy for this problem could be to increase the pH. However, operation at pH extremes is not recommended, owing to the risk of protein denaturation. Also, the pH is a crucial parameter for selectivity optimization, and optimum selectivity in CZE is usually achieved near the p*I*. Under such conditions, however, PLE is strongly adsorbed on the silica wall. Also, other complications, such as precipitation of the protein, could occur when the pH of the buffer is close to the p*I* of the protein.

We have shown previously that the use of a cationic fluorosurfactant buffer additive decreases the wall adsorption considerably [14,15]. Using this concept, we also noted a drastic decrease in the adsorption of PLE at pH con-

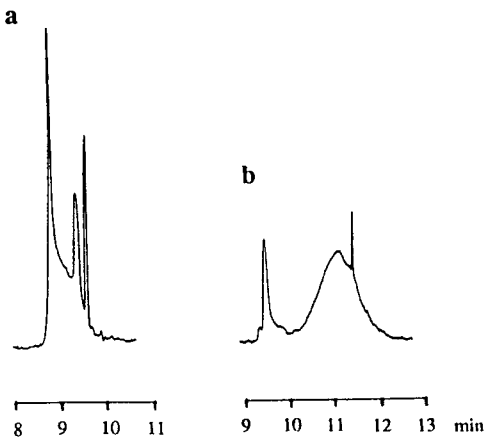

Fig. 1. Electropherograms of pig liver esterase in the presence of a cationic fluorosurfactant (FC134). Running buffer, 0.05 *M* acetate–phosphate with 100 μg/ml of FC134 added; buffer pH, (a) 4 and (b) 3.5; field strength, −30 kV; injection, electromigration at −20 kV for 10 s.

ditions just below the p*I* of the enzyme (Fig. 1). The reason for this improvement can in the first instance be explained by the formation of an admicellar bilayer or hemimicelles on the silica surface [15–19]. Thereby, the charge of the surface becomes positive. An indication of this is that the direction of the electroosmotic flow is reversed. PLE, which has a net positive charge under the actual pH conditions, should therefore be electrostatically repelled from the surface. However, negatively charged local regions of the protein molecules could still interact with the wall in different ways. We believe that these regions are shielded by bilayers and/or micelles of the fluorosurfactant and thus electrostatically repelled from the bilayer on the silica surface. Further, permanent adsorption of the protein on the bilayer is less probable, as the formation of the admicellar layer is a dynamic process, with a

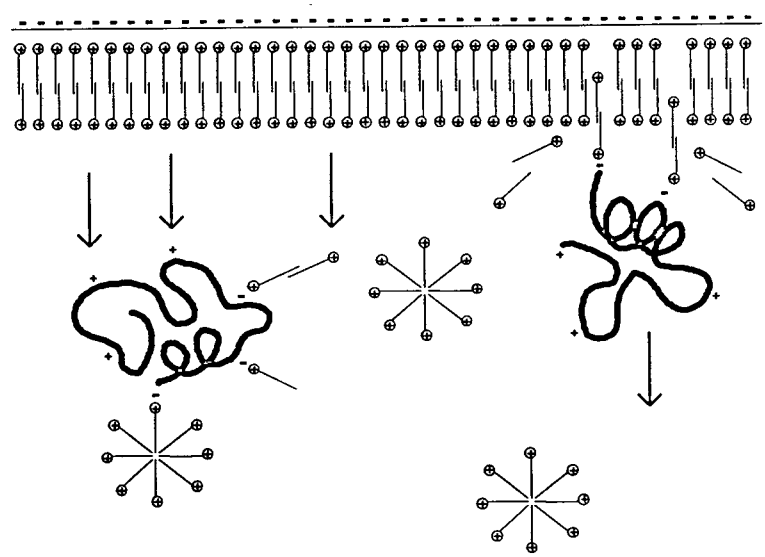

Fig. 2. Schematic diagram of some proposed interactions between a protein and the capillary wall in presence of a cationic fluorosurfactant. This must be seen as a dynamic process, with a continuous interchange of surfactant molecules. The negatively charged surface becomes positively charged owing to the formation of a bilayer of surfactant. The left part illustrates possible interactions between a protein molecule and the fluorosurfactant. The fluorosurfactant is present in the form of aggregates of different sizes up to complete micelles. The negatively charged centra of the protein will attract the positively charged surfactant monomers and aggregates. In its turn, these aggregates will attract other surfactant molecules by hydrophobic interaction. Thus the protein is shielded by positive charges, and consequently repelled from the positively charged wall. The right part shows the dynamic exchange of fluorosurfactant molecules between the surface bilayer and the protein molecule.

continuous interchange of the fluorosurfactant molecules. Fig. 2 shows a schematic diagram of these proposed mechanisms.

We also tested the effects of adding a zwitterionic fluorosurfactant. This amphoteric compound has a p*I* of about 8 [20]. Therefore, at a pH below this value, it will be positively charged and will act in a similar way to the cationic surfactant. However, significant changes in selectivity were observed on adding different combinations of the zwitterionic and the cationic fluorosurfactant to the running buffer for the PLE capillary electrophoretic separation (Fig. 3). We attribute these selectivity changes to the formation of mixed micelles in the buffer solution, on the silica surface and around the negatively charged local sites of the protein [21]. As the two fluorosurfactants have a different chemical composition and molecular structure, changes in the electrostatic interactions and corresponding electrophoretic mobility are to be expected.

As mentioned earlier, the buffer pH is a central parameter for optimization of the separation selectivity, as it affects the magnitude of the net charge and influences molecular conformations and charge distribution. For a complex protein such as PLE, this is further complicated by dissociation of the isoenzymes into subunits. It can therefore be expected that the separation patterns of PLE at different pH values of the running buffer will be very dissimilar. This can also be seen in Fig. 1.

Further, we attempted to improve the selectivity of the separation by adding a neutral fluorosurfactant. The results are shown in Fig. 4. Owing to their extremely non-polar character, one can expect a significant interaction between the fluorinated carbon chains of the charged and the neutral surfactants [22]. It is therefore likely that the neutral fluorosurfactant is also partially incorporated in the adsorbed admicellar double layer [21]. This would lead to a decrease in the

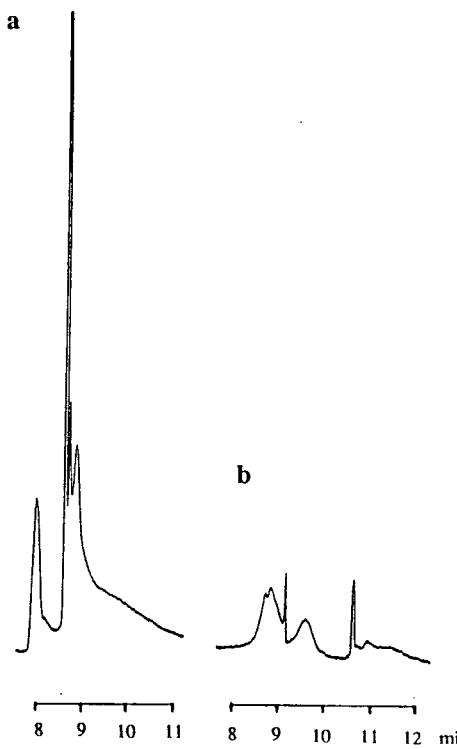

Fig. 3. (a) Electropherogram of PLE in the presence of a zwitterionic fluorosurfactant; (b) same as (a) but with addition of the cationic fluorosurfactant. Running buffer, 0.01 *M* acetate (pH 3.5) with (a) 400 μg/ml of zwitterionic fluorosurfactant added and (b) 200 μg/ml of zwitterionic and 50 μg/ml of cationic fluorosurfactant added; injection, electromigration at (a) −20 kV for 10 s and (b) −10 kV for 10 s. Other conditions as in Fig. 1.

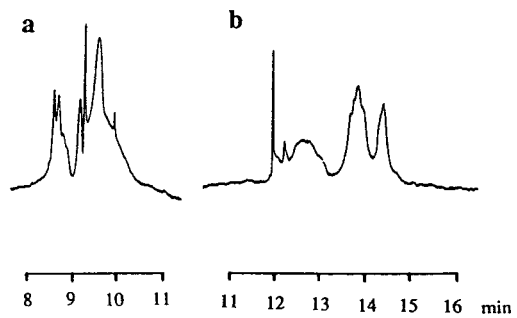

Fig. 4. Influence of the addition of a neutral fluorosurfactant on the separation of pig liver esterase. Running buffer: (a) 0.02 *M* acetate with 400 μg/ml of zwitterionic and 100 μg/ml of cationic fluorosurfactant added; (b) same as (a) but with an additional 200 μg/ml of neutral fluorosurfactant. Injection, electromigration at −10 kV for 10 s. Other conditions as in Fig. 1.

charge of the wall and result in a decrease in the electroosmotic flow. This is in accordance with our observations, as shown in Fig. 4. However, part of the decrease of the electroosmotic flow must also be attributed to an increased viscosity of the buffer solution.

Unfortunately, the PLE sample proved to be too complex to obtain a distinct separation of the enzyme units. The best results were obtained when a mixture of the three fluorosurfactants was added to the buffer (Fig. 4b), where about fifteen signals can be recognized. Several of the compounds overlap in the form of broad peaks. We believe that this could be partially due to the association and dissociation of subunits during the electrophoretic transport in the column. Another contributing factor is that the crude PLE sample is likely to contain a number of unspecified contaminants. The most feasible way to improve the separation would be to include a prefractionation, *e.g.*, by isoelectric focusing.

In previous studies [14], we assumed that hydrophobic interactions between fluorosurfactants and proteins are likely to be minimal, in view of the fact that the fluorocarbon chains have a lipophobic character. In order to investigate this assumption in practice, an enzymatic activity test with PLE in the presence of the fluorosurfactants was carried out. The results are presented in Table 1, and show that the enzymatic activity of PLE is completely preserved in the presence of the neutral fluorosurfactant. As expected, the charged fluorosurfactants interact with the proteins. However, at the low concentrations where wall deactivation for CZE is optimum, the enzymatic activity of PLE is to a large extent preserved.

4. Conclusions

CZE separation of native proteins such as PLE is not straightforward, owing to the complexity of such proteins and their unpredictable wall adsorption behaviour. Owing to the diversities in configuration, size, p*I* and charge distribution of the different isoenzymes and subunits, it is very difficult to design a model for optimum separation. Prefractionation schemes (*e.g.*, using isoelectric focusing) should be advantageous in this context.

Fluorosurfactants, used as buffer additives, can be successfully employed to suppress wall adsorption, while allowing operation at an optional buffer pH, preferably near the p*I* of the enzyme.

Significant differences in elution patterns are obtained with combinations of cationic, zwitterionic and neutral fluorosurfactants, which can be exploited for experimental optimization of the separation selectivity. Interactions between the fluorosurfactant additives and the enzyme were shown to be relatively moderate, as demonstrated by enzyme assays.

Several alternative methods to suppress adsorption, *e.g.*, the use of permanent wall coatings, could also prove to be effective. However, the advantage of the fluorosurfactant concept is

Table 1
Enzymatic activity of PLE in the presence of fluorosurfactants

Buffer additive	Activity (ΔA/min)	Relative activity
No additive	0.18	1
Cationic fluorosurfactant	0.11	0.61
Non-ionic fluorosurfactant	0.18	1
Zwitterionic fluorosurfactant	0.11	0.61

The enzymatic activity was monitored by the change in absorbance ($\lambda = 405$ nm) per minute (ΔA/min). Fluorosurfactant concentrations: 100 μg/ml for the cationic, 200 μg/ml for the non-ionic and 400 μg/ml for the zwitterionic surfactant. The results were corrected for non-enzymatic self-hydrolysis by running a parallel blank without enzyme.

its simplicity. Moreover, a very good reproducibility of migration times is obtained even with a sample such as crude PLE, because the surfactant layer on the wall is continuously renewed.

5. References

[1] E. Heymann and W. Junge, *Eur. J. Biochem.*, 95 (1979) 509.
[2] D. Farb and W.P. Jencks, *Arch. Biochem. Biophys.*, 203 (1980) 214.
[3] N. Öhrner, A. Mattson, T. Norin and K. Hult, *Biocatalysis*, 4 (1990) 81.
[4] H.H. Lauer and D. McManigill, *Anal. Chem.*, 58 (1986) 166.
[5] R.M. McCormick, *Anal. Chem.*, 60 (1988) 2322.
[6] J.S. Green and J.W. Jorgenson, *J. Chromatogr.*, 478 (1989) 63.
[7] M. Bushey and J.W. Jorgenson, *J. Chromatogr.*, 480 (1989) 301.
[8] S.A. Swedberg, *Anal. Biochem.*, 185 (1990) 51.
[9] G.J.M. Bruin, R. Huisden, J.C. Kraak and H. Poppe, *J. Chromatogr.*, 480 (1989) 339.
[10] J.K. Towns and F.E. Regnier, *J. Chromatogr.*, 516 (1990) 69.
[11] Z. Zhao, A. Malik and M.L. Lee, *J. Microcol. Sep.*, 4 (1992) 411.
[12] J.T. Smith and Z. El Rassi, *J. High Resolut. Chromatogr.*, 15 (1992) 573.
[13] M. Wahlgren and T. Arnebrant, *TIBTECH*, 9 (1991) 201.
[14] Å. Emmer, M. Jansson and J. Roeraade, *J. Chromatogr.*, 547 (1991) 544.
[15] Å. Emmer, M. Jansson and J. Roeraade, *J. High Resolut. Chromatogr.*, 14 (1991) 738.
[16] W.G.H.M. Muijselaar, C.H.M.M. de Bruijn and F.M. Everaerts, *J. Chromatogr.*, 605 (1992) 115.
[17] M.A. Yeskie and J.H. Harwell, *J. Phys. Chem.*, 92 (1988) 2346.
[18] H. Rupprecht and T. Gu, *Colloid Polym. Sci.*, 269 (1991) 506.
[19] J.M. Cases and F. Villieras, *Langmuir*, 8 (1992) 1251.
[20] Å. Emmer and J. Roeraade, *J. Liq. Chromatogr.*, in press.
[21] J.H. Harwell and J.F. Scamehorn, in K. Ogino and M. Abe (Editors), *Mixed Surfactant Systems* (*Surfactant Science Series*, Vol. 46), Marcel Dekker, New York, 1993, pp. 263–281.
[22] F. MacRitchie, *Adv. Colloid Interface Sci.*, 25 (1986) 341.

ELSEVIER

Journal of Chromatography A, 672 (1994) 237–241

JOURNAL OF CHROMATOGRAPHY A

Short Communication

Chromatographic separation of geometrical isomers using highly oriented polymer-immobilized silica gels

Takanori Fukumoto[a], Hirotaka Ihara[*,b] Shigeyoshi Sakaki[b], Hideto Shosenji[b], Chuichi Hirayama[b]

[a]*Chemical and Textile Industry Research Institute, Fukuoka Industrial Technology Centre, Kamikoga, Chikushino, Fukuoka 818, Japan*

[b]*Department of Applied Chemistry, Faculty of Engineering, Kumamoto University, 2-39-1 Kurokami, Kumamoto 860, Japan*

(First received January 18th, 1994; revised manuscript received March 8th, 1994)

Abstract

Poly(octadecyl acrylate) having a reactive group at one side of the terminal group was synthesized and immobilized on porous silica gels. Differential scanning calorimetric measurement indicated that the immobilized polymer underwent a crystal-to-isotropic phase transition on silica gels. Using a packed column, a remarkably high separation factor for geometrical isomers of stilbene was observed in the crystal-state temperature range, although no similar separation was observed with octadecylated silica gels. It was estimated by calculation of the HOMO that this specific retention includes charge-transfer interactions from double bonds of solutes to acrylate moieties of the stationary phase.

1. Introduction

We have developed novel stationary phases composed of grafted comb-shaped polymers and silica gels for high-performance liquid chromatography (HPLC) [1–4]. These packings are characterized by the fact that immobilized polymers are free from perturbation of supporting materials and thus show individual functions as the polymers can be chemically combined to silica gel at one side of the terminal groups. On the basis of this idea, the first example for HPLC use has been offered as shown in Fig. 1. This silica-supported comb-shaped polymer (Sil-**1**) showed various unique chromatographic sepa-

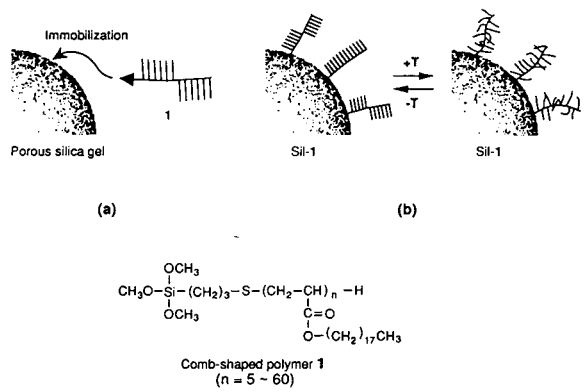

Fig. 1. (a) Structure of comb-shaped polymer **1** and immobilization on porous silica gels. (b) Silica-supported **1** (Sil-**1**) shows crystal-to-isotropic phase transition on silica gels.

* Corresponding author.

0021-9673/94/$07.00
SSDI 0021-9673(94)00245-5

rations; for example, the Sil-**1** column showed a remarkably high separation factor with a specific temperature dependence for polyaromatics, recognizing molecular planarity [1] and molecular length [2] of sample solutes. No similar behaviour was observed with conventional reversed-phase liquid chromatographic packings such as octadecylated (ODS) silica gels. These attributes of Sil-**1** are derived from the highly oriented structure of polymerized long-chain alkyl groups and their phase transition behaviour between the crystal and isotropic states (Fig. 1b).

In this paper, we report that Sil-**1** shows geometrically selective retention as an HPLC column and its separation mechanism is also discussed.

2. Experimental

2.1. Materials

Sil-**1** was prepared by telomerization of octadecyl acrylate with 3-mercaptotrimethoxysilane and subsequent immobilization on silica gels as reported previously [1,2]. The average degree of polymerization of grafted poly(octadecyl acrylate) was estimated as 27 by NMR spectroscopy. Elemental analysis indicated that 20.6 mass-% of organic phase was immobilized on porous silica gels (YMC SIL-120-S5; diameter 5 μm; pore size 120 Å; specific surface area 300 $cm^2\ g^{-1}$).

2.2. Measurements

Sil-**1** was packed into a stainless-steel column (250 mm × 4.6 mm I.D.) and its liquid chromatographic properties were examined using methanol–water as eluent. The chromatograph included a JASCO Model 880 PU pump and a Shimadzu SPD-M6A UV–visible photodiode-array detector. A 5-μl volume of the sample dissolved in methanol was injected through a Reodyne Model 7125 injector. Chromatography was carried out at flow-rate of 0.5 ml min^{-1}. Differential scanning calorimetric (DSC) thermograms of polymer **1** or Sil-**1** (5 mg) were obtained using a heating rate of 2°C min^{-1} with a Seiko I & E SSC-580 with a DSC-10 differential scanning calorimeter.

3. Results and discussion

3.1. Retention behaviour of stilbene

The Sil-**1** column gave a complete separation of a mixture of *trans*- and *cis*-stilbene at 25°C (Fig. 2). The theoretical plate number for the column and the separation factor (α, the ratio of the capacity factors of the *trans*- and *cis*-isomers) are 18 000 and 1.97, respectively. On the other hand, an ODS column (300 mm × 4.6 mm I.D.) (GL Science) provided a very small separation factor (α = 1.07 at 25°C). This large difference in α values indicates that Sil-**1** has a specific retention mechanism, although Sil-**1** includes a retention mode similar to that in reversed-phase liquid chromatography (RPLC) because the elution order is the same as that in ODS and the retention capacity increases with increase in mobile phase polarity.

The specificity of Sil-**1** was emphasized by examining the temperature dependence of its retention behaviour. Fig. 3 shows the temperature dependences of the capacity factors (k') of stilbenes. With ODS, the k' values decreased with increase in temperature. Such negative slopes as in Fig. 3 are commonly observed with the usual RPLC packings [5,6]. These can be explained by an increase in the solubility of solutes from the stationary to the mobile phase

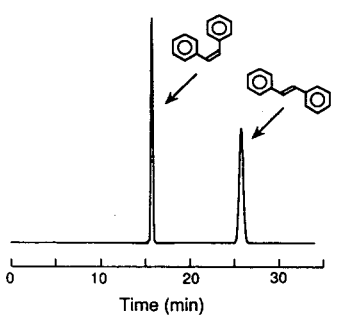

Fig. 2. Separation of a mixture of *trans*- and *cis*-stilbene with a Sil-**1** column. Mobile phase: methanol–water (7:3).

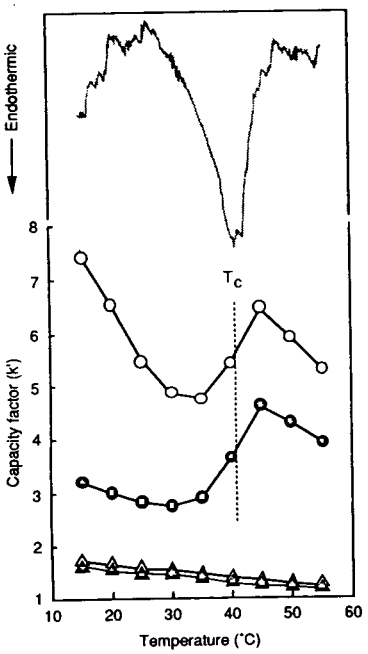

Fig. 3. Temperature dependences of the capacity factor of stilbene. DSC thermogram of Sil-**1** in a methanol–water (7:3) dispersion shown as a dotted line (top). T_c corresponds to the peak-top temperature of the phase transition. Methanol–water mixtures were used as mobile phases (7:3 with Sil-**1** and 9:1 with ODS). The k' value was determined by using the retention time of glycerol. ○ = *trans*-Stilbene with Sil-**1**; ● = *cis*-stilbene with Sil-**1**; △ = *trans*-stilbene with ODS; ▲ = *cis*-stilbene with ODS.

with increase in temperature [5,6]. In contrast, Sil-**1** provided critical bending points and positive slopes at temperatures between 35 and 45°C. Interestingly, this unusual temperature dependence includes a remarkable selectivity change. The α values are 2.33 (15°C), 1.97 (25°C), 1.64 (35°C), 1.55 (40°C), 1.40 (45°C), 1.38 (50°C) and 1.35 (55°C). With ODS, only small and constant α values (1.04–1.07 at 15–55°C) were observed.

3.2. Retention mechanism of Sil-1

The temperature shown as a dotted line in Fig. 3 indicates the phase transition behaviour (T_c, peak-top temperature) of the immobilized comb-shaped polymer **1** on silica gels, which was directly observed by DSC measurements in the methanol–water (7:3) dispersion state. Polarization microscopic observation indicated that this transition was from the crystalline to the isotropic state of the immobilized polymer **1**. This temperature lies in the temperature range at which the k' values increase in Fig. 3. Therefore, the unusual increase in retention is related to the phase transition of immobilized polymer **1** and the separation factor was much higher at crystal-state temperatures ($\alpha = 2.33$ at 15°C) than at isotropic-state temperatures ($\alpha = 1.35$ at 55°C). This indicates that the oriented structure of immobilized phase provides high selectivity for geometric isomers.

On the other hand, the positive slope of the k' *versus* temperature plots at 30–45°C does not show a change in the retention mechanism. For this unusual positive slope, we have following explanation: immobilized **1** forms a mixed phase containing both crystalline and isotropic phases and the ratio of isotropic **1** to crystalline **1** increases with increase in temperature at 30–45°C. Therefore, the capacity factor (k') also increases with increase in this ratio, because k' is larger in the isotropic than in the crystalline state.

In order to understand this unusual specificity, we have discussed previously that highly oriented structures of an immobilized phase can recognize the molecular planarity of solutes [1–3]. For example, a planar compound, triphenylene, is more strongly incorporated in a crystal-state medium than a corresponding non-planar compound, *o*-terphenyl [$\alpha = 4.0$ (25°C) and 1.5 (25°C) in Sil-**1** and ODS, respectively] [1,3]. In support of this, the stilbene isomers have very different molecular shapes. According to this assumption, it is considered that the steric bulkiness of *cis*-stilbene prevents it from being incorporated into a crystal medium.

However, in this study we encountered retention phenomena that cannot be explained only by this assumption. For example, Sil-**1** showed geometrically selective retention for 1,2-bis(phenylsulphonyl)ethylene isomers ($\alpha = 1.60$ at 25°C; Fig. 4), but showed almost no selectivity for geometrical isomers of 1,4-dichloro-2-butene (Fig. 4), 1,2-dimethylcyclohexane and deca-

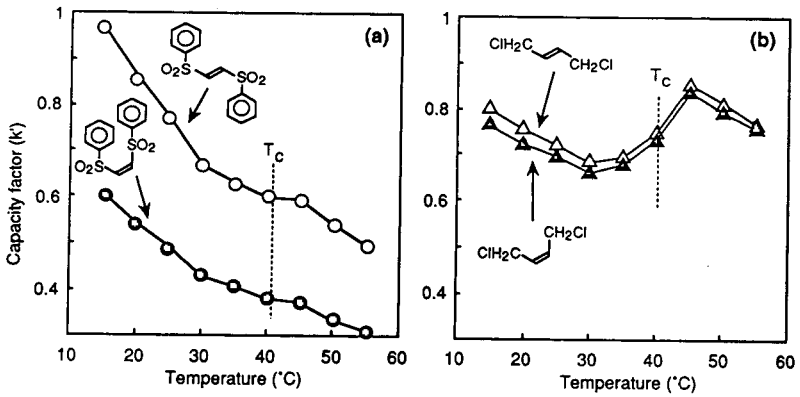

Fig. 4. Temperature dependences of the capacity factor of geometrical isomers of (a) 1,2-bis(sulphonyl)ethylene and (b) 1,2-dichloro-2-butene. Mobile phase: methanol–water (7:3).

hydronaphthalene ($\alpha = 1.04$, 1.05 and 1.08 at 25°C, respectively). However, the *k' versus* temperature plots showed a distinct jump at temperatures around the phase transition temperature in all samples. This indicates that the difference in bulkiness between *cis*- and *trans*-isomers is not always reflected in geometric selectivity.

On the basis of these results, our previously proposed mechanism for molecular recognition should be modified and developed as follows. (1) Immobilized polymer **1** forms a highly oriented structure at its crystal-state temperatures. A planar compound such as *trans*-stilbene can be easily incorporated in this oriented polymer. This mechanism is analogous to the fact that cholesterol as a rigid and planar compound is readily incorporated into lipid bilayer membranes which form a highly oriented structure. (2) Immobilized polymer **1** interacts with a double bond of the solutes, recognizing its π-electron density. Perhaps this interaction is derived from carbonyl π-electrons of acrylate moieties, which can work as electron-accepting groups. This assumption is supported by following facts: (i) it was confirmed that cross-linked poly(methyl acrylate) polymer (MA) particles as a reference showed higher selectivity for various isomeric aromatics compared with ODS, although these MA particles provided comparably small *k'* values because of the absence of a long-chain alkyl group; (ii) from calculation of the energy level of the HOMO (highest occupied molecular orbital) in stilbene, the *trans*-isomer is more electron donating (−8.63 eV) than the *cis*-isomer (−9.06 eV) [calculation of the energy level of the HOMO was carried out with Materia (MOPAC 6.00 with PM3 option) of Teijin System Technology (Japan)]. A similar interaction between benzene and formic acid was calculated by Bredás and Street [7]. On the other hand, geometrical isomerism for 1,4-dichloro-2-butene having non-conjugating substituent groups provides no significant difference in the energy level of the HOMO. In this case, Sil-**1** shows a small selectivity for retention of these isomers.

Acknowledgements

We are grateful to Mr. N. Nakamura for his capable assistance. We also thank Mr. Goda and Mr. Ohe of Sumitomo Seica Chemicals for the use of Materia. This study was supported in part by a Grant-in-Aid for Scientific Research from Fukuoka Science and Technology Foundation (Japan).

References

[1] C. Hirayama, H. Ihara and T. Mukai, *Macromolecules*, 25 (1992) 6375.

[2] H. Ihara, C. Hirayama and T. Fukumoto, *Anal. Sci.*, 9 (1993) 711.
[3] H. Ihara, T. Fukumoto and C. Hirayama, *Polyfiles*, 31 (1994) 60.
[4] C. Hirayama, H. Ihara, S. Nagaoka and T. Wada, *Polym. J.*, 26 (1994) 499.
[5] J.H. Knox and G. Vasvari, *J. Chromatogr.*, 83 (1973) 181.
[6] *Separation Report*, No. 077, Tosoh, Japan, p. 3.
[7] J.L. Bredás and G.B. Street, *J. Chem. Phys.*, 90 (1989) 7291.

ELSEVIER

Journal of Chromatography A, 672 (1994) 242–246

JOURNAL OF CHROMATOGRAPHY A

Short Communication

Determination of N^{ϵ}-carboxymethyllysine by a reversed-phase high-performance liquid chromatography method

J. Hartkopf, C. Pahlke, G. Lüdemann, H.F. Erbersdobler*

Institut für Humanernährung und Lebensmittelkunde, Christian-Albrechts-Universität zu Kiel, Düsternbrooker Weg 17, D-24105 Kiel, Germany

(First received January 24th, 1994; revised manuscript received March 29th, 1994)

Abstract

To determine N^{ϵ}-carboxymethyllysine (CML) in foods a RP-HPLC method after derivatisation with *o*-phthaldialdehyde was developed. To prevent an overestimation of the CML values by the formation of CML from Amadori products during hydrolysis a borohydride reduction precedes the hydrolysis. A comparison of the determination with and without reduction shows that during hydrolysis 2–12 times more CML than originally present can be formed. With the analytical conditions described in this paper it is possible to obtain measurable amounts of this trace substance in spite of the much higher values for other amino acids. The CML contents in selected processed food items varied between 11 mg in a preparation from mixed cereals for infants to 408 mg/kg protein in a processed malt product. CML is suitable as indicator of heat damage in processed or stored foods, being more stable than the Amadori compounds determined, *e.g.* in form of furosine.

1. Introduction

We recently published a comparison of modified HPLC and ion-exchange chromatography methods for the determination of furosine [1], an indicator for Maillard-type lysine damage. Another helpful indicator for heat damage is N^{ϵ}-carboxymethyllysine (CML), an oxidative derivative of the Amadori-compound ϵ-fructoselysine [2,3]. Additionally, CML is formed from the reaction of lysine and ascorbate [4,5] (Fig. 1).

Analysis of CML is complicated by the fact that CML is also formed from the Amadori products during acid hydrolysis normally applied for amino acid determination in foods, resulting in an overestimation of the CML values. However, by reducing the Amadori products it is possible to prevent the formation of CML during hydrolysis [6,7].

Methods for the determination of CML are gas–liquid chromatography of the heptafluorobutyryl isobutyl ester of CML [8,9] or GC–MS methods [4,6,7] and reversed-phase HPLC methods after derivatisation of CML with *o*-phthaldialdehyde (OPA) [10,11]. In this paper we describe a specific clean-up procedure followed by HPLC which is useful to determine specifically the CML concentration, arising from food processing.

* Corresponding author.

0021-9673/94/$07.00
SSDI 0021-9673(94)00306-T

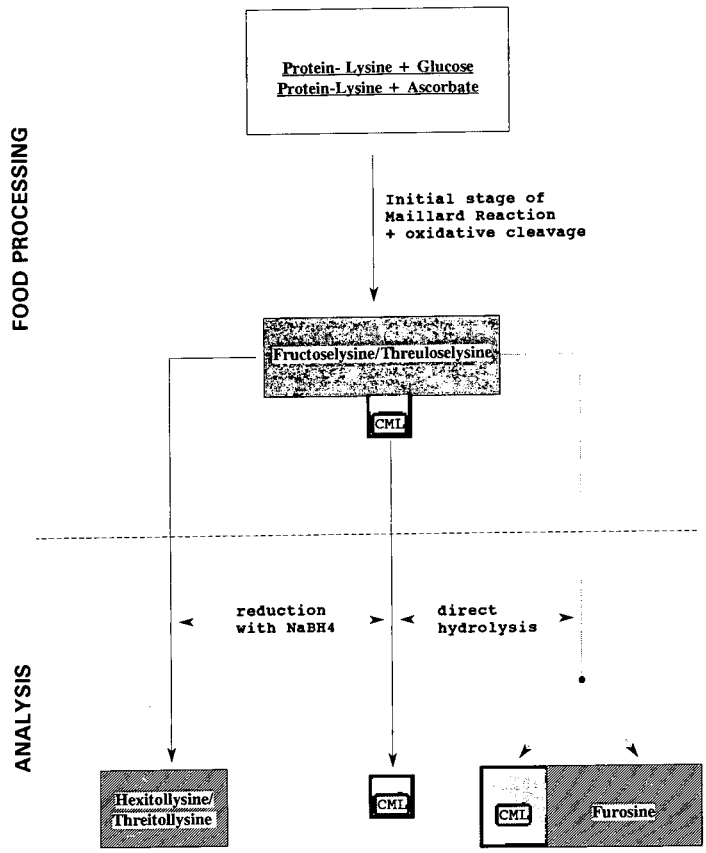

Fig. 1. Formation of CML during food processing and analysis (hydrolysis).

2. Experimental

The CML standard was synthesized by Lüdemann [10] and compared to another standard prepared by Liardon *et al.* [12]. The other reagents (all analytical grade or chromatographic grade) were obtained from Merck (Darmstadt, Germany).

An equimolar mixture of lysine monohydrochloride and glucose in an 88% (w/v) aqueous solution was used as a model sample, which was heated for 3 to 30 h, and then hydrolysed for 20 h with 7.8 *M* hydrochloric acid at 110°C.

The food samples were homogenised or pulverized before analysis. The initial masses of the food samples were chosen in a range between 2 and 5 g or ml, respectively. The sample masses were chosen according to the expected fructoselysine values in order to be sure that also high contents of fructoselysine will be reduced. Thus, all samples could be reduced with the same quantity of sodium borohydride. All foods were analysed either after direct hydrolysis or after borohydride reduction prior to hydrolysis.

The weighed samples were incubated with 20 ml of 0.2 *M* borate buffer (pH 9.1) and 10 ml of 1 *M* sodium borohydride (solved in 0.1 *M* sodium hydroxide). The incubation was continued for 3 h at room temperature. The reduced samples of solid foods were first adjusted with 50 ml 12.5 *M* hydrochloric acid to a molarity of 7.8 and then filled up to 90 ml with 7.8 *M* hydrochloric acid. The reduced samples of liquid foods were adjusted with 58 ml of 12.5 *M* hydrochloric acid and then filled up to 90 ml with 7.8 *M* hydrochloric acid. The samples without reduc-

tion were hydrolysed with 7.8 *M* hydrochloric acid (90 ml final volume). All samples were hydrolysed for 20 h under reflux. Afterwards the hydrolysates were concentrated by rotary evaporation to a volume of 10–20 ml and filled up with water to 50 ml. After filtration (Schleicher & Schüll 602H, Dassel, Germany) 5 ml of each filtrate were concentrated again by rotary evaporation nearly to dryness, resolved in 0.4 *M* borate buffer (pH 9.5) and filled up with borate buffer to make 10 ml, followed by an ultrafiltration (Schleicher & Schüll PH 79). The obtained ultrafiltrates were used for analysis after derivatisation with OPA.

The OPA reagent contained 54 mg OPA dissolved in 1 ml methanol, 50 μl 2-mercaptoethanol, and borate buffer (pH 9.5, 0.4 *M*) to make 10 ml.

CML was analysed using the reversed-phase HPLC-method after derivatisation with OPA. For the precolumn derivatization 100 μl of the standard solution or the hydrolysate were mixed with 500 μl of the OPA reagent in a 1.5-ml Eppendorf vial. This mixture was manually injected in a 20-μl sample loop (Rheodyne 7125, Cotati, USA). After a reaction time of exact 90 s the valve was switched into the inject position and the sample was injected onto the column (Spherisorb 5 C_{18} column; Promochem, Wesel, Germany). Two pumps (ConstaMetric III/IIIG), controlled by a gradient master (1601) from LDC (Gelnhausen, Germany) were used for a gradient elution at a flow-rate of 1.0 ml/min. The CML derivative was eluted with a gradient of the following buffers: (A) sodium acetate buffer (pH 6.70, 0.05 *M*)–methanol (96:4, v/v) and (B) methanol. A gradient was carried out from 15 to 70% B in 35 min, then hold for 4 min at 70% B, reset in 4 min to 15% B, and equilibrate for 12 min. The gradient was not linear but exponential ("exponent 3"). Therefore, the composition of the solvents during the gradient time is given in Table 1. The detection was evaluated with a fluorescence detector (F-1050) from Merck–Hitachi (Darmstadt, Germany), using an excitation wavelength at 340 nm and an emission wavelength at 455 nm. Data acquisition and peak integration were evaluated with an integrator C-R4A Chromatopac from Shimadzu (Duisburg, Germany).

Table 1
Composition of the solvent during the gradient time of the HPLC analysis

Time (min)	A (%)	B (%)
0	85	15
5	85	15
10	84	16
15	80	20
20	75	25
25	65	35
30	50	50
35	30	70

The whole analysis of CML lasted 55 min. Under the conditions described above clear and well separated CML peaks were obtained (Fig. 2).

3. Results and discussion

In our experiments with lysine–glucose model mixtures, treated by the reduction method with sodium borohydride, only 8–20% of the CML contents compared to the not reduced (direct hydrolysed) samples were determined (Fig. 3). This finding is very similar to results reported previously [13] comparing in the heated lysine–glucose models the samples without any hydrolysis with the not reduced, direct hydrolyzed counterparts. From the results a formation of 3.2–5.6% of fructoselysine to CML can be calculated. This is in agreement with reports of Dunn *et al.* [6] and Knecht *et al.* [7] from glycosylated biological material that a fraction of 3–5% fructoselysine undergoes oxidative cleavage to form CML during acid hydrolysis. The rate of formation during hydrolysis seems to be relatively small. However, due to the fact that the ratio of fructoselysine to CML is high a considerable amount of CML is formed.

These results demonstrate that all hydrolyses for CML must be performed after a borohydride reduction in order to transform fructoselysine to

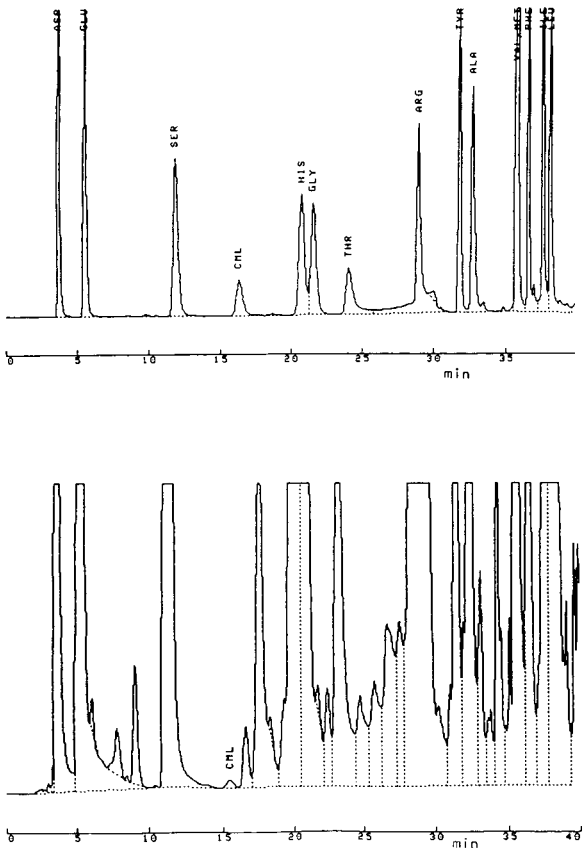

Fig. 2. HPLC chromatogram of a CML and amino acid standard and of a food sample.

hexitollysine, which does not produce CML (Fig. 1). With this procedure the formation of CML during hydrolysis can be prevented. As described elsewhere, the good correlation of $r = 0.996$ between the reduced and hydrolyzed samples and the equivalents without any hydrolysis of the heated lysine–glucose models demonstrated the accuracy of the reduction procedure [13]. Since furosine is also not formed from hexitollysine, efficiency of the reduction can be controlled by checking the absence of furosine.

To estimate the formation of CML during the hydrolysis in foods a comparison of not reduced (direct hydrolysed) and reduced food samples was carried out. The CML values in the food samples after reduction were only 8–55% of the data obtained in the samples without reduction (Fig. 4). All CML values obtained by the borohydride procedure were significantly lower than CML data in food samples described before. Due to the fact that the ratio of formation of CML during acid hydrolysis is not constant it seems to be not possible to correct mathematically older data from CML analyses of not reduced samples.

The lowest CML contents of the analyzed foods were determined in a preparation from mixed cereals for infants (11 mg) and in a sausage (23 mg CML/kg protein). This indicates a short and slight heat treatment during the processing. On the other hand, the highest CML contents were obtained in a condensed milk (390

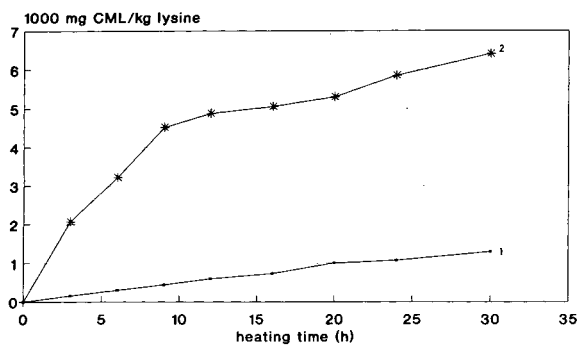

Fig. 3. Comparison of the CML levels (1000 mg CML/kg lysine) in the reduced (1) and not reduced (2) model samples.

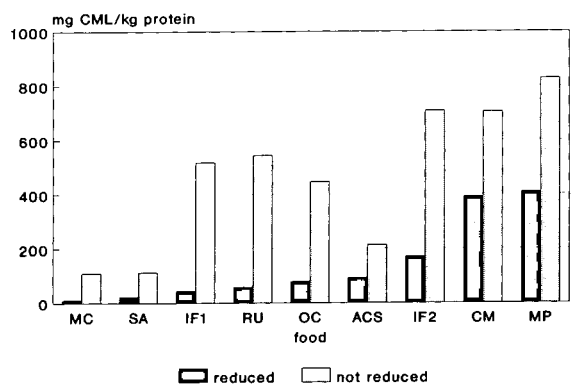

Fig. 4. Comparison of the CML levels (mg CML/kg protein) in the reduced and not reduced food samples. MC = Preparation from mixed cereals for infants; SA = sausage; IF1 = infant formula 1; RU = rusk; OC = oat cereals; ACS = asparagus creme-soup; IF2 = infant formula 2; CM = condensed milk; MP = processed malt product.

mg) and in a processed malt product (408 mg CML/kg protein), foods which were treated severely during processing. This confirms the conclusion that CML is suited as an indicator for heat damage in foods.

References

[1] J. Hartkopf and H.F. Erbersdobler, *J. Chromatogr.*, 635 (1993) 151–154.
[2] M.U. Ahmed, S.R. Thorpe and J.W. Baynes, *Fed. Proc.*, 44 (1985) 1621.
[3] M.U. Ahmed, S.R. Thorpe and J.W. Baynes, *J. Biol. Chem.*, 261 (1986) 4889–4894.
[4] J.A. Dunn, M.U. Ahmed, M.H. Murtiashaw, J.M. Richardson, M.D. Walla, S.R. Thorpe and J.W. Baynes, *Biochemistry*, 29 (1990) 10 964–10 970.
[5] U. Albrecht, J. Hartkopf and H.F. Erbersdobler, *Ernährungsumschau*, 39 (1992) 164.
[6] J.A. Dunn, D.R. McCance, S.R. Thorpe, T.J. Lyons and J.W. Baynes, *Biochemistry*, 30 (1991) 1205–1210.
[7] K.J. Knecht, J.A. Dunn, K.F. McFarland, D.R. McCance, T.J. Lyons, S.R. Thorpe and J.W. Baynes, *Diabetes*, 40 (1991) 190–196.
[8] W. Büser, H.F. Erbersdobler and R. Liardon, *J. Chromatogr.*, 387 (1987) 515–519.
[9] W. Büser and H.F. Erbersdobler, *Milchwisssenschaft*, 41 (1986) 780–785.
[10] G. Lüdemann, *Untersuchungen über Entstehen und Vorkommen von N^{ϵ}-Carboxymethyllysin in Lebensmitteln* (*Agr. Sci. Dissertation Series*, Vol. 6), Institut für Humanernährung und Lebensmittelkunde, University of Kiel, Kiel, 1989.
[11] R. Badoud, F. Hunston, L. Fay and G. Pratz, in P.A. Finot, H.U. Aeschbacher, R.F. Hurrell and R. Liardon (Editors), *The Maillard Reaction in Food Processing, Human Nutrition and Physiology* (*Advances in Life Sciences*), Birkhäuser, Basel, Boston, Berlin, 1990, pp. 79–84.
[12] R. Liardon, D. de Weck-Gaudard, G. Philippossian and P.-A. Finot, *J. Agric. Food Chem.*, 35 (1987) 427–431.
[13] J. Hartkopf and H.F. Erbersdobler, *Z. Lebensm.-Unters.-Forsch.*, 198 (1994) 15–19.

ELSEVIER

Journal of Chromatography A, 672 (1994) 247–253

JOURNAL OF CHROMATOGRAPHY A

Short Communication

High-performance liquid chromatographic separations of nystatin and their influence on the antifungal activity ☆

B. Sauer, R. Matusch *

Institut für Pharmazeutische Chemie, Philipps-Universität, Marbacher Weg 6, D-35032 Marburg/Lahn, Germany

(First received October 12th, 1993; revised manuscript received March 22nd, 1994)

Abstract

Several efficient analytical HPLC methods for the separation and comparison of the nystatin complex have been developed. These separations have been extended to the preparative scale in order to gain sufficient quantities of the purified nystatin components for testing antifungal activity. For the first time we describe a new HPLC method which does not affect the antifungal activity of nystatin.

1. Introduction

Polyenic antibiotics are very important substances for the treatment of fungal infections. The first member of this group of antibiotics was nystatin (Fig. 1), which was discovered in 1950 by Hazen and Brown [1]. It is produced by *Streptomyces noursei* and can be separated from the culture broth by extraction with organic solvents [2].

As a result of this methodology commercial available nystatin —as most of the other polyene antibiotics— is a complex mixture of closely related compounds. In order to obtain sufficient quantities of single, well purified antifungal substances it is therefore necessary to develop a method for the separation of the nystatin complex, which is rapid and selective and also preserves the antifungal activity of the isolated compounds.

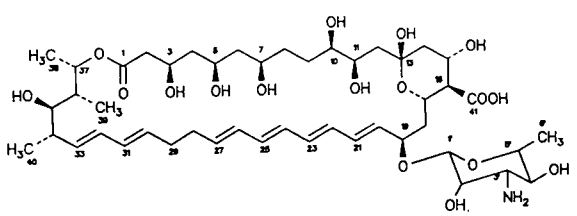

Fig. 1. Structure of nystatin A_1.

During the last twenty years methods using HPLC turned out to be the most efficient and reliable separation techniques for the isolation and analytical comparison of polyene antibiotics. Mechlinsky and Schaffner [3] were the first to publish analytical HPLC methods for the separation of polyene antibiotics. Hansen and Thomsen [4] described a HPLC technique for the comparison of some polyene antibiotics using phosphate buffer–methanol eluents as mobile phase. Thomas *et al.* [5] as well as Margosis and Aszalos [6] used mobile phases with reduced pH values by applying different buffers. Several authors described HPLC methods using acetonitrile instead of methanol [7–10].

* Corresponding author.

☆Dedicated to Professor Dr. B. Unterhalt, Münster, Germany, on the occasion of his 60th birthday.

0021-9673/94/$07.00
SSDI 0021-9673(94)00291-G

However, none of these analytical systems was adapted to the preparative scale, since the use of buffers causes great difficulties in removing the solvent after the separation, a step which is essential for further investigations with the separated substances. So far there are only two semi-preparative methods, which have been described by Gareil *et al.* [11] and by Milhaud *et al.* [12] who used methanol–water–dimethyl sulphoxide and methanol–water–dimethylformamide–acetic acid as mobile phases, respectively. However, both publications do not give any information about the antifungal activity after the separation.

In this paper we present three different efficient analytical HPLC methods, which are all extended to the preparative scale. Furthermore, we discuss the results of the microbiological assays, which were carried out with the different fractions after the separation. Finally, we present a rapid preparative HPLC method, that allows the purification of high amounts of nystatin and does not affect the antifungal activity of the isolated substances.

2. Experimental

2.1. Instruments

For the analytical separations we used a liquid chromatograph consisting of the following components all supplied by Waters (Milford, MA, USA): HPLC pump type 600 E, photodiode array detectors types 990 and 991 and graphic plotter. Data processing was conducted on a NEC APC III and IV.

The preparative separations were carried out on a liquid chromatograph consisting of two preparative ERC pumps type 64, an ERC UV detector type 7210 (Alteglofsheim, Germany) and a potentiometric recorder produced by Schoeffel (Westwood, NY, USA). Both chromatographs were equipped with a Rheodyne (Cotati, CA, USA) injection valve.

The solvents of the separated fractions were removed using a membrane pump and a vacuum controller constructed by Vaccuubrand (Wertheim, Germany).

2.2. Instrument operation

The detectors were started half an hour before the operation of the chromatograph. The column packings were conditioned with about 15 column volumes of the solvent system. After reaching a constant baseline on the screen or on the recorder, the samples were injected using a Hamilton HPLC syringe (Reno, NV, USA).

2.3. Solvent systems and columns

For the analytical separations we used two columns (250 × 4.0 mm), packed with LiChrospher RP-18 (5 μm) material or with LiChrosorb RP-18 (7 μm) material, respectively, both supplied by Merck (Darmstadt, Germany). The preparative separations were carried out on a column (250 × 25 mm), packed with LiChrosorb RP-18 (7 μm) material and supplied by Merck.

The following mobile phases were used: (I) methanol–water (90:10) + 1% formic acid, pH 3.5; (II) acetonitrile–trifluoroacetic acid 0.02 *M* (50:50), pH 2.7; (III) methanol–water–dimethylformamide (70:20:10), pH 7. All solvent mixtures were degassed with helium before operating the chromatograph.

2.4. Chemicals

The organic solvents were of analytical-reagent or LiChrosolv quality and were supplied by Merck. The water was bidistilled or purified by using a Seralpur Pro 90 C instrument of Seral (Ransbach-Baumbach, Germany). Nystatin was supplied by Serva (article No. 29870; Heidelberg, Germany). The samples were prepared by dissolving nystatin in the solvent mixture to concentrations of 1–5 mg/ml for analytical separations and 10 mg/ml for preparative separations.

2.5. Microbiological assay

Microbiological assays, measuring the activity against *Candida albicans* ATCC 10231 and *Candida tropicalis* ATCC 70156, were conducted by

Heumann (Nürnberg, Germany) using the agar-dilution method DIN 58940.

3. Results and discussion

3.1. Chromatography

The aim of this investigation was to develop a HPLC method which allows the separation of high amounts of nystatin without affecting the antifungal activity of the isolated substances. Therefore we had to take into consideration the poor solubility of the polyene antibiotics in most organic solvents when choosing the mobile phase. On the other hand the mobile phase had to be easily removable since the analytical method had to be extended to the preparative scale. Nystatin, as most of the polyene antibiotics, is an ampholyte (Fig. 1). Therefore its solubility is strongly pH-dependent. Solvent systems with lowered pH values have been shown to be useful for the separation of polyene antibiotics [5,6]. As it was not possible to use a buffer because of the difficulties in removing it after the separation, we chose two organic acids —formic acid (pK_a =

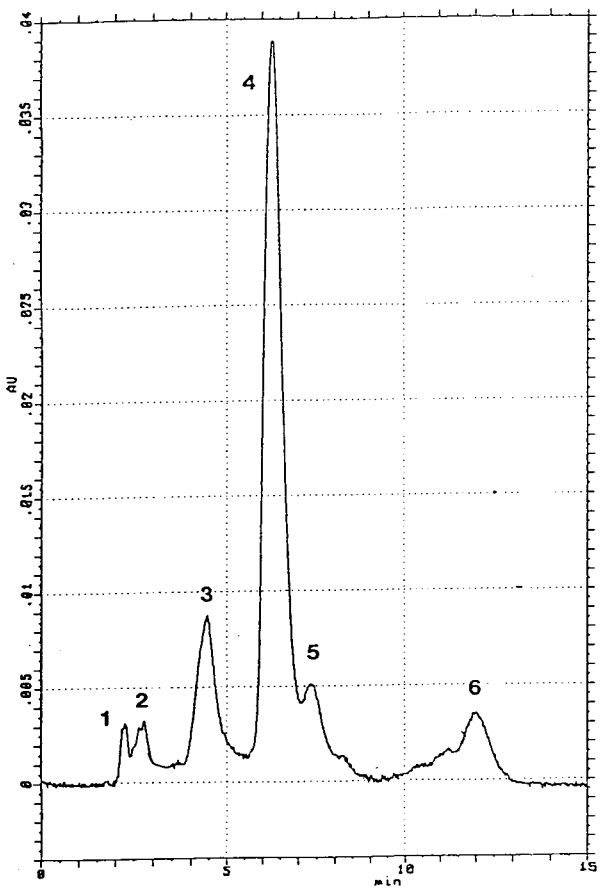

Fig. 2. Analytical chromatogram of nystatin. Stationary phase, LiChrosorb RP-18 (7 μm), 250 × 4.0 mm; mobile phase, methanol–water (90:10) + 1% formic acid, pH 3.5; flow-rate, 1 ml/min; UV at 340 nm; injection volume, 10 μl; sample, 1 mg/ml solution in the solvent mixture. Peaks numbered for comparison with other figures.

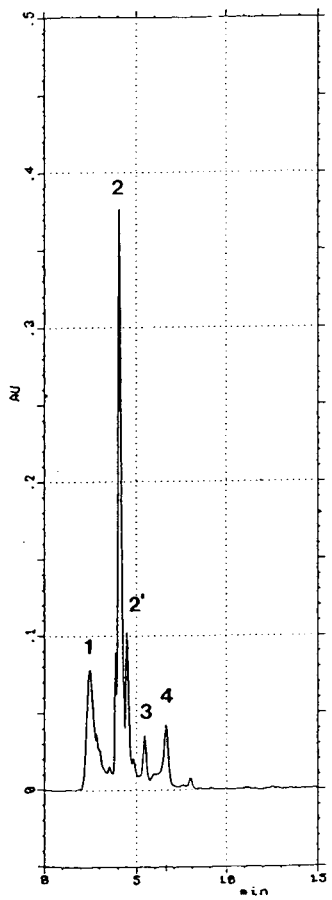

Fig. 3. Analytical chromatogram of nystatin. Stationary phase, LiChrospher RP-18 (5 μm), 250 × 4.0 mm; mobile phase, acetonitrile–trifluoroacetic acid 0.02 *M* (50:50), pH 2.7; flow-rate, 1 ml/min; UV at 340 nm; injection volume, 20 μl; sample, 5 mg/ml solution in the solvent mixture.

3.7) and trifluoroacetic acid ($pK_a = -3$)—which can both easily be removed together with the organic solvent. A major disadvantage of these solvent systems is the instability of polyene antibiotics in solutions with reduced pH values, and it is therefore necessary to work quickly and carefully.

To overcome this problem, we used a third mobile phase with pH 7 consisting of a methanol–water–dimethylformamide mixture, since dimethylformamide is a good organic solvent for polyene antibiotics.

Figs. 2–4a show the analytical chromatograms of nystatin and Fig. 4b its preparative chromatogram under different experimental conditions. All three solvent systems are very useful for the analytical HPLC of nystatin and allowed the separation of five to six peaks in a short time (12–18 min). The chromatogram in Fig. 4a was recorded at two different wavelengths (305 nm, 385 nm) in order to show the deviating structure of peak 5, which is a heptaene, whereas the main peak 3 is a tetraene and corresponds to nystatin A_1. The difference in the polyenic chain of the molecules is expressed in the very characteristic UV–Vis spectra, which are shown in Fig. 5. The

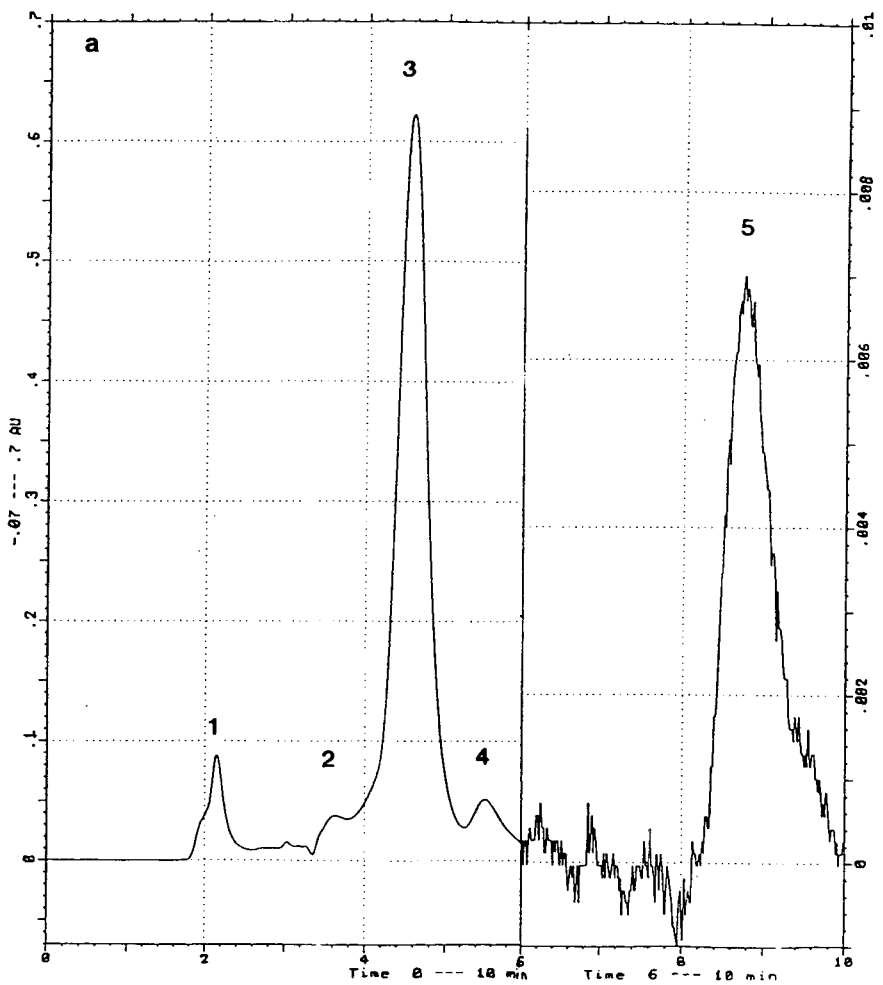

Fig. 4.

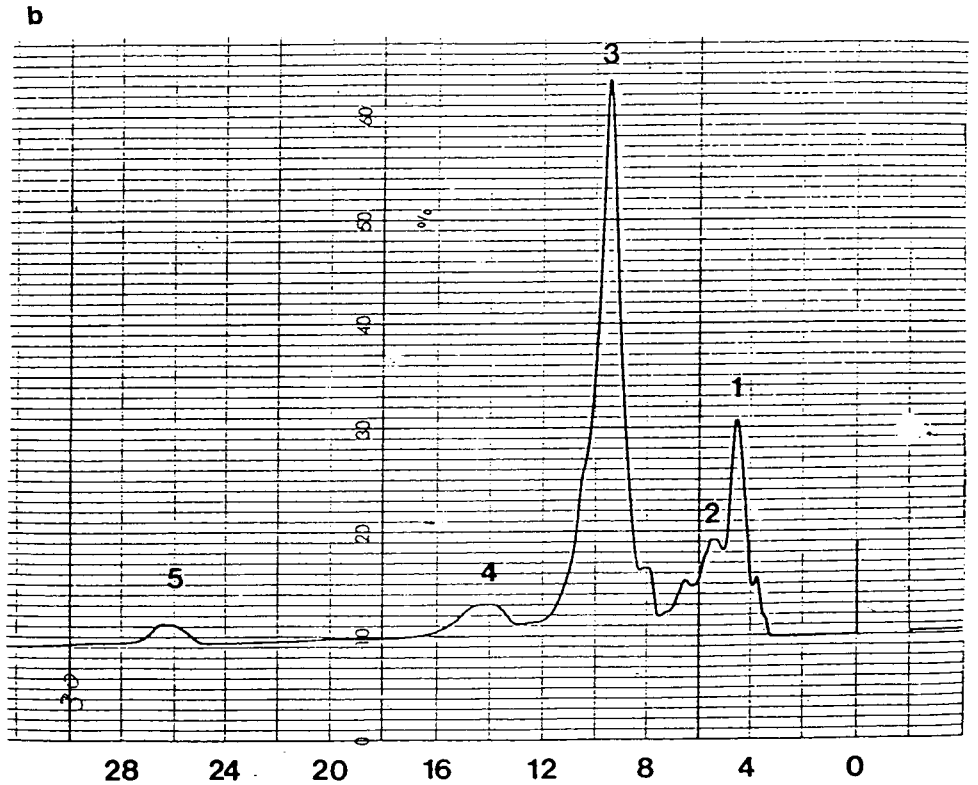

Fig. 4 (a) Analytical chromatogram of nystatin. Stationary phase, LiChrosorb RP-18 (7 μm), 250 × 4.0 mm; mobile phase, methanol–water–dimethylformamide (70:20:10); flow-rate, 1 ml/min; UV at 305 (left) and 385 (right) nm; injection volume, 5 μl; sample 1 mg/ml solution in the solvent mixture. (b) Preparative chromatogram of nystatin. Stationary phase, LiChrosorb RP-18 (7 μm), 250 × 25 mm; mobile phase, methanol–water–dimethylformamide (70:20:10); flow-rate, 15 ml/min; UV at 340 nm; injection volume, 5 ml; sample, 10 mg/ml solution in the solvent mixture.

presence of a heptaene in some nystatin complexes has been observed before [3,13] but its structure is still unknown.

The preparative chromatogram also shows a separation of five fractions in 28 min (Fig. 4b). Although there is an overlapping of some fractions, at least the main fraction (nystatin A_1) and the last fraction (the heptaene component) can be purely separated. This was checked by NMR spectroscopy and analytical HPLC with diode array detection. This method is also very efficient, as high amounts of nystatin can be purified by one separation (50 mg).

3.2. Microbiological assay

After the separation of 100 mg of nystatin with the different methods microbiological assays were carried out on the collected fractions in each case. Table 1 shows the minimal inhibitoric concentrations of the tested fractions against *Candida albicans* and *Candida tropicalis*. It is evident that the purification with the methanol–water–dimethylformamide mixture (pH 7) does not affect the antifungal activity of nystatin A_1 at all, whereas after the separation with the two acidic solvent systems all fractions have lost their antifungal activity (MIC of the reference = 2 μg/ml). Obviously the low pH value causes an

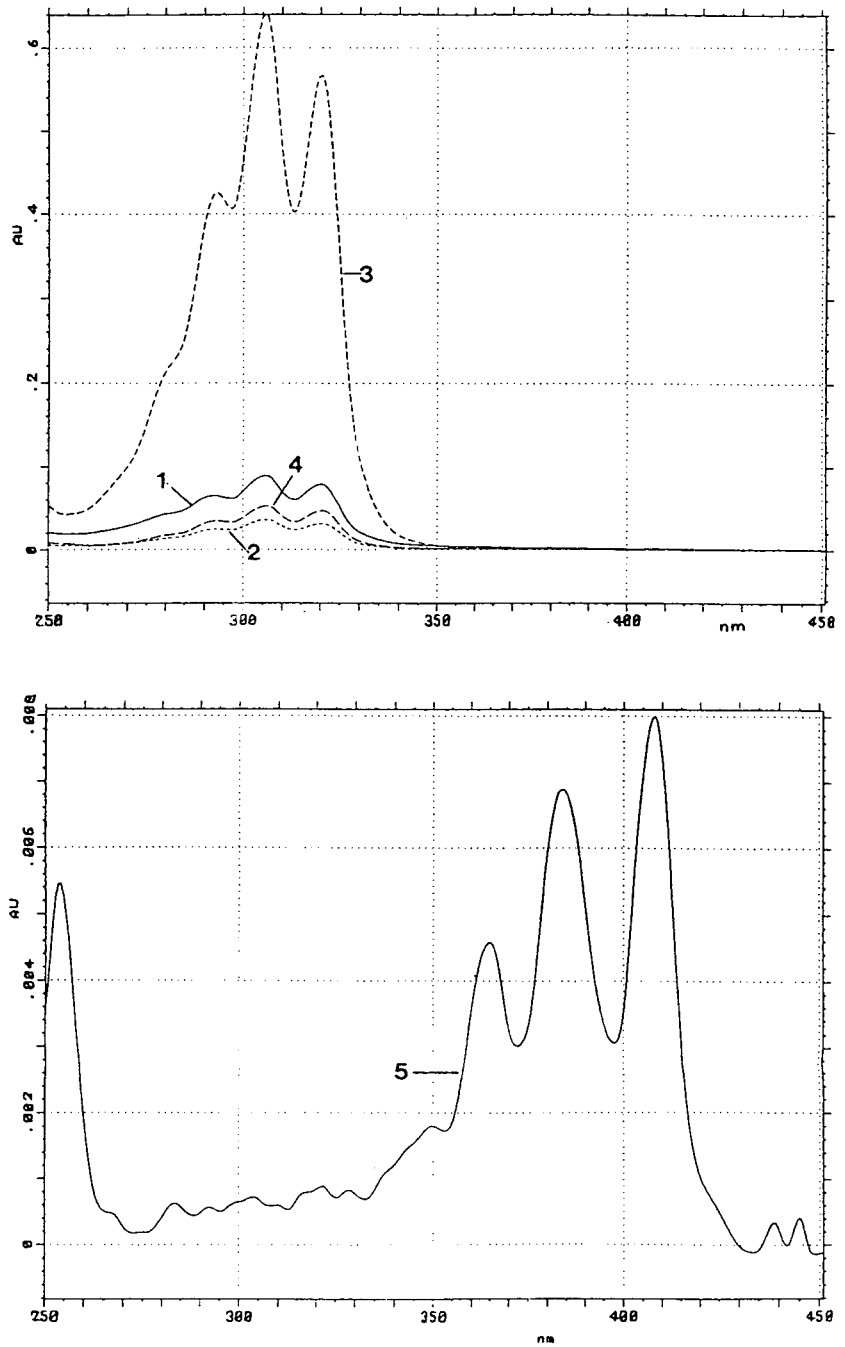

Fig. 5. UV–Vis spectra of the peaks 1–5 shown in Fig. 4a.

Table 1
Minimal inhibitory concentrations (MIC) of the nystatin fractions shown in Fig. 4b

Fraction	MIC (g/ml)	
	Candida albicans	*Candida tropicalis*
Fraction 1/2	>125	>125
Fraction 3	2	4
Fraction 4	3	4
Fraction 5	8	8
Reference (nystatin)	2	2

alteration in the structure of the molecules so that they are no longer able to form complexes with the membrane sterols, which is discussed to be their mode of action [14].

4. Conclusions

In conclusion, our data show that although all three presented HPLC methods are rapid and efficient for an analytical separation of nystatin, only the one using a methanol–water–dimethylformamide mixture with neutral pH value is applicable to the preparative purification of nystatin, since it is the only system which does not affect the antifungal activity of the separated components. The use of this method allows the separation of the nystatin complex into five fractions, of which the main component nystatin A_1 (fraction 3) and the heptaene component (fraction 5) can be obtained purely.

References

[1] E.L. Hazen and R. Brown, *Science*, 112 (1950) 423.
[2] G.W. Michel, in K. Florey (Editor), *Analytical Profiles of Drug Substances*, Academic Press, New York, 1977, Vol. 6, p. 341.
[3] W. Mechlinsky and C.P. Schaffner, *J. Chromatogr.*, 99 (1974) 619.
[4] S.H. Hansen and M. Thomsen, *J. Chromatogr.*, 123 (1976) 205.
[5] A.H. Thomas, P. Newland and G.J. Quinlan, *J. Chromatogr.*, 216 (1981) 367.
[6] M. Margosis and A. Aszalos, *J. Pharm. Sci.*, 73 (1984) 835.
[7] P. Helboe, M. Thomsen and S.H. Hansen, *J. Chromatogr.*, 189 (1980) 249.
[8] J.W. Mayhew, C. Fiore, T. Muray and M. Barza, *J. Chromatogr.*, 274 (1983) 271.
[9] A.H. Thomas and P. Newland, *J. Chromatogr.*, 354 (1986) 317.
[10] M.B. Swami, M.K. Sastry, A.G. Nirgudkar and R.K. Nanda, *Hind. Antibiot. Bull.*, 25 (1983) 81.
[11] P. Gareil, G. Salinier, M. Caude and R. Rosset, *J. Chromatogr.*, 208 (1981) 365.
[12] J. Milhaud, P. Gareil and R. Rosset, *J. Chromatogr.*, 358 (1986) 284.
[13] N. Porowska, L. Malski, Z. Plociennik, D. Kotiuszko, H. Morawska, Z. Kowszyk-Gindifer and H. Bojarska-Dahling, *Adv. Antimicrob. Antineoplast. Chemother.*, 1 (1972) 1031.
[14] R.W. Holz, *Ann. N.Y. Acad. Sci.*, 235 (1974) 469.

ELSEVIER

Journal of Chromatography A, 672 (1994) 254–260

JOURNAL OF CHROMATOGRAPHY A

Short Communication

Use of esterified and unesterified dipentylated γ-, β- and α-cyclodextrins as gas chromatographic stationary phases to indicate the structure of monoterpenoid constituents of volatile oils

T.J. Betts

School of Pharmacy, Curtin University of Technology, GPO Box U1987, Perth, Western Australia 6001, Australia

(First received January 4th, 1994; revised manuscript received March 11th, 1994)

Abstract

"Chiraldex-G-DA", unesterified dipentylated γ-cyclodextrin, yields a twenty-nine solute sequence distinctively different to other cyclodextrin modifications and to conventional stationary phases, particularly retaining bicyclic molecules. Percentage increases in relative retention times to *n*-undecane from the α-cyclodextrin corresponding phase are very indicative of solute structure: acyclics less than 60%, bicyclics over 150%, with monocyclics between. Percentage increases are also discussed from α- to γ-ester dipentylated cyclodextrins; from unesterified to esterified "G-PN" γ-phases; and between the two β-phases. With the lattermost pair, carbonyl solutes show increased values on the β-ester "B-TA" if not bicyclic, whilst alcohols increase on the unesterified phase except for some acyclics. Plots of values for some solutes on the three phases (both the esterified and unesterified) suggest that only sometimes may inclusion complexing be involved with the cyclodextrin rings —usually the largest. A solute is likely to have a different pattern on the esterified phases.

1. Introduction

Some modified cyclodextrins were introduced for the gas chromatography of enantiomers by Armstrong and Jin [1] in 1990. They used dipentylated cyclodextrins initially ("DA" meaning dialkyl), and then esterified the third glucose hydroxyl group to prepare dipentylated cyclodextrins with a 3-O-trifluoroacetyl ("TA") ester on each α-glucose unit in the rings [2]. The present author has used some of these phases since 1991 for non-enantiomeric studies of the constituents of volatile oils; on the dipentylated-hydroxy smallest ring α-cyclodextrin "Chiraldex-A-DA" [3–5], the similar intermediate-sized ring β-cyclodextrin ("B-DA") [4] and the esterified derivative "A-TA" [5].

Having noted some structurally informative graphic response patterns for terpenoids by comparing results for the dipentylated α- and β-cyclodextrins [4], it was of interest to try the largest eight-glucose (γ-) cyclodextrins for these solutes. The biggest ring phases are available as dipentylated Chiraldex-G-DA and -G-PN, where instead of the one free hydroxyl per α-glucose unit of DA, the PN phase is the 3-O-propionate. "This phase was designed to extend the scope of the (temperature-limited) Chiraldex-G-TA" phase, with some "enhanced selectivity" and "increased sensitivity" [6]. The β-cyclodextrin-

0021-9673/94/$07.00
SSDI 0021-9673(94)00286-I

TA phase was also studied, so that results could be compared on both sets of three dipentylated cyclodextrins, either with the remaining glucose hydroxyl present, or with this esterified.

2. Experimental

2.1. Materials

A Hewlett-Packard 5790A gas chromatograph was used, fitted with a capillary control unit, and a splitter injection port and flame ionisation detector, both set at 235°C. A Hewlett-Packard 3380A recorder/integrator was attached.

"Chiraldex" capillaries were obtained from Advanced Separation Technologies (ASTEC, Whippany, NJ, USA). A-TA and G-PN were purchased and G-DA and B-TA were kindly donated. They were all 10 m × 0.25 mm I.D. with film thickness given as 0.125 mm ± 10%. They were heated and cooled at 10°C min^{-1} to preserve the phases. Helium was the mobile phase, used at flow-rates of 0.55–0.95 ml min^{-1}, and also as the "makeup" gas to the detector.

Monoterpenoid solutes used were from various commercial sources.

2.2. Methods

Monoterpenoid solutes were injected as trace residues from a microsyringe which had been filled and "emptied". A few aromatic constituents found in some volatile oils were used for comparison. Main peaks were used if solutes were found to be impure. Holdup times were deducted, obtained by extrapolating to methane the retention times for *n*-heptane and *n*-hexane plotted on semi-logarithmic graph paper.

3. Results and discussion

Average results are presented in Table 1 and in Figs. 1 and 2, involving comparison with previous reports [4,7,8]. Ranges of values are quoted on Chiraldex-G-DA, being dose-dependent, in column 3 of Table 1. Berthod *et al.* [9] noted a group of solutes which "should not tolerate overloading . . . (as these) compounds or one of their enantiomers may be forming a dominant enantioselective inclusion complex. The large entropy decrease of the group . . . may be due to the loss of degrees of freedom for the compound included in the (cyclodextrin) cavity". Camphor gives unsharp peaks below 170°C; and the similarly bicyclic borneols emerge even more slowly, without giving good peaks, even at 190°C. The bicyclic sesquiterpene hydrocarbon caryophyllene also gives broad peaks. Relative retention times are used, having previously [5] proved more valuable than retention indices. Six solutes, citral to cuminal in the table, emerge in close sequence, and show ranges of values which overlap. Noteworthy features, which are special for Chiraldex-G-DA, are that (i) cineole is retained more strongly than linalol and citronellal, (ii) fenchone is retained after estragole and menthone, as well as the previous two solutes, (iii) menthol emerges after citral and pulegone and (iv) camphor is more strongly retained than all the other solutes (except borneols) in the table —yet on conventional phases, it would be no later than sixth in sequence after linalol (see column 16). The whole solute sequence on Chiraldex-G-DA is distinctive, compared to the other phases in Table 1, in showing relatively less retention of acyclic aldehydes citral and citronellal, and of aromatics estragole and *p*-cymene. Stronger retention is apparent for bicyclics, and monocyclic monoene ketones piperitone and pulegone.

The percentage increase in relative retention times on changing to the γ (G) from the α-dipentylated (A-DA) *hydroxy*cyclodextrin (Table 1, column 4) at 150°C seems spectacularly indicative of terpenoid structure. Acyclics (N) examined all show less than 60% increase with citral being as low as 13%. The monocyclics (M) at 150°C have increases of 65–91%; but the bicyclics (B) show much greater values, 157% and more. At 125°C bicyclic cineole also has a much higher relative retention value on the G-phase than limonene or other hydrocarbons, including γ-terpinene (see Table 1, column 6). Also the other rigid bicyclics, the pinenes and

camphene, emerge after γ-terpinene —they come first from conventional phases (see column 16 in Table 1). The bicyclic 3-carene, which is not rigid as it has a three-carbon side chain that can rotate, still shows a three figure percentage increase in relative retention times going to the G phase from A-DA (column 8). This is less than, but like other bicyclics (B) at 125°C (column 7). The two oxygenated aromatics show increases of only 20% or less at 150°C (cuminal and estragole, in column 4, Table 1).

In Fig. 1, a number of solutes show a virtual linear increase in relative retention time on changing from α- to β- to γ-*hydroxy*dipentylated cyclodextrins. Thus so for thujone, linalol, citronellal, menthone, menthol, carvone and citronellol (and the borneols?) on the unesterified phases (T, L, A, K, –, V, O, B, respectively in Fig. 1). In contrast, the upward angled plots of fenchone, pulegone, citral, geraniol, camphor (and piperitone?) reveal evidence of special interaction with the γ-phase, as their slope increases sharply from β-cyclodextrin values (F, P, C, G, H –, respectively). The manufacturers of these phases say that "inclusion complexing . . . is the basic driving mechanism" [6] for the dipentylhydroxycyclodextrins —not, it would appear, for monoterpenoids by the α-rings except possibly for citral and geraniol which are flexible acyclics and have higher values on this phase than on the larger B-DA rings. Fenchone, pulegone and camphor have rigid molecules, which could facilitate interaction with the γ-rings whereas thujone, menthone and menthol possess a rotatable three-carbon side chain (like piperitone!) and do not. The pattern in Fig. 1 for acylic citral (and geraniol?) suggests that the β-phase cavities may reject it, unlike citronellol (C, G, O, respectively); whilst this intermediate size ring phase could accept α-terpineol (and 4-terpineol?) equally as readily as the larger γ-ring phase (α, 4 in Fig. 1). Although monocyclic, α-terpineol is distinctive in having its oxygen "concealed" within the rotatable side chain. α-Terpineol and menthol enantiomers were separated by Kobor and Schomburg [10] on both the α- and β-rings (but not the γ-) of a different unesterified cyclodextrin (dimethyl, tertiary-butyldimethylsilyl) derivative. Their β modification gave highest α value separation for α-terpineols and thus agrees with the observation here, except that my unesterified γ-cyclodextrin is just as useful; but not the α-ring. My results for menthol indicate no favoured ring-size (see Fig. 2, M) and Kobor and Schomburg agreed by finding the same α-values on both the α- and β-cyclodextrins. They only obtained enantiomeric separation of linalols using their β-phase.

The γ-cyclodextrin with an *esterified* hydroxyl along with the dipentyl substitution (G-PN) shows some of the features seen above, but not all in Table 1, column 9. The dose-dependence is not a factor as it is for G-DA. Considering the solute elution sequence, citral and citronellal are relatively more strongly retained (acyclic aldehydes); but camphor, menthol, fenchone, thujone, cineole (mostly bicyclics) and some hydrocarbons less so than on G-DA. The change from the α-(A-TA) to γ-(G-PN) esterified cyclodextrins at 125°C (column 10) sees a three-figure percentage increase for oxygenated bicyclics other than cineole. This, and some hydrocarbon bicyclics still increase by 83% or more; but so do monocyclics piperitone and pulegone. Increases of less than 40% are typical of terminally oxygenated acyclics (*i.e.* not acyclics linalol and myrcene) particularly citral, which is thus distinctive on both esterified and non-esterified γ-cyclodextrin modifications. Fast-emerging solutes examined at 125°C have lower relative retention times on the esterified γ-cyclodextrin (PN) than on the corresponding hydroxyl DA phase (columns 6 and 9). The two α-cyclodextrin phases show closely similar values (columns 8 and 11).

Fig. 2, for α-, β- and γ-*esterified* dipentylated cyclodextrins shows similarities and differences to Fig. 1. As before, a number of solutes show a virtual linear increase in relative retention times. Menthol and citronellol again do this (but not the other solutes mentioned before) and also fenchone, α-terpineol and some more (M, O, F, α, respectively). There are upwardly angled plots, as before, now for camphor and the borneols (but not the others previously listed) and for some faster emerging bicyclics like

Table 1
Relative retention times (*n*-undecane = 1.00) on modified dipentyl cyclodextrin capillaries at two temperatures

Solute	Type[a]	Column No. in this table					
		3: Chiraldex-G-DA at 150°C	4: % increase ← α- to γ-CD	5: Chiraldex-A-DA at 150°C [4]	6: Chiraldex-G-DA at 125°C	7: % increase ← α- to γ-CD	8: Chiraldex-A-DA at 125°C [4]
Borneol	B	>12 at 170°C		*3.57*[b]			*3.84*
Isoborneol	B			*3.33*			*3.45*
Camphor	B	9.00 (±0.07)	341	*2.04*			*1.86*
Geraniol	N	7.15 (±0.18)	42	5.04			6.36
Piperitone	M	6.85 (±0.18)	91	*3.59*			*3.70*
Cuminal	A	6.00 (±0.11)	20	5.01[c]			5.09[c]
Citronellol	N	5.90 (±0.27)	38	4.27			5.11
Carvone	M	5.85 (±0.22)	65	3.54			3.54
Menthol	M	5.80 (±0.23)	74	3.33			↑ *3.73*
α-Terpineol	M	5.75 (±0.32)	80	3.19			3.47
Citral	N	5.70 (±0.20)	13	↑ *5.02*			↑ *5.93*
Pulegone	M	5.35 (±0.12)	88	*2.84*			2.77
4-Terpineol	M	4.95 (±0.25)	72	2.88			2.85
Fenchone	B	4.00 (±0.13)	210	*1.29*			*1.16*
Estragole	A	3.55 (±0.09)	12	↑ *3.18*[c]			↑ *3.19*[c]
Thujone	B	3.50 (±0.17)	157	*1.36*	3.76	203	*1.24*
Menthone	M	3.35 (±0.10)	81	1.85			1.73
Cineole	B	2.80 (±0.10)			2.95 (±0.16)	288	*0.76*
Linalol	N	2.40	54	1.56	2.72	73	1.57
Citronellal	N	2.40	34	↑ *1.79*	2.60 (±0.09)	44	↑ *1.81*
β-Pinene	B				1.84	268	*0.50*
Camphene	B				1.75	349	*0.39*
γ-Terpinene	M				1.27	69	0.75
3-Carene	B				1.27	115	*0.59*
Limonene	M				1.22	85	0.66
α-Pinene	B				1.12	203	*0.37*
p-Cymene	A				1.10	67	0.66
α-Terpinene	M				0.97	73	0.56
Myrcene	N				0.74	76	0.42

Using γ-(G), β-(B) or α-(A) cyclodextrins (CDs) with either one remaining hydroxyl group per α-glucose unit (-DA) or else esterified with trifluoracetic (-TA) or propionic (-PN) acid. Average values, with range for G-DA phase.
[a] A = Aromatic; B = bicyclic; M = monocyclic; N = acyclic.
[b] Values in italics are not in the sequence for Chiraldex-G-DA (lower, unless with an upward pointing arrow).
[c] Estimated from ref. 5.
[d] Direction of increase shown by arrow.

cineole, camphene and β-pinene which may be due to inclusion complexing with the γ-rings (H, B, N, E, –, respectively, in Fig. 2). A new feature is the large number of solutes on the β-esterified phase (B-TA) showing values almost as large as on the corresponding γ-cyclodextrin; hydrocarbons like α-terpinene and myrcene; linalol, menthone, pulegone and piperitone (R, Y, L, K, P, –, respectively, in Fig. 2). Several solutes are distinctive in exhibiting highest relative retention values preferentially for the β-esterified cyclodextrin (see Table 1, columns 9,

Column No. in this table							
9: Chiraldex-G-PN at 125°C	10: % increase ← α- to γ-CD	11: Chiraldex-A-TA at 125°C	12: Chiraldex-B-TA at 125°C	13: % increase[d] β-TA/DA-CD	14: Chiraldex-B-DA at 125°C [4]	15: % increase γ-PN to DA	16: Elution sequence [7,8] on methyl-polysiloxane
10.46	189	*3.62*	*4.68*	79→	8.36		18
9.78	187	*3.41*	*4.22*	84→	7.78		17
6.04	208	*1.96*	*3.19*	26→	*4.01*		14
7.69	36	5.66	7.13	← 8	6.60		28
7.17	99	*3.60*	*6.54*	←32	*4.96*		27
6.55	34	4.88	7.13				24
6.54	38	4.74	*5.81*	10→	6.40		23
5.98	74	3.43	6.34	←20	5.30		25
5.54	54	*3.59*	*4.45*	33→	↑ *5.92*		19
5.75	75	3.29	4.87	43→	↑ *6.96*		22
↑ *6.33*	5	↑ *6.03*	↑ *8.25*	←56	5.27		29
5.04	85	*2.73*	↑ *4.90*	←28	*3.83*		26
4.39	58	2.77	3.80	38→	5.26		20
2.59	123	*1.16*	*1.91*	6→	*2.02*		11
3.93	39	↑ *2.82*	3.78				21
2.85	126	*1.26*	*2.54*	6→	*2.69*	32	13
3.12	81	1.72	2.90	← 4	2.80		16
1.39	83	*0.76*	*0.98*			112	8
2.42	68	1.44	2.30	← 2	2.26	12	12
↑ *2.46*	39	↑ *1.77*	↑ *2.74*	←21	2.26	6	15
0.95	83	*0.52*	*0.69*			94	3
0.82	95	*0.42*	*0.56*			113	2
1.14	54	0.74	1.09			11	10
0.91	54	*0.59*	*0.82*			40	5
0.99	48	0.67	0.94			23	9
0.64	73	*0.37*	*0.48*			75	1
↑ *1.04*	53	↑ *0.68*	↑ *1.03*			6	7
0.87	55	0.56	0.86			11	6
0.67	56	0.43	0.63			10	4

11, 12) —citronellal, carvone, cuminal and citral (A, V, –, C, respectively) which have the common feature of a carbonyl-group that may facilitate inclusion in these medium-sized rings. Some other ketones exhibit a tendency towards this, but not all (not fenchone, nor camphor, which may have this effect counteracted by their bicyclic structures promoting enhanced γ-ring retention). The previously observed superiority of their β-cyclodextrin modification by Kobor and Schomburg [10] is seen here on the esterified phase with carbonyl-terpenoids; but not with alcoholic terpenoids, as they found. Their explanation for hydrocarbons was that their α-cyclodextrin "is too small to be entered by the pinene (and camphene) molecules whereas the cavity of (their γ-phase) is too big". No such preference was detected here for camphene (E) or other hydrocarbons (R, Y in Fig. 2). However, interactions with solutes must be influenced by the chemical modifications made to each set of three cyclodextrin phases. Andrews *et al.* [11] considered "with the larger γ cavity (of the trifluoroacetyl ester) all isomers (of naphthalene)

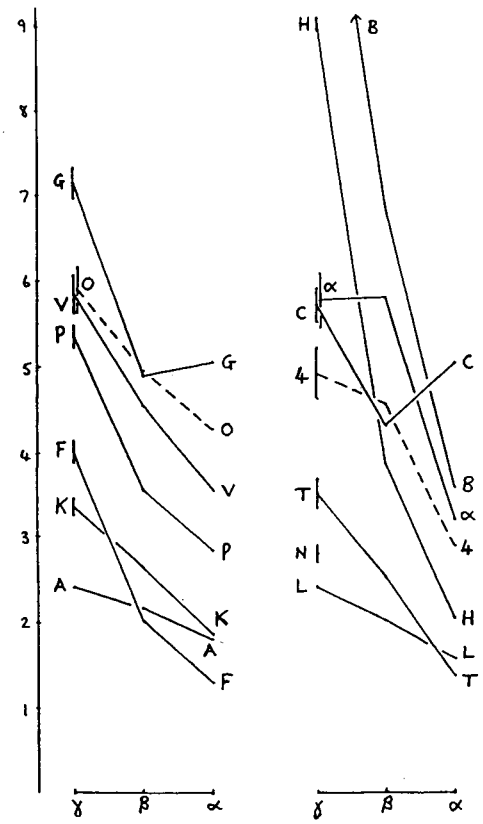

Fig. 1. Linked plots of average relative retention times (*n*-undecane = 1.00) (*y* axis) of some solutes on γ-, β- and α-hydroxy dipentylated cyclodextrins (Chiraldex DA phases) at 150°C. Ranges of results on the γ-phase shown by vertical lines. A = Citronellal; B = borneol; C = citral; F = fenchone; G = geraniol; H = camphor; K = menthone; L = linalol; N = cineole; O = citronellol; P = pulegone; T = thujone; V = carvone; α = α-terpineol; 4 = 4-terpineol. β-phase values come from ref. 4 and are not in Table 1.

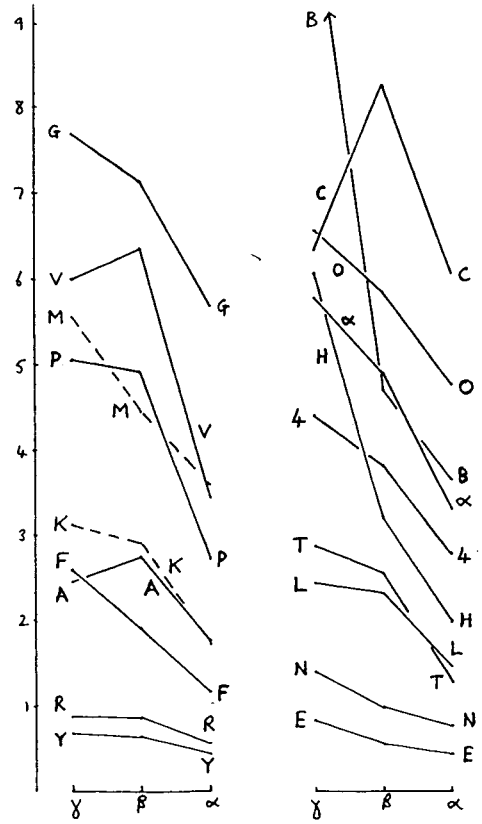

Fig. 2. Linked plots of average relative retention times (*n*-undecane = 1.00) (*y* axis) of some solutes on γ-(G-PN), β- and α-(TA) esterified dipentylated cyclodextrins (Chiraldex phases) at 125°C. Solute abbreviations as for Fig. 1 plus E = camphene; M = menthol; R = α-terpinene; Y = myrcene.

are equally able to fit into the cavity . . . However with the smaller β cavity (of permethylated, unesterified cyclodextrin!) some isomers are sterically hindered from fitting".

Bicyclic structure can also be detected by considering the percentage increase in relative retention time on changing γ-cyclodextrin modifications from Chiraldex-G-PN (column 9) to G-DA (column 6) in table 1, see column 15. At 125°C, considering the faster-emerging solutes, rigid-molecule bicyclics (four) show 75% or more increase (camphene and cineole being over 110%), greater than 3-carene which has the rotable side-chain. This solute still shows 40% increase, unlike the acyclic and monocyclics, which range from just 6 to 23%. By my *c* ratio method [12] the G-PN phase rates as more polar than G-DA (0.40 at 125°C against 0.26 at 170°C, respectively —"low" polarity values).

Considering the changes between the two β-cyclodextrin phases (Table 1, column 13) it is apparent that the increases are not all in one direction as previously found. Percentage increases from the ester (B-TA) to the alcohol (B-DA) phase of 84–10% are shown by alcohol solutes which should obviously have affinity for DA (apart from two acyclic alcohols); and by bicyclic ketones which increase by 26–6%. The

reverse increases, DA to TA, of 56–4% are given by non-bicyclic carbonyl-containing solutes. The *c* ratios of these intermediate size cyclodextrins confirm the ester phase as the more polar (0.61 for B-TA *versus* 0.28 for B-DA at 125°C. These "low" ratings are supported by considering the elution sequence of three of McReynolds' probe solutes, which is butanol, pyridine, then octyne [13].

In summary, for dipentylated cylcodextrin phases:

(i) The γ-phases can indicate molecular shape. They show high retention of many bicyclic monoterpenoids. There may also be delay-causing interaction with the acyclic dienes geraniol and citral. The esterified phase (G-PN) gives sharper, more reliable peaks, which are not dose-dependent as are those from the alcohol phase (G-DA).

Compared to the corresponding α-phase, the hydroxycyclodextrin (DA) gives over 100% increase in relative retention times to undecane for bicyclics, with some increases over 340%. In contrast, acyclics increase less than 55%, with citral only by 13%. Monocyclics fall in between, less than 100% increase.

(ii) The β-phases can indicate functional groups. The hydroxy phase (B-DA) shows equal relative affinity for α-terpineol to the corresponding γ-phase, and equally for geraniol to the α-phase —probably alcoholic responses. Citral is not favoured. The ester phase (B-TA) shows relatively higher affinity than the corresponding larger or smaller cyclodextrins for citral, carvone, citronellal (and cuminal) —probably carbonyl responses.

Comparing relative retention times on the ester with the alcoholic phase, carbonyl compounds show an increase unless bicyclic. Alcohols give a decrease unless possibly acyclic.

Acknowledgement

The donation of some "Chiraldex" capillaries by ASTEC (see Experimental) is gratefully acknowledged.

References

[1] D.W. Armstrong and H.L. Jin, *J. Chromatogr.*, 502 (1990) 154.
[2] W-Y. Li, H.L. Jin and D.W. Armstrong, *J. Chromatogr.*, 509 (1990) 303.
[3] T.J. Betts, *J. Chromatogr.*, 606 (1992) 281.
[4] T.J. Betts, *J. Chromatogr.*, 639 (1993) 366.
[5] T.J. Betts, *J. Chromatogr. A*, 653 (1993) 167.
[6] *Chiraldex Capillary GC Columns*, ASTEC, Whippany, NJ, 1993.
[7] N.W. Davies, *J. Chromatogr.*, 503 (1990) 1.
[8] T. Shibamoto, in P. Sandra and C. Bicchi (Editors), *Capillary Gas Chromatography in Essential Oil Analysis*, Hüthig, New York, 1987, p. 270.
[9] A. Berthod, W. Li and D.W. Armstrong, *Anal. Chem.*, 64 (1992) 873.
[10] F. Kobor and G. Schomburg, *J. High Resolut. Chromatogr.*, 16 (1993) 693.
[11] A.R.J. Andrews, Z. Wu and A. Zlatkis, *Chromatographia*, 34 (1992) 163.
[12] T.J. Betts, *J. Chromatogr.*, 628 (1993) 138.
[13] T.J. Betts, *J. Chromatogr.*, 354 (1986) 1.

ELSEVIER

Journal of Chromatography A, 672 (1994) 261–266

JOURNAL OF CHROMATOGRAPHY A

Short Communication

Gas chromatographic determination of trace amounts of aldehydes in automobile exhaust by a cysteamine derivatization methods☆

Akio Yasuhara*,[a], Takayuki Shibamoto[b]

[a]*Environmental Chemistry Division, National Institute for Environmental Studies, 16-2 Onogawa, Tsukuba, Ibaraki 305, Japan*
[b]*Department of Environmental Toxicology, University of California, Davis, CA 95616, USA*

(First received January 11th, 1994; revised manuscript received March 10th, 1994)

Abstract

Low-molecular-mass aldehydes present in automobile exhaust from vehicles with three different mileages were collected in a 1000-ml bottle and then determined as thiazolidine derivatives. Aldehydes were derivatized with cysteamine to the corresponding thiazolidines, which were subsequently determined using a gas chromatograph with a nitrogen–phosphorus detector. A car driven 50 000 km emitted high concentrations of formaldehyde (13.6 μg/l) and acetaldehyde (6.6 μg/l) and trace amounts of propionaldehyde, isobutyraldehyde, butyraldehyde, pentanal and benzaldehyde. Formaldehyde and acetaldehyde were also found in the exhaust from a car driven 20 000 km at levels of 4.33 and 1.32 μg/l, respectively. On the other hand, a car driven 5000 km did not emit any aldehydes.

1. Introduction

Some low-molecular-mass aldehydes such as formaldehyde and acetaldehyde may cause environmental problems because they are emitted from incinerator and automobile engines in large amounts. They are also known to produce photochemical smogs. It is therefore important to determine levels of these aldehydes emitted from automobile engines. However, it is extremely difficult to measure some of these low-molecular-mass aldehydes because they are highly volatile and reactive. Several methods have been reported [1–3] and the most commonly used methods involve derivatization with 2,4-dinitrophenylhydrazine (2,4-DNPH). However, chromatographic analysis of the 2,4-DNPH derivatives is difficult because they produce *syn* and *anti* forms, except in the case of formaldehyde. Moreover, this derivatization requires strongly acidic conditions, which may alter the chemicals of interest.

A simple and specific method that involves derivatization of aldehydes with cysteamine (2-aminoethanethiol) to form stable thiazolidines has been reported [4–6]. The resulting thiazolidines were determined by gas chromatography with a fused-silica capillary column and nitrogen-phosphorus detection (NPD). This method was applied successfully to determine various volatile aldehydes simultaneously in the headspace of heated pork fat [7] and cooking oils

* Corresponding author.

☆ Part of this work was presented at the *1st Symposium on Environmental Chemistry, Tsukuba, June 12, 1992.*

0021-9673/94/$07.00
SSDI 0021-9673(1994)00253-6

[8]. In this study, trace volatile aldehydes formed in exhaust from cars with gasoline engines were determined using this cysteamine method.

2. Experimental

2.1. Materials

Cysteamine and N-methylacetamide were purchased from Aldrich (Milwaukee, WI, USA). Analytical-reagent grade dichloromethane, anhydrous sodium sulphate, sodium hydroxide and aldehydes were obtained from Wako (Osaka, Japan). High-purity water was prepared by passing distilled water through an ion-exchange column and then through an activated carbon column. Thiazolidine derivatives from corresponding aldehydes except benzaldehyde were prepared according to the method reported previously [9]. A stock standard solution of cysteamine was prepared by dissolving 0.5 g of cysteamine hydrochloride in 15 ml of high-purity water. The solution was adjusted to pH 8.0 with 0.1 *M* sodium hydroxide solution and to 20 ml in volume with high-purity water. A GC internal standard solution was prepared by dissolving N-methylacetamide in benzene (13.8 mg/ml).

2.2. Synthesis of 2-phenylthiazolidine

Cysteamine hydrochloride (6.8 g) was dissolved in 100 ml of 50% methanol solution and the pH of the solution was adjusted to 7.5 with 1 *M* sodium hydroxide solution. Benzaldehyde (6.4 g) in 50 ml of methanol was added dropwise to the cysteamine solution while stirring at room temperature. After the reaction mixture had been stirred for 10 h, 30 ml of aqueous potassium carbonate solution (0.43 g/ml) were added dropwise to the reaction mixture while stirring. The reaction mixture was diluted with 150 ml of water and then extracted five times with 50-ml portions of dichloromethane. After the extract had been dried over anhydrous sodium sulphate, the solution was concentrated under atmospheric pressure by distillation with a fractionation column. The residual colourless crystals obtained were recrystallized from hexane–benzene (2:1). Colourless needles (7.7 g) with m.p. 112–113°C were obtained. NMR and mass spectral data for 2-phenylthiazolidine are given in Table 1.

2.3. Sampling of aldehydes from automobile exhausts

Cars run with regular unleaded gasoline were used. The exhaust gas was collected from an engine at idling speed after the car had been driven for *ca.* 8 km. A 1000-ml glass bottle sealed with a PTFE plug equipped with a PTFE stopcock was used for sample collection. A glass sample bottle, from which air had been evacuated with a vacuum pump prior to sampling, was placed over the exhaust pipe and the stopcock was opened gradually over 10 min. After exhaust gas had been drawn into the sample bottle, the stopcock was closed and the bottle was brought back to the laboratory. Three bottles were filled with exhaust gas from each car every day for 2 days.

Table 1
Spectral data for 2-phenylthiazolidine

^{1}H NMR (in C^2HCl_3)	δ (ppm): 7.57–7.54 (m, 2H, *o*-H on benzene ring), 7.43–7.32 (m, 3H, *m*- and *p*-H on benzene ring), 5.63 (s, 1H, methyne), 3.74–3.66 (m, 1H, one of methylene H), 3.22–3.12 (m, 3H, other methylene H), 2.04 (s, 1H, H on NH)
^{13}C NMR (in C^2HCl_3)	δ (ppm): 73.37 (position 2), 36.53 (position 4), 52.83 (position 5), 140.07 (position 1 of benzene ring), 128.13 (position 2 of benzene ring), 128.51 (position 3 of benzene ring), 127.22 (position 4 of benzene ring)
Mass spectrum	*m/z* (relative intensity, %): 15(3), 18(15), 27(4), 28(9), 30(100), 36(10), 38(3), 41(2), 42(9), 43(7), 44(44), 45(4), 46(3), 59(3), 60(2), 75(3), 76(3), 77(21), 78(3), 106(5), 109(22), 111(2), 123(4), 135(3)

2.4. Determination of aldehydes in exhaust gas

After sampling, 15 ml of cysteamine solution were injected into the sample bottle through the stopcock with a syringe. The bottle was shaken vigorously for 5 min and then allowed to stand for 1 h at room temperature. The reaction solution was extracted twice with 10-ml portions of dichloromethane using a separating funnel. The extracts were combined and passed through a small amount of sodium sulphate to remove water. The sodium sulphate was washed with 5 ml of dichloromethane. The dichloromethane solutions were combined and then concentrated to 1 ml under atmospheric pressure by distillation with a fractionation column. A 1-μl volume of N-methylacetamide solution was added to the sample solution as an internal standard prior to GC analysis.

2.5. Gas chromatography

A Hewlett-Packard Model 5890A gas chromatograph equipped with a DB-WAX fused-silica capillary column (30 m × 0.25 mm I.D., film thickness 0.25 μm) and was used with NPD. The oven temperature was held at 40°C for 2 min and then programmed to 200°C at 6°C/min. The GC peak areas were integrated with a System Instruments Model 7000B integrator. The injector temperature was 250°C and the detector temperature was 300°C. The linear velocity of helium carrier gas was 33.7 cm/s at 40°C. The injector splitting ratio was 1:20.

2.6. Measurement of NPD relative response factor

The relative response factor (*RRF*) for each thiazolidine derivative was defined by the following equation:

$$RRF = S_a / S_i$$

where S_a is peak area of each thiazolidine derivative per unit mass and S_i is peak area of 2-methylthiazolidine per unit mass. Measurements were performed for four consecutive days and five runs were carried out each day.

3. Results and discussion

The *RRF* values of 2-alkylthiazolidines are given in Table 2. The deviation in the *RRF*

Table 2
Deviations of relative response factors (*RRF*) of 2-alkylthiazolidines

2-Alkylthiazolidine	Deviation of *RRF* within a day							
	1st day		2nd day		3rd day		4th day	
	RRF[a]	R.S.D.[b]	*RRF*	R.S.D.	*RRF*	R.S.D.	*RRF*	R.S.D.
Unsubstituted	0.731	6.1	0.735	3.2	0.767	3.8	0.821	1.6
Ethylthiazolidine	0.913	0.34	0.902	1.2	0.902	0.47	0.897	0.79
Isopropylthiazolidine	0.911	0.81	0.882	2.3	0.810	1.8	0.869	1.6
Propylthiazolidine	0.740	0.75	0.768	0.60	0.771	0.89	0.764	1.1
Isobutylthiazolidine	0.710	0.72	0.694	1.3	0.694	1.3	0.686	1.4
Butylthiazolidine	0.690	0.79	0.679	0.85	0.682	1.2	0.678	1.1
Pentylthiazolidine	0.504	1.4	0.502	1.6	0.508	1.7	0.505	1.1
Hexylthiazolidine	0.459	1.8	0.457	2.4	0.469	2.5	0.466	1.8
Heptylthiazolidine	0.370	3.5	0.376	3.4	0.385	3.3	0.385	1.5
Octylthiazolidine	0.275	9.0	0.284	6.0	0.294	5.0	0.299	2.3
Phenylthiazolidine	0.950	4.4	0.916	3.8	0.943	4.6	0.966	4.4

[a] Values are averages of five replicates. Standard compound in *RRF* calculation is 2-methylthiazolidine.
[b] Relative standard deviation (%).

values is small, indicating that the use of a calibration graph for 2-methylthiazoline to determine other thiazolidine derivatives is acceptable.

A model study using standard chemicals showed that 2-alkylthiazolidines were sufficiently extracted with dichloromethane from an aqueous solution at pH 7 and exhaust gas did not change the pH of the sample solutions.

The recovery of formaldehyde using this method was checked by using a gas sample prepared by heating paraformaldehyde, and the average recovery was 89%. The average recoveries of propionaldehyde and butanal were 98% and 95%, respectively, in recovery experiments in which 10 μg of each aldehyde were added to clean air in a 1-l glass bottle.

Gas chromatograms of standard derivatives and a typical dichloromethane extract from a sample solution are shown in Fig. 1. The calibration graph for 2-methylthiazolidine is shown in Fig. 2.

Table 3 shows the results for the determination of aldehydes in exhaust gas; the values are means for three samples taken each day and corrected for the background. It is obvious that the older car (A) emitted a considerably high concentration of aldehydes, particularly formaldehyde (13.6 μg/l) and acetaldehyde (6.6 μg/l). It is noteworthy that there is an interference in the determination of formaldehyde and acetaldehyde due to the background of both aldehydes in the laboratory atmosphere and the reagents used. As the deviation of the background levels is fairly high (12–41%), the accuracy of the determination of both aldehydes becomes lower.

There are several reports on the determination of aldehydes in automobile exhaust [10–15]. Results of aldehyde determinations are summarized in Table 4. The presence of pentanal in automobile exhaust has not been reported prior to this study. Benzaldehyde, which has also been reported in exhaust gas by several researchers [12,13], may be formed from toluene in gasoline by oxidation. The amount of benzaldehyde determined in this study is consistent with those reported previously. The concentration levels of each aldehyde reported in many studies are fairly

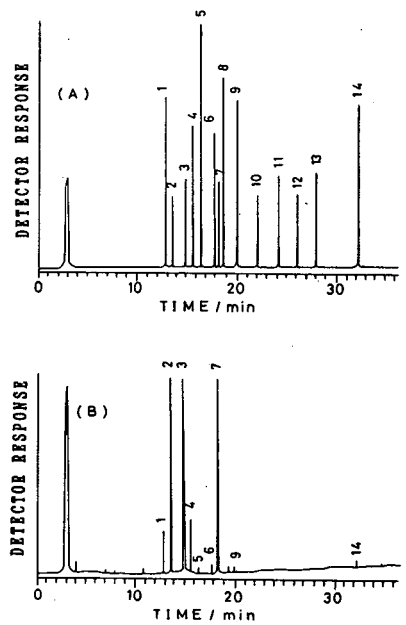

Fig. 1. Gas chromatograms of (A) a dichloromethane solution of thiazolidine standards and (B) a dichloromethane extract of automobile exhaust collected from car A. Peaks: 1 = 2,2-dimethylthiazolidine from acetone; 2 = 2-methylthiazoline from acetaldehyde; 3 = unsubstituted thiazolidine from formaldehyde; 4 = 2-ethylthiazolidine from propionaldehyde; 5 = 2-isopropylthiazolidine from isobutyraldehyde; 6 = 2-propylthiazolidine from butyraldehyde; 7 = N-methylacetamide (internal standard); 8 = 2-isobutylthiazolidine from isovaleraldehyde; 9 = 2-butylthiazolidine from valeraldehyde; 10 = 2-pentylthiazolidine from hexanal; 11 = 2-hexylthiazolidine from heptanal; 12 = 2-heptylthiazolidine from octanal; 13 = 2-octylthiazolidine from nonanal; 14 = 2-phenylthiazolidine from benzaldehyde.

similar and the relative abundances of the aldehydes show the same pattern.

The proposed method for the determination of low-molecular-mass aldehydes in exhaust gas is simple, highly sensitive and specific to aldehydes. Also, a simple quantitation method for various aldehydes was established using a single calibration graph and the relative response factor.

Acknowledgement

We thank Ms. Mutsumi Kataoka, a laboratory assistant at the National Institute for Environmental Studies, for technical assistance.

Table 3
Concentrations of formaldehyde (FA), acetaldehyde (AA), propionaldehyde (PA), isobutyraldehyde (IBA), butyraldehyde (BA), pentanal (PA) and benzaldehyde (BzA) found in exhaust gas from different cars

Model	Piston displacement (cm^3)	Year of manufacture	Mileage (km)	Sampled on	Aldehyde concentration ($\mu g/l$)						
					FA	AA	PA	IBA	BA	PA	BzA
A	550	1986	50 000	1st day	13.6	6.60	3.13	0.73	0.81	ND[a]	0.92
				2nd day	10.4	6.22	2.28	0.37	0.54	0.25	0.43
B	1800	1990	20 000	1st day	4.33	1.32	0.17	ND	ND	ND	ND
				2nd day	4.25	ND	ND	ND	ND	ND	ND
C	1500	1989	5000	1st day	ND	ND	ND	ND	ND	ND	ND
				2nd day	ND	ND	ND	ND	ND	ND	ND

[a] ND = Not detected.

Table 4
Concentration ranges of several aldehydes in car exhausts reported in the literature

Ref.	Year	Units[a]	Aldehyde concentration range								
			C_1	C_2	C_3	i-C_4	C_4	i-C_5	C_5	C_6	Benzaldehyde
12	1981	$\mu g/l$	5.1–6.1	1.8–5.7	0.5	0.1	0.1				3.5
10	1982	ppm	0.04–2.54	ND–0.59			ND–0.03				ND–0.10
14	1982	ppm	3.26–3.56	0.56–0.76	0.03–0.08	0.08–0.20		ND–0.03	ND–0.02	ND–0.01	0.05–0.07
11	1983	ppm	8.95–96.4	0.568–7.29	ND–0.756	ND–0.126					
15	1983	$\mu g/l$	17.2	4.03	0.644		0.588				0.886
13	1992	ppm	6.7–14.1	1.2–6.3	ND-1.1	ND–0.8					
This work	1992	$\mu g/l$	ND–13.6	ND–6.50	ND–3.13	ND–0.783	ND–0.805		ND–0.253		ND–0.924

[a] All ppm values are v/v.

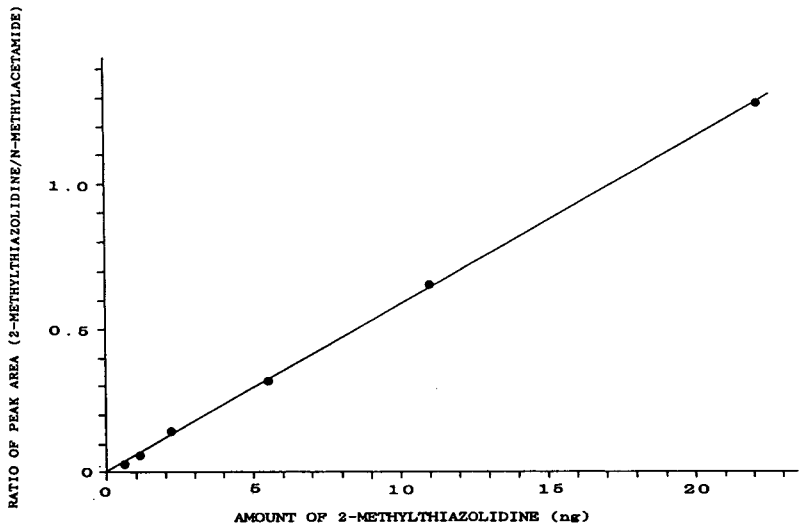

Fig. 2. Calibration graph for 2-methylthiazolidine. A 1-μl volume of standard solution was injected into the GC instrument. Each standard solution contained N-methylacetamide at 13.8 μg/ml as an internal standard. All thiazolidines were subsequently quantified using this calibration graph and the relative response factor (*RRF*).

References

[1] L.J. Papa and L.P. Turner, *J. Chromatogr. Sci.*, 10 (1972) 747.
[2] S. Selim, *J. Chromatogr.*, 136 (1977) 271.
[3] K. Kuwata, M. Uebori and Y. Yamasaki, *J. Chromatogr. Sci.*, 17 (1979) 264.
[4] T. Hayashi and T. Shibamoto, *J. Agric. Food Chem.*, 33 (1985) 1090.
[5] T. Hayashi, C.A. Reece and T. Shibamoto, *J. Assoc. Off. Anal. Chem.*, 69 (1986) 101.
[6] K. Umano and T. Shibamoto, *J. Agric. Food Chem.*, 35 (1987) 14.
[7] A. Yasuhara and T. Shibamoto, *J. Food Sci.*, 54 (1989) 1471.
[8] A. Yasuhara and T. Shibamoto, *J. Chromatogr.*, 547 (1991) 291.
[9] A. Yasuhara and T. Shibamoto, *Agric. Biol. Chem.*, 53 (1989) 2273.
[10] F. Lipari and S.J. Swarin, *J. Chromatogr.*, 247 (1982) 297.
[11] T. Saito, T. Takashina, S. Yanagisawa and T. Shirai, *Bunseki Kagaku*, 32 (1983) 33.
[12] L. Johnson, B. Josefsson, P. Marstorp and G. Elkund, *Int. J. Environ. Anal. Chem.*, 9 (1981) 7.
[13] A.C. Geng, Z.L. Chen and G.G. Siu, *Anal. Chim. Acta*, 257 (1992) 99.
[14] G. Creech, R.T. Johnson and J.O. Stoffer, *J. Chromatogr. Sci.*, 20 (1982) 67.
[15] K.T. Menzies, K.J. Beltis and C.M. Wong, *Development of sampling and analytical methods for toxicants in diesel exhaust streams*, U.S. Department of Commerce, PB84-196625, 1983.

ELSEVIER

Journal of Chromatography A, 672 (1994) 267–272

JOURNAL OF CHROMATOGRAPHY A

Short Communication

Determination of sterol content in different food samples by capillary gas chromatography

M. Rodríguez-Palmero[a], S. de la Presa-Owens[a], A.I. Castellote-Bargallo[a], M.C. López Sabater*[,a], M.Rivero-Urgell[b], M.C. de la Torre-Boronat[a]

[a]*Unitat de Nutrició i Bromatologia, Department de Ciències Fisiològiques i de la Nutrició, Facultat de Farmàcia, Universitat de Barcelona, Barcelona, Spain*

[b]*Departament Científic, ORDESA, Sant Boi de Llobregat, Barcelona, Spain*

(First received December 6th, 1993; revised manuscript received February 22nd, 1994)

Abstract

An accurate method for the determination of sterols by capillary gas chromatography was developed and applied to the analysis of food. The procedure includes the following steps: dichloromethane–methanol (2:1, v/v) lipid extraction, saponification at 80°C and separation of the unsaponifiable matter with cyclohexane, derivatization to form trimethylsilyl ethers and gas chromatography using 5α-cholestane as the internal standard. The method shows good accuracy, precision and sensitivity and is suitable for the determination of sterols in food.

1. Introduction

The accurate determination of the sterol content in food is of great importance, not only because adulteration can thus be detected, but also owing to the increasing interest in the possible link between arteriosclerotic and coronary diseases and cholesterol [1,2]. A rapid method is therefore needed to assist in research towards low-cholesterol or cholesterol-free diets. Moreover, owing to the relationship with coronary heart disease, the food industry has been focusing on the possibility of developing new products with low cholesterol content. Therefore, it is necessary to develop a rapid and accurate method to determine sterols in food.

Many methods have been published for the determination of cholesterol, including spectrophotometric, enzymatic, gas chromatographic and high-performance liquid chromatographic [3] techniques. Spectrophotometric and enzymatic methods are not strictly specific and are therefore subject to errors due to interfering substances, and they may overestimate the cholesterol content [4,5]. Nowadays, gas chromatography is the preferred method. Several groups [6–9] followed a direct saponification method. Using gas chromatography, some workers have avoided derivatization by dissolving the residue obtained from the unsaponifiable extraction in *n*-hexane [10]. Tsui [11] developed a gas chromatographic method in which, after saponification, the isolation was carried out by solid-phase

* Corresponding author. Address for correspondence: C/ Nicaragua 60–62, 3°4ª, Barcelona 08029, Spain.

* Presented at the *22nd Annual Meeting of the Spanish Chromatography Group, Barcelona, October 20–22, 1993.*

0021-9673/94/$07.00
SSDI 0021-9673(94)00183-A

extraction on a non-polar adsorbent, such as C_{18} packed in disposable polypropylene tubes. Fenton and Sim [12] reported an on-column capillary gas chromatographic method, also avoiding lipid extraction and derivatization.

Little information is available in the literature on the cholesterol value of multi-component food products.

This paper describes a rapid method for the determination of the sterol content in prepared food by means of capillary gas chromatography. The method was used to establish the sterol content of the diet in an old people's home, so that the daily cholesterol consumption could be evaluated. The procedure includes lipid extraction, separation of the unsaponifiable fraction, derivatization to form trimethylsilyl ethers and gas chromatography.

2. Experimental

2.1. Reagents and chemicals

5α-Cholestane, cholesterol, squalene, stigmasterol, campesterol, β-sitosterol and bis-(trimethylsilyl)trifluoroacetamide (BSTFA) containing 1% of trimethylchlorosilane (TMCS) were purchased from Sigma (St. Louis, MO, USA), 3-*tert.*-butyl-4-hydroxyanisole (BHA) from Fluka (Buchs, Switzerland), dried pyridine and *n*-hexane from Merck (Darnstadt, Germany), dichloromethane, methanol and anhydrous granulated Na_2SO_4 from Probus (Badalona, Spain), diethyl ether from SDS (Peypin, France) and cyclohexane and KOH pellets from Panreac (Barcelona, Spain).

2.2. Samples

The samples consisted of different cooked dishes on the menu in an old peoples' home. Each sample was analysed after homogenizing all the ingredients. The menu was representative of the mediterranean diet; vegetable oil was used for cooking and dressing the dishes. Some of the samples analysed were vegetable soup, hamburger with green salad, roast chicken and potatoes, fried fish, spaghetti bolognese, paella, turkey and eggs with tomato sauce.

2.3. Sample preparation and lipid extraction

Food samples were ground and homogenized individually. The samples were then thoroughly mixed with anhydrous granulated Na_2SO_4 to improve lipid extraction and kept at −20°C until further analysis.

First a quantitative fat determination of the sample was performed by means of acid hydrolysis followed by Soxhlet fat extraction.

The fat for the sterol determination was extracted using 225 ml of dichloromethane–methanol (2:1, v/v) with a magnetic stirrer, according to a modification of Folch *et al.'s* procedure [13]. Dichloromethane was chosen instead of chloroform owing to its lower toxicity and equal extraction capacity [14,15]. The extract was filtered into a separating funnel, 20 ml of distilled water were added and the funnel was shaken and left for the phases to separate. The organic phase was filtered through anhydrous granulated Na_2SO_4 into a dried flask and evaporated. The residue was dissolved in diethyl ether, in order to eliminate the non-lipidic substances retained by methanol, filtered and evaporated in a rotatory evaporator. Fat was kept in a dark vial. The vials were flushed with nitrogen, capped tightly and stored at −20°C until analysis.

2.4. Separation of the unsaponified fraction

The method proposed by Slover *et al.* [16] was used and modified as follows. About 100 mg of sample were placed in a 20 × 120 mm screw-capped test-tube (Trallero, Barcelona, Spain) and 8 ml of ethanolic BHA solution (115 mg of BHA in 100 ml of ethanol) and 0.25 ml of internal standard solution (200 μg/ml of 5-α-cholestane in *n*-hexane) were added, followed by 0.5 ml of 0.4 mg/ml KOH solution. The tubes were flushed with nitrogen and tightly closed. The samples were saponified by incubation in a water-bath at 80°C for 15 min with periodic shaking. The saponified solution was cooled

under tap water and 15 ml of cyclohexane were added, followed by 12 ml of distilled water. The tubes were shaken and centrifuged for 5 min at 360 *g*. The upper phase was carefully removed with a pipette and the cyclohexane extraction was repeated. The combined extracts were concentrated to a few millilitres in a rotatory evaporator and then transferred into a 10 × 100 mm screw-capped tube (Corning, New York, USA). The remaining solvent was removed using a stream of nitrogen. The sample was then ready for derivatization.

2.5. Derivatization

Sylon HTP (Supelco, Bellefonte, PA, USA) and BSTFA containing 1% of TMCS and dry pyridine were tested as derivatization reagents and the latter was chosen. Pure, dry pyridine (50 μl) and of BSTFA containing 1% of TMCS (50 μl) were added and the tubes were securely stoppered with PTFE-lined caps and mixed thoroughly. The samples were held at room temperature for at least 15 min before analysis.

2.6. Gas chromatography

A Shimadzu GC-14A gas chromatography, equipped with a flame ionization detector and a 30 m × 0.25 mm I.D. fused-silica capillary column coated with SPB-5 (Supelco) with a 0.25-μm film thickness was used under the following conditions: oven temperature, constant at 280°C; injector temperature, 265°C; helium carrier gas pressure, 15 p.s.i. (1 p.s.i. = 6894.76 Pa); helium flow-rate, 1 ml/min; air and hydrogen flow-rates, adjusted to give the maximum detector response; detector temperature, 290°C; injection volume, 0.3 μl; and injection, split mode with a splitting ratio of 1:100. A Shimadzu (Kyoto, Japan) C-R6A Chromatopac integrator was used.

3. Results and discussion

Many solvents were tested for their ability to extract the unsaponifiable matter. Cyclohexane was selected because it is less toxic, does not form peroxides as does diethyl ether and, above all, because it does not form stable emulsions during the procedure.

In the capillary gas chromatographic analysis of sterols, the derivatization process has the advantages of providing sharp peaks and improving their quantification. Two derivatizating reagents were tried. The first, Sylon HTP, gave turbidity and poor reproducibility. BSTFA containing 1% of TMCS with pyridine was tested. The latter gave high levels of all sterols and also better precision and recovery. Fig. 1 shows a typical chromatogram for a food sample. The resolution was satisfactory.

A plot of the ratio of peak area of cholesterol to that of 5α-cholestane *versus* amount of cholesterol (mg) gave a linear response in the range 0.05–0.5 mg of cholesterol ($r > 0.99$) (Fig. 2). Good linearity of the method for squalene and stigmasterol was also found, with $r > 0.99$ in both instances.

The precision of the method was tested by analysing ten aliquots of the same sample. The relative standard deviation for cholesterol, squalene and stigmasterol varied from 2.48 to 3.21%. This intra-laboratory precision is within the limits of acceptable variability in methods of analysis proposed of Horwitz [17] for analyte concentrations of the order of 0.2 mg/g sample.

The standard addition method was used to test the recovery of the analysis. Five levels of standard concentrations were added to a known mass of sample, and then they were carried through the entire procedure until the trimethylsilyl ethers of sterols were obtained, and then injected into the column. Recoveries between 100.63 and 80.33% were obtained. Details are given in Table 1.

The detection and quantification limits found were of the order of nanograms (Table 2). These limits show that the method has excellent sensitivity [18,19].

The method was applied for the analysis of 35 food samples, always with good results, and it may therefore be considered suitable for the routine determination of sterols in food. Moreover, it is rapid without the need to use separating funnels to obtain the unsaponifiable matter,

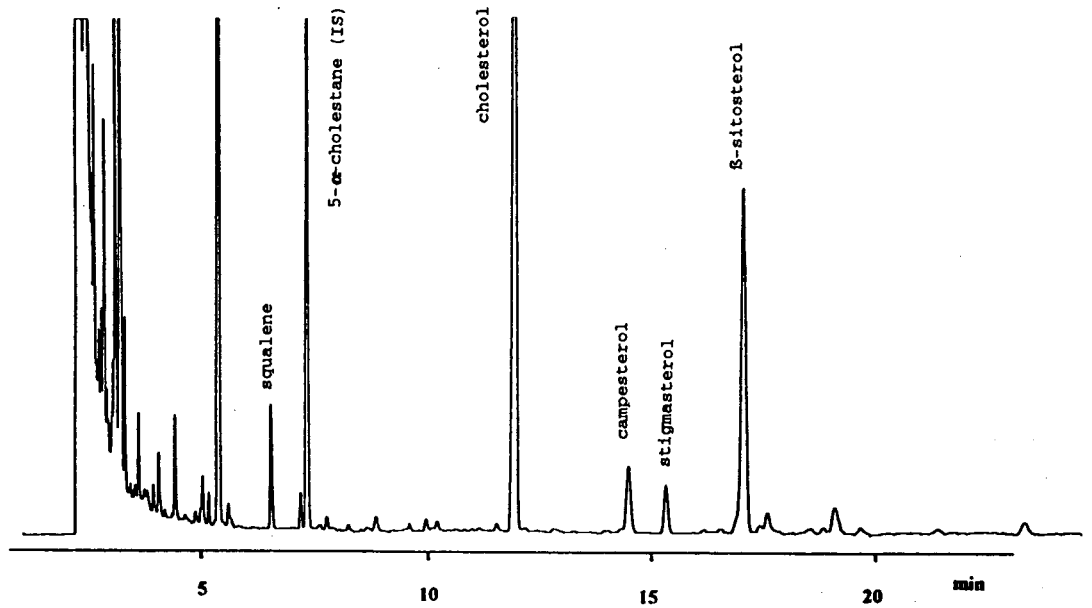

Fig. 1. Chromatogram of non-saponifiables isolated from a food sample (canned sardines with green salad).

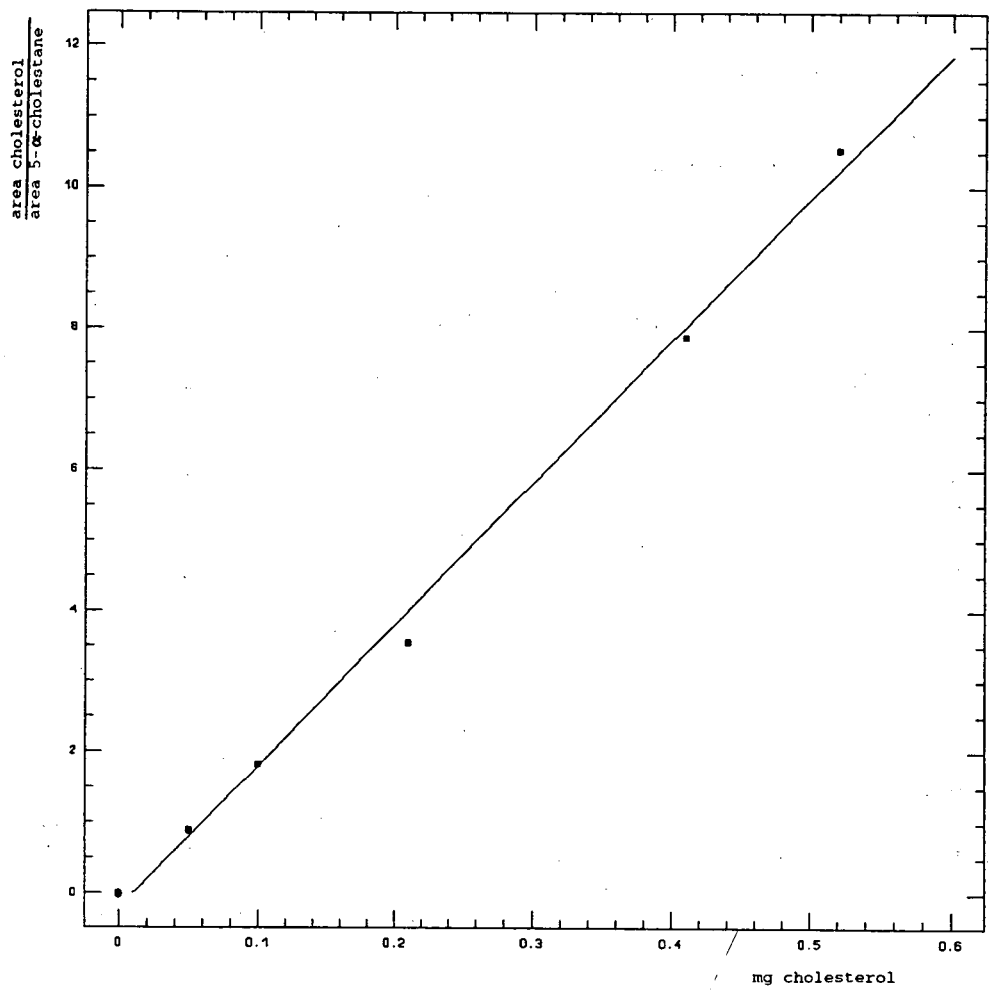

Fig. 2. Linearity of detector response for 0.05–0.5 mg of cholesterol: $y = 20.18x - 0.22$; $r > 0.99$.

Table 1
Recovery of the method

Cholesterol level (mg)	Recovery ($n = 2$) (%)	Squalene level (mg)	Recovery ($n = 2$) (%)	Stigmasterol level (mg)	Recovery ($n = 2$) (%)
1.1	95.65, 97.97	4.05	96.20, 96.95	1.67	99.18, 102.08
0.55	99.73, 100.27	2.02	94.62, 96.68	0.83	93.21, 93.75
0.22	93.04, 96.32	0.81	98.86, 100.12	0.33	86.26, 88.40
0.11	84.91, 87.27	0.40	94.31, 96.81	0.17	79.35, 81.31
0.02	92.41, 93.05	0.08	98.50, 98.78	0.03	93.10, 93.72
Mean	94.06 ± 5.2	Mean	97.18 ± 1.8	Mean	91.04 ± 7.6

Table 2
Limits of detection and quantification

Sterol	Detection limit[a] (ng)	Quantification limit[a] (ng)
Squalene	1.35	3.87
Cholesterol	1.08	3.09
Stigmasterol	1.12	3.18

[a] Signal-to-noise ratio = 3.
[b] Signal-to-noise ratio = 10.

Table 3
Sterol contents of some food samples (mg sterol per 100 g of sample)

Food	Squalene	Cholesterol	Campesterol	Stigmasterol	β-Sitosterol
Fried fish	1.7	40.3	2.4	1.9	15.1
Spaghetti bolognese	0.6	5.4	1.8	0.8	9.2
Paella	0.4	7.2	0.8	0.7	4.0
Turkey	1.6	22.4	3.0	1.2	1.83
Eggs with tomato sauce	1.4	242.0	0.1	1.2	7.0

and also avoids the necessity for thin-layer chromatography [20]. Table 3 gives the results obtained with different samples.

4. Acknowledgements

We thank Ordesa and CDTI for financial support. We also thank Fundació Garbí for their helpful assistance in collecting the samples.

5. References

[1] S.L. Connor, J.R. Gustafson and S.M. Artauwild, *Lancet*, i (1986) 1229.
[2] A. Bonanome and S.M. Grundy, *N. Engl. J. Med.*, 319 (1988) 1244.
[3] B. Holen, *J. Assoc. Off. Anal. Chem.*, 62 (1985) 1344.
[4] M.W. Marshal, R.H. Clevidence, T.T. Thompson and J. Judd, *J. Food Compos. Anal.*, 2 (1989) 2.
[5] C.E. Bohac, K.S. Rhee, H.R. Cross and K. Ono, *J. Food Sci.*, 53 (1988) 1642.

[6] M.L. Adams, D.M. Sullivan, R.L. Smith and E.F. Richter, *J. Assoc. Off. Anal. Chem.*, 69 (1986) 844.
[7] P. Oles, G. Gates, S. Kensinger, J. Patchell, D. Schumacher, T. Showers and A. Silcox, *J. Assoc. Off. Anal. Chem.*, 73 (1990) 724.
[8] J.D. Beyer, F.X. Milani, M.J. Dutelle and R.L. Bradley, *J. Assoc. Off. Anal. Chem.*, 72 (1989) 746.
[9] S.M. Al-Hasani, J. Hlavac and M.W. Carpenter, *J. Assoc. Off. Anal. Chem. Int.*, 76 (1993) 902.
[10] F. Ulberth and H. Reich, *Food Chem.*, 43 (1992) 387.
[11] I.C. Tsui, *J. Assoc. Off. Anal. Chem.*, 72 (1989) 421.
[12] M. Fenton and J.S. Sim, *J. Chromatogr.*, 540 (1991) 323.
[13] J. Folch, M. Less and G.H.S. Stanley, *J. Biol. Chem.*, 226 (1957) 497.
[14] I.S. Chen, C.-S.J. Shen and A.J. Sheppard, *J. Assoc. Off. Anal. Chem.*, 58 (1981) 599.
[15] W.W. Christie (Editor), *Gas Chromatography and Lipids*, Oily Press, Ayr, 1989, p. 31.
[16] H.T. Slover, R.H. Thompson and G.V. Merola, *J. Assoc. Off. Anal. Chem.*, 60 (1983) 1524.
[17] W. Horwitz, *Anal. Chem.*, 54 (1986) 67A.
[18] R. Kaiser, *Fresenius' Z. Anal. Chem.*, 189 (1962) 1.
[19] G.L. Long and J.D. Winefordner, *Anal. Chem.*, 55 (1983) 712A.
[20] V. Paganuzzi, *Riv. Ital. Sostanze Grasse*, 60 (1983) 116.

ELSEVIER

Journal of Chromatography A, 672 (1994) 273–277

JOURNAL OF CHROMATOGRAPHY A

Short Communication

Determination of thiols as sulphonic acids by capillary isotachophoresis

Mieczysław Wroński

Department of Chemical Technology and Environmental Protection, University of Łódź, Pomorska 18, 91-416 Łódź, Poland

(First received October 18th, 1993; revised manuscript received January 21st, 1994)

Abstract

The mobilities of sulphonic acids obtained by bromine oxidation of thiols and disulphides containing COOH, NH_2 and OH groups, from pH 3 to 9, the relative charges and apparent pK values of carboxylic groups were determined by means of capillary isotachophoresis.

1. Introduction

The problem of the determination of thiols and disulphides in trace concentrations in biological materials is often of prime importance and several techniques have been developed for this purpose.

Capillary isotachophoresis is a precise and accurate method for the determination of ions [1,2], and can be directly applied to mercaptoacids and aminothiols. This approach is of limited applicability, however, because natural samples in general contain many ionic compounds in great excess, which entirely overlap the small contribution of thiols. The derivatization of thiols as suggested by Holloway [3] is hardly applicable to natural samples and does not remove the ionic interferences.

The water-soluble thiols and disulphides can be readily and quantitatively oxidized to sulphonic acids, which are much more suitable for isotachophoretic analysis. Sulphonic acids are not or only slightly extractable from aqueous solution, which can be utilized for removal of foreign acids. The possible preparation of samples can be outlined as follows: (1) hydrolysis, oxidation and evaporation, *e.g.*, cysteine, homocysteine and penicillamine in protein hydrolysates; thiols and disulphides can be identified by comparison of isotachograms obtained before and after oxidation; (2) extraction, evaporation, oxidation and stripping of interferring materials with organic solvents, *e.g.*, thioctic acid in food; (3) reduction of disulphides, extraction of thiols as tributyltin mercaptides, stripping with hydrochloric acid, oxidation and stripping with tributyltin hydroxide, *e.g.*, thiols and disulphides in urine.

2. Theoretical

The effective mobility of an ion, u_X, can be calculated from isotachophoretic results using Boček *et al.*'s equation [2]:

$$\frac{1}{u_X} = \frac{1}{u_L} + \left(\frac{1}{u_S} - \frac{1}{u_L}\right)\frac{h_X}{h_S} \quad (1)$$

where u_L = mobility of the leading ion, usually

0021-9673/94/$07.00
SSDI 0021-9673(94)00251-4

chloride, $u_L = 79 \cdot 10^{-5}$ cm^2 s^{-1} V^{-1}, u_S = mobility of a standard, in this paper trichloroacetate, $u_S = 36.2 \cdot 10^{-5}$ cm^2 s^{-1} V^{-1} and h_X and h_S = step heights of the ion X and of the standard ion, respectively.

Inserting the mobilities of chloride and trichloracetate, Eq. 1 can be written in the form

$$u_X = \frac{79}{1 + 1.18h} \quad (2)$$

where h = relative step height of ion X, and $h = h_X/h_S$.

The relative charge of the ion X (effective charge) can be calculated from the equation [1,2]

$$Z_X = \frac{t_X i u_X}{n_X F(u_X + u_k)} \quad (3)$$

where t_X = zone length corresponding to ion X, i = driving current, F = Faraday constant, n_X = number of moles of ion X injected on to the column and u_k = the resulting mobility of the counter-buffer ion and protons. The value of u_k can be calculated from Eq. 3 using a standard such as trichloroacetate with the charge assumed to be −1. The charge is expressed as a positive number.

For monovalent acids the charge can also be calculated as the ratio of mobility u at a given pH to the mobility u_0 at full ionization:

$$Z = \frac{u}{u_0} \quad (4)$$

The relationship between charge, the pH of the leading buffer (pH_L) and the pK of the corresponding acid is given by

$$pK = pH_L + \log\left(\frac{1}{Z} - 1\right) \quad (5)$$

In order to avoid any misunderstanding, it is necessary to discriminate between some values of pK. The thermodynamic value pK_t is calculated for infinite dilution and is really constant. The apparent values calculated from Eqs. 3 and 5, pK_Z, or from Eqs. 4 and 5, pK_u, may depend on the composition of the solution.

Table 1 gives the pK values of some monovalent carboxylic acids. The pK_t values were taken from the literature [4], whereas the pK_Z and pK_u values calculated using data at pH 3.0 summarized in refs. 1 and 4 and with Eqs. 2–5. The determined value of u_k was $65.4 \cdot 10^{-5}$ cm^2 s^{-1} V^{-1} at pH 3.0. The results indicated a linear relationship between pK_t and pK_Z expressed by

Table 1
pK values of some monovalent carboxylic acids

Acid	pK_t	pK_Z	pK_u	pK'_t
Acetic	4.76	3.40	3.55	4.70
Benzoic	4.20	3.14	3.22	4.22
Butyric	4.82	3.47	3.55	4.83
Chloroacetic	2.87	2.39	2.41	2.86
Formic	3.75	2.87	3.02	3.73
Glyceric	3.74	2.87	2.94	3.73
Glycolic	3.89	2.96	3.06	3.90
Lactic	3.86	2.96	3.04	3.90
Levulinic	4.60	3.35	3.43	4.61
Nicotinic	4.82	3.44	3.54	4.77
p-Nitrobenzoic	3.52	2.74	2.79	3.50
Phenylacetic	4.41	3.25	3.33	4.42

pK_t = thermodynamic value; pK_Z = calculated from the charge at pH 3.0; pK_u = calculated from the mobility at pH 3.0; pK'_t = pK_t value calculated from pK_Z.

$$pK_t = 1.82\, pK_Z - 1.49 \quad (6)$$

The pK_t values calculated by means of Eq. 6 are given as pK'_t in the Table 1. The agreement is satisfactory.

The relationship between pK_Z and pK_u is expressed by the equation

$$pK_Z = 0.98\, pK_u \quad (7)$$

For the calculation of the apparent dissociation constant of a carboxylic group in the presence of a sulphonic group, full ionization of the sulphonic group above pH 2.8 may be assumed which results in the following equation for the pK of the carboxylic group:

$$pK = pH_L + \log\left(\frac{1}{Z - 1} - 1\right) \quad (8)$$

With two sulphonic groups in the molecule, the difference $Z - 2$ should be introduced.

On the basis of the established relationships, the identification and determination of unknown acids is possible by adopting the following steps:

determination of u_X and t_X at pH 3.0 and u_0, calculation of pK_u with Eqs. 4 and 5, pK_Z and Z_X with Eq. 5, n_X with Eq. 3 and pK_t with Eq. 6. The knowledge of pK_t can be evaluated for identification.

3. Experimental

Relative step heights were measured using an isotachophoretic analyser from Labeco (Slovak Republic), at a concentration of leading chloride ions of 0.01 *M* and a driving current of 50 μA in the analytical column. The mobilities were calculated from relative step heights using Eq. 2. The leading electrolytes were prepared from β-alanine (pH 3.0 and 3.5), aminocaproic acid (pH 4.5), histidine (pH 6.0), imidazole (pH 7.0) and methyldiethanolamine (pH 9.0), using 0.2% of PEG 200 as an additive. The terminating electrolytes were prepared from caproic acid (pH 3.0, 3.5 and 4.5) and 2-(N-morpholino)ethanesulphonic acid (MES) (pH 6, 7 and 9).

The sulphonic acids were prepared by oxidation of thiols in aqueous solution of known concentration by shaking with a 1 *M* solution of bromine in carbon tetrachloride until a stable yellow colour was just formed. The sample was evaporated under vacuum, the residue dissolved in water and an aliquot of the solution applied to the column. The method was applied to the determination cystine and cysteic acid in wool, as described in Section 4.1.

4. Results and discussion

Table 2 summarizes the mobilities determined for sulphonic acids obtained by oxidation of listed thiols. The mobility of a sulphonic acid not containing a carboxylic group (No. 1) does not depend on pH. The presence of sulphonic and carboxylic groups (Nos. 2–9) results in an increase in mobility with increase in pH, but tending to a constant value corresponding to complete ionization. The presence of one carboxylic and one amino group in the sulphonic acid (Nos. 10, 11 and 12) results in a slight increase in mobility from pH 3 to 7 and a strong increase at higher pH. The presence of two carboxylic groups and one amino group (No. 13) is reflected by a marked increase in mobility from pH 3 to 6, small change between pH 6 and 7 and a strong increase at higher pH. The results

Table 2
Mobilities (10^{-5} cm^2 s^{-1} V^{-1}) of sulphonic acids obtained by oxidation of thiols as a function of pH_L

No.	Parent thiol	Sulphonic acid	pH_L					
			3.0	3.5	4.5	6.0	7.0	9.0
1	Mercaptoethanol	2-Hydroxyethanesulphonic acid	39.4	39.5	39.3	39.6	39.7	39.4
2	Mercaptoacetic acid	Sulphoacetic acid	44.7	48.4	58.4	62.1	63.8	64.0
3	Thiolactic acid	2-Sulphopropionic acid	37.9	40.7	51.2	54.3	56.9	57.0
4	3-Mercaptopropionic acid	3-Sulphopropionic acid	36.1	37.9	47.6	53.3	55.7	56.0
5	Mercaptolactic acid	3-Sulpholactic acid	43.5	45.5	56.0	57.2	57.0	57.1
6	Thioctic acid	6,8-Disulphooctanoic acid	41.4	42.1	44.3	48.1	52.3	52.5
7	N-Acetylcysteine	N-Acetylcysteic acid	37.3	40.7	44.5	47.0	47.6	47.6
8	N-(2-Mercaptopropionyl)-glycine	N-(2-Sulphopropionyl)glycine	35.4	38.5	45.0	46.0	46.8	47.0
9	Captopril	1-(3-Sulpho-2-methyl-1-oxopropyl)-proline	30.0	32.7	37.8	38.6	38.8	39.0
10	Cysteine	Cysteic acid	32.0	33.4	33.8	33.9	34.5	46.2
11	Homocysteine	Homocysteic acid	28.6	29.5	30.0	30.7	31.2	41.8
12	Penicillamine	Dimethylcysteic acid	27.6	29.2	29.5	30.0	31.0	41.5
13	Glutathione	γ-Glutamylsulphoalanylglycine	28.8	31.4	36.5	38.0	38.3	40.8

Table 3
Relative charges Z and apparent pK_Z values of carboxylic groups in sulphonic acids as a function of pH of the leading electrolyte

Sulphonic acid	Parameter	pH_L		
		3.0	3.5	4.5
2-Sulphopropionic acid	Z	1.12	1.24	1.77
	pK_Z	3.87	4.00	3.98
3-Sulphopropionic acid	Z	1.01	1.14	1.58
	pK_Z	–	4.29	4.36
N-Acetylcysteic acid	Z	1.31	1.54	1.81
	pK_Z	3.35	3.43	3.71
N-(2-Sulphopropionyl) glycine	Z	1.22	1.38	1.84
	pK_Z	3.55	3.71	3.78
1-(3-Sulpho-2-methyl-1-oxopropyl)proline	Z	1.31	1.58	1.91
	pK_Z	3.35	3.36	3.50

presented can be utilized to select the best pH for the separation of the sulphonic acids.

Table 3 demonstrates some charges determined using Eq. 3 and pK_Z values calculated with Eq. 8. The u_k values (10^{-5} cm^2 s^{-1} V^{-1}), found were as follows: pH 3.0, 67.4; pH 3.5, 53.3; pH 4.5, 39.6; pH 6.0, 38.9. At pH 9.0 the complete ionization results in $Z = 2$. The calculated pK_Z values are independent of pH.

4.1. Determination of cystine and cysteic acid in wool

Of many methods suggested for determination of cystine in protein hydrolysates, the most familiar is that developed by Schram *et al.* [5] based on oxidation followed by isolation of the resulting cysteic acid on an ion-exchange resin and its determination by the ninhydrin spectrophotometric procedure. Another approach involves the separation of cysteic acid using paper chromatography or paper electrophoresis and ninhydrin spectrophotometry [6].

The determination of cysteic acid using the capillary isotachophoretic method suggested in this paper simplifies the whole procedure and extends its field of application. One part of the hydrolysate is examined for cysteic acid and the other, after oxidation with bromine, for total cysteic acid, and the cystine content is calculated by difference. At the same time aspartic acid and glutamic acid can be determined and used to characterize the sample.

About 10 mg of sample was placed in a test-tube (80 mm × 10 mm I.D.), 2 ml of 6 *M* hydrochloric acid were added and the contents were heated by placing the tube in a hole in an iron plate at 120°C. After 18 h the hydrolysate was diluted to 5 ml and a 2-ml portion was transferred into an ampoule (44 mm × 17 mm I.D.) and evaporated at 65°C at normal pressure. The other part of the hydrolysate was oxidized by shaking with 1 *M* bromine in carbon tetrachloride and a 1-ml volume was evaporated to dryness at 65°C in a second ampoule. To each ampoule 1 ml of water and 1 ml of 0.1 *M* tributyltin hydroxide in octane were added and, after shaking and separation, the aqueous phase was examined at pH 3.5.

A calibration graph for cysteic acid was prepared with a standard solution of cysteine after oxidation in 0.2 *M* hydrochloric acid with bromine, evaporation and dilution. The established relationship between the zone length (t, s) and the number of nanomoles of cysteic acid applied to the column at pH 3.5 and a driving current of 50 μA (n_C) can be expressed by the following empirical equations:

$$n_C = 0.191\,t - 0.295 \quad \text{for } t < 40$$

$$n_C = 0.203\,t - 0.76 \quad \text{for } t > 40$$

The relative step heights with the use of 0.2% (v/v) isocapronic acid as terminating electrolyte were found to be cysteic acid 0.26, aspartic acid 0.49 and glutamic acid 0.72. In addition, at relative step heights of 0.19, 0.22, 0.30, 0.34 and 0.41 small amounts of unidentified acids were observed.

The results obtained for a sample of Merino wool on a moisture-free basis, with standard deviations for six independent determinations, were cystine 11.5 ± 0.2 and cysteic acid 0.48 ± 0.04%.

References

[1] F.M. Everaerts, J.L. Beckers and Th.P.E.M. Verheggen, *Isotachophoresis*, Elsevier, Amsterdam, 1976.
[2] P. Boček, M. Deml, P. Gebauer and V. Dolnik, in B.J. Radola (Editor), *Analytical Isotachophoresis*, VCH, New York, 1988, p. 73.
[3] C.J. Holloway, *J. Chromatogr.*, 390 (1987) 101.
[4] T. Hirokawa, M. Nishino, N. Aoki, Y. Kiso, Y. Sawamoto, T. Yagi and J.-I. Akiyama, *J. Chromatogr.*, 271 (1983) D_1.
[5] E. Schram, S. Moore and E.J. Bigwood, *Biochem. J.*, 57 (1954) 33.
[6] M. Baunters, L. Lefebvre and M. Van Overbeine, *Bull. Inst. Text. Fr.*, 80 (1959) 7.

ELSEVIER

Journal of Chromatography A, 672 (1994) 278–279

JOURNAL OF CHROMATOGRAPHY A

Book Review

Theoretical advancement in chromatography and related separation techniques, edited by F. Dondi and G. Guiochon, Kluwer, Dordrecht, Boston, London, 1992, XX + 641 pp., price Dfl. 390.00, US$ 249.00, £136.00, ISBN 0-7923-1991-5.

The reviewed volume contains proceedings of the NATO Advanced Study Institute (ASI) on theoretical aspects of chromatography and related separation technique, organized by Dondi and Guiochon in Ferrara, Italy on August 18–30, 1991. It is listed as Vol. 383 of the *NATO ASI Series C: Mathematical and Physical Science*, which has a well established position in scientific literature.

Because of a great number of articles published each year on theoretical and applied aspects of chromatography and related separation techniques, the investigation of current achievements in this field is very difficult. Thus, the volumes which present the current status of a given research area and address its future developments, are of great interests for readers. The present volume is especially interesting because it contains a unique collection of twenty review articles on recent advancements in the theory of chromatography and related separation techniques, which have been written by outstanding scientists.

The volume starts with three articles by Golshan-Shirazi and Guiochon, in which various models of ideal and linear chromatography are critically reviewed. A special emphasis has been given on the equilibrium-dispersive model of chromatography. The review gives a comprehensive survey of recent progress in this area, to which the authors contributed significantly. The successive three contributions deal with the theory of zonoids and its application to chromatographic processes (two articles by Valentin) and with the stochastic theory of chromatography (work by Dondi *et al.*).

The above mentioned series of articles is followed by very interesting contributions devoted to the retention mechanisms in gas, liquid and supercritical fluid chromatography as well as their applications in physicochemical studies. Four articles by Martire, Findenegg, Riedo and Kováts cover some theoretical aspects of the retention mechanism, which are common to gas–solid and liquid–solid chromatography. For instance, two contributions by Martire present a unified approach to the theory of chromatography and are a continuation of his excellent previous works in this area. The principles of adsorption at solid surfaces and their significance to gas–solid and liquid–solid chromatography have been discussed by Findenegg. However, Conder and Katsanos in their articles reviewed physicochemical measurements by chromatography.

The remaining contributions are devoted to the separation of polymers and biomolecules, using hydrophobic interaction chromatography, affinity chromatography, field flow fractionation, classical or capillary electrophoresis.

The volume is well organized and contains many useful figures, tables and references. As

SSDI 0021-9673(94)00293-I

the editors wrote in preface, the contributions were prepared at the graduate level, accessible to all those who have a good general background in the thermodynamics of phase equilibria and the mass transfer theory. Thus, the book seems to be suitable for scientists and engineers who are interested in the theoretical foundations of chromatographic processes.

Kent, OH, USA M. Jaroniec

Author Index

Journal of Chromatography A

Request for Manuscripts

Susumu Honda will edit a special, thematic issue of the *Journal of Chromatography A* entitled

Chromatographic and Electrophoretic Analyses of Carbohydrates

Both reviews and research articles will be included.
Topics such as the following will be covered:

- Gas chromatography and gas chromatography–mass spectrometry of carbohydrates
- Supercritical fluid chromatography of carbohydrates
- Thin-layer chromatography of carbohydrates
- Liquid chromatography of carbohydrates
  - Separations based on various modes including adsorption, hydrophilic interaction, hydrophobic interaction, ion exchange, ligand exchange, size exclusion, bioaffinity, etc.
  - Derivatization
  - Preparative liquid chromatography
  - High-performance liquid chromatography–mass spectrometry
- Electrophoresis of carbohydrates
  - Gel electrophoresis
  - Capillary zone electrophoresis
  - Micellar electrokinetic capillary chromatography
  - Ultrasensitive detection
  - Derivatization
  - Capillary electrophoresis–mass spectrometry
- Chromatography and electrophoresis in glycobiology
  - Release of carbohydrates from glycoconjugates
  - Monosaccharide composition analysis
  - Oligosaccharide mapping
  - Oligosaccharide sequencing
  - Automated analysis of carbohydrates

Potential authors of reviews should contact Roger Giese, Editor, prior to any submission. Address: Mugar Building Rm 122, Northeastern University, Boston, MA 02115, USA; tel.: (+1-617) 373-3227; fax: (+1-617) 373-8720.

The deadline for receipt of submissions is **November 15, 1994**. Manuscripts submitted after this date can still be published in the Journal, but then there is no guarantee that an accepted article will appear in this special, thematic issue. Four copies of the manuscript, citing this issue, should be submitted to the Editorial Office, *Journal of Chromatography A*, P.O. Box 681, NL-1000 AR Amsterdam, The Netherlands. All manuscripts will be reviewed and acceptance will be based on the usual criteria for publishing in the *Journal of Chromatography A*.

Announcing...

International Ion Chromatography Symposium 1994

19-22 September , 1994
Turin, Italy

Program Chairman:
Corrado Sarzanini
Analytical Chemistry
University of Turin
Via Giuria 5
I - 10125 Turin, Italy
Telephone: +39-11-670-7628
Fax: +39-11-670-7615

Session Topics

- Separation Selectivity and Column Technology
- Developments in Separation Methodology
- Advances in Detection
- Special Sample Treatment Procedures
- Novel Applications
- Process Monitoring and Control
- Separation of Metal Ions
- Pharmaceutical Applications
- Environmental Applications
- Ion analysis in the Electrical Generating Industry
- Standard Methods and Data Processing

For more information, contact:

Century International, Inc.
P.O.Box 493 • 25 Lee Road
Medfield, MA 02052-0493 USA
508/359-8777 • 508/359-8778 (FAX)

Directory of Capillary Electrophoresis

(TrAC Supplement No. 1)

©1994 Paperback 156 pages Price:Dfl.137.00(US$ 70.00)

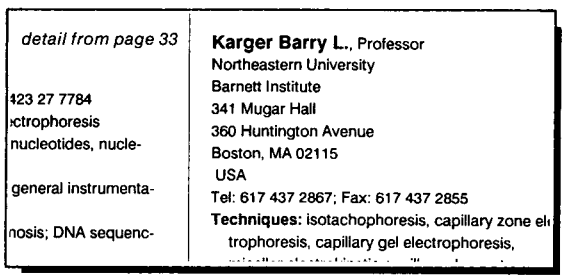

detail from page 33

423 27 7784
ctrophoresis
nucleotides, nucle-

general instrumenta-

nosis; DNA sequenc-

Karger Barry L., Professor
Northeastern University
Barnett Institute
341 Mugar Hall
360 Huntington Avenue
Boston, MA 02115
USA
Tel: 617 437 2867; Fax: 617 437 2855
Techniques: isotachophoresis, capillary zone el
trophoresis, capillary gel electrophoresis,

- **Containing over 450 V.I.P.s Worldwide**
- **Including Complete Addresses, Fax and Phone Numbers, and E-Mail Addresses (where available)**
- **Giving Techniques, Applications and Research Topics**
- **Providing an Extensive Subject Index**

This directory of researchers in capillary electrophoresis not only contains the names and addresses of most leading scientists in this rapidly developing field. The papers in this area that each listed scientist considers as his or her most significant contribution are given. A geographical index with techniques and application areas shows who is doing what in each country. Instrument manufacturers and suppliers are also listed on a country by country basis, along with the products or services they offer.

The editors have endeavoured to collect together, in this one source, information on who's who and the major research trends in the field of capillary electrophoresis.

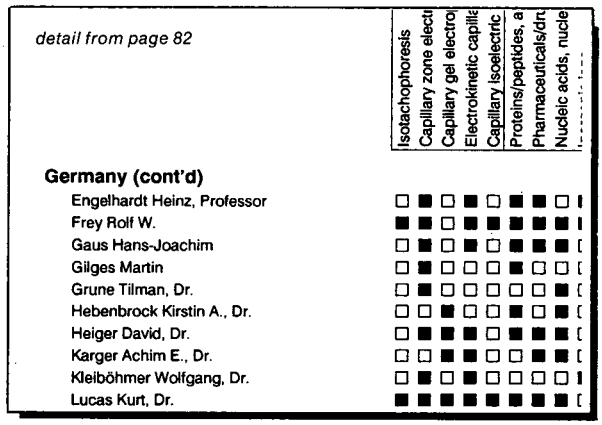

detail from page 82

	Isotachophoresis	Capillary zone electi	Capillary gel electro	Electrokinetic capill	Capillary isoelectric	Proteins/peptides, a	Pharmaceuticals/dn	Nucleic acids, nucle
Germany (cont'd)								
Engelhardt Heinz, Professor	□	■	□	■	□	■	■	□
Frey Rolf W.	■	■	□	■	■	■	■	■
Gaus Hans-Joachim	□	■	□	■	□	■	■	■
Gilges Martin	□	■	□	□	□	■	□	□
Grune Tilman, Dr.	□	■	□	□	□	□	□	■
Hebenbrock Kirstin A., Dr.	□	□	■	□	□	■	□	■
Heiger David, Dr.	□	■	■	■	□	■	■	■
Karger Achim E., Dr.	□	□	■	■	□	□	■	■
Kleiböhmer Wolfgang, Dr.	□	■	□	■	□	□	□	□
Lucas Kurt, Dr.	■	■	■	■	■	■	■	■

ORDER FORM

Please send this form to your regular supplier or to:

Elsevier Science B.V.
Attn. Eugene P.M. Wijnhoven
P.O. Box 330, 1000 AH Amsterdam The Netherlands
Fax: +31 (20) 586 2845

☐ **Yes,** Please send me a copy of **Directory of Capillary Electrophoresis**

☐ Please charge my credit card:
☐ Eurocard ☐ Mastercard ☐ American Express ☐ VISA ☐ Access

Card number: _____ Expiry Date: _____

Vat registration number: _____ Signature: _____

Name: _____

Address: _____

US$ prices are valid only for the USA & Canada and are subject to exchange rate fluctuations; in all other countries the Dutch guilder price (Dfl.) is definitive. Customers in the European Union should add the appropriate VAT rate applicable in their country to the price(s). Books are sent postfree if prepaid.

PUBLICATION SCHEDULE FOR THE 1994 SUBSCRIPTION

Journal of Chromatography A and *Journal of Chromatography B: Biomedical Applications*

MONTH	1993	J	F	M	A	M	J	
Journal of Chromatography A	652–657	658/1 658/2 659/1 659/2	660/1 + 2 661/1 + 2 662/1 662/2	663/1 663/2 664/1	664/2 665/1 665/2 666/1 + 2 667/1 + 2	668/1 668/2 669/1 + 2	670/1 + 2 671/1 + 2 672/1	The publication schedule for further issues will be published later.
Bibliography Section				681/1			681/2	
Journal of Chromatography B: Biomedical Applications		652/1	652/2 653/1	653/2 654/1	654/2 655/1	655/2	656/1 656/2	

INFORMATION FOR AUTHORS

(Detailed *Instructions to Authors* were published in *J. Chromatogr. A*, Vol. 657, pp. 463–469. A free reprint can be obtained by application to the publisher, Elsevier Science B.V., P.O. Box 330, 1000 AH Amsterdam, Netherlands.)

Types of Contributions. The following types of papers are published: Regular research papers (full-length papers), Review articles, Short Communications and Discussions. Short Communications are usually descriptions of short investigations, or they can report minor technical improvements of previously published procedures; they reflect the same quality of research as full-length papers, but should preferably not exceed five printed pages. Discussions (one or two pages) should explain, amplify, correct or otherwise comment substantively upon an article recently published in the journal. For Review articles, see inside front cover under Submission of Papers.

Submission. Every paper must be accompanied by a letter from the senior author, stating that he/she is submitting the paper for publication in the *Journal of Chromatography A* or *B*.

Manuscripts. Manuscripts should be typed in **double spacing** on consecutively numbered pages of uniform size. The manuscript should be preceded by a sheet of manuscript paper carrying the title of the paper and the name and full postal address of the person to whom the proofs are to be sent. As a rule, papers should be divided into sections, headed by a caption (*e.g.*, Abstract, Introduction, Experimental, Results, Discussion, etc.). All illustrations, photographs, tables, etc., should be on separate sheets.

Abstract. All articles should have an abstract of 50–100 words which clearly and briefly indicates what is new, different and significant. No references should be given.

Introduction. Every paper must have a concise introduction mentioning what has been done before on the topic described, and stating clearly what is new in the paper now submitted.

Experimental conditions should preferably be given on a *separate* sheet, headed "Conditions". These conditions will, if appropriate, be printed in a block, directly following the heading "Experimental".

Illustrations. The figures should be submitted in a form suitable for reproduction, drawn in Indian ink on drawing or tracing paper. Each illustration should have a caption, all the *captions* being typed (with double spacing) together on a *separate sheet*. If structures are given in the text, the original drawings should be provided. Coloured illustrations are reproduced at the author's expense, the cost being determined by the number of pages and by the number of colours needed. The written permission of the author and publisher must be obtained for the use of any figure already published. Its source must be indicated in the legend.

References. References should be numbered in the order in which they are cited in the text, and listed in numerical sequence on a separate sheet at the end of the article. Please check a recent issue for the layout of the reference list. Abbreviations for the titles of journals should follow the system used by *Chemical Abstracts*. Articles not yet published should be given as "in press" (journal should be specified), "submitted for publication" (journal should be specified), "in preparation" or "personal communication".

Vols. 1–651 of the *Journal of Chromatography*; *Journal of Chromatography, Biomedical Applications* and *Journal of Chromatography, Symposium Volumes* should be cited as *J. Chromatogr.* From Vol. 652 on, *Journal of Chromatography A* (incl. Symposium Volumes) should be cited as *J. Chromatogr. A* and *Journal of Chromatography B: Biomedical Applications* as *J. Chromatogr. B.*

Dispatch. Before sending the manuscript to the Editor please check that the envelope contains four copies of the paper complete with references, captions and figures. One of the sets of figures must be the originals suitable for direct reproduction. Please also ensure that permission to publish has been obtained from your institute.

Proofs. One set of proofs will be sent to the author to be carefully checked for printer's errors. Corrections must be restricted to instances in which the proof is at variance with the manuscript.

Reprints. Fifty reprints will be supplied free of charge. Additional reprints can be ordered by the authors. An order form containing price quotations will be sent to the authors together with the proofs of their article.

Ovomucoid Bonded Column for Direct Chiral Separation

ULTRON ES-OVM

Narrow-Bore Column (2.0 I.D. x 150 mm) for Trace Analyses
Analytical Column (4.6 I.D. , 6.0 I.D. x 150 mm) for Regular Analyses
Semi-Preparative Column (20.0 I.D. x 250 mm) for Preparative Separation

Analysis of Trace FLURBIPROFEN in Metabolite with NARROW-BORE COLUMN

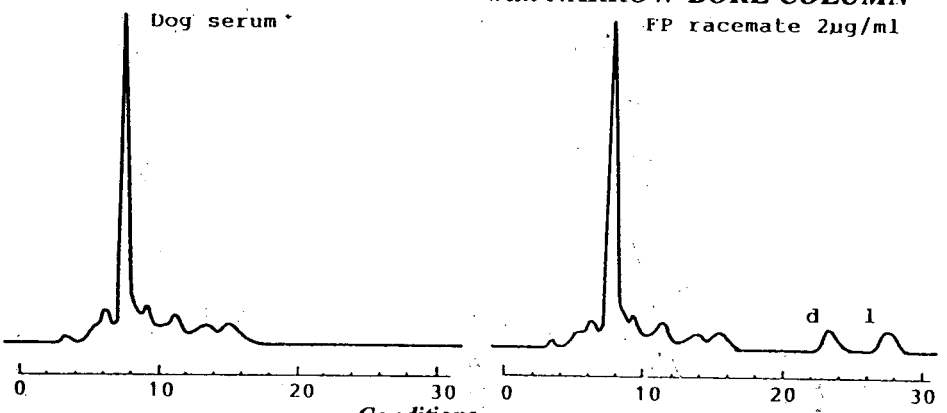

Conditions

Column: ULTRON ES-OVM(2.0I.D. x 150mm)
Mobile Phase: 20mMPhosphate Buffer(pH=3.0)/CH3CN =100/15
Flow Rate: 0.1ml/min
Temperature: 25°C
Injection: 5µl
Detection: UV- 247nm(0.05AUFS)

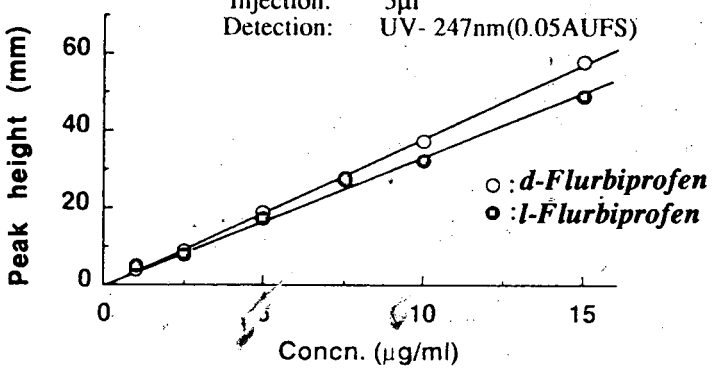

Calibration Curve for Each Enantiomer of Flurbiprofen

SHINWA CHEMICAL INDUSTRIES, LTD.

50 Kagekatsu-cho, Fushimi-ku, Kyoto 612, JAPAN
Phone:+81-75-621-2360 Fax:+81-75-602-2660

In the United States and Europe, please contact:

Rockland Technologies, Inc.

538 First State Boulevard, Newport, DE 19804, U.S.A.
Phone: 302-633-5880 Fax: 302-633-5893

This product is licenced by Eisai Co., Ltd.